

HELICAL TRANSITION METAL COMPLEXES AS  
CATALYSTS FOR ASYMMETRIC SULFOXIDATIONS  
AND ALDOL ADDITION REACTIONS

by

SANMITRA BARMAN

M. Sc., Jadavpur University, 2003

AN ABSTRACT OF A DISSERTATION

submitted in partial fulfillment of the requirements for the degree

DOCTOR OF PHILOSOPHY

Department of Chemistry  
College of Arts and Sciences

KANSAS STATE UNIVERSITY  
Manhattan, Kansas

2010

## Abstract

Stepped helical salen complexes with vanadium as the central metal were synthesized and characterized. The helicity in these complexes arise from the fused phenyl rings (phenanthryl and benz[a]anthryl) as sidearms, whereas the chirality arises from the chiral cyclohexyl diamine or binaphthyl diamine backbones. These complexes showed good yields and moderate enantioselectivity in asymmetric sulfoxidation reactions with methylphenyl sulfide as the substrate and H<sub>2</sub>O<sub>2</sub> or cumene hydroperoxide as the oxidants. To further improve the closed nature of these complexes with a tetradentate salen ligand, we synthesized and characterized vanadium complexes with tridentate (*S*)-NOBIN backbone Schiff base ligands with phenanthryl and benz[a]anthryl as the sidearms. After initial catalytic study, we concluded that these catalysts are too open in nature to impose face selection during asymmetric induction. We also synthesized and characterized vanadium and titanium salen complexes. These complexes can adopt  $\beta$ -*cis* geometry, thereby making the complex “*chiral at metal*” and they are known for better catalysts in terms of asymmetric induction than their unreduced counterparts. However, these complexes showed better catalytic activity than their unreduced counterparts in sulfoxidation reactions with methylphenyl sulfide as the substrate and H<sub>2</sub>O<sub>2</sub> or cumene hydroperoxide as the oxidants. We also put an effort to synthesize mixed salen complexes with vanadium as the central metal. These complexes have two different sidearms attached to one backbone unit. However, our method did not work well to produce pure mixed salen ligands. The catalysis results for mixed salen vanadium complexes are also comparable to the unreduced vanadyl salen complexes. Lastly, we synthesized and characterized new helical titanium Schiff base complexes with (*S*)-NOBIN backbone and phenanthryl and benz[a]anthryl sidearms. Single crystal studies showed that these complexes exist in the *M* helical conformation in the solid state. These complexes showed moderate activity in asymmetric aldol addition reactions between 2-methoxy propene and different aldehydes.

HELICAL TRANSITION METAL COMPLEXES AS  
CATALYSTS FOR ASYMMETRIC SULFOXIDATIONS  
AND ALDOL ADDITION REACTIONS

by

SANMITRA BARMAN

M. Sc., Jadavpur University, 2003

A DISSERTATION

submitted in partial fulfillment of the requirements for the degree

DOCTOR OF PHILOSOPHY

Department of Chemistry  
College of Arts and Sciences

KANSAS STATE UNIVERSITY  
Manhattan, Kansas

2010

Approved by:

Major Professor  
Dr. Christopher J. Levy

## Abstract

Stepped helical salen complexes with vanadium as the central metal were synthesized and characterized. The helicity in these complexes arise from the fused phenyl rings (phenanthryl and benz[a]anthryl) as sidearms, whereas the chirality arises from the chiral cyclohexyl diamine or binaphthyl diamine backbones. These complexes showed good yields and moderate enantioselectivity in asymmetric sulfoxidation reactions with methylphenyl sulfide as the substrate and H<sub>2</sub>O<sub>2</sub> or cumene hydroperoxide as the oxidants. To further improve the closed nature of these complexes with a tetradentate salen ligand, we synthesized and characterized vanadium complexes with tridentate (*S*)-NOBIN backbone Schiff base ligands with phenanthryl and benz[a]anthryl as the sidearms. After initial catalytic study, we concluded that these catalysts are too open in nature to impose face selection during asymmetric induction. We also synthesized and characterized vanadium and titanium salan complexes. These complexes can adopt  $\beta$ -*cis* geometry, thereby making the complex “*chiral at metal*” and they are known for better catalysts in terms of asymmetric induction than their unreduced counterparts. However, these complexes showed better catalytic activity than their unreduced counterparts in sulfoxidation reactions with methylphenyl sulfide as the substrate and H<sub>2</sub>O<sub>2</sub> or cumene hydroperoxide as the oxidants. We also put an effort to synthesize mixed salen complexes with vanadium as the central metal. These complexes have two different sidearms attached to one backbone unit. However, our method did not work well to produce pure mixed salen ligands. The catalysis results for mixed salen vanadium complexes are also comparable to the unreduced vanadyl salen complexes. Lastly, we synthesized and characterized new helical titanium Schiff base complexes with (*S*)-NOBIN backbone and phenanthryl and benz[a]anthryl sidearms. Single crystal studies showed that these complexes exist in the *M* helical conformation in the solid state. These complexes showed moderate activity in asymmetric aldol addition reactions between 2-methoxy propene and different aldehydes.

## Table of Contents

List of Figures .....	viii
List of Tables .....	xiv
Acknowledgements.....	xvi
CHAPTER 1 - Helical Vanadium Salen Complexes for Asymmetric Sulfoxidations .....	1
1.1 Abstract.....	1
1.2 Introduction.....	1
1.3 Results and discussions.....	12
1.3.1 General Synthesis Scheme For The Vanadium-Salen Complexes .....	12
1.3.2 Characterization of the vanadyl complexes (C-1 to C-4) .....	14
1.3.2.1 <sup>1</sup> H NMR spectra of the complexes.....	14
1.3.2.2 IR spectra of the complexes.....	14
1.3.2.3 EPR spectra of complexes C-1 and C-2.....	15
1.3.2.4 Mass spectra of vanadyl(IV)-salen complexes C-1 to C-4 .....	18
1.3.2.5 Solid state X-ray structures of complexes C-1 and C-3.....	23
1.3.2.6 Solution property studies: CD spectroscopy for complexes C-1, C-3 and C-2 ....	29
1.3.2.7 Sulfoxidation Results By Helical Complexes.....	33
1.4 Conclusions.....	38
1.5 Experimental Section .....	38
1.6 References.....	41
CHAPTER 2 - Asymmetric Sulfoxidations By Helical Ti, V, Al, Fe Salan Complexes .....	45
2.1 Abstract.....	45
2.2 Introduction.....	45
2.3 Results and discussions.....	53
2.3.1 General scheme for synthesis of (R,R)-5, (R,R)-6, (R,R)-7 and (R,R)-8 .....	53
2.3.2 Characterization of the ligands .....	54
2.3.3 Synthesis and characterization of Fe(II)-(R,R)-8 (C1) and Al(III)-(R,R)-8 (C2) complexes .....	64

2.3.4 Synthesis and characterization of V(IV)-(R,R)-8 (C-2), V(IV)-(R,R)-7 (C-4) and V(IV) (R,R)-5 (C-5) complexes.....	67
2.3.5 Synthesis and characterization of Ti(IV)-(R,R)-5 (C-6), Ti(IV)-(R,R)-6 (C-7), Ti(IV)-(R,R)-7 (C-8) and Ti(IV)-(R,R)-8 (C-9) complexes.....	71
2.3.6 Sulfoxidation by Al, Fe, V and Ti-salan complexes.....	79
2.4 Conclusions.....	87
2.5 Experimental Section.....	88
2.6 References:.....	95
<b>CHAPTER 3 - Chiral Helical <math>C_1</math>-Symmetrical Vanadium And Zinc Salen Complexes For</b>	
Asymmetric Sulfoxidations.....	98
3.1 Abstract.....	98
3.2 Introduction.....	98
3.3 Results and Discussion.....	104
3.3.1 Synthesis of non-symmetrical salen ligands.....	104
3.3.2 Synthesis and characterization of non-symmetrical Zn and V salen complexes.....	109
3.3.3 Asymmetric sulfoxidations by non-symmetrical vanadyl(IV) salen complexes.....	112
3.4 Conclusions.....	115
3.5 Experimental Section.....	115
3.6 References.....	120
<b>CHAPTER 4 - Sulfoxidations by <math>C_1</math> Symmetric (S)-Nobin Backbone Helical Vanadium Schiff</b>	
Base Complexes.....	122
4.1 Abstract.....	122
4.2 Introduction.....	122
4.3 Results and discussions.....	127
4.3.1 Synthesis of ligands (S)-3 and (S)-5.....	127
4.3.2 Characterization of ligands (S)-3 and (S)-5.....	128
4.3.3 Synthesis of vanadium(IV) complexes (C-1 and C-2) with ligands (S)-3 and (S)-5.....	132
4.3.4 Characterization of complexes C-1 and C-2.....	132
4.3.5 Asymmetric sulfoxidations by catalysts C-1 and C-2.....	138
4.4 Conclusions.....	142
4.6 References.....	146

CHAPTER 5 - Catalytic Enantioselective Acetone Aldol Additions With 2-Methoxypropene	148
5.1 Abstract.....	148
5.2 Introduction.....	148
5.3 Results and discussions.....	152
5.3.1 Synthesis of (S)-NOBIN backbone isoquinualdehyde side arm tridentate Schiff base ligand.....	152
5.3.2 Characterization of ligand (S)-4.....	152
5.3.3 Synthesis of complexes C-3, C-4 and C-5.....	155
5.3.4 Characterization of complexes C-3, C-4 and C-5.....	156
5.3.5 Catalytic asymmetric aldol condensations.....	168
5.4 Conclusions.....	175
5.5 Experimental Section.....	175
5.6 References.....	183
CHAPTER 6 - Overall Conclusions And Future Work.....	185
Reference:.....	186
Appendix A - Chapter 1.....	187
Appendix B - Chapter 2.....	196
Appendix C - Chapter 3.....	219
Appendix D - Chapter 4.....	227
Appendix E - Chapter 5.....	231

## List of Figures

1.1. General scheme for the synthesis of salen ligands.....	2
1.2. Possible configurations of metallosalen complexes .....	2
1.3. Equilibrium between two conformers.....	3
1.4. Helical units as opposed to planar units.....	4
1.5. Minimized <i>P</i> (left) and <i>M</i> (right) conformations of monohelical Zn(II) salen complex.....	4
1.6. Ligand directed complex conformation preference in solution.....	5
1.7. Shows different trajectories of the approaching reactant molecule to the metal center.....	6
1.8. Binaphthyl backbone salen ligand coordinated to Pd(II).....	7
1.9. Trajectory for the approach of the substrate molecule to the catalyst center of copper(II) salen catalyst.....	7
1.10. "S" isomer of omeprazole.....	8
1.11. First salen vanadium catalyst for thioanisole oxidation with cumene hydroperoxide.....	8
1.12. Vanadium(IV) salen catalyst system introduced by Bolm et al.....	9
1.13. Sulfoxidation catalyst system introduced by Katsuki et al.....	9
1.14. Schematic of the titanium(IV) salen catalyst responsible for high asymmetric induction...10	
1.15. Salen ligands used in this study.....	11
1.16. Synthesis of vanadyl complexes <b>C-1</b> to <b>C-4</b> .....	12-13
1.17. <sup>1</sup> H NMR (CDCl <sub>3</sub> , 400 MHz) of complex <b>C-1</b> .....	14
1.18. EPR spectrum of complex <b>C-1</b> .....	16
1.19. EPR spectrum of complex <b>C-2</b> .....	17
1.20. Sketch of the general orientation of the principal axis system for g on proton hyperfine tensors for complex <b>C-2</b> .....	18
1.21. Observed (top) and simulated (bottom) mass spectra of complex <b>C-1</b> .....	19
1.22. Observed (top) and simulated (bottom) mass spectra of complex <b>C-2</b> .....	20
1.23. Observed (top) and simulated (bottom) mass spectra of complex <b>C-3</b> .....	21
1.24. Observed (top) and simulated (bottom) mass spectra of complex <b>C-4</b> .....	22
1.25. Thermal ellipsoid plot of complex <b>C-1</b> (first molecule: <i>P</i> , second molecule: <i>M</i> ).....	24
1.26. Space filling models of <b>C-1</b> showing the <i>P</i> and the <i>M</i> conformers.....	25



1.27. Thermal ellipsoid plot of <b>C-3</b> (top: <i>P</i> , bottom: <i>M</i> ).....	26
1.28. Space filling models of <b>C-3</b> showing the <i>P</i> and the <i>M</i> conformers.....	27
1.29. Experimental and corrected CD spectra of zinc salen complex.....	30
1.30. CD spectra for complex <b>C-1</b> and <b>C-3</b> .....	31
1.31. CD spectra of zinc salen complex (top) and vanadyl salen complex (bottom).....	32
1.32. Exposure of the vanadium(IV) center for the substrate attack.....	33
1.33. % conversion with time (hr) plot for all the catalysts in CHCl <sub>3</sub> and MeOH mixture.....	34
1.34. Proposed mechanism of vanadium(IV) salen catalyzed sulfoxidations.....	36
1.35. Three dimensional structure (left) and two dimensional representation (right) of the transition state leading to one possible isomer ( <i>R</i> or <i>S</i> ).....	37
1.36. Three dimensional structure (left) and two dimensional representation (right) of the transition state leading to one possible isomer ( <i>R</i> or <i>S</i> ).....	37
1.37. Hydrogen bonding assisted face selectivity.....	38
2.1. Sulfoxidation catalytic system introduced by Kagan and Modena.....	46
2.2. Katsuki's titanium(IV)-salen complex for sulfoxidations.....	47
2.3. Vanadium(IV) salen catalyzed sulfoxidation of thioanisole.....	48
2.4. Fe(II) salen catalyzed asymmetric sulfoxidations.....	49
2.5. Al(III) salen catalyzed asymmetric sulfoxidations.....	49
2.6. Possible geometries of an octahedral metal salen complex.....	50
2.7. Diastereomers after complexation with titanium.....	50
2.8. Two isomers of <i>fac-fac</i> octahedral titanium salen complex.....	51
2.9. Ball and stick model of octahedral titanium(IV) salen complex.....	52
2.10. Stick model of vanadium(IV) salen complex.....	52
2.11. Salan ligands used in this study.....	53
2.12. Synthesis of salan ligands used in this study.....	54
2.13. AB pattern from the two protons of the CH <sub>2</sub> group.....	54
2.14. Proton NMR (CDCl <sub>3</sub> , 400 MHz) spectrum of ( <b><i>R,R</i></b> )- <b>6</b> .....	55
2.15. <sup>1</sup> H- <sup>1</sup> H COSY spectrum (top) of the salan ligand showing the couplings.....	56
2.16. <sup>1</sup> H- <sup>1</sup> H NOESY spectrum (top) of the salan ligand showing the through space couplings.....	57
2.17. <sup>1</sup> H NMR (CDCl <sub>3</sub> , 400 MHz) peak assignments for ( <b><i>R,R</i></b> )- <b>8</b> .....	59
2.18. <sup>1</sup> H- <sup>1</sup> H COSY spectrum for ligand ( <b><i>R,R</i></b> )- <b>8</b> .....	60

2.19. NOESY spectrum of <b>(R,R)-8</b> .....	62
2.20. HMQC spectrum of <b>(R,R)-8</b> .....	63
2.21. A correlation between the aromatic carbons and protons numbering for table 2.3.....	63
2.22. Synthesis of iron ( <b>C-1</b> ) and aluminum ( <b>C-3</b> ) complexes from <b>(R,R)-8</b> .....	65
2.23. <sup>27</sup> Al NMR spectrum for complex <b>C-3</b> .....	66
2.24. UV (left) and CD (right) spectra of complex <b>C-3</b> .....	66
2.25. Synthesis of vanadium(IV) salen complexes.....	67
2.26. Two possible conformations of a helix ( <i>M</i> and <i>P</i> ).....	69
2.27. Model zinc salen complex with <i>M</i> conformation.....	70
2.28. Vanadium(IV) salen complex ( <b>C-4</b> ) with <i>P</i> conformation.....	70
2.29. Synthesis of complexes <b>C-6</b> , <b>C-7</b> , <b>C-8</b> and <b>C-9</b> .....	72
2.30. <sup>1</sup> H NMR (CDCl <sub>3</sub> , 400 MHz) spectrum of <b>C-6</b> .....	73
2.31. Δ and Λ isomers of complex <b>C-6</b> .....	73
2.32. Experimental and simulated CD spectra of <i>P</i> and <i>P+M</i> conformations.....	74
2.33. CD spectrum of titanium(IV) salen complex ( <b>C-6</b> ) in the <i>P</i> conformation in THF.....	75
2.34. <sup>1</sup> H- <sup>1</sup> H COSY spectrum of <b>C-6</b> .....	76
2.35. <sup>1</sup> H- <sup>1</sup> H NOESY spectrum of complex <b>C-6</b> .....	77
2.36. Effect of temperature on ee of the product, tested with catalyst <b>C-8</b> .....	81
2.37. Effect of time on % conversions by different catalysts.....	81
2.38. Working hypothesis for an effective catalyst for oxidation with H <sub>2</sub> O <sub>2</sub> .....	82
2.39. Effect of oxidant/substrate ratio on yields and stereoselectivity of the product.....	84
2.40. Site for the substrate to approach the titanium metal center.....	85
2.41. Hydrogen bonding in titanium salen complex.....	86
2.42. Mechanism of titanium salen catalyzed sulfoxidations.....	87
3.1. Salen ligand introduced by Jacobsen.....	98
3.2. Retrosynthetic analyses of unsymmetrical salen ligands.....	99
3.3. Problems encountered during the synthesis of non-symmetrical salen ligands.....	100
3.4. Formation of <i>racemic</i> mixed salen ligand.....	101
3.5. Salt formation in case of <i>non-racemic</i> 1,2-diamino cyclohexane.....	101
3.6. Mixed salen ligand synthesized by Jacobsen et al.....	102
3.7. Synthesis of unsymmetrical salen ligands by protecting group approach.....	103

3.8. Metal template approach for the synthesis of unsymmetrical zinc salen complex.....	104
3.9. Non-symmetric salen ligands used in this study.....	104
3.10. Scheme for the synthesis of salen ligands.....	105
3.11. Molecular ion peak of ligand ( <b>R,R</b> )- <b>2</b> at ESI-MS.....	106
3.12. UV (left) and CD (right) spectra of ( <b>R,R</b> )- <b>2</b> .....	107
3.13. UV and CD spectra of symmetric salen ligand.....	107
3.14. <sup>1</sup> H NMR (CDCl <sub>3</sub> , 400 MHz) (top) with some assigned peaks (bottom) for ( <b>R,R</b> )- <b>3</b> .....	108
3.15. Synthesis of complexes <b>C-1</b> , <b>C-2</b> and <b>C-3</b> .....	109
3.16. Comparison of the chemical shifts of the ligand and the zinc(II) complex.....	110
3.17. Observed isotopic pattern (left) for unsymmetrical vanadyl(IV) salen complex ( <b>C-3</b> ) with simulated isotopic pattern (right).....	111
3.18. Sulfoxidation by catalysts <b>C-2</b> and <b>C-3</b> .....	112
3.19. Three dimensional structure (left) and two dimensional representation (right) of the transition state leading to one possible isomer ( <i>R</i> or <i>S</i> ).....	114
3.20. Three dimensional structure (left) and two dimensional representation (right) of the transition state leading to one possible isomer ( <i>R</i> or <i>S</i> ).....	114
4.1. C <sub>1</sub> symmetric vanadium(IV) Schiff base complex.....	123
4.2. C <sub>1</sub> symmetric vanadium(IV) Schiff base complex for asymmetric sulfoxidations.....	123
4.3. Bolm and Bienewald's tridentate ligand for vanadium(IV) catalyzed sulfoxidations.....	124
4.4. Diastereomeric vanadium(V) species (a) and (b).....	124
4.5. BINOL, BINAM and NOBIN structures.....	125
4.6. Possible directions of approach of the nucleophile to the metal center.....	126
4.7. Tridentate salen ligands used for the complexation with vanadium(V).....	126
4.8. Synthesis scheme of ( <i>S</i> )-NOBIN backbone salen ligand.....	127
4.9. <sup>1</sup> H NMR (CDCl <sub>3</sub> , 400 MHz) for ligand ( <b>S</b> )- <b>3</b> .....	128
4.10. <sup>1</sup> H NMR (CDCl <sub>3</sub> , 400 MHz) for ligand ( <b>S</b> )- <b>5</b> .....	129
4.11. Molecular ion peak of ( <b>S</b> )- <b>3</b> in ESI-MS.....	130
4.12. Molecular ion peak of ( <b>S</b> )- <b>5</b> in ESI-MS.....	130
4.13. Thermal ellipsoid plot of ligand ( <b>S</b> )- <b>5</b> .....	131
4.14. Space filling model of the crystal packing for ligand ( <b>S</b> )- <b>5</b> .....	131
4.15. Synthesis scheme for complexes <b>C-1</b> and <b>C-2</b> .....	132

4.16. <sup>1</sup> H NMR (CDCl <sub>3</sub> , 400 MHz) spectrum of complex <b>C-1</b> .....	133
4.17. <sup>1</sup> H NMR (CDCl <sub>3</sub> , 400 MHz) spectrum of complex <b>C-2</b> .....	133
4.18. ESI-MS of complex <b>C-1</b> .....	134
4.19. ESI-MS for complex <b>C-2</b> .....	135
4.20. UV spectra of the ligand ( <b>S</b> )- <b>3</b> (left) and the complex <b>C-1</b> (right).....	137
4.21. CD spectra of the ligand ( <b>S</b> )- <b>3</b> (left) and the complex <b>C-1</b> (right).....	137
4.22. UV spectra of the ligand ( <b>S</b> )- <b>5</b> (left) and the complex <b>C-2</b> (right).....	138
4.23. CD spectra of the ligand ( <b>S</b> )- <b>5</b> (left) and the complex <b>C-2</b> (right).....	138
4.24. Sulfoxidations catalyzed by catalysts <b>C-1</b> and <b>C-2</b> .....	139
4.25. Mechanism for sulfoxidations reactions catalyzed by complex <b>C-1</b> .....	141
5.1. Scheme for an aldol reaction.....	148
5.2. Acetone aldol addition by titanium Schiff base complex introduced by Carreira.....	149
5.3. Two different coordination environments of the ligands around the metal center.....	151
5.4. Two possibilities of approach for the nucleophile to the aldehyde moiety.....	151
5.5. Scheme for the synthesis of ligand ( <b>S</b> )- <b>4</b> .....	152
5.6. <sup>1</sup> H NMR (CDCl <sub>3</sub> , 400 MHz) spectrum of ligand ( <b>S</b> )- <b>4</b> .....	153
5.7. Crystal structure with atom numbering for ligand ( <b>S</b> )- <b>4</b> .....	154
5.8. Space filling model of ligand ( <b>S</b> )- <b>4</b> (oxygen in red and nitrogen in blue).....	154
5.9. Titanium(IV) complexes ( <b>C-3</b> , <b>C-4</b> and <b>C-5</b> ) with ( <b>S</b> )-NOBIN backbone ligands.....	156
5.10. MALDI-TOF mass spectrum of the complex <b>C-3</b> (top) and simulated spectrum (bottom).....	157
5.11. <sup>1</sup> H NMR (CDCl <sub>3</sub> , 400 MHz) peak assignments for complex <b>C-4</b> .....	158
5.12. <sup>1</sup> H NMR (CDCl <sub>3</sub> , 400 MHz) peak assignments for complex <b>C-5</b> .....	159
5.13. Observed (left) and simulated (right) mass spectra of the complex <b>C-4</b> .....	160
5.14. Observed (left) and simulated (right) mass spectra of the complex <b>C-5</b> .....	161
5.15. CD spectrum of the ligand ( <b>S</b> )- <b>3</b> (left) and the complex <b>C-4</b> (right).....	162
5.16. CD spectrum of the ligand ( <b>S</b> )- <b>5</b> (left) and the complex <b>C-5</b> (right).....	163
5.17. One pair of molecules with atom numbering for complex <b>C-4</b> .....	164
5.18. Thermal ellipsoid model of the arrangement of one pair of molecules in the complex <b>C-4</b> .....	165
5.19. Structure of complex <b>C-5</b> with atom numbering.....	166

5.20. Space filling model of complex <b>C-5</b> (front view and the back view).....	166
5.21. Schematic of aldol addition reactions catalyzed by Ti complexes.....	169
5.22. Proposed mechanism for aldol condensation.....	170
5.23. Preference of attack by the nucleophile on the aldehyde moiety.....	171
5.24. Reaction of ( <i>R</i> )- <i>O</i> -acetyl mandelic acid with $\beta$ -hydroxy ketone.....	172
5.25. $^1\text{H}$ NMR ( $\text{CDCl}_3$ , 400 MHz) of ( <i>R</i> )- <i>O</i> -acetyl mandelic acid derivative of the $\beta$ -hydroxy ketone derived from 3-phenyl propanaldehyde.....	174

## List of Tables

1.1. IR stretching frequencies of different complexes.....	15
1.2. Spin Hamiltonian parameters calculated for the EPR spectrum of <b>C-2</b> in DMSO.....	17
1.3. Crystal data for <b>C-1</b> .....	24
1.4. Crystal data for <b>C-3</b> .....	26
1.5. Comparison of bond lengths and bond angles of <i>M</i> and <i>P</i> isomers of <b>C-1</b> .....	28
1.6. Comparison of bond lengths and bond angles of <i>M</i> and <i>P</i> isomers of <b>C-3</b> .....	29
1.7. Sulfoxidation results by different catalysts.....	35
2.1. Correlation between aliphatic protons from 1D and 2D NMR.....	58
2.2. Correlation between few protons in ligand ( <b><i>R,R</i></b> - <b>8</b> ) from 1D and 2D NMR.....	61
2.3. Correlation between aromatic carbons and protons from HSQC.....	64
2.4. Calculated and found mass spectral data for <b>C-2</b> .....	68
2.5. Calculated and found mass spectral data for <b>C-4</b> .....	68
2.6. ESI-MS data for <b>C-5</b> .....	71
2.7. <sup>1</sup> H- <sup>1</sup> H NMR correlation between the aromatic protons in <b>C-6</b> shown in figure 2.34.....	78
2.8. Comparison between calculated and observed mass spectral data for <b>C-8</b> .....	79
2.9. Comparison between calculated and observed mass spectral data for <b>C-9</b> .....	79
2.10. Sulfoxidation results by different catalysts.....	83
2.11. Comparative activity study of all the catalysts in terms of conversions and selectivity.....	85

3.1. Assigned protons (molecule shown with marked protons) chemical shifts.....	106
3.2. Chemical shifts and splitting patterns (comparison between the ligand and the complex)..	110
3.3. Sulfoxidation results by catalysts <b>C-2</b> and <b>C-3</b> .....	113
4.1. Sulfoxidation results by different catalysts.....	140
4.2. Comparison of the ee of the sulfoxide with the ee of the ligand ( <b>S</b> )- <b>5</b> (catalyst <b>C-2</b> ).....	142
5.1. Yields and ee's from the reaction of 2-methoxy propene with different aldehydes.....	150
5.2. Some basic parameters for complexes <b>C-4</b> and <b>C-5</b> .....	167
5.3. Selected bond lengths and bond angles for complexes <b>C-4</b> and <b>C-5</b> .....	167
5.4. Aldol addition results by catalysts <b>C-4</b> and <b>C-5</b> .....	173
5.5. Ratio of different characteristic protons in the product ester from different aldehydes.....	174

## **Acknowledgements**

I would like to thank my advisor Dr. Christopher Levy for his help, advice and support, while a member of his research group. Thanks also go to my committee members Dr. Eric Maatta, Dr. Stefan Bossmann, Dr. John Tomich and Dr. Larry Erickson. Also deserving of praise are the support of the chemistry department of KSU- thank you Jim for many repairs, thank you Earline for being so nice throughout and thank you Tobe for all your help.

I would also like to thank the coworkers who have made my time and experience a positive one, and other graduate students, whom I have known in the time that I have spent here.



# CHAPTER 1 - Helical Vanadium Salen Complexes for Asymmetric Sulfoxidations

## 1.1 Abstract

Chiral oxovanadium(IV) salen complexes, [VO(salen)], were prepared by ligand replacement reactions starting from vanadyl(IV) acetylacetonate as the source of vanadyl. The complexes were characterized by  $^1\text{H}$  NMR (nuclear magnetic resonance), IR (infra-red), EPR (electron paramagnetic resonance), MALDI-TOF-MS (time-of-flight mass spectrometry), UV-Vis and circular dichroism (CD) spectra. Single crystals were grown to understand the active site of the catalysts in the asymmetric oxidation reactions. Single crystal XRD showed the unique mono-helical nature of these catalysts with a good possibility of face selectivity after the binding of the reactant molecules in the transition state. All the oxovanadium(IV) complexes catalyze the asymmetric oxidation of sulfides to sulfoxides with good selectivity for sulfoxides and low to moderate enantiomeric excess ranged between 8 to 33% with hydrogen peroxide as the terminal oxidant in  $\text{CHCl}_3$  and 5% MeOH mixture. The enantiomeric excess in the product sulfoxides are found to be better when the reactions were carried out in chloroform with 5% methanol than in dichloromethane.

## 1.2 Introduction

Chiral organic molecules have great importance in pharmaceuticals and agrochemical industries.<sup>1</sup> A handful of drug molecules obtained from a natural source or made in the laboratory, are chiral.<sup>2</sup> Therefore, there has been a huge effort to synthesize these important chiral molecules in the laboratory to meet societal needs. One versatile way to make chiral molecules is by asymmetric catalysis, where a transition metal based chiral complex or a chiral organic molecule act as the source of asymmetric induction.<sup>3</sup> Transition metals have shown promising activity to act as effective catalysts due to their Lewis acidity, binding capability, redox nature and easy availability. For many years, chiral transition metal complexes have been very useful in various types of asymmetric induction reactions.<sup>4</sup> One class of reactions that is very important to the pharmaceutical industries, is asymmetric oxidation reactions. In this category asymmetric sulfoxidation is widely useful as many drugs have sulfoxide functional groups in their active structure.<sup>5</sup>

Salen ligands, which are diimine-diphenolate ligands bearing a linkage between two imine donors, have emerged as one of the most versatile synthetic ligands.<sup>6</sup> These ligands are generally synthesized by condensation between a chiral diamine and salicylaldehyde moiety in a 1:2 ratio (figure 1.1). The chiral diamine imparts chirality in the complex and acts as backbone whereas the derivative of salicylaldehyde acts as the sidearm of the entire molecule. Since a wide variety of chiral diamines and derivatives of salicylaldehydes are readily available or easily synthesizable, plethora of chiral ligands can be produced with tetradentate ONNO donor center.

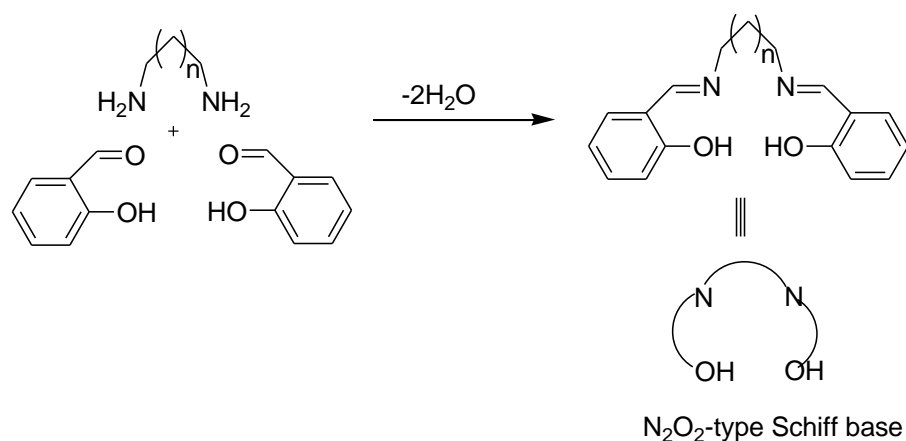


**Figure 1.1.** General scheme for the synthesis of salen ligand.

The conformations of the salen catalysts play a crucial role in asymmetric induction. First row transition metals often display octahedral geometry with tetradentate ONNO donor atoms and two ancillary ligands.<sup>7</sup> The metal salen complexes normally have three possible configurations: *trans*, *cis-β* and *cis-α* (figure 1.2).<sup>7</sup>

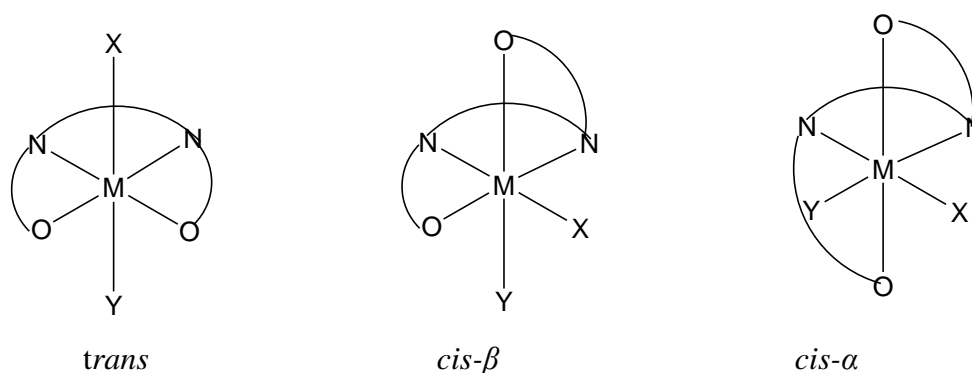


**Figure 1.2.** Possible configurations of metallosalen complexes.

In the *trans* isomer the two ancillary ligands occupy the apical positions in the complex. *Trans* metallo-salen complexes with the flexible backbones, exist in “stepped conformation” (figure 1.3).<sup>7</sup> If there is significant flexibility, the stepped conformation can equilibrate between two conformers, depending on the orientation of the R group in the backbone. Normally the conformer with the two R groups equatorial is more stable on steric grounds (figure 1.3).<sup>7</sup>

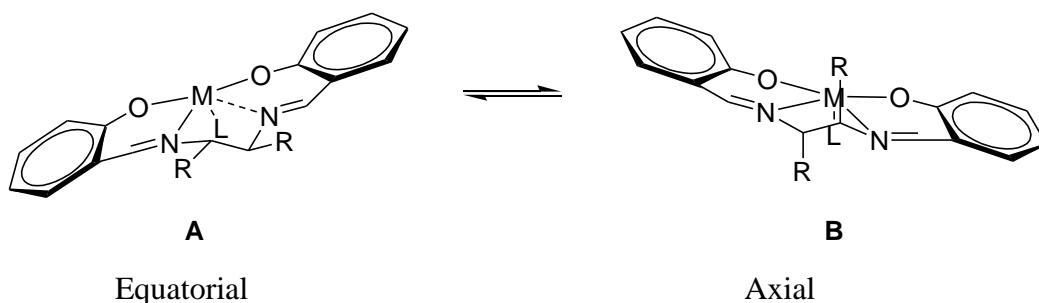


**Figure 1.3.** Equilibrium between two conformers.

The stepped conformations of salen ligands are closely related to helical structures. Helical molecules are chiral and have great potential as asymmetric building blocks and catalysts. Inspired from nature, a helical molecule is a coil shaped molecule like DNA (figure 1.4).<sup>8</sup> Diimine backbone chirality can influence the helicity in metal-salen complexes, and in some models it has been argued that helical chirality plays a crucial role in asymmetric catalysis. For example, elegant studies by Katsuki have showed that chiral donor ligands can induce high enantiomeric excess catalyzed by achiral manganese-salen catalysts.<sup>9</sup> Computational studies also have showed that the high enantiomeric excess in the product comes from the folding of the catalysts.<sup>7</sup> So, folding or helicity itself can act as a source of chiral induction compared to a planar unit where there is no directional property (figure 1.4). Depending on the direction of the rotation of the coil, a helix can have *P* (direction of rotation is clockwise) or *M* (direction of rotation is anticlockwise). Helical complexes with one metal ion are called monohelices and when one metal center binds to one ligand and the resulting complex gets a helical shape, it is called a single stranded mono helix (figure 1.5).<sup>7</sup>

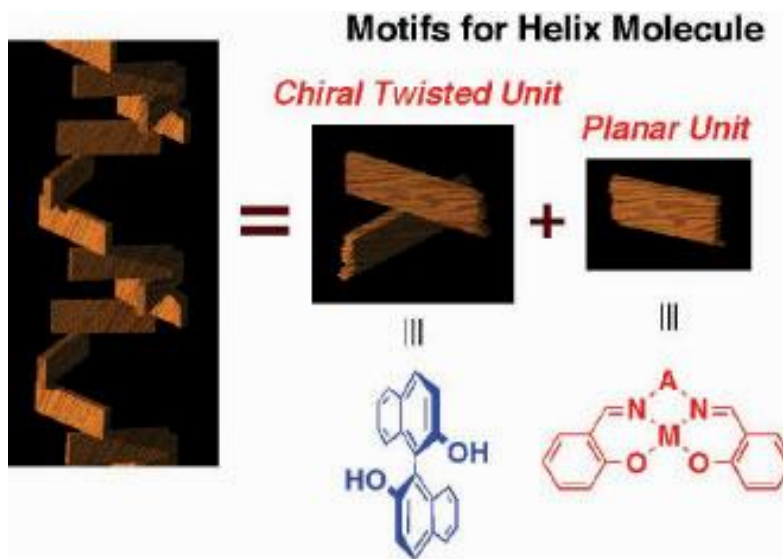


**Figure 1.4.** Helical units as opposed to planar unit.<sup>(7)</sup>

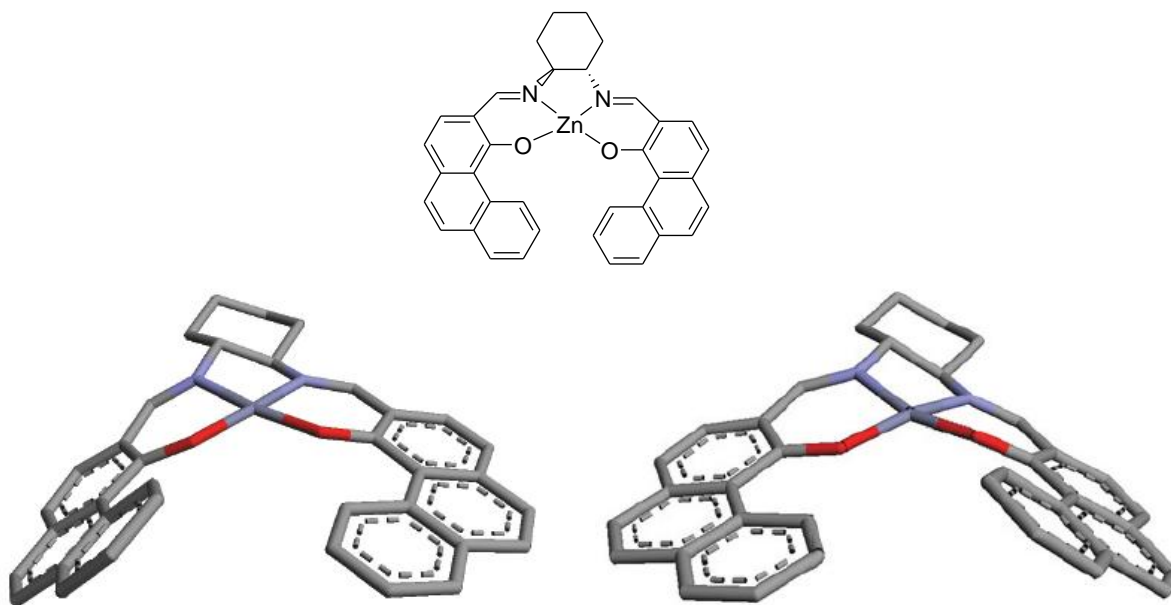


**Figure 1.5.** Minimized *P* (left) and *M* (right) conformations of monohelical Zn(II)-salen complex

It has been shown that the coordination geometry as well as the conformations of the salen ligands can be changed by changing the diamine linkage, leading to unique reactivity.<sup>10</sup> Also salicylidene rings can be appropriately modified to create a helical nature in the entire complex leading to enhanced chirality resulting from the backbone as well as the helical folding in the molecule.<sup>10</sup> It has been observed that the amount of chiral induction increases

proportionately with the amount of chirality in the chiral catalysts.<sup>11</sup> In our group, we have synthesized the helical metal salen complexes by appropriately modifying the salicylidene rings in which intramolecular hydrogen bonding,  $\pi$ - $\pi$  stacking can take place; giving the complex a rigid helical structure. Also, the preferred orientation of the metal binding sites is an important factor which gives the complex stability and an unique helical nature with extended sidearms overlap with each other.

In previous studies, it has been seen that the (*R,R*)-1,2-cyclohexyldiamine backbone biases these salen complexes to form *M* helix preferentially to the *P* form (figure 1.6). In some cases only one type of helix is formed while in other cases there is evidence for both in the solid state. Circular dichroism studies showed the preferential formation of the *M* helix in solution and facile conversion between *M* and *P* forms.<sup>12</sup>

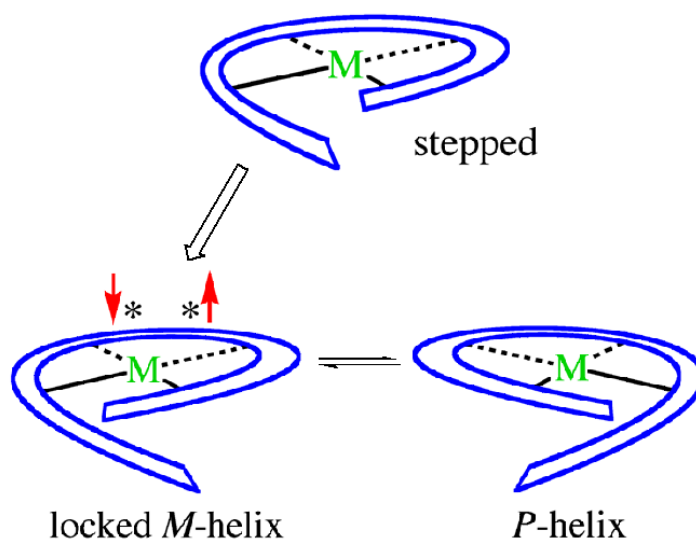


**Figure 1.6.** Ligand directed complex conformation preference in solution (actual structures of the *M* and *P* conformers of a zinc salen complex are shown in figure 1.5).

Figure 1.7 shows the different trajectories in which the incoming nucleophile can approach the Lewis acidic metal center. Vanadium as the central metal has been successfully used as the central metal for asymmetric reactions. Vanadyl complexes of tetradentate ONNO chelating ligands tend to be square pyramidal with one apical position occupied by the oxo group. After it forms a locked conformation facilitated by the  $\pi$ - $\pi$  stacking of the extended fused phenyl ring sidearms and the rigid backbone unit, there seems to be only three possible

trajectories of approach from the nucleophile to the central metal in the transition state. These areas are marked as “A”, “B” and “C”. Area “A” is marked as the gap between the two side arms when they cross each other, Area “B” is marked as the empty space underneath the sidearm in the locked *M* conformation of the complex and the last direction is marked as “C”, which is directly from the bottom of the square plane. Among all the trajectories proposed, “A” is the most acceptable one due to the availability of the free space in this direction and the empty  $d_{xy}$ ,  $d_{yz}$  and the  $d_{zx}$  orbitals in the metal center. Although, direction “C” seems to have the most empty space available for the nucleophile to approach the central metal, but there is no available empty orbital in this direction as the  $d_z^2$  orbital is already involved in bonding with axial oxygen atom.

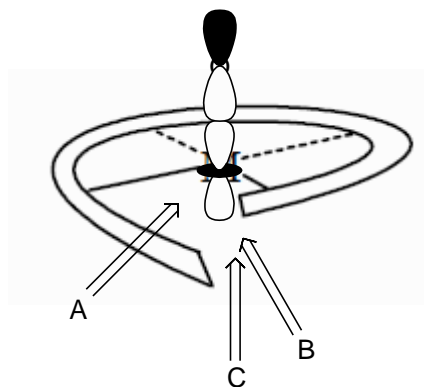


**Figure 1.7.** Shows different trajectories of the approaching reactant molecule to the metal center.

The second chiral backbone used in this research investigation, is the *R* binaphthyl moiety. Salen ligands with binaphthyl backbone generally tend to coordinate with the metal center with a distorted tetrahedral geometry.<sup>13</sup> Exceptions are found for Pd-salen complexes, which tend to have a square pyramidal geometry with the binaphthyl moiety as the backbone. This is presumably due to the high affinity of Pd for square planar geometry (figure 1.8).<sup>14</sup> A few binaphthyl salen metal complexes (with coordination numbers 5 and 6) have been also reported.<sup>15</sup> These mostly have distorted trigonal bipyramidal and octahedral geometries.<sup>15</sup>

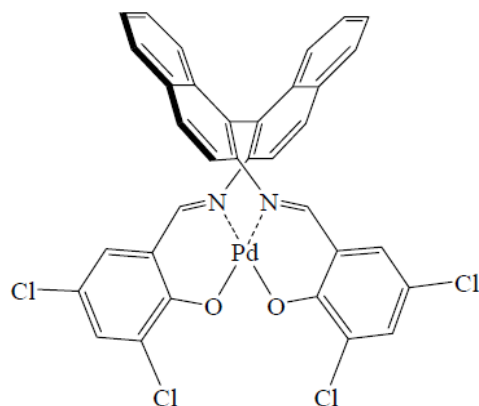


**Figure 1.8.** Binaphthyl backbone salen ligand coordinated to Pd(II).

Binaphthyl salen ligands show axial chirality due to the restricted rotation of the naphthyl rings.<sup>16</sup> The extended fused phenyl ring sidearms can lock the complex structure very effectively due to the high rotational barrier from the binaphthyl backbone and  $\pi$ - $\pi$  overlapping from the sidearms. These two combined factors can lead to one rigid diastereomeric form of the catalyst molecule with a sterically congested environment. The binaphthyl group and a helical conformation (figure 1.9) can influence the directionality of the incoming nucleophile to an appreciable amount (figure 1.9). Binaphthyl salen metal complexes appear to have well defined chiral environment and this phenomenon can lead to the acceptable facial selection of the substrate molecule at the catalyst surface resulting in good enantiomeric excess in the product.

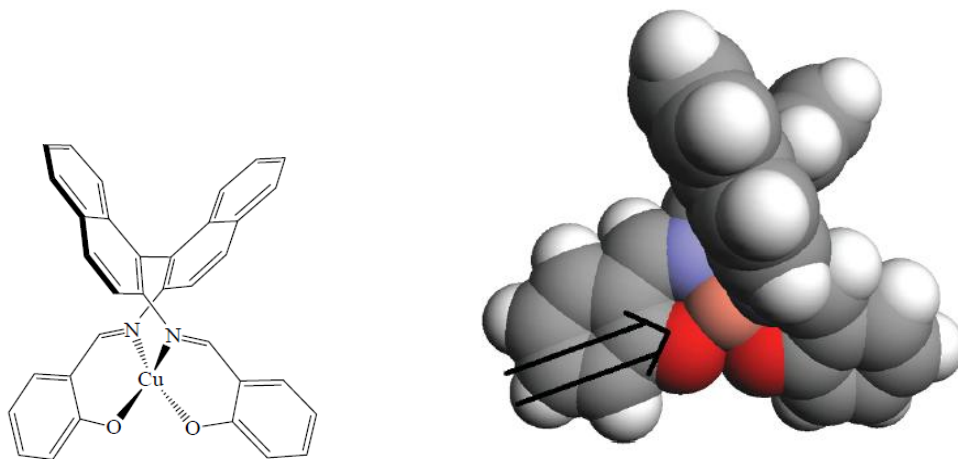


**Figure 1.9.** Trajectory for the approach of the substrate molecule to the catalyst center of copper(II) salen catalyst.

Chiral sulfoxidation catalyzed by helical vanadium salen complexes is the focus of this research.<sup>17</sup> One example of a drug containing a chiral sulfoxide unit is omeprazole.<sup>18</sup> The *S* isomer is an active drug whereas the *R* isomer is not active (figure 1.10). So far, mostly Ti, V and Mn salen complexes are the most studied as catalysts for asymmetric sulfoxidation reactions. In 1986, Nakajima et al. reported on the application of catalysts bearing chiral salen type ligands in enantioselective sulfide oxidations.<sup>19</sup> Using 10 mol% of a salen-oxovanadium(IV) complex as catalyst and cumene hydroperoxide (CHP) as oxidant they achieved an enantioselectivity (“ee” is defined as the excess amount of the one isomer over the other) of 42% ee in the oxidation of methyl phenyl sulfide to the corresponding sulfoxide (figure 1.11).<sup>19</sup>

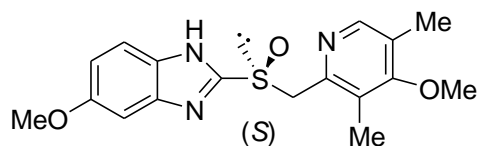


**Figure 1.10.** “*S*” isomer of omeprazole (prilosec).

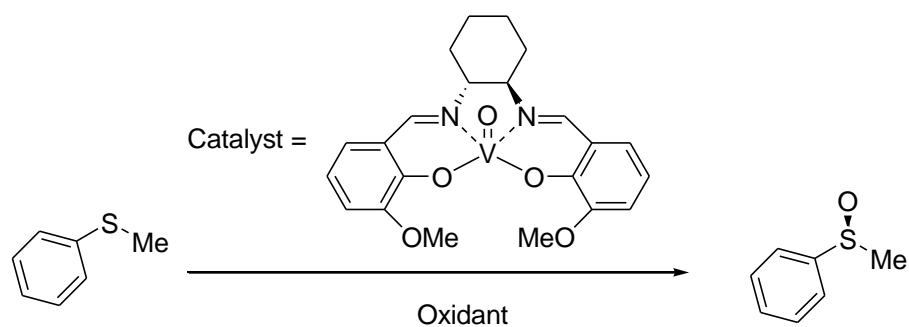


**Figure 1.11.** First salen vanadium catalyst for thioanisole oxidation with cumene hydroperoxide.

Since the first development of a vanadyl salen complex which can effectively catalyze sulfide oxidation with reasonable stereoselectivity, there has been enormous amount of research to modify the salen ligand to obtain better results in this oxidation reaction. A notable breakthrough in designing the salen ligand was reported in 1995 by Bolm et al.<sup>20</sup> They showed that as the bulkyness (*t*-Butyl group) increases at the 3, 3' positions in the salicylidene rings the chiral induction by the vanadyl salen catalyst increases. Also, the presence of electron withdrawing groups (like nitro) at the 5, 5' positions of the salicylidene sidearms is necessary to produce high stereoselectivity. Increase in stereoselectivity with the introduction of the bulky



substituents in the 3, 3' position of the salicylidene sidearm establishes the idea that the approach of sulfide happens through direction “A” mentioned earlier (figure 1.7). The optimum catalyst structure which produces upto 85% ee is shown in figure 1.12.<sup>20</sup>

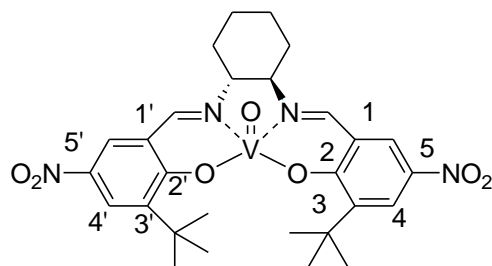


**Figure 1.12.** Vanadium salen catalyst system introduced by Bolm et al.

Katsuki et al. studied catalysis by cyclohexyl salen ligands with several metals including Al, Ti, Mn and Fe.<sup>21,22,23</sup> In the sulfoxidation reaction of phenyl methyl sulfide, 2 mol% of the catalyst produces very high ee (99%) in methanol by using hydrogen peroxide as the source of oxygen at 0 °C in 24 hrs. They proposed the active structure of the Ti-salen catalyst system as the *cis-β*-peroxo-Ti-salen dimer (figure 1.13).<sup>22</sup> In methanol, the catalyst transforms to a *trans* monomer. This converts to a peroxo species with a *β-cis* configuration in presence of oxidant. The high asymmetric induction by the complex is attributed to the participation of the peroxo species in a concave shape that is formed by the *β-cis* salen ligand, to which sulfide can approach only from one side due to the presence of a bulky 2-phenyl naphthyl group (figure 1.14). To date this is the most effective catalyst system discovered for asymmetric sulfoxidation reactions.

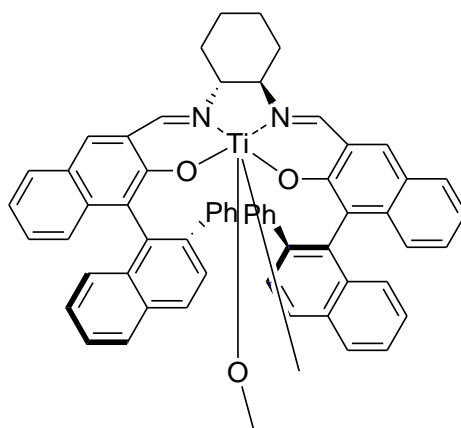


**Figure 1.13.** Sulfoxidation catalyst system introduced by Katsuki et al.<sup>22</sup>

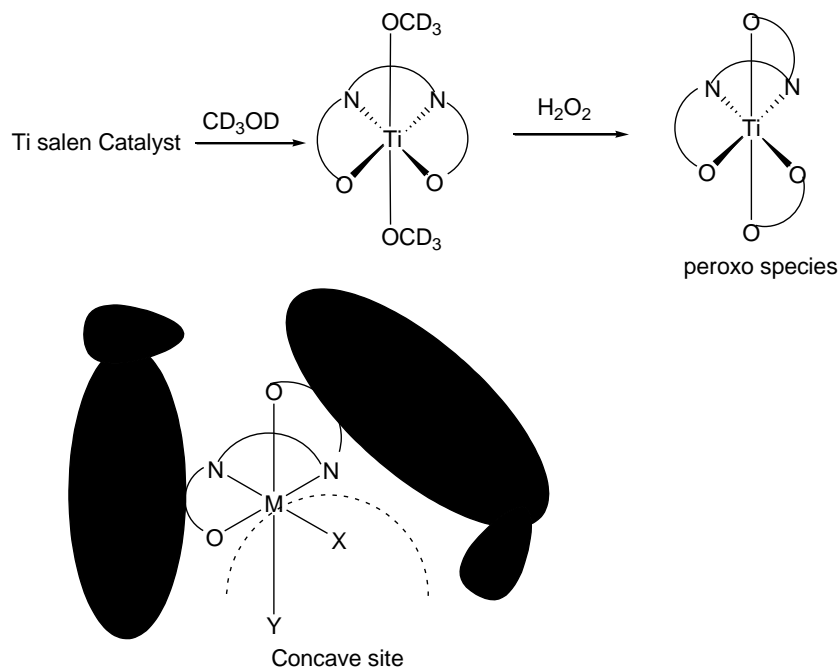


**Figure 1.14.** Schematic of the Ti-salen catalyst responsible for high asymmetric induction.<sup>22</sup>

The source of oxygen is an important aspect to consider in asymmetric catalysis. The most common oxidants used so far in asymmetric sulfoxidation reactions are hydrogen peroxide, cumene hydroperoxide and *t*-butyl hydroperoxide.<sup>23</sup> Depending on the catalyst system, solvent and temperature of the reaction, they all showed good activity. However, the two important aspects that any industry in present days and in future will focus are sustainability and pollution prevention. From this standpoint, hydrogen peroxide is the best oxidant other than using air as the source of oxygen. Hydrogen peroxide produces water as the by product and has a high content of active oxygen.

The main goal of this research project is to synthesize rigid helical vanadium complexes with chiral helix directing ligands, characterize them and to explore their catalytic activity in asymmetric sulfoxidation reactions. To accomplish this goal, we have synthesized four ligand systems with 1*R*,2*R*-cyclohexyl and 2,2'-*R*-binaphthyl (BINAM) as the backbones and phenanthryl and benz[*a*]anthryl sidearms. These polyaromatic side arms can overlap and hence make the system more rigid (figure 1.15). The helicity induced by the extended sidearms can increase the asymmetry of the overall complex. Four ligands (**1-4**) are used in this research to explore how helicity can influence the chiral induction. Ligands **1** and **3** have the cyclohexyl backbone and ligands **2** and **4** have the binaphthyl backbone. These ligands were synthesized by

Schiff base condensation between the corresponding diamine backbone and the salicylidene backbone. The detailed steps for the synthesis of the sidearms and the ligands were reported previously from our group.<sup>12</sup>

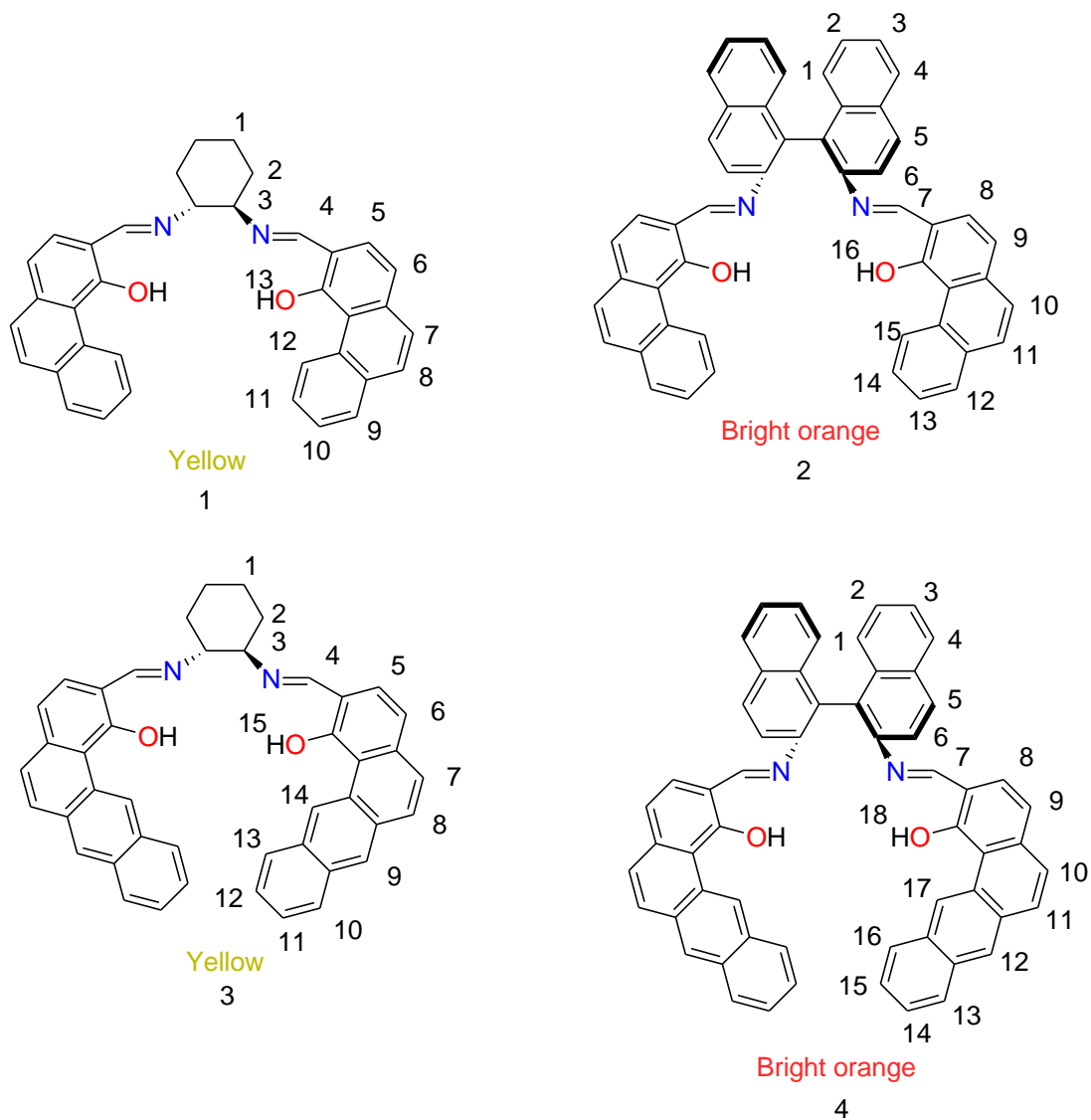
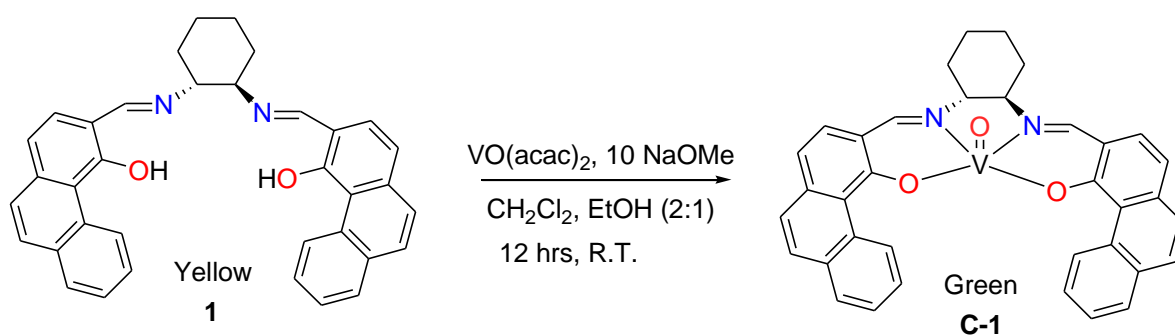


**Figure 1.15.** Salen ligands used in this study.

## 1.3 Results and discussions

### 1.3.1 General Synthesis Scheme For The Vanadium-Salen Complexes

The synthesis scheme for the vanadyl-salen complexes is shown in figure 1.16. To the solution of the ligand in  $\text{CH}_2\text{Cl}_2$  and ethanol mixture, were added vanadyl acetylacetonate and sodium methoxide. The solution was stirred for 12 to 16 hrs at room temperature. Green colored precipitate for complexes **C-1** and **C-3** and brown colored precipitate for complexes **C-2** and **C-4** were separated out. The precipitate was purified by a soxhlet extraction in  $\text{CH}_2\text{Cl}_2$ . These complexes are poorly soluble in most of the common organic solvents. Attempts were made to synthesize these complexes from vanadyl sulfate, however, its poor solubility in any of the common organic solvent, prevented reactions from occurring. Vanadyl acetyl acetate was used as a source of the metal due to its improved solubility in dichloromethane. It was observed that the amount of base plays a crucial role in the formation of these complexes. The acidic phenolic protons in these ligands system require at least 10 equivalents of strong base like NaOMe to deprotonate and to coordinate with the metal. The acidic nature of the phenolic protons can be seen in  $^1\text{H}$  NMR spectrum, where they shift highly downfield around 15 ppm. Previously from our group, it is observed that these protons are involved in intra-molecular hydrogen bond with the nearby OH group and the imine nitrogen.<sup>12</sup>



Continued.....

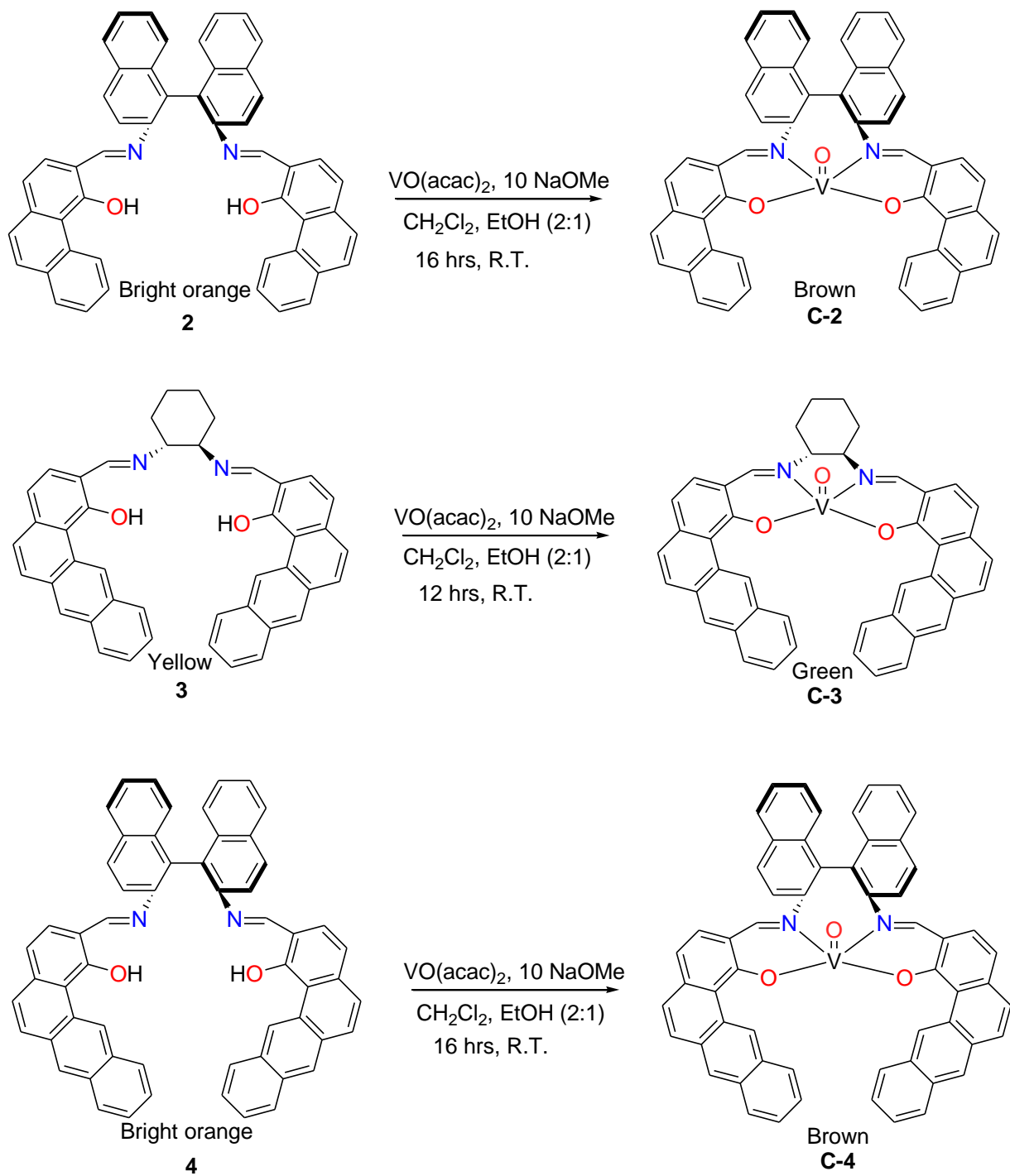


**Figure 1.16.** Synthesis of vanadyl complexes **C-1** to **C-4**.

### 1.3.2 Characterization of the vanadyl complexes (C-1 to C-4)

#### 1.3.2.1 $^1\text{H}$ NMR spectra of the complexes

All the vanadyl complexes showed broad  $^1\text{H}$  NMR spectra. These spectra are characteristic of paramagnetic complexes. As an example, Figure 1.17 shows the  $^1\text{H}$  NMR ( $\text{CDCl}_3$ , 400 MHz) of complex **C-1**.

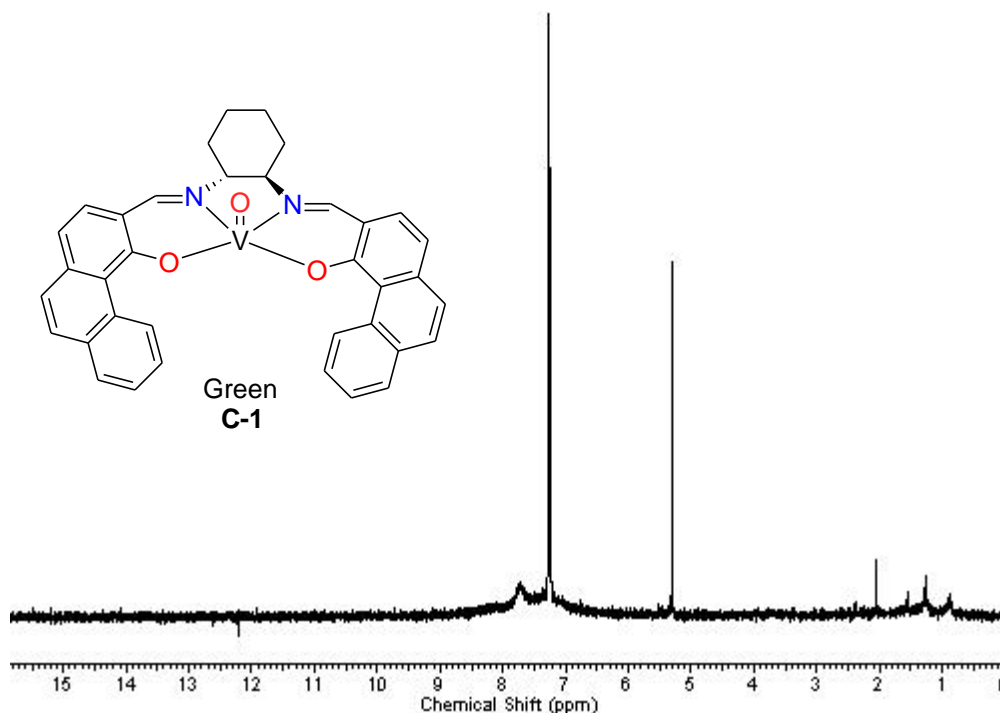


**Figure 1.17.**  $^1\text{H}$  NMR ( $\text{CDCl}_3$ , 400 MHz) of complex **C-1**.

#### 1.3.2.2 IR spectra of the complexes

For complexes **C-1** and **C-3**,  $\nu_{\text{V=O}}$  (stretching frequency) is observed at 1033.81 and 1035.71  $\text{cm}^{-1}$  respectively. These stretches are characteristic of green colored monomeric square pyramidal vanadyl salen complexes studied previously.<sup>13</sup> The  $\nu_{\text{V=O}}$  stretch for octahedral complexes generally comes in the range between 970 to 1000  $\text{cm}^{-1}$ . For octahedral complexes with similar tetradentate ONNO ligands, the  $\nu_{\text{V=O}}$  is lower due to the expected weakening of the V=O bond by the *trans* influence of the other axial ligand. The somewhat lower V=O stretching

frequency in case of **C-3** indicates slightly weaker and longer V=O than for **C-1**. The slight difference in stretching frequency might be attributed to the fact that one extra fused phenyl ring in the side arm of complex **C-3** creates more electron delocalization into the ligand system, causing the metal center more electron rich and henceforth slightly lower  $\nu_{V=O}$  results.<sup>14</sup> However, in case of **C-2** and **C-4**, the  $\nu_{V=O}$  was observed at 1016.03 and 1035.71  $\text{cm}^{-1}$  respectively. These stretching frequency numbers show that there might be polymeric nature of these brown colored complexes due to extensive  $V=O \cdots V=O$  formation between the nearby molecules thereby reducing the double bond character of the axial V=O bond.<sup>14</sup> The comparative IR stretching frequencies and corresponding bond lengths of important bonds are described in Table 1.1.

**Table 1.1.** IR stretching frequencies of different complexes

Complexes	$\nu_{V=O}$ $\text{cm}^{-1}$ Bond length (C=O)	$\nu_{C=N}$ $\text{cm}^{-1}$ Bond length (C=N)
<b>C-1</b>	1036.81    1.581 (4) Å	1608.00    1.271 (7)
<b>C-2</b>	1016.03	1613.00
<b>C-3</b>	1035.71    1.584 (5) Å	1609.51    1.291 (9)
<b>C-4</b>	1008.50	1606.00

### 1.3.2.3 EPR spectra of complexes C-1 and C-2

The EPR spectrum of complex **C-1** was recorded at room temperature in dichloromethane. It shows a broad EPR spectrum with  $g$  value 2.00, typical for a paramagnetic  $d^1$  electronic configuration.<sup>17</sup> There are few possible reasons for this broadness in the EPR spectrum. One reason for the broadness is possibly due to the rapid interconversions between the  $M$  and the  $P$  isomers in the solution at room temperature. The other possible reason for the broadness is believed to be due to the degeneracy of the other  $d$  orbitals ( $d_{yz}$ ,  $d_{zx}$ ,  $d_x^2 - y^2$  and  $d_z^2$ ) with the ground state  $d_{xy}$  orbital in which the single electron on metal center initially resides.<sup>15</sup> The single electron delocalization might cause the broadness at room temperature EPR spectrum.

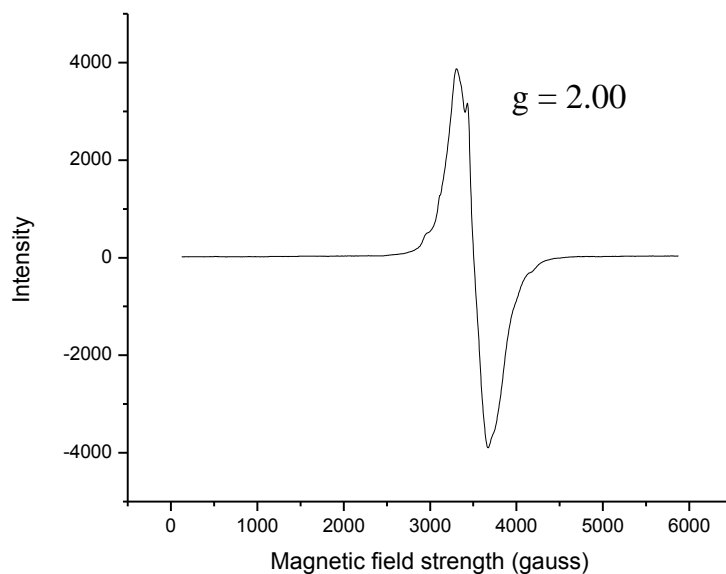


**Figure 1.18.** EPR spectrum of complex **C-1**.

The EPR spectrum of the complex **C-2** was recorded under nitrogen at liquid nitrogen temperature by dissolving in DMSO (figure 1.18). The X-band EPR spectra  $V^{IV}O$  complex was simulated using a computer program from Rockenbauer and Korecz.<sup>24</sup> The system was simulated considering the molecule as a octahedral geometry where the fifth coordinate is occupied by the axial oxygen atom and the sixth coordination mode is occupied by the DMSO. The EPR spectrum helps to elucidate which groups coordinate in solution. For  $V^{IV}O$  system, the hyperfine coupling arises from the interaction of the magnetic moment for the unpaired electron on the vanadium(IV) with the nuclear spin of vanadium. For  $V^{IV}O$  system, we used the additivity rule to estimate the hyperfine coupling constant  $A_{\parallel}^{est}$ , based on the contributions  $A_{\parallel,i}$  of each of the four equatorial donor groups [ $A_{\parallel}^{est} = \sum A_{\parallel,i} (i = 1 \text{ to } 4)$ ]. The estimated accuracy of the  $A_{\parallel}^{est}$  is  $\pm 3 \times 10^{-4} \text{ cm}^{-1}$ .<sup>24</sup> The data can be used to establish the most probable binding mode of the  $V^{IV}$  complex. However, it may not be accurate as contribution of the donor groups in hyperfine splitting depend on their orientation and charge of the ligand. The influence of the axial oxygen was not taken into account, since it is not relevant in the present system.



The X-band 1<sup>st</sup> derivative EPR spectrum at liquid nitrogen temperature for complex **C-2** in DMSO was measured and simulated.<sup>24</sup> Table 1.2 shows the comparison between the simulated and experimental data. The complex was envisioned as in the octahedral environment with solvent DMSO occupying the sixth coordination site. Among the three different possible geometric isomers, complex **C-2** shows best match with the  $\beta$ -*cis* geometry (figure 1.19).

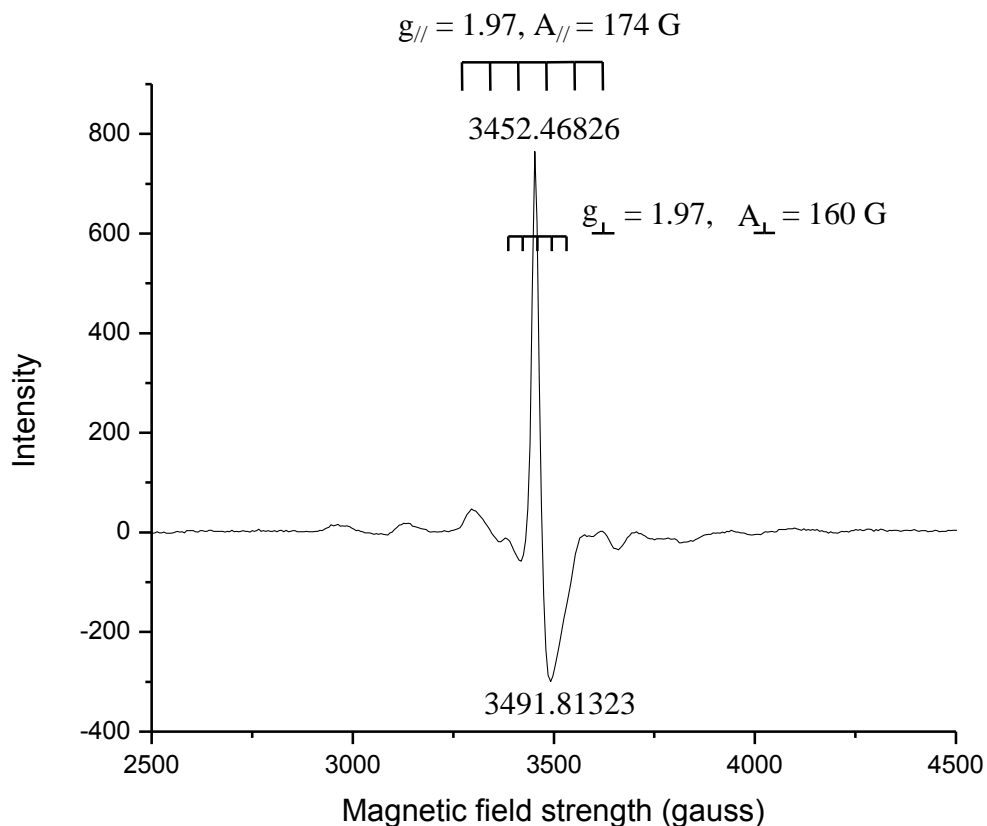


**Figure 1.19.** EPR spectrum of complex **C-2**.

**Table 1.2.** Spin-Hamiltonian parameters calculated for the EPR spectrum of **C-2** in DMSO

Complex	$g_{\perp}$	$A_{\perp} \times 10^4 \text{ cm}^{-1}$	$g_{\parallel}$	$A_{\parallel} \times 10^4 \text{ cm}^{-1}$	Binding mode ( $A_{\parallel}^{\text{est}} \times 10^4 \text{ cm}^{-1}$ )
<b>C-2</b>	1.97	160	1.97	174	<i><math>\alpha</math>-cis</i> (165) <i><math>\beta</math>-cis</i> (174.3) <i>trans</i> (160)

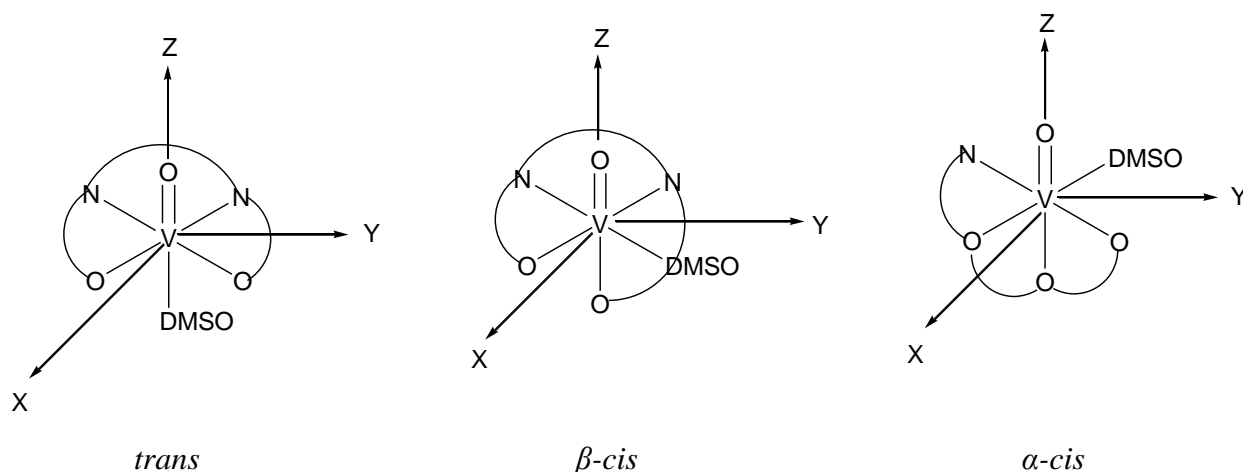
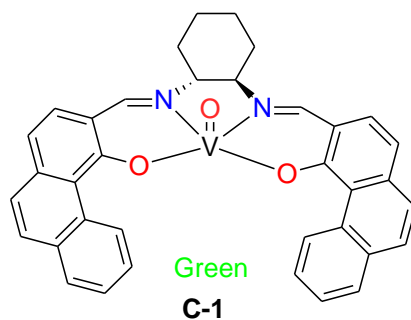


**Figure 1.20.** Sketch of the general orientation of the principal axis system for  $g$  on proton hyperfine tensors for complex **C-2**.

#### 1.3.2.4 Mass spectra of vanadyl(IV)-salen complexes **C-1** to **C-4**

The MALDI-TOF mass spectra of these complexes showed the expected molecular ion peaks that compared with the simulated values to 4<sup>th</sup> decimal places. The molecular ion peak for all the complexes (both calculated and found) and the isotopic pattern peak numbers are shown in the experimental section. The isotopic pattern also matches very close with the simulated isotopic pattern. This is strong evidence that we have successfully synthesized these molecules. The mass spectra of the complexes **C-1** to **C-4** are shown in figures 1.21 to 1.24.



$M+1$  ( $C_{36}H_{29}N_2O_3V_1$ ) = 588.1624 (% Abundance = 64)  
 $M+2$  ( $C_{36}H_{30}N_2O_3V_1$ ) = 589.1673 (% Abundance = 27)  
 $M+3$  ( $C_{36}H_{31}N_2O_3V_1$ ) = 590.1726 (% Abundance = 8)  
 $M+4$  ( $C_{36}H_{32}N_2O_3V_1$ ) = 591.1753 (% Abundance = 1)

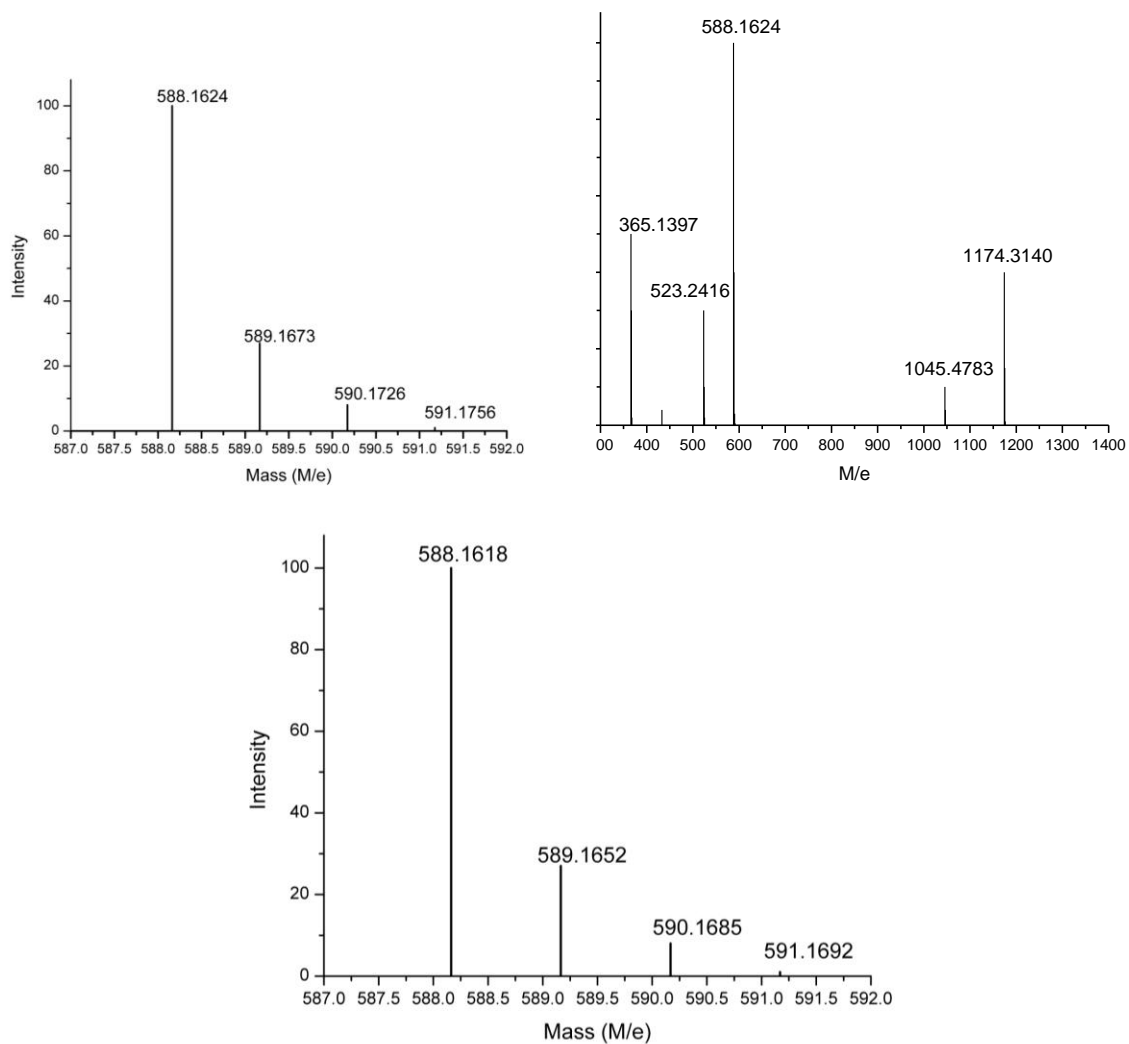
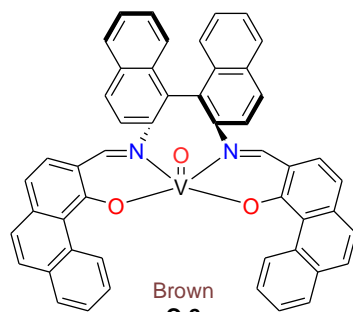


**Figure 1.21.** Structure of catalyst **C-1** with % abundance (previous page), observed isotopic pattern (top left), entire spectrum (top right) and simulated pattern (bottom) mass spectra.



M+1 ( $C_{50}H_{31}N_2O_3V_1$ ) = 758.2069 (% Abundance = 60)  
M+2 ( $C_{50}H_{32}N_2O_3V_1$ ) = 759.2354 (% Abundance = 31)  
M+3 ( $C_{50}H_{33}N_2O_3V_1$ ) = 760.2368 (% Abundance = 8)  
M+4 ( $C_{50}H_{34}N_2O_3V_1$ ) = 761.2438 (% Abundance = 1)

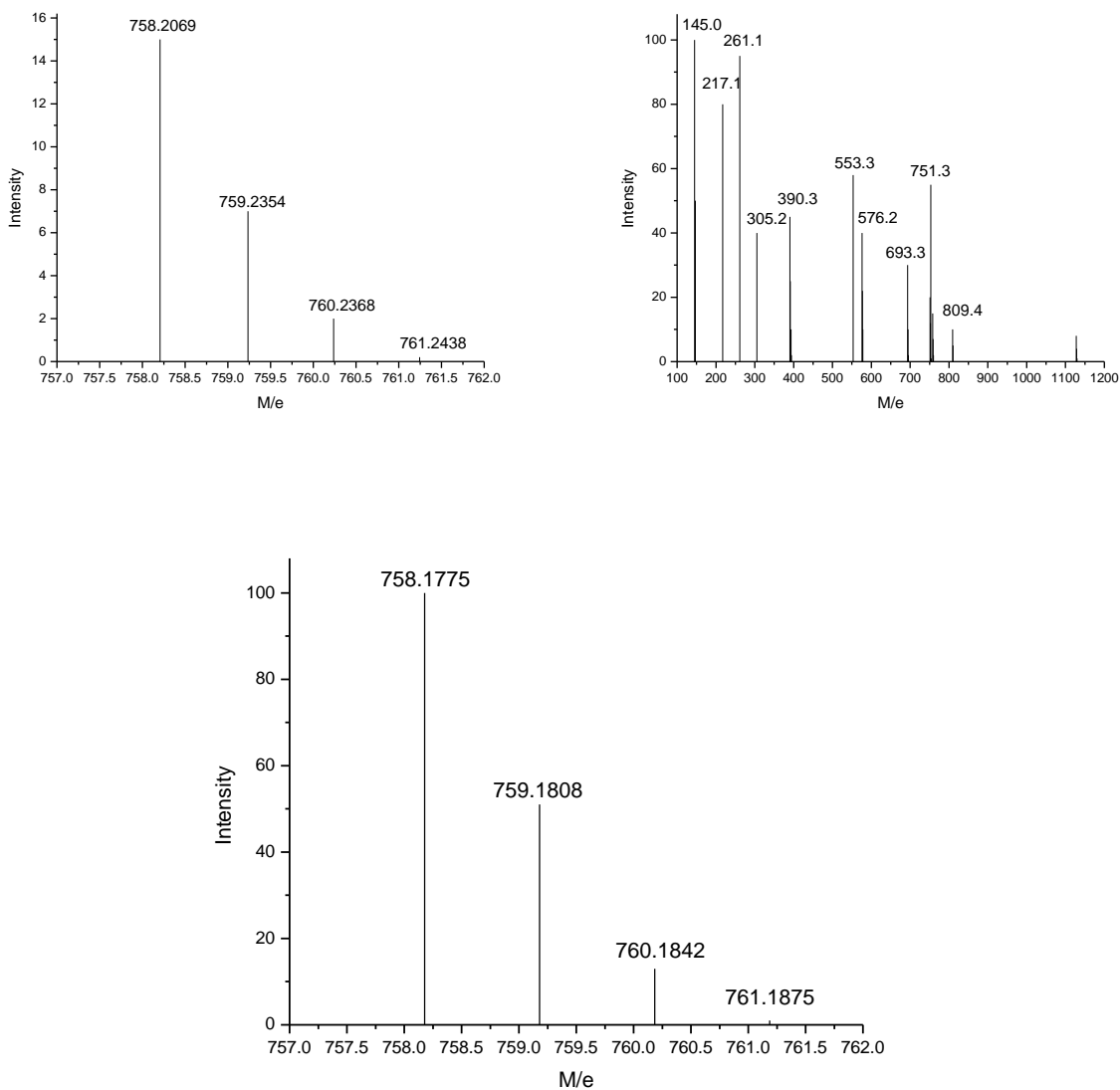
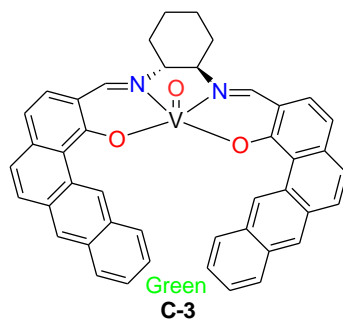


**Figure 1.22.** Structure of catalyst **C-2** with % abundance (previous page), observed isotopic pattern(top left), entire spectrum (top right) and simulated pattern (bottom) mass spectra.



M+1 (C<sub>44</sub>H<sub>33</sub>N<sub>2</sub>O<sub>3</sub>V) = 688.1919 (%Abundance = 76)  
 M+2 (C<sub>44</sub>H<sub>34</sub>N<sub>2</sub>O<sub>3</sub>V) = 689.1962 (%Abundance = 18)  
 M+3 (C<sub>44</sub>H<sub>35</sub>N<sub>2</sub>O<sub>3</sub>V) = 690.2012 (%Abundance = 5)  
 M+4 (C<sub>44</sub>H<sub>36</sub>N<sub>2</sub>O<sub>3</sub>V) = 691.2012 (%Abundance = 1)

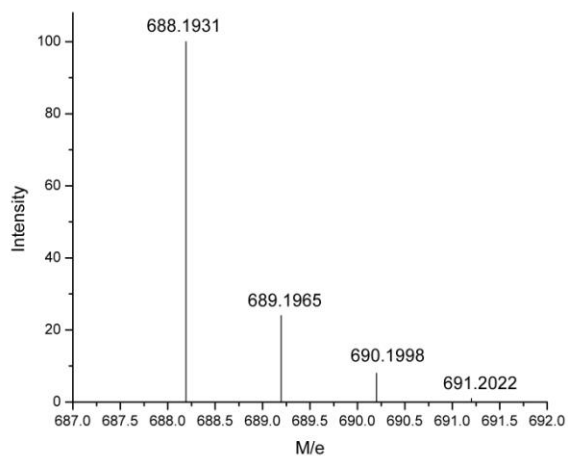
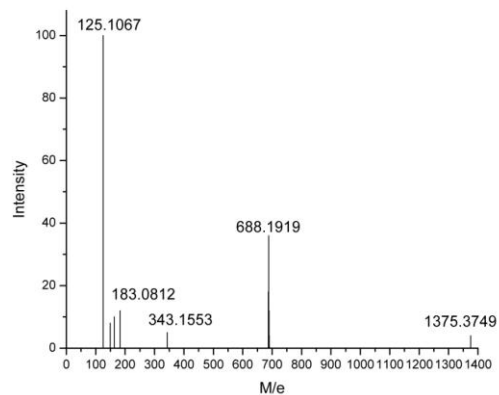
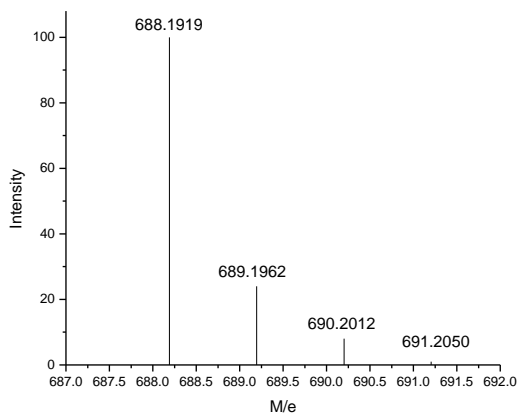
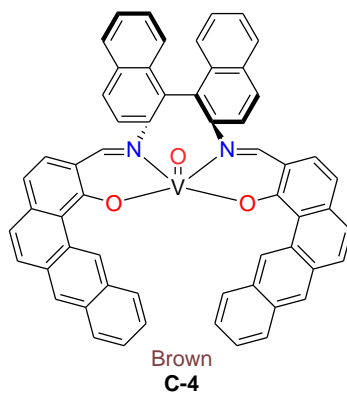


**Figure 1.23.** Structure of catalyst **C-3** with % abundance (top), observed isotopic pattern (top left), entire spectrum (top right) and simulated isotopic pattern (bottom) mass spectra.



M+1 (C<sub>58</sub>H<sub>45</sub>N<sub>2</sub>O<sub>3</sub>V) = 858.2091 (%Abundance = 52)  
M+2 (C<sub>58</sub>H<sub>46</sub>N<sub>2</sub>O<sub>3</sub>V) = 859.1785 (%Abundance = 34)  
M+3 (C<sub>58</sub>H<sub>47</sub>N<sub>2</sub>O<sub>3</sub>V) = 860.6641 (%Abundance = 12)  
M+4 (C<sub>58</sub>H<sub>48</sub>N<sub>2</sub>O<sub>3</sub>V) = 861.6643 (%Abundance = 2)

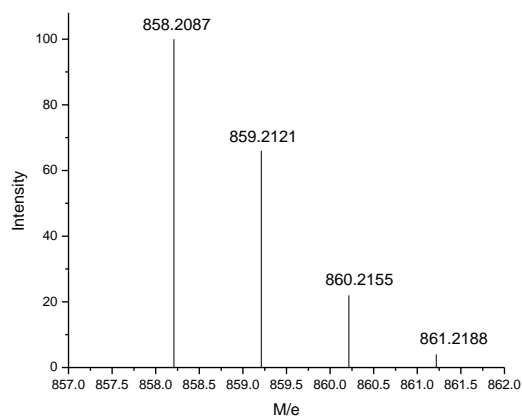
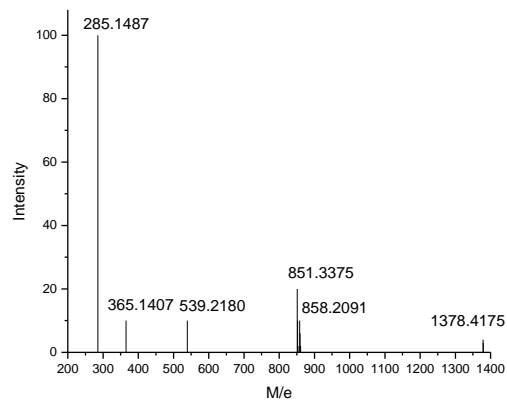
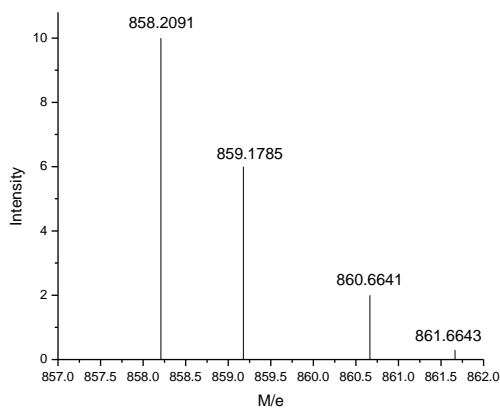
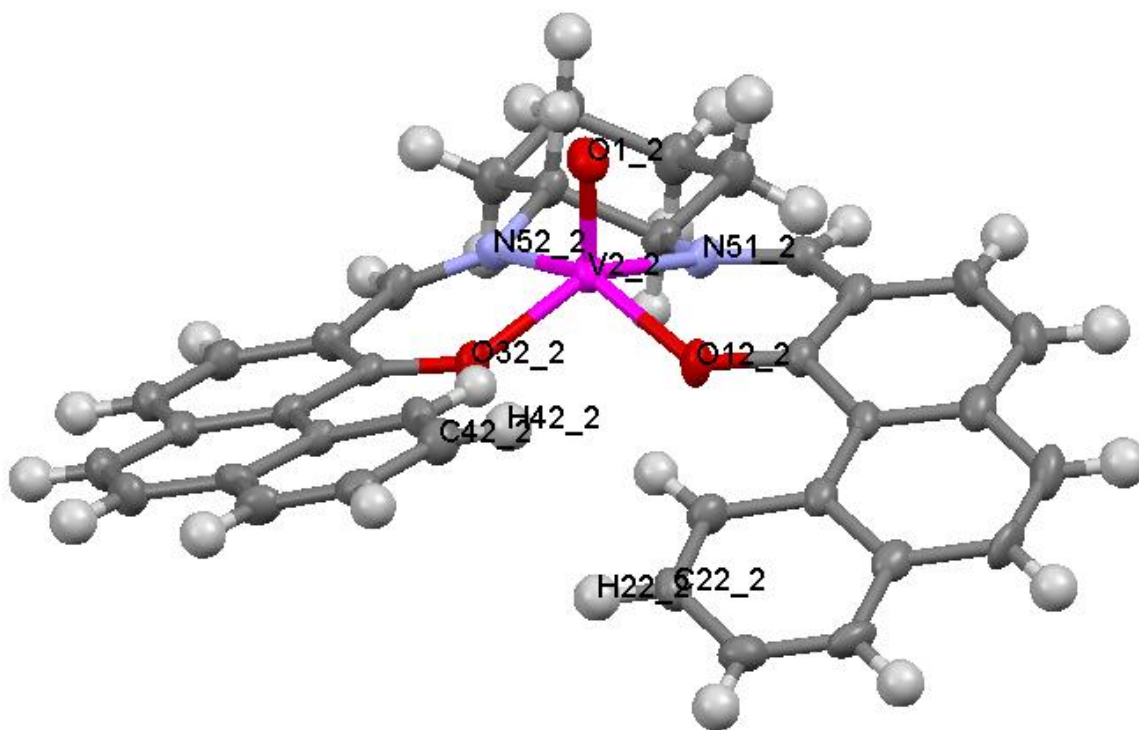


**Figure 1.24.** Structure of catalyst **C-4** with % abundance(top), observed isotopic pattern (top left), entire spectrum (top right) and simulated isotopic pattern (bottom) mass spectra.

### 1.3.2.5 Solid state X-ray structures of complexes C-1 and C-3

Single crystals were grown by the slow diffusion method by layering hexane above dichloromethane solutions of cyclohexyl salen complexes **C-1** and **C-3**. Both the structures show that vanadium is penta-coordinated with the salen ligand occupying the square plane and the oxo group at the axial position. The geometry of the complexes found to be slightly distorted square pyramidal. Both the complexes showed polyaromatic sidearms that are wrapped around the metal giving the complexes a rigid stepped monohelical structure. The overlap by the benz[a]anthryl sidearms causes  $\pi$ - $\pi$  stacking in complex **C-3** as observed from the crystal structure.

The thermal ellipsoid plot of **C-1** in the *M* and *P* conformations with atom numbering is shown in figure 1.25. We can see that the vanadium situated slightly above (0.33 Å) the square plane formed by the tetradentate ONNO donor salen ligand. The crystal system is monoclinic with space group P2(1). The basic crystal parameters are shown in table 1.3. Figure 1.26 shows the space filling model of **C-1** which has a 1:1 ratio of *P* and *M* helices in the solid state.



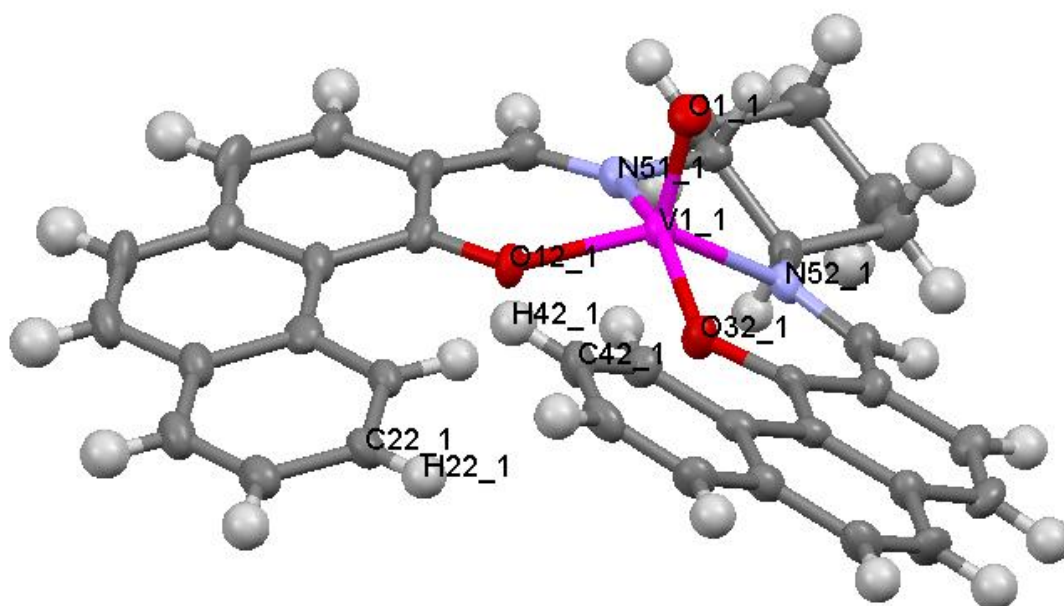


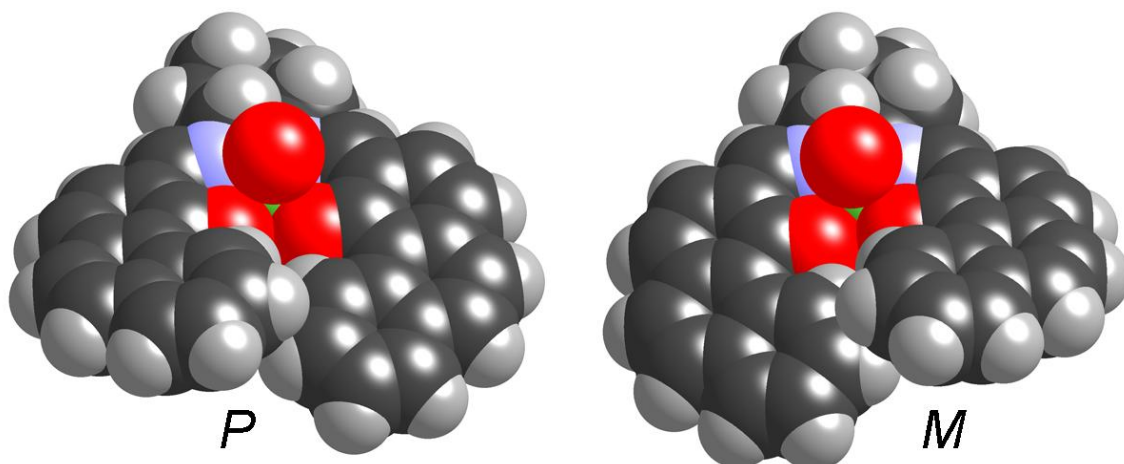
**Figure 1.25.** Thermal ellipsoid plot of complex **C-1** (first molecule: *P*, second molecule: *M*).

**Table 1.3.** Crystal data for **C-1**

Identification code	<b>C-1</b>	
Empirical formula	$C_{36} H_{28} N_2 O_3 V$	
Formula weight	587.54	
Temperature	173(2) K	
Wavelength	0.71073 Å	
Crystal system	Monoclinic	
Space group	P2(1)	
Unit cell dimensions	$a = 9.668(3)$ Å	$\alpha = 90^\circ$ .
	$b = 10.827(3)$ Å	$\beta = 99.717(14)^\circ$ .
	$c = 25.450(7)$ Å	$\gamma = 90^\circ$ .
Volume	$2625.8(13)$ Å <sup>3</sup>	
Z	4	
Density (calculated)	1.486 g/cm <sup>3</sup>	
Absorption coefficient	0.422 mm <sup>-1</sup>	
F(000)	1220	
Crystal size	0.25 x 0.20 x 0.15 mm <sup>3</sup>	
Refinement method	Full-matrix least-squares on F <sup>2</sup>	
Data / restraints / parameters	10225 / 1 / 757	

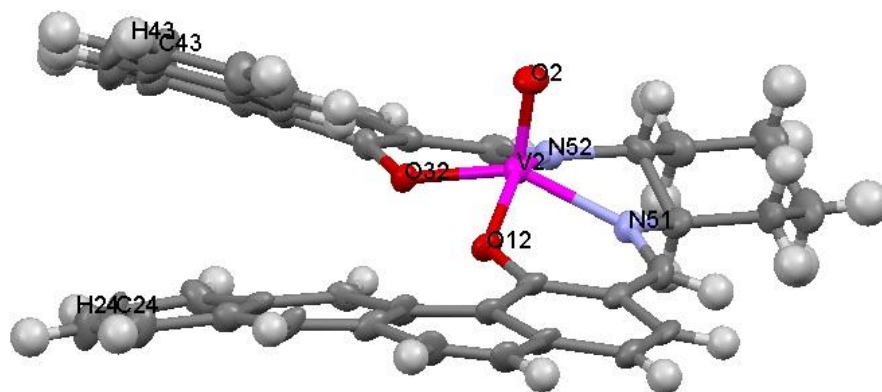


Goodness-of-fit on $F^2$	1.012
Final R indices [ $I > 2\sigma(I)$ ]	R1 = 0.0579, wR2 = 0.1553
R indices (all data)	R1 = 0.0830, wR2 = 0.1752
Absolute structure parameter	0.03(3)
Largest diff. peak and hole	0.447 and $-0.540 \text{ e.}\text{\AA}^{-3}$



**Figure 1.26.** Space filling models of **C-1** showing the *P* and the *M* conformers .

The single crystal structure (ellipsoid model) of **C-3** with the benz[*a*]anthryl sidearm, also showed that *P* and *M* conformations are both present in the solid state (figure 1.27). The space filling model of the *M* and the *P* conformations are shown in figure 1.28. The vanadium metal center is slightly above ( $23.11^\circ$  or  $0.31 \text{ \AA}$ ) the ONNO square plane. From the space filling model shows that there is  $\pi$ - $\pi$  stacking between the benz[*a*]anthryl sidearms. The crystal system is triclinic in nature with a *P1* space group. The basic crystal parameters are shown in table 1.4.



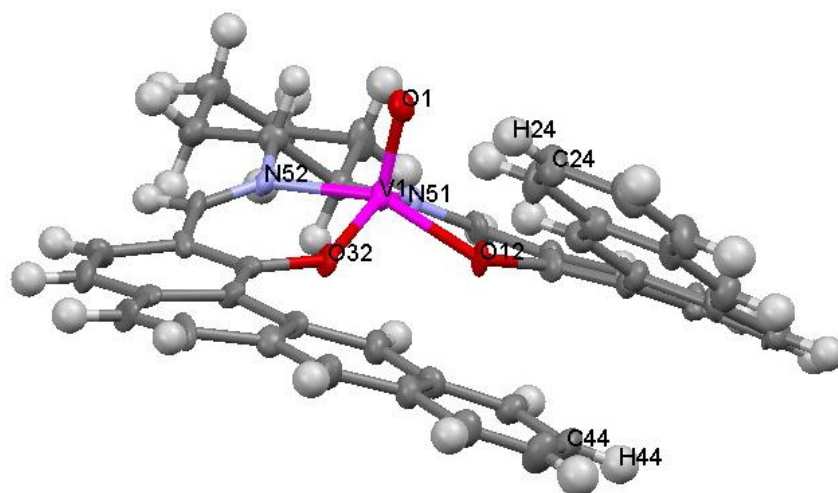


**Figure 1.27.** Thermal ellipsoid plot of **C-3** (top: *P*, bottom: *M*).

**Table 1.4.** Crystal data for **C-3**

Identification code	<b>C-3</b>	
Empirical formula	C <sub>45</sub> H <sub>34</sub> C <sub>12</sub> N <sub>2</sub> O <sub>3</sub> V	
Formula weight	772.58	
Temperature	100(2) K	
Wavelength	0.71073 Å	
Crystal system	Triclinic	
Space group	P1	
Unit cell dimensions	a = 12.0364(9) Å	a = 89.1610(10)°.
	b = 16.8357(12) Å	b = 77.6150(10)°.
	c = 17.9974(13) Å	g = 85.9340(10)°.
Volume	3553.2(4) Å <sup>3</sup>	
Z	4	
Density (calculated)	1.444 Mg/m <sup>3</sup>	
Absorption coefficient	0.476 mm <sup>-1</sup>	
F(000)	1596	
Crystal size	0.35 x 0.07 x 0.04 mm <sup>3</sup>	
Refinement method	Full-matrix least-squares on F <sup>2</sup>	
Data / restraints / parameters	23786 / 673 / 1900	
Goodness-of-fit on F <sup>2</sup>	1.068	

Final R indices [I>2sigma(I)]	R1 = 0.0690, wR2 = 0.1670
R indices (all data)	R1 = 0.1107, wR2 = 0.1905
Absolute structure parameter	0.02(3)
Largest diff. peak and hole	0.843 and -0.980 e.Å <sup>-3</sup>

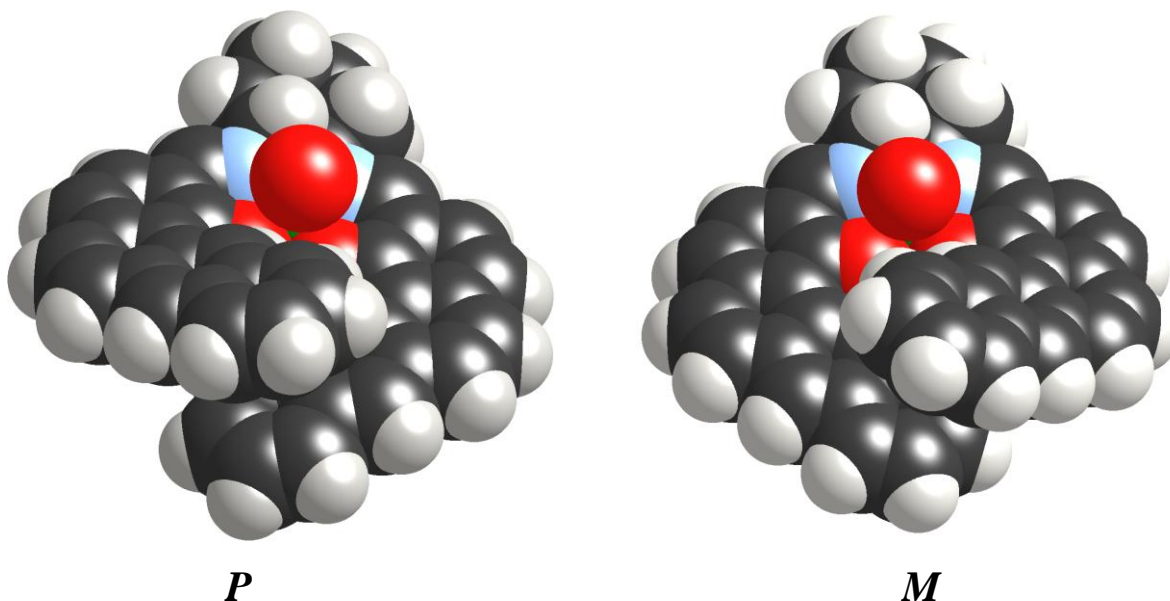


**Figure 1.28.** Space filling models of **C-3** showing the *P* and the *M* conformers.

Comparison of bond lengths and bond angles between the *M* and *P* isomers is presented for complexes **C-1** and **C-3** are presented in table 1.5 and 1.6 respectively. From the space filling model for complex **C-3**, it is clear that the benz[a]anthryl sidearms are significantly overlapped. Indeed, centroid-to-carbon distances are well within the 3.4-3.6 Å range expected for attractive  $\pi$ - $\pi$  stacking. The angle between the sidearms in complex **C-3** is 24.1° for the *M* and 23.8° for the *P* isomer. However, the large angle difference (22.2° for the *M* and 22.7° for the *P*) between the phenanthryl sidearms and the relatively large spacing suggest a little face to face  $\pi$ - $\pi$  interaction is present for complex **C-1**. Both the complexes form a 1:1 mixture of *P* and *M* isomers in the solid state. Since  $\pi$ - $\pi$  interactions appear nearly identical for the two conformers, they do not result any significant thermodynamic preference for one over the other. A comparison of the two space filling model for both the complexes **C-1** and **C-3** reveals that they are nearly enantiomeric and that the main difference is the relative positions of phenanthryl and benz[a]anthryl sidearms.

**Table 1.5.** Comparison of bond lengths and bond angles of *M* and *P* isomers of **C-1**

Bond lengths (Å) ( <i>M</i> isomer)	Bond lengths (Å) ( <i>P</i> isomer)	Bond angles (°) ( <i>M</i> isomer)	Bond angles (°) ( <i>P</i> isomer)
V11-O11 1.581(4)	V22-O22 1.574(4)	O11-V11-O121 112.84(18)	O22-V22-O122 107.05(18)
V11-O121 1.930(3)	V22-O122 1.942(3)	O11-V11-O321 90.16(16)	O22-V22-O322 91.07(16)
V11-O321 1.944(4)	V22-O322 1.935(4)	O121-V11-N511 86.34(15)	O122-V22-N512 85.40(14)
V11-N511 2.030(4)	V22-N512 2.052(4)	O121-V11-N521 136.21(16)	O122-V22-N522 147.04(16)
V11-N521 2.038(4)	V22-N522 2.032(4)	N511-V11-N521 78.25(17)	N512-V22-N522 78.07(16)
		N511-V11-O321 153.82(17)	N512-V22-O322 145.37(18)
		N511-V11-O11 98.7(2)	N512-V22-O22 104.5(2)
		N521-V11-O11 109.89(18)	N522-V22-O22 104.62(18)

**Table 1.6.** Comparison of bond lengths and bond angles of *M* and *P* isomers of **C-3**

Bond lengths (Å) ( <i>M</i> isomer)	Bond lengths (Å) ( <i>P</i> isomer)	Bond angles (°) ( <i>M</i> isomer)	Bond angles (°) ( <i>P</i> isomer)
V1-O1 1.584(5)	V2-O2 1.576(5)	O1-V1-O12 104.6(3)	O2-V2-O12 110.0(3)
V1-O12 1.923(5)	V2-O12 1.920(5)	O1-V1-O32 88.0(2)	O2-V2-O32 85.8(2)
V1-O32 1.918(5)	V2-O32 1.925(6)	O12-V1-N51 87.5(3)	O12-V2-N51 86.9(3)
V1-N51 2.058(7)	V2-N51 2.018(7)	O12-V1-N52 151.2(3)	O12-V2-N52 145.5(3)
V1-N52 2.068(7)	V2-N52 2.054(6)	N51-V1-N52 78.2(17)	N51-V2-N52 79.6(3)
		N51-V1-O32 140.2(3)	N51-V2-O32 143.6(3)
		N51-V1-O1 109.8(3)	N51-V2-O2 107.3(3)
		N52-V1-O1 103.8(3)	N52-V2-O2 104.3(3)

The single crystals of **C-2** were grown from dichloromethane and hexane mixture but analysis showed that only the pure ligand has crystallized out, so for the crystallization of X-ray quality single crystals of **C-2** and **C-4** has been unsuccessful.

#### 1.3.2.6 Solution property studies: CD spectroscopy for complexes **C-1**, **C-3** and **C-2**

The electronic spectra of all complexes were recorded in THF solution with concentration in the  $10^{-5}$  M range. Complexes **C-1** and **C-3** shows the predominance of *M* conformation in the solution. Previously from our group, we reported the simulated and experimental CD spectra of

the zinc salen complex in the *M* conformation (figure 1.29).<sup>25</sup> The CD pattern (figure 1.30) of complexes **C-1** and **C-3** match quite well with the CD spectrum of the zinc salen complex in its *M* conformation. It is important to mention that the CD pattern for the *P* conformation is just the mirror image CD spectrum of the *M* conformer. We can conclude that both vanadium salen complexes **C-1** and **C-3** exist mostly in the *M* conformation in the solution. The broad negative peak at 410-450 nm for complexes **C-1** and **C-3**, is the characteristic CD peak for the *M* conformation and this peak arises due to the  $\pi\text{-}\pi^*$  transitions in the imine group.<sup>28</sup> The broad negative peak at 410-450 nm confirms the diequatorial 1*R*, 2*R* configuration and non-coplanar imines.<sup>29</sup> The phenanthryl chromophore in complex **C-1** absorbs in the 225-350 nm region with the strongest absorption from 220-240 nm region, whereas the benz[a]anthryl chromophore in complex **C-3** absorbs in the 230-360 nm region with the strongest absorption from 230-260 nm region.<sup>28</sup>

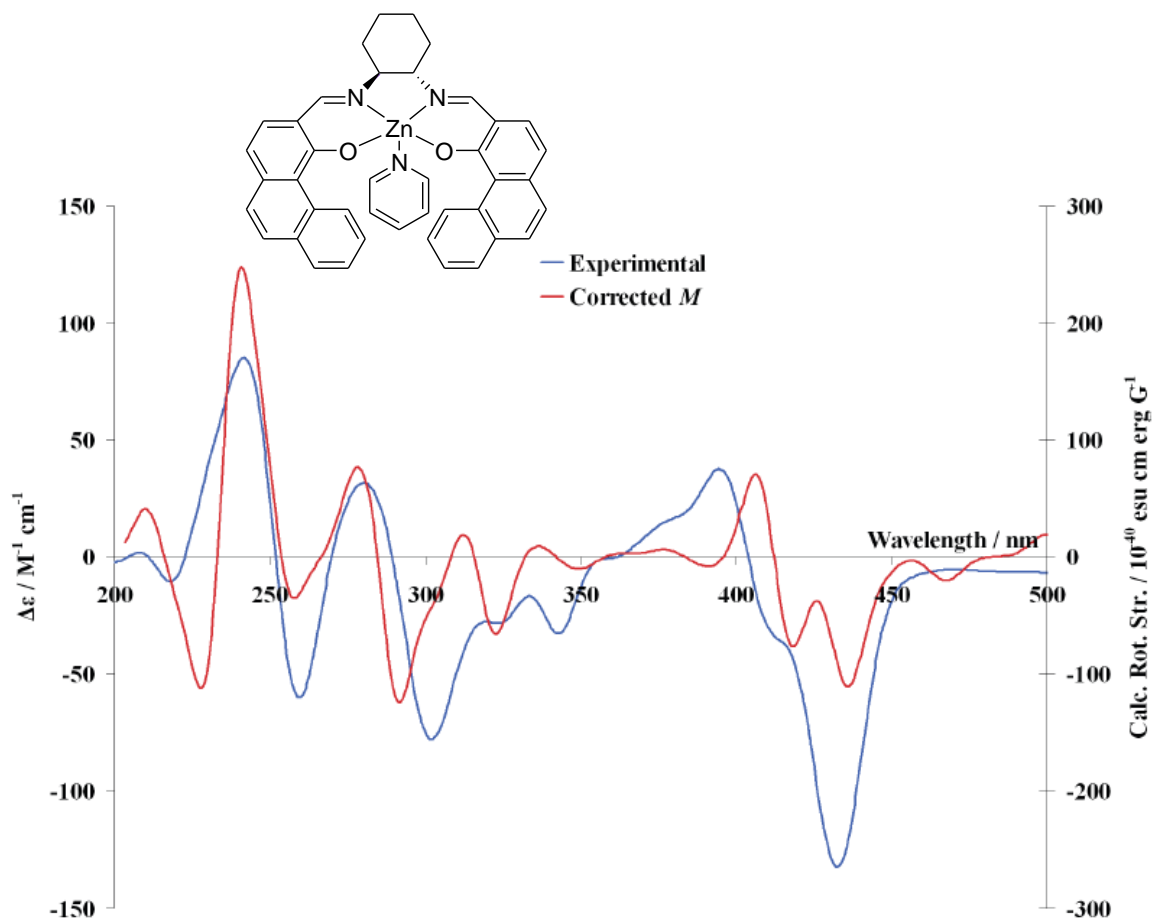


**Figure 1.29.** Experimental and corrected CD spectra of zinc salen complex.

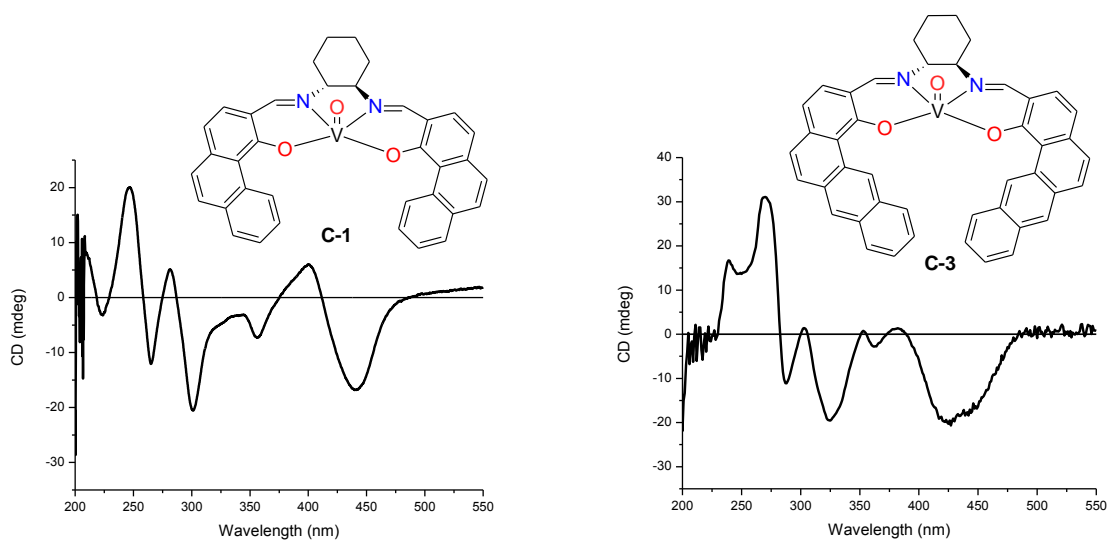


**Figure 1.30.** CD spectra for complex **C-1** and **C-3**.

Complex **C-2** shows CD spectrum exactly opposite to the CD spectrum zinc salen complex with the similar binaphthyl salen ligand (figure 1.31).<sup>25</sup> However, so far there has been no report about the helicity of the complex **C-2** from the particular CD pattern. So, we can not assign the helical conformation for this particular CD pattern for complex **C-2**. In the solid state, zinc salen complex with binaphthyl backbone exist in the *M* helical conformation. Simulation studies needs to be done to understand the helical chirality for binaphthyl salen metal complexes. The broad negative CD peak at 435-490 nm for the zinc salen complex, and broad positive peak at 425-500 nm for the vanadium salen complex, is believed to arise due to the  $\pi$ - $\pi^*$  transitions in the non-coplanar imine bonds.<sup>28</sup> The region from 220-360 nm in the CD spectrum for the binaphthyl backbone salen complexes is mainly due to the absorptions by the binaphthyl rings in their mutually perpendicular orientations. However, the characteristics strongest absorption by the binaphthyl rings arises in the region 240-260 nm.<sup>28</sup>

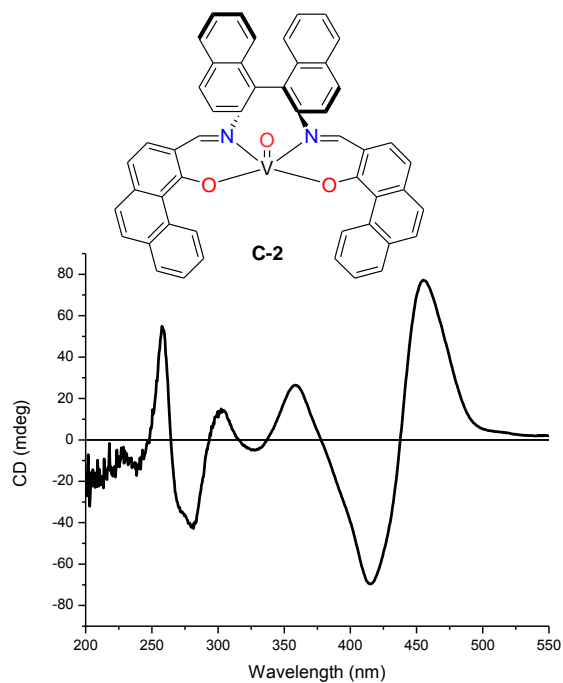
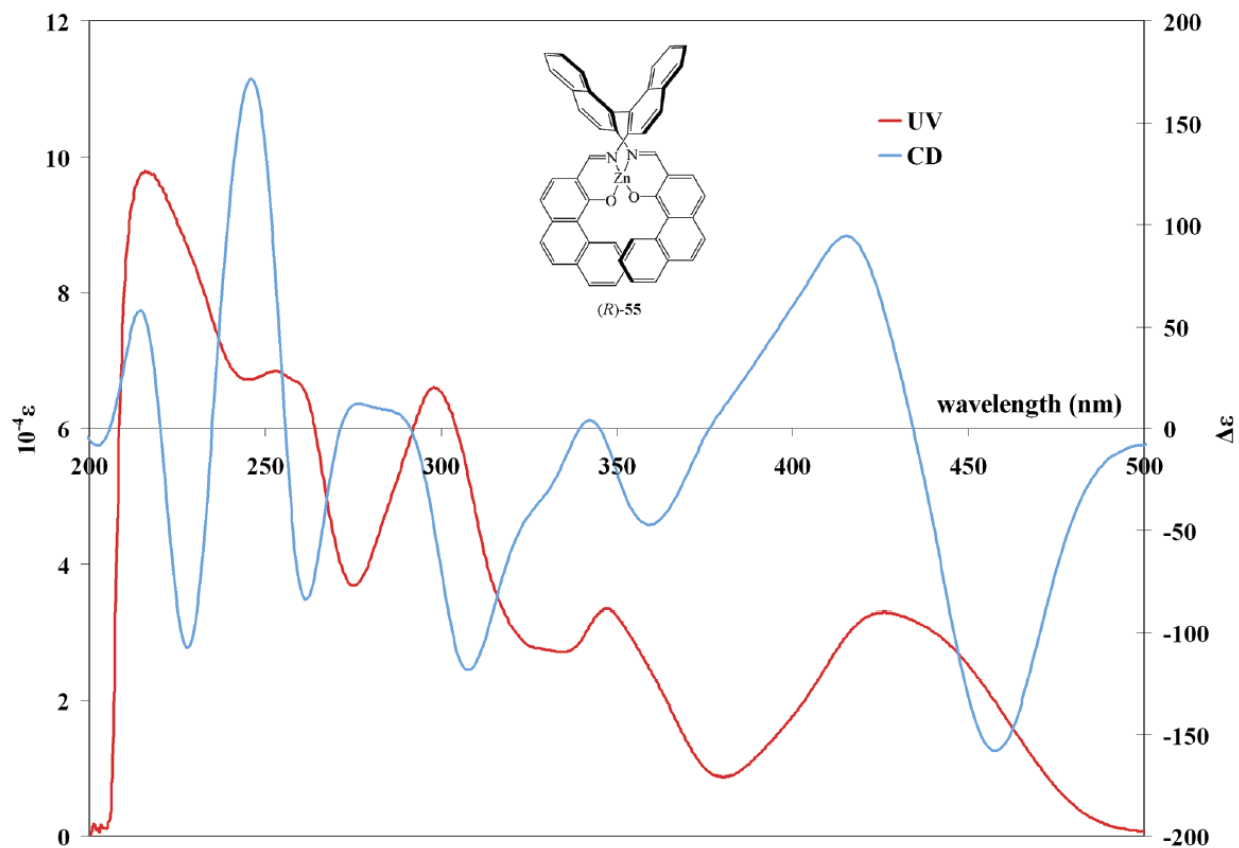


**Figure 1.31.** CD spectra of zinc salen complex (top) and vanadyl salen complex (bottom).



### 1.3.2.7 Sulfoxidation Results By Helical Complexes

The potential of the vanadium complexes as enantioselective catalysts was tested in the asymmetric oxidation with  $\text{H}_2\text{O}_2$  of a simple model compound, thioanisole. The reactions were carried out in  $\text{CH}_2\text{Cl}_2$  and in chloroform with methanol (5% volume/volume) mixture as well as acetonitrile the stereoselectivity was much lower. In all the cases the products were either *R* or *S*-methyl phenyl sulfoxide, or the sulfone resulting from the oxidation of sulfoxides. All addition of reagents was done at 0 °C. The reactions were carried out for 16 hrs under nitrogen. A few control reactions were performed to test the noncatalytic oxidation of thioanisole by  $\text{H}_2\text{O}_2$  in the absence of a catalyst. The change in reaction temperature from room temperature to 0 °C increases the stereoselectivity only a small extent. However, time has a great influence on both the yield as well as the stereoselectivity of the product. It is observed that when the reaction was carried out for 16 hrs the conversion and the enantiomeric excess reached the highest levels. After 16 hrs the conversion and the enantioselectivity levels off, indicating that after this time period the catalysts has likely decomposed in presence of excess oxidant and water. Figure 1.33 shows the comparison of the conversions of four catalysts with time (in  $\text{CHCl}_3$  and 5% MeOH mixture). For catalysts **C-2** and **C-4**, the conversion reaches over 90%. In this solvent combination, catalysts with the binaphthyl backbone are more active than the catalysts with cyclohexyl backbone. This may be due to the presence of more exposure of the reaction site for the binaphthyl backbone vanadyl salen complex (figure 1.32).

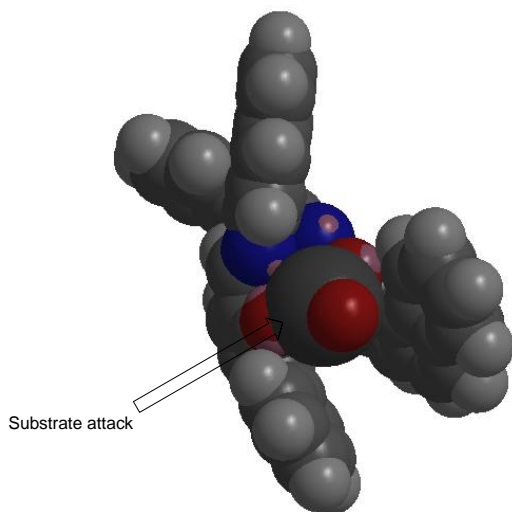


**Figure 1.32.** Exposure of the vanadium(IV) center for the substrate attack.

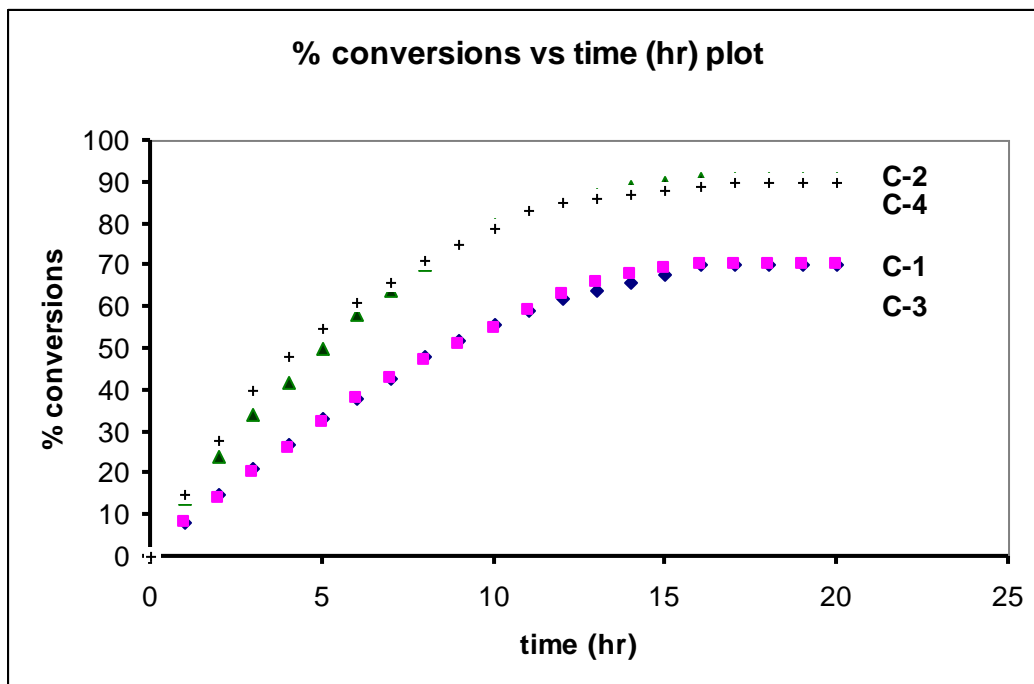


**Figure 1.33.** Percent conversion with time (hr) plot for all catalysts in  $\text{CHCl}_3$  and MeOH mixture.

Solvent plays an important role in terms of conversion and stereoselectivity. In acetonitrile, although the conversion is fairly high, the enantiomeric excess of the product was very low (maximum ee reached 5%). For all the catalysts except **C-4**, the conversion is almost comparable in dichloromethane as well as in chloroform. In dichloromethane we used cumene hydroperoxide as the oxidant. Reactions with 30%  $\text{H}_2\text{O}_2$  in dichloromethane solution gave very similar enantiomeric excesses. From the conversion data it is clear that the larger benz[a]anthryl sidearm or more rigid helical structure does not make much difference. Catalysts with binaphthyl backbone produce better conversion than catalysts with cyclohexyl backbones. All catalysts produce better enantiomeric excesses in the methanol chloroform mixture. This suggests that polarity of the solvent has a profound effect on the enantiomeric excess of the product. The binaphthyl salen complexes are comparable to the cyclohexyl backbone salen complexes in terms of chiral induction. In all the cases the major isomer produced was the *R* form of phenyl methyl sulfoxide. The data is presented in table 1.7.

**Table 1.7.** Sulfoxidation Results By Different Catalysts

Catalyst	Oxidant	Solvent	Temp (°C)	Time (hr)	Sulfoxide (%)	Sulfone (%)	Sulfide (%)	ee (%)	Main isomer
<b>C-1</b>	H <sub>2</sub> O <sub>2</sub>	CHCl <sub>3</sub> and 5% MeOH	0 to R.T.	16	69	5	26	30	<i>R</i>
<b>C-1</b>	CHP	CH <sub>2</sub> Cl <sub>2</sub>	0 to R.T.	16	70	7	23	11	<i>R</i>
<b>C-2</b>	H <sub>2</sub> O <sub>2</sub>	CHCl <sub>3</sub> and 5% MeOH	0 to R.T.	16	88	6	6	32	<i>R</i>
<b>C-2</b>	CHP	CH <sub>2</sub> Cl <sub>2</sub>	0 to R.T.	16	91	2	7	13	<i>R</i>
<b>C-3</b>	H <sub>2</sub> O <sub>2</sub>	CHCl <sub>3</sub> and 5% MeOH	0 to R.T.	16	65	5	30	33	<i>R</i>
<b>C-3</b>	CHP	CH <sub>2</sub> Cl <sub>2</sub>	0 to R.T.	16	69	8	23	14	<i>R</i>
<b>C-4</b>	H <sub>2</sub> O <sub>2</sub>	CHCl <sub>3</sub> and 5% MeOH	0 to R.T.	16	79	12	9	33	<i>R</i>
<b>C-4</b>	CHP	CH <sub>2</sub> Cl <sub>2</sub>	0 to R.T.	16	66	10	24	13	<i>R</i>

ee of the product were measured by HPLC analysis. HPLC analysis was carried out with a DAICEL OD-H column (isopropanol:hexane 5:95). Retention times 17.82 mins for (*R*) and 20.91 mins for (*S*) isomers.

Our proposed mechanism for sulfoxidation with catalyst **C-1** is shown in figure 1.34. The catalytic cycle starts from A. In presence of hydrogen peroxide and sulfide, one of the equatorial vanadium oxygen bond breaks and hydrogen peroxide and thioanisole coordinate to the metal center *cis* to each other. The coordination of the sulfide to the metal center is believed to be the rate determining step of the catalytic cycle.<sup>30</sup> The oxidation state of the vanadium stays the same (IV) throughout the catalytic cycle. In the step B of the catalytic cycle, the oxygen atom in the hydroperoxide ligand can attack the coordinated sulfur from either of the prochiral faces of the planar thioanisole. This phenomenon of face selectivity can produce isomers *R* or *S*. In this state the oxygen atom of the hydroperoxo has partial negative charge and the sulfur from phenyl methyl sulfide has partial positive charge. In the step C, facile oxygen transfer to sulfide from peroxide followed by bond rearrangement produces the product phenyl methyl sulfoxide and the catalyst molecule goes back to the initial step. However, the product selectivity (in terms of the *R* or *S* isomers of the product methylphenyl sulfoxide) can be guided by many factors. Most of the

literature reports reveal that the product selectivity is determined in the sulfide to metal binding step.<sup>30</sup> Another hypothesis reveals that the selectivity is guided by the oxo transfer rate while going from step B to step C. If the rate of oxo transfer is faster from one face of the thioanisole over the other, then this results in preferential formation of one isomer over the other.<sup>30</sup>

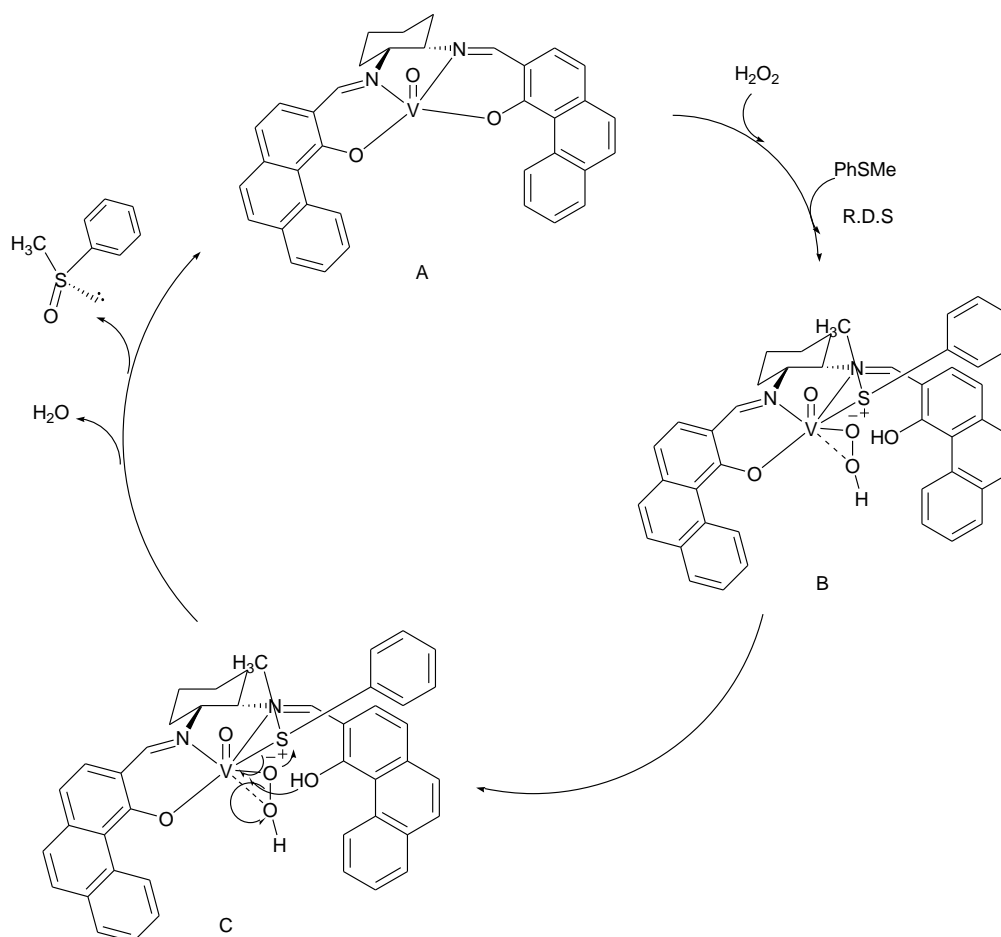


**Figure 1.34.** Proposed mechanism of vanadium(IV) salen catalyzed sulfoxidation.

Based upon the first hypothesis that the product selectivity is guided by the sulfide to metal binding step, we have calculated (MM2 method) the energy of two possible sulfide to metal adducts described in figure 1.35 and 1.36 of state B, which leads to two different isomers (*R* or *S*). In this step, if the energy difference between the two possible binding modes of sulfide to the metal center is small, then the catalyst will give rise to low enantioselectivity in the product sulfoxides. Our calculated energy difference between the two possible adducts give rise to a small number (0.56 kcal/mol) and this explains the low enantioselectivity in sulfoxidation

reactions. Also, the most plausible explanation for the increase of enantiomeric excess in the presence of methanol, can be explained by the hydrogen bonding interaction between proton from peroxide and the metal coordinated oxygen from the methoxide, leading to lock the position of the peroxide and therefore enhancement in facial selectivity (figure 1.37).

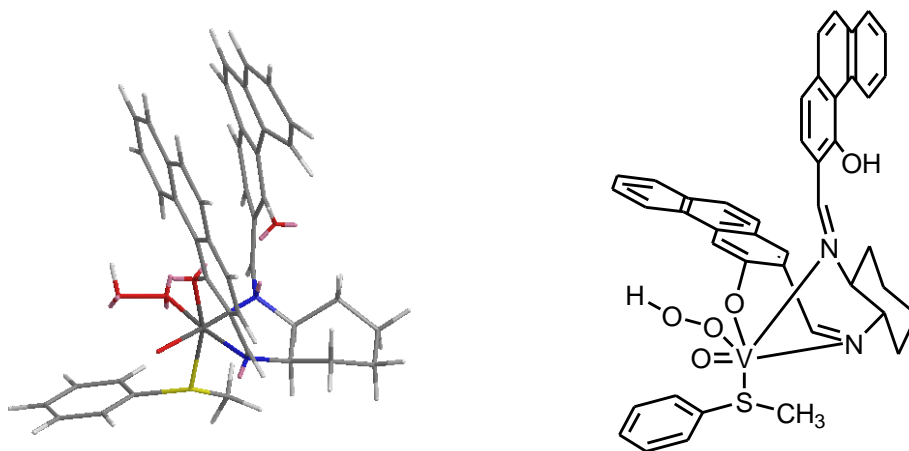


**Figure 1.35.** Three dimensional structure (left) and two dimensional representation (right) of the transition state leading to one possible isomer (*R* or *S*) ( $E = 32.4391$  kcal/mol).

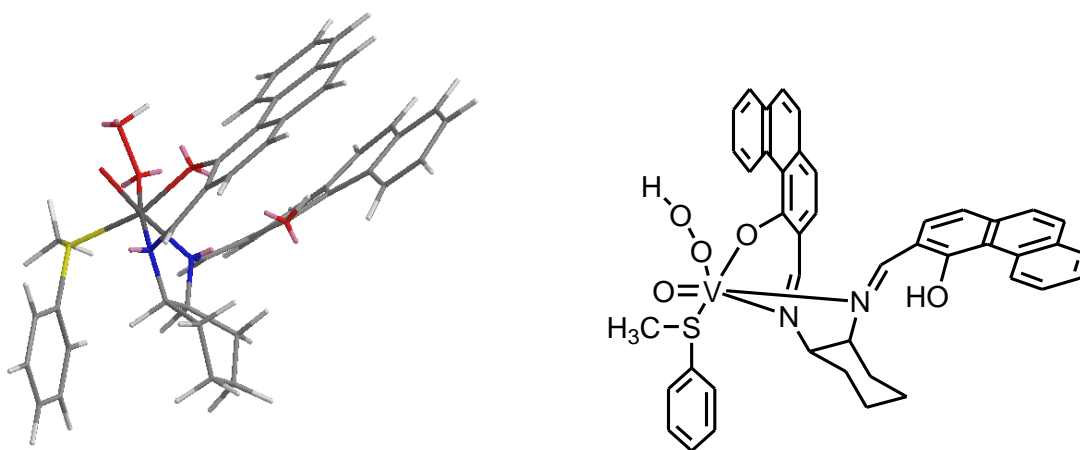


**Figure 1.36.** Three dimensional structure (left) and two dimensional representation (right) of the transition state leading to one possible isomer (*R* or *S*) ( $E = 31.8676$  kcal/mol).

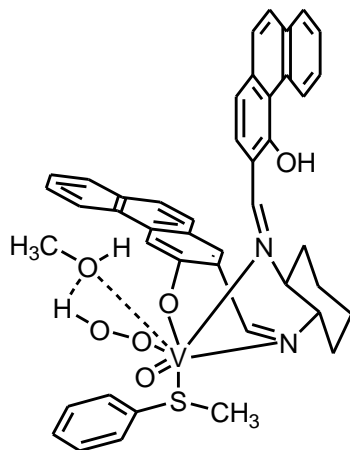


**Figure 1.37.** Hydrogen bonding assisted face selectivity.

## 1.4 Conclusions

Chiral rigid helical vanadium salen complexes were prepared and characterized. Chirality of the backbone can be enhanced due to the rigid helical nature of these molecules. For the cyclohexyl backbone complexes the *M* isomer is predominant in solution. Chemists tried to answer the question for long “how helicity induced chirality can incorporate chiral induction in asymmetric reactions?” As we know from the previous work by Fox et al that, cyclohexyl diamine is a weak director of chirality, and this hypothesis is true in our case as well.<sup>26</sup> We saw both cyclohexyl diamine and binaphthyl diamine failed to produce high enantiomeric excess under the current reaction conditions. Helicity does not have much impact in the chiral induction. Among all the solvent and reaction conditions tried, our catalysts showed modest chiral induction when methanol was added in the solvent mixture. So, solvent polarity appears to play a critical role in asymmetric induction in the present condition.

## 1.5 Experimental Section

### *General Methods*

All reactions were run under inert atmospheres unless otherwise noted. Solvents used in metallation reactions were stored over sodium benzophenone ketyl or calcium hydride, and degassed prior to transfer via high-vacuum line techniques. Inert gasses were purified by passage

through 4 Å molecular sieves and a Engelhard Q5 catalyst bed. Preparation and workup of V(IV) compounds were completed under rigorously inert conditions to prevent oxidation or decomposition.

Elemental analyses were carried out by Desert Analytics of Tucson, Arizona. UV-vis spectra were obtained on a Varian Cary 500 spectrometer, and CD spectra (5 scans, 1mm path length cell) on a JASCO 720 spectropolarimeter. Solution samples for these two techniques were prepared using dried spectroscopic grade THF, at concentrations that ranged between 1.5 and 2.5 × 10<sup>-5</sup> M. A 1 cm path length quartz cell was employed for the analysis. <sup>1</sup>H and <sup>13</sup>C NMR spectra were obtained on a Varian Unity 400 MHz spectrometer employing residual solvent protons or in some cases TMS as an internal standard. Crystallographic data was collected using either a Bruker SMART 1000 CCD or a Bruker-AXS SMART APEX CCD. Full structural information is included in appendix II. EPR spectroscopy of the vanadium complexes were measured in Varian E-4 EPR spectrometer.

**V(IV)-(R,R)-1 complex (C-1).** Ligand **1** (0.100 g, 0.192 mmol) and sodium methoxide (0.103 g, 1.920 mmol) were dissolved into a mixture (2:1 ratio) of dichloromethane (10 mL) and ethanol (5 mL). The mixture was dissolved by stirring. Vanadyl(IV) acetylacetonate (0.052 g, 0.192 mmol) added to the mixture and the entire solution was stirred overnight. A green colored precipitate separated out and the solution was filtered. The precipitate was washed with 5 mL of dichloromethane. The precipitate was dried under vacuum to afford **C-1** (0.100 g, 89% yield). <sup>1</sup>H NMR (CDCl<sub>3</sub>, 400 MHz): δ 0.9 (broad, 4H, CH), 1.25 (broad, 4H, CH), 2.1 (broad, 2H, CH), 7.0-7.7 (broad, 16H, CH), 7.8-7.9 (broad, 2H, CH). C:H:N (found 63.55:3.78:4.00; calculated 63.54:3.79:4.01). IR (ν<sub>V=O</sub> 1032.45 cm<sup>-1</sup>). MS: (C<sub>36</sub>H<sub>28</sub>N<sub>2</sub>O<sub>3</sub>V)<sup>+</sup> 588.1624 (75%), 589.1673 (18%), 590.1726 (5%), 591.1756 (2%). EPR (g=2.0, paramagnetic). CD (at 10<sup>-5</sup>M in THF, *M* isomer of the helix predominates in solution). Single crystals were grown from diffusion method from dichloromethane and hexane mixture.

**V(IV)-(R)-2 complex (C-2).** Ligand **2** (0.100 g, 0.145 mmol) and sodium methoxide (0.086 g, 1.590 mmol) were dissolved into a mixture (2:1 ratio) of dichloromethane (10 mL) and ethanol (5 mL). The mixture was dissolved by stirring. Vanadyl(IV) acetylacetonate (0.039 g, 0.145 mmol) added to the mixture and the entire solution was stirred overnight. After overnight

stirring, the solution turned deep brown. Solution was filtered. Solvent was evaporated under reduced pressure to afford deep brown colored solid. Soxhlate extraction was performed in dichloromethane to afford after drying pure deep brown colored **C-2** (0.089 g, 91% yield).  $^1\text{H}$  NMR ( $\text{CDCl}_3$ , 400 MHz):  $\delta$  7.0-8.1 (broad, 30H, CH). MS:  $(\text{C}_{50}\text{H}_{30}\text{N}_2\text{O}_3\text{V})^{+1}$  758.2069 (71%), 759.2354 (21%), 760.2691 (6%), 761.2842 (2%). EPR ( $g=2.0$ , paramagnetic), IR ( $\nu_{\text{V=O}}$  1016.03  $\text{cm}^{-1}$ ,  $\nu_{\text{C=C}}$  1573.28  $\text{cm}^{-1}$ ). UV (broad absorption peak for LMCT at 440 nm). CD (at  $10^{-5}\text{M}$  in THF, *M* isomer of the helix predominates in solution).

**V(IV)-(R,R)-3 complex (C-3)**. Ligand **3** (0.600 g, 0.965 mmol) and sodium methoxide (0.521 g, 9.650 mmol) were dissolved into a mixture (2:1 ratio) of dichloromethane (20 mL) and ethanol (10 mL). The mixture was dissolved by stirring. Vanadyl(IV) acetylacetonate (0.261 g, 0.965 mmol) added to the mixture and the entire solution was stirred overnight. A deep green colored precipitate was separated out. Solution was filtered. Soxhlate extraction was done in dichloromethane to purify the green colored solid. The solid was dried under reduced pressure to obtain **C-3** (0.490 g, 81% yield).  $^1\text{H}$  NMR ( $\text{CDCl}_3$ , 400MHz): 1.25 (broad, 2H), 1.6-1.8 (broad, 4H), 3.75 (broad, 2H), 7.9 (broad singlet, imine proton, 2H), 7.0-8.0 (broad, 20H). MS:  $(\text{C}_{44}\text{H}_{32}\text{O}_3\text{N}_2\text{V})^{+1}$  688.1919 (75%), 689.1962 (21%), 690.2012 (3%), 691.2050 (1%). IR ( $\nu_{\text{V=O}}$  1008.50  $\text{cm}^{-1}$ ,  $\nu_{\text{C=C}}$  1606.50  $\text{cm}^{-1}$ ). UV (in THF) shows for LMCT at 350 nm. CD spectrum (in THF at  $10^{-5}\text{M}$ ) shows the presence of *M* helix in the solution. Single crystal was grown from diffusion method from dichloromethane and hexane.

**V(IV)-(R)-4 complex (C-4)**. Ligand **4** (0.650 g, 0.821 mmol) and sodium methoxide (0.488 g, 9.028 mmol) were dissolved in a mixture (2:1 ratio) of dichloromethane (20 mL) and ethanol (10 mL). The mixture was dissolved by stirring. Vanadyl(IV) acetylacetonate (0.222 g, 0.821 mmol) added to the mixture and the entire solution was stirred overnight. The solution became dark reddish brown on the next day. Solution was filtered and the solvent evaporated from the filtrate part to obtain reddish brown colored solid. The solid was subjected to the soxhlate extraction in dichloroethane followed by solvent removal under reduced pressure to obtain pure brown colored **C-4** (0.480 g, 80% yield).  $^1\text{H}$  NMR ( $\text{CDCl}_3$ , 400 MHz):  $\delta$  7.0-8.0 (broad, 40H). MS:  $(\text{C}_{58}\text{H}_{34}\text{N}_2\text{O}_3\text{V})^{+1}$  858.2091 (65%), 859.1785 (29%), 860.6641 (5%), 861.6937 (1%). IR ( $\nu_{\text{V=O}}$



1035.71  $\text{cm}^{-1}$ ). UV (three LMCT transitions at 395, 445 and 482 nm). CD (shows the predominance of *M* helix in the solution).

### ***General Procedure for Sulfoxidations:***

All sulfoxidation reactions are carried out by 1 mol% of catalyst. 1 mol% of catalyst was dissolved in dichloromethane (3mL) inside a two neck R.B. under argon. The mixture was stirred in inert atmosphere for 10 minutes. 100 mol% phenyl methyl sulfide was added followed by additional 15 minutes of stirring. The entire system was cooled to 0 °C. 110 mol% oxidant (hydrogen peroxide or cumene hydroperoxide) was added to the mixture slowly for a period of 2 hrs. The mixture was additionally stirred for 16 hrs. A saturated solution of sodium sulfite was added to quench the reaction. The reaction mixture was extracted with dichloromethane followed by drying over sodium sulfate. The product was purified by flash column chromatography in 1:3 ethyl acetate:hexane. Pure sulfoxide was analysed by  $^1\text{H}$  NMR ( $\text{CDCl}_3$ , 400 MHz): 3.72 (s, 3H,  $\text{CH}_3$ ), 7.5 (m, 3H, CH), 7.6 (m, 2H, CH). Enantiomeric excess of the phenyl methyl sulfoxide was determined by HPLC analysis with a Daicel Chiralcel OD-H column. Hexane and isopropanol mixture (90:10) was used as the eluent. The *R* isomer and the *S* isomer elutes at 17 and 20 minutes respectively.

## **1.6 References**

1. "Vanadium catalyzed asymmetric oxidation of sulfides using Schiff base ligands derived from  $\beta$ -amino-alcohols with two stereogenic centers" Chan, A. S. C.; Li, X.; Liu, J.; Wu, Y. *Eur. J. Org. Chem.* **2009**, 2607-2610.
2. "Highly enantioselective oxidative couplings of 2-naphthols catalyzed by chiral bimetallic oxovanadium complexes with either oxygen or air as oxidant" Gong, L. Z.; Cun, L. F.; Luo, S. W.; Ye, J. L.; Liu, Q. Z.; Luo, Z. B.; Wu, Z. J.; Guo, Q. X. *J. Am. Chem. Soc.* **2007**, 129, 13927-13938.
3. "Efficient asymmetric oxidation of sulfides and kinetic resolution of sulfoxides catalyzed by a vanadium salan system" Hu, H.; Pan, Y.; Yang, M.; Dai, Z.; Zhu, C.; Sun, J. *J. Org. Chem.* **2004**, 99, 2500-2504.

4. "Chiral distortion in a Mn(IV)-(salen)(N<sub>3</sub>)<sub>2</sub> derived from Jacobsen's catalyst as a possible conformation model for its enantioselective reactions" Fujii, H.; Kurahashi, T. *Inorg. Chem.* **2008**, *47*, 7556-7567.
5. "Catalytic enantioselective oxidation of sulfides to sulfoxides with a renewable hydroperoxides" Scettri, A.; Siniscalchi, F. R.; Lattanzi, A.; Massa, A. *Tetrahedron: Asymmetry.* **2001**, *12*, 2775-2777.
6. "Material application of salen frameworks" Kleij, A. W.; Wezenberg, S. J. *Angew. Chem. Int. Ed.* **2008**, *47*, 2354-2364.
7. "Critical role of external axial ligands in chirality amplification of *trans*-cyclohexane-1,2-diamine in salen complexes" Fujii, H.; Hada, M.; Kurahashi, T. *J. Am. Chem. Soc.* **2009**, *131*, 12394-12405.
8. "Vanadium catalyzed enantioselective sulfoxidations: rational design of biocatalytic and biomimetic systems" Sheldon, R. A.; Arends, I. W. C. E.; Velde, F. V. D. *Topics in Catalysis.* **2000**, *13*, 259-265.
9. "The first asymmetric epoxidation using a combination of achiral (salen)-manganese(III) complex and chiral amine" Ito, Y.; Hashihayata, T.; Katsuki, T. *Tetrahedron.* **1997**, *53*, 9541-9552.
10. "Control of absolute helicity in single-stranded abiotic metallofoldamers" Dong, Z.; Karpowicz, R. J. Jr.; Bai, S.; Yap, G. P. A.; Fox, J. M. *J. Am. Chem. Soc.* **2006**, *128*, 14242-14243.
11. "Abiotic metallofoldamers as electrochemically responsive molecules" Zhang, F.; Bai, S.; Yap, G. P. A.; Tarwade, V.; Fox, J. M. *J. Am. Chem. Soc.* **2005**, *127*, 10590-10599.
12. "Iron and zinc(II) monohelical binaphthyl salen complexes with overlapping benz[a]anthryl sidearms" Wiznycia, A. V.; Desper, J.; Levy, C. J. *Dalton Trans.* **2007**, 1520-1527.
13. "Five coordinate compounds-.....:synthesis and properties of [O-.....-OC<sub>6</sub>H<sub>4</sub>CHNCH<sub>2</sub>C(CH<sub>3</sub>)<sub>2</sub>NCHC<sub>6</sub>H<sub>4</sub>O-.....-O]VO" Daughdrill, D. L.; Martin D. F.; Binford, J. S. Jr. *J. Inorg. Nucl. Chem.* **1970**, *32*, 2885-2890.

14. "Synthesis, characterization and study of vanadyl tetradentate Schiff base complexes as catalysts in aerobic selective oxidation of olefins" Mohebi, S.; Boghaei, D. M. *J. Mol. Catal. A: Chemical* **2002**, *179*, 41-51.
15. "1,1'-binaphthyl-2,2'-diol and 2,2'-diamino-1,1'-binaphthyl: versatile frameworks for chiral ligands in coordination and metallocsupramolecular chemistry" Telfer, S. G.; Kuroda, R. *Coordination. Chem. Rev.* **2003**, *242*, 33-46.
16. "Mono and dinuclear complexes of chiral tri and tetradentate Schiff base ligands derived from 1,1'-binaphthyl-2,2'-diamine" Telfer, S. G.; Sato, T.; Harada, T.; Kuroda, R.; Lefebvre, J.; Leznoff, D. G. *Inorg. Chem.* **2004**, *43*, 6168-6176.
17. "Metal complexes of chiral binaphthyl Schiff base ligands and their application in stereoselective organic transformations" Che, M. C.; Huang, J. S. *Coordination. Chem. Rev.* **2003**, *243*, 97-113.
18. "Preparation and characterization of optically active Schiff base oxovanadium(IV) and oxovanadium(V) complexes and catalytic properties of these complexes on asymmetric oxidation of sulfides into sulfoxides with organic hydroperoxides" Nakajima, K.; Kojima, K.; Kojima, M.; Fujita, J. *Bull. Chem. Soc. Jpn.* **1990**, *63*, 2620-2630.
19. "Asymmetric synthesis of esomeprazole" Cotton, H.; Elebring, T.; Larson, M.; Li, L.; Sorenson, H.; Unge, S. V. *Tetrahedron: Asymmetry.* **2000**, *11*, 3819-3825.
20. "Tetradentate Schiff base oxovanadium(IV) complexes: structures and reactivities in the solid state" Kojima, M.; Taguchi, H.; Tsuchimoto, M.; Nakajima, K. *Coordination. Chem. Rev.* **2003**, *237*, 183-196.
21. "Vanadium catalyzed asymmetric oxidations" Bolm, K. *Coordination. Chem. Rev.* **2003**, *237*, 245-256.
22. "Asymmetric catalysis of metal complexes with non-planar ONNO ligands: salen, salalen and salan" Matsumoto, K.; Saito, B.; Katsuki, T. *Chem. Commun.* **2007**, 3619-3627.
23. "Asymmetric epoxidation of olefins catalyzed by Ti(salen) complexes using aqueous hydrogen peroxide as the oxidant" Matsumoto, K.; Sawada, Y.; Katsuki, T. *Pure. Appl. Chem.* **2008**, *80*, 1071-1077.

24. "Fe(salan) catalyzed asymmetric oxidation of sulfides with hydrogen peroxide in water" Egami, H.; Katsuki, T. *J. Am. Chem. Soc.* **2007**, *129*, 8940-8941.
25. Rockenbauer, A.; Korecz, L. *Appl. Magn. Reson.* **1996**, *10*, 29-43.
26. "Monohelical iron(II) and zinc(II) complexes of a (1*R*,2*R*)-cyclohexyl backbone salen ligands with benz[*a*]anthryl sidearms" Wiznycia, A. V.; Desper, J.; Levy, C. J. *Inorg. Chem.* **2006**, *45*, 10034-10036.
27. "*trans*-cyclohexane-1,2-diamine is a weak director of absolute helicity in chiral nickel salen complexes" Dong, Z.; Yap, G. P. A.; Fox, J. M. *J. Am. Chem. Soc.* **2007**, *129*, 11850-11853.
28. "Optically active complexes of Schiff bases: an analysis of the circular dichroism spectra of some complexes of different coordination numbers with quadridentate Schiff bases of optically active diamines" Pasini, A.; Gullotti, M.; Ugo, R. *J. Chem. Soc., Dalton Trans.* **1977**, 346.
29. "Some factors influencing the ultraviolet absorption spectra of polynuclear aromatic compounds: a general survey" Jones, R. N. *J. Am. Chem. Soc.* **1945**, *67*, 2127.
30. "Synthesis, characterization, and application of vanadium salan complexes in oxygen transfer reactions" Adao, P.; Pessoa, J. C.; Henriques, R. T.; Kuznetsov, M. L.; Avecilla, F.; Maurya, M. R.; Kumar, U.; Correia, I. *Inorg. Chem.* **2009**, *48*, 3542-3561.

# CHAPTER 2 - Asymmetric Sulfoxidations by Helical Ti, V, Al, Fe Salan Complexes

## 2.1 Abstract

New chiral salan ligands with a 1,2-(*R,R*)-diamine-cyclohexyl backbone, and either phenanthryl or benz[*a*]anthryl sidearms are synthesized. Both secondary N-H and tertiary N-Me versions have produced and characterized by 2D NMR techniques. Due to the enhanced flexibility of these ligands compared to their salen counterparts, they have the potential to generate helical  $\beta$ -*cis* geometries upon complexation with a metal center. Complexations of these ligands were done with Ti(IV), V(IV), Al(III) and Fe(II) as the central metal ions. These complexes were characterized by  $^1\text{H}$  NMR, IR, CD and MS techniques and were tested as catalysts for chiral induction in sulfoxidation. Due to the inherent asymmetry in  $C_1$ -symmetric  $\beta$ -*cis* geometry, these complexes produce better chiral inductions than their salen counterparts.

## 2.2 Introduction

In the late 20<sup>th</sup> century, chemists witnessed remarkable advancements in catalytic asymmetric synthesis.<sup>1</sup> Asymmetric synthesis is one of the most important field of organic chemistry and it has vast importance in pharmaceutical, oil and fine chemicals industry etc.<sup>2, 3</sup> Most of the drug molecules contain one or more functional groups, and sulfoxide is one of the important groups present in a number of drugs.<sup>4</sup> The presence of sulfoxide generates a chiral center (provided the two R groups attached to the sulfur are different) in the pharmaceutically important molecule. The orientation of the sulfoxide group plays a crucial role on the activity in those pharmaceutically important molecule.<sup>4</sup> Depending on the chirality (*R* or *S*) of the sulfoxide, a molecule can be active or inactive.<sup>4</sup> One example of a drug containing chiral sulfoxide is omeprazol (prilosec) which is widely used to treat acid reflux conditions related to the esophagus, stomach and intestines (figure 1.10).<sup>4</sup> There are several possible approaches to synthesizing enantiomerically pure organic compounds: (a) resolution of racemic mixtures, (b) chemical modifications of chiral objects available from the “chiral pool”, and (c) asymmetric synthesis. Among them the most efficient is catalytic asymmetric synthesis, because one chiral catalyst molecule can (in principle) produce millions of chiral product molecules.<sup>5</sup> To make these important chiral molecules, significant efforts have been made developing efficient catalysts

composed of chiral metal-organic frameworks or chiral organic molecules (organocatalysis).<sup>6</sup> Among chiral metal organic framework,<sup>5</sup> chiral metal-salen complexes have been established some of the most versatile catalysts. They are relatively easy to prepare, have high complexation ability with a wide variety of metal (M) ions, and complexes tend to be stable and have structural diversity.<sup>7</sup>

The first catalytic systems used for asymmetric sulfoxidation were those of Kagan and Modena (figure 2.1).<sup>7</sup> They applied the “Katsuki-Sharpless reagent”  $\text{Ti}(\text{O}^i\text{Pr}_4)$ /diethyl tartrate/alkyl hydroperoxide, with appropriate modifications, to the asymmetric oxidation of prochiral sulfides by alkyl hydroperoxide.<sup>7</sup> However, soon after modifications of the Ti-tartrate systems were developed, which can produce with 90% yields and 90% ee values for certain sulfides.<sup>8</sup> However, these systems have certain disadvantages, such as cost, low catalysts turnover numbers and activity (4-16 mol% catalysts required) and complexity.<sup>9</sup>

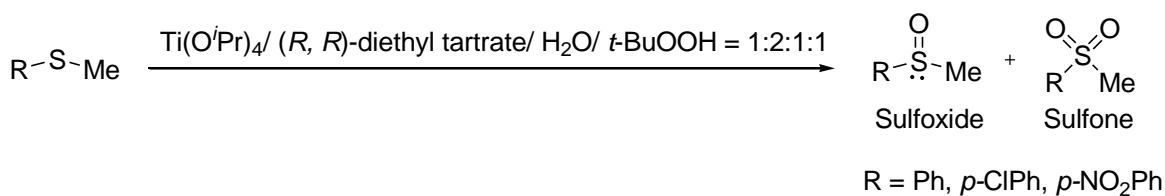


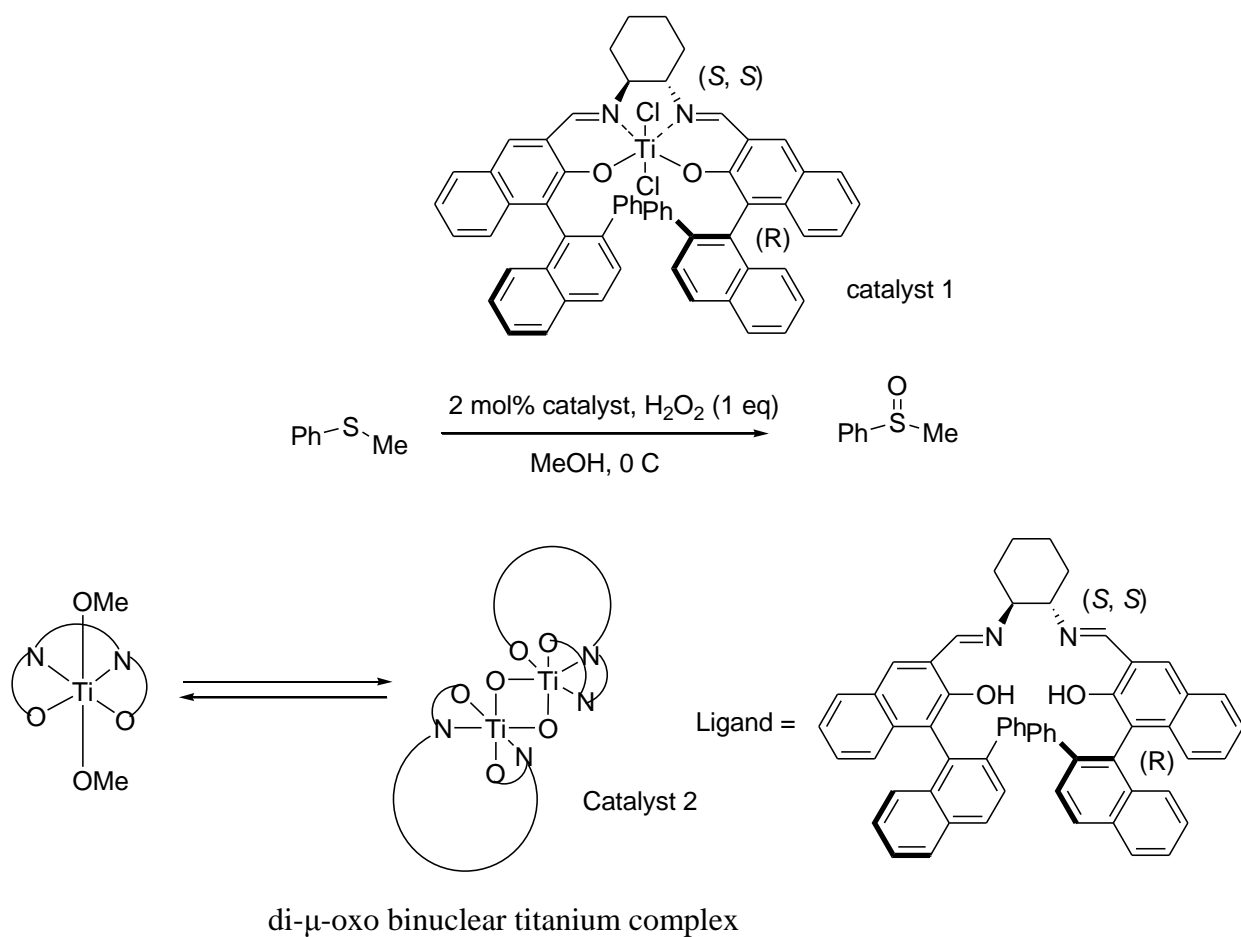
**Figure 2.1.** Sulfoxidation catalytic system introduced by Kagan and Modena.<sup>7</sup>

From the pharmaceutical research viewpoint, there has been an enormous need to find an ideal catalytic system for catalytic asymmetric sulfoxidation. A simple catalytic system, which is inexpensive, robust, environmentally safe, efficient (in terms of turnover numbers), highly enantioselective, and can be usable with environmentally benign oxidant like  $\text{H}_2\text{O}_2$  is most desirable. Catalytic systems based on nontoxic metals such as titanium or low toxicity metals such as vanadium, aluminum or iron in combination with hydrogen peroxide as the oxidant are of interest.

The first attempts to find the effective catalytic system with titanium as the central metal and hydrogen peroxide as the oxidant was made by Pasini et al. in 1986.<sup>10</sup> They used a titanium(IV)-salen system with  $\text{H}_2\text{O}_2$  and achieved ee  $\leq$  18%. Fifteen years later, in 2001, Katsuki introduced a mononuclear “second generation” titanium-salen complex (bearing additional elements of chirality at the 3,3’positions of the salen ligand) as a sulfoxidation

catalysts and found poor selectivity (catalyst 1, figure 2.2).<sup>11</sup> However, when this complex was converted into its di- $\mu$ -oxo binuclear titanium counterpart, this catalyst became very active and produced enantioselectivities to 99% with aryl alkyl sulfides as the substrate (catalyst 2, figure 2.2).<sup>12</sup> The monomeric complex becomes dimeric with oxo bridges in methanol with added  $\text{H}_2\text{O}_2$ . This catalyst system was successfully applied to the asymmetric oxidation of cyclic dithioacetals (with ee values of the resulting monosulfides ranging from 39 to 99%).<sup>12</sup> Recently, a family of titanium(IV) catalysts with  $\beta$ -amino-alcohol derived Schiff bases produced chiral sulfoxides between 40 to 72% ee with  $\text{H}_2\text{O}_2$  as the oxidant.<sup>13</sup>

Vanadium(IV)-salen has been a well known catalyst system for asymmetric sulfoxidation.<sup>14</sup> However, so far only a few examples are available about vanadium-salen system used for asymmetric sulfoxidation. The first vanadium salen system successfully used as chiral



sulfoxidation catalyst was by Zhu et al. in 1995.<sup>12</sup> Their catalyst system involves (*R,R*)-1,2-diamino cyclohexane and (*R,R*)-1,2-diamino diphenyl ethane as the backbone and salicyl or 3,5-di-*tert*-butyl salicyl as the side arm. The catalyst system produced up to 98% ee in CH<sub>2</sub>Cl<sub>2</sub> or in CHCl<sub>3</sub> at 0 °C with alkyl aryl sulfides as the substrate.<sup>12</sup> However, when the reduced version of salen, (salan) complexed with vanadium, it produces better results in terms of asymmetric inductions in sulfoxidations, than the unreduced similar vanadium salen system.<sup>13</sup> More recently (2004), Correia et al were able to fully characterize the (*R,R*)-1,2-diamino cyclohexyl vanadium salan complexes and used them in different asymmetric oxidation reactions such as sulfoxidations, and the oxidation of alkenes.<sup>13</sup> They reported moderate activity of these vanadium salan complexes in the oxidation of thioanisole. The enantioselectivity reached to 50% (figure 2.3). The stability of these complexes is a big issue. These vanadyl salan complexes are very prone to oxidation to V(V) complexes. This might be the factor for the low activity in catalytic reactions.

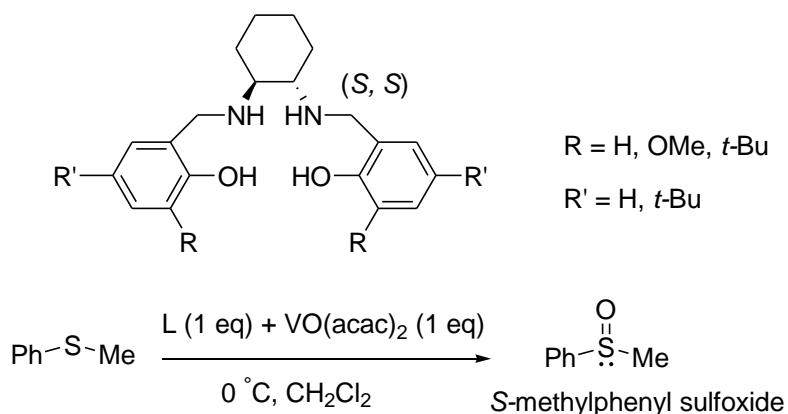


**Figure 2.3.** Vanadium(IV)-salan catalyzed sulfoxidation of thioanisole

In recent years, salan [*N,N'*-bis(salicylamine)] and salalen (*N*-salicylamine-*N'*-salicylimine) complexes of different transition metals have been applied in different asymmetric catalytic processes.<sup>13</sup> One example of a recently discovered successful metal salan complex, is shown in figure 2.4.<sup>14</sup> The complex has additional chirality in the aromatic ring sidearms of the iron(III) salan complex, and was found to effectively catalyze the oxidation of aryl alkyl sulfides with H<sub>2</sub>O<sub>2</sub> in aqueous media (in 81-96% ee) (figure 2.4).<sup>14</sup>



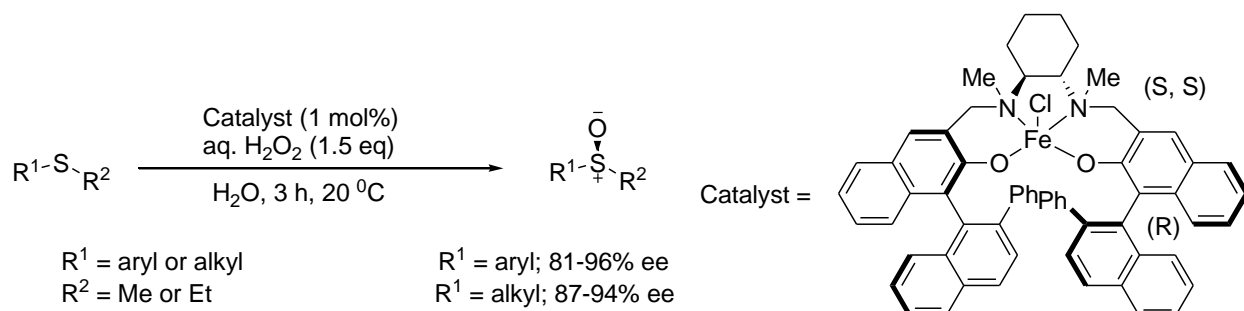


**Figure 2.4.** Fe(III) salan catalyzed asymmetric sulfoxidation<sup>14</sup>

A salalen-Al(III) complex proved to be even more efficient chiral catalyst in sulfoxidation reactions (figure 2.5).<sup>15</sup> This catalyst work in the synergistic way which is a combination of initial enantioselective oxidation of the aryl alkyl sulfide followed by the oxidative kinetic resolution process, showed even more remarkable results in methanolic solution: alkyl aryl sulfoxides were obtained with 94-99% ee value.<sup>15</sup>

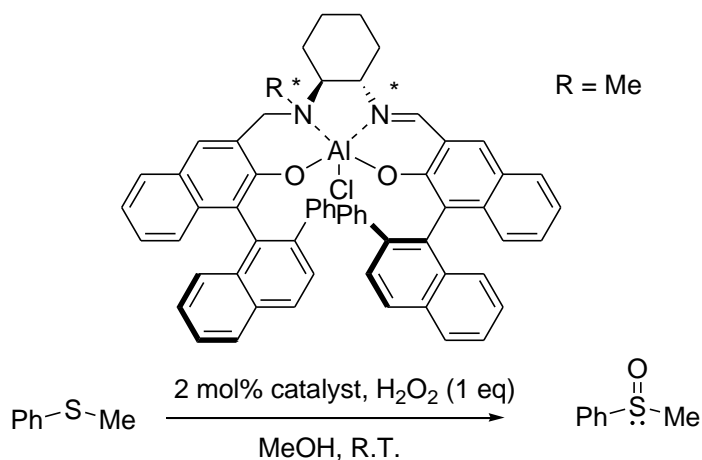


**Figure 2.5.** Al(III)-salalen complex for asymmetric sulfoxidation

There are a few advantages and disadvantages of using salans as chiral ligands compared to salens. In solution, salen ligands have the disadvantage of the hydrolysis of the C=N bond, particularly in water containing solvents. The reduced derivative of salen: called tetrahydrosalen or salan are much less studied than their salen counterparts. The presence of a  $sp^3$  carbon attached to an amine group, results in a more flexible structure, which is also more resistant to the hydrolysis. The flexibility of the carbon-nitrogen single bond causes salan ligands to bind to

a metal ion in a non-planar arrangement and often either a *cis-α* or a *cis-β* conformation is dominant in octahedral coordination. For the salen analogue a *trans* configuration is more common (figure 2.6).<sup>16</sup> These conformations are chiral and it is observed that *cis-β* conformation induces chirality transfer to the product. Therefore, salen ligands are better in terms of chiral induction than their imine analogue.

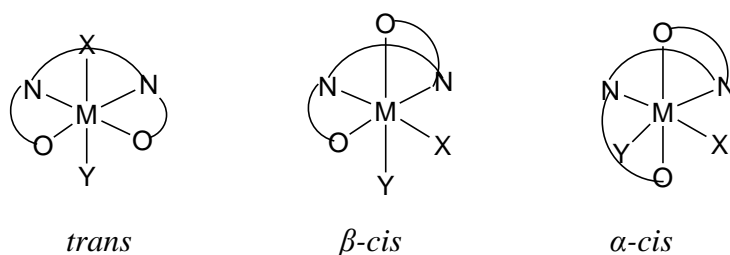


**Figure 2.6.** Possible geometries of an octahedral metal salen complex

The flexibility of the salen ligands can also be a drawback in terms of regulating the stereochemistry of these complexes. It was observed that the *cis-α* or *cis-β* isomers can equilibrate between all three isomers described above.<sup>16</sup> Thus, due to the difficulty in controlling their stereochemistry, there are few reports on asymmetric catalysis with M(salen) complexes. For example, Walsh and co-workers reported that treatment of  $\text{Ti}(\text{O}^i\text{-Pr})_4$  with a salen ligand gave a diastereomeric mixture of two isomers shown in figure 2.7.<sup>17</sup> However, if their stereochemistry can somehow be regulated M(salen) complexes should be as attractive chiral catalysts as their salen analogues.

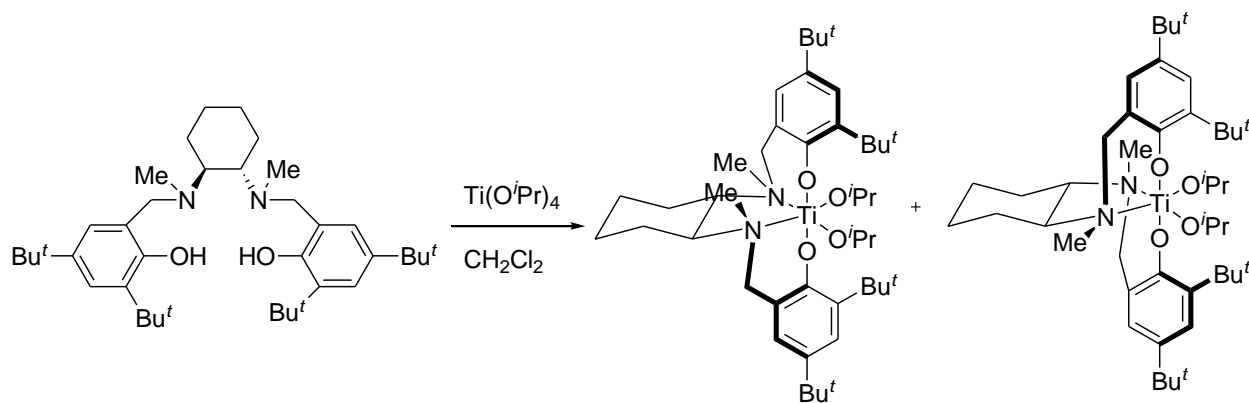


**Figure 2.7.** Diastereomers after complexation with titanium<sup>17</sup>

Most of the salen ligands used so far have the chirality source coming from the ligand backbone and not the ligand wrapping mode around the metal; that is these complexes are not *chiral-at-the-metal*. In contrast, most of the isotactic polymerization catalysts *ansa*-metallocenes and salan complexes are  $C_2$  chiral as a result of ligand wrapping around the metal center.<sup>18</sup> Unfortunately, due to the lack of chirality at the ligand backbone, this leads to racemic catalyst mixtures. However, unraveling the factors that determine the cause of chirality due to chiral ligand wrapping around the metal centers may lead to asymmetric catalysts with *predetermined* chirality at the metal center. Here, in this article, we discuss the asymmetric sulfoxidation by enantiomerically pure diastereotopic salan complexes of titanium, vanadium aluminum and iron.

The preferred wrapping mode of the salan ligand around the octahedral titanium, aluminum and iron is *fac-fac* in nature.<sup>18</sup> This specific wrapping mode gives rise to  $C_2$  chiral complexes. The introduction of chirality at the backbone of the salan ligand will give rise to two diastereotopic isomers ( $\Delta$  and  $\Lambda$ ) shown in figure 2.8.<sup>18</sup>

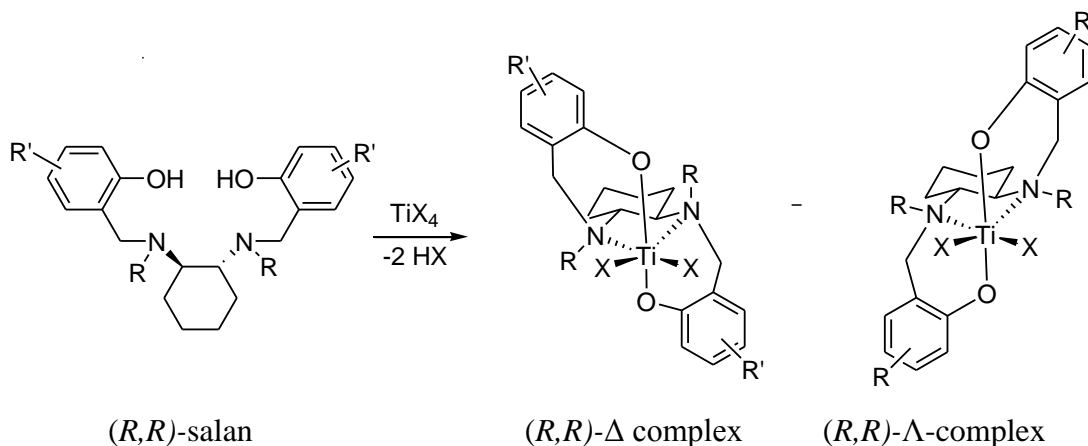


**Figure 2.8.** Two isomers of *fac-fac* octahedral titanium salan complex

The four chiral salan ligands described in this work are assembled around *trans*-1,2-diaminocyclohexane, featuring either N-H or N-Me groups, and either phenanthryl or benz[a]anthryl as the sidearms. A three dimensional ball and stick model of one isomer of an octahedral titanium salan complex that we will deal with in this article is shown in figure 2.9. From the figure it is clear that the molecule is predicted to have a *cis- $\beta$*  geometry rather than a *trans* geometry. One model of a vanadyl salan complex is also shown in figure 2.10. The

molecular model predicts a stepped helical square pyramidal geometry in the *P* conformation for the vanadium salan complex.

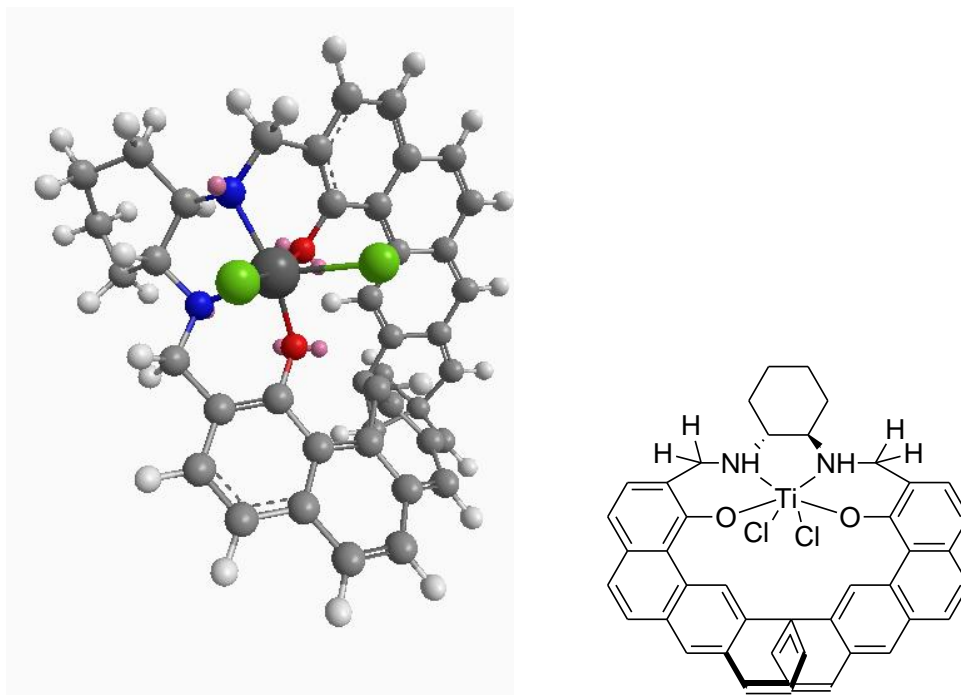


**Figure 2.9.** Ball and stick model of octahedral titanium(IV) salan complex

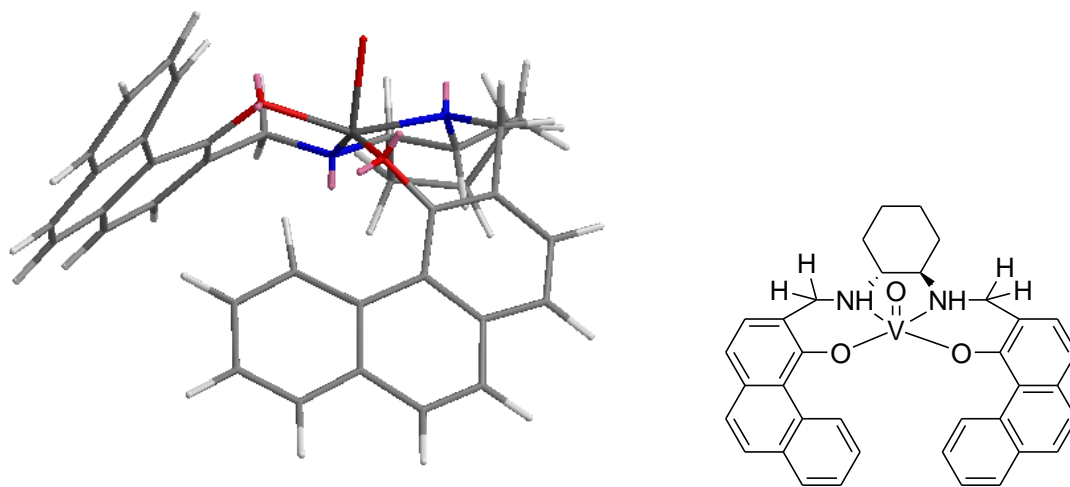


**Figure 2.10.** Stick model of vanadium(IV) salan complex

The salan ligands used in this study are shown in figure 2.11. These ligands were synthesized from their salen precursors and characterized by 2D NMR. Different salan ligands were used to form complexes with titanium(IV), vanadium(IV), iron(II) and aluminum(III).

These complexes were characterized by different analytical techniques:  $^1\text{H}$  NMR, IR, UV, CD and MS. These complexes were used as the asymmetric catalysts in sulfoxidation reactions with  $\text{H}_2\text{O}_2$  as the terminal oxidant. A comparative study was done depending on the catalytic activity of these catalysts.

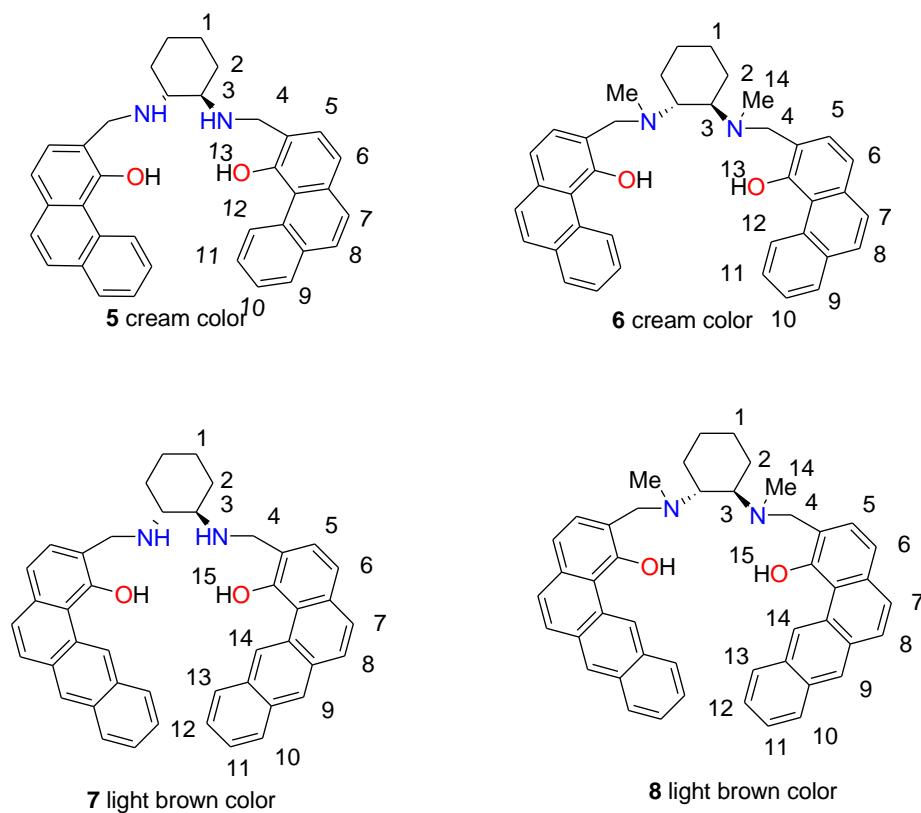


**Figure 2.11.** Salan ligands used in this study.

## 2.3 Results and discussions

### 2.3.1 General scheme for synthesis of (*R,R*)-5, (*R,R*)-6, (*R,R*)-7 and (*R,R*)-8

All four ligands were synthesized from their salen precursors. They were first reduced with  $\text{NaBH}_4$  followed by formylation by the treatment of the reduced ligand with formaldehyde, acetic acid and finally methylated  $\text{NaBH}_4$  to obtain the desired salan ligand with N-Me groups (figure 2.12). The yields of all the ligands are fairly high. All the ligands were characterized by 1D and 2D NMR.

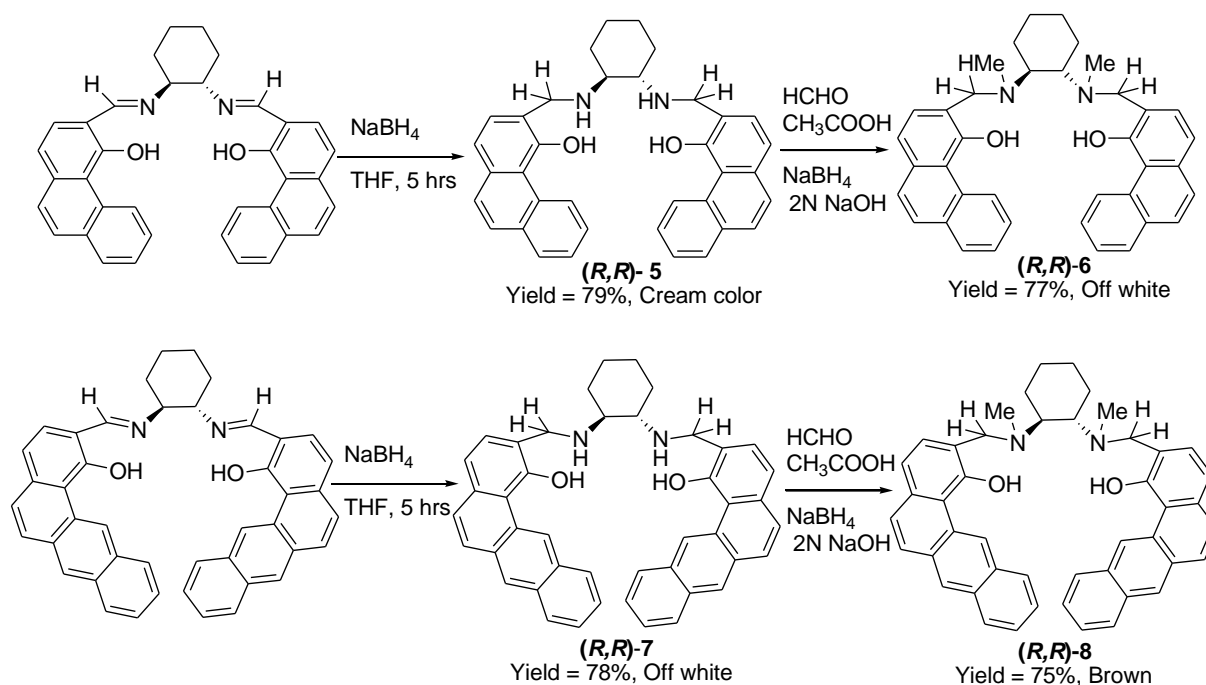


**Figure 2.12.** Synthesis of salan ligands used in this study.

### 2.3.2 Characterization of the ligands

For ligands **(R,R)-5** and **(R,R)-7**, the proton NMR showed characteristics second order AB peak pattern for the two enantiotopic protons in the  $\text{CH}_2$  group. Due to the chirality of the backbone, the two protons in the  $\text{CH}_2$  group became enantiotopic (figure 2.13). The protons in the  $\text{CH}_2$  group for the ligand **7** appeared slightly upfield than for **5**. This is due to the enhanced electron delocalization imposed by the extra phenyl ring side arm in case of **7**, and thereby making the amine bond more electron rich. The imine peak has completely disappeared in the reduced product indicating the formation of the reduced salen. The proton peak in hydroxyl group has an upfield shift than the salen analogues due to the reduction of the imine bond.



**Figure 2.13.** Second order AB pattern from the two protons of the  $\text{CH}_2$  group.

For ligand (*R,R*)-**6**, proton NMR showed the presence of the characteristics AB pattern for the CH<sub>2</sub> protons adjacent to the *N*-methyl group. There is an appearance of a sharp singlet around 3.7 ppm and this peak is assigned to the *N*-methyl group. The appearance of a larger number of peaks than expected in the aliphatic region is due to the coupling of each aliphatic protons with the adjacent protons and through space couplings as can be confirmed by 2D NMR spectroscopy. The bay proton appears at 9.94 ppm as a doublet by coupling with the nearest aromatic proton. The proton NMR spectrum with each peak assignment is shown in figure 2.14. To understand the long range through space coupling, 2D NMR experiments were carried out.

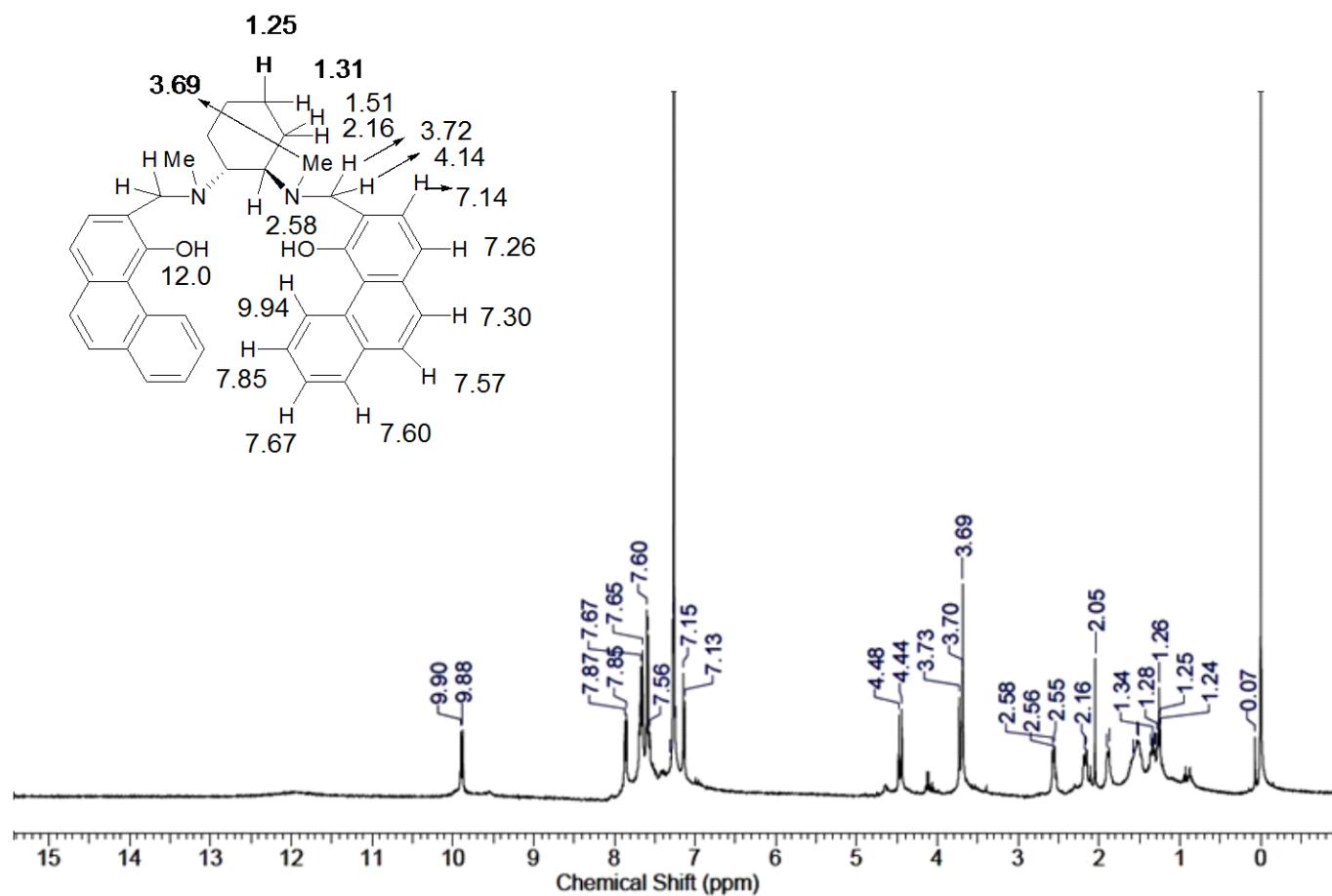


**Figure 2.14.** Proton NMR (CDCl<sub>3</sub>, 400 MHz) spectrum of (*R,R*)-**6**.

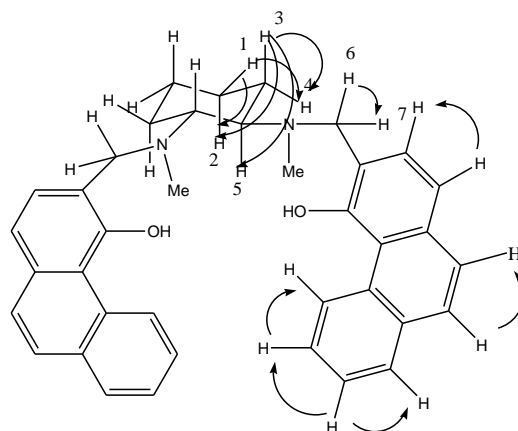
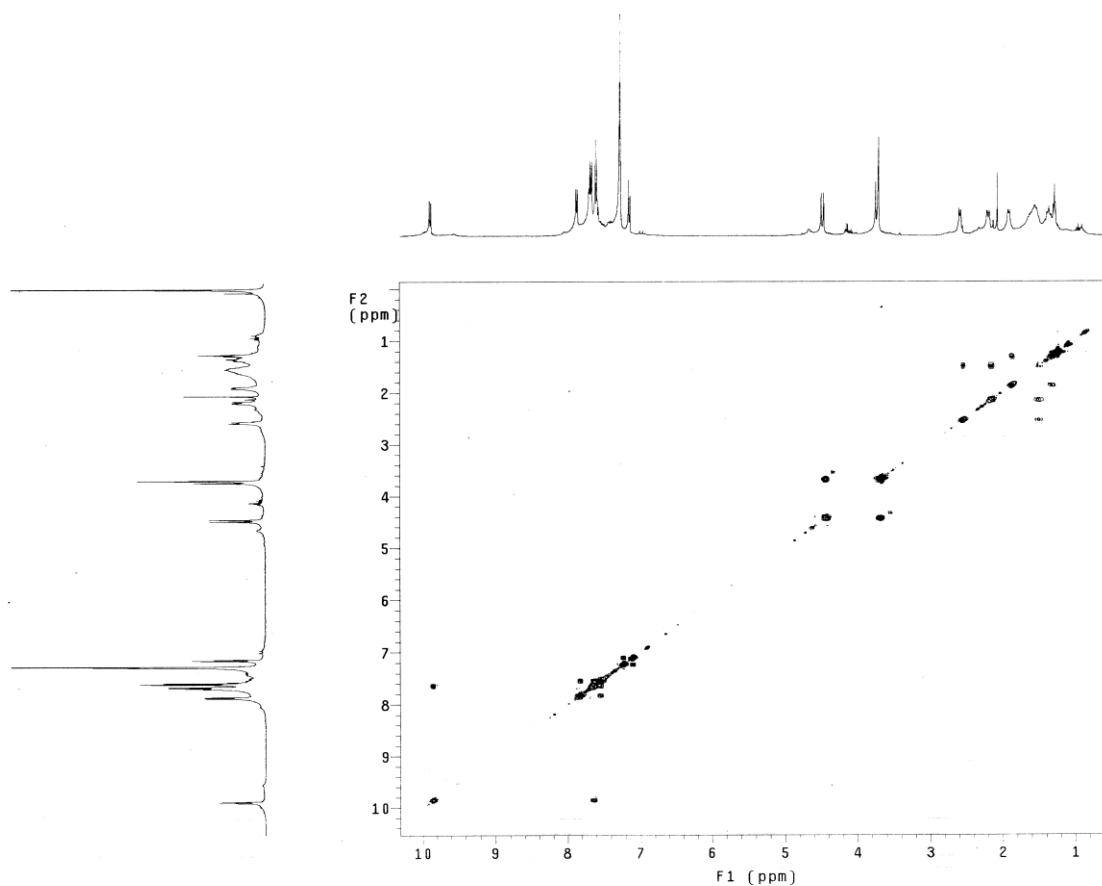


**Figure 2.15.**  $^1\text{H}$ - $^1\text{H}$  COSY spectrum (top) of the salan ligand showing the couplings.

$^1\text{H}$ - $^1\text{H}$  correlation spectroscopy (figure 2.15) showed that there are extensive couplings between the protons which are two bonds away (protons 1 and 2) from each other and the protons which are 1,2 diaxially oriented three bonds away (protons 2 and 3) from each other in the cyclohexyl ring backbone. Also, in the fused aromatic ring sidearm, there exist three bond



couplings between the adjacent protons (figure 2.15). A correlation between the aliphatic protons is shown in table 2.1 from 1D and 2D NMR spectroscopy.

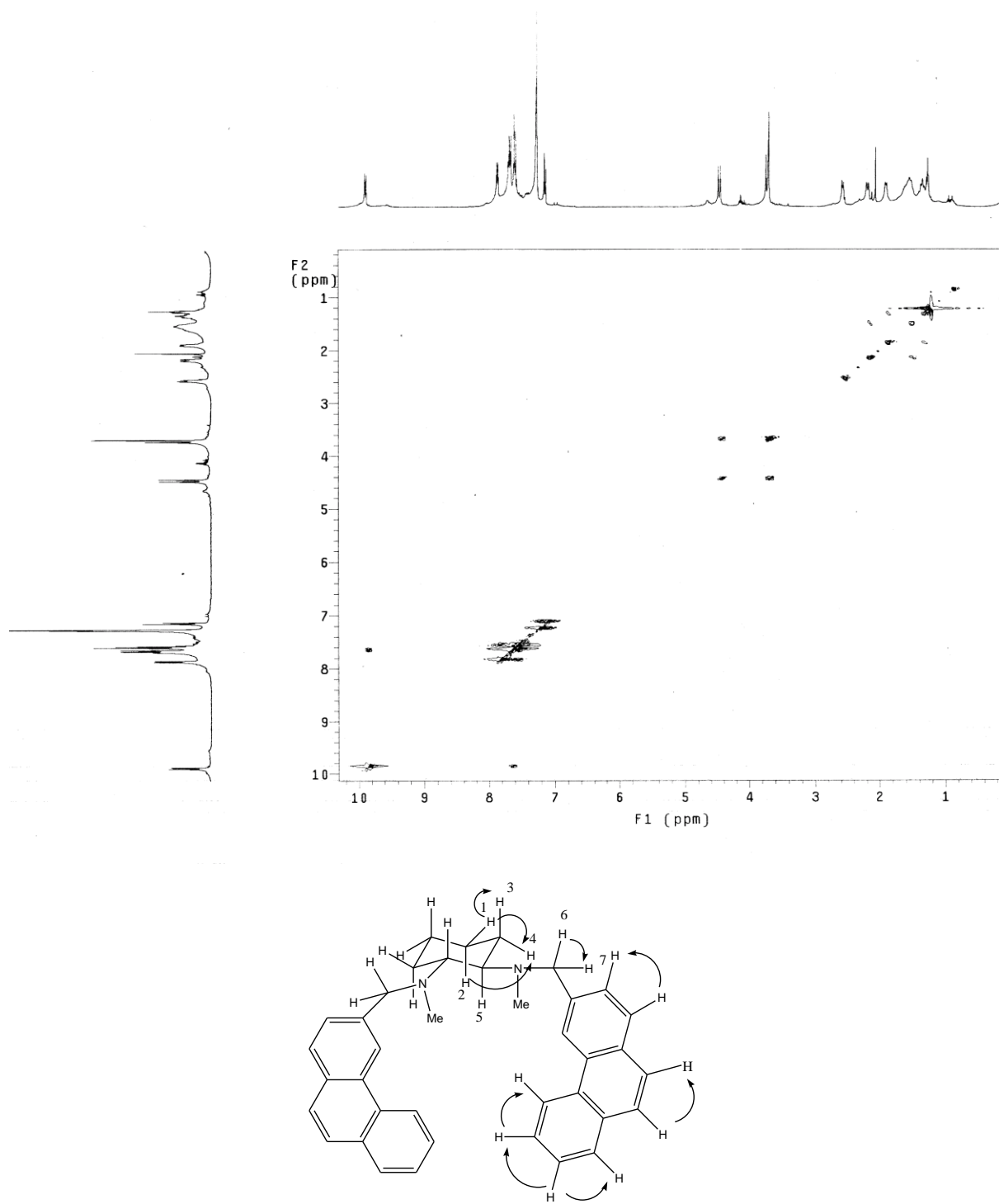


**Figure 2.16.**  $^1\text{H}$ - $^1\text{H}$  NOESY spectrum of the salan ligand showing the through-space couplings.

**Table 2.1.** Correlation between aliphatic protons from 1D and 2D NMR

Proton number	Chemical shift (ppm) (splitting pattern)	Coupling constant $^3J_{HH}$ (Hz)
1	1.24 (m)	6.4
2	1.85 (m)	6.6
3	2.16 (m)	6.6
4	2.55 (m)	6.4
5	2.82 (m)	6.8
6	8.2 (dd, AB)	8.2 ( $^2J_{HH}$ )

$^1\text{H}$ - $^1\text{H}$  NOESY spectrum shows the through space coupling between the protons (figure 2.16). From this spectrum, it is clear that there are some through space couplings between the adjacent (3 bonds away) axial and equatorial protons in the cyclohexyl backbone. These through space couplings along with the through bond couplings in the cyclohexyl backbone produces a very complicated  $^1\text{H}$  NMR spectrum of the salan ligand in the aliphatic region of the proton NMR.

Ligand (***R,R***)-**8** was characterized by the 2D NMR techniques COSY, NOESY and HMQC. The  $^1\text{H}$  NMR spectrum ( $\text{CDCl}_3$ , 400MHz) is shown in figure 2.17 with the peak assignments.

Note: Full names of some used terms,

COSY: correlation spectroscopy

NOESY: nuclear overhauser effect spectroscopy

HMQC: heteronuclear multiple quantum coherence spectroscopy

ppm: parts per million

ee: enantiomeric excess

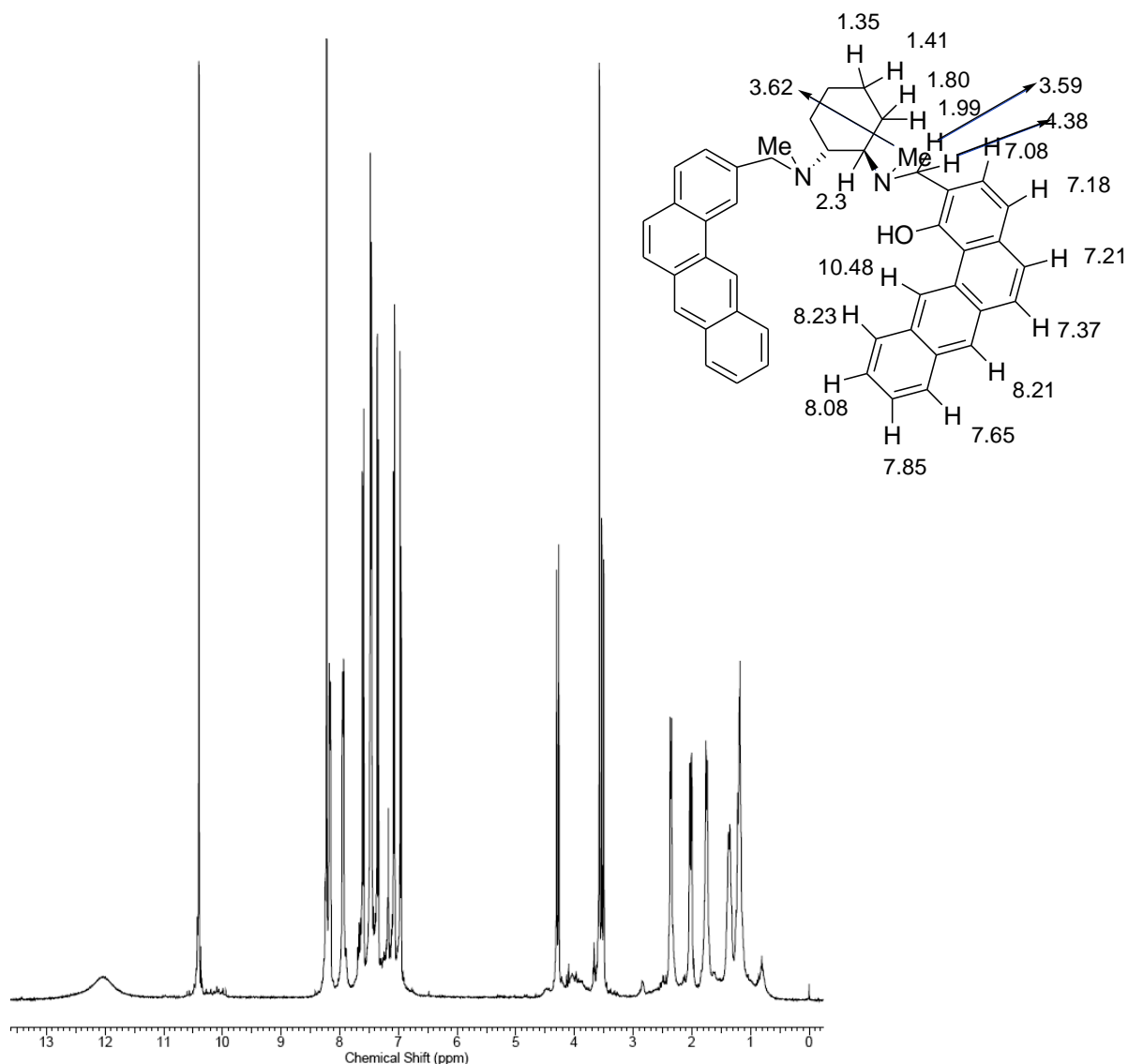


**Figure 2.17.**  $^1\text{H}$  NMR ( $\text{CDCl}_3$ , 400 MHz) peak assignments for **(*R,R*)-8**

The  $^1\text{H}$ - $^1\text{H}$  COSY spectrum is shown in figure 2.18. In comparison to the COSY of **(*R,R*)-6**, in the case of **(*R,R*)-8**, the cyclohexyl backbone of the ligand showed less through bond coupling. However, there is only coupling (in the cyclohexyl backbone) between  $\text{H}^2$ - $\text{H}^3$  protons aligned anti to each other (figure 2.18). There is also a new coupling observed between one of the protons in the methylene group (attached with the nitrogen) with the  $\text{H}^8$  proton in the phenyl ring sidearm (figure 2.18). This coupling was absent for **(*R,R*)-6**. The couplings between the adjacent protons ( $^3J_{\text{HH}}$ ) in the fused phenyl ring side arms are present for ligand **(*R,R*)-8** as well.

A correlation between the few protons from the 1D and 2D NMR spectra for ligand (*R,R*)-**8** is shown in table 2.2.

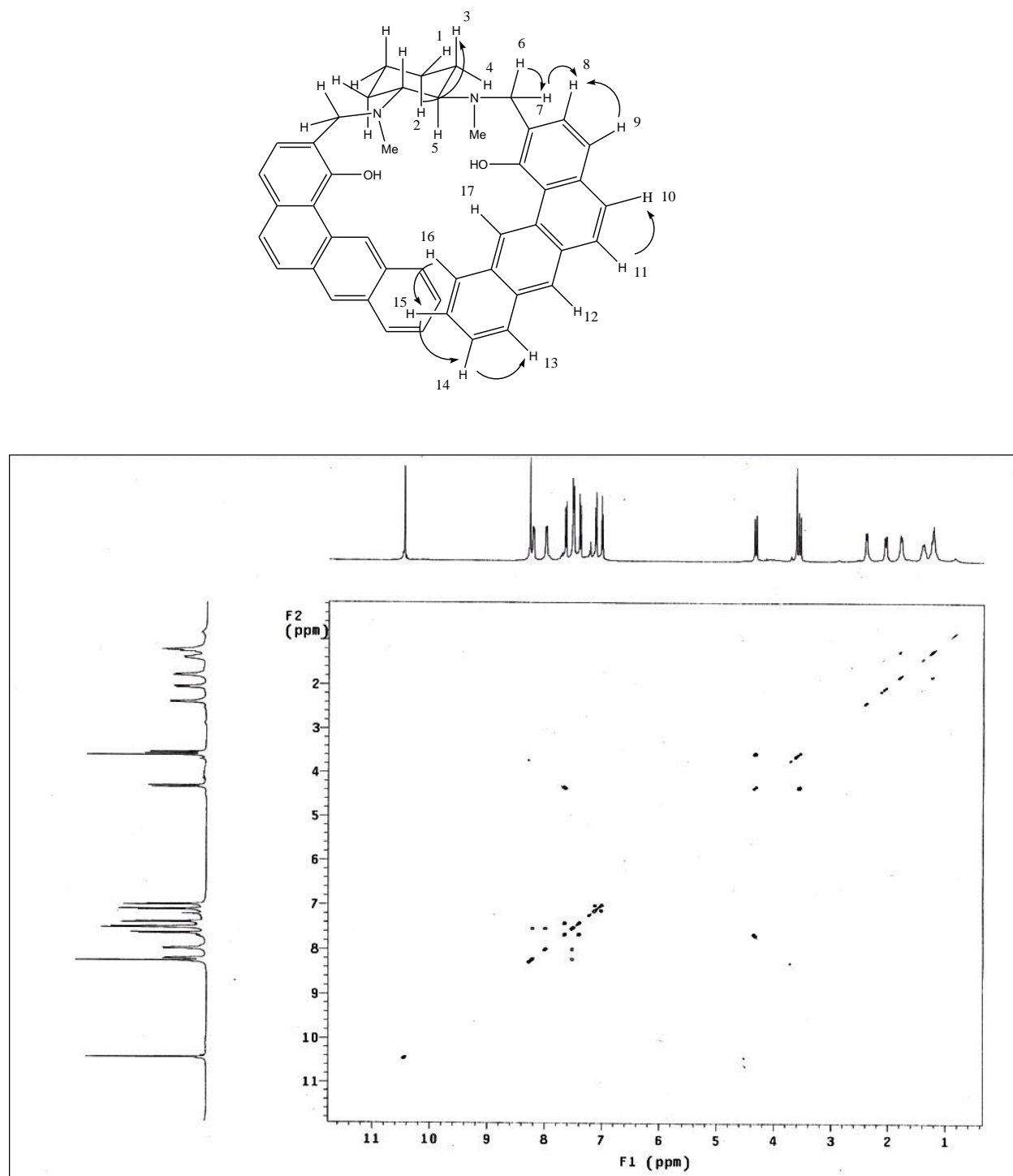


**Figure 2.18.** <sup>1</sup>H-<sup>1</sup>H COSY spectrum for ligand (*R,R*)-**8** (showing at the top).

**Table 2.2.** Correlation between protons in ligand (***R,R***)- **8** from 1D and 2D NMR

Proton number	Chemical shift (ppm) Splitting pattern	Coupling constant ( $^nJ_{HH}$ ) (Hz)
2	1.41 (m)	(n = 3) 6.2
3	1.80 (m)	(n = 3) 6.2
6	3.59 (dd, AB)	(n = 2) 8.2
7	4.38 (dd, AB)	(n = 2) 8.2; (n = 4) 4.8
8	7.08 (dd)	(n = 2) 8.6; (n = 4) 4.8
9	7.18 (d)	(n = 3) 6.8
10	7.21 (d)	(n = 3) 6.6
11	7.37 (d)	(n = 3) 7.0
13	7.65 (d)	(n = 3) 7.0
14	7.85 (m)	(n = 3) 7.2; (n = 3) 7.4
15	8.08 (m)	(n = 3) 7.2; (n = 3) 7.4
16	8.23 (d)	(n = 3) 7.6

Figure 2.19 is showing the through space coupling (NOESY) between the protons in ligand (***R,R***)-**8**. In the cyclohexyl backbone two axial protons and two equatorial protons are coupled with each other. There is coupling between the two singlet protons in the fused phenyl ring side arm ( $H^{12}$  and  $H^{17}$ ). This coupling between protons marked as  $H^{12}$  and  $H^{17}$  is a long range coupling only observed in this kind of fused ring systems. Also, protons  $H^{13}$  and  $H^{15}$  are coupled between each other through space. The NOESY spectrum for this molecule is shown in figure 2.19.

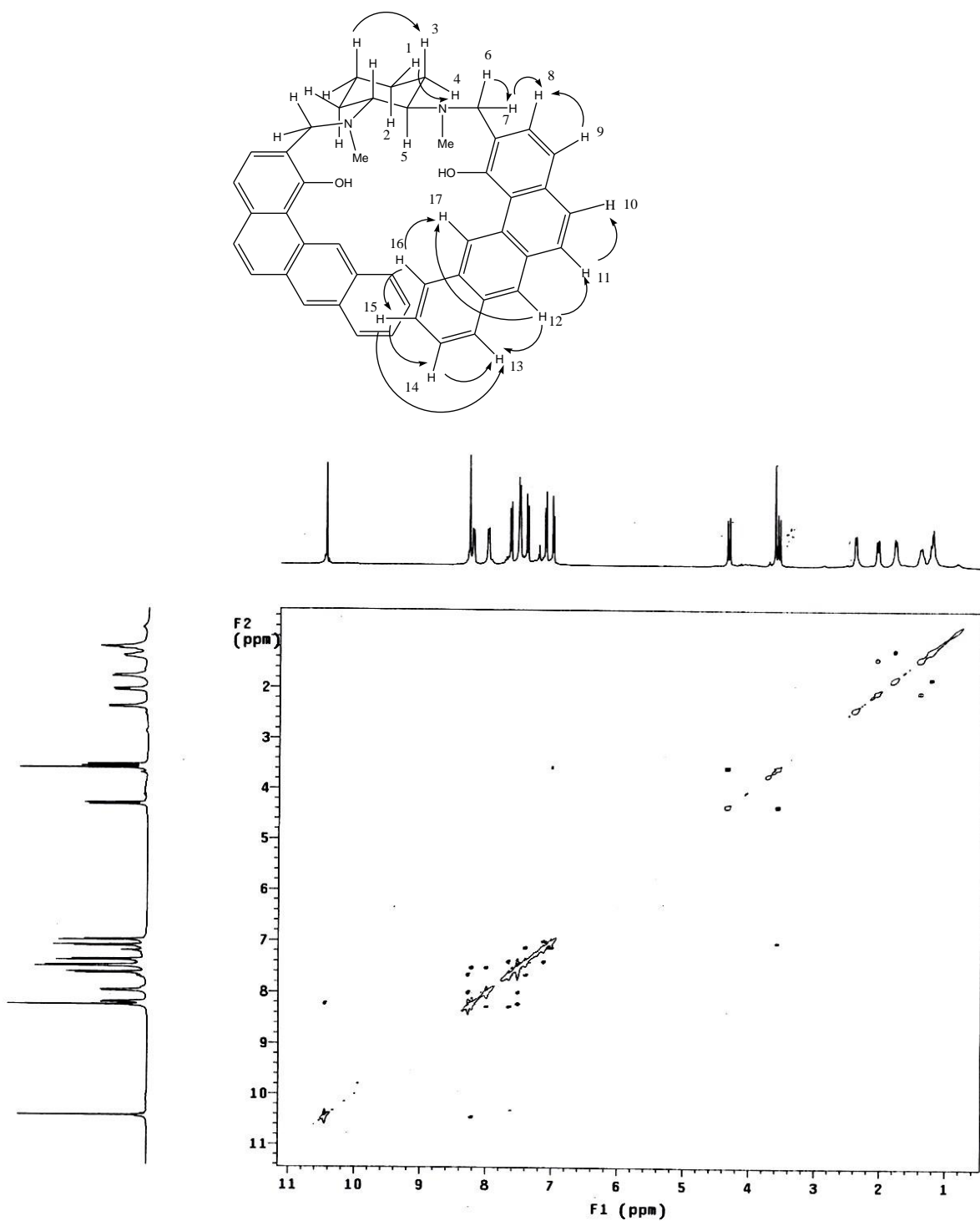


**Figure 2.19.** NOESY spectrum of *(R,R)*-8 (showing at the top).

The proton-carbon HMQC spectrum of the salan ligand for the aromatic region is shown in figure 2.20. The ten carbon atoms attached to protons showed in figure 2.21 are represented in

table 2.3. Two carbon signals at 127.90 and 128.05 are overlapped showing a single mark in the HMQC spectrum.

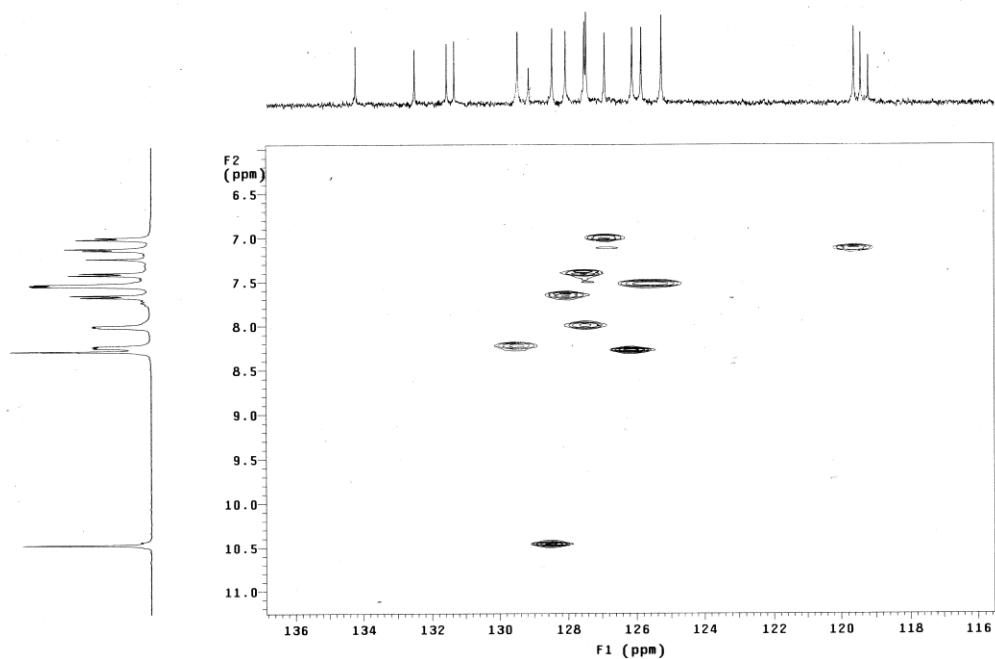


**Figure 2.20.** HMQC spectrum of (*R,R*)-8.

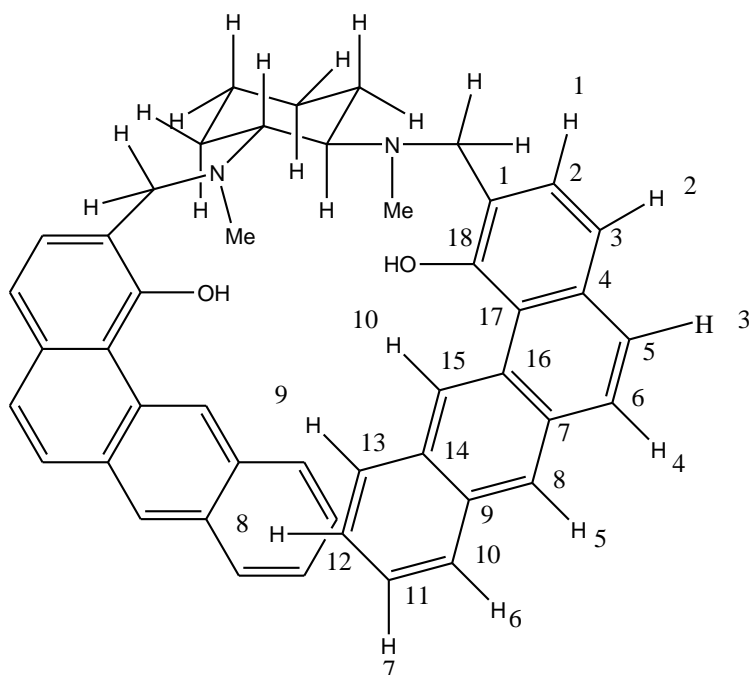


**Figure 2.21.** A correlation between the aromatic carbons and protons numbering for table 2.3.

**Table 2.3.** Correlation between aromatic carbons and protons from HSQC

Carbon number (chemical shift)(ppm)	Proton number (chemical shift)(ppm)
2 (119)	1 (7.08)
3 (125)	2 (7.18)
5 (126)	3 (7.21)
6 (127)	4 (7.37)
8 (128)	5 (8.21)
10 (128)	6 (7.65)
11 (129)	7 (7.85)
12 (130)	8 (8.08)
13 (131)	9 (8.23)
15 (132)	10 (10.48)

### ***2.3.3 Synthesis and characterization of Fe(II)-(R,R)-8 (C1) and Al(III)-(R,R)-8 (C2) complexes***

Complex **C-1** was synthesized in good yield (71%), by dissolving FeCl<sub>2</sub> and sodium methoxide in the ligand solution in CH<sub>2</sub>Cl<sub>2</sub> and EtOH mixture at room temperature (figure 2.22). The greenish brown colored precipitate came out of solution after stirring for 8 hrs. The precipitate was washed with hexane to obtain the pure product.

Complex **C-3** was synthesized by dropwise addition of Et<sub>2</sub>AlCl to a solution of the ligand in toluene at room temperature. An off-white colored precipitate formed after stirring for 6 hrs. The precipitate was washed with hexane to obtain pure **C-3** in good yield (70%).



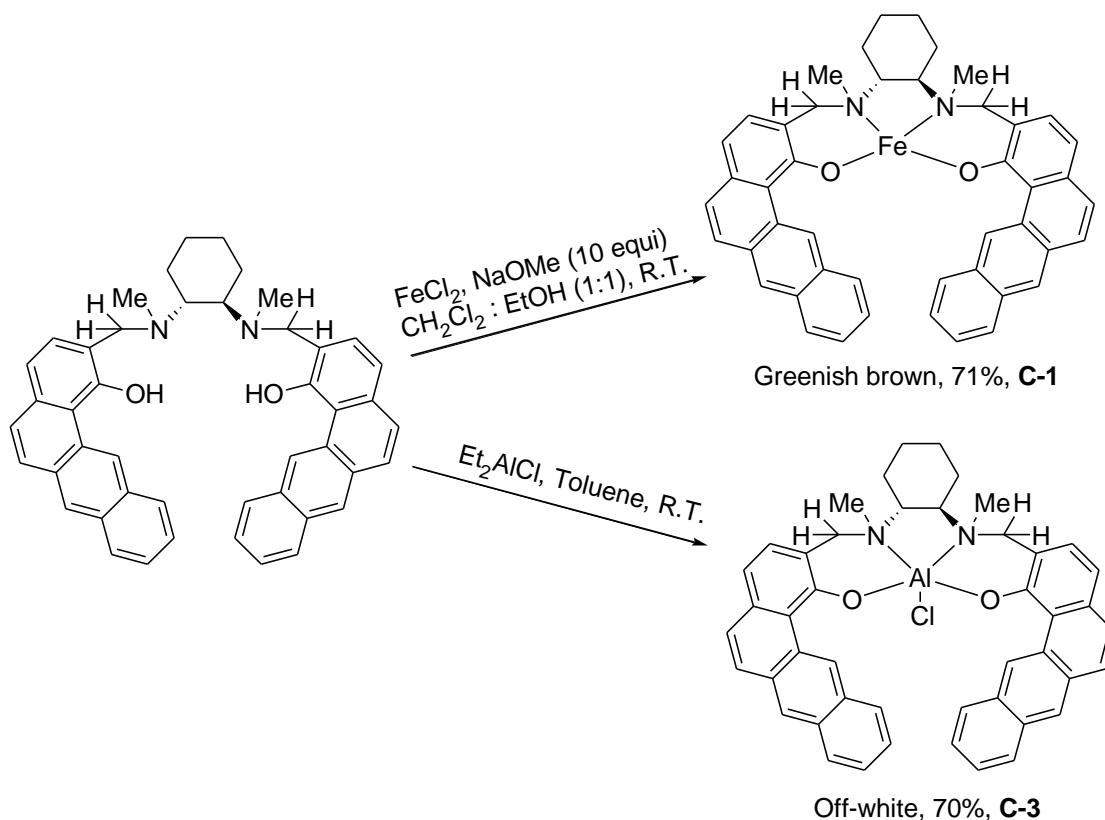


**Figure 2.22.** Synthesis of iron (**C-1**) and aluminum (**C-3**) complexes from (*R,R*)-**8**.

The  $^1\text{H}$  NMR spectrum of the iron salan complex showed few but significant characteristic changes from the pure ligand spectrum. The *N*-Me signal is shifted downfield (by 0.30 ppm) compared to the pure ligand. This indicates that the nitrogen atoms are involved in binding with the metal. The hydroxyl proton peak in the pure ligand disappeared completely after complexation. This is a strong indication that the phenolic oxygens are bound to the metal center. There is also a significant downfield shift (about 1.92 ppm) for the bay protons compared to the pure ligand.

$^1\text{H}$  NMR ( $\text{CDCl}_3$ , 400 MHz) shows the absence of the broad peak for the phenolic hydroxyl proton and there are downfield shifts (by 2.0 ppm) for the bay protons indicating the coordination of aluminum inside the ligand core. The  $^{27}\text{Al}$  NMR spectrum showed a single peak at 172 ppm. The presence of one peak at this region on  $^{27}\text{Al}$  NMR denotes that Al has a single symmetric tetrahedral coordination environment in the complex (figure 2.23).

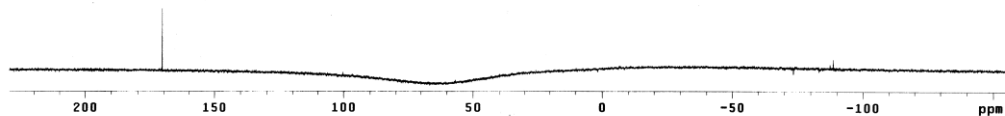


**Figure 2.23.**  $^{27}\text{Al}$  NMR spectrum for complex **C-3**.

The UV and the CD spectra for the complex **C-3** is shown in figure 2.24. The CD spectrum for the complex is distinctly different from the CD spectrum of the pure ligand. The peak at 315 nm in the UV, is due to the  $\pi\text{-}\pi^*$  transition in the side arm of the salan ligand. Also, the broad peak around 400 nm is due to phenolate oxygen to aluminum charge transfer ( $n\rightarrow\pi^*$ ) transitions. The positive CD peak at 330 nm is due to the  $\pi$  conjugation in the ligand sidearm and the peak nature arises due to particular chiral environment (*P* or *M*) of the complex. However, further studies and calculations need to be done to predict the absolute helicity of the salan aluminum complex. The absence of a broad peak around 350-450 nm region in the CD spectrum shows the absence of non-coplanar imine groups. The peaks arise due the presence of benz[a]anthryl sidearms are present in the 300-410 nm region in the CD spectrum of complex **C-3**, however, this region for the salan complexes significantly shifted towards higher wavelength than for the salen complexes. Although, the pattern for the absorption due to the benz[a]anthryl sidearms remain the same with the strongest absorption peak arise at 330 nm.

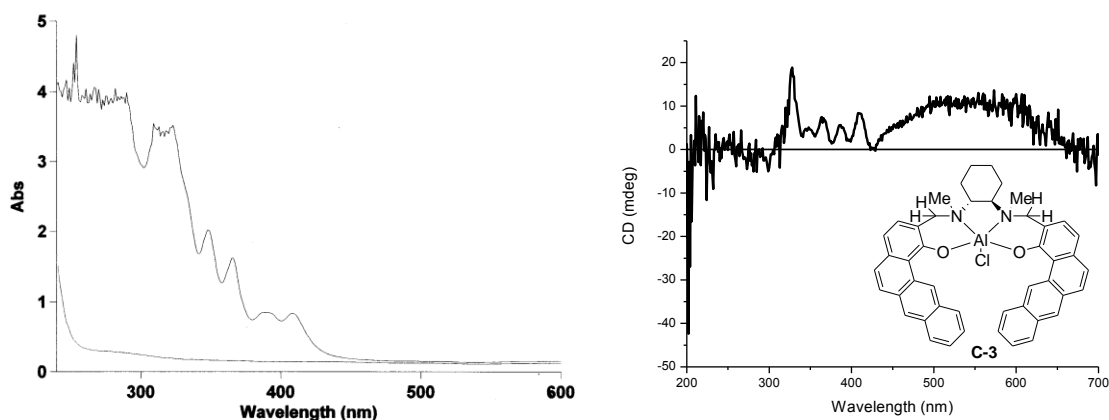


**Figure 2.24.** UV (left) and CD (right) spectra of complex **C-3**.

### 2.3.4 Synthesis and characterization of V(IV)-(R,R)-8 (C-2), V(IV)-(R,R)-7 (C-4) and V(IV) (R,R)-5 (C-5) complexes

All vanadyl salan complexes were synthesized from vanadyl acetylacetonate. In a solution of the ligand in CH<sub>2</sub>Cl<sub>2</sub> and ethanol mixtures were added excess sodium methoxide and vanadyl acetylacetonate. The solution was stirred overnight followed by filtration and then drying under reduced pressure to obtain brown colored precipitate with moderate yield (60-70%) (figure 2.25).

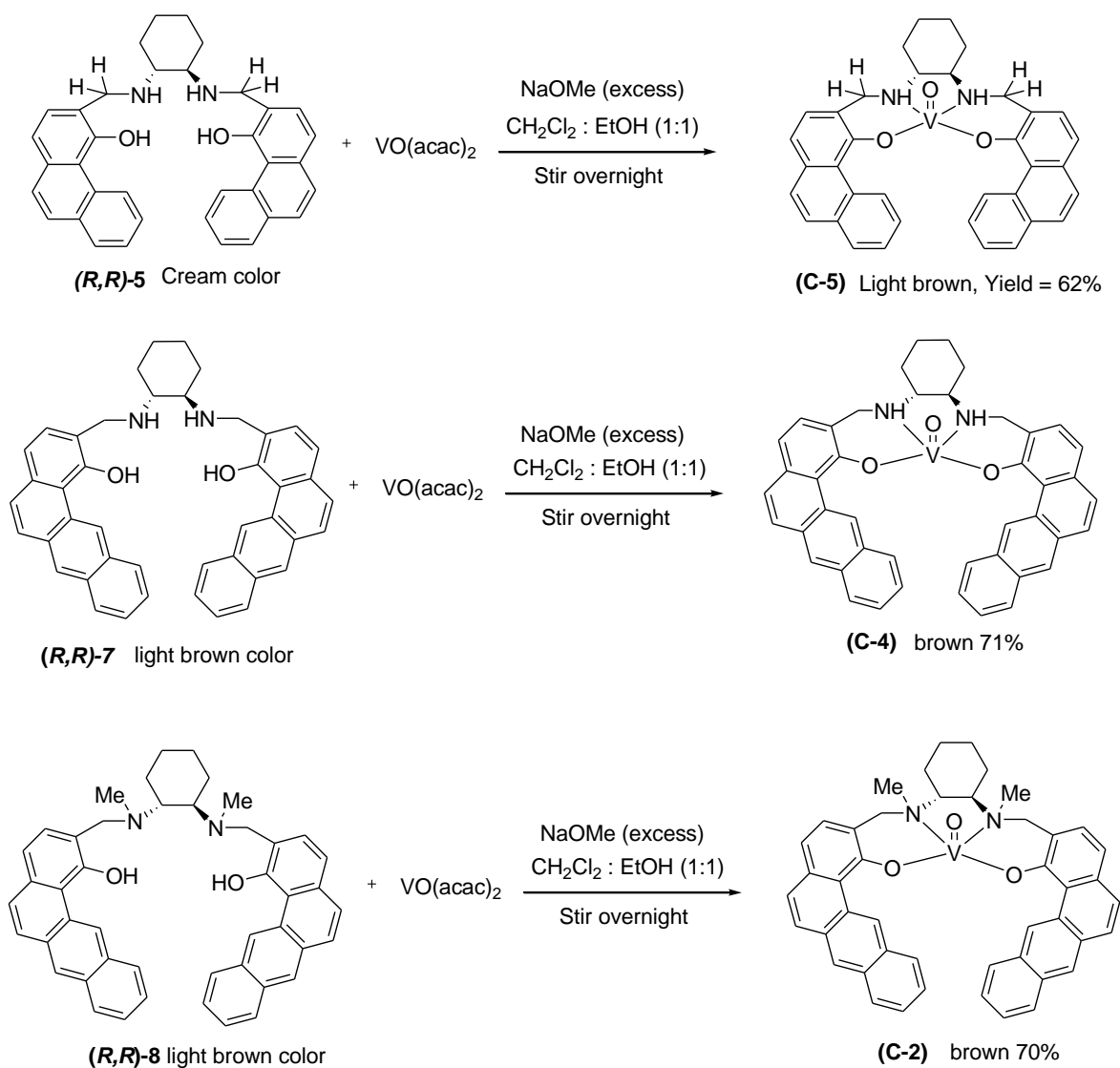


**Figure 2.25.** Synthesis of vanadium(IV) salan complexes.

All these complexes showed very broad difficult to assign  $^1\text{H}$  NMR signals ( $\text{CDCl}_3$ , 400 MHz). This shows the presence of a paramagnetic ( $d^1$ ) metal center. It proved difficult to get crystal structures for these vanadium salan complexes as they decompose rapidly when exposed to air during mounting process. The ESI mass spectrum of the complex **C-2** was taken in  $\text{CH}_2\text{Cl}_2$  solution and it showed the presence of V(V)-salan species in solution with an axially attached chloride satisfying the charge of the vanadium(V)-salan species. A comparison of calculated and observed mass spectral data with the percentage abundance of the octahedral vanadium(V) salan complex is presented in table 2.4. V(IV) is oxidized to V(V) under the conditions of the experiment.

**Table 2.4.** Calculated and experimentally observed mass spectral data for **C-2**

Calculated mass for $(\text{C}_{46}\text{H}_{40}\text{N}_2\text{O}_3\text{V}_1\text{Cl}_1)^{+1}$	Observed mass for $(\text{C}_{46}\text{H}_{40}\text{N}_2\text{O}_3\text{V}_1\text{Cl}_1)^{+1}$
755.976 (100%)	755.974 (45%)
756.974 (52%)	756.978 (26%)
757.979 (16%)	757.982 (8%)
758.980 (4%)	758.986 (2%)

Complex **C-4** showed characteristics IR stretches for V=O at  $829\text{ cm}^{-1}$  and for N-H at  $3400\text{ cm}^{-1}$ . The molecular ion peak was observed in the ESI mass spectrum for complex **C-4**. The molecular ion peak showed the presence of V(IV)-salan species in the complex. A comparison of the calculated and observed mass spectral data with the percentage abundance of the square pyramidal vanadium(IV) salan complex is presented in table 2.5.

**Table 2.5.** Calculated and experimentally observed mass spectral data for **C-4**

Calculated mass for $(\text{C}_{44}\text{H}_{34}\text{N}_2\text{O}_3\text{V}_1)^{+1}$	Observed mass for $(\text{C}_{44}\text{H}_{34}\text{N}_2\text{O}_3\text{V}_1)^{+1}$
691.056 (100%)	691.058 (100%)
692.059 (62%)	692.062 (62%)
693.064 (14%)	693.062 (14%)
694.067 (2%)	694.068 (2%)

The CD spectrum of the complex **C-4** was recorded in THF with a concentration of  $1 \times 10^{-5}$  M. The CD spectrum of a model zinc(II) salen complex was previously calculated in our group (figure 2.27). Salan ligands are more flexible than the salen ligand and due to this flexibility, they often adopt  $\beta$ -*cis* geometry. Also, due to the presence of the extended fused phenyl ring side arm and rigid backbone, these ligand molecules prefer to form *P* helix after complexation with vanadium(IV) in a distorted square planar geometry. This observation is clear after comparing the simulated CD spectrum of the zinc salen complex (figure 2.27) with the CD spectrum of vanadium salan complex (figure 2.28).<sup>19</sup> The sharp strongest negative absorption peak at 280 nm and another negative peak at 335 nm with two short positive absorption peaks at 375 and 385 nm are the marker peaks to assign the *P* helical conformation to the vanadyl salan complex. The pattern for the CD absorption peaks for the *M* helix would be exactly the mirror image of the absorption peaks for *P* helix. Due to the presence of an imine group in the salen ligand, there are UV/CD absorptions around 450 nm. This broad peak is absent in case of salan ligand. However, the peak pattern of the vanadium(IV) salan matches quite well with the simulated *P* isomer of the zinc salen complex. Henceforth, we can reasonably conclude that the vanadium(IV) salan complexes exist in *P* helical conformations in solution. In solution vanadyl salan complexes exist in the *P* helical conformation and this conformation can be seen as the thermodynamically stable locked conformation in solution (figure 2.26).

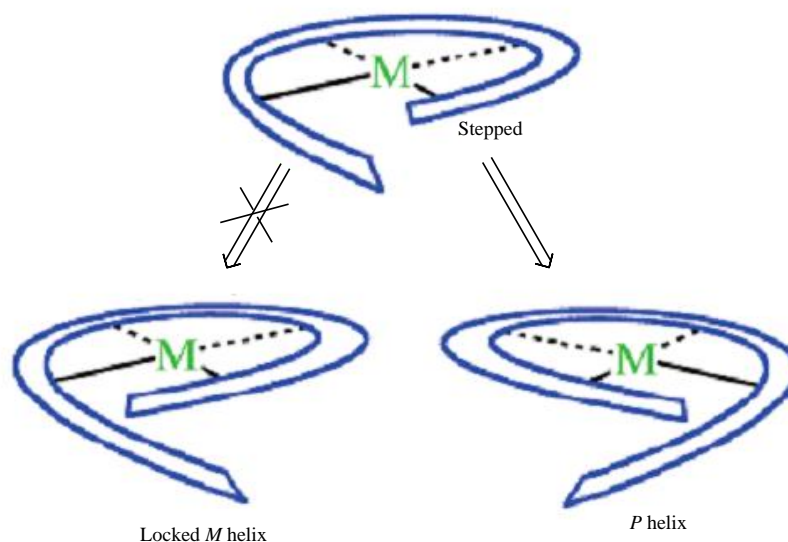


**Figure 2.26.** Two possible conformations of a helix (*M* and *P*).

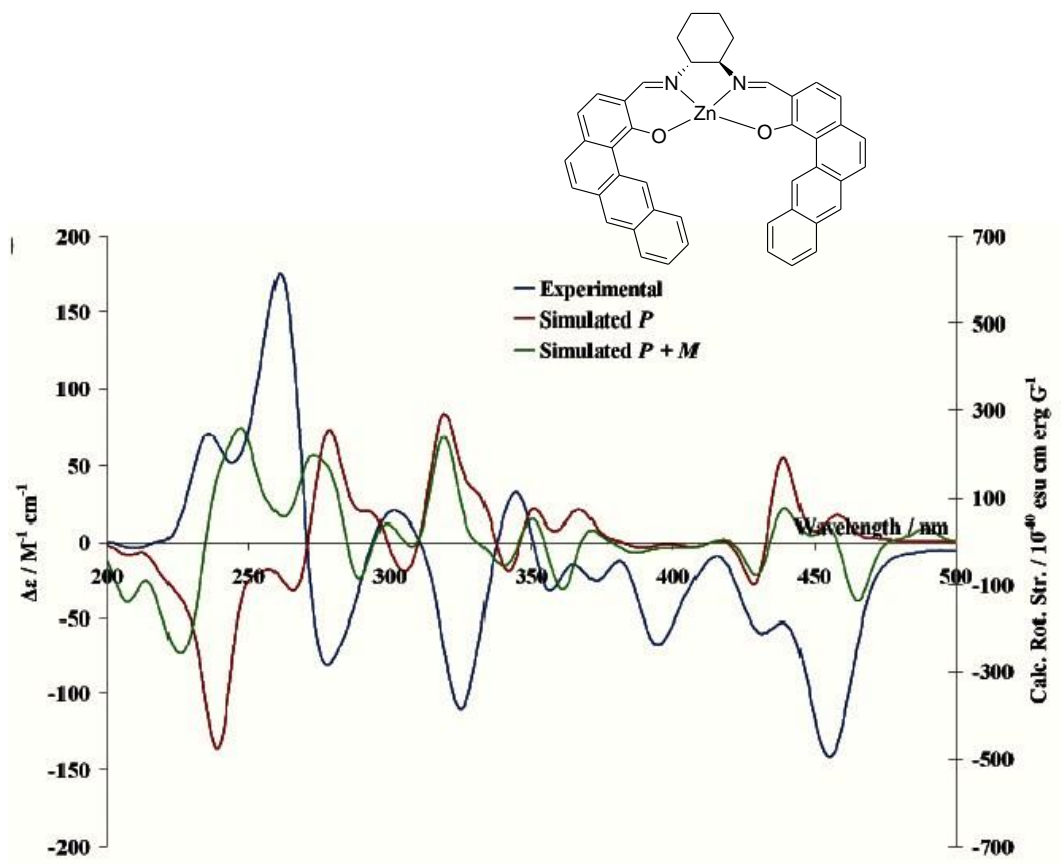


Figure 2.27. Model Zn-salen complex with *M* conformation.

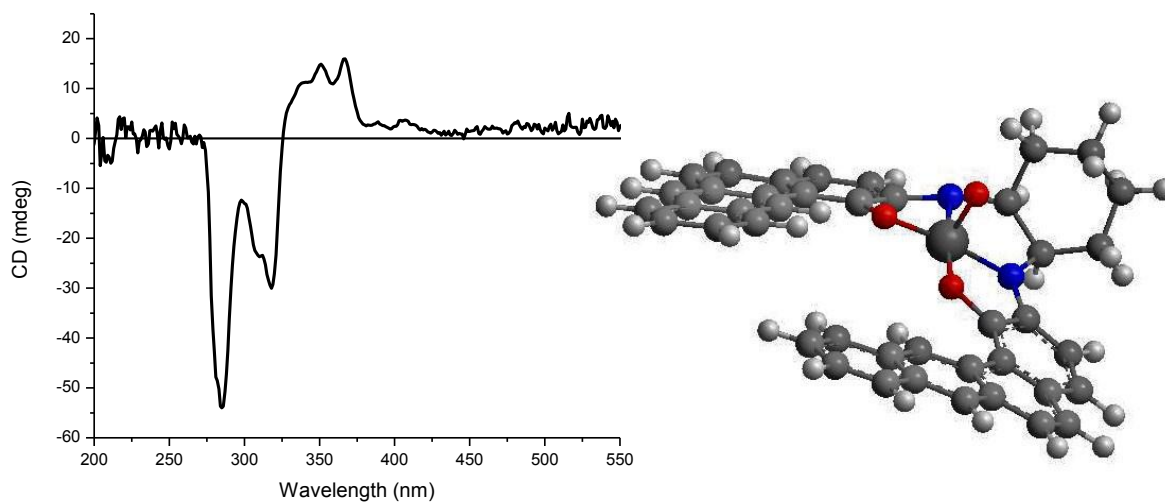
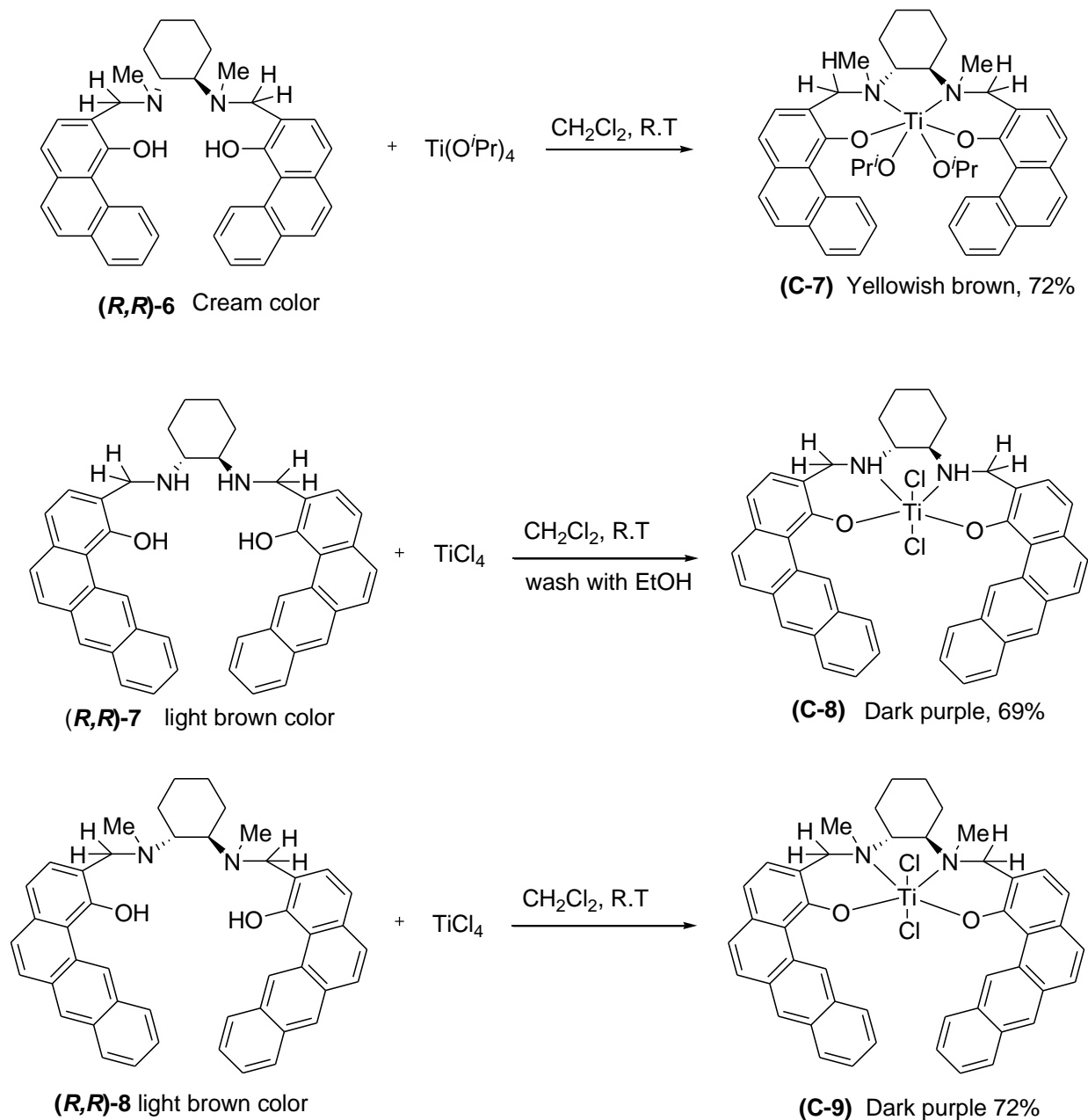


Figure 2.28. Vanadium(IV) salen complex (C-4) with *P* conformation.





**Figure 2.29.** Synthesis schemes of complexes **C-6**, **C-7**, **C-8** and **C-9**.

The aromatic region of the  $^1\text{H}$  NMR ( $\text{CDCl}_3$ , 400 MHz) spectrum with peak assignment, for **C-6**, is shown in figure 2.30. It is clear that there are two sets of peaks of similar splitting pattern with an intensity ratio 2:1. Due to the flexibility of the salen ligands to adopt different geometries than the salen ligands, it is possible that the molecule has adopted a  $\beta$ -*cis* geometry and two isomers  $\Delta$  and  $\Lambda$  exist with an intensity ratio of 2:1 (figure 2.31).



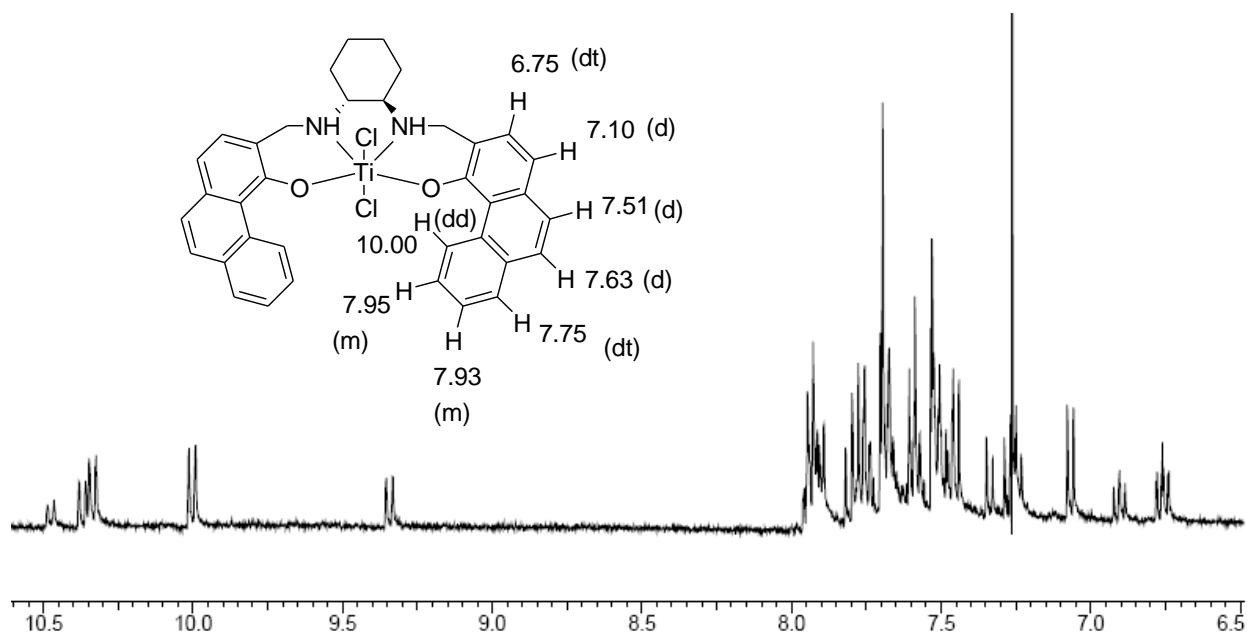


**Figure 2.30.** <sup>1</sup>H NMR (CDCl<sub>3</sub>, 400 MHz) spectrum of C-6.

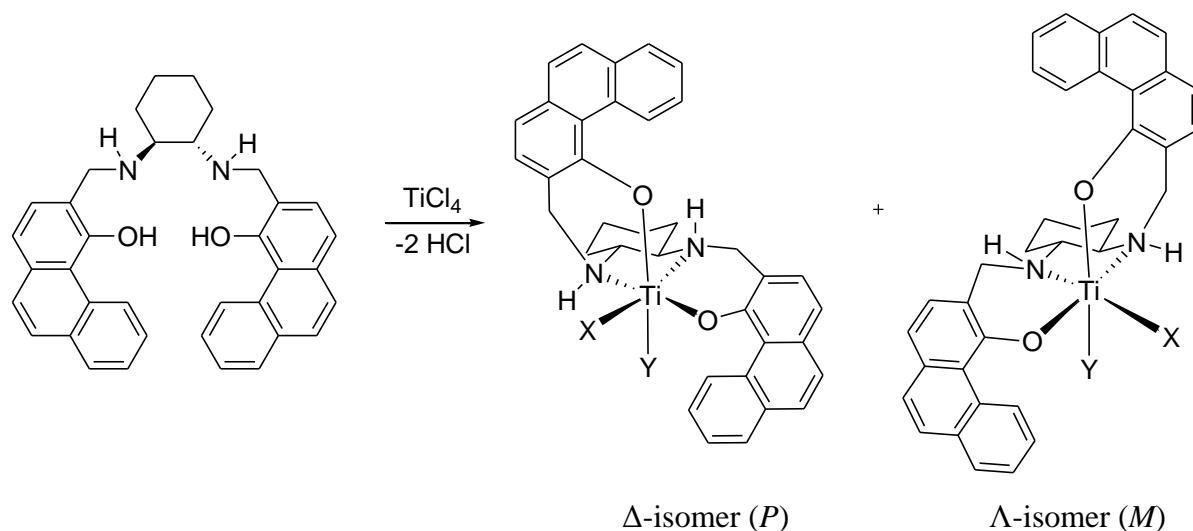


**Figure 2.31.** Δ and Λ isomers of complex C-6.

The CD spectrum of the complex (C-6) was recorded in THF ( $1 \times 10^{-5}$  M) (figure 2.33). The CD spectrum of the complex was compared to the CD spectrum of the model zinc salen complex (figure 2.32).<sup>19</sup> Figure 2.32 is showing the CD spectral pattern of the experimentally obtained, simulated pattern for the *P* conformer and simulated pattern for the 1:1 mixture of the *P* and *M* conformers. A closer look can show the differences between the metal salen complex

with a metal salan complex. The absence of a broad peak around 400 nm in the titanium salan complex is attributed to the absence of imine bond in this complex. Apart from the difference in geometry of the two complexes and the presence of imine bond in the zinc complex, the simulated  $M+P$  conformer's CD spectrum matches quite well with the CD spectrum of the octahedral Ti-salan complex (figure 2.33) and this proves the existence of both  $\Delta$  and  $\Lambda$  isomers in the solution for the titanium salan complexes. The positive cotton effect peaks at 250 nm, 275-300 nm and at 310 nm are characteristics of a  $P+M$  conformation. The sharp negative CD peak at 237 nm for the titanium salan complex is attributed to the main absorption peak from the phenanthryl sidearms. This peak at 237 nm is purely ligand based as the same peak was observed in free ligand as well.

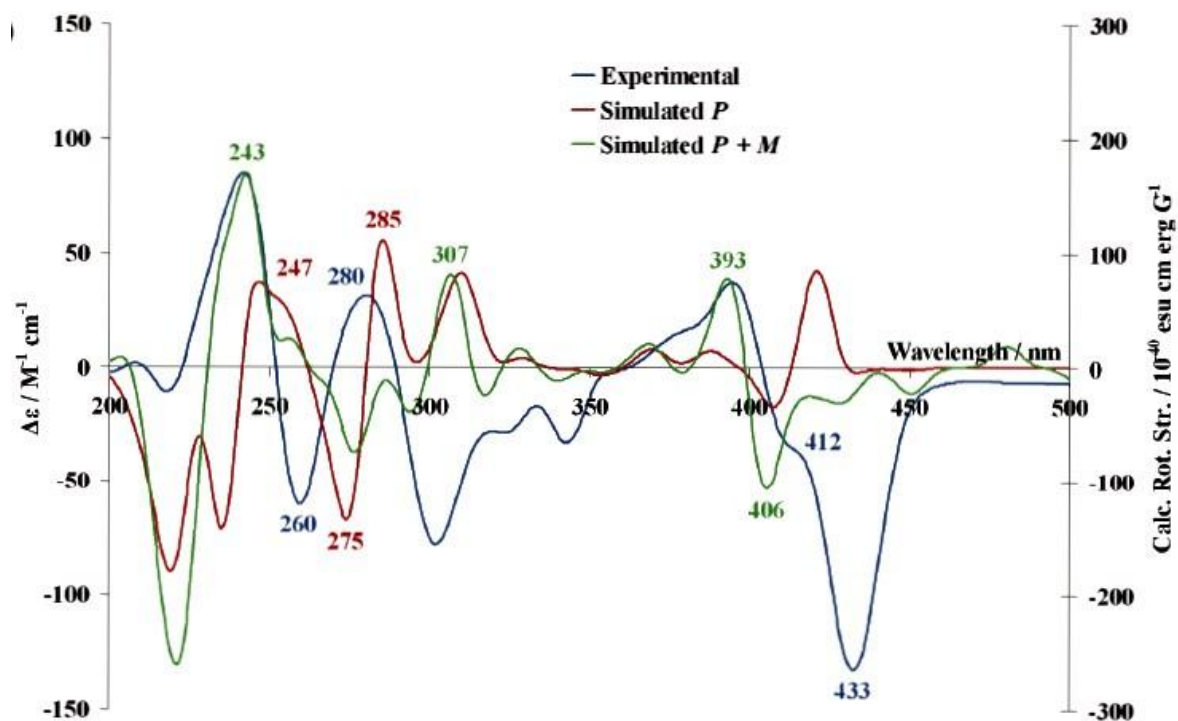
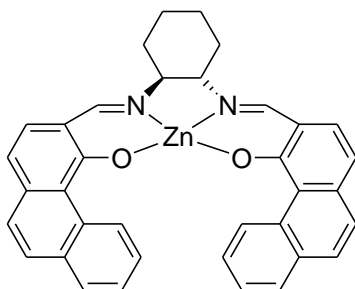


**Figure 2.32.** Experimental and simulated CD spectrum of  $P$  and  $P+M$  conformations.

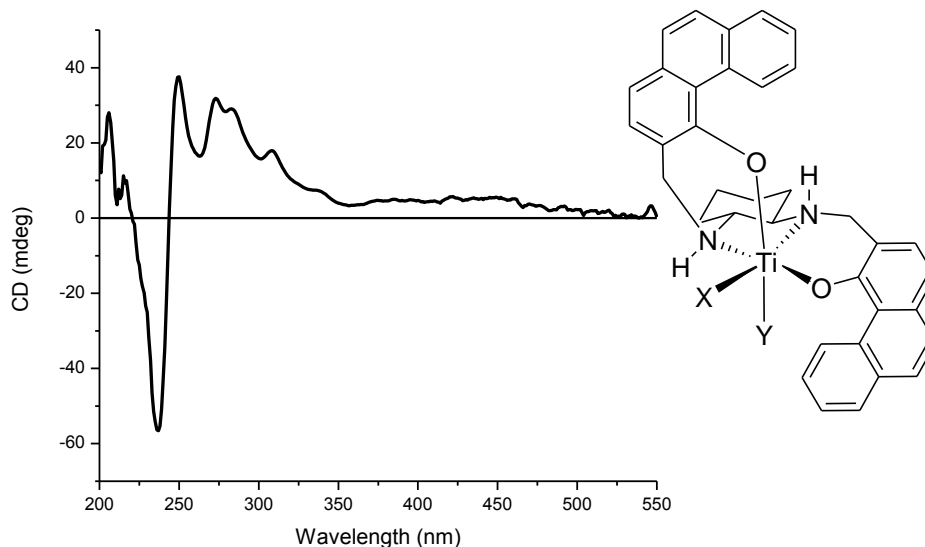


**Figure 2.33.** CD spectrum of the titanium(IV) salan complex (**C-6**) in *P* conformation in THF.

The COSY and NOESY spectra for complex **C-6** are shown in figure 2.34 and 2.35. Also table 2.7 is showing the chemical shifts and coupling constants for the aromatic protons in the sidearms. One interesting observation is the occurrence of broadening of  $^1\text{H}$  NMR peaks with time. After dissolving the compound in NMR solvent, first we did COSY experiment and then NOESY. During the long experiment time for NOESY, we can see the relatively sharp peaks which we obtained in COSY, got broader in NOESY. Eventually we observe slight through space  $^1\text{H}$ - $^1\text{H}$  couplings in NOESY after intensifying the spectrum window. This suggests that there is a rapid interconversion between the different isomers of the complex which is no longer recognizable in the NMR time scale.

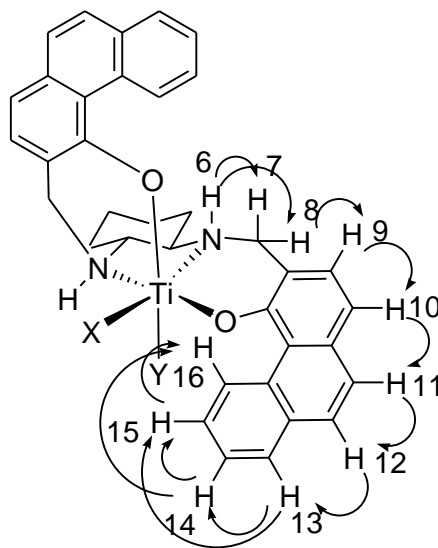
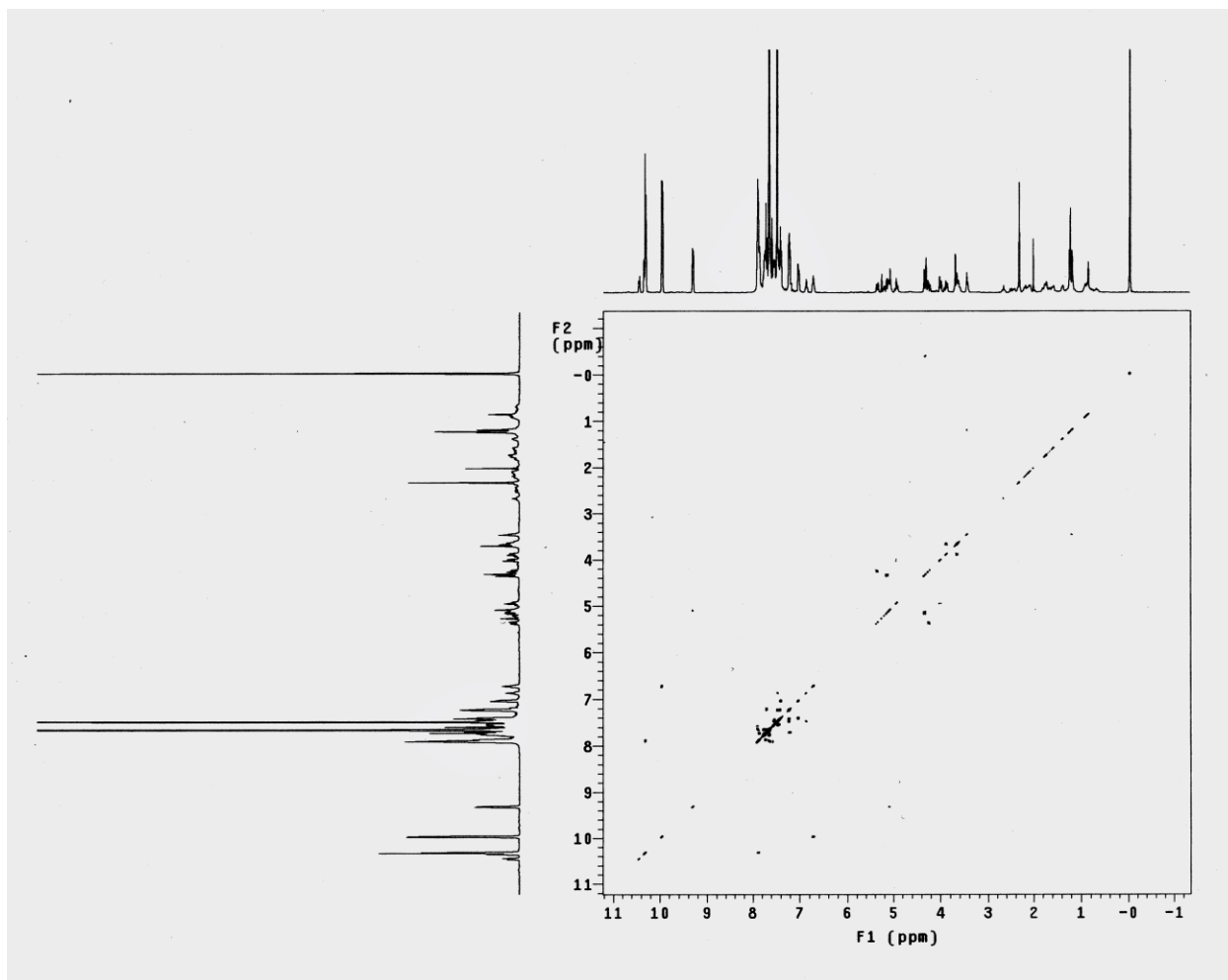


**Figure 2.34.**  $^1\text{H}$ - $^1\text{H}$  COSY spectrum of C-6 (couplings are shown above).

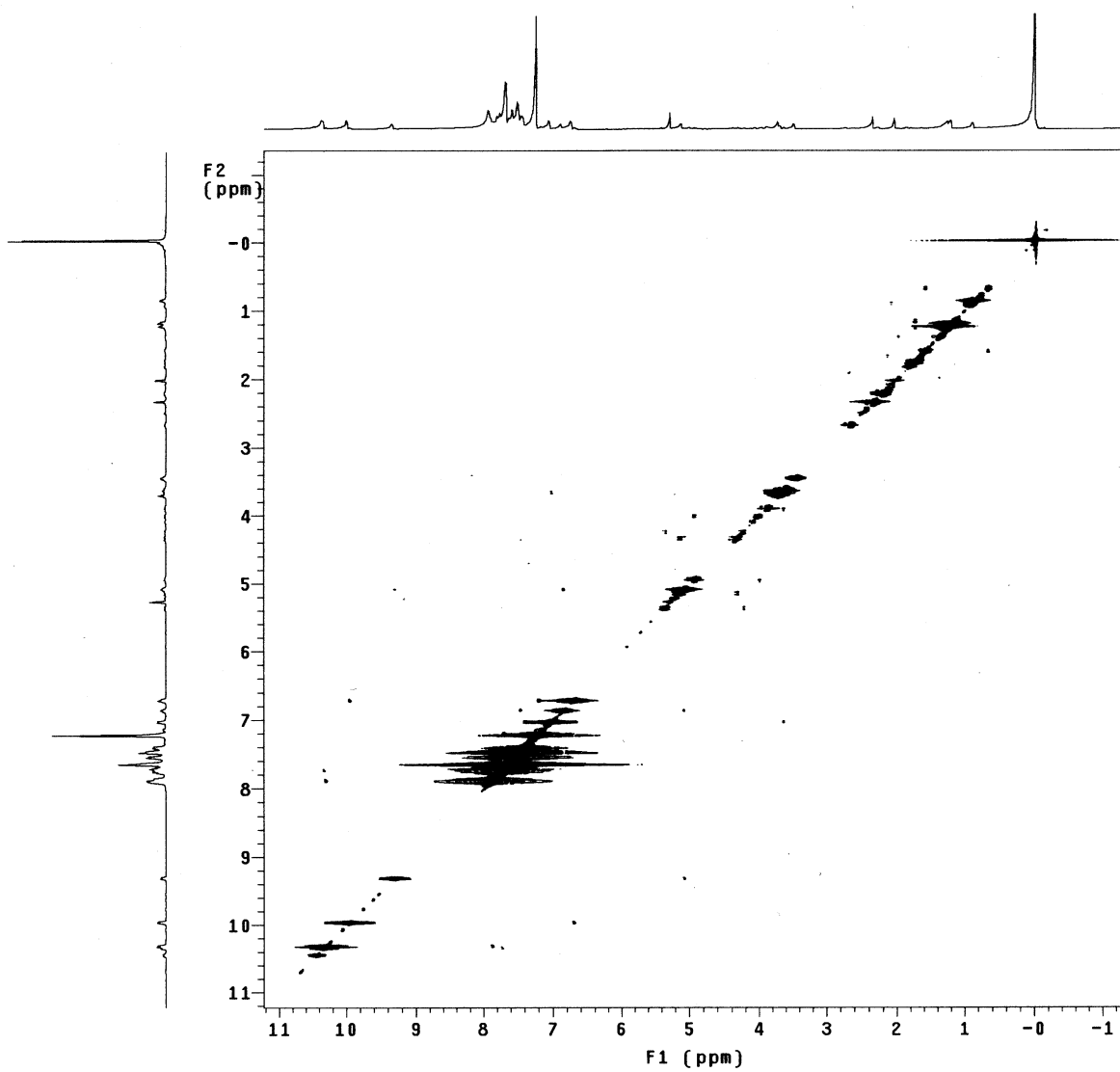


Figure 2.35.  $^1\text{H}$ - $^1\text{H}$  NOESY spectrum for complex C-6.

**Table 2.7.**  $^1\text{H}$ - $^1\text{H}$  NMR correlation between the aromatic protons in **C-6** shown in figure 2.34

Proton numbers	Chemical shifts (ppm) (Splitting pattern)	Coupling constant ( $^nJ_{\text{HH}}$ ) (Hz)
6	5.2 (m)	n = 3, 6.6 (with 7); and 6.8 (with 8)
7	3.45 (m)	n = 3, 6.2; n = 2, 8.4
8	4.16 (m)	n = 3, 6.8; n = 2, 8.8
9	7.25 (m)	n = 3, 6.4; n = 4, 4.8
10	7.30 (m)	n = 3, 6.4; n = 4, 5.2
11	7.50 (m)	n = 3, 6.6; n = 4, 4.6
12	7.51 (m)	n = 3, 6.6; n = 4, 4.8
13	7.61 (m)	n = 3, 6.8; n = 4, 5.2
14	7.75 (m)	n = 3, 6.6; n = 4, 5.0
15	9.8 (m)	n = 3, 6.6; n = 4, 5.2
16	10.2 (m)	n = 3, 6.6; n = 4, 4.8

Complex **C-7** gave comparatively broad  $^1\text{H}$  as well as  $^{13}\text{C}$  NMR spectra in  $\text{CDCl}_3$ . However, we can still clearly assign the peaks in the NMR. The broad nature of the spectrum believed to be due to fast isomerization between  $\Delta$  and  $\Lambda$  geometry, which is a common occurrence for the Ti-salan complexes.  $^1\text{H}$  NMR and mass spectrum of the molecule supports the presence of isopropoxide group in the molecular structure.

Complex **C-8** gave broad  $^1\text{H}$  and  $^{13}\text{C}$  NMR spectra in DMSO. However, we can still clearly assign the peaks in the NMR. Again, the broad nature is believed to be due to fast isomerization between  $\Delta$  and  $\Lambda$  isomers in  $\beta$ -*cis* geometry. High resolution mass spectrum showed the presence of molecular ion peak with the correct isotopic pattern. The mass spectral isotopic patterns for the calculated and observed peaks are given in table 2.8.

**Table 2.8.** Comparison between calculated and observed mass spectral data for **C-8**

Calculated mass for (C <sub>46</sub> H <sub>41</sub> N <sub>2</sub> O <sub>3</sub> Ti <sub>1</sub> ) <sup>+1</sup>	Observed mass for (C <sub>46</sub> H <sub>41</sub> N <sub>2</sub> O <sub>3</sub> Ti <sub>1</sub> ) <sup>+1</sup>
715.2568 (14%)	715.2570 (6%)
716.2571 (19%)	716.2572 (8%)
717.2575 (100%)	717.2574 (40%)
718.2620 (50%)	718.2618 (20%)
719.2621 (22%)	719.2618 (9%)
720.2653 (7%)	720.2649 (3%)

Complex **C-9** gave broad <sup>1</sup>H and <sup>13</sup>C NMR spectra in CDCl<sub>3</sub>. Again, the broad nature is believed to be due to fast isomerization between Δ and Λ isomers in β-*cis* geometry. Observed and simulated molecular ion peaks with the isotopic patterns are presented in table 2.9.

**Table 2.9** Comparison between calculated and observed mass spectral data for **C-9**

Calculated mass for (C <sub>47</sub> H <sub>43</sub> N <sub>2</sub> O <sub>3</sub> Ti <sub>1</sub> ) <sup>+1</sup>	Observed mass for (C <sub>47</sub> H <sub>43</sub> N <sub>2</sub> O <sub>3</sub> Ti <sub>1</sub> ) <sup>+1</sup>
729.2750 (14%)	729.2753 (8%)
730.2814 (19%)	730.2815 (12%)
731.2678 (100%)	731.2681 (57%)
732.2724 (55%)	732.2726 (33%)
733.2730 (25%)	733.2728 (14%)
734.2733 (6%)	734.2730 (4%)

### 2.3.6 Sulfoxidation by Al, Fe, V and Ti-salan complexes

The potential of the vanadium, aluminum, iron and titanium salan complexes as enantioselective catalysts were tested in the asymmetric oxidation with H<sub>2</sub>O<sub>2</sub> of a simple model compound, thioanisole. The reactions were carried out in CH<sub>2</sub>Cl<sub>2</sub> since with acetonitrile the stereoselectivity was much lower (maximum ee reached was 8 %). Cumene hydroperoxide (CHP) or hydrogen peroxide was used as the source of oxygen. In all the cases the products were

either *R*-methyl phenyl sulfoxide, or the sulfones resulting from the oxidation of sulfoxides. All additions of reagents were done at 0 °C. The reactions were done for 30 hrs under nitrogen in order to estimate the activity of each catalyst in terms of conversions. Control reactions were made to test the noncatalytic oxidation of thioanisole by H<sub>2</sub>O<sub>2</sub> in the absence of a catalyst. The change in reaction temperature from 20 °C to 0 °C increases the stereoselectivity to a small extent (figure 2.36). This phenomenon was tested with catalyst **C-8**. When the oxidation was carried out at 0 °C, 39 % ee in the phenylmethyl sulfoxide was obtained. However, when the same reaction was carried out at 20 °C, 36.5% ee was obtained. Temperature has only a slight effect in changing the ee of the product and the catalyst was almost equally active at 20 °C as well.

However, time has a significant influence on the conversions (figure 2.37). In this figure, comparisons of all the catalysts were done with respect to conversions over time, using H<sub>2</sub>O<sub>2</sub> as the oxidant. It is observed that, for the iron salan complex (**C-1**), the maximum conversions (88%) were attained at 22 hrs and the catalyst activities do not change as time progresses after 22 hrs. For the aluminum salan catalyst (**C-3**) maximum conversion (82%) was attained in 24 hours with no change in catalytic activity to 30 hours. It was observed that when the reaction was carried out for 16 hrs, the conversions reached the highest and remained almost constant for next few hours for vanadium salan (**C-2**, **C-4** and **C-5**) catalysts. The vanadium salan catalyst with N-H groups (**C-5**), shows better activity than with N-methyl group vanadium salan systems (**C-2** and **C-4**). Among the N-methyl vanadium salan complexes (**C-2** and **C-4**), **C-2** with bigger extended side arms (benz[a]anthryl), showed less activity than **C-4**. This may be due to the steric effect created by the benz[a]anthryl side arms hinders the approach of the sulfide to the metal center. Vanadium based catalytic systems showed lower activity than the aluminum, iron or titanium analogues. However, the activity of the titanium salan complexes decreased after 16 hours. This can be explained by the formation of the oxo-bridged titanium salan dimeric species, which does not show any catalytic activity due to the unavailability of any vacant coordination site (figure 2.42).<sup>11</sup>Titanium based catalysts, **C-7** and **C-9** showed very high initial rate of conversions compared to the other catalysts. Under the current reaction conditions iron, titanium and aluminum based catalysts systems are most effective in terms of conversions. The loss of activity for the iron, aluminum and vanadium salan catalysts after reaching the maximum activity might be due to the decomposition of the catalysts in the presence of excess oxidant and water.



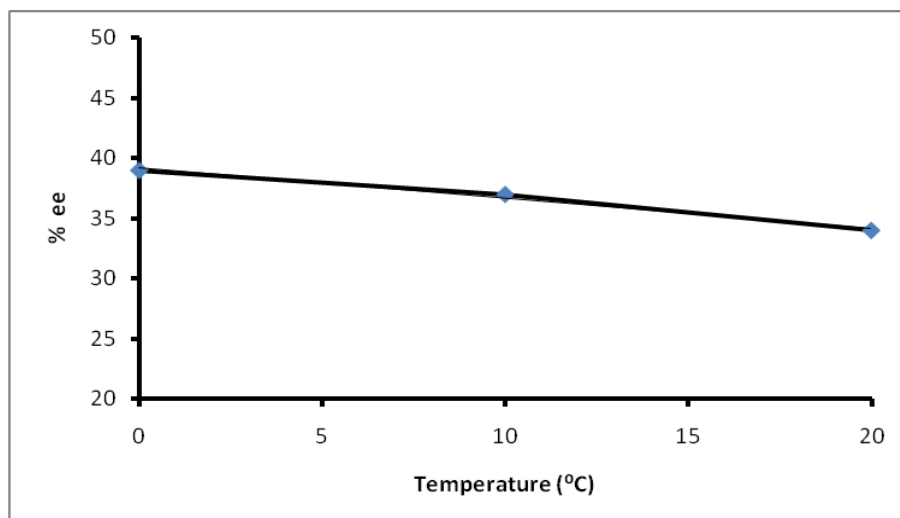


**Figure 2.36.** Effect of temperature on % ee of the product, tested with catalyst C-8.

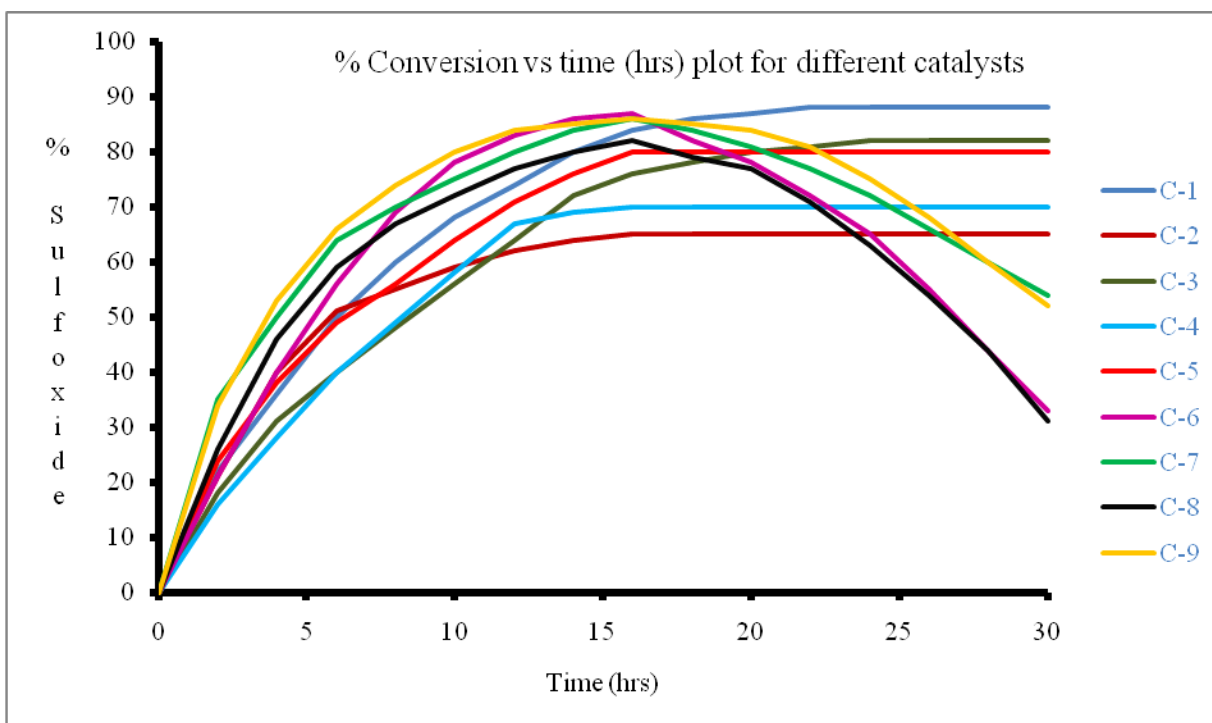


**Figure 2.37.** Effect of time on % conversions by different catalysts.

The sulfoxidation results with all the catalysts were presented in table 2.10. Titanium, iron and aluminum catalysts produced (*R*) phenylmethylsulfoxide as the major product whereas vanadium salan catalysts produced (*S*) phenylmethylsulfoxide as the product. In the previous chapter we observed that the vanadium salen complexes with *M* helical conformations produced

the *R* isomer as the major product. From this fact, it is understandable that the vanadium(IV) salan complexes having *P* helical conformations can produce (*S*) phenylmethylsulfoxide as the major isomer. However, further studies need to be carried out to understand the mechanism of formation of *S* isomers with the vanadium(IV) salan catalysts. In terms of ee of the product, all the catalysts showed better activity when H<sub>2</sub>O<sub>2</sub> was used as the oxidant whereas all the catalysts showed better activity in terms of conversions when CHP was used as the oxidant. Overall, titanium based catalysts showed good activity towards conversions. The iron salan catalyst **C-1** showed better product selectivity when CHP was used as the oxidant and comparable ee of the product in both CHP and in H<sub>2</sub>O<sub>2</sub>. The iron salan catalyst showed poor ee compared to other metal salan catalysts. Further investigations need to be done in order to find out the reason for poor ee in the product when the reaction was catalyzed by iron-salan complex. The aluminum salan catalyst **C-3** showed good product selectivity as well as acceptable ee in CH<sub>2</sub>Cl<sub>2</sub> using H<sub>2</sub>O<sub>2</sub> as the oxidant. Katsuki et. al proposed, aluminum, being a trivalent metal, tends to form *cis-β* structure would be better catalyst for oxidation with aqueous hydrogen peroxide, because the hydroperoxide species with a neutral aqua ligand should be easily transformed into an η<sup>2</sup>-coordinated hydroperoxo species, and the participation of a monodentate hydroperoxide species should be significantly decreased (figure 2.38).<sup>12</sup> Vanadium complex with N-methyl salan ligand (**C-2**) are less active in terms of asymmetric induction than the complexes with N-H group (**C-4** and **C-5**).

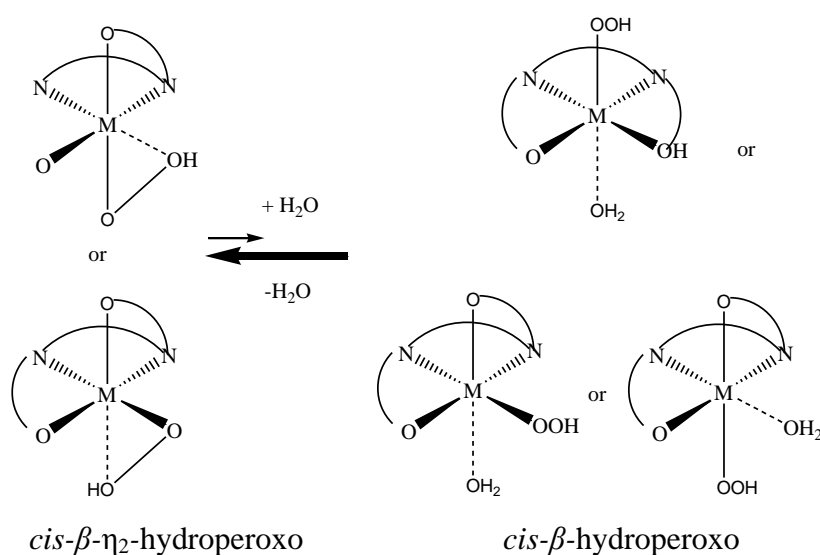


**Figure 2.38.** Working hypothesis for an effective catalyst for oxidation with aqueous H<sub>2</sub>O<sub>2</sub>.<sup>23</sup>

**Table 2.10.** Sulfoxidation results by different catalysts

Catalyst	oxidant	solvent	Temp (°C)	Time (hr)	Sulfoxide (%)	Sulfone (%)	Sulfide (%)	ee (%)	Main isomer
<b>C-1</b>	H <sub>2</sub> O <sub>2</sub>	CH <sub>2</sub> Cl <sub>2</sub>	0	16	64	24	12	14	<i>R</i>
<b>C-1</b>	CHP	CH <sub>2</sub> Cl <sub>2</sub>	0	16	71	22	7	9	<i>R</i>
<b>C-2</b>	H <sub>2</sub> O <sub>2</sub>	CH <sub>2</sub> Cl <sub>2</sub>	0	16	59	6	35	33	<i>S</i>
<b>C-2</b>	CHP	CH <sub>2</sub> Cl <sub>2</sub>	0	16	70	8	22	18	<i>S</i>
<b>C-3</b>	H <sub>2</sub> O <sub>2</sub>	CH <sub>2</sub> Cl <sub>2</sub>	0	16	73	9	18	35	<i>R</i>
<b>C-3</b>	CHP	CH <sub>2</sub> Cl <sub>2</sub>	0	16	79	11	10	23	<i>R</i>
<b>C-4</b>	H <sub>2</sub> O <sub>2</sub>	CH <sub>2</sub> Cl <sub>2</sub>	0	16	64	6	30	38	<i>S</i>
<b>C-4</b>	CHP	CH <sub>2</sub> Cl <sub>2</sub>	0	16	80	9	11	25	<i>S</i>
<b>C-5</b>	H <sub>2</sub> O <sub>2</sub>	CH <sub>2</sub> Cl <sub>2</sub>	0	16	71	9	20	36	<i>S</i>
<b>C-5</b>	CHP	CH <sub>2</sub> Cl <sub>2</sub>	0	16	79	9	12	24	<i>S</i>
<b>C-6</b>	H <sub>2</sub> O <sub>2</sub>	CH <sub>2</sub> Cl <sub>2</sub>	0	16	78	9	13	38	<i>R</i>
<b>C-6</b>	CHP	CH <sub>2</sub> Cl <sub>2</sub>	0	16	84	14	2	27	<i>R</i>
<b>C-7</b>	H <sub>2</sub> O <sub>2</sub>	CH <sub>2</sub> Cl <sub>2</sub>	0	16	76	8	16	28	<i>R</i>
<b>C-7</b>	CHP	CH <sub>2</sub> Cl <sub>2</sub>	0	16	82	16	2	15	<i>R</i>
<b>C-8</b>	H <sub>2</sub> O <sub>2</sub>	CH <sub>2</sub> Cl <sub>2</sub>	0	16	75	7	18	39	<i>R</i>
<b>C-8</b>	CHP	CH <sub>2</sub> Cl <sub>2</sub>	0	16	86	14	0	29	<i>R</i>
<b>C-9</b>	H <sub>2</sub> O <sub>2</sub>	CH <sub>2</sub> Cl <sub>2</sub>	0	16	79	7	15	29	<i>R</i>
<b>C-9</b>	CHP	CH <sub>2</sub> Cl <sub>2</sub>	0	16	87	13	0	18	<i>R</i>

ee of the product were measured by HPLC analysis. HPLC analysis was carried out with a DAICEL OD-H column (isopropanol:hexane 5:95). Retention times 17.82 mins for (*R*) and 20.91 mins for (*S*) isomers.

The oxidant and substrate mole ratio plays a critical role in terms of yields and ee of the product (figure 2.39). Experiments were performed by changing the equivalents of oxidants (H<sub>2</sub>O<sub>2</sub> and CHP), and it was observed that when the mole ratio of oxidant to substrate was 1.5, the product selectivity and the ee are the maximum. Increasing the amount of oxidant generates more sulfone at the expense of sulfoxide and the ee of the sulfoxide decreases. However, when the mole ratio of oxidant to substrate was 0.5, the yield of sulfoxide is affected drastically in

comparison to when the ratio reached 0.75 but the ee of the product sulfoxide have affected to a small extent. Changing the mole ratio to 0.75, increases the yields of sulfoxide to acceptable levels with small change in ee of the product. This experiment shows the active oxygen content in H<sub>2</sub>O<sub>2</sub>. The yields of sulfoxide does not change much with a mole ratio of oxidant to substrate changes from 0.75 to 1.5.

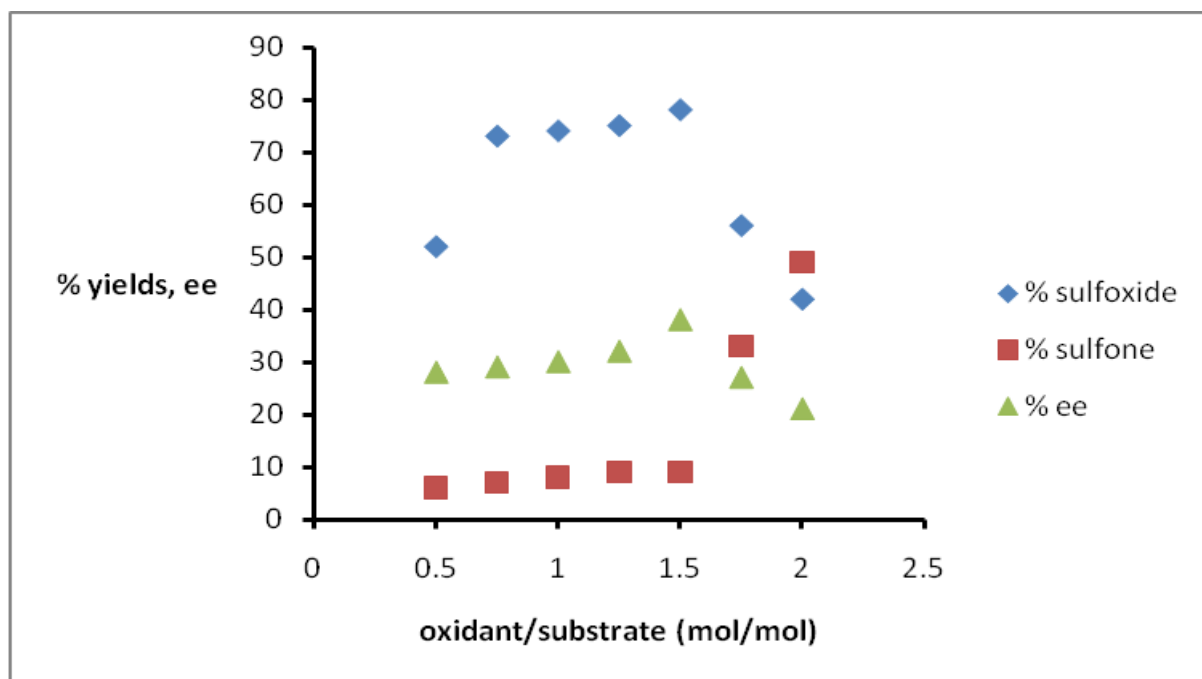


**Figure 2.39.** Effect of oxidant/substrate ratio on yields and stereoselectivity of the product.

A comparative activity of all the catalysts in terms of conversion and selectivity of the desired product sulfoxide is presented in table 2.11. Vanadium salan catalysts (**C-2**, **C-4** and **C-5**) are relatively less active than the titanium, aluminum and iron analogues in terms of conversions. Complexes of titanium and vanadium which contain *N*-methyl derivative of salan ligands, are less active in terms of conversions compared to their *N*-H salan complexes. The iron complex (**C-1**) shows high conversions with poor selectivity as well as ee and this suggests the propensity of the complex towards racemization. The aluminum complex showed high conversions, good selectivity and acceptable ee.

**Table 2.11.** Comparative activity study of all the catalysts in terms of conversion and selectivity

Catalyst	Time (hrs)	Conversions (%)	Selectivity (% Sulfoxide:% Sulfone)
C-1	16	88	64:24
C-2	16	65	59:6
C-3	16	82	73:9
C-4	16	70	64:6
C-5	16	80	71:9
C-6	16	87	78:9
C-7	16	86	76:8
C-8	16	82	75:7
C-9	16	86	79:7

The moderate stereoselectivity of the titanium salan complexes can be explained by the steric blocking by the extended side arms and backbone in the *cis-β* geometry and as a result of that, the molecule can only have an open concave site for the nucleophile to attack the metal center (figure 2.40). The preference for the substrate to attack the metal center from a specified direction increases the possibility of asymmetric inductions. Also the *cis-β* geometry can better act as an effective catalyst than the *trans* geometry (mainly adopted by the salen-transition metal complexes) as in *cis-β* geometry, a bidentate peroxy ligand has an easy access to coordinate to the metal center as observed by Katsuki et. al<sup>12</sup>

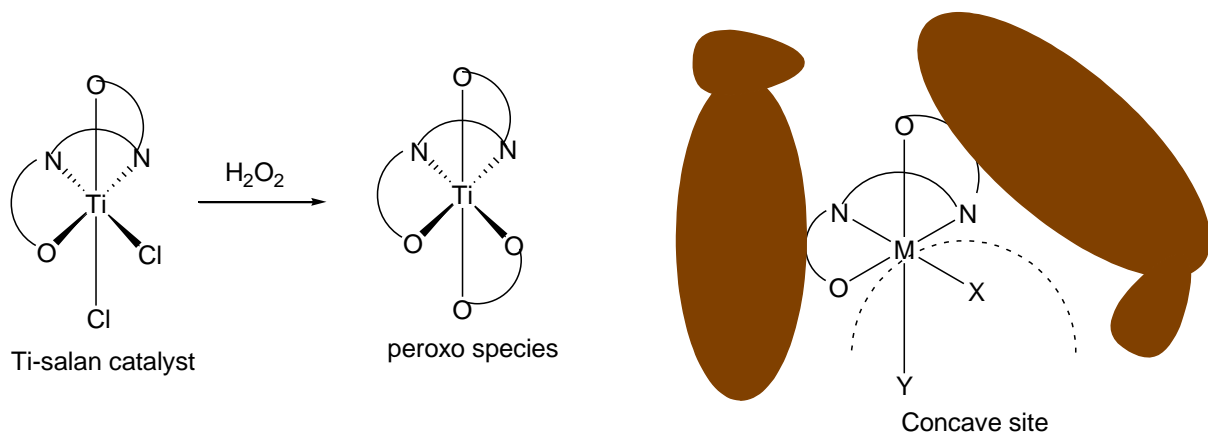


**Figure 2.40.** Site for the substrate to approach the titanium metal center.

The reason for the higher activity for the titanium salan complexes with N-H groups compared to those with the *N*-methyl groups was explained by Katsuki<sup>20</sup>. We can explain the slightly higher activity, by the possible activating effect of the complex by the hydrogen bonding between the N-H group and the oxygen from the coordinated peroxo ligand (figure 2.41). This hydrogen bonding is possible if the complex adopts *cis-β* conformation.

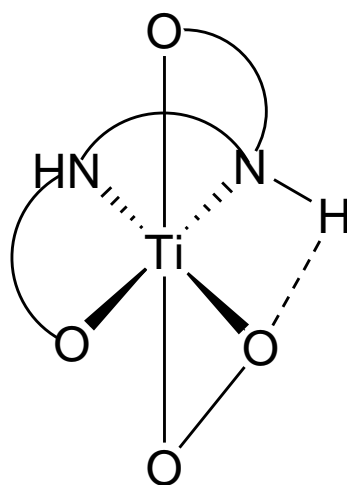


**Figure 2.41.** Hydrogen bonding in titanium salan complex.

The mechanism of titanium salan catalyzed sulfoxidation is shown in figure 2.42. The addition of sulfide is the rate determining step of the entire reaction cycle. Throughout the reaction process, the oxidation state of titanium remains same (IV). In the first step peroxo ligand attaches to the titanium center replacing two chloride ligands. Consequently after the addition of the sulfide, titanium complex forms a distorted octahedral geometry with the sulfide and the hydro-peroxide are in close proximity to each other (marked as B in figure 2.42). In the next step, the oxygen from peroxide attacks the sulfide and after bond rearrangement, product phenylmethyl sulfoxide is released and titanium complex forms a dimeric  $\eta^2$ -oxo bridged complex.<sup>20</sup> The formation of the dimeric  $\eta^2$ -oxo bridged titanium complex, explains the decrease of activity of titanium salan based catalysts after a certain time.

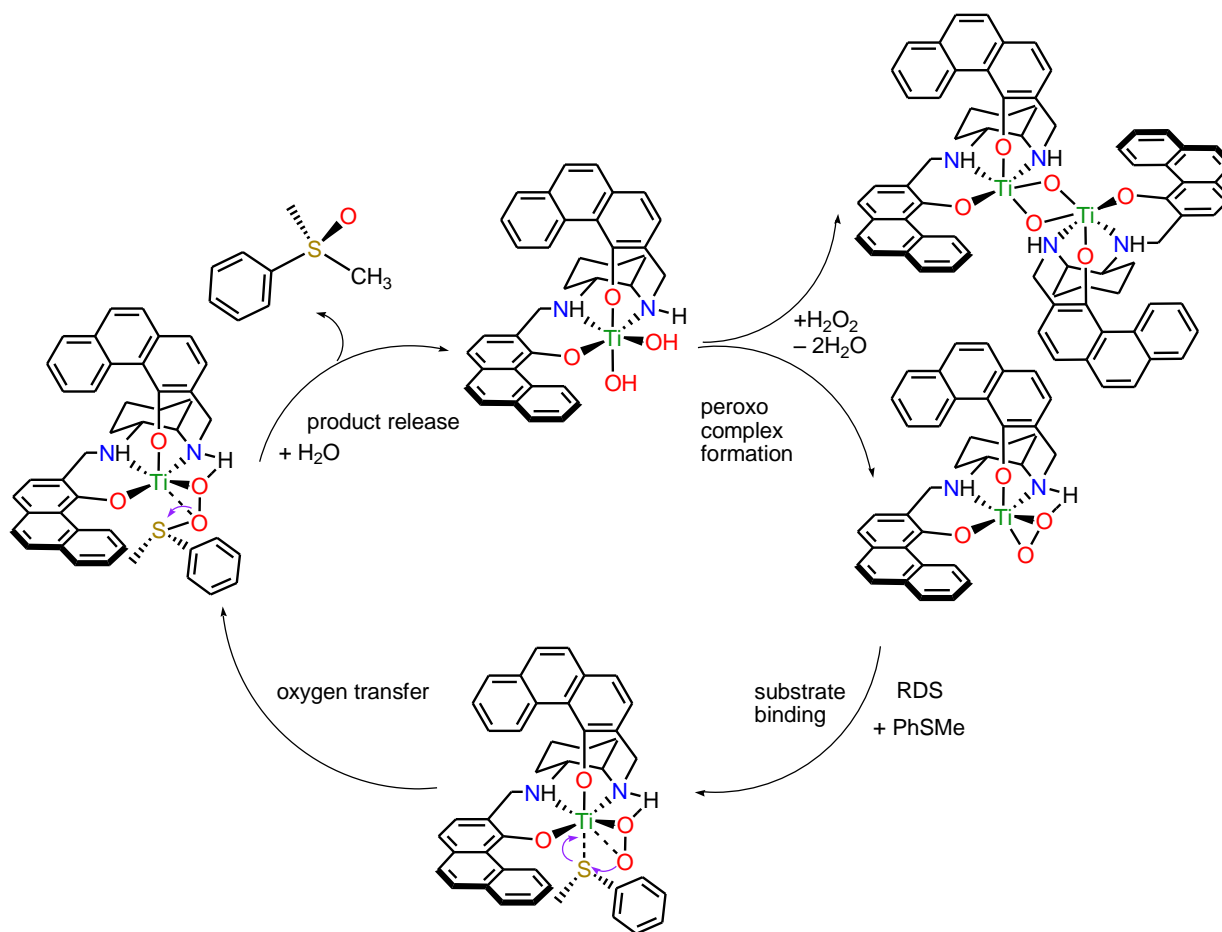


**Figure 2.42.** Mechanism of titanium salan catalyzed sulfoxidations.

## 2.4 Conclusions

Four salan ligands were synthesized and characterized. Complexations were prepared with aluminum(III), iron(II), vanadium(IV) and with titanium(IV) and these complexes were characterized by  $^1\text{H}$  and  $^{27}\text{Al}$  NMR, IR, MS, and CD. It is observed that the salan complexes of vanadium are really unstable in air. Titanium salan complexes are hard to dissolve in most of the common organic solvents. One of the goals of this chapter was to investigate whether there is any effect of extended phenyl ring side arm on the catalyst's asymmetric induction ability. As we observed, increasing the number of phenyl rings in the side arm of the salan ligand has no effect on the catalyst's stereoselectivity. The other goal was to compare the effect of N-methylated salan ligands with N-H salan ligands, on the catalysts. We observed that the N-H salan ligands

are better ligands in terms of catalytic activity. There is a possibility of hydrogen bonding in N-H salan complexes and that makes the catalyst more active. Aluminum salan complexes showed promising activity in terms of product selectivity and ee. The decrease in activity of the titanium salan complexes after 16 hrs, possibly due to the formation of the dimeric oxo bridged titanium complexes. All vanadium complexes produce *S* phenylmethyl sulfoxides as the major product whereas all other catalysts produce *R* isomer as the major one. Further investigations needs to be carried out to understand the solid state structure of these catalysts as well as the mechanism of sulfoxidations.

## 2.5 Experimental Section

### *General Methods*

All reactions were run under inert atmospheres unless otherwise noted. Solvents used in metallation reactions were stored over sodium benzophenone ketyl or calcium hydride, and degassed prior to transfer via high-vacuum line techniques. Inert gasses were purified by passage through 4 Å molecular sieves and an Engelhard Q5 catalyst bed. Preparation and workup of V(IV) and Ti(IV) compounds were completed under rigorously inert conditions to prevent oxidation or decomposition.

All mass spectra were recorded in LCT Premier (Waters corp, Milford, MA) mass spectrometer. All IR spectra were recorded in Nicolet 6700 FT-IR spectrometer. <sup>1</sup>H and <sup>13</sup>C and <sup>27</sup>Al NMR spectra were obtained on a Varian Unity 400 MHz spectrometer employing residual solvent protons (CDCl<sub>3</sub>) or in some cases TMS as an internal standard. CD spectroscopic study was performed in JASCO 720 spectropolarimeter with 5 scans and in a cell size of 1 cm path-length.

### **3,3'-[(1*R*,2*R*)-1,2-Cyclohexanediylbis(nitrilomethane)]bis-4-phenanthrenol (*R,R*)-5.**

Previously reported from our lab, salen ligand-1 (0.453g, 0.868 mmol) was dissolved in THF (10 mL) and methanol (3 mL) mixture. After stirring for 30 minutes NaBH<sub>4</sub> (0.066 g, 1.74 mmol) was added. The reaction mixture was stirred for 8 hrs at room temperature followed by the addition of aqueous saturated NH<sub>4</sub>Cl. The reaction mixture was extracted with ethyl acetate. The



organic phase was dried over anhydrous sodium sulfate and filtered over a pad of celite. The filtrate was concentrated under reduced pressure. The crude product was purified by a flash column chromatography in ethyl acetate and hexane (1:5) mixture. The pure product obtained was off white colored solid powder (0.341 g, 79 % yield).  $^1\text{H}$  NMR ( $\text{CDCl}_3$ , 400 MHz):  $\delta$  1.24-1.28 (m, 4H, CH); 1.75 (m, 2H, CH); 2.28 (m, 2H, CH); 2.61-2.62 (m, 2H, CH); 4.19 (dd, AB pattern, 2H,  $\text{CH}_2$ ); 4.33 (dd, AB pattern, 2H,  $\text{CH}_2$ ); 7.17-7.31 (dd, 4H, CH); 7.42-7.51 (dd, 4H, CH); 7.47 (d, 2H, CH); 7.60-7.66 (q, 2H, CH); 7.80-7.82 (dd, 2H, CH); 9.77 (d, 2H, CH); 12.45 (br, 2H, OH).  $^{13}\text{C}$  NMR ( $\text{CDCl}_3$ , 400 MHz):  $\delta$  24.92, 31.00, 50.00, 59.85, 119.52, 119.81, 120.43, 125.10, 126.52, 127.46, 128.37, 128.40, 129.31, 129.54, 131.46, 132.25, 134.57, 159.15. MS:  $[\text{M}]^{+1}$  ( $\text{C}_{36}\text{H}_{34}\text{N}_2\text{O}_2$ ) $^{+1}$  527.2621 (59%), 528.2656 (23%), 529.2661 (10%), 530.2691 (8%). UV and CD spectra were recorded. CD shows chirality of the ligand system.

### **3,3'-[(1*R*,2*R*)-*N,N'*-dimethyl-1,2-cyclohexanediyl]bis(nitrilomethane)]bis-4-phenanthrenol (*R,R*)-6**

To a solution of (*R,R*)-6 (1.50 G, 2.852 mmol) in acetonitrile (50 mL) were added aqueous formaldehyde (37%, 0.79047 ml, 28.52 mmol) and formic acid (4.96 mL) at room temperature. The mixture was stirred for 30 minutes followed by the addition of  $\text{NaBH}_4$  (0.539 g, 14.26 mmol). After stirring for another 16 hrs at room temperature, acetonitrile was removed in vacuo and the residue was treated with 2N NaOH (5 mL). The aqueous phase was extracted with ethyl acetate and the organic phase was dried over anhydrous sodium sulfate. Purification of the crude product was done by a flash column chromatography in ethyl acetate and hexane (1:5) mixture to obtain a off-white powder (1.29 g, 77% yield).  $^1\text{H}$  NMR ( $\text{CDCl}_3$ , 400 MHz):  $\delta$  1.24-1.28 (m, 4H, CH); 1.85 (m, 2H, CH); 2.16 (m, 2H, CH); 2.55-2.58 (m, 2H, CH); 3.69 (s, 6H,  $\text{CH}_3$ ); 3.71 (dd, AB, 2H,  $\text{CH}_2$ ); 4.56 (dd, AB, 2H,  $\text{CH}_2$ ); 7.13 (d, 2H, CH); 7.15 (d, 2H, CH); 7.60 (d, 2H, CH); 7.65 (m, 2H, CH); 7.67 (m, 2H, CH); 7.85 (d, 2H, CH); 7.87 (d, 2H, CH); 9.88-9.90 (d, 2H, bay proton); 12.00 (br, 2H, OH).  $^{13}\text{C}$  NMR ( $\text{CDCl}_3$ , 400 MHz):  $\delta$  24.25, 29.18, 57.09, 69.29, 76.84, 118.35, 119.62, 125.95, 126.58, 126.69, 127.26, 127.76, 127.91, 128.28, 128.78, 132.75, 135.51, 139.96, 157.01. MS:  $[\text{M}]^{+1}$  ( $\text{C}_{38}\text{H}_{38}\text{N}_2\text{O}_2$ ) $^{+1}$  555.2930 (58%), 556.2941 (30%), 557.2971 (8%), 558.2982 (4%).

**2,2'-[(1*R*,2*R*)-1,2-Cyclohexanediylbis(nitrilomethane)]bisbenz[*a*]anthracen-1-ol (R,R)-7.**

Previously reported from our lab salen ligand-2 (1.00 g, 1.607 mmol) was dissolved in THF (15 mL) and methanol (5 mL) mixture. After stirring for 30 minutes NaBH<sub>4</sub> (0.122 g, 3.215 mmol) was added. The reaction mixture was stirred for 8 hrs at room temperature followed by the addition of aqueous saturated NH<sub>4</sub>Cl. The reaction mixture was extracted with ethyl acetate. The organic phase was dried over anhydrous sodium sulfate and filtered over a pad of celite. The filtrate was concentrated under reduced pressure. The crude product was purified by a flash column chromatography in ethyl acetate and hexane (1:5) mixture. The pure product obtained was off white colored solid powder (0.800 g, 78% yield). <sup>1</sup>H NMR (CDCl<sub>3</sub>, 400 MHz): δ 1.34-1.49 (m, 2H, CH); 1.62-1.80 (m, 4H, CH); 1.99-2.08 (m, 2H, CH); 3.99-4.10 (AB pattern dd, 4H, *J*=8.0 Hz); 7.11 (d, 2H, *J*= 8.2 Hz, CH); 7.37 (d, 2H, *J*= 8.1Hz, CH); 7.51 (d, 2H, *J*= 8.8 Hz, CH); 7.56-7.63 (m, 4H, CH); 7.91 (d, 2H, *J*= 8.8 Hz, CH); 8.09-8.16 (m, 2H, CH); 7.56-7.63 (m, 4H, CH); 7.91 (d, 2H, *J*=8.8 Hz, CH); 8.09-8.16 (m, 2H, CH); 8.27-8.34 (m, 2H, CH); 8.46 (s, 2H, CH); 8.63 (s, 2H, CH); 10.15 (s, 2H, CH); OH signal not observed. <sup>13</sup>C δ 23.01, 32.30, 50.00, 59.50, 118.89, 121.11, 125.50, 126.50, 126.72, 127.44, 128.21, 128.41, 128.99, 130.08, 130.41, 131.00, 131.51, 132.51, 133.67, 134.55, 135.00, 158.01, one signal not observed. MS: [M]<sup>+</sup> (C<sub>44</sub>H<sub>38</sub>N<sub>2</sub>O<sub>2</sub>)<sup>+</sup> 627.2930 (56%), 628.2932 (27%), 629.2940 (14%), 630.2942 (3%).

**2,2'-[(1*R*,2*R*)-N,N'-dimethyl-1,2-Cyclohexanediylbis(nitrilomethane)]bisbenz[*a*]anthracen-1-ol (R,R)-8.**

To a solution of (R,R)-7 (0.15 g, 0.239 mmoles) in acetonitrile (5mL) were added aqueous formaldehyde (37%, 0.07 mL, 2.39 mmols) and acetic acid (0.5 mL) at room temperature. The mixture was stirred for 30 mins followed by addition of NaBH<sub>4</sub> (0.0452 g, 1.195 mmols). After stirring for another 16 hrs, acetonitrile was removed in vacuo and the residue was treated with 2N NaOH (0.45 mL). The aqueous phase was extracted with ethyl acetate and the organic phase was dried over anhydrous sodium sulfate. The solution was evaporated in vacuo and the dark brown colored residue collected as a crude product (0.122 g, 75% yield). The crude product was purified by column chromatography on silica gel (hexane/ethyl acetate = 4:1) to give the pure product (R,R)-8 (0.11 g, 71% yield). <sup>1</sup>H NMR (CDCl<sub>3</sub>, 400 MHz): δ 1.35 (m, 2H, CH), 1.41 (m, 2H, CH); 1.80 (m, 2H, CH); 1.99 (m, 2H, CH); 2.3 (m, 2H, CH); 3.59-4.38 (AB pattern, dd, 4H); 3.62 (s, 6H, CH<sub>3</sub>); 7.08 (d, 2H, CH); 7.18 (d, 2H, CH); 7.21 (d, 2H, CH); 7.37 (d, 2H, CH); 7.65

(m, 2H, CH); 7.85 (m, 2H, CH); 8.08 (m, 2H, CH); 8.21 (s, 2H, CH); 8.23 (m, 2H, CH); 10.48 (s, 2H, bay proton, CH); 12.10 (br, 2H, OH).  $^{13}\text{C}$   $\delta$  24.01, 29.03, 57.15, 69.85, 75.21, 119.15, 121.85, 124.20, 125.91, 126.68, 127.10, 127.56, 128.10, 128.29, 128.68, 128.99, 129.27, 130.10, 130.89, 131.56, 131.96, 132.10, 158.00. MS  $[\text{M}]^{+1}$  ( $\text{C}_{46}\text{H}_{42}\text{N}_2\text{O}_2$ ) $^{+1}$  655.3239 (56%), 656.3301 (30%), 657.3349 (12%), 658.3367 (2%).

### **Fe(II)-(R,R)-8 complex (C-1)**

Ligand **8** (0.05 g, 0.07645 mmoles) was dissolved in 1:1 mixture of ethanol (5 mL) and dichloromethane (5 mL). To this, at room temperature  $\text{FeCl}_2$  was added (0.0097 g, 0.07645 mmoles) followed by the addition of sodium methoxide (0.041 g, 0.7645 mmoles). After stirring the solution for 16 hrs, it was filtered and the filtrate concentrated to obtain the greenish brown color product (0.04 g, 71% yield).  $^1\text{H}$  NMR ( $\text{C}_6\text{D}_5\text{N}$ , 400 MHz):  $\delta$  1.18 (m, 2H, CH); 1.36 (m, 2H, CH); 1.61 (m, 2H, CH); 2.06 (m, 2H, CH); 2.49 (m, 2H, CH); 3.68-4.21 (AB pattern, dd, 4H); 3.92 (s, 6H,  $\text{CH}_3$ ); 7.10 (d, 2H, CH); 7.37 (m, 2H, CH); 7.39 (d, 2H, CH); 7.41 (d, 2H, CH); 7.77 (d, 2H, CH); 7.80 (s, 2H, CH); 7.84 (m, 2H, CH); 7.92 (m, 2H, CH); 8.04 (m, 2H, CH); 8.32 (s, imine CH, 2H); 12.43 (s, 2H, bay proton, CH). IR:  $\nu_{\text{Fe-O}}$  515.82  $\text{cm}^{-1}$ .

### **V(IV)-(R,R)-8 complex (C-2)**

Ligand **8** (0.081 g, 0.1245 mmol) was dissolved in a mixture of  $\text{CH}_2\text{Cl}_2$  (10mL) and EtOH (5mL). To this solution vanadyl acetyl acetonate (0.033g, 0.1245 mmol) and sodium methoxide (0.067g, 0.1245 mmol) were added. The solution was stirred for 16 hrs followed by filtration. The complex collected as a brown colored precipitate. The crude compound was purified by soxalate extraction in dichloro ethane. After drying under reduced pressure a brown colored powder was collected (0.061 g, 70% yield).  $^1\text{H}$  NMR ( $\text{CDCl}_3$ , 400 MHz): broad peaks show the presence of paramagnetic compound. MS  $[\text{M}]^{+1}$  ( $\text{C}_{46}\text{H}_{38}\text{N}_2\text{O}_3\text{V}_1\text{Cl}_1$ ) $^{+1}$  753.972 (45%), 754.974 (30%), 755.978 (17%), 756.980 (8%).

### **Al(III)-(R,R)-8 complex (C-3)**

Ligand **8** (0.07 g, 0.107 mmol) was dissolved in a mixture of toluene (1mL). To this solution diethyl aluminum chloride (100  $\mu\text{L}$ , 0.107 mmoles) was added. The solution was stirred for 16 hrs. Then the solution was suspended in hexane followed by filtration. The complex collected as

off-white colored precipitate. The precipitate was washed with hexane. It was dried under vacuum (0.049 g, 70% yield).  $^1\text{H}$  NMR ( $\text{CDCl}_3$ , 400 MHz): 1.25 (m, 2H, CH); 1.39 (m, 2H, CH); 1.81 (m, 2H, CH); 2.1 (m, 2H, CH); 2.6 (m, 2H, CH); 3.91-4.5 (AB pattern, dd, 4H,  $\text{CH}_2$ ); 4.48 (broad singlet, 6H,  $\text{CH}_3$ ); 7.28 (d, 2H, CH); 7.35 (d, 2H, CH); 7.37 (d, 2H, CH); 7.56 (m, 2H, CH); 7.82 (d, 2H, CH); 8.10 (m, 2H, CH); 8.25 (m, 2H, CH); 8.52 (s, 2H, CH); 10.48 (s, 2H, CH); 12.60 (broad singlet, 2H, CH).  $^{27}\text{Al}$  NMR:  $\delta$  172.00 (confirms the presence of Al in the complex). MS:  $[\text{M-Cl}]^+$  OR  $(\text{C}_{46}\text{H}_{40}\text{N}_2\text{O}_2\text{Al}_1)^{+1}$  679.010 (55%), 680.008 (30%), 681.014 (5%). UV (LMCT absorption bands at 390 and 410 nm were observed). CD shows that *P* isomer is predominant in solution.

#### **V(IV)-(R,R)-7 complex (C-4)**

Ligand **7** (0.10 g, 0.159 mmol) was dissolved in a mixture of  $\text{CH}_2\text{Cl}_2$  (10 mL) and EtOH (5 mL). To this solution vanadyl acetyl acetonate (0.042 g, 0.159 mmol) and sodium methoxide (0.086 g, 1.59 mmol) were added. The solution was stirred for 16 hrs followed by filtration to obtain a brown colored precipitate. The compound was further purified by soxalate extraction in  $\text{CH}_2\text{Cl}_2$ . Pure brown colored compound was obtained after solvent removal at reduced pressure (0.69 g, 71% yield).  $^1\text{H}$  NMR ( $\text{CDCl}_3$ , 400 MHz): broad unassignable peaks suggest paramagnetic compound. MS:  $[\text{M}]^{+1}$  OR  $(\text{C}_{44}\text{H}_{34}\text{O}_3\text{N}_2\text{V}_1)^{+1}$  691.058 (56%), 692.062 (34%), 693.062 (8%), 694.068 (2%). IR:  $\nu_{\text{V=O}}$  829  $\text{cm}^{-1}$  (sharp single peak),  $\nu_{\text{N-H}}$  3400  $\text{cm}^{-1}$ . CD shows the predominance of *P* helix in the solution.

#### **V(IV)-(R,R)-5 complex (C-5)**

Ligand **5** (0.50 g, 0.7947 mmol) was dissolved in a mixture of  $\text{CH}_2\text{Cl}_2$  (15 mL) and EtOH (5 mL). To this solution vanadyl acetyl acetonate (0.212 g, 0.7947 mmol) and sodium methoxide (0.4313 g, 7.95 mmol) were added. The solution was stirred for 16 hrs followed by filtration to obtain a light green colored precipitate. The compound was further purified by soxalate extraction in dichloro ethane. Pure light green colored compound was obtained after solvent removal under reduced pressure (0.345 g, 69% yield).  $^1\text{H}$  NMR ( $\text{CDCl}_3$ , 400 MHz): broad unassignable peaks suggest paramagnetic compound. MS:  $[\text{M-H+Na}]^{+1}$  OR  $(\text{C}_{36}\text{H}_{32}\text{N}_2\text{O}_3\text{V}_1\text{Na}_1)^{+1}$  613.771(52%), 614.773 (28%), 615.775 (13%), 616.810 (7%). IR:  $\nu_{\text{V=O}}$  826.72  $\text{cm}^{-1}$ .

### Ti(IV)-(R,R)-5 complex (C-6)

In the solution of the ligand **5** (0.50 g, 0.9506 mmol) (in 8 mL of dry CH<sub>2</sub>Cl<sub>2</sub>) was added TiCl<sub>4</sub> (1 M in CH<sub>2</sub>Cl<sub>2</sub>, 0.9506 mmol, 0.9506 mL) dropwise. Instantly, the solution turned purple. The entire mixture was stirred for additional 2 hrs before removing the solvent. The precipitate was decanted with ether and ether/hexane (1:1) mixture respectively. The purple colored precipitate was dried under vacuum to get pure complex (0.39 g, 78% yield). <sup>1</sup>H NMR (CDCl<sub>3</sub>, 400 MHz): 1.1 (m, 2H, CH, ratio 2); 1.2 (m, 2H, CH, ratio 1); 1.26 (m, 2H, CH, ratio 2); 1.31 (m, 2H, CH, ratio 1); 1.75(m, 2H, CH, ratio 2); 2.02 (m, 2H, CH, ratio 1); 2.24 (m, 2H, CH, ratio 2); 2.50 (m, 2H, CH, ratio 1); 3.51 (m, 2H, CH, ratio 2); 4.16 (m, 2H, CH, ratio 1); 3.95-4.00 (dd, AB pattern, 2H, CH<sub>2</sub>); 5.1-5.26 (dd, AB pattern, 2H, CH<sub>2</sub>); 6.75 (t, 2H, CH, ratio 2); 6.85 (t, 2H, CH, ratio 1); 7.1 (d, 2H, CH, ratio 2); 7.30 (d, 2H, CH, ratio 1); 7.25 (m, 2H, CH, ratio 1); 7.50 (m, 2H, CH, ratio 2); 7.51 (d, 2H, CH, ratio 1); 7.52 (d, 2H, CH, ratio 2); 7.61 (m, 2H, CH, ratio 1); 7.75 (m, 2H, CH, ratio 2); 7.95 (m, 2H, CH, ratio 1); 9.37 (d, 2H, CH, ratio 1); 10.00 (d, 2H, CH, ratio 2); 10.32 (d, 2H, CH, ratio 1); 10.35 (d, 2H, CH, ratio 2); 10.49 (d, 2H, CH, ratio 1). <sup>13</sup>C NMR (CD<sub>2</sub>Cl<sub>2</sub>, 400 MHz): δ 23.00, 24.52, 29.61, 30.71, 49.72, 51.22, 63.21, 119.00, 123.43, 124.95, 125.00, 125.47, 127.31, 127.83, 128.83, 129.00, 129.57, 130.00, 131.94, 161.22, 162.00. MS: [M-2Cl+2,5-dihydroxy benzoic acid (component from matrix)] (C<sub>43</sub>H<sub>36</sub>O<sub>6</sub>N<sub>2</sub>Ti<sub>1</sub>) 722.803 (2%), 723.801 (4%), 724.814 (52%), 725.824 (30%), 726.808 (12%), 727.811 (1%). IR: ν<sub>Ti-O</sub> 711.32 cm<sup>-1</sup>. UV and CD data showed significant change from the ligand's spectrum. Possibly, *M* conformer predominates in solution.

### Ti(IV)-(R,R)-6 complex (C-7)

0.210 g (0.379 mmol) of ligand **6** was dissolved in 5 mL of CH<sub>2</sub>Cl<sub>2</sub> inside the glove box. Slowly dropwise 111 μL of Titanium isopropoxide was added in the reaction mixture. The entire mixture was stirred for overnight. Solvent was removed under reduced pressure and the yellowish brown colored solid was decanted with hexane followed by drying under reduced pressure to get the pure product (0.124 g, 72% yield). <sup>1</sup>H NMR (CDCl<sub>3</sub>, 400 MHz): 1.20 (m, 2H, CH); 1.52 (m, 2H, CH); 1.87 (m, 2H, CH); 2.15 (m, 2H, CH); 2.56 (m, 2H, CH); 3.68 (s, 6H, CH<sub>3</sub>); 3.70-3.72 (dd, AB, 2H, CH<sub>2</sub>); 4.43-4.47 (dd, AB, 2H, CH<sub>2</sub>); 7.13 (d, 2H, CH); 7.26 (d, 2H, CH); 7.57-7.60 (d, 2H, CH); 7.65-7.67 (d, 2H, CH); 7.71 (m, 2H, CH); 7.87 (m, 2H, CH); 9.88-9.90 (m, 2H, CH);

10.23 (m, 2H, CH). MS: (C<sub>44</sub>H<sub>45</sub>O<sub>4</sub>N<sub>2</sub>Ti)<sup>+</sup> 712.760 (1%), 713.784 (12%), 714.790 (60%), 715.727 (18%), 716.754 (6%), 717.811 (2%), 718.807 (1%). IR:  $\nu_{\text{Ti-O}}$  745.57 cm<sup>-1</sup>.

#### **Ti(IV)-(R,R)-7 complex (C-8)**

In the solution of the ligand **7** (0.560 g, 0.8945 mmol) in approximately 20 mL of CH<sub>2</sub>Cl<sub>2</sub> was added TiCl<sub>4</sub> (1M in CH<sub>2</sub>Cl<sub>2</sub>, 0.8945 mmol). The solution turned dark purple within few seconds. The entire mixture was stirred for 2 hours before removing the solvent. The precipitate was decanted with ether and ether/hexane (1:1) mixture followed by ethanol before drying. Dark purple colored product obtained which was mostly insoluble in almost all common organic solvents (0.382 g, 69% yield). <sup>1</sup>H NMR (DMSO-d<sub>6</sub>, 400 MHz): 1.20 (broad, 2H, CH); 1.35 (broad, 2H, CH); 1.60-2.0 (broad, 4H, CH), 2.10-2.18 (broad, 2H, CH); 4.56-4.79 (broad, 2H, CH); 7.12 (m, 1H, CH); 7.15 (d, 1H, CH); 7.21 (m, 1H, CH); 7.24-7.68 (m, 8H, CH); 7.80-7.95 (m, 4H, CH); 8.05-8.18 (m, 4H, CH); 8.22-8.35 (m, 2H, CH); 10.42 (s, 2H, bay proton). <sup>13</sup>C NMR (CDCl<sub>3</sub>, 400 MHz): very broad spectrum in the aromatic region (around 130 ppm). MS: (C<sub>46</sub>H<sub>41</sub>O<sub>3</sub>N<sub>2</sub>Ti)<sup>+</sup> 715.2570 (4%), 716.2572 (5%), 717.2574 (52%), 718.2618 (32%), 719.2618 (6%), 720.2649 (1%). IR: 743.14 cm<sup>-1</sup>(Ti-O bond), 716.93 cm<sup>-1</sup>(Ti-Cl bond).

#### **Ti(IV)-(R,R)-8 complex (C-9)**

In the solution of the ligand **8** (0.300 g, 0.458 mmol) in approximately 13 mL of CH<sub>2</sub>Cl<sub>2</sub> was added TiCl<sub>4</sub> (1M in CH<sub>2</sub>Cl<sub>2</sub>, 0.457 mmol). The solution turned dark purple within few seconds. The entire mixture was stirred for 2 hours before removing the solvent. The precipitate was decanted with ether and ether/hexane (1:1) mixture before drying. Dark purple colored product obtained which was mostly insoluble in almost all common organic solvents (0.214 g, 72% yield). <sup>1</sup>H NMR (CDCl<sub>3</sub>, 400 MHz): broad proton NMR spectrum. Can not assign the peaks due to the broadness. <sup>13</sup>C NMR (CDCl<sub>3</sub>, 400 MHz): very broad spectrum in the aromatic region (around 132 ppm). MS: (C<sub>47</sub>H<sub>43</sub>O<sub>3</sub>N<sub>2</sub>Ti) 729.2753 (8%), 730.2815 (10%), 731.2681 (43%), 732.2726 (25%), 733.2728 (12%), 734.2730 (2%). IR: 743.59 cm<sup>-1</sup>(Ti-O bond).

**General Procedure for Sulfoxidations:** All sulfoxidation reactions are carried out by 1 mol% of catalyst. 1mol% of catalyst was dissolved in dichloromethane (3mL) inside a two neck R.B. under argon. The mixture was stirred in inert atmosphere for 10 minutes. 100 mol% phenyl

methyl sulfide was added followed by additional 15 minutes of stirring. The entire system was cooled to 0 °C. 110 mol% oxidant (hydrogen peroxide or cumene hydroperoxide) was added to the mixture slowly for a period of 2 hrs. The mixture was additionally stirred for 16 hrs. A saturated solution of sodium sulfite was added to quench the reaction. The reaction mixture was extracted with dichloromethane followed by drying over sodium sulfate. The product was purified by flash column chromatography in 1:3 ethyl acetate:hexane. Pure sulfoxide was analysed by <sup>1</sup>H NMR (CDCl<sub>3</sub>, 400 MHz): 3.72 (s, 3H, CH<sub>3</sub>); 7.5 (m, 3H, CH); 7.6 (m, 2H, CH). Enantiomeric excess of the phenyl methyl sulfoxide was determined by HPLC analysis with a Daicel Chiralcel OD-H column. Hexane and isopropanol mixture (90:10) was used as the eluent. The *R* isomer and the *S* isomer elutes at 17 and 20 minutes respectively.

## 2.6 References:

1. "Synthesis of an optically active Al(salalen) complex and its application to catalytic hydrophosphonylation of aldehydes and aldimines" Saito, B.; Egami, H.; Katsuki, T. *J. Am. Chem. Soc.* **2007**, *129*, 1978-1986.
2. "Epoxidation of olefins catalyzed by vanadium salan complexes: a theoretical mechanistic study" Kuznetsov, L. M.; Pessoa, J. C. *Dalton. Trans.* **2009**, 5460-5468.
3. "Asymmetric catalysis of metal complexes with non-planar ONNO ligands: salen, salalen and salan" Matsumoto, K.; Saito, B.; Katsuki, T. *Chem. Commun.* **2007**, 3619-3627.
4. "Asymmetric synthesis of esomeprazole" Cotton, H.; Elebring, T.; Larson, M.; Li, L.; Sorensen, H.; Unge, S.V. *Tetrahedron: Asymmetry.* **2000**, *11*, 3819-3825.
5. "Diastereomerically specific zirconium complexes of chiral salan ligands: isospecific polymerization of 1-hexene and 4-methyl-1-pentene and cyclopolymerization of 1,5-hexadiene" Yeori, A.; Goldberg, I.; Shuster, M.; Kol, M. *J. Am. Chem. Soc.* **2006**, *128*, 13062-13063.
6. "Salan complexes of the group 12, 13 and 14 elements" Atwood, D. A. *Coordn. Chem. Rev.* **1997**, *165*, 267-296.
7. "An efficient asymmetric oxidation of sulfides to sulfoxides" Pitchen, P.; Kagan, H. B. *Tetrahedron Lett.* **1984**, *25*, 1049.

8. "Synthesis of chiral sulfoxides by metal catalyzed oxidation with *tert*-butyl hydroperoxides" Di Furia, S. H.; Modena, G.; Seraglia, G. *Synthesis*. **1984**. 325.
9. "Highly enantioselective oxidation of sulfides mediated by a chiral titanium complex" Brunel, J. M.; Diter, P.; Duetsch, M.; Kagan, H. B. *J. Org. Chem.* **1995**. *60*. 8086-8088.
10. Colombo, A.; Maturano, G.; Pasini, A. *Gazz. Chim. Ital.* **1986**. *116*. 35.
11. "Ti(salan) catalyzed enantioselective sulfoxidation using hydrogen peroxide as a terminal oxidant" Saito, B.; Katsuki, T.; *Tetrahedron Lett.* **2001**. *42*. 3873-3876.
12. "Mechanistic consideration of Ti(salan) catalyzed asymmetric sulfoxidation" Saito, B.; Katsuki, T. *Tetrahedron Lett.* **2001**. *42*. 8333-8336.
13. "Titanium salan catalyzed asymmetric oxidation of sulfides and kinetic resolution of sulfoxides with H<sub>2</sub>O<sub>2</sub> as the oxidant" Bryliakov, K. P.; Talsi, E.P. *Eur. J. Org. Chem.* **2008**. 3369-3376.
14. "Synthesis, characterization, and application of vanadium salan complexes in oxygen transfer reactions" Adao, P.; Costa, J. P.; Henriques, R. T.; Kuznetsov, M. L.; Avecilla, F.; Maurya, M. R.; Kumar, U.; Correia, I. *Inorg. Chem.* **2009**. *48* (8). 3542-3561.
15. Matsumoto, K.; Yamaguchi, T.; Fujisaki, J.; Saito, B.; Katsuki, T. *Chem. Asian. J.* **2008**. DOI: 10.1002/asia.200700328.
16. "Diastereomerically selective enantiomerically pure titanium complexes of salan ligands: synthesis, structure, and preliminary activity studies" Yeori, A.; Groysman, S.; Goldberg, I.; Kol, M. *Inorg. Chem.* **2005**. *44* (13). 4466-4468.
17. "Achiral tetrahydrosalen ligands for the synthesis of C<sub>2</sub> symmetric titanium complexes: a structure and diastereoselectivity study" Balsells, J.; Carroll, P. J.; Walsh, P. J. *Inorg. Chem.* **2001**. *40*. 5568
18. "Predetermined chirality at metal centers" Mamula, O.; von Zelewsky, A. *Angew. Chem. Int. Ed.* **1999**. *38*. 302.
19. "Iron(II) and zinc(II) monohelical binaphthyl salen complexes with overlapping benz[a]anthryl sidearms" Wiznycia, A. V.; Desper, J.; Levy, C. J. *Dalton Trans.* **2007**, 1520-1527.



20. "Titanium salan catalyzed asymmetric epoxidation with aqueous hydrogen peroxide as the oxidant" Sawada, Y.; Matsumoto, K.; Kondo, S.; Watanabe, H.; Ozawa, T.; Suzuki, K.; Saito, B.; Katsuki, T. *Angew. Chem. Int. Ed.* **2006**, *45*, 3478-3480.

# CHAPTER 3 - Chiral Helical $C_1$ -Symmetrical Vanadium and Zinc Salen Complexes for Asymmetric Sulfoxidations

## 3.1 Abstract

Efforts were made to develop  $C_1$ -symmetrical salen ligands and to characterize them by common analytical methods. These  $C_1$ -symmetrical salen ligands were complexed with zinc(II) and vanadium(IV) and characterized. The [VO-salen] complexes were used as catalysts in sulfoxidation reactions and the results were compared with the  $C_1$ -symmetrical analogues of [VO-salen].

## 3.2 Introduction

Salen ligands are comprised of a tetradentate  $N_2O_2$  coordination set and the ligands are synthesized by a double condensation between a diamine and two equivalents of a salicylaldehyde.<sup>1</sup> The discovery of the salen ligands as potential source of asymmetric catalysis by Jacobsen and Katsuki has been a landmark in the industrial research.<sup>2,3</sup> The properties of the salen ligands can be easily altered by structural changes in the diamine or salicylaldehyde components.<sup>4</sup> This offers great diversity in the salen ligands that can be obtained and offers a valuable toolkit for the fine-tuning of the steric and electronic properties. Also, appropriate selection of chiral molecules provide the opportunity to vary the non-symmetrical environment around the metal center.<sup>5</sup> The first generation of salen ligands with  $C_2$  symmetry were constructed by Jacobsen with two salicylidene fragments having the same substitution pattern on the aromatic side rings (figure 3.1).<sup>2</sup> However, the use of different salicylaldehydes can create a way to vary the ligand properties to some extent, but the diversity of structures that can be achieved is limited.

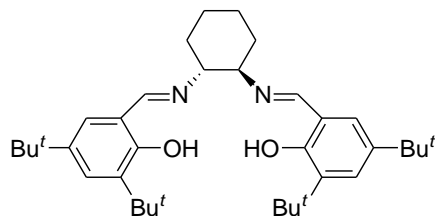


**Figure 3.1.** Salen ligand introduced by Jacobsen.

The presence of two distinct salicylideneimine groups in the salen ligand can be beneficial for a number of reasons (figure 3.2). First of all, immobilization of the salen ligands over a homogeneous or heterogeneous support is a well known way in catalysis and the immobilization allows the recovery of the catalyst systems and reuse in the subsequent catalytic campaigns.<sup>5</sup> Unsymmetrical salen ligands equipped with a single functional group useful for such immobilization procedures would thus be required.<sup>6</sup> The presence of a single connection to a support permits the substrate to freely approach the catalytic site which may be difficult in doubly immobilized, symmetrical salen derivatives eventually leading to lower reaction rates and selectivities.<sup>6</sup> Another advantage of non-symmetry in the salen scaffold is the possibility of further fine tuning its structures by introducing different electron withdrawing and electron donating groups both in the backbone as well as in the side arms.<sup>7</sup> Lastly, the desymmetrization of the salen ligands has been reported to produce, at least in some cases improved enantioselective behavior in different organic transformations as compared to the symmetrical ones.<sup>8</sup>

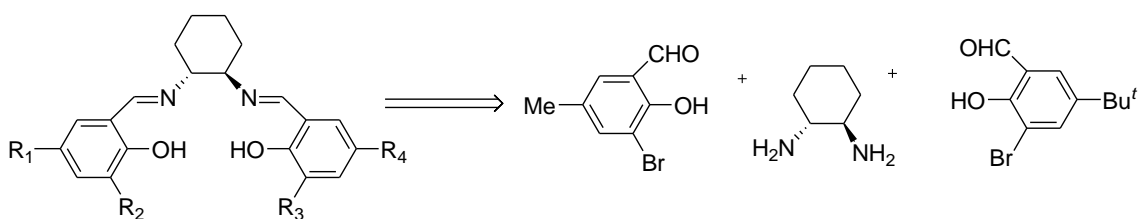


**Figure 3.2.** Retrosynthetic analyses of unsymmetrical salen ligand.

In the last decade, numerous groups have devoted their research to synthesize non-symmetrical salen ligands and complexes.<sup>9</sup> However, most of the groups faced the same problem while synthesizing non-symmetrical salen ligands. When a chiral 1,2 cyclohexyl diamine refluxed with a 1:1 mixture of two different salicylaldehyde, it often results in the formation of two symmetrical salen ligands with each having the same side arms (figure 3.3).<sup>10</sup> The stability of the salen ligands comes from the same electronic and steric environment in the symmetric salen ligands as opposed to different steric and electronic environment in non-symmetrical salen ligands having two different side arms.<sup>10</sup>

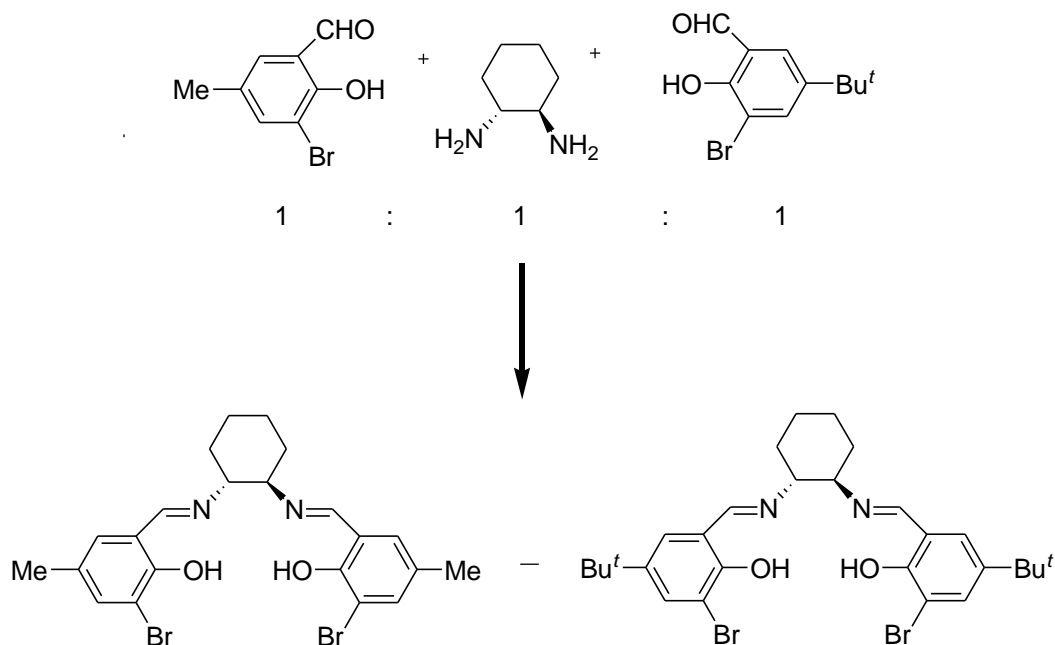


**Figure 3.3.** Problems encountered during the synthesis of non-symmetrical salen ligands.

There are many approaches to synthesize the non-symmetrical salen ligands. Among them the direct stepwise synthesis is the most straightforward approach.<sup>10</sup> Gilheany has reported that a *racemic* 1,2-diamino-cyclohexane when treated with two distinctly different salicylaldehyde sidearms with a large electronic and steric differences, can lead to a possible isolation of the monoamine salt intermediate (A). In the following step, the non-symmetrical salen ligand forms in a substantial quantity (figure 3.4).<sup>11</sup> This phenomenon was observed when tartaric acid was used as the salt forming agent. However, when the same reaction sequence were carried out with the *non-racemic* 1,2-diamino cyclohexane, only the the salt (B) was isolated (figure 3.5). It appeared that in case of *non-racemic* 1,2-diaminocyclohexane, perhaps the steric requirements of the system were such that they did not allow the formation of a salt such as (A) containing two “half-units” of the same enantiomer. Also, electronic and steric differences in the side arms play a crucial role in the synthesis of non-symmetrical salen ligands.

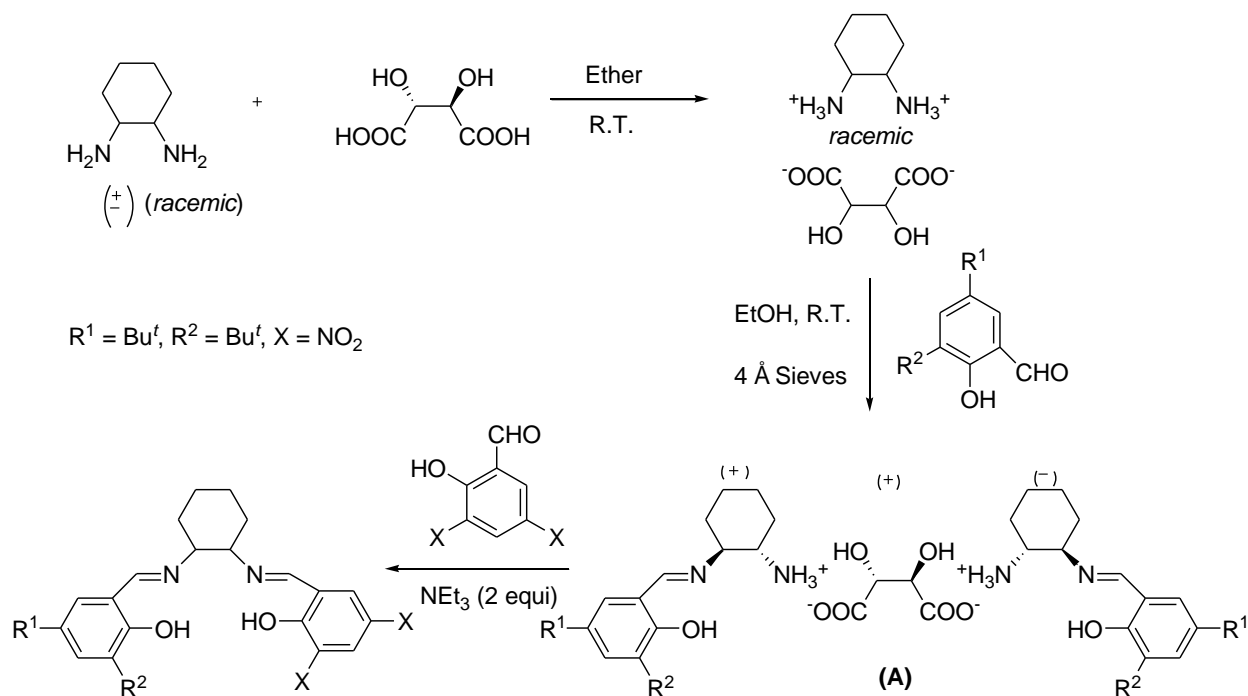


**Figure 3.4.** Formation of *racemic* mixed salen ligand.

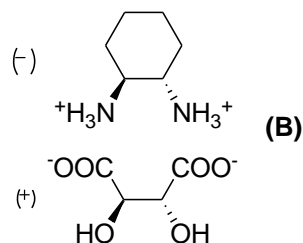


**Figure 3.5.** Salt formation in case of *non-racemic* 1,2-diamino cyclohexane.

There are three principal ways of preparing non-symmetrical salen ligands: direct preparation, using a protecting group approach and a metal template approach.<sup>12, 13, 14</sup> Here we described in short each of these approaches.

Direct preparation is defined as the condensation between the amine and the aldehyde without the use of any other (in)organic reagents or any templating metal ions or any protection/deprotection sequences during the condensation stage(s). The first example of the direct preparation of non-symmetrical salen ligands was presented by Jacobsen. The synthesis of the dissymmetric salen ligand was reported with two distinct salicylideneimine groups (figure

3.6). The statistical mixture of salen ligands (both homo-combinations and the hetero-combination) was separated using column chromatography. The reported yield of the hetero-combination was 40%. This method is not widely used because of the tedious chromatographic separation of the desired product from the mixture.<sup>12</sup>

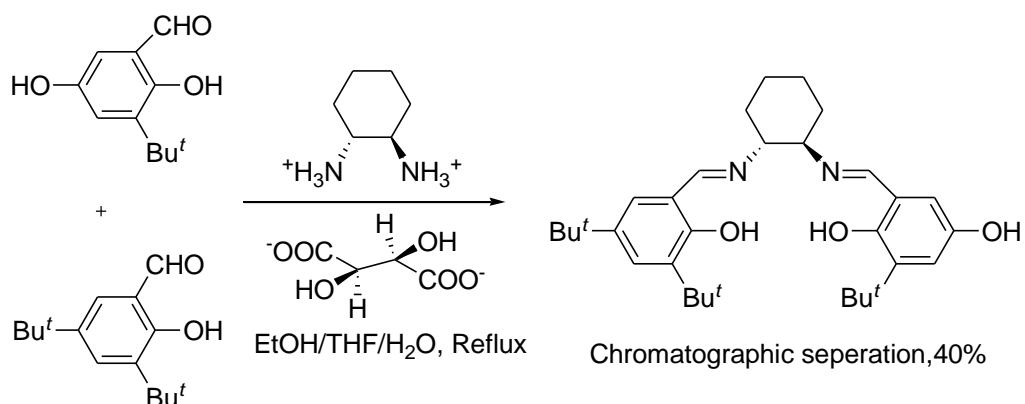


**Figure 3.6.** Mixed salen ligand synthesized by Jacobsen et al.

Synthesis of non-symmetrical salen ligands by a protecting group approach is the most widely used as this method produces good yields of the desired unsymmetrical ligand. This method is described as the selective protection of one of the two amine groups in the diamine reagent. The protected reagent is then subjected to a step-wise condensation with distinct salicylaldehydes to give the non-symmetrical salen ligands; the second Schiff base function is introduced after deprotection of the protected amine group.

Nguyen et al reported a general one pot high yielding synthesis of non-symmetrical salen ligands using mono-ammonium salt derived from diamines and anhydrous hydrochloric acid.<sup>12</sup> The ammonium salts are rather insoluble in ether and can be isolated and treated with one equivalent of salicylaldehyde to yield mono-imine reagents in high yields. The mono-imino ammonium salt can in turn be added to a second salicylaldehyde in the presence of triethylamine to produce the desired non-symmetrical salen ligands in high yields. The major advantage of this procedure is that large scale synthesis can be carried out without the need for tedious chromatographic separations. One limitation of this procedure is that, this process so far showed success only when the differences in electronic and steric properties are large in the two side arms of the non-symmetrical salen ligands (figure 3.7).

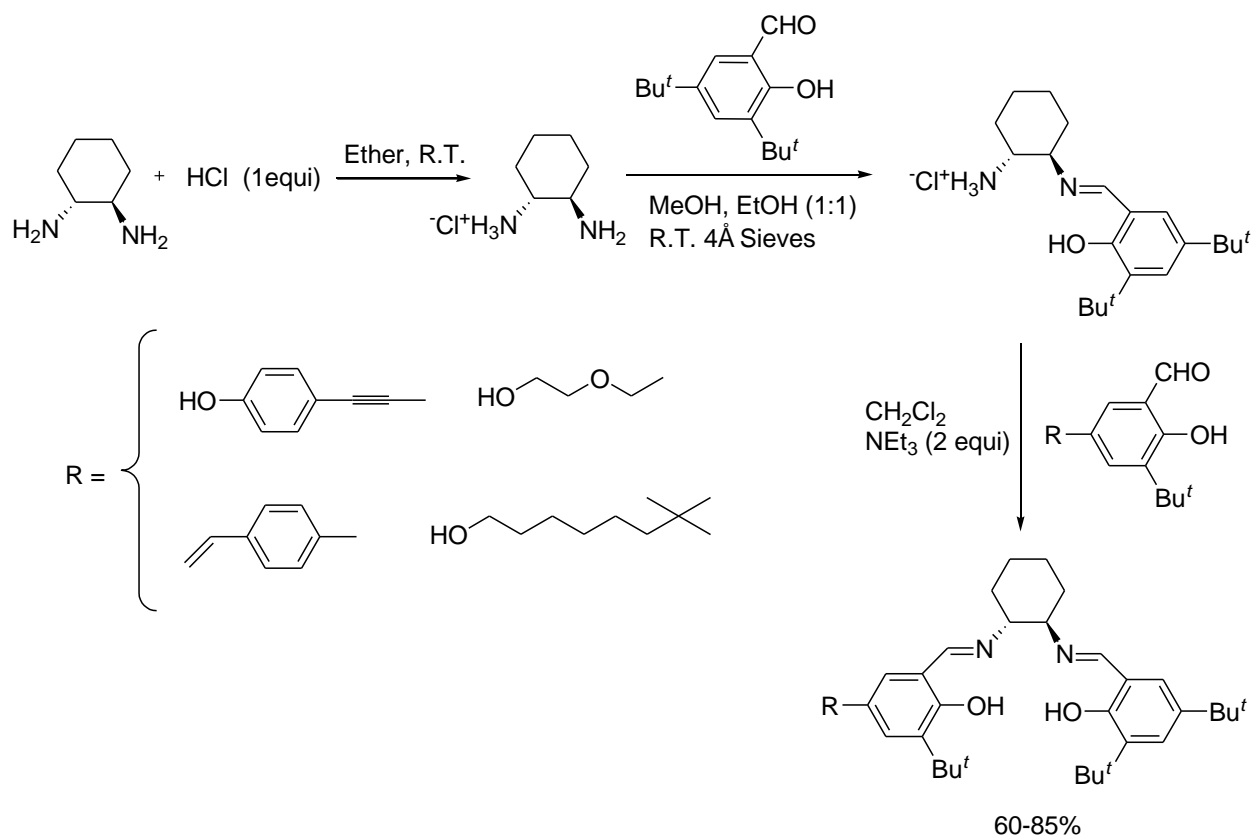


**Figure 3.7.** Synthesis of unsymmetrical salen ligands by protecting group approach.

The last common approach to the synthesis of unsymmetrical salen ligands is the metal template approach.<sup>14</sup> In order to arrive at non-symmetrical metal-salen complexes, the equilibrium between mono- and diimine species, and the diamine upon dissolution in subsequent stages needs to be controlled. One way to control the equilibrium during the second condensation step is to make use of templation. Kleij et al have used the mono-imine synthon to prepare, in a one pot procedure, non-symmetrical metal-salen complexes (figure 3.8).<sup>14</sup> The mono-imine reactant is treated with a mixture of another salicylaldehyde and a zinc diacetate to afford exclusively the non-symmetrical zinc-salen complex in high yields. However, this template procedure has not been as successful with chiral diamines. The reasons are still unclear for the propensity of chiral diamines to produce a mixture of symmetrical and non-symmetrical salen ligands in the metal-template approach.

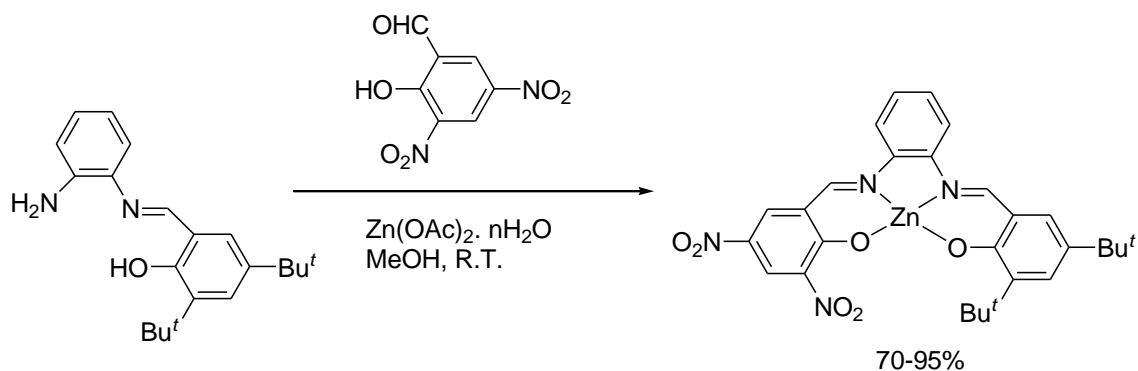


**Figure 3.8.** Metal template approach for the synthesis of unsymmetrical zinc-salen complex.

The three non-symmetrical salen ligands discussed in this chapter are shown in figure 3.9. All of these ligands have (*R,R*)-1,2-diaminocyclohexane as the backbone. The helicity induced by the extended fused phenyl ring side arms can create a highly asymmetric environment in the complex. We already reported the effect of helicity on the chiral induction by the  $C_2$ -symmetric [VO-salen] (with the symmetric version of these ligands) complexes. However, these classes of helical unsymmetric salen ligands may show better activity in chiral catalysis than their symmetric counter-parts.

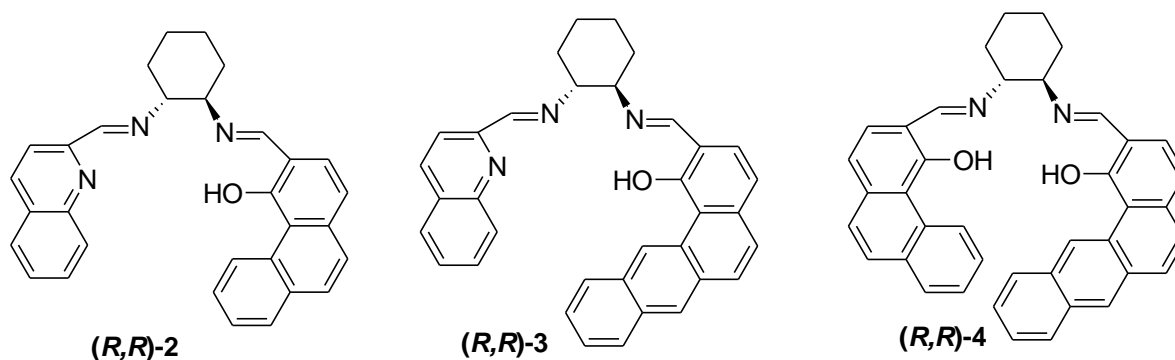


**Figure 3.9.** Non-symmetric salen ligands used in this study.

### 3.3 Results and Discussion

#### 3.3.1 Synthesis of non-symmetrical salen ligands

All the ligands used in this chapter (figure 3.10) were synthesized by the protecting group method introduced by Nguyen et al.<sup>12</sup> First mono-ammonium salt of 1,2-diamino cyclohexane



was synthesized. This mono-iminium salt was condensed with the less bulky sidearm first to produce mono-imine reagent. Then the mono-imino ammonium salt in turn added to the second salicylaldehyde in the presence of triethylamine to produce the desired non-symmetrical salen ligands. Ligands **(R,R)-2** and **(R,R)-3** were obtained as a brown colored powder, where as ligand **(R,R)-4** was isolated as a yellow colored powder.

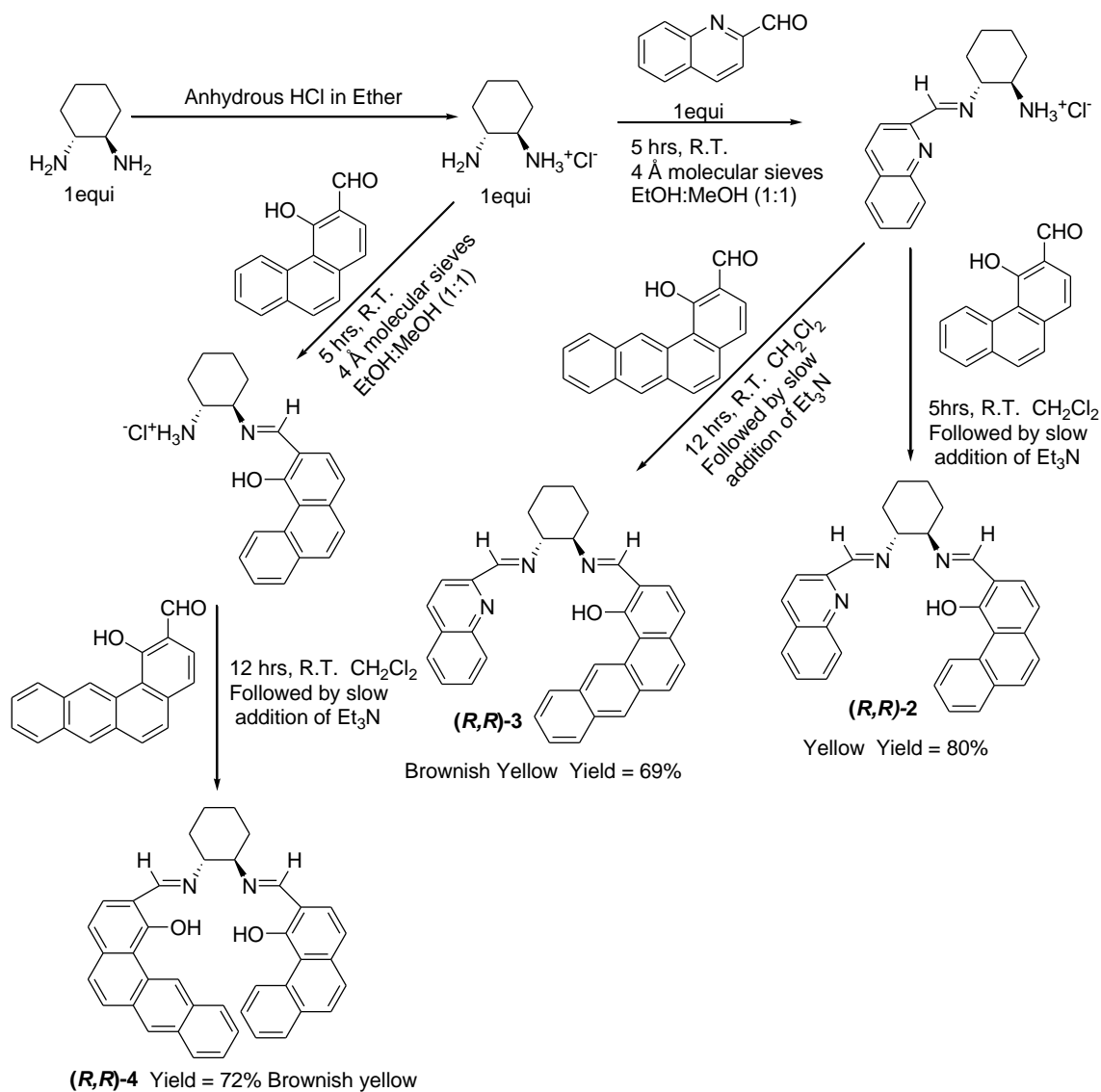


**Figure 3.10.** Scheme for the synthesis of salen ligands.

The <sup>1</sup>H NMR (CDCl<sub>3</sub>, 400 MHz) showed that the synthesis of these ligands produced a mixture of symmetrical and unsymmetrical salen ligands. However, the ratio of the hetero to

homo combination is 60:40. To date, there are no reports for a successful synthesis of non-symmetrical salen ligands by any known synthesis methods when the differences of electronic and steric properties of the two side arms are small. Also, the chemical nature of the symmetric and unsymmetric salen ligands are so similar that it is difficult to separate them by chromatographic techniques or recrystallization. The important assigned peaks from the  $^1\text{H}$  NMR spectrum for ligand (*R,R*)-**2** are shown in table 3.1. ESI-MS spectrum shows the presence of molecular ion peak for the desired non-symmetrical salen ligand at  $M/Z$  458.776 (figure 3.11).

**Table 3.1.** Assigned protons (molecule shown below with marked protons) chemical shifts

Protons	1a	2a	1b	2b
Chemical shifts	8.30 (s)	8.55 (s)	8.05 (d)	10.07 (d)
(splitting patterns)				

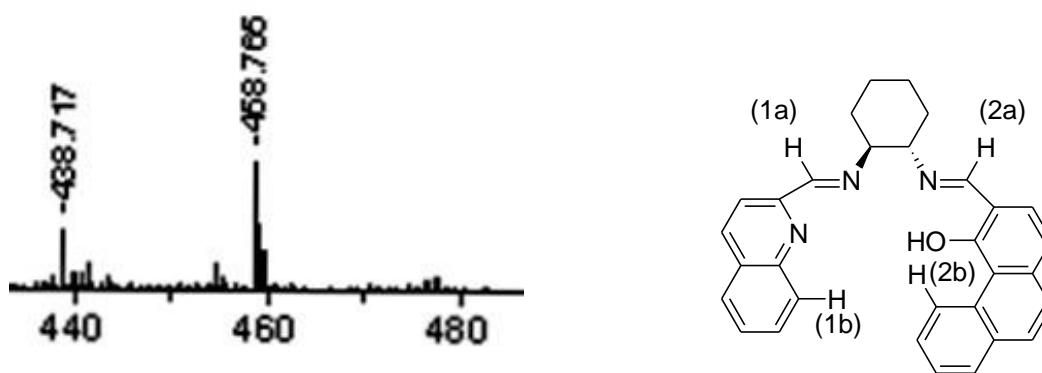


**Figure 3.11.** Molecular ion peak of ligand (*R,R*)-**2** at ESI-MS.

Comparison of the UV and CD spectra of the symmetrical salen ligand (with phenanthryl sidearms on both sides of the salen ligand (figure 3.13), with the non-symmetric one (ligand (*R,R*)-**2** shown in figure 3.12), showed that the chirality is very similar in both the cases.<sup>15</sup> The broad negative peak around 450 nm in UV is due to the absorption by the non-planar imine groups. The region from 220nm to 350 nm in the CD spectrum, is for the absorption by the phenanthryl and isoquinoline sidearms for ligand (*R,R*)-**2**. The strongest positive absorption peak is shifted to lower wavelength (245 nm) for the non-symmetric ligand (figure 3.11) compared to

the similar peak (255 nm) for the symmetric ligand (figure 3.12). However, the chirality is same for both symmetric and non-symmetric salen ligands.

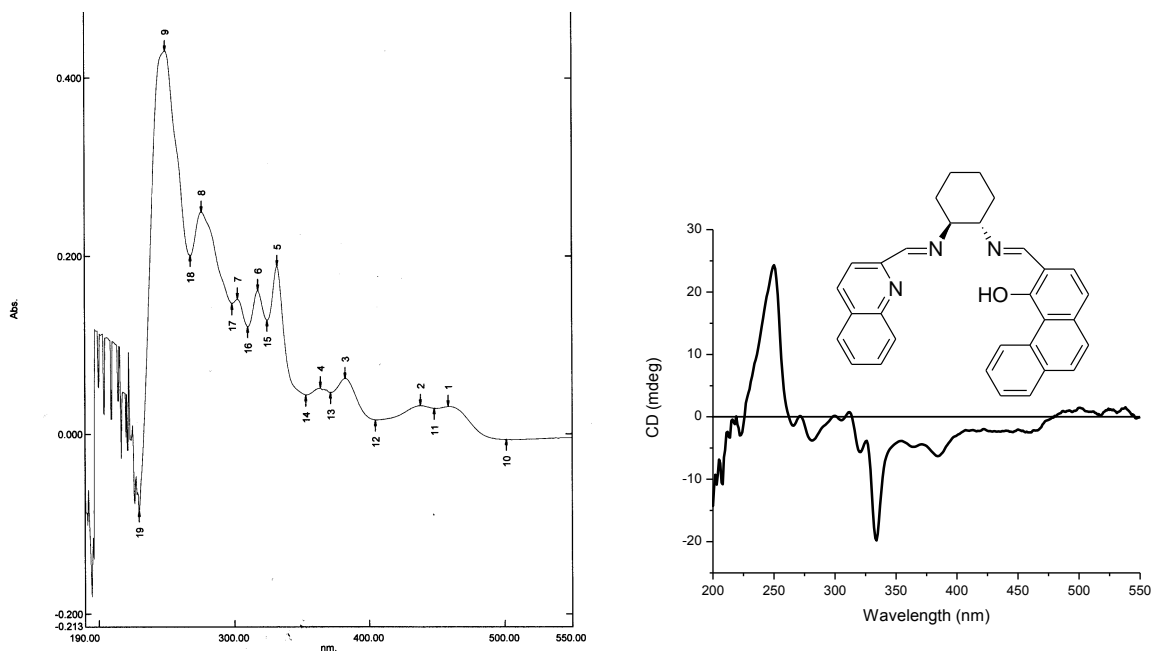


Figure 3.12. UV (left) and CD (right) spectra of *(R,R)*-2.

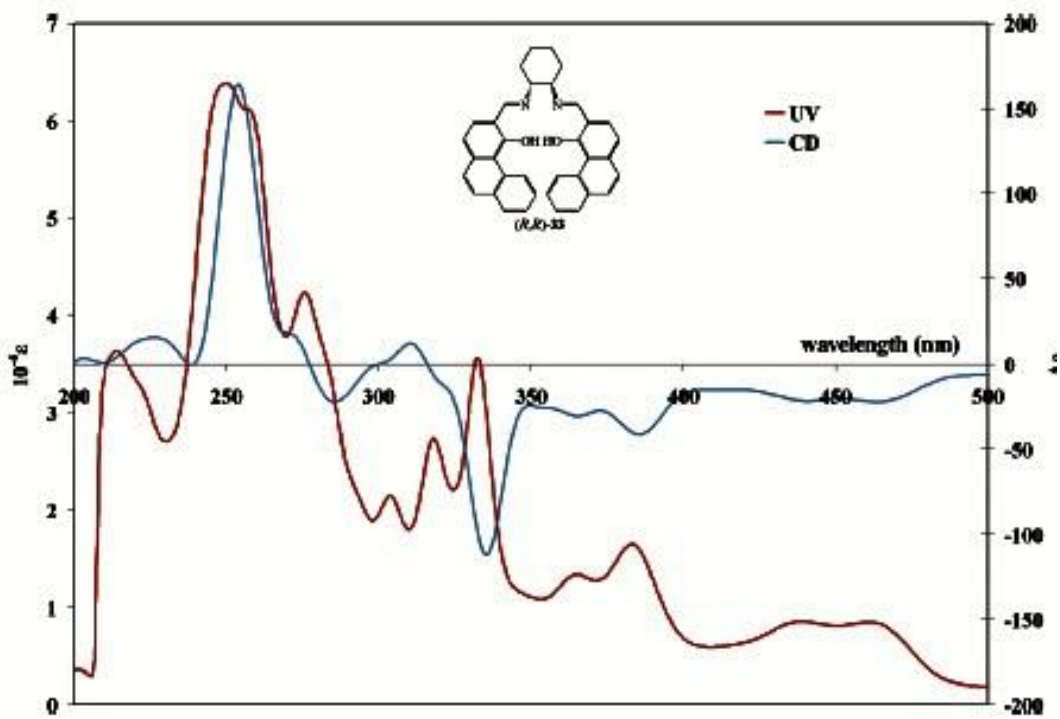
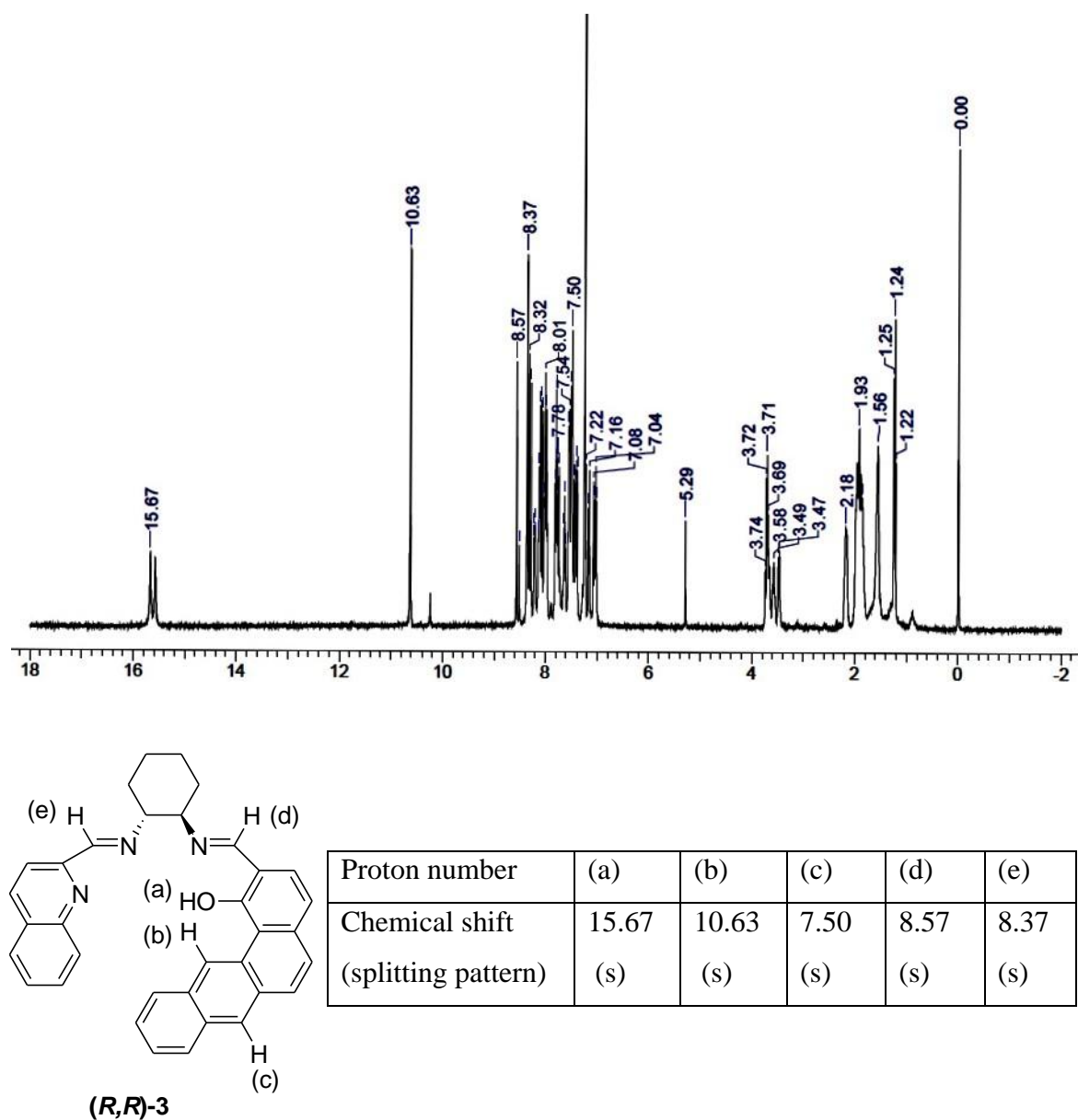


Figure 3.13. UV and CD spectra of symmetric salen ligand.<sup>15</sup>

Ligand **(R,R)-3** showed the presence of a molecular ion peak for the non-symmetrical salen ligand and the peak for symmetrical salen ligand with benz[a]anthryl sidearm on both sides in the high resolution MALDI-TOF.  $^1\text{H}$  NMR ( $\text{CDCl}_3$ , 400 MHz) showed the presence of a mixture of one symmetrical ligand (with benz[a]anthryl sidearms) and non-symmetrical ligand in the ratio of 20%:80%.  $^1\text{H}$  NMR ( $\text{CDCl}_3$ , 400 MHz) for ligand **(R,R)-3** with some assigned peaks are shown in figure 3.14. However, it is difficult to analyze from the  $^1\text{H}$  NMR data as most of the peaks overlap with each other. Ligand **(R,R)-3** was complexed with vanadyl(IV) acetylacetonate.



**Figure 3.14.**  $^1\text{H}$  NMR ( $\text{CDCl}_3$ , 400 MHz) (top) with some assigned peaks (bottom) for **(R,R)-3**.

Ligand **(R,R)-4** showed the presence of molecular ion peaks for both symmetrical and non-symmetrical salen ligands in ESI MS. <sup>1</sup>H NMR (CDCl<sub>3</sub>, 400 MHz) showed the presence of a mixture of symmetrical and non-symmetrical ligands. However, it is difficult to analyze their proportions from the NMR data as the peaks overlap with each other.

### 3.3.2 Synthesis and characterization of non-symmetrical Zn and V salen complexes

The zinc complex **C-1** was synthesized by stirring a solution containing zinc triflate and ligand **(R,R)-2** in ethanol at 55 °C for 24 hours (figure 3.15). A brown colored precipitate separated out from the solution. Vanadyl complexes were synthesized by stirring a mixture containing vanadyl acetylacetonate, ligand and excess sodium methoxide in 1:1 ethanol and CH<sub>2</sub>Cl<sub>2</sub> mixture for 12 hours (figure 3.15). A green colored precipitate separated out. Soxhlet extraction in CH<sub>2</sub>Cl<sub>2</sub> was done to purify the vanadyl complexes.

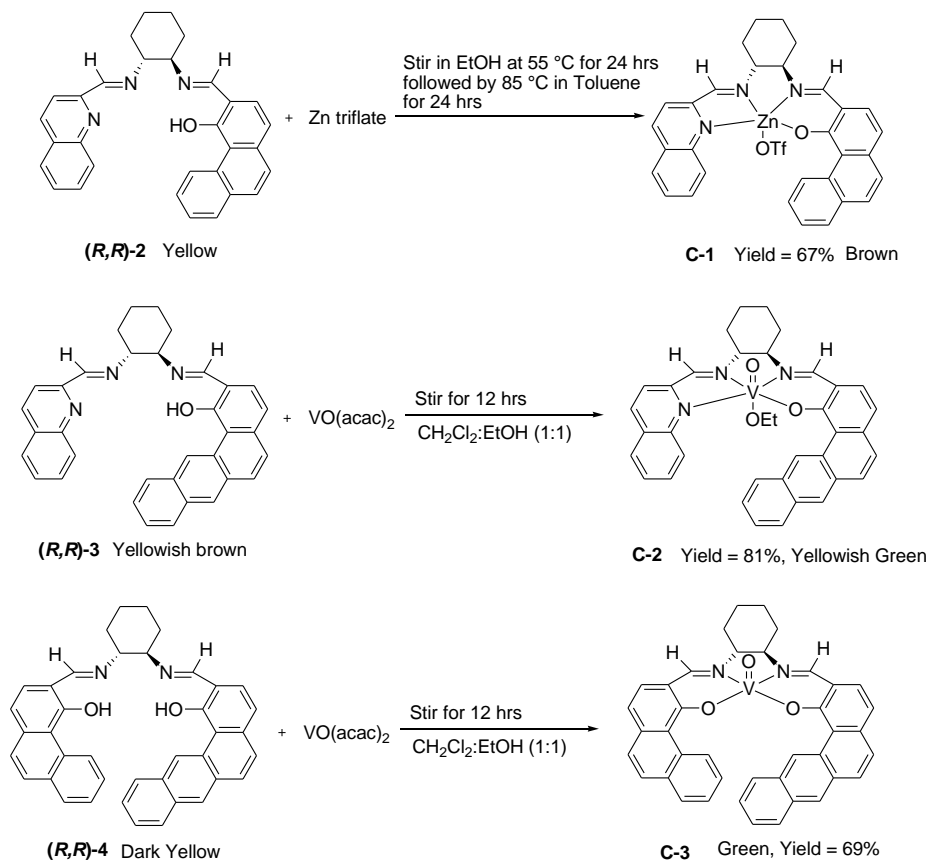


**Figure 3.15.** Synthesis of complexes **C-1**, **C-2** and **C-3**.

The chemical shifts and the splitting patterns of the easily identifiable protons from ligand (**R,R**)-**2** with the complex **C-1** were compared and showed in figure 3.16 and table 3.2. It is clear from the  $^1\text{H}$  NMR data that after complexation the imine protons as well as the bay proton showed downfield shifts. The absence of the phenolic-OH proton peak showed the involvement of the phenolic-OH group after complexation.

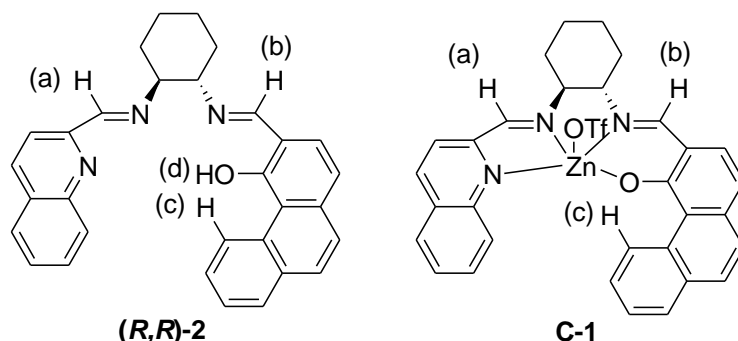


**Figure 3.16.** Comparison of the chemical shifts for few marked protons of the ligand and the zinc(II) complex for table 3.2.

**Table 3.2.** Chemical shifts and splitting patterns of the ligand and the complex (figure 3.14)

Proton number	(a)	(b)	(c)	(d)
Chemical shifts (ppm) (splitting pattern) ( <b>R,R</b> )- <b>2</b>	8.30 (s)	8.55 (s)	10.07 (s)	15.42 (s)
Chemical shifts (ppm) (splitting pattern) ( <b>C-1</b> )	9.82 (s)	10.00 (s)	13.58 (s)	none

Both complexes **C-2** and **C-3** showed broad  $^1\text{H}$  NMR spectra which are characteristics of paramagnetic complexes. The hydroxyl proton peaks have disappeared in the  $^1\text{H}$  NMR spectra after complexation and this shows the participation of the hydroxyl protons during complexation. The high resolution mass spectra for complex **C-3** showed the molecular ion peaks with appropriate isotopic ratios of both symmetrical and unsymmetrical vanadium(IV) salen complexes. Figure 3.17 is showing the molecular ion peak with the isotopic patterns for the desired unsymmetrical vanadyl(IV) salen complex (**C-3**) in the high resolution mass spectroscopy. The IR spectra of **C-2** and **C-3** showed the presence of  $\nu_{\text{V=O}}$  at  $824.08\text{ cm}^{-1}$  and at  $830.07\text{ cm}^{-1}$  respectively.

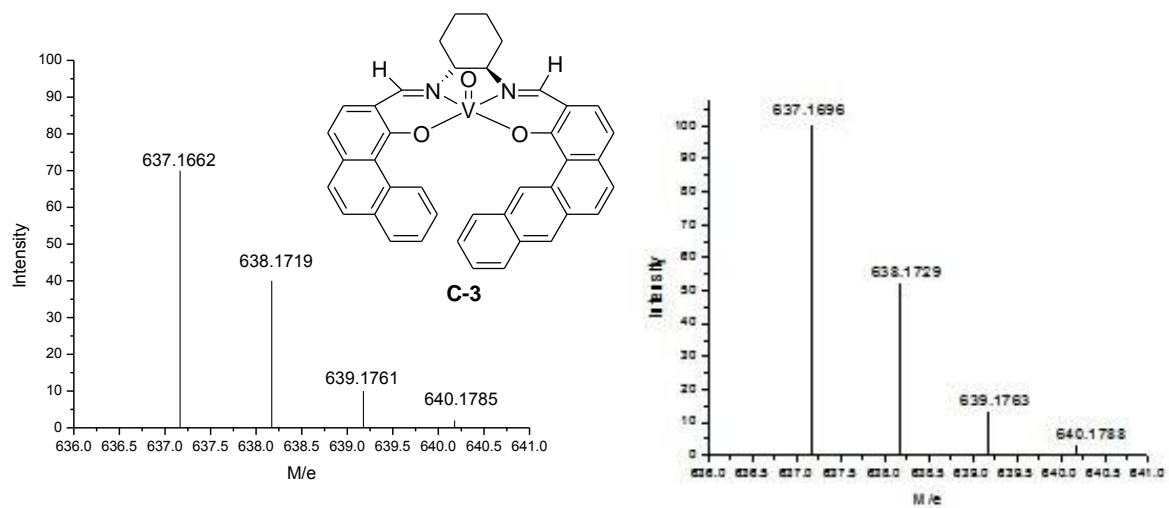
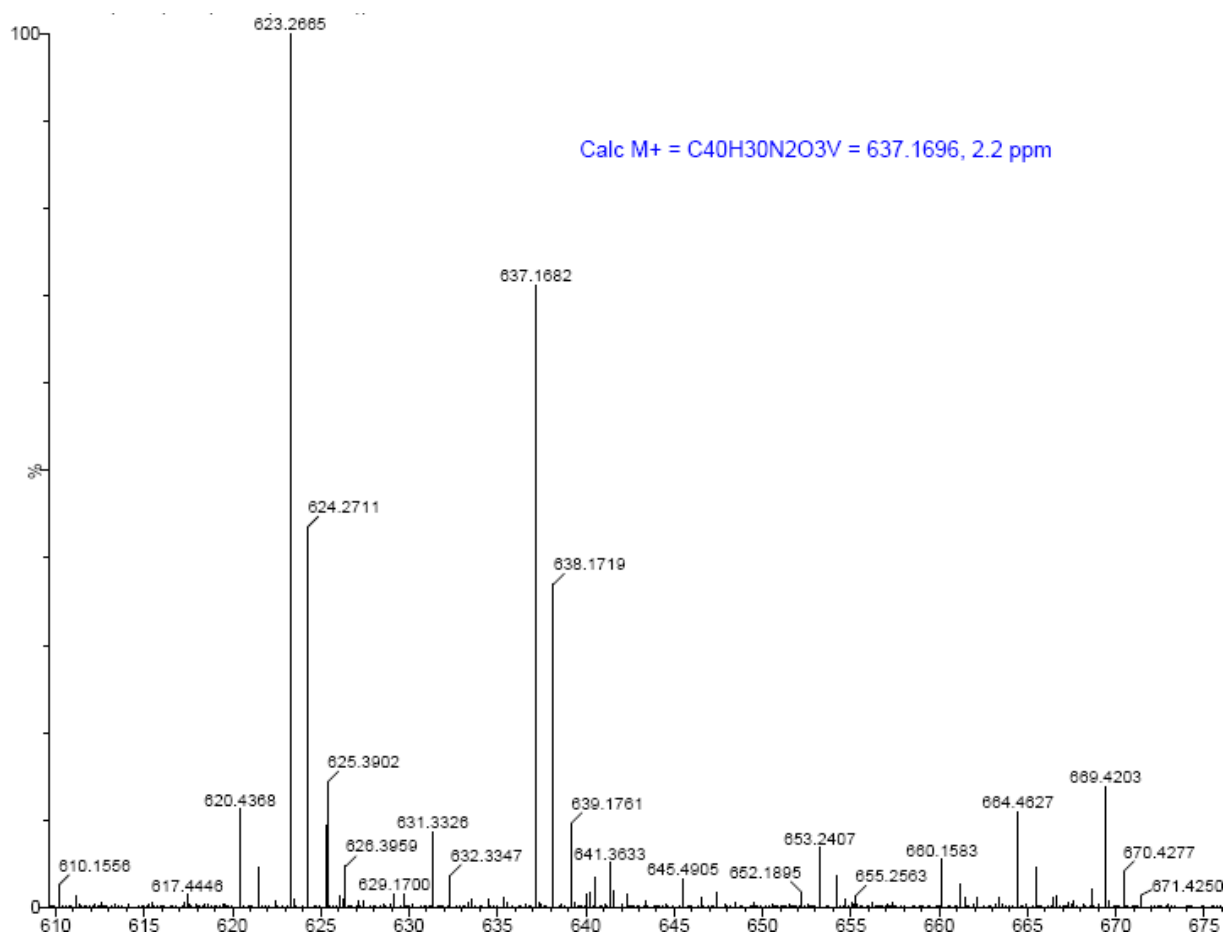


**Figure 3.17.** Complete mass spectrum (top) for unsymmetrical vanadyl(IV) salen complex (**C-3**) with simulated isotopic pattern (bottom right) and observed isotopic pattern (bottom left).

### 3.3.3 Asymmetric sulfoxidations by non-symmetrical vanadyl(IV) salen complexes

$C_1$  and  $C_2$  symmetric vanadyl(IV) salen complexes are well known chiral catalysts for asymmetric sulfoxidation reactions.<sup>16</sup> However,  $C_1$ -symmetric vanadyl(IV) salen complexes with two different sidearms in the salen ligand have not explored as chiral catalysts in asymmetric sulfoxidations to date. Due to the increased asymmetry in the ligand, these  $C_1$ -symmetric salen ligands may act as better chiral catalysts than their symmetric counterparts and this observation has reported many times in the literature.<sup>17</sup> Unfortunately, the mass spectral data showed that we failed to avoid the synthesis of a mixture of both symmetric and non-symmetrical salen ligands and so our sulfoxidation data looks quite similar to the previous data presented in chapter 1 with the symmetrical vanadyl(IV) salen complexes.

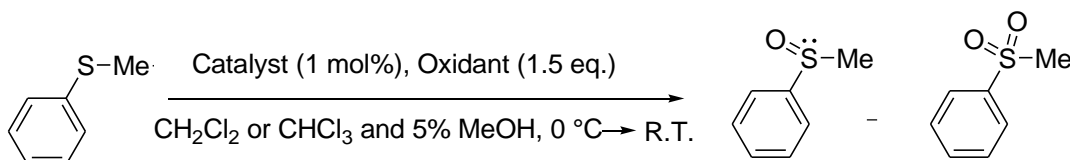


**Figure 3.18.** Sulfoxidation by catalysts **C-2** and **C-3**.

Catalytic activities of the vanadyl(IV) salen complexes (**C-2** and **C-3**) were examined in the sulfoxidation of phenylmethyl sulfide with H<sub>2</sub>O<sub>2</sub> and cumene hydroperoxide (CHP) as the terminal oxidants (figure 3.18). To compare the activities, these reactions were carried out for 16 hours and the temperature was monitored from 0 °C to room temperature. The reactions were performed in CH<sub>2</sub>Cl<sub>2</sub> and in CHCl<sub>3</sub> with 5% methanol (v/v) mixture. In acetonitrile, although the conversions were very high (up to 99%) the enantioselectivities (ee) were very low (around 2 to 3%).

Solvent polarity has a profound effect on the enantioselectivity of the product sulfoxide. It is observed that high polarity solvents such as acetonitrile or ethanol gave negligible ee (2 to 3%). The enantioselectivity increases to a small extent, when the reactions were carried out in a less polar solvent such as CH<sub>2</sub>Cl<sub>2</sub> and CHCl<sub>3</sub>. However, as the polarity of the CHCl<sub>3</sub> was increased by the addition of methanol from 0% to 5% (v/v), the enantioselectivity was increased and after 5% there were no significant changes in the enantioselectivity observed for the product



phenylmethyl sulfoxide. This phenomenon suggests that solvent polarity plays a crucial role in the enantioselectivity of the product.

Both catalysts **C-2** and **C-3** produce the *R* isomer of the phenylmethyl sulfoxide. Better conversions were observed when CHP was used as the oxidant rather than H<sub>2</sub>O<sub>2</sub>. However, the enantioselectivity was better when H<sub>2</sub>O<sub>2</sub> was used as the oxidant in the MeOH and CHCl<sub>3</sub> mixture. The reason might be the same as mentioned in chapter 1 (figure 1.37). The hydrogen bonding between the coordinated methanol and the oxidant may lock the geometry and therefore the oxidant can approach the coordinated sulfide from one particular side leading to the preferential formation of one isomer over the other. Catalyst **C-3** is a better catalyst overall both in terms of enantioselectivity and conversions than catalyst **C-2** and this implied that the catalyst with more extended sidearms act as a better catalyst than the one with less extended side arms. In table 3.3, we can see that the difference in conversions and enantioselectivity is small between catalysts **C-2** and **C-3**. For catalyst **C-3**, the selectivity for sulfoxide in the product is higher compared to catalyst **C-2**. The best catalytic results were observed for both the catalysts when the mole ratio of oxidant/substrate was 1.5.

**Table 3.3.** Sulfoxidation results by catalysts **C-2** and **C-3**

Catalyst	Oxidant	Solvent	Temp (°C)	Time (hr)	Sulfoxide (%)	Sulfone (%)	Sulfide (%)	ee (%)	Main isomer
<b>C-2</b>	H <sub>2</sub> O <sub>2</sub>	CHCl <sub>3</sub> and 5% MeOH	0 to R.T.	16	73	5	22	30	<i>R</i>
<b>C-2</b>	CHP	CH <sub>2</sub> Cl <sub>2</sub>	0 to R.T.	16	81	14	5	9	<i>R</i>
<b>C-3</b>	H <sub>2</sub> O <sub>2</sub>	CHCl <sub>3</sub> and 5% MeOH	0 to R.T.	16	89	6	5	35	<i>R</i>
<b>C-3</b>	CHP	CH <sub>2</sub> Cl <sub>2</sub>	0 to R.T.	16	94	2	4	16	<i>R</i>

ee of the product were measured by HPLC analysis. HPLC analysis was carried out with a DAICEL OD-H column (isopropanol:hexane 5:95). Retention times 17.82 mins for (*R*) and 20.91 mins for (*S*) isomers.

The proposed mechanism for the sulfoxidations catalysed by [VO-salen] has already been established.<sup>17</sup> We have predicted the mechanism for sulfoxidation catalysed by our C<sub>2</sub> symmetric [VO-salen] in figure 1.34 in chapter 1. It is believed that the binding of the sulfide to the

vanadium center is the rate determining step in the overall reaction sequence. We proposed that, at this step, the phenylmethyl sulfide can bind to the vanadium center in two possible ways shown in figures 3.19 and 3.20, leading to the two possible isomers (*R* or *S*) of the phenylmethyl sulfoxide. In this step, if the energy difference between the two possible binding modes of sulfide to the metal center is small, then the catalyst will give rise to low enantioselectivity in the product sulfoxides. Our calculated energy (by MM2 method) difference between the two possible ways of attachment of the sulfide to the vanadium center is only 0.45 kcal/mol and this small energy difference explains the generation of low enantiomeric excess in the product sulfoxides.

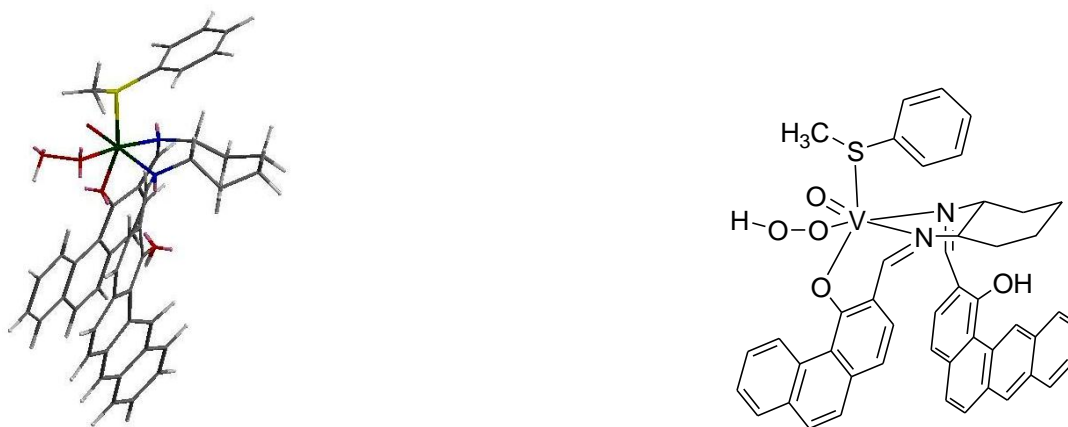


**Figure 3.19.** Three dimensional structure (left) and two dimensional representation (right) of the transition state leading to one possible isomer (*R* or *S*) ( $E = 22.9099$  kcal/mol).



**Figure 3.20.** Three dimensional structure (left) and two dimensional representation (right) of the transition state leading to the other possible isomer (*R* or *S*) ( $E = 23.3573$  kcal/mol).

### 3.4 Conclusions

An effort was made to synthesize the non-symmetrical salen complexes of zinc and vanadium, by the protecting group approach. This approach was successfully developed to synthesize non-symmetrical salen ligands when there are large differences in the electronic and steric properties of the two side arms as described by Weck et.al.<sup>18</sup> However, from our observations and results, it is clear that this approach of synthesizing non-symmetrical salen ligands are less effective when the electronic and steric differences between the two distinct side arms are not very high. From the high resolution mass spectra, it is clear that both symmetrical and non-symmetrical [VO-salen] complexes have formed. Further characterizations of these complexes will be only carried out after we develop a procedure to successfully synthesize these non-symmetrical salen ligands with our side arms where the electronic and steric differences are not high. Sulfoxidation by the non-symmetrical [VO-salen] complexes showed slightly better results (conversions and enantioselectivity) than the symmetrical counterparts but again these reported catalysis results are for the catalysts mixture (symmetrical and non-symmetrical). The slightly higher enantioselectivity by our catalytic systems proves that the non-symmetric salens are better chiral ligands than the symmetric ones.

### 3.5 Experimental Section

#### *General Methods*

All reactions were run under inert atmospheres unless otherwise noted. Solvents used in metallation reactions were stored over sodium benzophenone ketyl or calcium hydride, and degassed prior to transfer via high-vacuum line techniques. Inert gasses were purified by passage through 4 Å molecular sieves and a Engelhard Q5 catalyst bed. Preparation and workup of V (IV) compounds were completed under rigorously inert conditions to prevent oxidation or decomposition.

Elemental analyses were carried out by Desert Analytics of Tucson, Arizona. UV-vis spectra were obtained on a Varian Cary 500 spectrometer, and CD spectra on a JASCO 720 spectropolarimeter. Solution samples for these two techniques were prepared using dried spectroscopic grade THF, at concentrations that ranged between 1.5 and  $2.5 \times 10^{-5}$  M. A 1 cm path length

quartz cell was employed for the analysis.  $^1\text{H}$  and  $^{13}\text{C}$  NMR spectra were obtained on a Varian Unity 400 MHz spectrometer employing residual solvent protons or in some cases TMS as an internal standard. All mass spectra were recorded in LCT Premier (Waters corp, Milford, MA) mass spectrometer. All IR spectra were recorded in Nicolet 6700 FT-IR spectrometer.

***Trans*-1,2-diaminocyclohexane monohydrochloride (1)**

0.60 g (5.26 mmol) of *trans*-1,2 cyclohexyl-diamine was dissolved in 14 mL of ether. The solution was stirred vigorously while adding anhydrous HCl (1.22 M in ether, 4.2 mL, 5.26 mmol) dropwise over a period of 15 minutes. After complete addition of the acid, the solution was stirred for 10 hrs. The precipitate was collected by vacuum filtration, wash with excess ether and dry under vacuum to get a white powder (0.50 g, 80%).  $^1\text{H}$  NMR ( $\text{CDCl}_3$ , 400 MHz): 1.25 (m, 4H,  $\text{CH}_2\text{-CH}_2\text{-}$ ); 1.70 (m, 2H,  $\text{CH}_2\text{-CH-NH}_2$ ); 1.96 (m, 2H,  $\text{CH}_2\text{-CH-NH}_3^+$ ); 2.84 (m, 2H, CH-CH). MS:  $[\text{M}]^+$  (calculated 115.1235, found 115.1235).

**(1*R*,2*R*)(*N,N'*)-1,2-cyclohexanediiimine-(2-quinoline)(4-phenanthrenol) (*R,R*)-2**

*Trans*-1,2 cyclohexyldiamine monohydrogenchloride (0.096 g, 0.640 mmol), 2-quinoline carboxaldehyde (0.100 g, 0.640 mmol) and activated 4 Å molecular sieves were added to a 50 mL round bottom flask with a septum and a stir bar. Anhydrous ethanol and methanol (4 mL each) were added and the solution was stirred for 5 hrs. A brownish yellow colored precipitate appeared after 5 hrs. A solution of phenanthrolinaldehyde-1-ol (0.140 g, 0.640 mmol) in  $\text{CH}_2\text{Cl}_2$  (10 mL) was added, followed by the slow addition of triethyl amine (0.177 mL, 1.28 mmol) into the reaction mixture. The reaction mixture was allowed to stir for another 5 hrs. The reaction mixture was filtered through a pad of silica gel. Solvent was removed under reduced pressure to obtain a brownish yellow colored powder (0.150 g, 80% yield).  $^1\text{H}$  NMR ( $\text{CDCl}_3$ , 400 MHz):  $\delta$  1.20 (m, 2H, CH); 1.31 (m, 2H, CH); 1.95 (m, 2H, CH); 2.21 (m, 2H, CH); 3.60 (m, 2H, CH); 6.95 (d, 1H, CH); 7.10-7.15 (dd, 1H, CH); 7.10-7.20 (dd, 1H, CH); 7.22 (d, 1H, CH); 7.52 (m, 4H, ABMX pattern); 7.70 (m, 2H, CH); 7.76 (m, 2H, CH); 7.76 (dd, 1H, CH); 7.78 (dd, 1H, CH); 8.0 (m, 1H, CH); 8.05 (d, 1H, CH); 8.13 (d, 1H, CH); 8.23 (d, 1H, CH); 8.30 (s, 1H, imine proton); 8.49 (d, 1H, CH); 8.52 (s, 1H, imine proton, CH); 10.07 (d, 1H, bay-CH); 15.42 (s, 1H, OH).  $^{13}\text{C}$  NMR ( $\text{CDCl}_3$ , 400 MHz): 24.04, 30.00, 33.03, 34.00, 46.07, 69.32, 70.09, 72.03, 113.14, 114.03, 117.21, 118.24, 118.92, 124.51, 126.31, 126.53, 126.95, 128.10, 128.95, 129.21,

130.01, 130.85, 131.11, 132.00, 137.31, 137.94, 161.93, 163.14, 163.92, 164.34, 168.38. MS:  $[M]^{+1}$  458.765 (64%), 459.801 (22%), 460.851 (10%), 461.916 (4%). UV: several absorption peaks in pairs with higher and lower intensity due to  $\pi$  to  $\pi^*$  transition in two different side arms. CD: showed the chirality of the ligand in solution.

### **Zn(II)-(R,R)-2 complex (C-1)**

Zinc trifluoromethane sulfonate (0.103 g, 0.285 mmol) and **(R,R)-2** (0.130 g, 0.285 mmol) were suspended into dry ethanol (15 mL). The mixture was stirred for 24 hrs at 55 °C. After 24 hrs, ethanol was removed followed by addition of toluene (15 mL). The reaction mixture was heated to 80 °C and stirred for another 24 hrs. Toluene was removed under reduced pressure and the resulting brown precipitate was washed with toluene to afford the complex (0.914 g, 67% yield).  $^1\text{H}$  NMR ( $\text{CDCl}_3$ , 400 MHz): 1.24 (m, 1H, CH); 1.31 (m, 1H, CH); 1.53 (m, 1H, CH); 1.62 (m, 1H, CH); 1.87 (m, 1H, CH); 1.99 (m, 1H, CH); 2.4 (m, 1H, CH); 2.6 (m, 1H, CH); 2.7 (m, 1H, CH); 2.82 (m, 1H, CH); 7.20 (dd, 1H, CH); 7.45 (d, 1H, CH); 7.49 (d, 1H, CH); 7.71 (m, 4H, CH, ABMX pattern); 7.94 (d, 1H, CH); 8.21 (d, 1H, CH); 8.49 (m, 3H, CH, ABX pattern); 9.82 (s, 1H, CH, imine); 10.00 (s, 1H, CH); 13.58 (s, 1H, CH, bay proton).

### **(1R,2R)(N,N')-1,2-cyclohexanediimine-(2-quinoline)(2-benz[a]anthracen-1-ol)(R,R)-3**

*Trans*-1,2 cyclohexyldiamine monohydrogenchloride (0.096 g, 0.640 mmol), 2-quinoline carboxaldehyde (0.100 g, 0.640 mmol) and activated 4 Å molecular sieves were added to a 50 mL round bottom flask with a septum and a stir bar. Anhydrous ethanol and methanol (4 ml each) were added and the solution was stirred for 8 hrs. A brownish yellow colored precipitate appeared after 8 hrs. A solution of benzantracenaldehyde-1-ol (0.174 g, 0.640 mmol) in  $\text{CH}_2\text{Cl}_2$  (10 mL) was added, followed by the slow addition of triethyl amine (0.177 mL, 1.28 mmol) into the reaction mixture. The reaction mixture was allowed to stir for another 8 hrs. The reaction mixture was filtered through a pad of silica gel. Solvent was removed under reduced pressure to obtain a brownish yellow colored powder (0.128 g, 69% yield).  $^1\text{H}$  NMR ( $\text{CDCl}_3$ , 400 MHz):  $\delta$  1.21 (m, 2H, CH); 1.82-1.95 (m, 4H, CH); 2.21 (m, 2H, CH); 3.42 (m, 2H, CH); 7.02 (d, 1H, CH); 7.06 (d, 1H, CH); 7.16 (d, 1H, CH); 7.41 (d, 1H, CH); 7.45 (m, 2H, BM from ABMX system of isoquinoline ring); 7.50 (d, 1H, CH); 7.51 (m, 1H, CH); 7.54 (m, 1H, CH); 7.72 (d, 1H, CH); 8.03 (m, 2H, AX from ABMX system of isoquinoline ring); 8.10 (m, 2H, BM from

ABMX system of benzanthracene ring); 8.12 (s, 1H, imine proton attached to isoquinoline ring); 8.14 (m, 2H, AX from ABMX system of benzanthracene ring); 8.37 (s, 1H, imine proton attached to benzanthracene ring); 8.57 (s, 1H, CH); 10.68 (s, 1H, bay proton); 15.68-15.74 (d, 1H, O-H).  $^{13}\text{C}$  NMR ( $\text{CDCl}_3$ , 400 MHz):  $\delta$  24.48, 27.08, 33.02, 69.92, 70.99, 74.03, 114.94, 115.25, 117.68, 118.45, 118.53, 120.06, 120.66, 125.40, 125.55, 126.43, 126.60, 127.44, 127.55, 128.09, 129.86, 129.90, 130.86, 130.98, 131.28, 132.82, 136.59, 136.68, 137.25, 154.65, 163.13, 164.36, 165.39, 165.88, 168.06. MS:  $[\text{M}]^{+1}$  506.2221(66%), 507.2301 (20%), 508.2457 (10%), 509.2571 (4%).

#### **V(IV)-(R,R)-3 complex (C-2)**

Ligand **(R,R)-3** (0.101 g, 0.199 mmol) was dissolved in a mixture of  $\text{CH}_2\text{Cl}_2$  (5 mL) and EtOH (3 mL). To this solution vanadyl acetyl acetonate (0.053 g, 0.199 mmol) and sodium methoxide (0.043 g, 0.796 mmol) were added. The solution was stirred for 16 hrs followed by filtration to obtain a brown colored precipitate. The compound was further purified by soxalate extraction in dichloromethane. Pure brown colored compound was obtained after solvent removal under reduced pressure (0.953 g, 81% yield).  $^1\text{H}$  NMR ( $\text{CDCl}_3$ , 400 MHz): broad peaks suggest paramagnetic compound. MS:  $[\text{C}_{70}\text{H}_{56}\text{N}_6\text{O}_3\text{VLi}]^+$  1086.3458 (79%), 1087.3671 (16%), 1088.3841 (4%), 1089.3871 (1%). IR:  $\nu_{\text{V=O}}$  824.07  $\text{cm}^{-1}$ .

**(1R,2R)(N,N')-1,2-cyclohexanediimine-(2-phenanthrene)(2'-benz[a]anthracen-1-ol) (R,R)-4**  
*Trans*-1,2 cyclohexyldiamine monohydrogenchloride (0.150 g, 1.00 mmol), phenanthraldehyde-1-ol (0.222 g, 1.00 mmol) and activated 4 Å molecular sieves were added to a 50 mL round bottom flask with a septum and a stir bar. Anhydrous ethanol and methanol (4 mL each) were added and the solution was stirred for 8 hrs. A brownish yellow colored precipitate appeared after 8 hrs. A solution of benzanthracenaldehyde-1-ol (0.272 g, 1.00 mmol) in  $\text{CH}_2\text{Cl}_2$  (10 mL) was added, followed by the slow addition of triethyl amine (0.279 mL, 2.00 mmol) into the reaction mixture. The reaction mixture was allowed to stir for another 10 hrs. The reaction mixture was filtered through a pad of silica gel. Solvent was removed under reduced pressure to obtain a brownish yellow colored powder (0.280 g, 72% yield).  $^1\text{H}$  NMR ( $\text{CDCl}_3$ ):  $\delta$  0.87 (m, 2H, CH); 1.26 (m, 2H, CH); 2.0 (m, 2H, CH); 2.18 (m, 2H, CH); 3.10 (m, 2H, CH); 7.0 (d, 1H, CH); 7.07 (s, 1H, CH); 7.13 (m, 2H, CH); 7.21 (d, 1H, CH); 7.30 (m, 2H, BM from ABMX

system); 7.56 (m, 2H, AX from the ABMX system); 7.59 (m, 1H, CH); 7.73 (dt, 1H, CH); 7.77 (d, 1H, CH); 7.80 (d, 1H, CH); 7.86 (d, 1H, CH); 8.05 (m, 1H, CH); 8.20 (m, 1H, CH); 8.21 (s, 1H, imine proton); 8.34 (s, 1H, imine proton); 8.42 (m, 2H, BM from ABMX system); 10.06-10.09 (m, 2H, AX from ABMX system); 10.37 (s, 1H, bay proton); 10.59 (s, 1H, bay proton); 15.46 (s, 1H, O-H); 15.66 (s, 1H, O-H).  $^{13}\text{C}$  NMR ( $\text{CDCl}_3$ , 400 MHz): 32.09, 45.87, 70.14, 70.34, 71.19, 117.87, 117.98, 118.56, 120.43, 124.75, 125.32, 126.11, 126.47, 127.10, 127.33, 127.86, 127.96, 128.06, 128.16, 128.52, 128.77, 128.96, 129.10, 129.26, 129.87, 130.01, 130.23, 130.69, 130.99, 131.29, 131.79, 132.21, 132.47, 137.26, 162.32, 163.96 (1 signal is missing). MS:  $[\text{M}]^+$  573.2542 (66%), 574.2575 (20%), 575.2609 (10%), 576.2705 (4%).

#### **V(IV)-(R,R)-4 complex (C-3)**

Ligand **(R,R)-4** (0.700 g, 1.22 mmol) was dissolved in a mixture of  $\text{CH}_2\text{Cl}_2$  (10 mL) and EtOH (5 mL). To this solution vanadyl acetylacetonate (0.324 g, 1.22 mmol) and sodium methoxide (0.727 g, 12.23 mmol) were added. The solution was stirred for 16 hrs followed by filtration to obtain a green colored precipitate. The compound was further purified by soxalate extraction in dichloromethane. Pure green colored compound was obtained after solvent removal under reduced pressure (0.502 g, 69% yield).  $^1\text{H}$  NMR ( $\text{CDCl}_3$ , 400 MHz): broad peaks suggest paramagnetic compound. MS:  $[\text{M}]^+$  637.1682 (53%), 638.1719 (35%), 639.1761 (12%). IR:  $\nu_{\text{V=O}}$  830.08  $\text{cm}^{-1}$ .

**General Procedure for Sulfoxidations:** All sulfoxidation reactions are carried out by 1 mol% of catalyst. 1mol% of catalyst was dissolved in dichloromethane (3mL) inside a two neck R.B. under argon. The mixture was stirred in inert atmosphere for 10 minutes. 100 mol% phenyl methyl sulfide was added followed by additional 15 minutes of stirring. The entire system was cooled to 0 °C. 110 mol% oxidant (hydrogen peroxide or cumene hydroperoxide) was added to the mixture slowly for a period of 2 hrs. The mixture was additionally stirred for 16 hrs. A saturated solution of sodium sulfite was added to quench the reaction. The reaction mixture was extracted with dichloromethane followed by drying over sodium sulfate. The product was purified by flash column chromatography in 1:3 ethyl acetate:hexane. Pure sulfoxide was analysed by  $^1\text{H}$  NMR ( $\text{CDCl}_3$ , 400 MHz): 3.72 (s, 3H,  $\text{CH}_3$ ); 7.5 (m, 3H, CH); 7.6 (m, 2H, CH). Enantiomeric excess of the phenyl methyl sulfoxide was determined by HPLC analysis with a

Daicel Chiralcel OD-H column. Hexane and isopropanol mixture (90:10) was used as the eluent. The *R* isomer and the *S* isomer elutes at 17 and 20 minutes respectively.

### 3.6 References

1. "Utilization of homogeneous and supported chiral metal(salen) complexes in asymmetric catalysis" Canali, L.; Sherrington, D. C. *Chem. Soc. Rev.* **1999**, 28, 85-93.
2. "Enantioselective epoxidation of unfunctionalized olefins catalyzed by salen manganese complexes" Zang, W.; Loebach, L. J.; Wilson, S. R.; Jacobsen, E. N. *J. Am. Chem. Soc.* **1990**, 112, 2801-2803.
3. "Catalytic asymmetric epoxidation of unfunctionalized olefins" Irie, R.; Noda, K.; Ito, Y.; Matsumoto, N.; Katsuki, T. *Tetrahedron Lett.* **1990**, 31, 7345-7348.
4. "Electronic effects in (salen)Mn-based epoxidation catalysts" Cavallo, L.; Jacobsen, H. *J. Org. Chem.* **2003**, 68, 6202-6207.
5. "Application of new unsymmetrical chiral Mn(III), Co(II, III) and Ti(IV) salen complexes in enantioselective catalytic reactions" Kim, G. J.; Shin, H. J. *Catal. Lett.* **1999**, 63, 83-90.
6. "Polymer bound chiral (salen)Mn(III) complex as heterogeneous catalyst in rapid and clean enantioselective epoxidation of unfunctionalized olefins" Minutolo, F.; Pini, D.; Salvadori, P. *Tetrahedron Lett.* **1996**, 37, 3375-3378.
7. "Salalen: a hybrid salen/salen tetradentate [ONNO] type ligand and its coordination behavior with group IV metals" Yeori, A.; Gendler, S.; Groysman, S.; Goldberg, I.; Kol, M. *Inorg. Chem. Commun.* **2004**, 7, 280-282.
8. "Unsymmetrical chiral salen Schiff base ligands: synthesis, and use in metal based asymmetric epoxidation reactions" Renehan, M. F.; Schanz, H. J.; Mc Gariggle, E. M.; Dalton, C. T.; Daly, A. M.; Gilheany, D. G. *J. Mol. Catal. A* **2005**, 231, 205-220.
9. "Selective epoxidation of unfunctionalized olefins catalyzed by unsymmetric Mn(III) Schiff base complexes" Du, X. D.; Yu, X. D. *J. Mol. Catal. A* **1997**, 126, 109-133.
10. Kureshi, R. I.; Khan, N. H.; Abdi, S. H. R.; Iyer, P.; Patel, S. T. *Polyhedron*, **1996**, 110, 33-40.



11. "Unsymmetrical salen ligands: synthesis and use in chromium mediated asymmetric epoxidation" Daly, A. M.; Dalton, C. T.; Renehan, M. F.; Gilheany, D. G. *Tetrahedron Lett.* **1999**, *40*, 3617-3620.
12. "Unsymmetrical salen type ligands: high yield synthesis of salen type Schiff bases containing two different benzaldehyde moieties" Campbell, E. J.; Nguyen, S. T. *Tetrahedron Lett.* **2001**, *42*, 1221-1224.
13. "Copper(II) and nickel(II) complexes of unsymmetrical tetradentate Schiff base ligands" Atkins, R.; Brewer, G.; Kokot, E.; Mockler, G. M.; Sinn, E. *Inorg. Chem.* **1985**, *24*, 127-134.
14. "A convenient synthetic route for the preparation of *non*-symmetric metallo-salphen complexes" Kleij, A. W.; Tooke, D. M.; Spek, A. L.; Reek, J. N. H. *Eur. J. Inorg. Chem.* **2005**, 4626-4634.
15. "Iron(II) and zinc(II) monohelical binaphthyl salen complexes with overlapping benz[a]anthryl sidearms" Wiznycia, A. V.; Desper, J.; Levy, C. J. *Dalton Trans.* **2007**, 1520-1527.
16. "Synthesis of an optically active Al(salalen) complex and its application to the catalytic hydrophosphonylation of aldehydes and aldimines" Saito, B.; Egami, H.; Katsuki, T. *J. Am. Chem. Soc.* **2007**, *129*, 1978-1986.
17. "Catalytic asymmetric oxidations using optically active (salen)manganese(III) complexes as catalysts" Katsuki, T. *Coord. Chem. Rev.* **1995**, *140*, 189-214.
18. "Enhanced cooperativity in hydrolytic kinetic resolution of epoxides poly(styrene) resin-supported dendronized Co-(salen) catalysts" Goyal, P.; Zheng, X.; Weck, M. *Adv. Synth. Catal.* **2008**, *350*, 1816-1822.

# CHAPTER 4 - Sulfoxidations by $C_1$ Symmetric (*S*)-Nobin Backbone Helical Vanadium Schiff Base Complexes

## 4.1 Abstract

$C_1$  symmetric (*S*)-NOBIN backbone helical Schiff base ligands with phenanthryl and benz[a]anthryl sidearms having tridentate ONO donor sites, were synthesized and characterized. Vanadium(IV) complexes were synthesized with these tridentate Schiff base ligands and characterized. These complexes were used as asymmetric catalysts in sulfoxidations reactions. They showed moderate activity as chiral catalysts compared to other vanadium(IV) tridentate ligands used so far.

## 4.2 Introduction

Chiral sulfoxides are very important compounds as chiral auxiliaries in asymmetric carbon-carbon bond formation reactions and as bioactive reagents in the pharmaceuticals industry.<sup>1, 2</sup> One example of a drug containing chiral sulfoxide group in its structure is esomeprazole.<sup>3</sup> It is observed that, esomeprazole, which is a very important drug for the treatment of stomach ulcers, only the *S* form is active as a drug whereas the *R* form and the racemic are not. Recently, enantioselective oxidation of sulfides catalyzed by the different transition metals like titanium,<sup>4</sup> vanadium,<sup>5</sup> manganese,<sup>6</sup> iron,<sup>7</sup> has been extensively studied. Salen ligands with tetradentate  $N_2O_2$  coordination mode are widely used as chiral ligands for asymmetric reactions with transition metals.<sup>8</sup> Typically the tetradentate with  $N_2O_2$  coordination mode salen ligands are synthesized by the double condensations between the diamine backbone with the two side arms which are generally derivatives of benzaldehyde.<sup>8</sup> Vanadium(IV) complexed with the tetradentate salen ligands are well known as chiral catalysts in asymmetric sulfoxidations. However, instead of double condensations to form a tetradentate  $N_2O_2$  donor salen ligand, if the backbone contains one amine and one hydroxyl group, then monocondensation occurs between the amine and the derivative of salicylaldehyde, producing a Schiff base unit with a tridentate ONO donor sites (figure 4.8). There are not many reports of vanadium(IV) complexed with tridentate ONO-donor Schiff base ligands used in asymmetric

sulfoxidations. Monomeric vanadium(IV) complexes derived from vanadyl(IV) acetylacetonate with tridentate (ONO donor) Schiff base ligands are usually  $C_1$  symmetric. Apart from the tridentate Schiff base ligand with the ONO donor set, the other two positions in the square pyramidal geometry of the central vanadium(IV) are usually occupied by the axially coordinated oxygen atom and a coordinating molecule, such as a solvent molecule in this case (figure 4.1). In some cases it is known that the chiral induction by catalysts increase with the asymmetry in the catalyst's structure. This phenomenon stimulated us to synthesize  $C_1$  symmetric vanadium(IV) Schiff base complexes and to test their activity in the chiral sulfoxidations reactions.

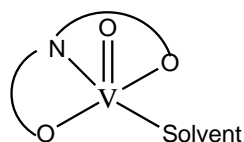


**Figure 4.1.**  $C_1$  symmetric vanadium(IV) schiff base complex.

The structurally well characterized oxo-vanadium(V) complex having an amino acid-derived tridentate O-N-O type Schiff base ligand was reported by Fujita and coworkers as an effective catalyst that produce optically active phenylmethyl sulfoxide in the asymmetric oxidation of the phenylmethyl sulfide with *tert*-butyl hydroperoxide as the oxidant (figure 4.2).<sup>9</sup> However, even with 10 mol% of catalyst, the highest enantioselectivity reached was only 14% ee.

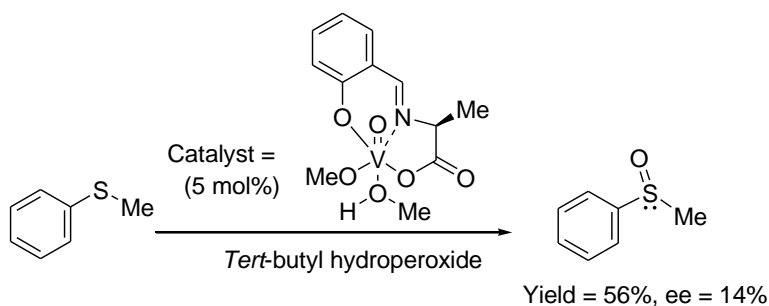


**Figure 4.2.**  $C_1$  symmetric vanadium(IV) Schiff base complex for asymmetric sulfoxidations.

In the light of this result, the behavior of the oxidation catalyst formed in-situ from Schiff base and vanadyl(IV) acetylacetonate introduced by Bolm and Bienewald in 1995 was

remarkable (figure 4.3).<sup>10</sup> For example, this system with 1 mol% of the catalyst was sufficient to produce optically active methylphenyl sulfoxides with 85% ee. Furthermore, the simple reaction conditions which allow one to perform the catalysis in open vessels and the use of environmentally benign oxidant, such as, H<sub>2</sub>O<sub>2</sub> make this catalysis particularly attractive for the large scale applications. However, it is observed that the ligand structure plays a crucial role in determining the enantioselectivity of the product phenylmethyl sulfoxide. An aryl ring at the 6 position and an electron withdrawing NO<sub>2</sub> group at the 4 position of the parent salicylaldene ring with a bulky *tert*-butyl group in the side arm of the ligand (as shown in figure 4.3) is the most active catalyst in the chiral sulfoxidations reactions.<sup>10</sup>

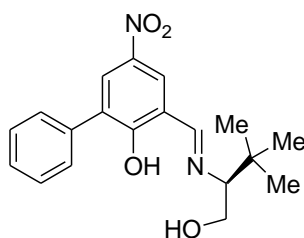


**Figure 4.3.** Bolm and Bienewald's tridentate ligand for vanadium(IV) catalyzed sulfoxidation.<sup>10</sup>

Since the discovery of the simple tridentate Schiff base ligands, readily available from salicylaldehydes and amino alcohols, introduced by Bolm and Bienewald, a number of research groups have tried to modify the tridentate Schiff base ligand system to achieve better enantioselectivity in asymmetric sulfoxidations.<sup>10</sup> However, a number of studies were made in order to elucidate the mechanism of sulfoxidations catalyzed by tridentate vanadium(IV) Schiff base complexes. <sup>51</sup>V NMR studies revealed the presence of various species under catalytic conditions. On the basis of the <sup>51</sup>V NMR data Bolm and Bienewald suggested the formation of diastereomeric vanadium(V) species (a) and (b) with oxoperoxo group as the active species in the oxidation of sulfides (figure 4.4).<sup>10</sup>

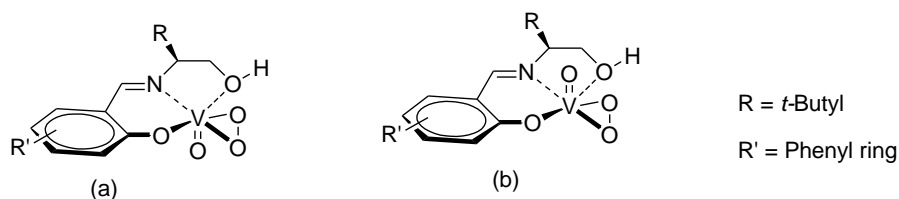


**Figure 4.4.** Diastereomeric vanadium(V) species (a) and (b).

Two important  $C_2$  symmetric scaffolds of chiral molecules used extensively for the synthesis of chiral catalysts, with axial chirality are 1,1'-bi-2-naphthol (BINOL) and 1,1'-bi-2-naphthylamine (BINAM).<sup>11</sup> 2-Amino-2'-hydroxy-1,1'-binaphthyl (NOBIN) could be considered as the hybrid analogue of BINOL and BINAM (figure 4.5). In 1991, Kocovsky first reported about NOBIN and since then it has been recognized as an important molecule for constructing chiral ligands for asymmetric catalysis.<sup>12</sup> In the last 10 years enantiopure NOBIN has been widely used in asymmetric catalysis in many different reactions, such as alkyl addition to aldehydes and  $\alpha$ ,  $\beta$ -unsaturated ketones, Mukaiyama type aldol reactions, hetero-Diels-Alder reactions, and cyclopropanations.<sup>13, 14, 15, 16</sup>

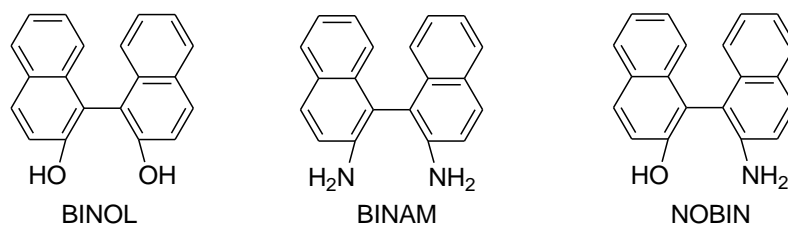


**Figure 4.5.** Structures of BINOL, BINAM and NOBIN.

Enantiopure BINAM is a well known chiral synthon used to synthesize vanadium salen complexes and these complexes showed moderate to good activities in asymmetric sulfoxidation reactions.<sup>11</sup> However, so far, no reports are found with enantiopure NOBIN used as chiral synthon to synthesize vanadium(IV) Schiff base complexes which were used as asymmetric catalysts in sulfoxidations reactions. In this chapter we wanted to investigate the chiral induction ability of these vanadium(IV) Schiff base complexes with the (*S*)-NOBIN backbone, in sulfoxidation reactions. Moreover, we wanted to investigate the effect of the helicity on the chiral induction by extending the side arm of the tridentate Schiff base ligands. An example of one of the  $C_1$  symmetric catalysts used in this chapter is shown in figure 4.6. The fifth coordination position is occupied by the coordinating solvent molecule and the oxidation state of the central vanadium is +4. There are three trajectories (a, b and c) in which the incoming nucleophile can approach the central metal are shown in the figure 4.6. Among the three possible directions, “a” and “b” have partial blocking by the backbone and from the side arm respectively. Direction “c” seems to be the most probable approach of the incoming nucleophile to the metal center. The two Schiff base ligands used to synthesize complexes with vanadium(IV) are shown

in figure 4.7. Both of them having the tridentate ONO donor sites, however, the only difference lies in their side arms.

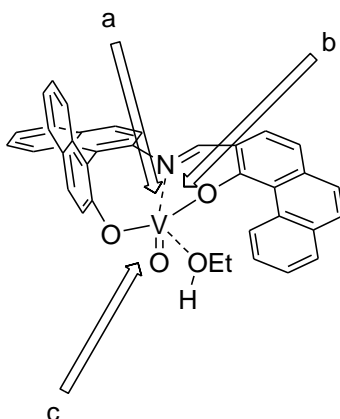


**Figure 4.6.** Possible directions of approach of the nucleophile to the metal center.

We observed that (*S*)-NOBIN backbone vanadium(IV) Schiff base complexes are unstable with prolonged air exposure. So, we can conclude that due to the lack of a tetradentate salen ligand, vanadium(IV) oxidizes to form vanadium(V) where the fifth coordination position is occupied by the methoxide group from the excess sodium methoxide (figure 4.7). Complex **C-2** has more helical nature than complex **C-1** due to the presence of a benz[*a*]anthryl sidearm.

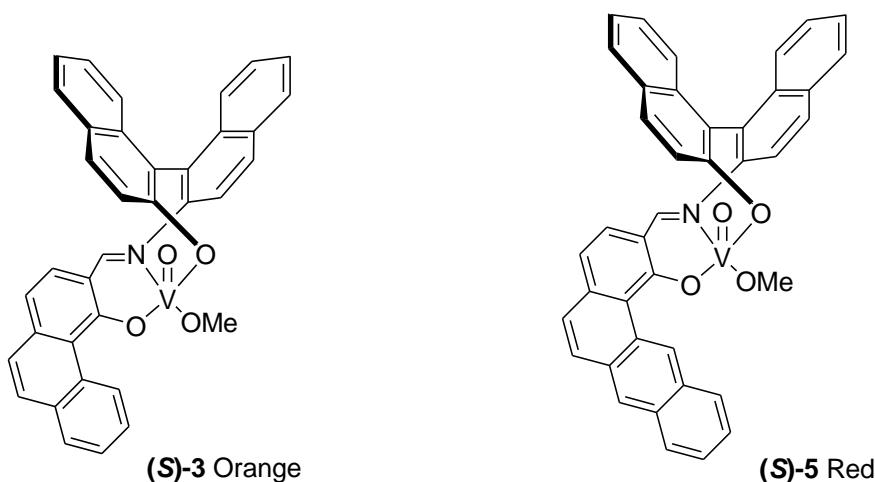
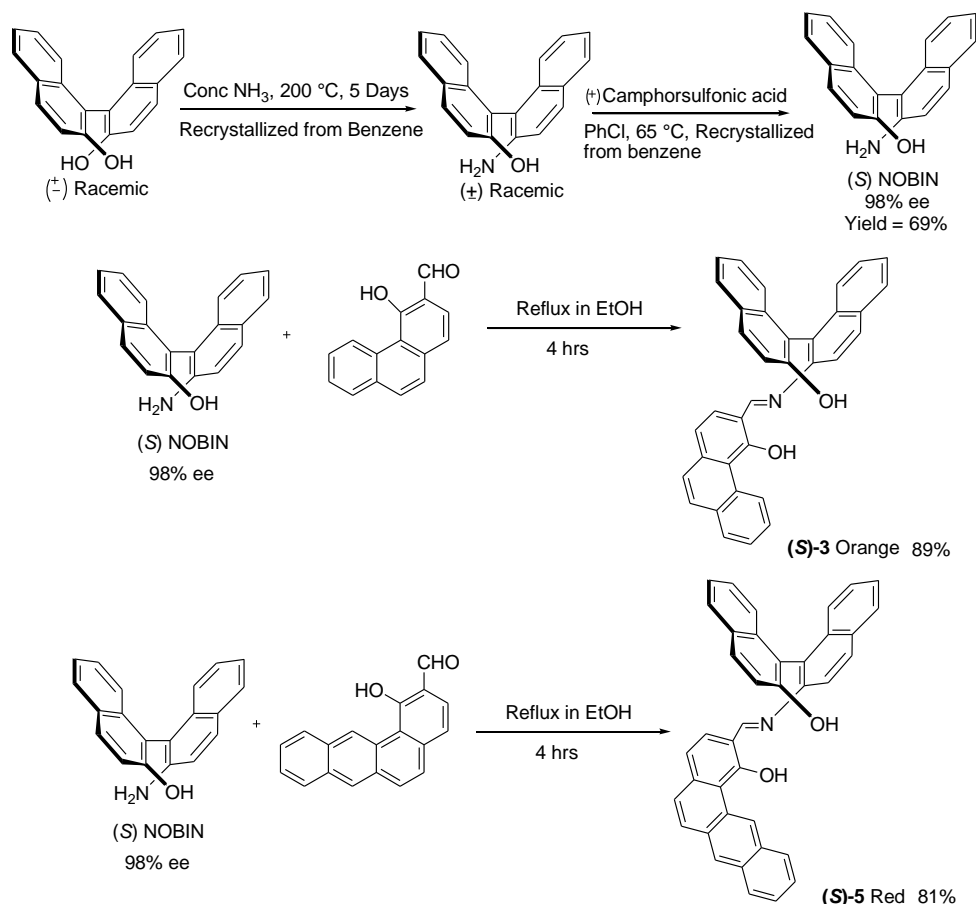


**Figure 4.7.** Tridentate Schiff base ligands used for the complexation with vanadium(V).

## 4.3 Results and discussions

### 4.3.1 Synthesis of ligands (S)-3 and (S)-5

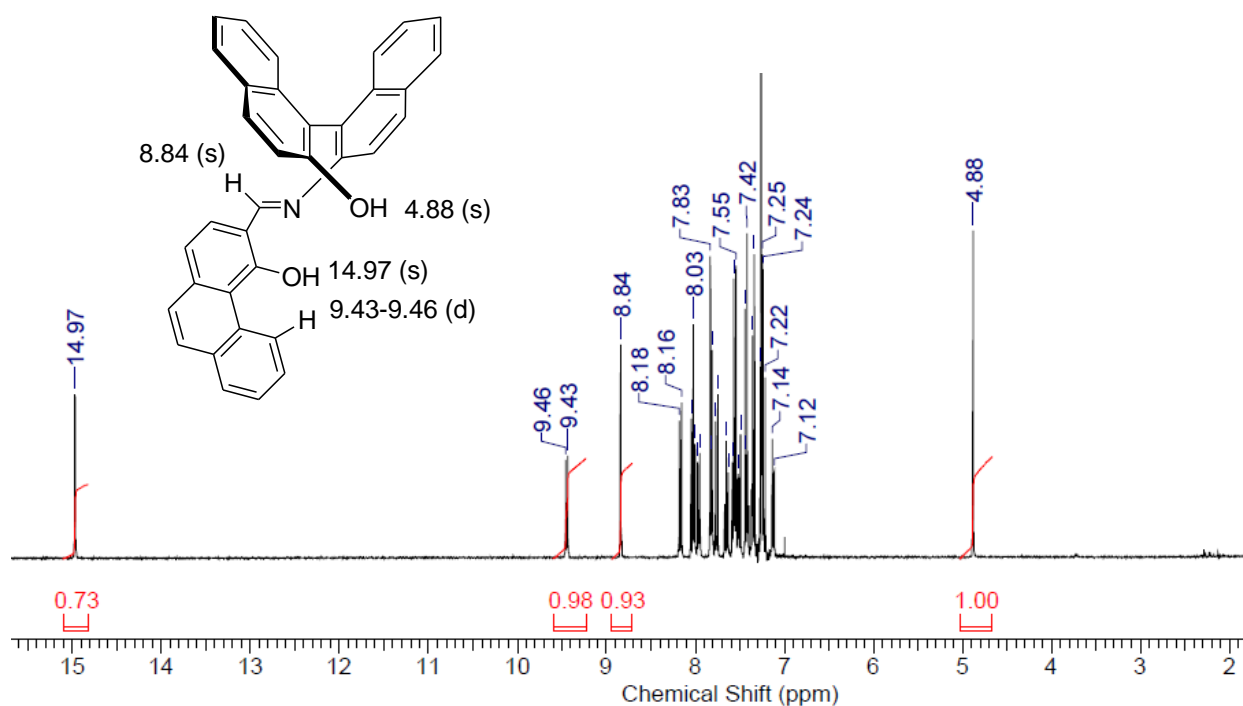
Ligands (S)-3 and (S)-5 were synthesized starting from racemic 1,1'-bi-2-naphthol (figure 4.8). The racemic binaphthol was first converted into racemic 1-amino-1'-hydroxy-binaphthyl by the treatment of concentrated ammonia at 200 °C for 5 days. Intramolecular hydrogen bonding is the driving force for the reaction to stop after replacing one hydroxyl group with one amine to produce 1-amino-1'-hydroxy-binaphthyl.<sup>6</sup> In the next step, chiral resolution was carried out to synthesize (S)-NOBIN from *racemic* 1-amino-1'-hydroxy-binaphthyl. The product (S)-NOBIN was synthesized in three separate batches with 81%, 90% and 98% ee to evaluate the effect of chiral backbone on the enantioselectivity of the product chiral sulfoxides. The chiral NOBIN was condensed with phenanthryl and benz[a]anthryl to produce the desired tridentate ligands (S)-3 and (S)-5 as orange and the red colored powders respectively.



**Figure 4.8.** Synthesis scheme of (S)-NOBIN backbone Schiff base ligand.

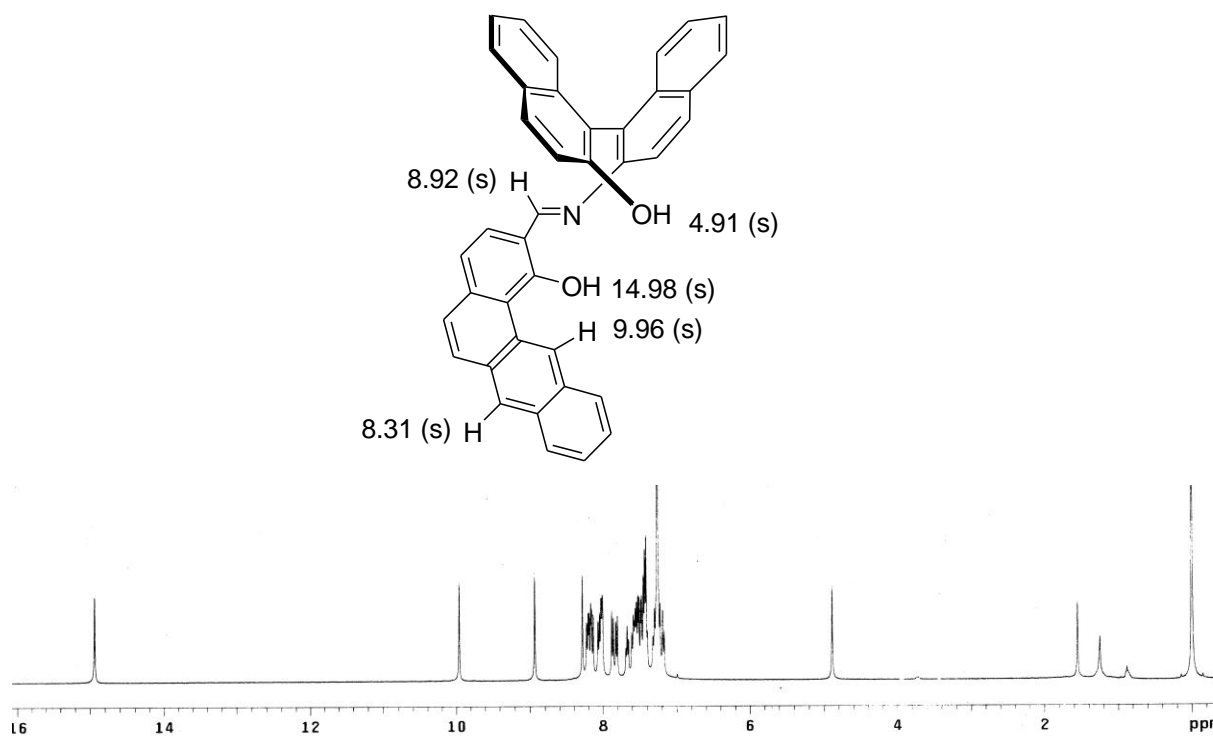
### 4.3.2 Characterization of ligands (S)-3 and (S)-5

$^1\text{H}$  NMR ( $\text{CDCl}_3$ , 400MHz) spectrum with a few important peaks for ligand (S)-3 and (S)-5 are shown in figure 4.9 and 4.10 respectively. Due to the presence of fused phenyl rings there are extensive couplings between the adjacent protons and this causes a complicated second order spectrum. The bay proton (the most deshielded proton in the side arm) for (S)-3 (figure 4.9) shows a doublet at 9.43-9.46 ppm whereas the bay proton for (S)-5 (figure 4.10) comes as a singlet at 9.96 ppm.



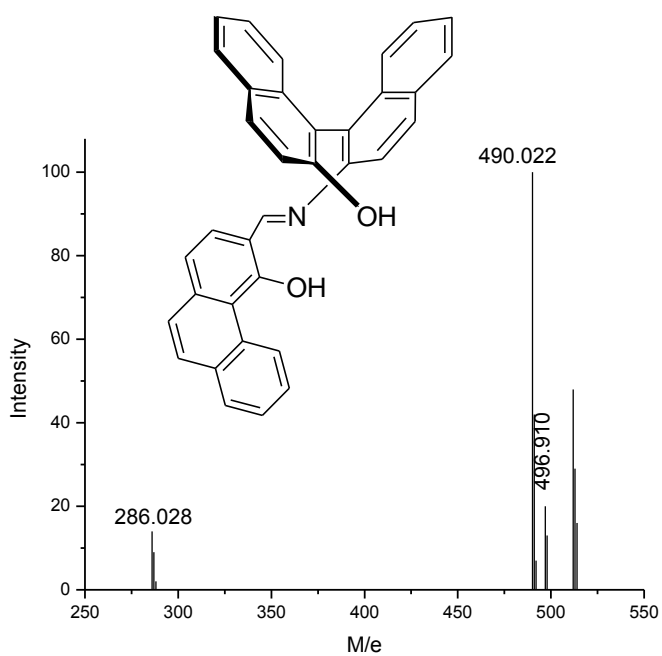
**Figure 4.9.**  $^1\text{H}$  NMR ( $\text{CDCl}_3$ , 400 MHz) for ligand (S)-3.





**Figure 4.10.**  $^1\text{H}$  NMR (CDCl<sub>3</sub>, 400 MHz) for ligand (S)-5.

Both the ligands (S)-3 and (S)-5, showed the required number of peaks in the  $^{13}\text{C}$  NMR. They showed molecular ion peak in the ESI-MS (figure 4.11 and 4.12).



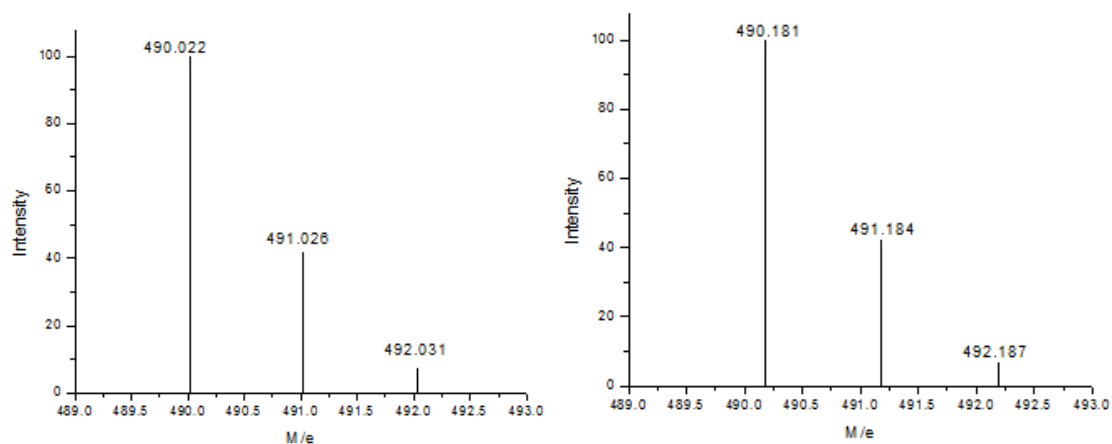


**Figure 4.11.** Entire ESI-mass spectrum of (*S*)-**3** (previous page), observed isotopic pattern of the molecular ion peak (top left), and simulated isotopic pattern (top right).

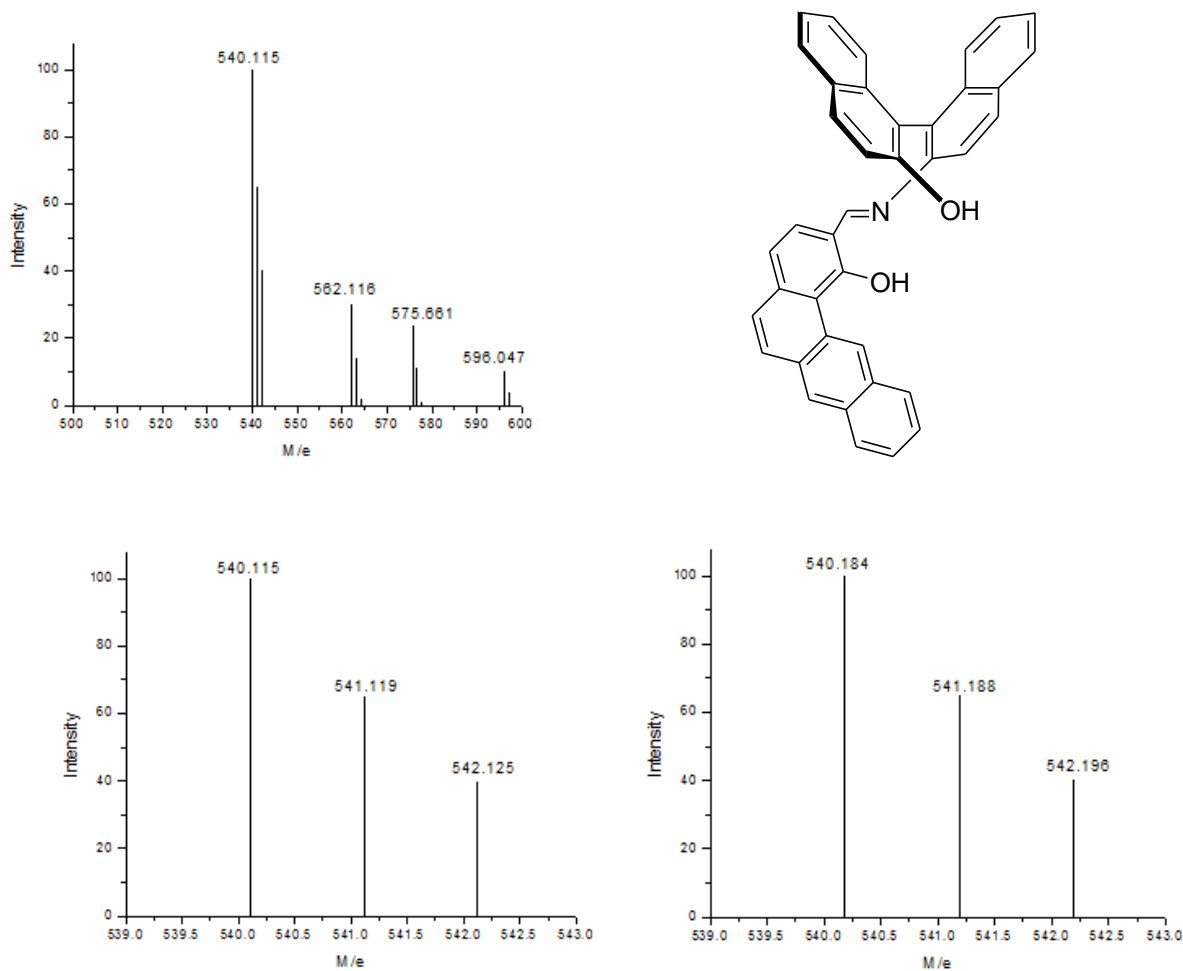


**Figure 4.12.** Entire ESI-MS of (*S*)-**5** (top), observed isotopic pattern of the molecular ion peak (bottom left), and simulated isotopic pattern (bottom right).

Single crystals of the ligand (*S*)-**5** were grown from CH<sub>2</sub>Cl<sub>2</sub> by slow diffusion method. The torsional angle between the two naphthyl rings in the ligand backbone is -100.6°. This value shows the almost perpendicular orientation of the two naphthyl rings in the backbone. There is hydrogen bonding between the hydroxyl proton from the benz[*a*]anthryl side arm and the imine nitrogen. The crystal system is triclinic with P-1 space group. The thermal ellipsoid model and the space filling model of the crystal packing are shown in the figure 4.13 and 4.14 respectively.

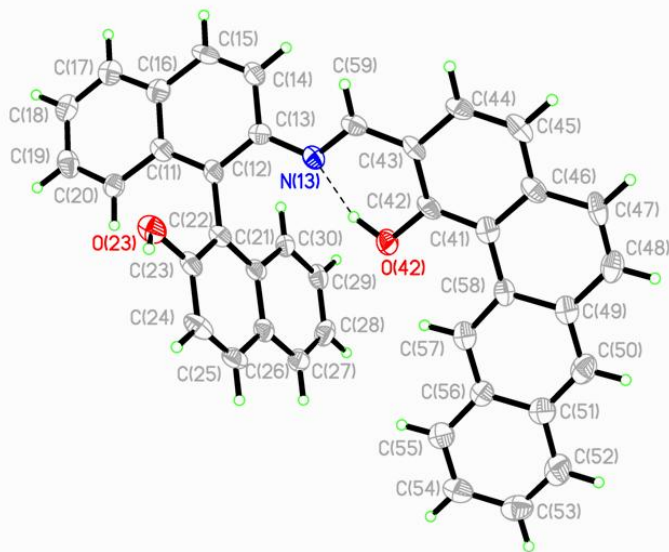


**Figure 4.13.** Thermal ellipsoid plot of ligand (*S*)-**5**.

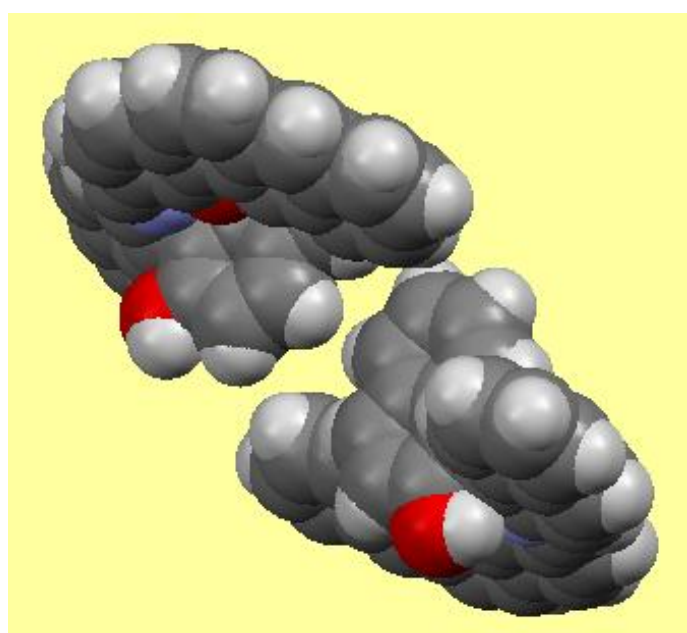


**Figure 4.14.** Space filling model of crystal packing for ligand (*S*)-**5**.

### 4.3.3 Synthesis of vanadium(IV) complexes (C-1 and C-2) with ligands (S)-3 and (S)-5

Synthesis of these complexes were performed under nitrogen by stirring for 16 hours a mixture of the ligand, vanadyl(IV) acetylacetonate and excess sodium methoxide in CH<sub>2</sub>Cl<sub>2</sub> and ethanol mixture (2:1 ratio). A precipitate was separated out. It was filtered to obtain the crude product. The crude product was purified by soxalate extraction in CH<sub>2</sub>Cl<sub>2</sub> to obtain a brown colored pure compound. The fifth coordination position of the vanadium(IV) complex can be occupied by a neutral coordinating solvent molecule like CH<sub>2</sub>Cl<sub>2</sub> or EtOH.

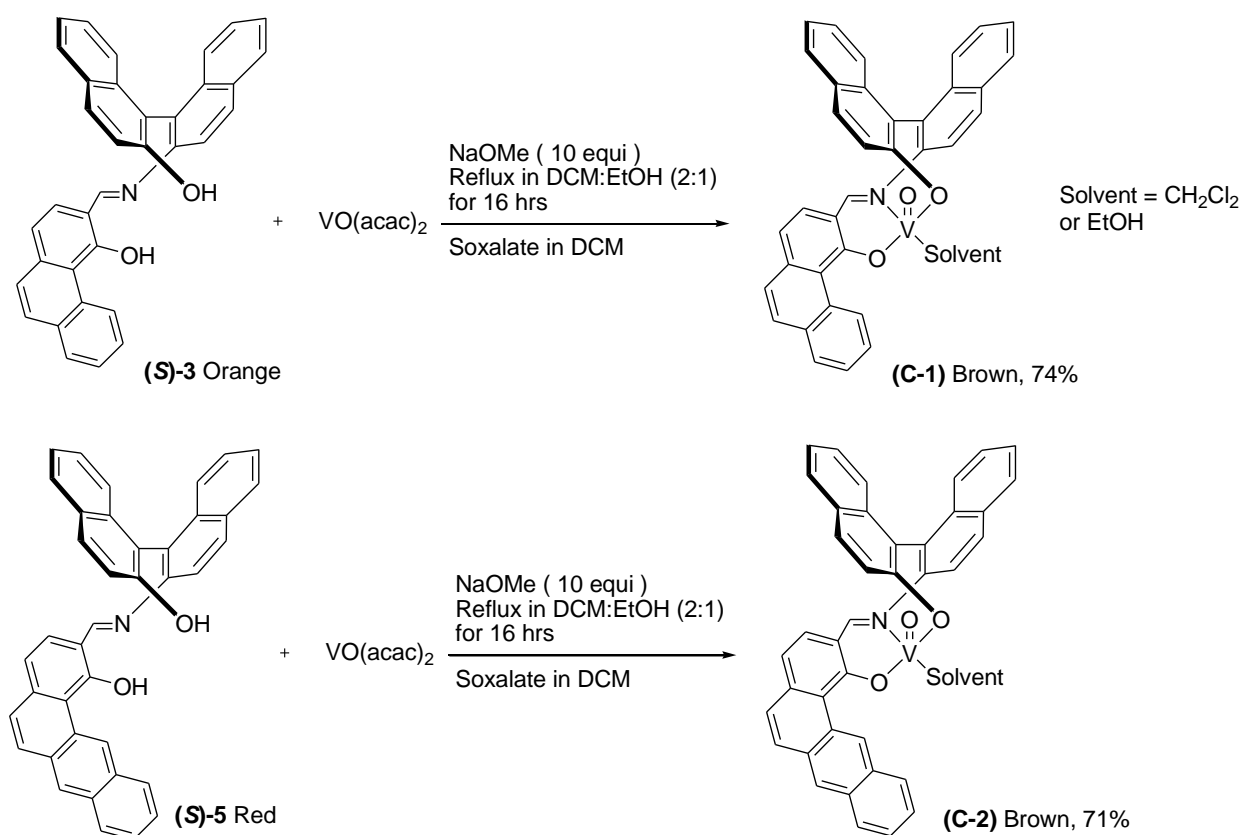
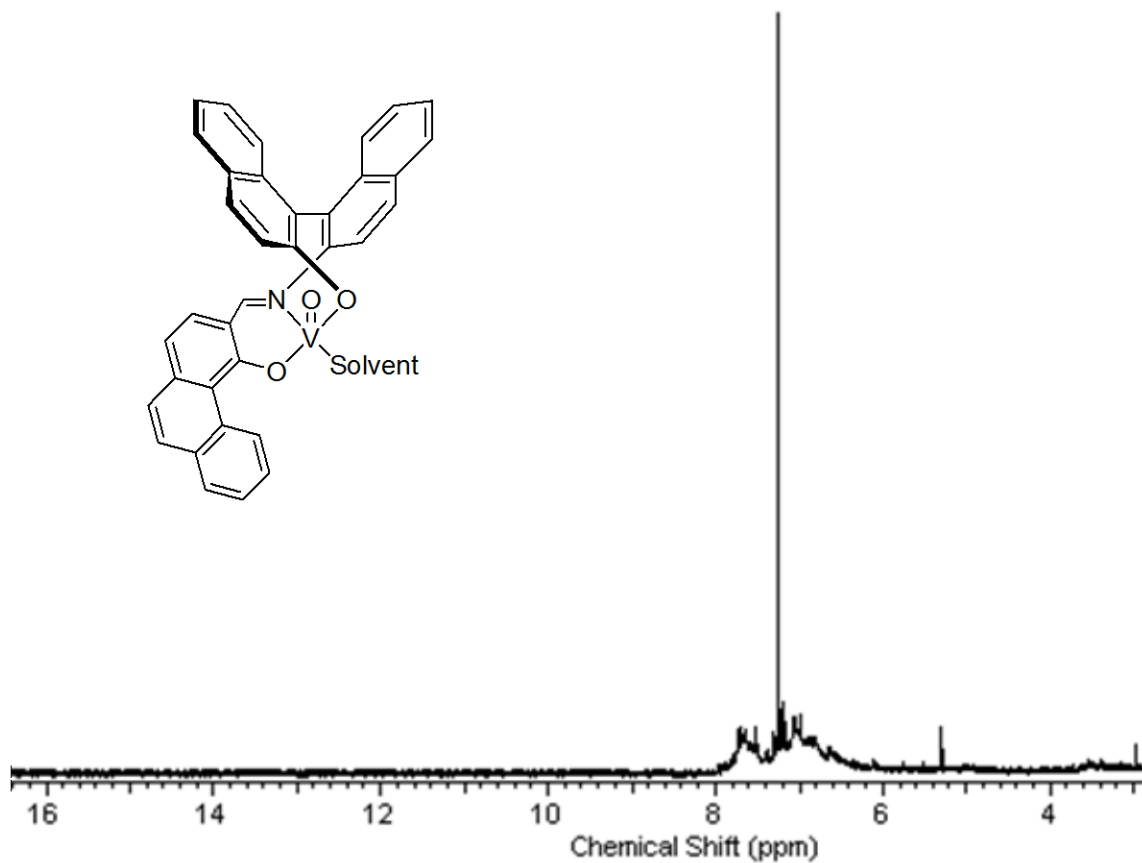


Figure 4.15. Synthesis scheme for complexes C-1 and C-2.

### 4.3.4 Characterization of complexes C-1 and C-2

Both the complexes showed broad nature in <sup>1</sup>H NMR (CDCl<sub>3</sub>, 400 MHz)(figures 4.16 and 4.17) suggesting the presence of paramagnetic vanadium(IV) center in the complexes.



**Figure 4.16.** <sup>1</sup>H NMR (CDCl<sub>3</sub>, 400 MHz) spectrum of complex C-1.

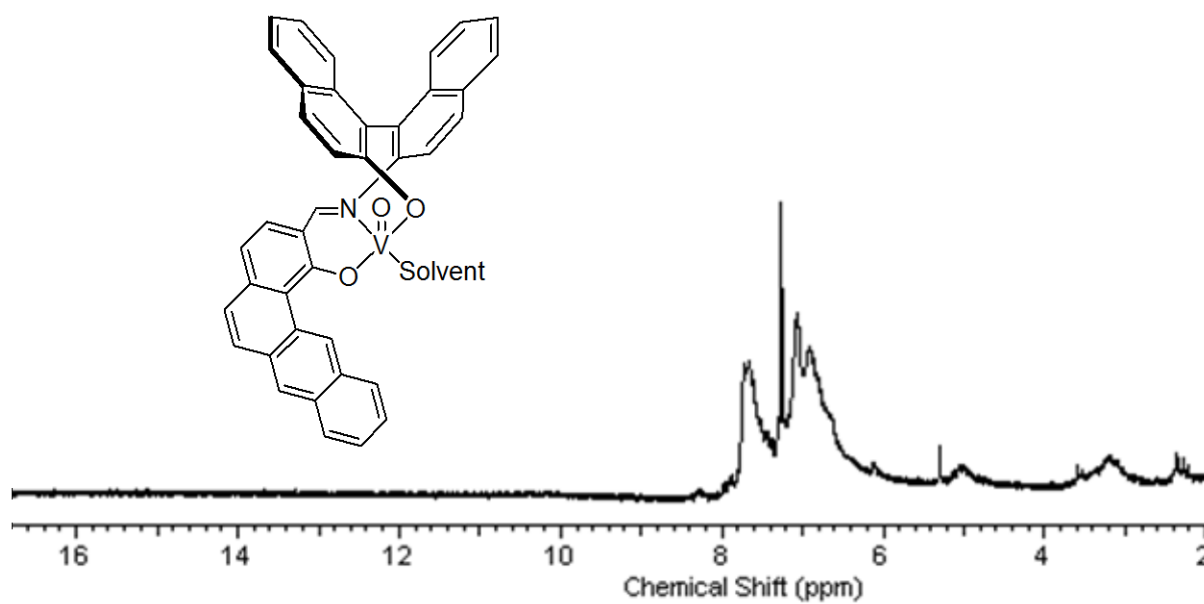


**Figure 4.17.** <sup>1</sup>H NMR (CDCl<sub>3</sub>, 400MHz) spectrum of complex C-2.

MALDI-TOF mass spectra showed the presence of a vanadium(V) complex with the fifth coordination position of the vanadium is occupied by a methoxy group (figure 4.18 and 4.19). IR shows the presence of V=O bond at 818.87 and 816.91  $\text{cm}^{-1}$  for complexes **C-1** and **C-2** respectively.

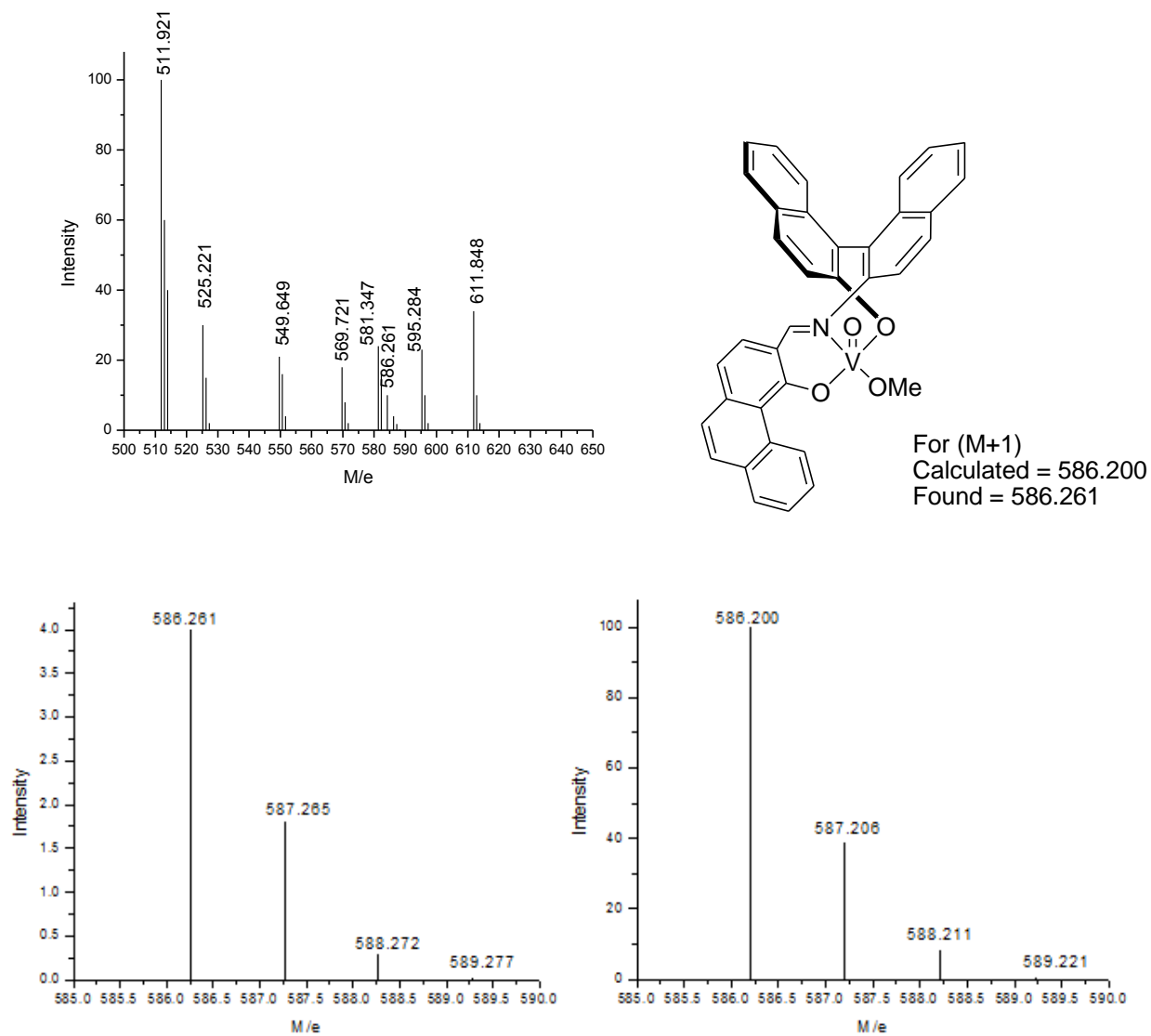


**Figure 4.18.** Entire ESI-MS of complex **C-1** (top left), observed isotopic pattern of the molecular ion peak (bottom left), and simulated isotopic pattern (bottom right).

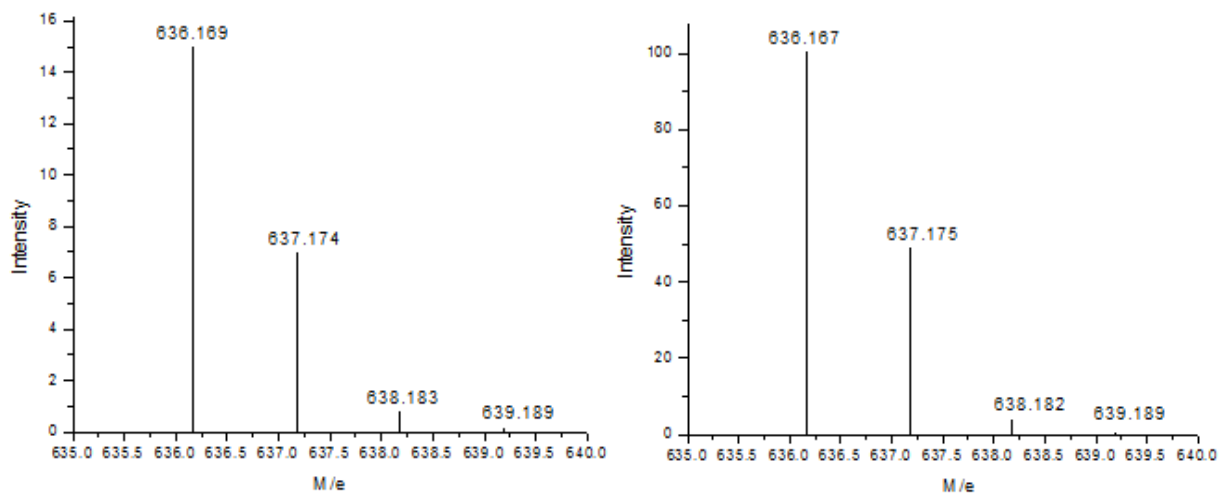
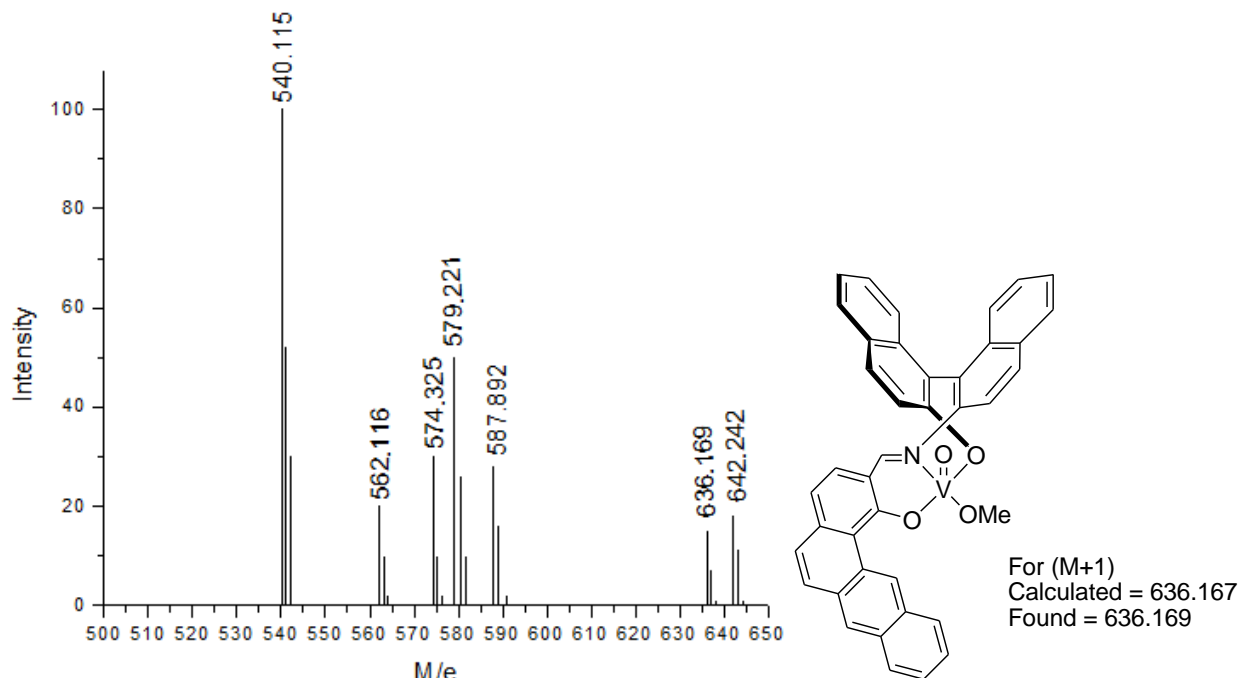


**Figure 4.19.** Entire ESI-MS for complex **C-2** (top left), observed isotopic pattern of the molecular ion peak (bottom left), and simulated isotopic pattern (bottom right).

In the ultraviolet range, the (*S*)-NOBIN solutions in THF display the absorption spectra and circular dichroism (CD), typical for 2, 2'-substituted 1, 1'-binaphthyls. Systems of three absorption bands are observed, which corresponds to three basic absorption bands of  $\beta$ -mono-substituted naphthalene, and they can be conventionally assigned to three electron transitions of naphthalene:  $^1B_b$ ,  $^1L_a$ , and  $^1L_b$ .<sup>17</sup> Significant circular dichroism occurs for all of these transitions.

The most clearly expressed absorption band in the CD spectrum for the ligand (**S**)-**3** in figure 4.20 is at 235 nm and is attributed to allowed  ${}^1B_b$  transition of naphthyl chromophores whose rotation relative to each other is restricted. The sharp positive peak at 235 nm in the CD spectrum of ligand (**S**)-**3** is due to the *S*-enantiomer of NOBIN.

${}^1L_a$  and  ${}^1L_b$  transitions in the CD spectrum for (*S*)-NOBIN generally occur at 265-340 nm range. They are decomposed into two systems (265-280 nm and 310-340 nm) and both of these transitions give rise to negative peaks with small intensity in the CD spectrum. The vibronic structures in the observed absorption spectra typical of the L-transitions are expressed weakly due to the lack of symmetry in the (*S*)-NOBIN and this result in peaks with feeble intensity at this wavelength (265-340 nm) range (CD spectrum of the ligand (**S**)-**3** in figure 4.21).

There are a few differences between the UV and the CD spectra for the ligand (**S**)-**3** and complex **C-1** (figures 4.20 and 4.21). All the peaks both in the UV and in the CD for the complex **C-1**, have shifted towards higher wavelength than for the ligand (**S**)-**3**. This suggests either the lowering in the energy of the anti-bonding orbital or the raise in energy of the bonding orbitals in the ligand after complexation. There are two sharp negative peaks at 285 nm and 335 nm in the CD spectrum of the complex **C-1** suggest the incorporation of more symmetry in the two naphthyl units of the NOBIN backbone after complexation (figure 4.21). Also there appears a new peak in the CD spectrum, for the imine part in the complex **C-1** at 360 nm with the negative intensity (figure 4.21). Overall, the similarity in the CD spectrum for the ligand (**S**)-**3** and the complex **C-1** suggests no significant change in ligand orientation before and after complexation.

The nature of the CD spectra for both the ligand (**S**)-**5** and complex **C-2** (figure 4.23) are very similar to the CD spectra of ligand (**S**)-**3** and complex **C-1** discussed above. So, the same explanations are valid for ligand (**S**)-**5** and complex **C-2**. However, due to the almost perpendicular orientation of the two naphthyl units in the NOBIN backbone ligand (**S**)-**5**, there appears two sharp absorption peaks with almost equal intensities in the UV (figure 4.22).



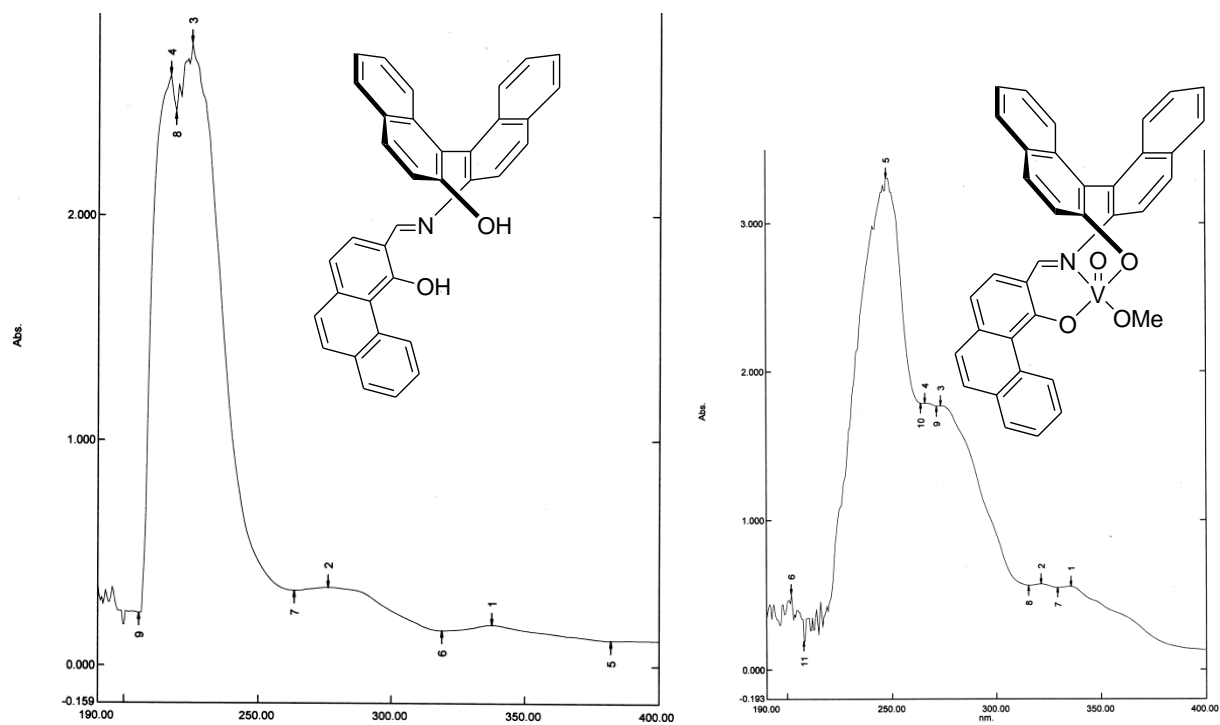


**Figure 4.20.** UV spectra of the ligand (S)-3 (left) and the complex C-1 (right).

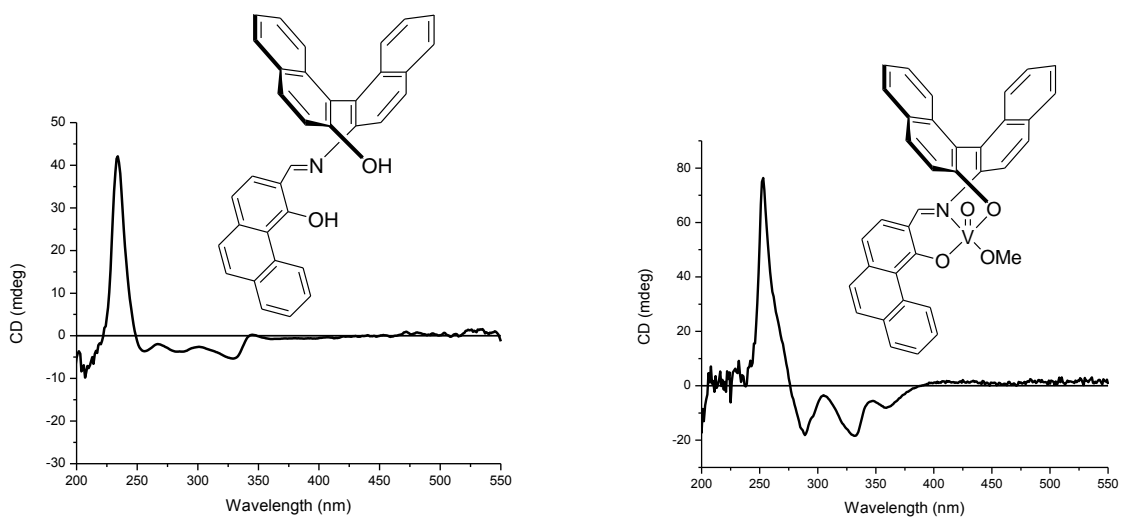


**Figure 4.21.** CD spectra of the ligand (S)-3 (left) and the complex C-1 (right).

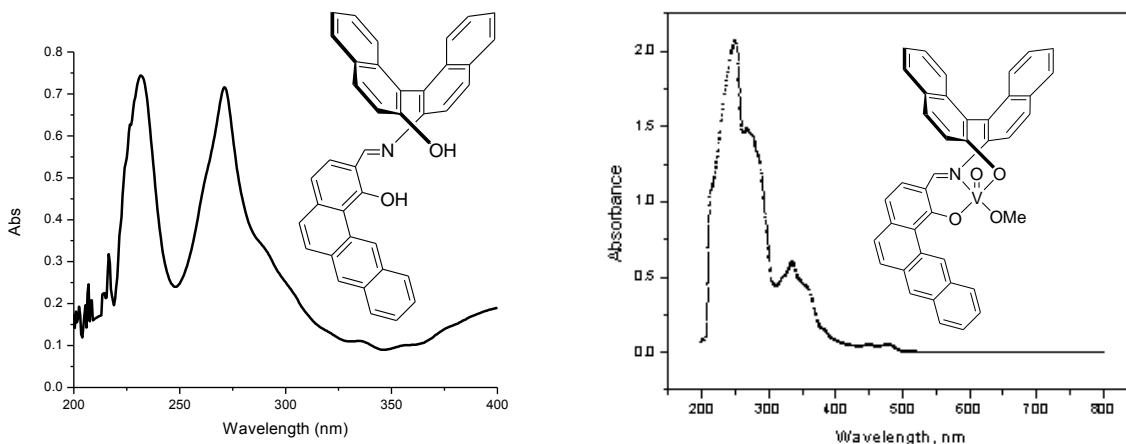


**Figure 4.22.** UV spectra of ligand (*S*)-**5** (left) and the complex **C-2** (right).

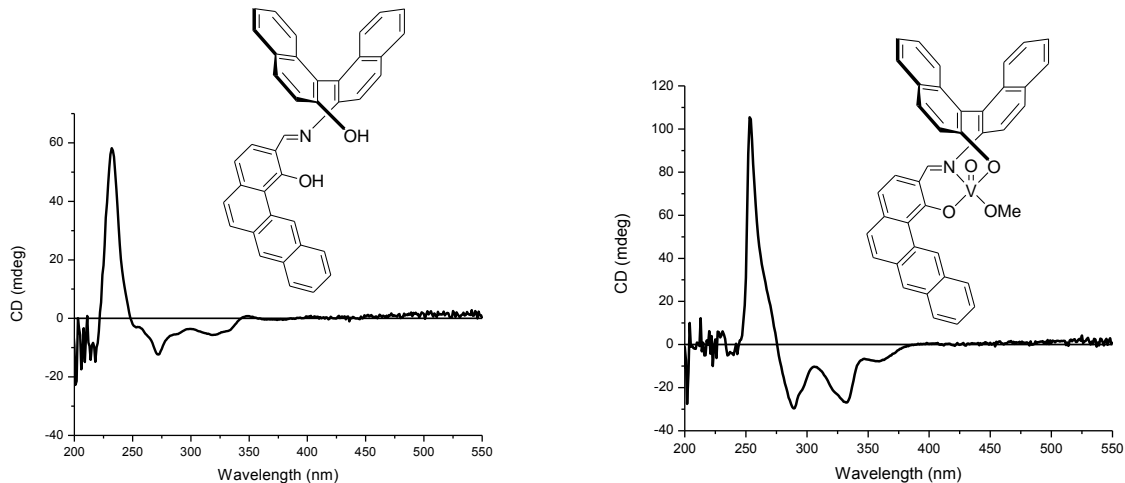


**Figure 4.23.** CD spectra of ligand (*S*)-**5** (left) and the complex **C-2** (right).

#### 4.3.5 Asymmetric sulfoxidations by catalysts *C-1* and *C-2*

The potential for the vanadium(IV) Schiff base complexes as enantioselective catalysts for sulfoxidations has been a well researched topic. Most of these vanadium(IV) Schiff base complexes studied so far have a chiral diamine backbone.<sup>5</sup> Although NOBIN is a well known chiral backbone used in chiral synthesis, there are no reports of using chiral NOBIN as the backbone in vanadium(IV) Schiff base complexes used for sulfoxidations. In this chapter we investigated the potential of the chiral NOBIN backbone  $C_1$  symmetric vanadium(IV) Schiff base complexes to act as enantioselective catalysts in the asymmetric sulfoxidations reactions. All the

reactions were carried out in  $\text{CH}_2\text{Cl}_2$ . The enantioselectivity reached a maximum value 7%, when using acetonitrile as the solvent. A low to moderate polarity solvent such as  $\text{CH}_2\text{Cl}_2$  showed the best enantioselectivity among all the solvents tried for the sulfoxidations reactions. We did not observe any enhancement of enantioselectivity by increasing the polarity of  $\text{CH}_2\text{Cl}_2$  after the addition of methanol. All the reactions were performed at 0 °C for 16 hours.

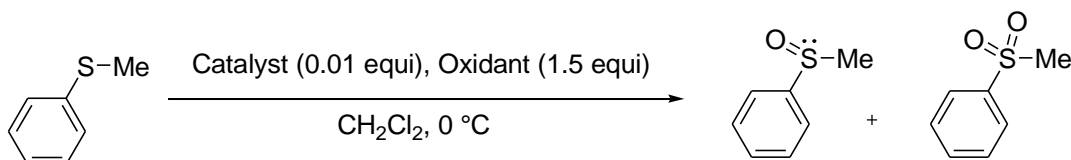


**Figure 4.24.** Sulfoxidations catalyzed by catalysts **C-1** and **C-2**.

In all cases the major isomer produced was *R* methylphenyl sulfoxide (table 4.1). Three oxidants were used in the oxidation of methylphenyl sulfide. They are  $\text{H}_2\text{O}_2$ , cumene hydroperoxide (CHP), and *tert*-butyl hydroperoxide (TBHP). The best enantioselectivity in the product sulfoxide was achieved using  $\text{H}_2\text{O}_2$  as the oxidant. The maximum enantioselectivity attained with catalyst **C-2** was 25% using  $\text{H}_2\text{O}_2$  as the oxidant whereas for catalyst **C-1**, it was 23%. This shows that extending the side arm has very little effect on the enantioselectivity of the sulfoxides. With all the three oxidants used in this reaction, catalyst **C-2** showed slightly higher enantioselectivity than catalyst **C-1**. The enantioselectivity in the product sulfoxide was least while using *tert*-butyl hydroperoxide as the oxidant. This might be due to the monophasic reactions in case of CHP and TBHP, making the oxidation faster with less site selectivity while delivering the oxygen to the substrate. However, the conversions are higher in case of two organic oxidants (CHP and TBHP) than in case of  $\text{H}_2\text{O}_2$  with both the catalysts. For both the catalysts, using CHP or TBHP results in comparable conversions and selectivity. However, with catalyst **C-1**, the selectivity to sulfoxides (76%) reached the highest value with CHP oxidant among all the reactions as shown in the table 4.1.

**Table 4.1** Sulfoxidation results by different catalysts

Catalyst	Oxidant	Solvent	Temp (°C)	Time (hr)	Sulfoxide (%)	Sulfone (%)	Sulfide (%)	ee (%)	Main isomer
<b>C-1</b>	H <sub>2</sub> O <sub>2</sub>	CH <sub>2</sub> Cl <sub>2</sub>	0	16	69	13	18	23	<i>R</i>
<b>C-1</b>	TBHP	CH <sub>2</sub> Cl <sub>2</sub>	0	16	72	16	12	9	<i>R</i>
<b>C-1</b>	CHP	CH <sub>2</sub> Cl <sub>2</sub>	0	16	76	14	10	17	<i>R</i>
<b>C-2</b>	H <sub>2</sub> O <sub>2</sub>	CH <sub>2</sub> Cl <sub>2</sub>	0	16	65	14	21	25	<i>R</i>
<b>C-2</b>	TBHP	CH <sub>2</sub> Cl <sub>2</sub>	0	16	73	20	7	5	<i>R</i>
<b>C-2</b>	CHP	CH <sub>2</sub> Cl <sub>2</sub>	0	16	74	16	10	19	<i>R</i>

ee of the product were measured by HPLC analysis. HPLC analysis was carried out with a DAICEL OD-H column (isopropanol:hexane 5:95). Retention times 17.82 mins for (*R*) and 20.91 mins for (*S*) isomers.

The *C*<sub>2</sub>-symmetric vanadium(IV) salen complexes with tetradentate salen ligands (from chapter 1) showed better enantioselectivity in sulfoxidations under similar experimental conditions than the *C*<sub>1</sub>-symmetric vanadium(IV) Schiff base complexes with tridentate (*S*)-NOBIN backbone ligands. In chapter 1, we have seen that opening up a coordination site at the vanadium is necessary for the formation of the hydroperoxo complex, which is a necessary step in the catalytic cycle. This observation initiates us to synthesize tridentate NOBIN based ligands to reduce the steric congestion at the vanadium site to make room for the substrates to attach to metal center without any steric burden. However, the initial results suggest that the complexes are too open and they do not provide enough interaction with the substrate sulfide to discriminate between the enantiofaces. The mechanism of sulfoxidations by catalyst **C-1** is explained in figure 4.25. It is believed that under the experimental conditions vanadium(IV) gets oxidized to vanadium(V) with hydroxyl group occupying the fifth coordination position of the square pyramidal *C*<sub>1</sub>-symmetric complex. In the consequent step, after the additions of the H<sub>2</sub>O<sub>2</sub> and the sulfide, the complex first transforms to a hydroperoxo unit and then attains a pseudo octahedral

configuration with the sulfide occupying the sixth coordination position. The binding of the sulfide to the vanadium center is the rate determining step of the overall reaction. In the following step, oxo transfer occurs from hydroperoxide to the sulfide and this leads to the product release and the catalyst regeneration to finally go back to its original form.

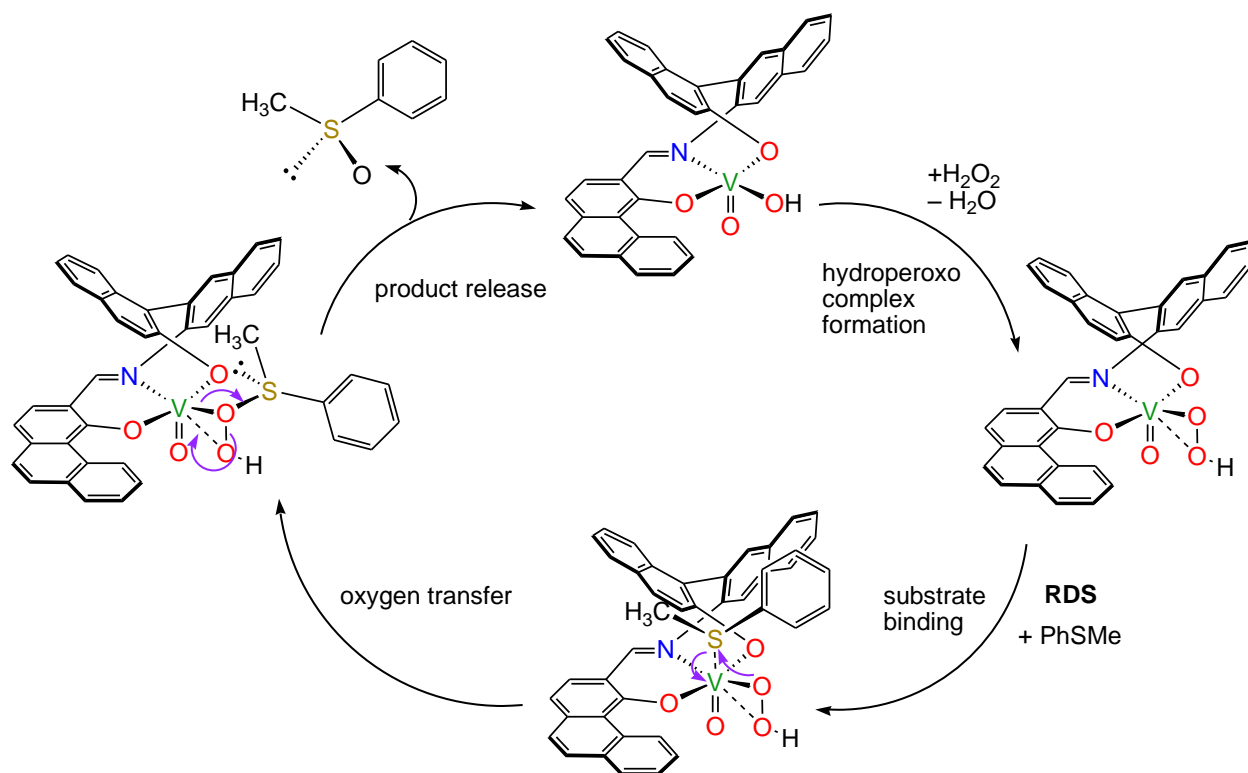


**Figure 4.25.** Mechanism for sulfoxidations reactions catalyzed by complex C-1.

It is observed that the enantioselectivity of the sulfoxide is ligand accelerated (table 4.2). With the increase in the enantiomeric excesses of the ligand, the sulfoxide enantiomeric excess increases. (*S*)-NOBIN backbone prepared in three different batches with different enantiomeric excesses were applied as catalyst C-2 for sulfoxidations reactions with  $\text{H}_2\text{O}_2$  as the oxidant in  $\text{CH}_2\text{Cl}_2$ . The highest enantioselectivity obtained was 25% with the ligand having the highest ee 98%.

**Table 4.2** Comparison of the ee of the sulfoxide with the ee of the ligand (*S*)-**5** (catalyst **C-2**)  
(Oxidant = H<sub>2</sub>O<sub>2</sub>, Solvent = CH<sub>2</sub>Cl<sub>2</sub>, Time = 16 hrs)

ee (%) of the ( <i>S</i> )- <b>5</b> ligand	ee (%) of the sulfoxide
82	14
90	21
98	25

## 4.4 Conclusions

We synthesized C<sub>1</sub>-symmetric (*S*)-NOBIN backbone tridentate phenanthryl and benz[a]anthryl sidearm Schiff base ligands. The vanadium complexes of these ligands have open coordination sites so that substrate can bind to the metal center. We observed high values of conversions (90%) in the vanadium-NOBIN complex catalyzed sulfoxidations. However, the enantiomeric excess attained in the product sulfoxide was low. This suggests that these complexes do not provide enough interaction with the substrate sulfide to discriminate between the enantiofaces. The enantioselectivity in the product sulfide is ligand accelerated. The more extended side arm with higher helical nature has a small effect on the enantioselectivity of the product sulfoxides.

## 4.5 Experimental Section

### *General Methods*

All reactions were performed under inert atmospheres unless otherwise noted. Solvents used in metallation reactions were stored over sodium benzophenone ketyl or calcium hydride, and degassed prior to transfer via high-vacuum line techniques. Inert gasses were purified by passage through 4 Å molecular sieves and an Engelhard Q5 catalyst bed. Preparation and workup of V (IV) and Ti(IV) compounds were completed under rigorously inert conditions to prevent oxidation or decomposition. All aldehydes used in the aldol-condensation were freshly distilled

before use. 2-methoxy propene was passed through basic alumina and then freshly distilled to ensure the complete absence of any acidic nature.

UV-vis spectra were obtained on a Varian Cary 500 spectrometer, and CD spectra on a JASCO 720 spectropolarimeter. Solution samples for these two techniques were prepared using dried spectroscopic grade THF, at concentrations that ranged between 1.5 and  $2.5 \times 10^{-5}$  M. A 1 cm path length quartz cell was employed for the analysis.  $^1\text{H}$  and  $^{13}\text{C}$  NMR spectra were obtained on a Varian Unity 400 MHz spectrometer employing residual solvent protons or in some cases TMS as an internal standard. Crystallographic data was collected using either a Bruker SMART 1000 CCD or a Bruker-AXS SMART APEX CCD. Full structural information is included in appendix II. EPR spectroscopy of the vanadium complexes were measured in Varian E-4 EPR spectrometer. All mass spectra were recorded in LCT Premier (Waters corp, Milford, MA) mass spectrometer. All IR spectra were recorded in Nicolet 6700 FT-IR spectrometer.

**(±)-2-Amino-2'-hydroxy-1,1'-binaphthyl (±)(1).** To a 150 mL Teflon lined autoclave was added 5.00 g (17.5 mL) of 1,1'-bi-2-naphthol, 23.5 g (175 mmol) of  $(\text{NH}_4)_2\text{SO}_3 \cdot \text{H}_2\text{O}$  and 65 mL of concentrated aqueous ammonia. The mixture was stirred at 200 °C in an oil bath for 5 days. It was then cooled down to ambient temperature and filtered. The resulting white solid was washed with water followed by recrystallization from toluene to afford 4.30 g (87% yield) of pure (±)-2-amino-2'-hydroxy-1,1'-binaphthyl.  $^1\text{H}$  NMR has already been reported in literature.<sup>6</sup>

**(S)-2-Amino-2'-hydroxy-1,1'-binaphthyl (2).** (±)(1) (0.10 g, 0.3508 mmol) dissolved in a mixture of 1.2 mL of chlorobenzene and 0.25 mL of ethanol, was placed in a 100 mL flask. The mixture was heated to 65 °C with rapid stirring. (S)-camphor-10-sulfonic acid (0.085 g, 0.367 mmol) (freshly recrystallized from ethyl acetate) was added to the reaction mixture. The dark colored reaction mixture became homogeneous immediately after the addition of camphor-sulfonic acid. Stirring was continued and the temperature was maintained at 65 °C for 30 minutes, during which time a precipitate began to form. The well stirred solution was then allowed cooled gradually to room temperature over 3 hours. The precipitate formed was isolated by filtration and washed three times with 0.5 mL chlorobenzene. The filter cake was suspended in a mixture of 1.6 mL of  $\text{CH}_2\text{Cl}_2$  and 0.8 mL of 5% aq.  $\text{NaHCO}_3$  solution. The mixture was rapidly stirred for 10 minutes, over which time the organic phase become homogeneous. The

organic layer was separated and extracted with another 0.5 mL of CH<sub>2</sub>Cl<sub>2</sub>. The combined organic layers are dried over Na<sub>2</sub>SO<sub>4</sub> and concentrated in vacuo to produce (*S*)-**2**. Recrystallization of the product from toluene affords pure (*S*)-**2** (0.045 g, 87% yield) with 97% ee [ $\alpha$ ]<sub>D</sub> = +122 (c = 1.04, THF), M.P. 169 °C. <sup>1</sup>H NMR has already been reported in literature.

**(*S*)-2-hydroxy-1,1'-binaphthyl-2'-imine-phenanthrene-1-ol (*S*)-3.** A mixture of 0.10 g (0.351 mmol) of (*S*)-**2** and 0.115 g (0.422 mmol) of 2-phenanthraldehyde-1-ol were refluxed in absolute ethanol (15 mL) under argon for 10 hours. The solution became reddish orange after 10 hours. The mixture was hot filtered and washed with boiling ethanol to produce red colored pure ligand (*S*)-**3** (0.210 g, 89% yield). <sup>1</sup>H NMR (CDCl<sub>3</sub>, 400 MHz):  $\delta$  4.82 (s, 1H, OH from NOBIN); 7.12-7.14 (d, 1H, CH); 7.26 (m, 2H, BM from ABMX system in NOBIN ring); 7.34-7.42 (d, 1H, CH); 7.35 (dt, AX protons from ABMX system, 2H, CH); 7.36-7.44 (d, 1H, CH); 7.42 (dt, 2H, AX protons from ABMX system, CH); 7.49 (d, 1H, CH); 7.53 (m, 2H, BM protons from ABMX system, CH); 7.56 (m, 2H, AX protons from ABMX system); 7.64 (dt, 2H, AX protons from ABMX system, CH); 7.75-7.77 (d, 1H, CH); 7.82 (m, 2H, BM protons from ABMX system, CH); 7.95-7.97 (d, 2H, CH); 8.03 (t, 1H, CH); 8.16-8.18 (d, 2H, CH); 8.84 (s, 1H, CH); 9.43-9.46 (d, 1H, CH); 14.95 (s, 1H, OH, from the sidearm). <sup>13</sup>C NMR (CDCl<sub>3</sub>, 400 MHz):  $\delta$  117.31, 118.52, 119.00, 120.84, 124.35, 125.53, 126.10, 126.31, 126.42, 126.47, 126.51, 127.00, 127.04, 127.34, 127.48, 127.93, 128.00, 128.09, 128.14, 128.21, 128.29, 128.38, 128.47, 129.49, 129.67, 130.12, 130.97, 131.45, 132.58, 134.17, 137.09, 144.00, 151.67, 161.71, 166.04. MS: [M]<sup>+1</sup> (C<sub>35</sub>H<sub>23</sub>O<sub>2</sub>N<sub>1</sub>)<sup>+1</sup> 540.115 (82%), 541.117 (16%), 542.124 (2%). UV:  $\Pi$  to  $\Pi^*$  (C=N) at 180 nm,  $\Pi$  to  $\Pi^*$  (C=C) at 185 nm. CD shows chirality of the ligand in solution.

**(*S*)-2-hydroxy-1,1'-binaphthyl-2'-imine-benz[a]anthracene-1-ol (*S*)-5**

A mixture of 0.100 g (0.351 mmol) of (*S*)-**2** and 0.115 g (0.422 mmol) of 2-benz[a]anthraldehyde-1-ol were refluxed in absolute ethanol (10 mL) under argon for 10 hours. The solution became dark red after 10 hours. The mixture was hot filtered and washed with boiling ethanol to produce dark red colored pure ligand (*S*)-**5** (0.591g, 81% yield). <sup>1</sup>H NMR (CDCl<sub>3</sub>, 400 MHz):  $\delta$  4.91 (s, 1H, O-H); 7.31 (d, 1H, CH); 7.37 (m, 4H, CH, complex ABMX pattern); 7.41 (d, 1H, CH); 7.43 (d, 1H, CH); 7.61 (m, 4H, CH, complex ABMX pattern); 7.71 (d, 1H, CH); 8.05 (m, 4H, CH, from the side arm, complex second order pattern); 8.20 (d, 1H,



CH); 8.28 (s, 1H, CH); 8.34 (d, 1H, CH); 8.39 (d, 1H, CH); 8.41 (d, 1H, CH); 8.88 (s, 1H, imine proton); 9.92 (s, 1H, bay proton).  $^{13}\text{C}$  NMR ( $\text{CDCl}_3$ , 400 MHz):  $\delta$  116.00, 117.59, 118.12, 118.60, 119.04, 123.21, 125.01, 125.17, 125.49, 125.67, 125.93, 126.01, 126.59, 126.67, 126.91, 127.04, 127.19, 127.23, 127.48, 127.84, 127.99, 128.31, 128.37, 128.48, 128.59, 129.11, 129.48, 129.91, 130.11, 130.56, 130.91, 131.41, 131.49, 132.01, 134.00, 137.14, 142.00, 151.94, 161.32, 164.04. MS:  $[\text{M}]^{+1}$  ( $\text{C}_{39}\text{H}_{25}\text{O}_2\text{N}_1$ ) $^{+1}$  490.022 (84%), 491.032 (14%), 492.068 (2%). UV:  $\Pi$  to  $\Pi^*$  ( $\text{C}=\text{N}$ ) at 225 nm,  $\Pi$  to  $\Pi^*$  ( $\text{C}=\text{C}$ ) at 265 nm. CD shows chirality of the ligand in solution. Crystals obtained from the diffusion of  $\text{CH}_2\text{Cl}_2$  in hexane layer.

### **V(IV)(S)-3 complex (C-1)**

Ligand (S)-3 (0.100 g, 0.205 mmol) was dissolved in a mixture of  $\text{CH}_2\text{Cl}_2$  (15 mL) and EtOH (5 mL). To this solution vanadyl acetyl acetonate (0.054 g, 0.205 mmol) and sodium methoxide (0.100 g, 2.04 mmol) were added. The solution was refluxed for 16 hrs followed by filtration to obtain a brown colored precipitate. The compound was further purified by soxalate extraction in dichloromethane. Pure brown colored compound was obtained after solvent removal under reduced pressure (0.702 g, 74% yield).  $^1\text{H}$  NMR ( $\text{CDCl}_3$ , 400 MHz): broad peaks suggest paramagnetic compound. MS:  $[\text{M}+\text{OMe}]^{+1}$  ( $\text{C}_{36}\text{H}_{24}\text{N}_1\text{O}_4\text{V}_1$ ) $^{+1}$  586.2113 (64%), 587.3157 (24%), 588.3467 (8%), 589.3965 (4%). IR:  $\nu_{\text{V}=\text{O}}$  818.87  $\text{cm}^{-1}$ ,  $\nu_{\text{C}=\text{N}}$  1612.72  $\text{cm}^{-1}$ . UV: L  $\rightarrow$  M charge transfer at 365 nm (broad peak). CD: The chirality is intact in the complex with increase in intensity of the CD peaks.

### **V(IV)(S)-5 complex (C-2)**

Ligand (S)-5 (0.063 g, 0.116 mmol) was dissolved in a mixture of  $\text{CH}_2\text{Cl}_2$  (8 mL) and EtOH (3 mL). To this solution vanadyl acetyl acetonate (0.031g, 0.116 mmol) and sodium methoxide (0.063 g, 1.16 mmol) were added. The solution was stirred for 16 hrs followed by filtration to obtain a deep brown colored precipitate. The compound was further purified by soxalate extraction in dichloromethane. Pure deep brown colored compound was obtained after solvent removal under reduced pressure (0.049 g, 71% yield).  $^1\text{H}$  NMR ( $\text{CDCl}_3$ , 400 MHz): broad peaks in the aromatic region suggest paramagnetic compound. MS:  $[\text{M}+\text{OMe}]^{+1}$  ( $\text{C}_{40}\text{H}_{26}\text{N}_1\text{O}_4\text{V}_1$ ) $^{+1}$  636.169 (66%), 637.261 (26%), 638.257 (7%), 639.421 (1%). IR:  $\nu_{\text{V}=\text{O}}$  816.91  $\text{cm}^{-1}$ ,  $\nu_{\text{C}=\text{N}}$  1613.33  $\text{cm}^{-1}$ . UV: Characteristic broad peak at 365 nm for more delocalization of the  $\Pi$

electrons from ligand to metal. CD: The chirality is intact in the complex compared to that of the ligand with red shift of the CD peaks.

**General Procedure for Sulfoxidations:** All sulfoxidation reactions are carried out by 1 mol% of catalyst. 1 mol% of catalyst was dissolved in dichloromethane (3mL) inside a two neck R.B. under argon. The mixture was stirred in inert atmosphere for 10 minutes. 100 mol% phenyl methyl sulfide was added followed by additional 15 minutes of stirring. The entire system was cooled to 0 °C. 110 mol% oxidant (hydrogen peroxide or cumene hydroperoxide) was added to the mixture slowly for a period of 2 hrs. The mixture was additionally stirred for 16 hrs. A saturated solution of sodium sulfite was added to quench the reaction. The reaction mixture was extracted with dichloromethane followed by drying over sodium sulfate. The product was purified by flash column chromatography in 1:3 ethyl acetate:hexane. Pure sulfoxide was analysed by <sup>1</sup>H NMR (CDCl<sub>3</sub>, 400 MHz): 3.72 (s, 3H, CH<sub>3</sub>), 7.5 (m, 3H, CH), 7.6 (m, 2H, CH). Enantiomeric excess of the phenyl methyl sulfoxide was determined by HPLC analysis with a Daicel Chiralcel OD-H column. Hexane and isopropanol mixture (90:10) was used as the eluent. The R isomer and the S isomer elutes at 17 and 20 minutes respectively.

## 4.6 References

1. "Recent developments in the synthesis and utilization of chiral sulfoxides" Fernandez, I.; Khair, N. *Chem. Rev.* **2003**, *103*, 3651-3705.
2. "Applications of catalytic asymmetric sulfide oxidations to the synthesis of biologically active sulfoxides" Legros, J.; Dehli, J. R.; Bolm, C. *Adv. Synth. Catal.* **2005**, *347*, 19-31.
3. "Catalytic asymmetric synthesis of *tert*-butanesulfonamide: Application to the asymmetric synthesis of amines" Liu, G.; Cogan, D. A.; Ellman, J. A. *J. Am. Chem. Soc.* **1997**, *119*, 9913-9914.
4. "Ti(salen) catalyzed enantioselective sulfoxidation using hydrogen peroxide as a terminal oxidant" Saito, B.; Katsuki, T. *Tetrahedron. Lett.* **2001**, *42*, 3873-3876.
5. "Asymmetric sulfide oxidation with vanadium catalysts and hydrogen peroxide" Bolm, C.; Bienewald, F. *Angew. Chem. Int. Ed.* **1995**, *34*, 2640-2642.

6. "Construction of highly efficient Mn-salen catalyst for asymmetric epoxidation of conjugated *cis*-olefins" Sasaki, H.; Irie, R.; Ito, Y.; Katsuki, T. *Synlett*. **1994**, 356.
7. "Highly enantioselective iron catalyzed sulfide oxidation with aqueous hydrogen peroxide under simple reaction conditions" Legros, J.; Bolm, C. *Angew. Chem. Int. Ed.* **2004**, *43*, 4225-4228.
8. Palucki, M.; Hanson, P.; Jacobsen, E. N. *Tetrahedron. Lett.* **1992**, *33*, 711-714.
9. <sup>51</sup>V and <sup>13</sup>C NMR spectroscopic study of the peroxo vanadium intermediates in vanadium catalyzed enantioselective oxidation of sulfides" Bryliakov, K. P.; Karpyshev, N. N.; Fominsky, S. A.; Toltsikov, A. G.; Talsi, E. P. *J. Mol. Catal. A: Chem.* **2001**, *171*, 73.
10. "Iron catalyzed asymmetric sulfide oxidation with aqueous hydrogen peroxide" Legros, J.; Bolm, C. *Angew. Chem. Int. Ed.* **2003**, *42*, 5487-5489.
11. Mikami, K.; Okubu, Y.; Terada, M.; Wu, Y.; Liu, J.; Yun, H.; Wang, Y.; Ding, K. *Chem. Eur. J.* **1995**, *5*, 1734-1737.
12. "A facile synthesis of 2-amino-2'-hydroxy 1,1'-binaphthyl and 2,2'-diamino-1,1'-binaphthyl by oxidative coupling using copper(II) chloride" Smreina, M.; Lovenc, M.; Hanus, V.; Kocovsky, P. *Synlett*. **1991**, 231.
13. "Catalytic asymmetric organozinc additions to carbonyl compounds" Pu, L.; Yu, H. *B. Chem. Rev.* **2001**, *101*, 757.
14. "Catalytic enantioselective aldol additions with methyl and ethyl acetate *o*-silyl enolates: a chiral tridentate chelate as a ligand for titanium(IV)" Carreira, E. M.; Singer, R. A.; Wheesong, L. *J. Am. Chem. Soc.* **1994**, *116*, 8837.
15. "To probe the origin of activation effect of carboxylic acid and (+) NLE in tridentate titanium catalyst systems" Yuan, Y.; Li, X.; Sun, J.; Ding, K. *J. Am. Chem. Soc.* **2002**, *124*, 14866.
16. "A new chiral ruthenium complex for catalytic asymmetric cyclopropanation" Tang, W.; Hu, X.; Zhang, X. *Tetrahedron. Lett.* **2002**, *43*, 3075.
17. "Optical rotatory power of 2,2'-dihydroxy-1,1'-binaphthyl and related compounds" Hanazaki, I.; Akimoto, H. *J. Am. Chem. Soc.* **1972**, *94*, 4102.

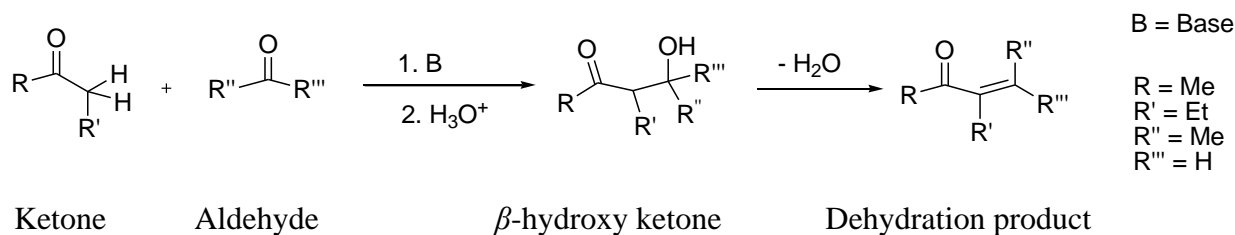
# CHAPTER 5 - Catalytic Enantioselective Acetone Aldol Additions with 2-Methoxypropene

## 5.1 Abstract

New helical  $C_2$ -symmetric (*S*)-NOBIN (2-amino-2'-hydroxy-1,1'-binaphthyl) backbone titanium(IV) Schiff base complexes were synthesized and characterized by common analytical methods. These complexes exist in the *M* helical conformation in the solution. These complexes can catalyze asymmetric aldol addition reactions of 2-methoxy propene with different aldehydes and produces moderate enantioselectivity. First time (*R*)-*O*-acetyl mandelic acid was used to determine the enantioselectivity of the aldol addition products  $\beta$ -hydroxy ketones.

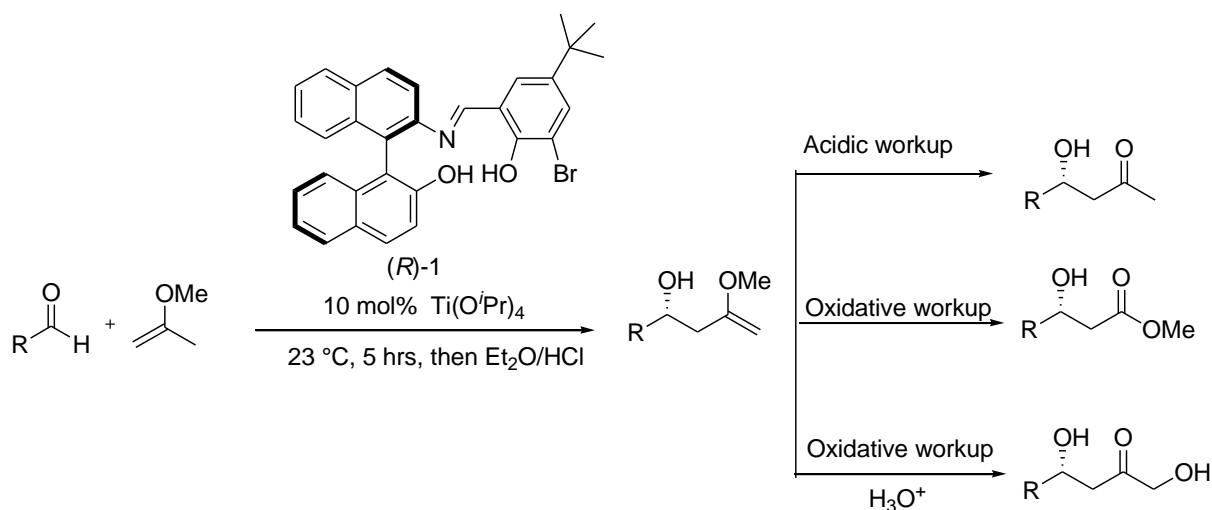
## 5.2 Introduction

Carbon-carbon bond formation reactions are one of the most important categories of reactions in organic chemistry.<sup>1</sup> Among all the carbon-carbon bond formation reactions, aldol condensation is one of the important classes of reactions widely used in pharmaceuticals industry.<sup>2</sup> Usually, aldol condensation involves the nucleophilic addition of a ketone enolate to an aldehyde to form a  $\beta$ -hydroxyketone, or "aldol" (aldehyde + alcohol), a structural unit found in many naturally occurring molecules and pharmaceuticals (figure 5.1).<sup>3</sup> In aldol condensations, an enol or an enolate ion reacts with a carbonyl compound to form a  $\beta$ -hydroxyaldehyde or  $\beta$ -hydroxyketone, followed by a dehydration to produce a conjugated enone.<sup>2</sup> The  $\beta$ -hydroxyaldehyde or  $\beta$ -hydroxyketone: a chiral aldol addition product formed during aldol addition reactions, is a very important structural motif in many drug molecules in the pharmaceuticals industry.<sup>3</sup> Catalytic asymmetric aldol additions are one of the most popular ways to synthesize these chiral  $\beta$ -hydroxy aldehydes or  $\beta$ -hydroxy ketones.<sup>4</sup>



**Figure 5.1.** Scheme for an aldol reaction.

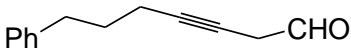
A breakthrough in asymmetric aldol chemistry to synthesize enantioselective  $\beta$ -hydroxy aldehydes was achieved by Carreira, using titanium complexes of chiral NOBIN derived Schiff base ligand ((*R*)-**1**) as catalysts in this reaction (figure 5.2).<sup>3</sup> This also represents the first application of NOBIN by taking the advantage of its propensity to form tridentate imines.<sup>3</sup> They examined the aldol condensation with an inexpensive, commodity chemical 2-methoxypropene (as an acetone enolate equivalent) in catalytic, enantioselective aldol addition reactions with different aldehydes to produce chiral  $\beta$ -hydroxy ketones (figure 5.2). The catalyst was generated by mixing ligand (*R*)-**1** and  $\text{Ti}(\text{O}^i\text{Pr})_4$  with subsequent removal of the released isopropanol. This catalyst was found to be effective for the enantioselective addition of 2-methoxypropene, a weak nucleophile to the aldehydes, affording aldol addition adduct in good to excellent enantioselectivity (table 5.1). The unique feature of the titanium complex derived from ligand (*R*)-**1** results from the fact that, the complex is sufficiently electrophilic to activate the bound aldehyde towards the addition of a weak nucleophile: 2-methoxypropene (“C” in figure 5.22). However, the main problem with this reaction is the high propensity for the 2-methoxypropene towards self polymerization. Trace quantities of  $\text{H}^+$  can initiate the self polymerization of 2-methoxypropene. So, it is very important to remove any  $\text{H}^+$  during the reaction. 2-methoxypropene filtered through Activity 1 basic alumina followed by distillation prior to use work best for this reaction. One advantage of this reaction results from the fact that, different workup conditions give rise to different products. For example, acidic workup produces  $\beta$ -hydroxy ketones, oxidative workup give rise to  $\beta$ -hydroxy esters and  $\beta$ -hydroxy acids.<sup>3</sup>



**Figure 5.2.** Acetone aldol addition by titanium-Schiff base complex introduced by Carreira.

However, it is observed that, it is necessary to have steric bulk at the *ortho*-position to the phenolic hydroxyl group in the side arm of the ligand to obtain good enantioselectivity (ee) in the acetone aldol addition reaction. Also, 5-10 mol% of the catalyst is required to produce the aldol addition product.<sup>3</sup>

**Table 5.1.** Yields and ee's from the reaction of 2-methoxypropene with different aldehydes

Aldehydes	Yield (%)	ee (%)
	99	98
$\text{Ph}-\overset{\text{H}_2}{\text{C}}-\text{C}\equiv\text{C}-\text{CHO}$	85	93
$\text{Ph}-\text{C}\equiv\text{C}-\text{CHO}$	99	91
$\text{PhCH}_2\text{CH}_2\text{CHO}$	98	90
$\text{PhCHO}$	83	66
$c\text{-C}_6\text{H}_{11}\text{CHO}$	79	75

The ee was determined by preparation of the (*S*)-MTPA ester of the corresponding  $\beta$ -hydroxy ketone. Analysis was done by <sup>1</sup>H NMR (CDCl<sub>3</sub>, 400 MHz) spectroscopy.

Ding and coworkers explored the solid state structure of the catalyst.<sup>5</sup> From the crystal structure of the NOBIN backbone tridentate titanium Schiff base complex, it is clear that two ligands are bound to a single metal center in an octahedral environment. There exists two different coordination environments for the ligand around the metal center, for example either the complex exist in a homochiral (both the ligands have *S* chiral configuration) environment or in a heterochiral (one ligand is *R* and the other one is *S*) environment (figure 5.3).<sup>5</sup>

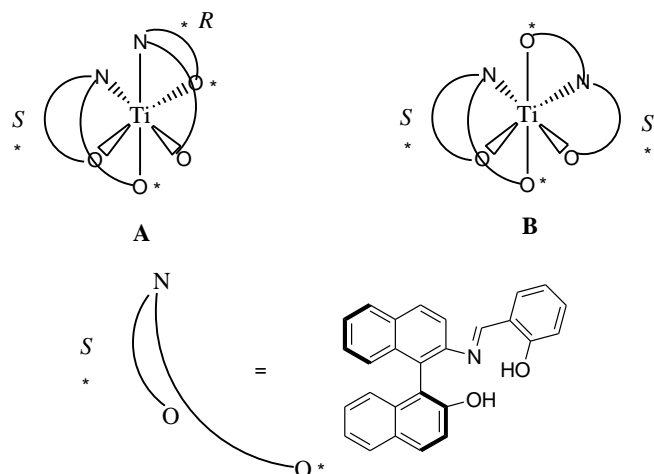


**Figure 5.3.** Two different coordination environments of the ligands around the metal center.

Figure 5.4 shows the preference of the nucleophile to choose one face of the aldehyde relative to the other. Carreira et al. proposed this structural factor of the catalyst to be the key reason for getting enantioselectivity in aldol addition reactions.<sup>6</sup> Considering the fact that, it is necessary to have steric bulk at the *ortho* position of the phenol unit in the side arm to get high enantioselectivity, we wanted to explore the effect of helicity by extending the side arm with fused phenyl rings. We synthesized new helical NOBIN backbone tridentate helical titanium Schiff base complexes and wanted to explore the effect of helicity on the enantioselectivity of the acetone aldol addition reaction between the 2-methoxypropene and aldehydes. These complexes have isoquininaldehyde-1-ol, phenanthryl, and benz[a]anthryl side arms. The presence of fused phenyl ring side arms can generate helical nature in these complexes which can be beneficial for getting high enantioselectivity in the asymmetric aldol reactions.

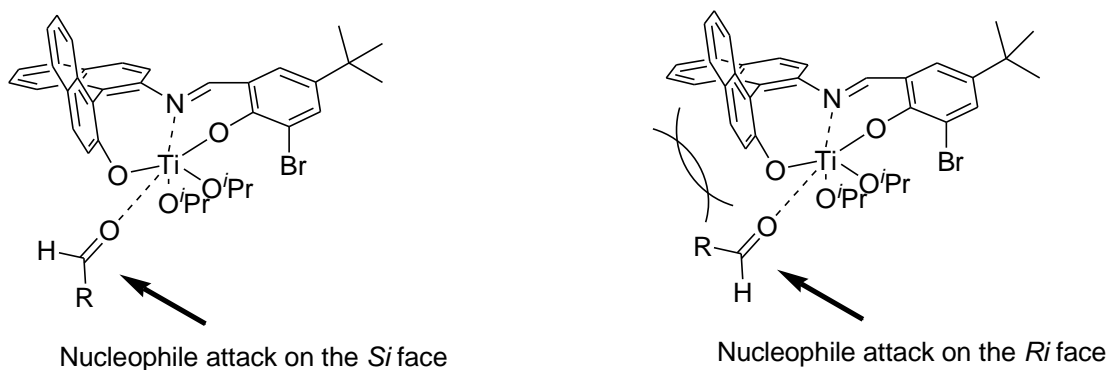


**Figure 5.4.** Two possibilities of approach for the nucleophile to the aldehyde moiety.

## 5.3 Results and discussions

### 5.3.1 Synthesis of (*S*)-NOBIN backbone isoquininaldehyde side arm tridentate Schiff base ligand

Synthesis of the ligand (*S*)-**4** was performed by refluxing a mixture of (*S*)-NOBIN and 2-quininaldehyde in ethanol for 8 hours. A cream colored precipitate came out of solution with 81% yield (figure 5.5).

Synthesis of ligands (*S*)-**3** and (*S*)-**5** were described in the previous chapter. In this chapter, we will describe the synthesis of the titanium complexes with these ligands in details.

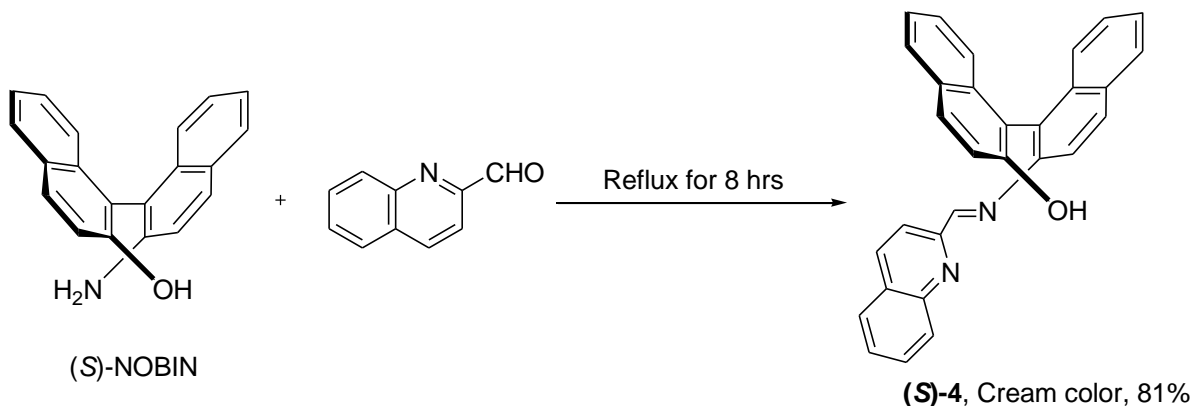


**Figure 5.5.** Scheme for the synthesis of ligand (*S*)-**4**.

### 5.3.2 Characterization of ligand (*S*)-**4**

<sup>1</sup>H NMR (CDCl<sub>3</sub>, 400MHz) spectral assignment is shown in figure 5.6. However, most of the peaks for the aromatic protons produce long range splitting pattern in the spectrum due to the presence of fused aromatic rings.



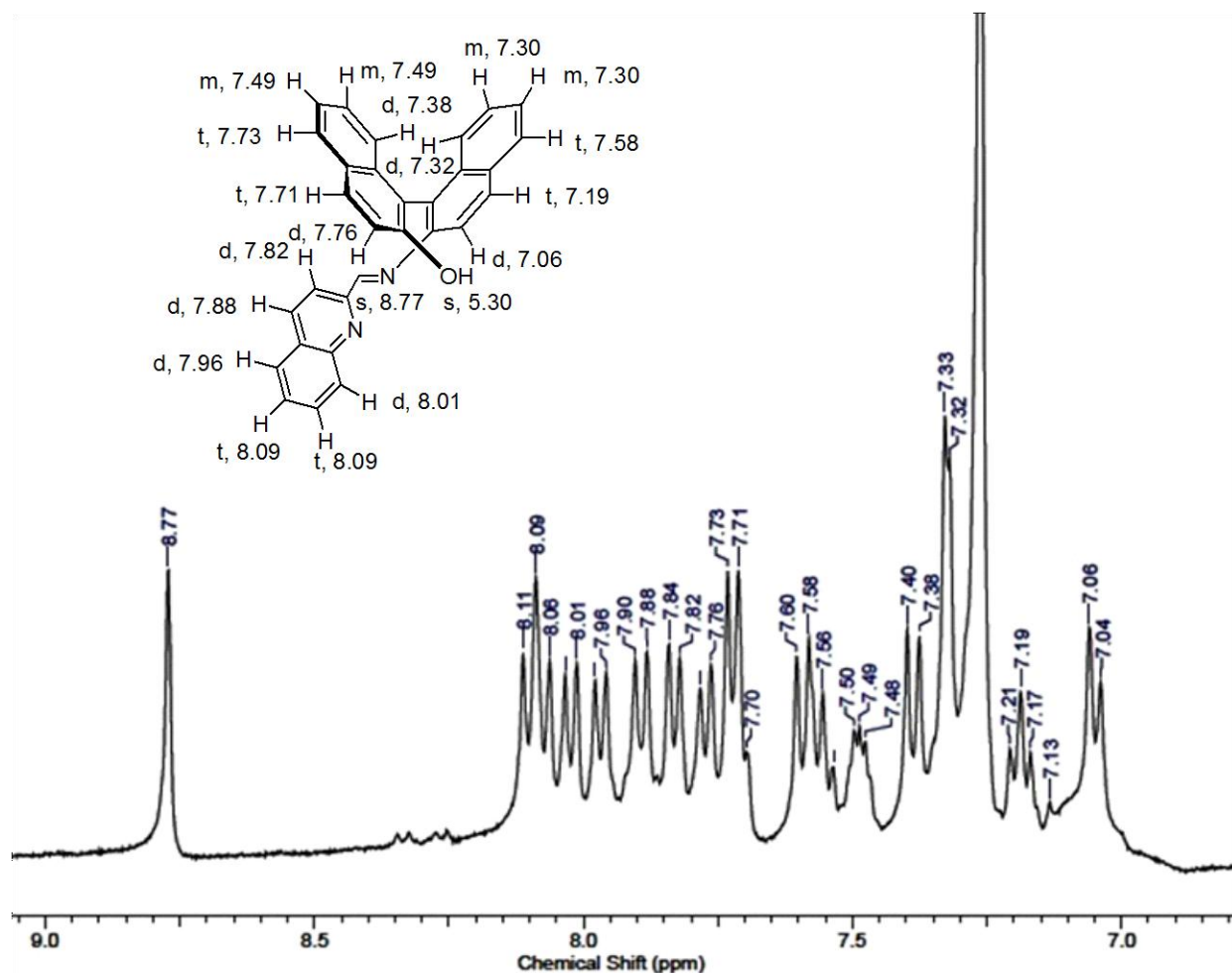


**Figure 5.6.** <sup>1</sup>H NMR (CDCl<sub>3</sub>, 400 MHz) spectrum of ligand (S)-4.

Single crystals of ligand (S)-4 were grown from slow diffusion method from dichloromethane and hexane solvent mixture. The crystal system is hexagonal in nature with P6(5) space group. It is evident from the crystal structure that the two naphthyl rings in the NOBIN backbone are almost perpendicular to each other (figure 5.7). The space filling model is shown in figure 5.8.

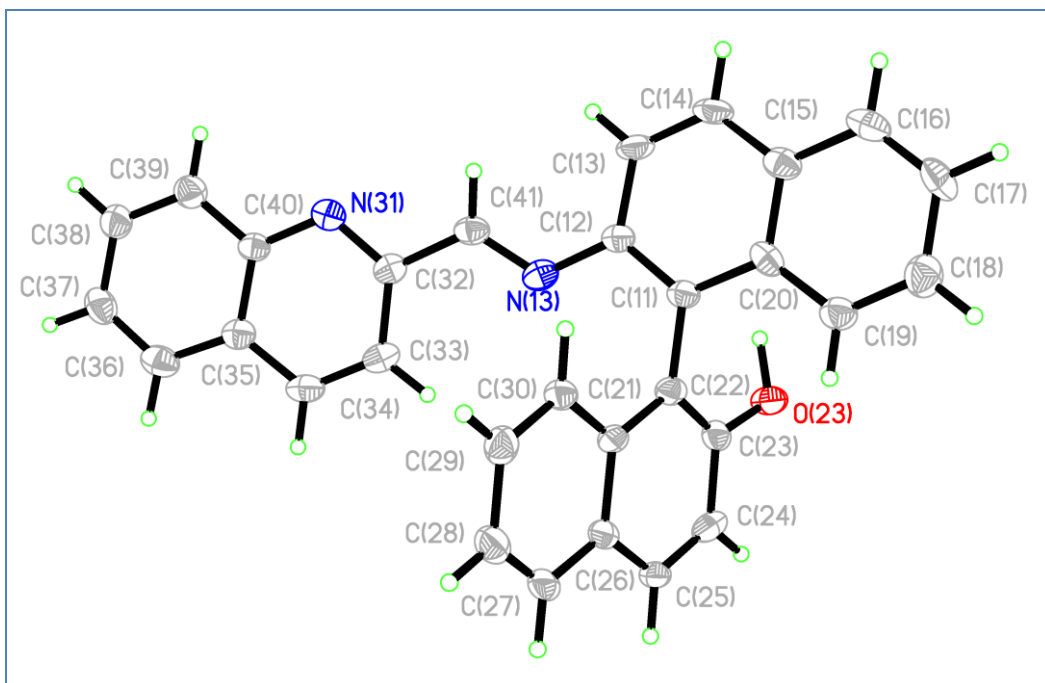


**Figure 5.7.** Crystal structure with atom numbering for ligand (S)-4.

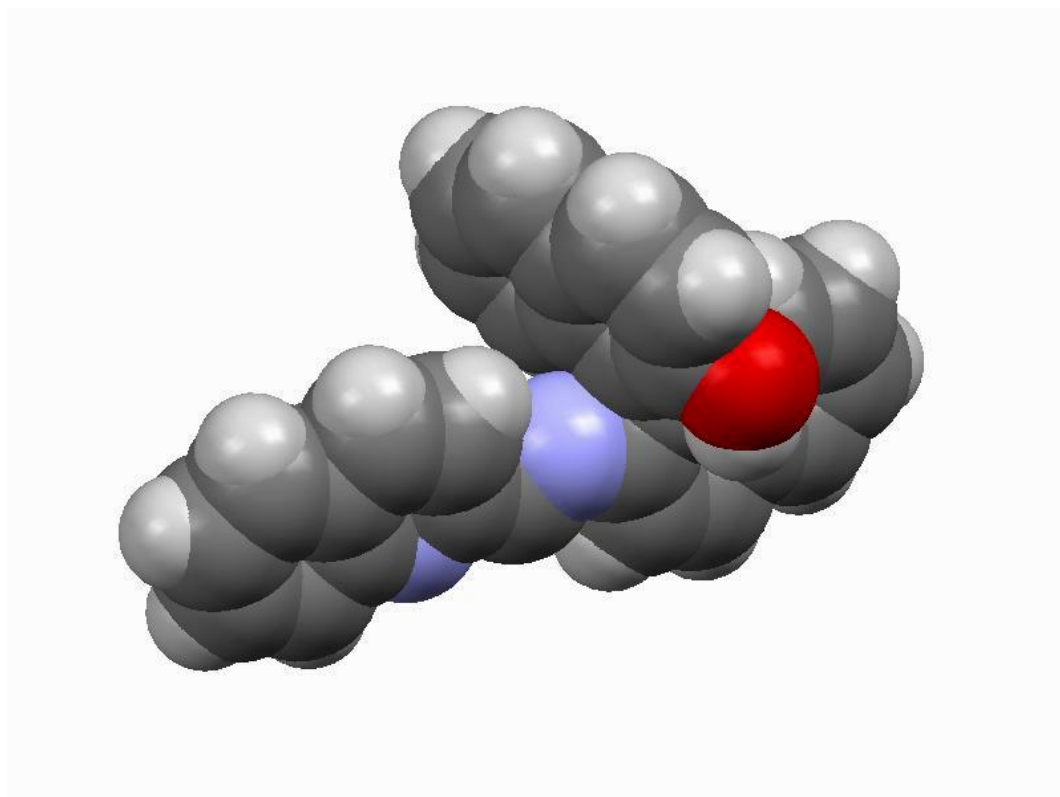
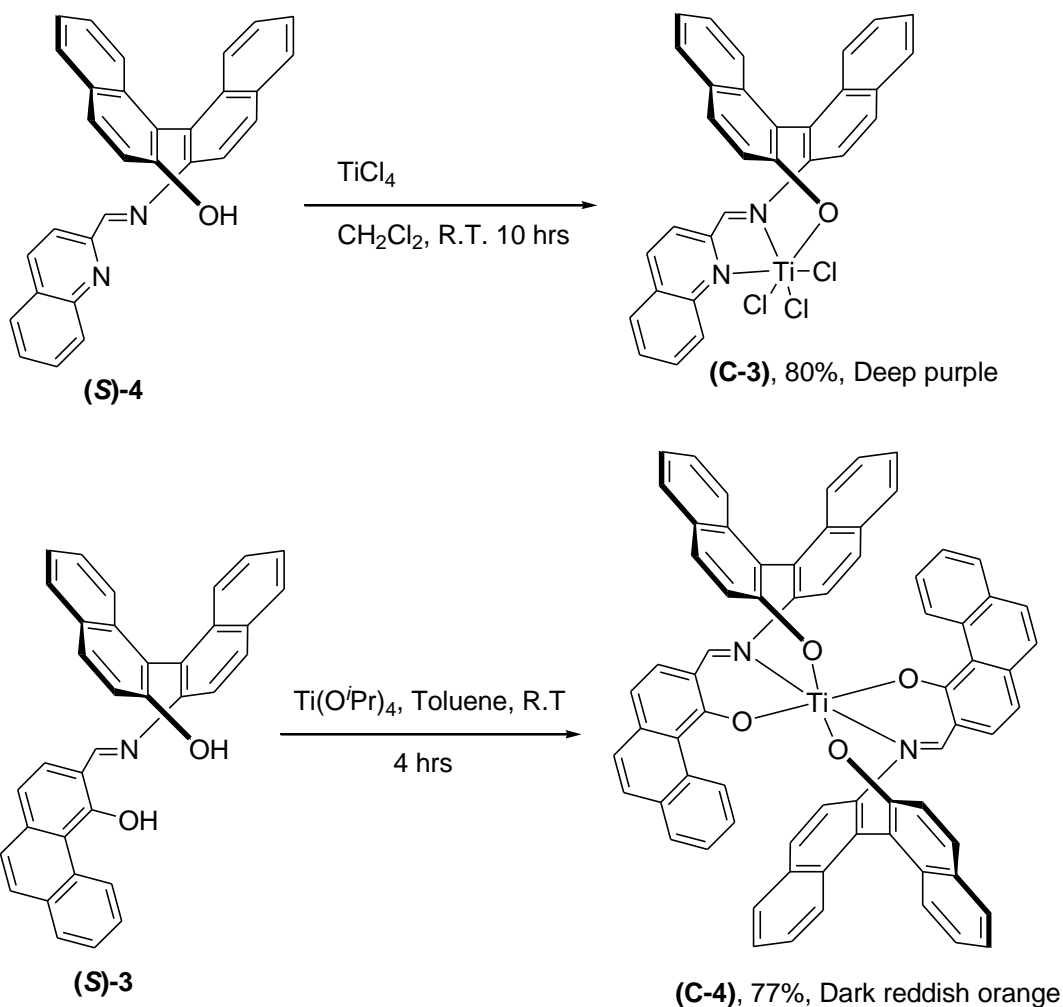


**Figure 5.8.** Space filling model of ligand (S)-4 (oxygen in red and nitrogen shown in blue).

### 5.3.3 Synthesis of complexes C-3, C-4 and C-5

Complex **C-3** was synthesized from  $\text{TiCl}_4$  and ligand **(S)-4** (figure 5.9). A mixture of the metal salt and the ligand were stirred for 10 hours at room temperature in  $\text{CH}_2\text{Cl}_2$ . A deep purple colored solid separated out from the solution. The solid was purified by washing with hexane and ether respectively. However, complexes **C-4** and **C-5** were synthesized from  $\text{Ti}(\text{O}^i\text{Pr})_4$  with ligands **(S)-3** and **(S)-5** respectively (figure 5.9). A mixture of  $\text{Ti}(\text{O}^i\text{Pr})_4$  and the ligand were stirred in the toluene solution at room temperature for 4 hrs. A bright red colored solid formed after solvent evaporation. These complexes were purified by washing with hexane.



Contd.....

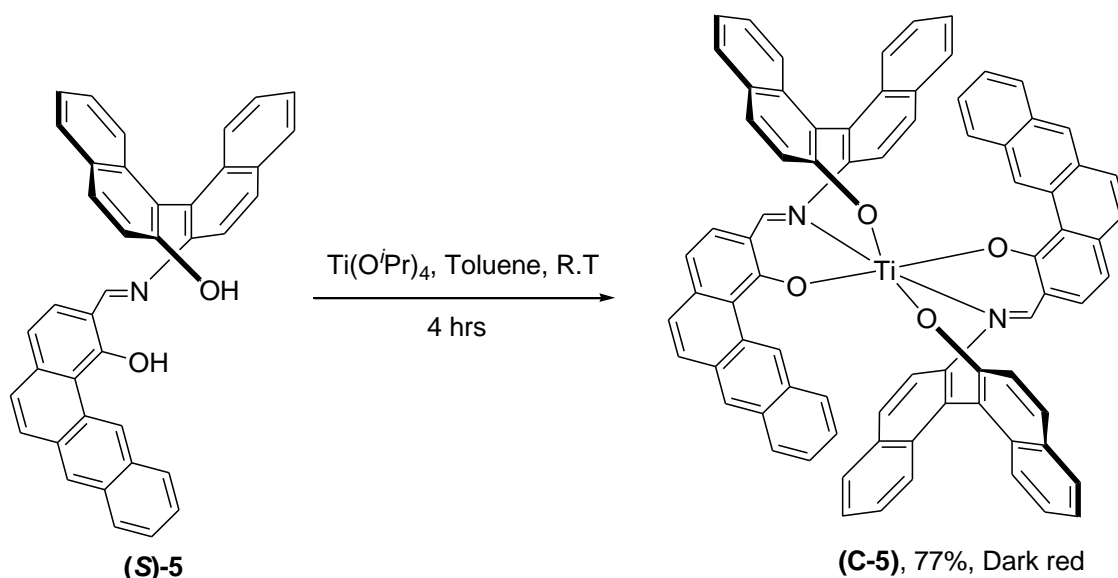


**Figure 5.9.** Titanium(IV) complexes (**C-3**, **C-4** and **C-5**) with (*S*)-NOBIN backbone ligands.

#### 5.3.4 Characterization of complexes **C-3**, **C-4** and **C-5**

Complex **C-3** showed a broad  $^1\text{H}$  NMR ( $\text{CDCl}_3$ , 400 MHz) spectrum. The reason for this broad NMR spectrum may be attributed due to the fluxional behavior arising from the rapid interconversion between the different isomers (facial and meridional) characteristics of an octahedral tridentate ligand-metal complex. We observed this broad  $^1\text{H}$  NMR spectrum for many of the Ti(IV)-salan complexes with tetradentate ( $\text{N}_2\text{O}_2$  donor sites) salan ligands and this phenomenon for Ti(IV)-salan complexes is attributed to the rapid interchange between the  $\Delta$  and the  $\Lambda$  isomers in the  $\beta$ -cis geometry.<sup>5</sup>

The mass spectrum of the complex **C-3**, showed the presence of a mono-cationic Ti(IV)-salan (imine bond reduced version) monochloride complex (figure 5.10). We believe, that the complex **C-3** is highly unstable in air and in the appropriate solvent medium (probably ethanol), the imine bond in the Schiff base reduces to form an amine bond (salan ligand). It is possible that during the purification step, we washed the complex with ethanol and during this washing step ethanol reduces the imine bond to form a Ti(IV)-salan complex. The simulated isotopic pattern of the complex (bottom figure, 5.10) and the isotopic pattern obtained from the mass spectrum of the complex (top figure 5.10) matches quite well. The IR spectrum of the complex showed the presence of Ti-O and Ti-Cl bonds ( $\nu_{\text{Ti-O}}$  at  $747.00\text{ cm}^{-1}$ ,  $\nu_{\text{Ti-Cl}}$  at  $696.26\text{ cm}^{-1}$ ).

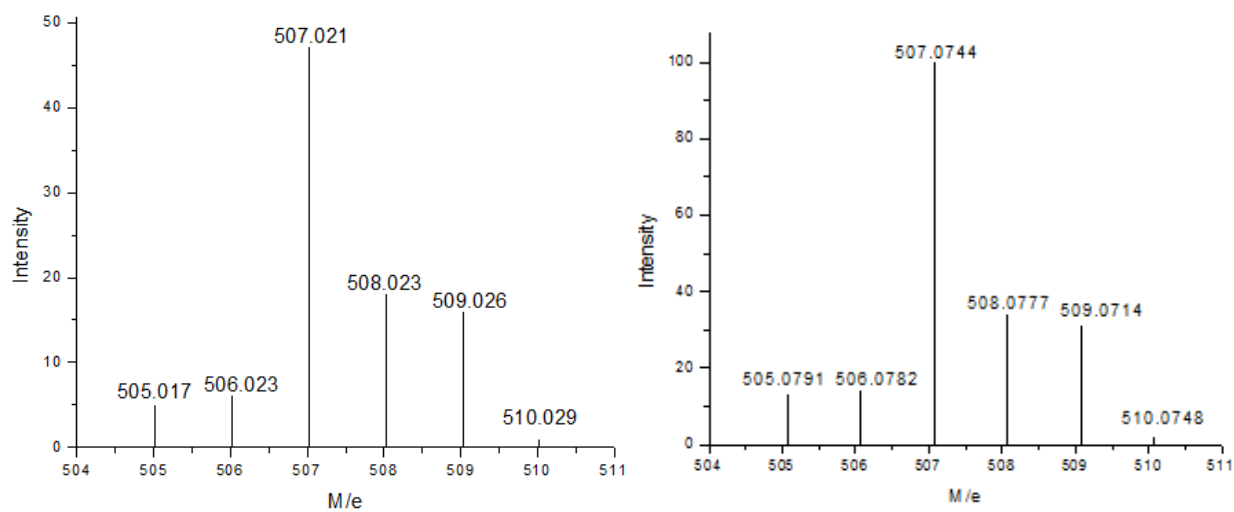
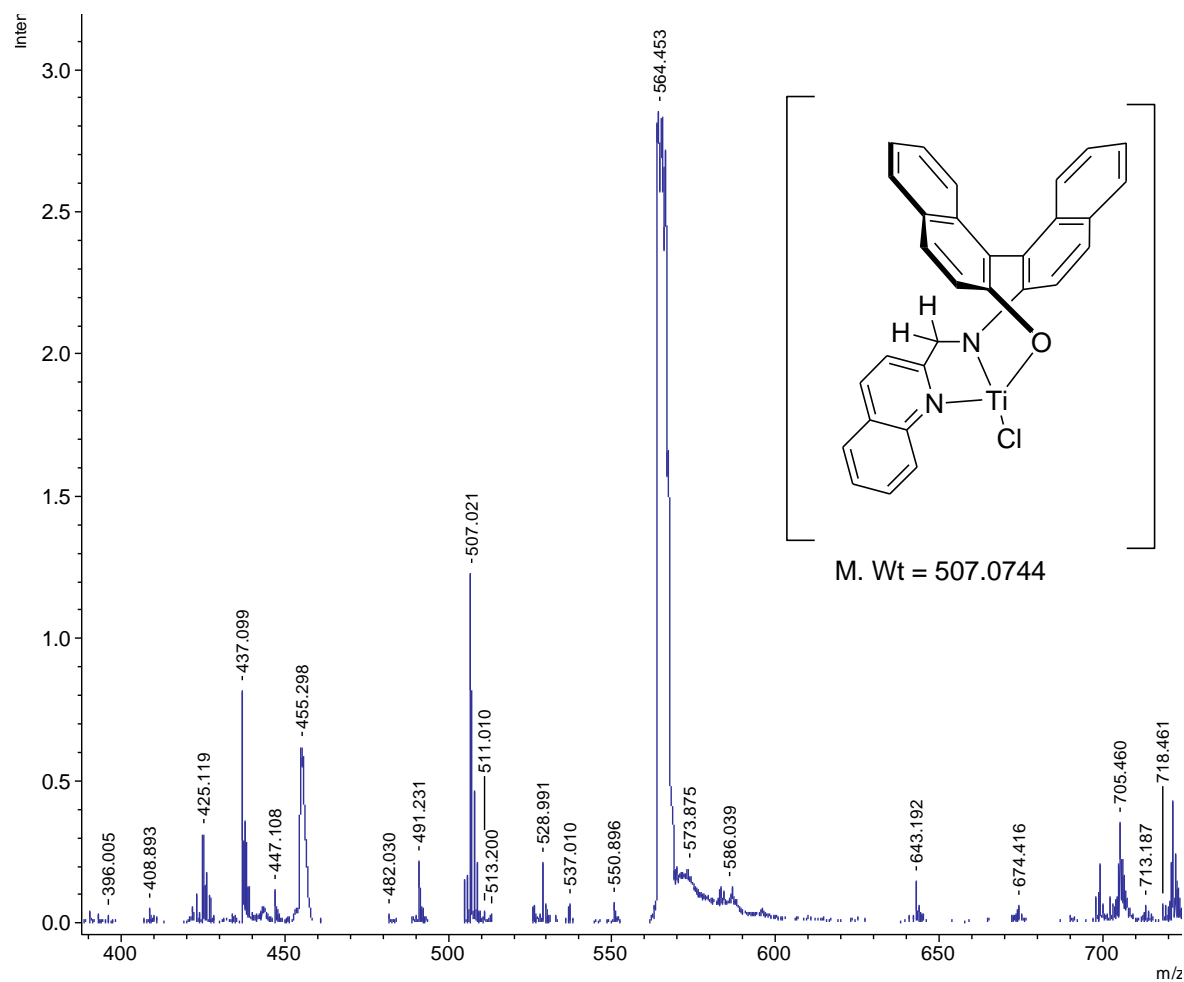


**Figure 5.10.** Entire MALDI-TOF spectrum of complex **C-3** (top), observed molecular ion peak with isotopic pattern (bottom left), and simulated pattern (bottom right).

Complexes **C-4** and **C-5** were characterized by  $^1\text{H}$  NMR ( $\text{CDCl}_3$ , 400 MHz), IR, mass spectrometry, circular dichroism (CD) and single crystal analysis methods.  $^1\text{H}$  NMR spectra of complexes **C-4** and **C-5** showed the presence of  $C_2$  symmetry in the molecule. All the peak assignments for molecules **C-4** and **C-5** are shown in figures 5.11 and 5.12 respectively. However, some of the peaks are difficult to assign due to the presence of long range couplings and the complicated nature of the spectrum. Both the molecules showed the absence of the aromatic hydroxyl peaks and this can be attributed due to the involvement of these aromatic hydroxyl groups in the complexations.

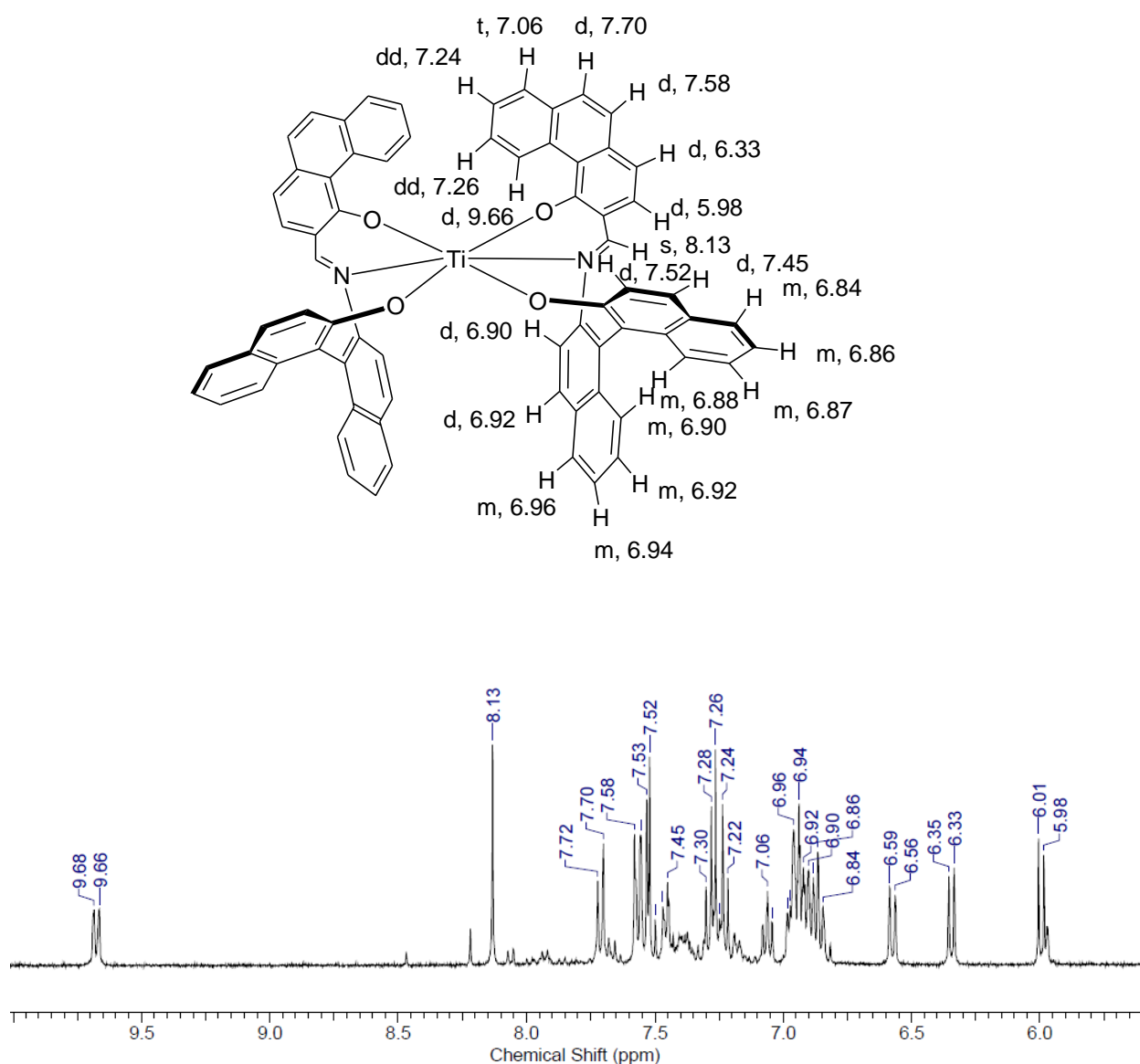


**Figure 5.11.**  $^1\text{H}$  NMR ( $\text{CDCl}_3$ , 400 MHz) peak assignments for complex **C-4** (top).

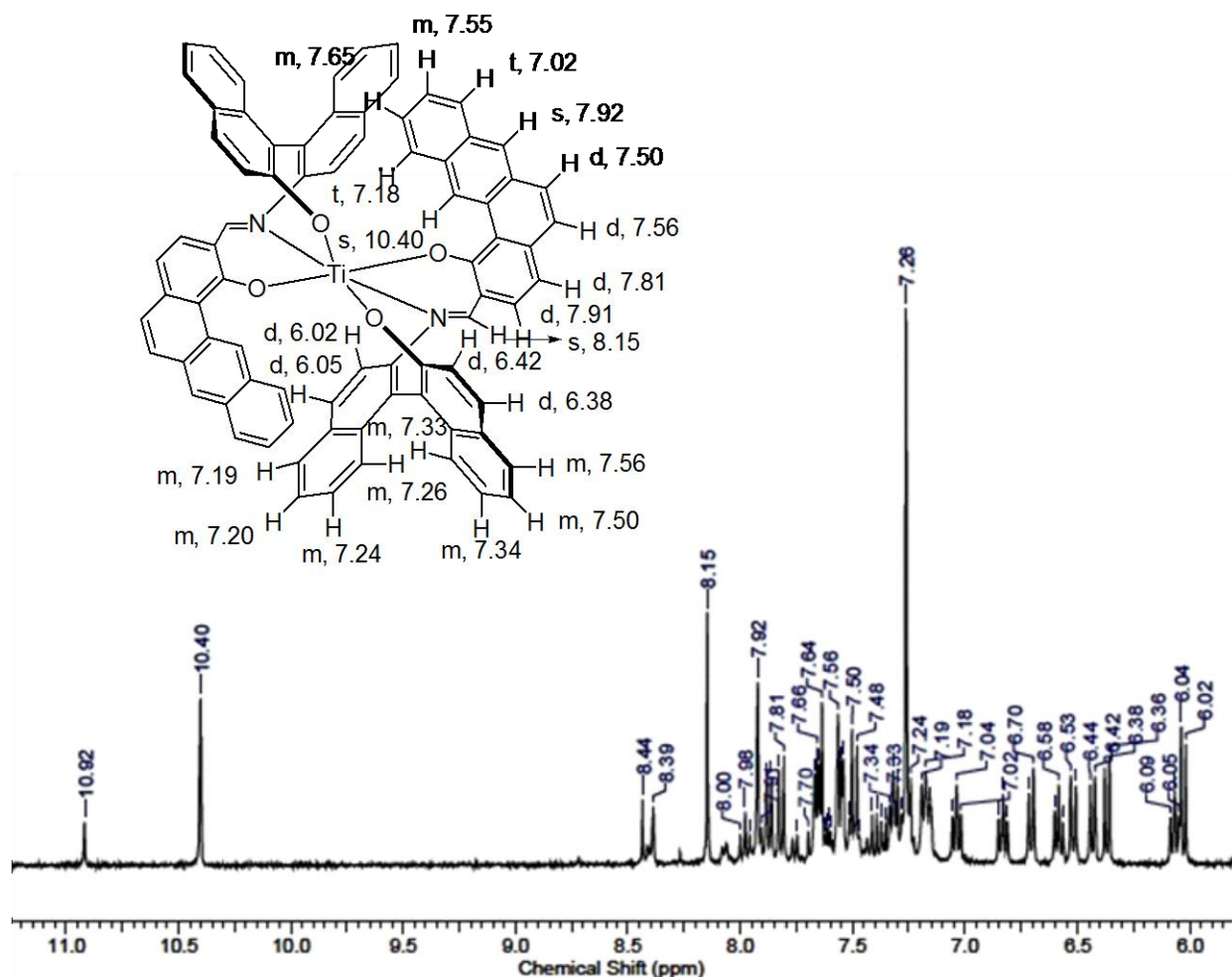


**Figure 5.12.**  $^1\text{H}$  NMR ( $\text{CDCl}_3$ , 400 MHz) peak assignments for complex **C-5**.

Mass spectra (ESI-MS) of the complexes **C-4** and **C-5** are shown in figures 5.13 and 5.14 respectively. The observed and the simulated isotopic pattern of the mass spectra of the molecules match quite well. From the mass spectral data, we can conclude that there are two ligands coordinated to one metal center in an octahedral environment.

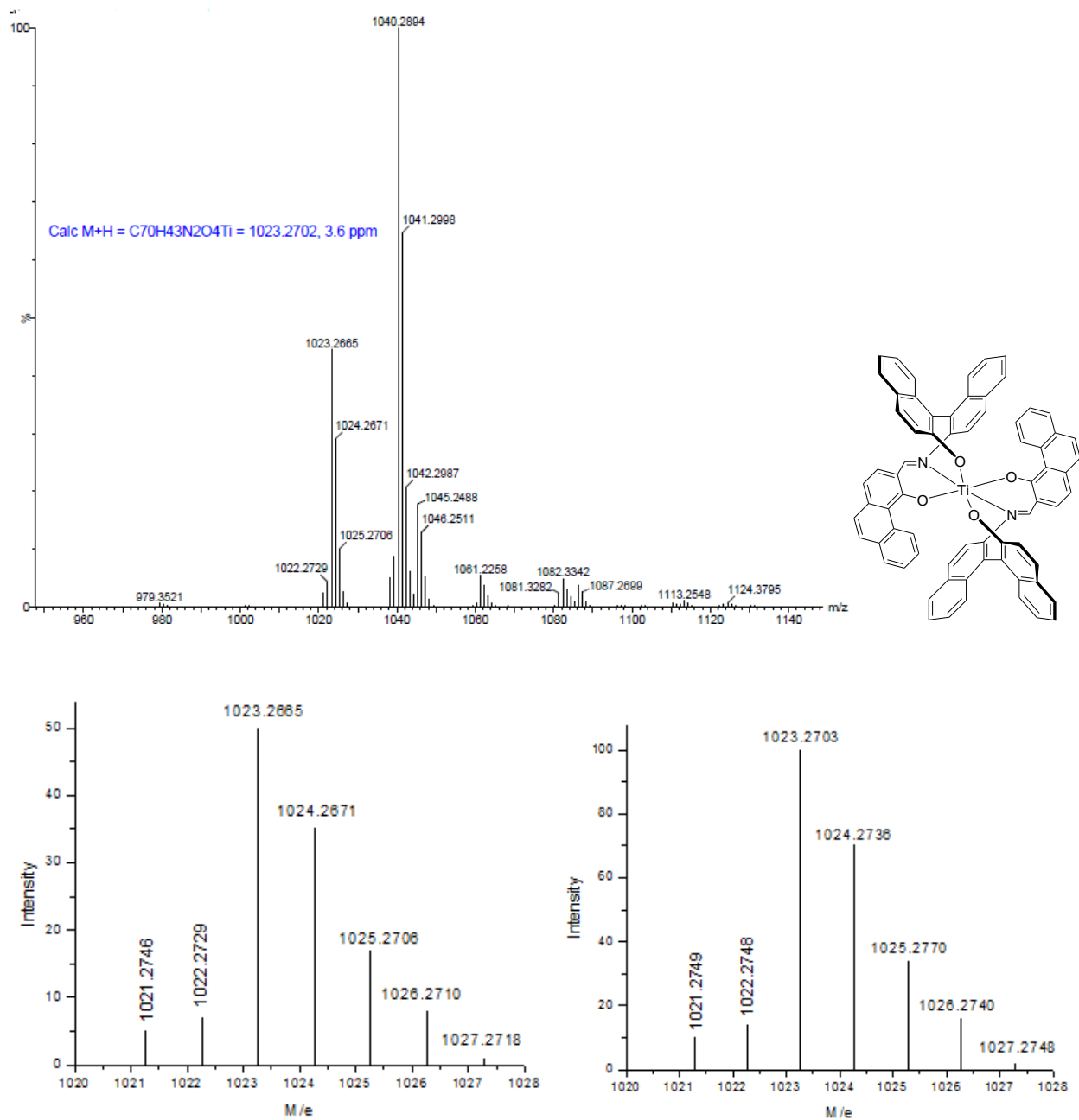


**Figure 5.13.** Entire ESI-MS of complex C-4 (top), observed molecular ion peak with isotopic pattern (bottom left), and simulated isotopic pattern (bottom right).



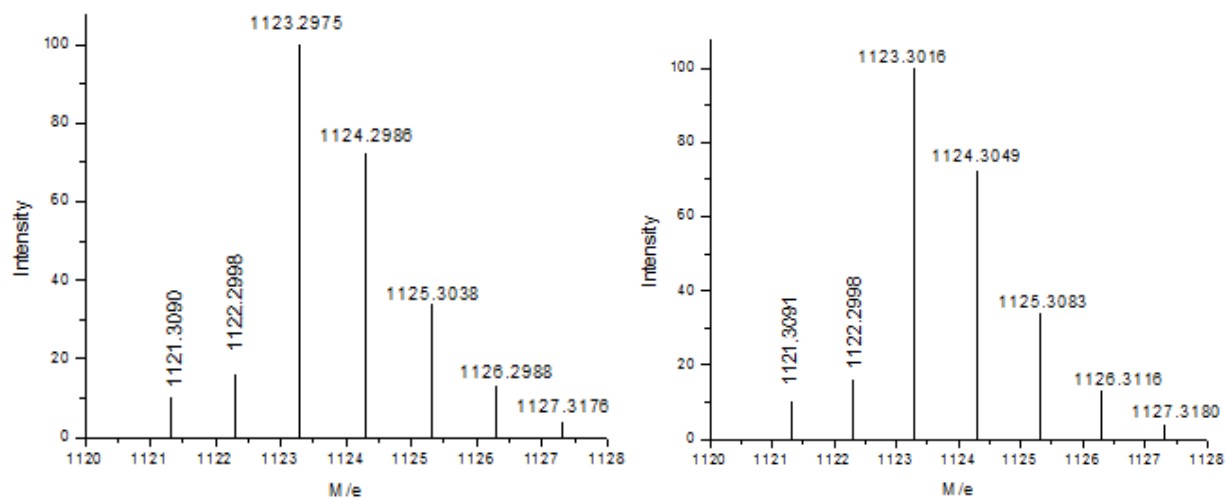
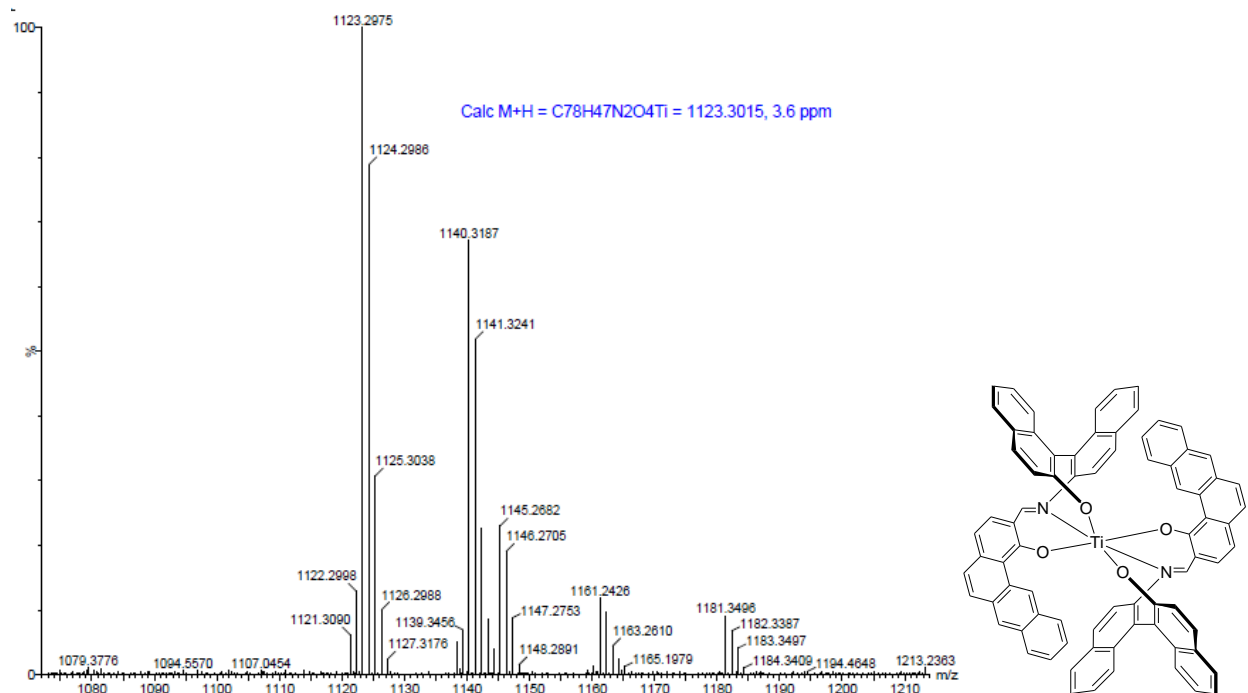


**Figure 5.14.** Entire ESI-MS of **C-5** (top), observed isotopic pattern for the molecular ion peak (bottom left), and simulated isotopic pattern (bottom right).

The CD spectra of complexes **C-4** and **C-5** with the CD spectra of the corresponding free ligands are shown in figures 5.15 and 5.16 respectively. There are significant changes between the CD spectrum of the free ligand (**S-3**) and the complex **C-4** (figure 5.15). The CD peaks have shifted towards higher wavelength in the complex **C-4** than in the free ligand (**S-3**). This phenomenon can be attributed to the lowering in the energy of the antibonding orbitals or the

increase in the energy level of the bonding orbitals after complexation.<sup>7</sup> The sharp positive absorption peak at 235 nm in the free ligand (*S*)-**3** has transformed into a positive peak at 252 nm with a shoulder at 265 nm in the complex **C-4** and this can be attributed to the dipole dipole interactions of the two naphthyl rings in the (*S*)-NOBIN backbone in two different spatial environment in the octahedral complex **C-4**.<sup>7</sup> The two other negative peaks due to the L-transitions at 275 nm and at 335 nm are expressed weakly in the ligand (*S*)-**3** due to the complete absence of symmetry in the NOBIN backbone, whereas these two transitions (at 290 nm and at 335 nm) are quite sharp in the complex **C-4** due to the symmetrical environment of the two NOBIN units after complexation ( $C_2$  symmetric complex). The broad negative peak at 375-425 nm in the complex arises due to the absorption by the imine bond and the side arms in the complex **C-4**.<sup>7</sup>

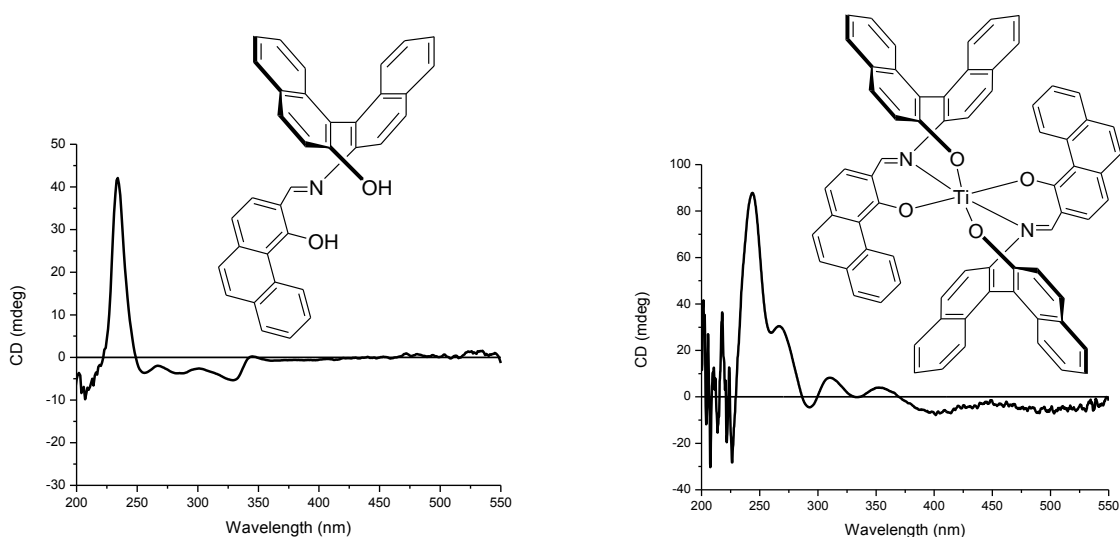


**Figure 5.15.** CD spectrum of the ligand (*S*)-**3** (left) and the complex **C-4** (right).

The interpretations of the CD spectra for the ligand (*S*)-**5** and the complex **C-5** are quite similar to the CD spectra of the ligand (*S*)-**3** and the complex **C-4**. However, there are two shoulders at 265 nm and at 280 nm for the main positive absorption peak at 245 nm in the complex **C-5**. Also, the two negative CD peaks at 330 nm and at 350 nm for the complex **C-5** have lower intensity than the corresponding peaks for the ligand. This suggests the less symmetric environment of the two naphthyl rings in the NOBIN backbone after complexation.

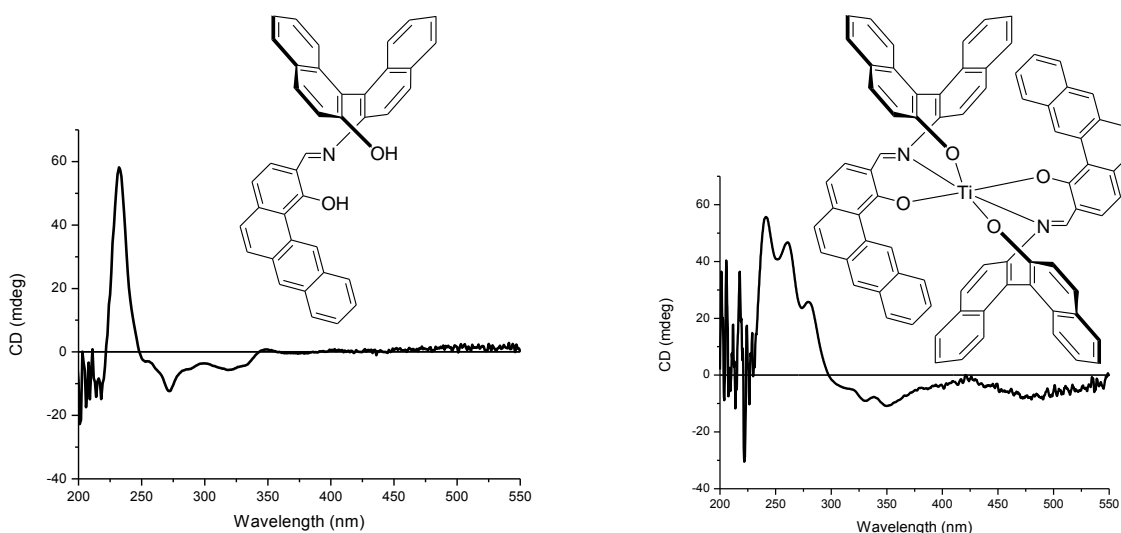


**Figure 5.16.** CD spectrum of the ligand (*S*)-**5** (left) and the complex **C-5** (right).

Single crystals of both the complexes **C-4** and **C-5** are grown by heating cooling method from ethanol solution. From the crystal structures of these complexes, it is clear that both of these complexes adopt an octahedral geometry with *M* configuration in the solid state. Two tridentate ligands bound to one metal center generating an octahedral geometry. Complex **C-4** crystallizes out as eight identical molecules present in one unit cell (figure 5.17). The geometry and the atom numbering around the two titanium centers in the two molecules present in the unit cell are shown in figure 5.17. The eight molecules in one unit cell distributed as four identical pairs. The titanium center denoted as Ti(1) of one molecule in a pair is shown in figure 5.17 and for the other molecule in the same pair, denoted as Ti(2). Both the molecules have homochiral (*R, R*) coordination geometry of the ligand centers around the central titanium. Each individual molecule in the unit cell has  $C_2$  symmetry. Capped stick arrangement for complex **C-4** with one pair of molecules are shown in figure 5.18. From the spatial arrangement of the two molecules in one pair, it is clear that there is  $\pi$ - $\pi$  stacking between the side arms of the two molecules in each pair. From figure 5.18, it is clear that each pair is  $C_2$ -symmetric as well.

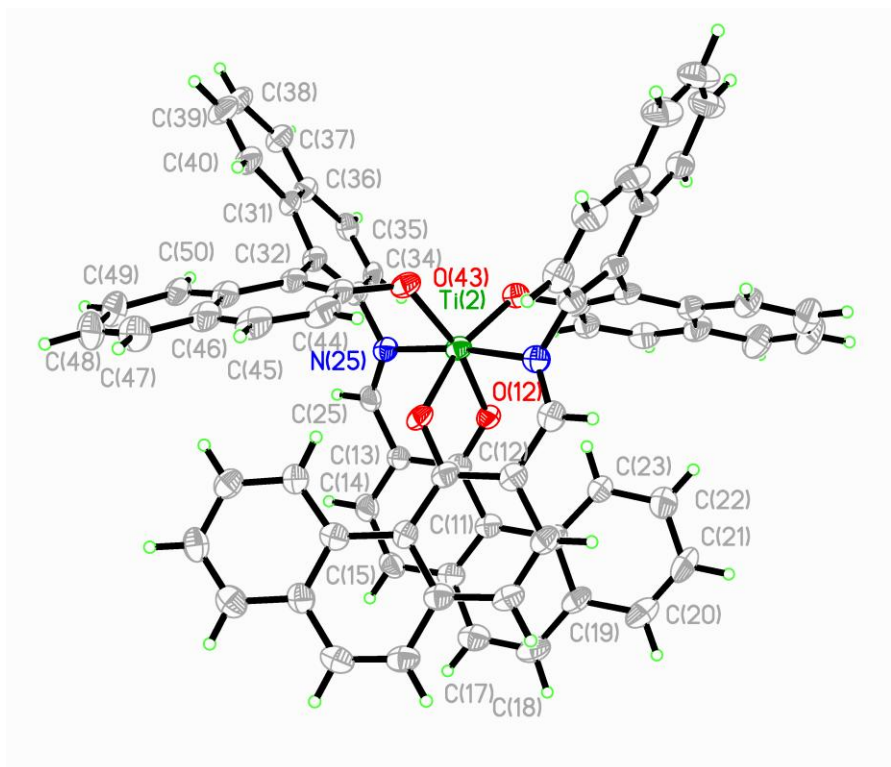
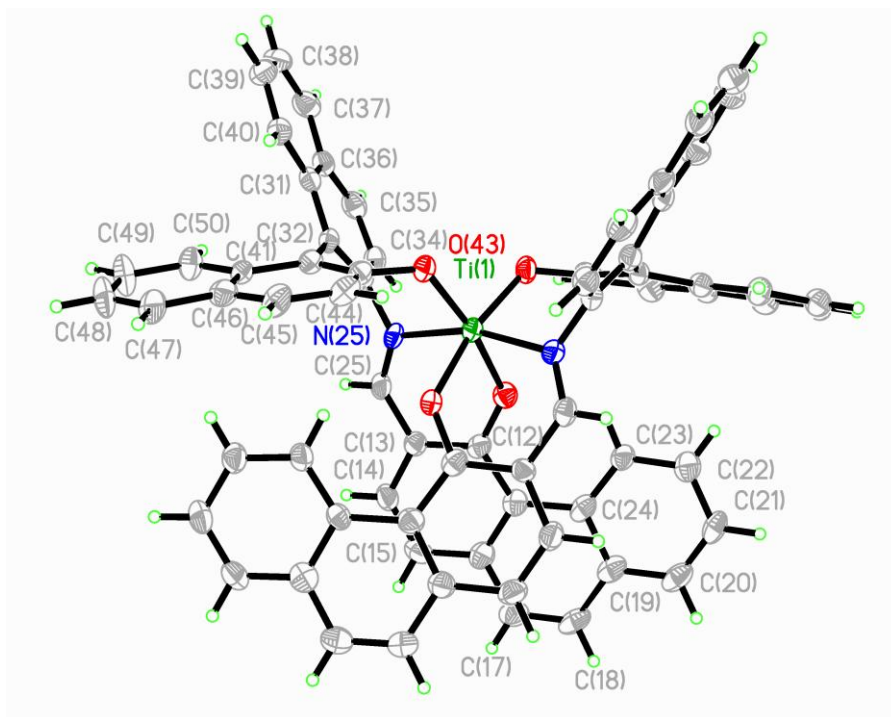


**Figure 5.17.** One pair of molecules with atom numbering for complex C-4.

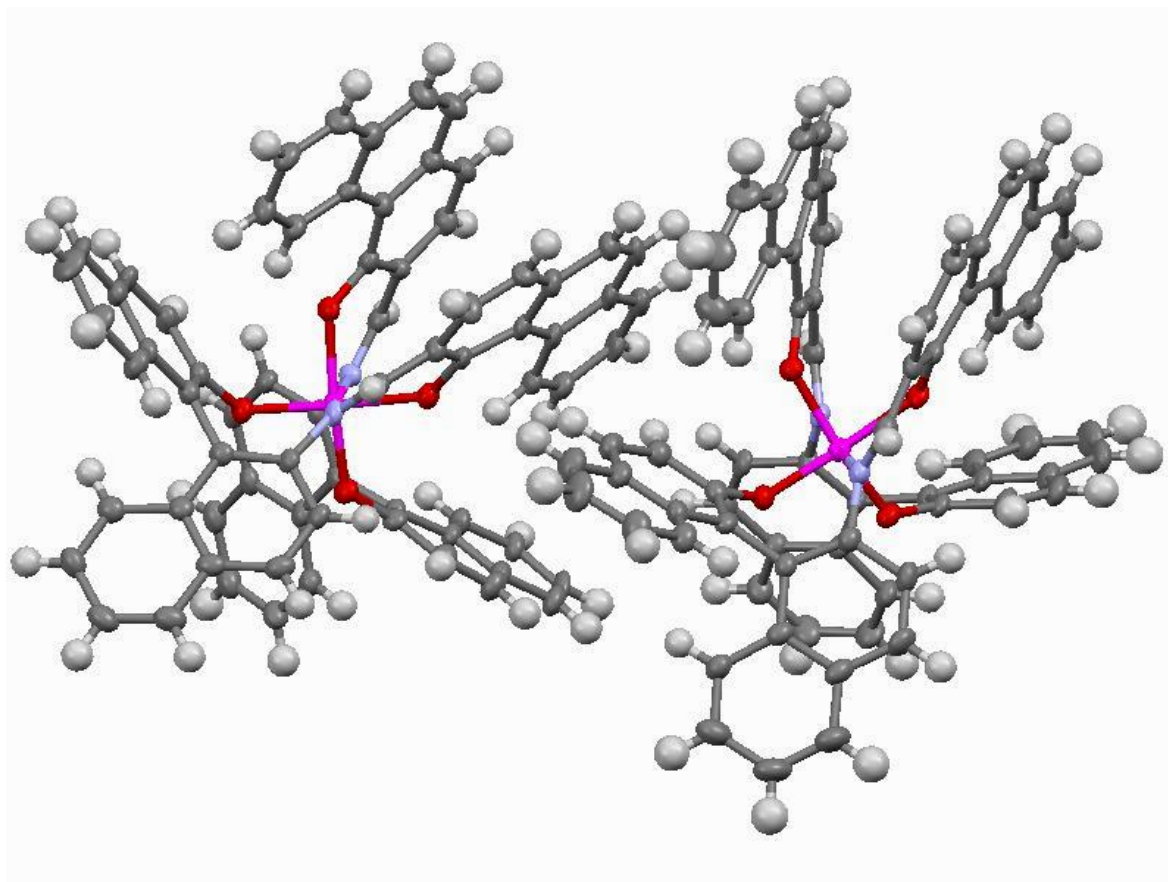
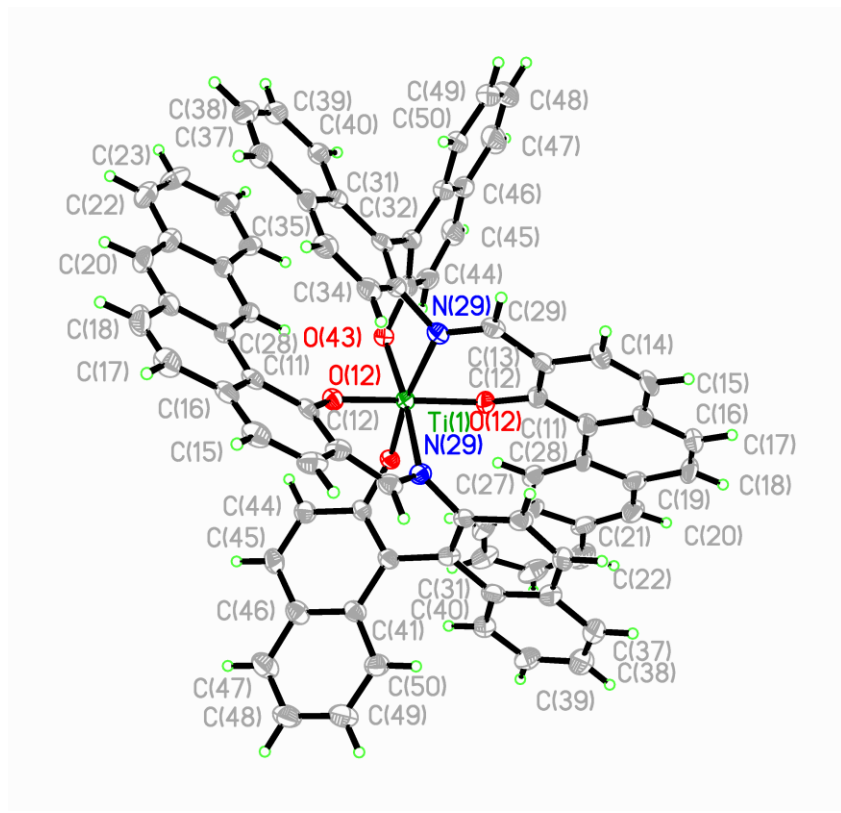


**Figure 5.18.** Thermal ellipsoid (50%) model of the arrangement of one pair of molecules in the complex **C-4**.

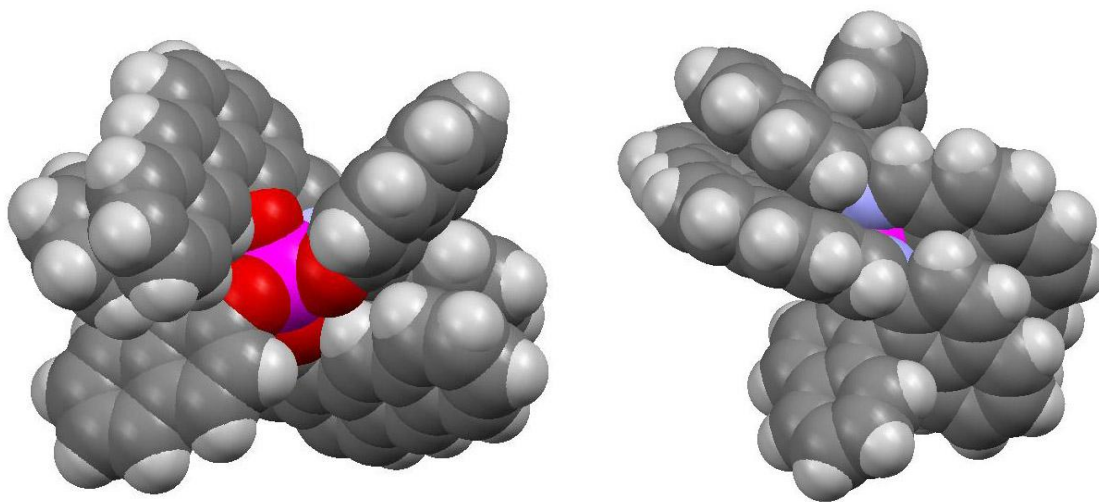
Complex **C-5** exists in the octahedral geometry with two tridentate ligands occupying the meridional positions in the octahedron. The significant difference between the two solid state structures of complexes **C-4** and **C-5** comes from the fact that, there is no  $\pi$ - $\pi$  stacking observed between the benz[a]anthryl side arms in the complex **C-5**, instead, the two side arms oriented exactly opposite to each other. Complex **C-5** has  $C_2$  symmetry present in its molecular structure, as can be predicted from the figure 5.19. There are four identical molecules present in the unit cell for complex **C-5**. The space filling model of complex **C-5** is shown in the figure 5.20. From the space filling model it is clear that there is  $\pi$ - $\pi$  stacking between the benz[a]anthryl side arm and the naphthyl ring in the NOBIN backbone.

Table 5.2 shows some basic structural parameters of complexes **C-4** and **C-5**. Both the complexes form orthorhombic crystal systems with  $P2(1)2(1)2(1)$  space group.

Table 5.3 shows a comparison of the selected bond lengths and bond angles of complexes C-4 and C-5. It is observed that the average bond lengths of the Ti-O bonds ( $\approx 1.9 \text{ \AA}$ ) are shorter than the average Ti-N bond lengths ( $\approx 2.2 \text{ \AA}$ ). Also, the bond angles support the octahedral structures for both the molecules.



**Figure 5.19.** Structure of complex C-5 with atom numbering.



**Figure 5.20.** Space filling model of complex C-5 (front view on left and back view on right).

**Table 5.2.** Some basic parameters for complexes **C-4** and **C-5**

Complex <b>C-4</b>		Complex <b>C-5</b>	
Empirical formula	C <sub>148</sub> H <sub>108</sub> N <sub>4</sub> O <sub>12</sub> Ti <sub>2</sub>	Empirical formula	C <sub>86</sub> H <sub>70</sub> N <sub>2</sub> O <sub>8</sub> Ti <sub>1</sub>
Formula weight	2230.18	Formula weight	1307.34
Temperature	120(2) K	Temperature	120(2) K
Wavelength	0.71073 Å	Wavelength	0.71073 Å
Crystal system	Orthorhombic	Crystal system	Orthorhombic
Space group	P2(1)2(1)2(1)	Space group	P2(1)2(1)2(1)
Unit cell dimensions a = 16.0470 (7) Å    α = 90 b = 22.6153 (10) Å    β = 90 c = 31.1102 (15) Å    γ = 90		Unit cell dimensions a = 15.5874 (14) Å    α = 90 b = 17.2424 (16) Å    β = 90 c = 24.5188 (17) Å    γ = 90	
Volume	11290.1 (9) Å <sup>3</sup>	Volume	6589.8 (10) Å <sup>3</sup>
Z	4	Z	4
Density (calculated)	1.312 g/cm <sup>3</sup>	Density (calculated)	1.318 mg/m <sup>3</sup>

**Table 5.3.** Selected bond lengths and bond angles for complexes **C-4** and **C-5**

Bond lengths ( <b>C-4</b> ) [Å]	Bond lengths ( <b>C-5</b> ) [Å]	Bond angles ( <b>C-4</b> )	Bond angles ( <b>C-5</b> )
Ti(1)-O(43) 1.846 (3)	Ti(1)-O(431) 1.864 (3)	O(12)-Ti(2)-O(43) 89.40 (12)	O(12)-Ti(1)- O(43) 91.71 (14)
Ti(1)-O(12) 1.940 (3)	Ti(1)-O(432) 1.858 (3)	O(12)-Ti(2)-N(25) 80.75 (12)	O(12)-Ti(1)- N(29) 87.16 (14)
Ti(1)-N(25) 2.148 (3)	Ti(1)-O(121) 1.878 (3)	O(43)-Ti(2)-N(25) 83.89 (13)	O(43)-Ti(1)- O(29) 91.71 (14)
Ti(2)-O(43) 1.837 (3)	Ti(1)-O(122) 1.884 (3)	O(43)-Ti(1)-N(25) 86.99 (12)	O(43)-Ti(1)- N(29) 84.62 (14)
Ti(2)-O(12) 1.938 (3)	Ti(1)-N(291) 2.200 (4)		
Ti(2)-N(25) 2.167 (3)	Ti(1)-N(292) 2.219 (4)		

### 5.3.5 Catalytic asymmetric aldol condensations

We investigated the catalytic ability of the titanium complexes (**C-4** and **C-5**) in the asymmetric aldol condensation reactions between cheap, commercially available 2-methoxypropene and different aldehydes. Previously in 1994, Carreira et al. observed that to obtain high value of enantioselectivity in the aldol additions between 2-methoxypropene and aldehydes, bulkiness at the *ortho* position of the phenol ring in the side arm of the ligand is an important factor.<sup>2</sup> We wanted to investigate the effect of helicity on the NOBIN backbone tridentate Schiff base derived titanium complexes on the asymmetric acetone aldol addition reactions. Complexes **C-4** and **C-5** were used as the catalysts in the aldol addition reactions between 2-methoxypropene and four different aldehydes (figure 5.21).

The reaction was carried out with 10 mol% of the catalyst. The catalyst was synthesized by stirring a solution containing the ligand and Ti(O<sup>*i*</sup>Pr)<sub>4</sub> in toluene at 23 °C for 4 hrs followed by the removal of toluene (figure 5.21). The reaction mixture was cooled to 0 °C and 2-methoxypropene was added. In this reaction, 2-methoxypropene is acting as a reactant as well as a solvent. 2, 6-di-*tert*-butyl-4-methyl pyridine and the aldehyde were added sequentially and the reaction was allowed to carry out for 16 hours for aromatic aldehydes and for 20 hours for aliphatic aldehydes. The reaction mixture was concentrated in vacuo and treated with a biphasic mixture of ether and 2N HCl to obtain the required  $\beta$ -hydroxy ketone in 67-80% yields.

The crystal structures of both the complexes (**C-4** and **C-5**) showed the formation of the octahedral complexes where all the six coordination sites are occupied by two tridentate ligands. This unique structural feature of titanium complexes clearly explained the reason why the aldol addition between the 2-methoxypropene and aldehydes proceeds slowly. With the addition of the 2-methoxypropene, the coordination sphere of the octahedral titanium complex must break to accommodate the substrate molecules. However, to elucidate the actual mechanism, we need more experimental evidences. In figure 5.22, we proposed a reaction mechanism for the aldol addition reactions.



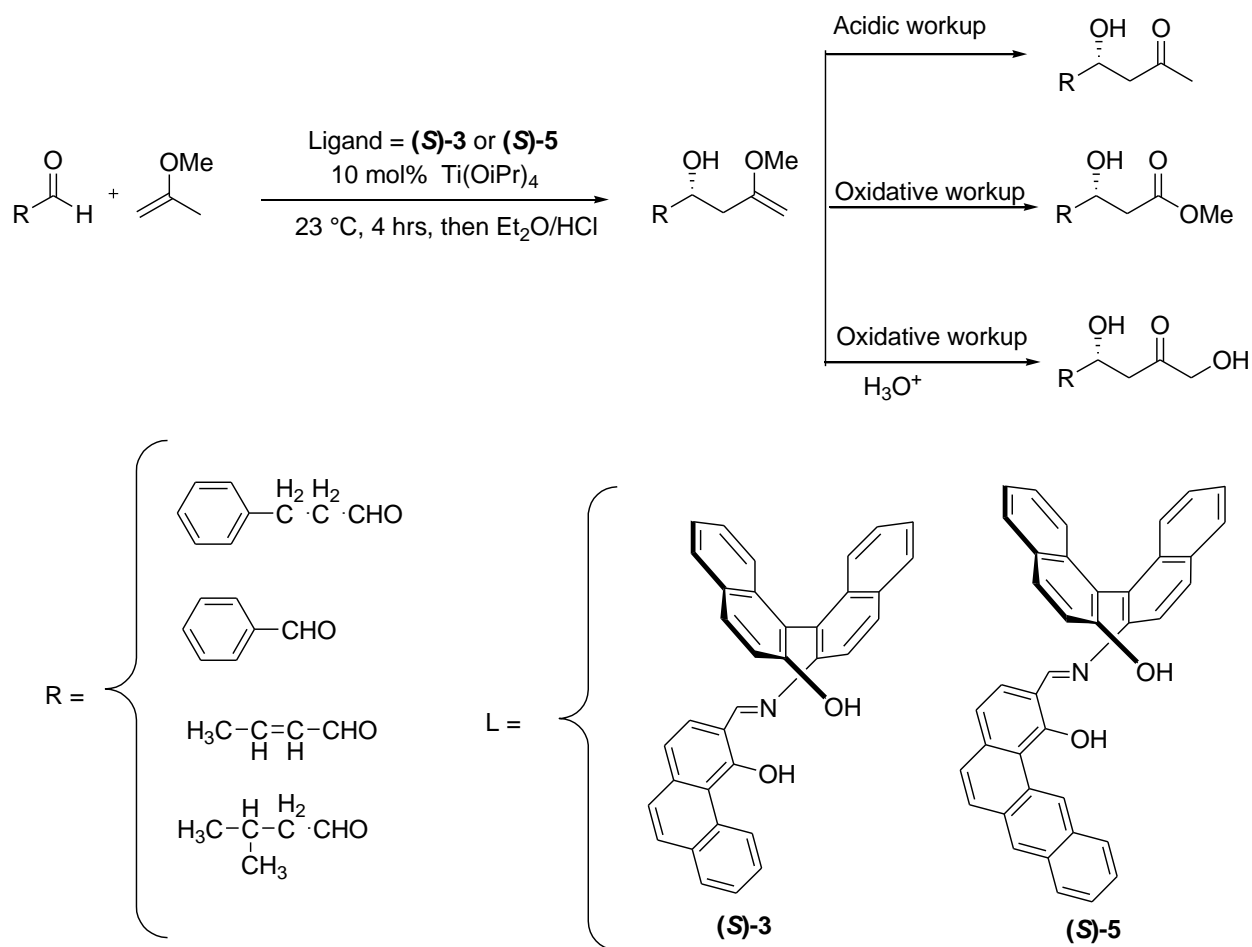


**Figure 5.21.** Schematic of aldol addition reactions catalyzed by Ti complexes.

In figure 5.22, the octahedral titanium complex with two tridentate coordinating ligands is represented as **A**. After the addition of the 2-methoxypropene, one ligand dissociates and the isopropanol ligands coordinates the titanium center and the geometry of the complex transforms to a trigonal bipyramidal, represented as **B**. The source of isopropanol is believed to be from the inside of the crystal lattice in the octahedral titanium complexes as we have observed the presence of uncoordinated isopropanol inside the crystal lattices of octahedral titanium complexes. With the addition of the aldehyde the complex again transform to an octahedral complex **C** where the R group in the aldehyde is facing away from the NOBIN backbone of the Schiff base ligand (figure 5.23). The nucleophilic attack by the deprotonated 2-methoxypropene on the aldehyde and subsequent bond rearrangement followed by acidic workup shown in step **D** leads to the formation of the  $\beta$ -hydroxy ketone adduct. The complex goes back to its original state **A** by the subsequent attack by the tridentate Schiff base ligand.

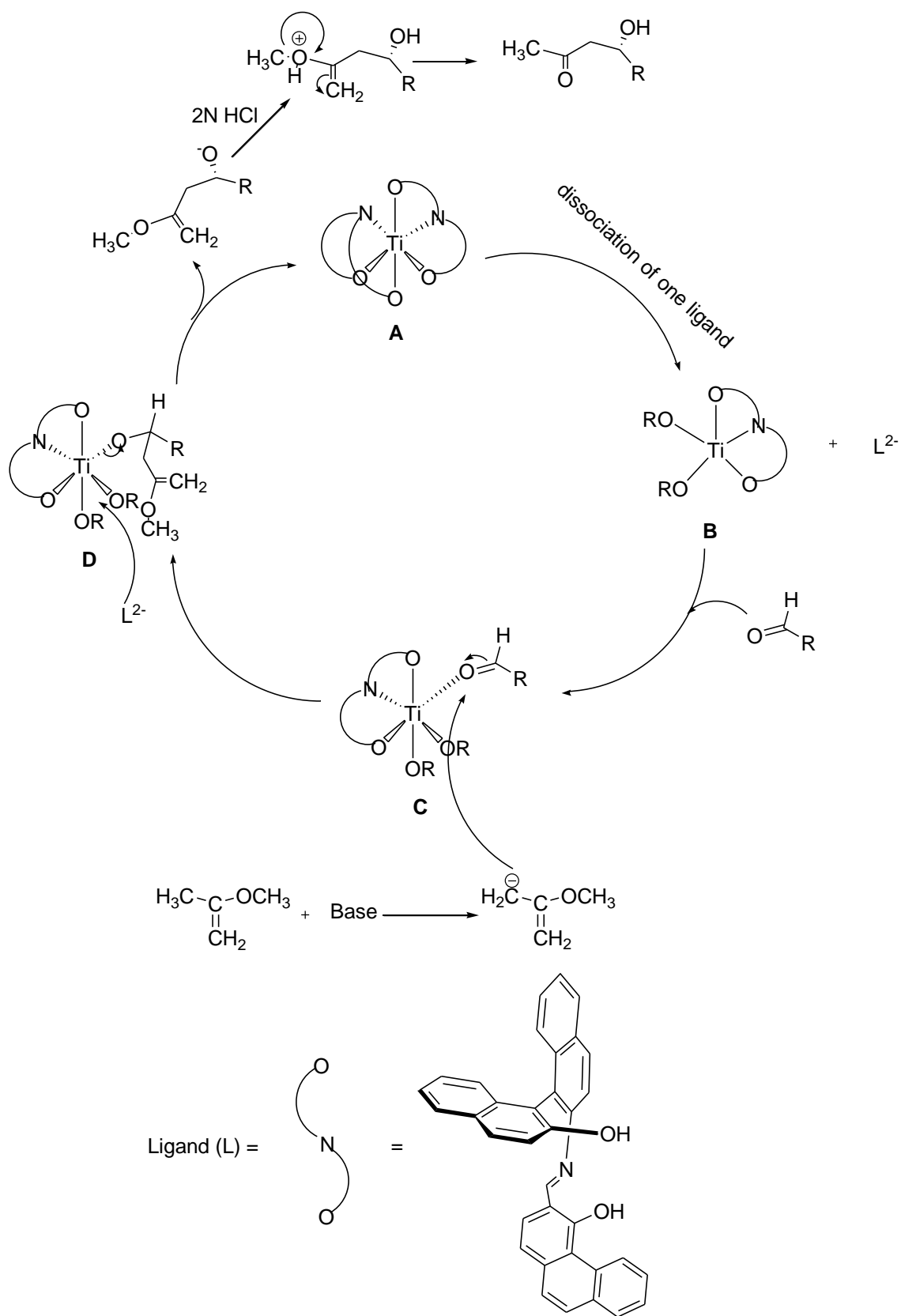


**Figure 5.22.** Proposed mechanism for aldol condensation.

During the reaction, the source of the enantioselectivity can be explained from the orientation of the coordinated aldehyde with respect to the NOBIN backbone (figure 5.23). Due to the perpendicular orientation of the two naphthyl rings in the NOBIN backbone, there are steric limitations, and thus it is more energetically favorable for the R group from the aldehyde to orient away from the NOBIN backbone leaving only the *Si* face of the aldehyde exposed towards the nucleophile. It was observed that the steric bulk at the *ortho* position of the phenolic hydroxyl group in the side arm of the Schiff base ligand is an important factor for obtaining high enantioselectivity in the acetone aldol addition reactions. Our objective was to investigate the effect of the helicity by extending the side arm of the ligand on the enantioselectivity of the aldol addition adducts. We observed the enantioselectivity reached as high as 55%, which is still less than by the ligand system introduced by Carreira (figure 5.2).<sup>2</sup> This shows that the energy difference between the two possible geometries leading to the two different isomers shown in figure 5.23 is not high enough to produce one enantiomer exclusively.

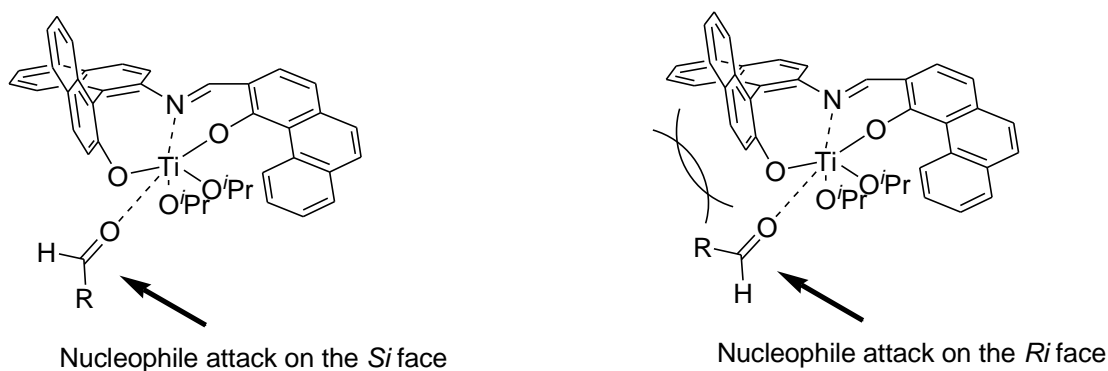


**Figure 5.23.** Preference of attack by the nucleophile on the aldehyde moiety.

The enantioselectivity was measured by forming a derivative of the  $\beta$ -hydroxy ketone with (*R*)-*O*-acetyl mandelic acid.<sup>6</sup> (*R*)-*O*-acetyl mandelic acid forms ester by reacting with the hydroxyl group of the  $\beta$ -hydroxy ketone. One model reaction is shown in figure 5.24. The chiral  $\beta$ -hydroxy ketone formed from the reaction of benzaldehyde and 2-methoxy propene, reacts with (*R*)-*O*-acetyl mandelic acid forming esters with (*R,R*) and (*R,S*) configurations with a ratio that depends on the ratio of two isomers of  $\beta$ -hydroxy ketone. The two protons marked as (a) and (b), adjacent to the chiral center in the ester are used as the markers to determine the enantiomeric excess in the aldol addition reaction. This proton shows a multiplet peak in the <sup>1</sup>H NMR (CDCl<sub>3</sub>,

400MHz). We can also use the methyl groups marked as (a) and (b) in the ester derivative to determine the enantiomeric excess in the aldol addition reaction.

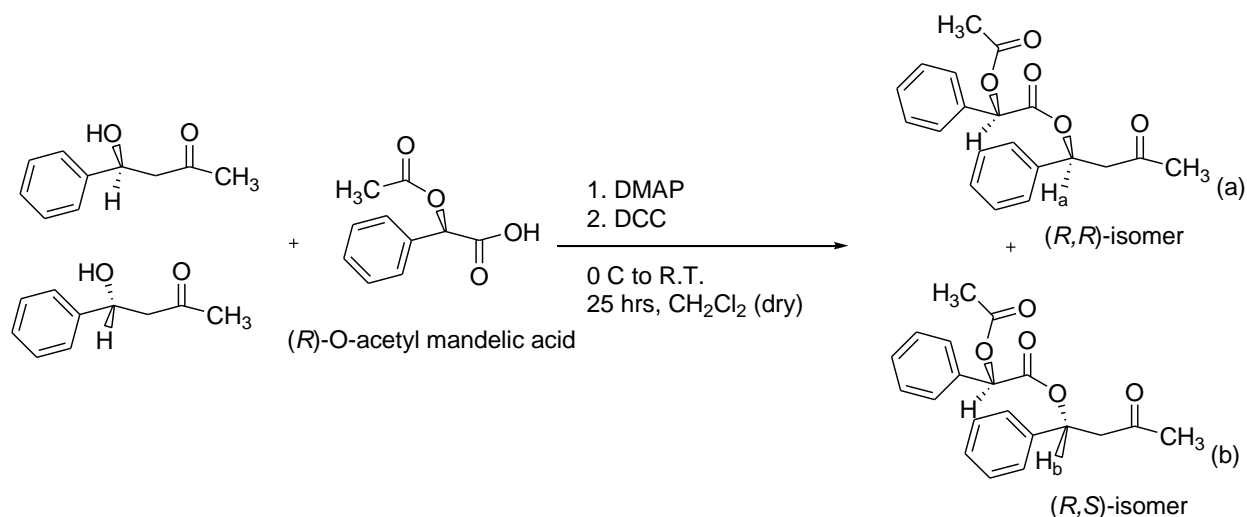


**Figure 5.24.** Reaction of  $(R)$ -O-acetyl mandelic acid with  $\beta$ -hydroxy ketone.

Table 5.4 shows the aldol addition results by different catalysts. It is observed that catalyst **C-5** with benz[a]anthryl side arm is very similar to the catalyst **C-4** in terms of the enantioselectivity of the product. This shows us that extending the side arm of the Schiff base ligand to give it more helical character does not play any role in the chiral induction during aldol addition reactions. However, catalyst **C-5** with more extended side arm reduces the yield of the product to a small extent for almost all the aldehydes. This may be attributed to the fact that an extended side arm produces greater steric congestion, and therefore it is difficult for the nucleophile to approach the titanium bound aldehyde molecule (step **C** in figure 5.22). For aromatic aldehydes, it takes less time (16 hours) for the reaction to reach completion but for the aliphatic aldehydes, it takes longer time (20 hours) to complete. For long chain aromatic aldehyde, for example 3-phenyl propanaldehyde, the catalysts works better in terms of enantioselectivity and yields than for small aromatic aldehydes like benzaldehyde. Among all the aldehydes, aldol addition product with crotonaldehyde showed the lowest enantioselectivity.

Table 5.5 is showing the ratio of different characteristic protons in the product ester generating from different aldehydes as shown in figure 5.24 with benzaldehyde as an example. There are no literature reports on the determination of the enantioselectivity of these aldol

addition products by derivatizing with (*R*)-*O*-acetyl mandelic acid. So, we are unable to determine the absolute configuration of these  $\beta$ -hydroxy ketones. However, we calculated the ee values reported in table 5.5 for each aldehyde, by comparing the ratio of two protons (either H<sub>a</sub> and H<sub>b</sub> or CH<sub>3(a)</sub> with CH<sub>3(b)</sub>) listed in figure 5.24. One example of the <sup>1</sup>H NMR (CDCl<sub>3</sub>, 400 MHz) spectrum of the (*R*)-*O*-acetyl mandelic acid derivative of  $\beta$ -hydroxy ketone derived from 3-phenyl propanaldehyde is shown in figure 5.25. The two protons (H<sub>a</sub> and H<sub>b</sub>) directly attached to the chiral center has a ratio of 1:3.38 for the two possible isomers of the  $\beta$ -hydroxy ketone.

**Table 5.4.** Aldol addition results by catalysts **C-4** and **C-5**

Aldehyde	Catalyst	Temperature (°C)	Time (hr)	Yield (%)	ee (%)
3-phenyl propanaldehyde	<b>C-4</b>	0 to R.T.	16	80	53
3-phenyl propanaldehyde	<b>C-5</b>	0 to R.T.	16	72	54
Benzaldehyde	<b>C-4</b>	0 to R.T.	16	70	43
Benzaldehyde	<b>C-5</b>	0 to R.T.	16	68	45
3-methyl butyraldehyde	<b>C-4</b>	0 to R.T.	20	67	55
3-methyl butyraldehyde	<b>C-5</b>	0 to R.T.	20	64	56
Crotonaldehyde	<b>C-4</b>	0 to R.T.	20	71	31
Crotonaldehyde	<b>C-5</b>	0 to R.T.	20	67	32

The ee was determined by synthesizing the ester derivative of (*R*)-*O*-acetyl mandelic acid. Analysis by <sup>1</sup>H NMR (CDCl<sub>3</sub>, 400 MHz) spectroscopy shows the ratio of the intensity of the protons (either H<sub>a</sub> and H<sub>b</sub> or CH<sub>3(a)</sub> and CH<sub>3(b)</sub>) marked in figure 5.24, gave an estimate of ee.

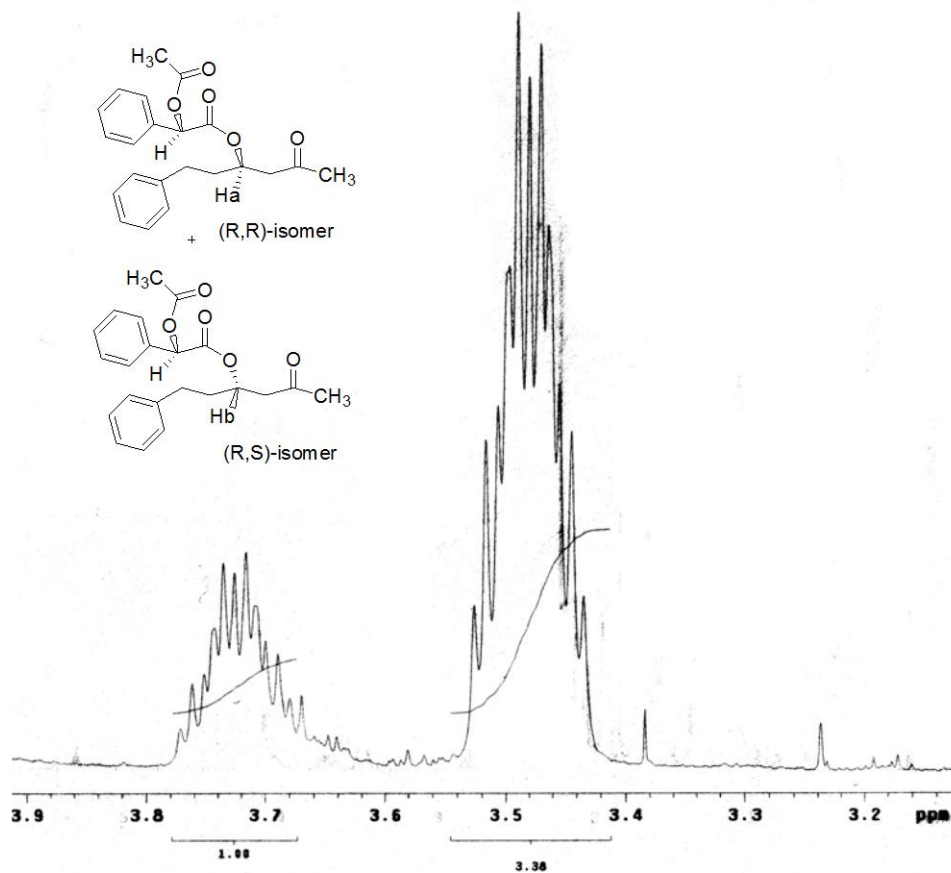


**Figure 5.25.**  $^1\text{H}$  NMR ( $\text{CDCl}_3$ , 400 MHz) of (*R*)-*O*-acetyl mandelic acid derivative of the  $\beta$ -hydroxy ketone derived from 3-phenyl propanaldehyde.

**Table 5.5.** Ratio of different characteristics protons in the product ester from different aldehydes

Aldehyde	Catalyst	Ratio of $\text{H}_a\text{:H}_b$ (in the ester) or vice versa	Ratio of $\text{CH}_3(a)\text{:CH}_3(b)$ (in the ester) or vice versa	ee %
3-Phenyl propanaldehyde	<b>C-4</b>	1:3.37		53
3-Phenyl propanaldehyde	<b>C-5</b>	1.3.38		54
Benzaldehyde	<b>C-4</b>		1:0.40	43
Benzaldehyde	<b>C-5</b>		1:0.38	45
3-Methyl butyraldehyde	<b>C-4</b>	1:3.59		55
3-Methyl butyraldehyde	<b>C-5</b>	1:3.61		56
Crotonaldehyde	<b>C-4</b>	0.51:1.0		31
Crotonaldehyde	<b>C-5</b>	0.52:1.0		32

## 5.4 Conclusions

Schiff base tridentate NOBIN backbone helical ligands were synthesized and characterized. Octahedral titanium(IV) complexes with these ligands were synthesized and characterized. Solution studies (CD) showed the predominance of the *M* helical conformations in the solution. These complexes were used as catalysts in asymmetric aldol addition reaction between 2-methoxy propene and different aldehydes. These complexes can catalyze the asymmetric aldol addition of both aromatic and aliphatic aldehydes with a weak nucleophile, 2-methoxy propene. However, the yields of these reactions reached moderate to high values whereas the enantioselectivities were modest in comparison to the Carreira's catalyst. First time (*R*)-*O*-acetyl mandelic acid was used as the chiral derivatizing agent to discriminate between the *R* and the *S* isomers of  $\beta$ -hydroxy ketones.

## 5.5 Experimental Section

### *General Methods*

All reactions were performed under inert atmospheres unless otherwise noted. Solvents used in metallation reactions were stored over sodium benzophenone ketyl or calcium hydride, and degassed prior to transfer via high-vacuum line techniques. Inert gasses were purified by passage through 4 Å molecular sieves and an Engelhard Q5 catalyst bed. Preparation and workup of V (IV) and Titanium (IV) compounds were completed under rigorously inert conditions to prevent oxidation or decomposition. All aldehydes used in the aldol-condensation were freshly distilled before use. 2-methoxy propene was passed through basic alumina and then freshly distilled to ensure the complete absence of any acidic nature.

UV-vis spectra were obtained on a Varian Cary 500 spectrometer, and CD spectra on a JASCO 720 spectropolarimeter. Solution samples for these two techniques were prepared using dried spectroscopic grade THF, at concentrations that ranged between  $1.5$  and  $2.5 \times 10^{-5}$  M. A 1 cm path length quartz cell was employed for the analysis.  $^1\text{H}$  and  $^{13}\text{C}$  NMR spectra were obtained on a Varian Unity 400 MHz spectrometer employing residual solvent protons or in some cases TMS as an internal standard. Crystallographic data was collected using either a Bruker SMART 1000

CCD or a Bruker-AXS SMART APEX CCD. Full structural information is included in appendix II. EPR spectroscopy of the vanadium complexes were measured in Varian E-4 EPR spectrometer. All mass spectra were recorded in ESI-MS instrument. All IR spectra were recorded in Nicolet 6700 FT-IR spectrometer.

#### **(S)-2-hydroxy-1,1'-binaphthyl-2'-imine-quinoline (4)**

A mixture of 0.240 g (0.842 mmol) of (S)-2 and 0.132 g (0.842 mmol) of 2-quinolaldehyde were refluxed in absolute ethanol (15 mL) under argon for 8 hours. The solution became cream colored after 8 hours. The mixture was hot filtered and washed with boiling ethanol to produce cream colored pure ligand **4** (0.201 g, 81% yield).  $^1\text{H}$  NMR ( $\text{CDCl}_3$ , 400 MHz):  $\delta$  7.04-7.06 (d, 1H, CH); 7.17-7.21 (t, 2H, CH); 7.26-7.27 (d, 1H, CH); 7.32-7.33 (d, 1H, CH); 7.38-7.40 (d, 1H, CH); 7.49 (m, 2H, CH); 7.58 (t, 2H, CH); 7.71-7.73 (d, 1H, CH); 7.78-7.80 (d, 1H, CH); 7.82-8.84 (d, 1H, CH); 7.89-7.90 (d, 1H, CH); 7.98-8.00 (d, 1H, CH); 8.01-8.02 (d, 1H, CH); 8.09 (t, 2H, CH); 8.77 (s, 1H, imine proton).  $^{13}\text{C}$  NMR ( $\text{CDCl}_3$ , 400 MHz):  $\delta$  118.12, 118.49, 118.91, 122.97, 123.57, 124.71, 125.53, 126.00, 127.61, 128.31, 128.57, 129.03, 129.41, 129.72, 129.91, 130.00, 130.95, 131.12, 131.61, 131.82, 137.13, 141.57, 142.00, 147.91, 148.13, 150.27, 151.13, 153.72, 154.92, 162.00. MS:  $[\text{M}]^{+1}$  ( $\text{C}_{30}\text{H}_{20}\text{N}_2\text{O}_1$ ) $^{+1}$  424.1575 (81%), 425.1671 (18%), 426.1682 (1%). Single crystals are grown from  $\text{CH}_2\text{Cl}_2$  solution after cooling to 0 °C.

#### **Ti(IV)(S)-4 complex (C-3)**

In the solution of the ligand **4** (0.030 g, 0.071 mmol) in approximately 2 mL of  $\text{CH}_2\text{Cl}_2$  was added  $\text{TiCl}_4$  (1M in  $\text{CH}_2\text{Cl}_2$ , 0.071 mmol). The solution turned dark purple within few seconds. The entire mixture was stirred for 3 hours before removing the solvent. The precipitate was decanted with ether and ether/hexane (1:1) mixture before drying. Dark purple colored product obtained (0.025 g, 80% yield).  $^1\text{H}$  NMR ( $\text{CDCl}_3$ , 400 MHz):  $\delta$  7.10 (broad, 4H, CH), 7.50 (broad, 2H, CH), 7.80-8.05 (broad, 12H, CH), 8.91 (s, 1H, imine proton). MS: ( $\text{C}_{30}\text{H}_{20}\text{N}_2\text{O}_1\text{TiCl}$ ) $^{+1}$  505.011 (4%), 506.017 (10%), 507.021 (68%), 508.032 (15%), 509.102 (2%), 510.057 (1%). IR:  $\nu_{\text{Ti-O}}$  747.00  $\text{cm}^{-1}$ ,  $\nu_{\text{Ti-Cl}}$  696.26  $\text{cm}^{-1}$ .



### Ti(IV)(S)-3 complex (C-4)

In the solution of the ligand **3** (0.120 g, 0.246 mmol) in approximately 3 mL of toluene was added Ti(O<sup>*i*</sup>Pr)<sub>4</sub> (0.036 mL, 0.123 mmol) slowly at room temperature. The solution turned dark red within few seconds. The entire mixture was stirred for 4 hours. Solvent was removed under reduced pressure to obtain dark red colored pure complex (0.097 g, 77% yield). <sup>1</sup>H NMR (CDCl<sub>3</sub>, 400 MHz): δ 5.98-6.00 (d, 2H, CH); 6.33-6.35 (d, 2H, CH); 6.56-6.59 (d, 2H, CH); 6.84-6.98 (m, 16H, CH, ABMX protons of backbone); 7.06 (t, 2H, CH); 7.22-7.24 (d, 2H, CH); 7.26-7.28 (d, 2H, CH); 7.39 (m, 2H, CH); 7.45-7.47 (d, 2H, CH); 7.52-7.53 (d, 2H, CH); 7.58-7.60 (d, 2H, CH); 7.70-7.72 (d, 2H, CH); 8.13 (s, 2H, imine proton); 9.66-9.68 (d, 2H, CH). <sup>13</sup>C NMR (CDCl<sub>3</sub>, 400 MHz): 105.00, 115.41, 119.44, 119.69, 119.81, 119.95, 121.43, 122.00, 123.31, 123.16, 123.91, 125.00, 125.17, 125.29, 126.04, 126.43, 126.84, 127.00, 127.13, 127.43, 127.85, 128.09, 129.10, 131.66, 133.07, 133.59, 133.87, 136.71, 138.17, 148.38, 149.19, 159.00, 163.71, 163.98, 165.77. MS: (C<sub>70</sub>H<sub>42</sub>O<sub>4</sub>N<sub>2</sub>Ti)<sup>+</sup> 1021.2701 (3%), 1022.2729 (6%), 1023.2665 (48%), 1024.2671 (30%), 1025.2706 (9%), 1026.2715 (3%), 1027.3146 (1%). IR: ν<sub>C=N</sub> 1614.26 cm<sup>-1</sup>, ν<sub>Ti-O</sub> 523.92 cm<sup>-1</sup>, ν<sub>Ti-N</sub> 509.61 cm<sup>-1</sup>. UV: broad peak at 425 nm due to LMCT. CD: *M* isomer is the predominant one in solution. Single crystal was grown from boiling ethanol solution.

### Ti(IV)(S)-5 complex (C-5)

In the solution of the ligand **5** (0.200 g, 0.371 mmol) in approximately 5 mL of toluene was added Ti(O<sup>*i*</sup>Pr)<sub>4</sub> (0.054 mL, 0.186 mmol) slowly at room temperature. The solution turned dark red within few seconds. The entire mixture was stirred for 4 hours. Solvent was removed under reduced pressure to obtain dark red colored pure complex (0.160 g, 77% yield). <sup>1</sup>H NMR (CDCl<sub>3</sub>, 400 MHz): δ 6.02-6.04 (d, 2H, CH); 6.06 (t, 2H, CH); 6.36-6.38 (d, 2H, CH); 6.42-6.44 (d, 2H, CH); 6.58 (t, 2H, CH); 6.70-6.72 (d, 2H, CH); 6.8 (t, 2H, CH); 7.04 (t, 2H, CH); 7.18-7.19 (m, 4H, CH); 7.33 (m, 2H, CH); 7.34-7.36 (d, 2H, CH); 7.48-7.50 (d, 2H, CH); 7.56 (m, 2H, CH); 7.56-7.64 (d, 2H, CH); 7.66 (m, 4H, CH); 7.71-7.72 (d, 2H, CH); 7.81-7.82 (d, 2H, CH); 7.90-7.91 (d, 2H, CH); 7.92 (s, 2H, CH); 8.15 (s, 2H, imine proton); 10.40 (s, 2H, CH, bay proton). <sup>13</sup>C NMR (CDCl<sub>3</sub>, 400 MHz): 118.00, 119.10, 120.27, 120.48, 121.41, 121.59, 122.61, 122.93, 124.45, 124.91, 125.31, 125.37, 125.43, 125.57, 125.69, 125.71, 125.86, 126.00, 126.10, 126.17, 126.78, 127.09, 127.18, 127.29, 128.10, 128.30, 128.41, 128.99, 129.72, 130.46, 130.97,

131.14, 131.77, 139.20, 148.71, 163.72, 164.06, 166.00. MS:  $(C_{78}H_{46}N_2O_4Ti)^+$  1121.3090 (3%), 1122.2998 (6%), 1123.2975 (48%), 1124.2986 (30%), 1125.3058 (9%), 1126.2988 (3%), 1127.3176 (1%). IR:  $\nu_{Ti-O}$  546.15  $cm^{-1}$ ,  $\nu_{Ti-N}$  518.98  $cm^{-1}$ ,  $\nu_{C=N}$  1607.43  $cm^{-1}$ . UV: broad peak at 450 nm, is due to L→M charge transfer. CD: *M* conformer is predominant in solution. Single crystal is grown from boiling ethanol by heating cooling method.

### ***Catalytic Asymmetric Aldol Condensations***

#### ***Reaction between 3-phenyl propanaldehyde and 2-methoxy propene by catalyst C-4***

To a solution of Schiff's base ligand **3** (0.015 g, 0.028 mmol) in toluene (3 mL) was added  $Ti(O^iPr)_4$  (4.5  $\mu$ L, 0.014 mmol). The orange solution was stirred for 1 hr at 23 °C. The solvent was removed in vacuo and the solid orange residue was taken up in 2-methoxy propene (2mL) at 0 °C. 2,6-di-*t*-butyl 4 methyl pyridine (0.012 g, 0.056 mmol) and 3-phenyl propanaldehyde (20.39  $\mu$ L, 0.14 mmol) were added sequentially. After 16 hrs, the reaction was concentrated in vacuo and the resulting residue was treated with a biphasic mixture of ether and aqueous 2(N) HCl for 30 minutes. It was extracted with ether and the combined organic extracts were dried over anhydrous sodium sulfate. The organic extracts were concentrated in vacuo. Purification by chromatography using 4:1 hexane:ethyl acetate elutes the ligand first followed by 1:1 mixture to elute the  $\beta$ -hydroxy ketone adduct (0.015 g, 80% yield).  $^1H$  NMR ( $CDCl_3$ , 400 MHz): 1.62-1.74 (m, 1H); 1.76-1.86 (m, 1H); 2.17 (s, 3H); 2.61 (d, 1H); 2.65 (d, 1H); 2.68-2.78 (m, 1H); 2.82-2.91 (m, 1H); 3.17 (s, 1H); 4.10 (m, 1H); 7.16-7.31 (m, 5H).  $^{13}C$  NMR ( $CDCl_3$ , 400 MHz):  $\delta$  30.7, 31.7, 37.9, 49.9, 66.7, 125.8, 128.4, 128.5, 141.8, 210.0. Enantiomeric excess was determined by forming an ester with (*R*)-*O*-acetyl mandelic acid.

***Procedure for formation of (R)-O-acetylmandelic acid ester:*** To a solution of (*R*)-*O*-acetyl mandelic acid (0.02 g, 0.104 mmol), 0.02 g of aldol product (0.104 mmol) and DMAP (0.003 g, 0.021 mmol) in 1mL of  $CH_2Cl_2$  at 0 °C was added dropwise over 10 minutes with stirring under Ar, DCC (0.024 g, 0.115 mmol) in 2mL of  $CH_2Cl_2$ . A white precipitate should observe before the addition is complete. The reaction then allowed to proceed at 25 °C for an additional 22 hrs. The urea was removed by filtration and the resulting solution was washed successively with 5mL of 0.5 N HCl, 2N  $Na_2CO_3$  and brine. The organic layer was dried over  $MgSO_4$ , and concentrated. The crude product was purified by flash column chromatography with 6:1 hexane:ethyl acetate

mixture. The CH proton adjacent to the chiral hydroxyl group in  $\beta$ -hydroxy ketone-(*R*)-*O*-acetyl mandelic acid adduct integrates in  $^1\text{H}$  NMR ( $\text{CDCl}_3$ , 400 MHz) at 3.47 and 3.72 ppm as multiplet with an intensity ratio of 1.0 to 3.32 (ee 53 %).

#### ***Reaction between 3-phenyl propanaldehyde and 2-methoxy propene by catalyst C-5***

To a solution of Schiff's base ligand **5** (0.016 g, 0.029 mmol) in toluene (3 mL) was added  $\text{Ti}(\text{O}^i\text{Pr})_4$  (4.21  $\mu\text{L}$ , 0.014 mmol). The orange solution was stirred for 1 hr at 23 °C. The solvent was removed in vacuo and the solid orange residue was taken up in 2-methoxy propene (2mL) at 0 °C. 2,6-di-*t*-butyl 4 methyl pyridine (0.012 g, 0.058 mmol) and 3-phenyl propanaldehyde (18.5  $\mu\text{L}$ , 0.15 mmol) were added sequentially. After 16 hrs, the reaction was concentrated in vacuo and the resulting residue was treated with a biphasic mixture of ether and aqueous 2(N) HCl for 30 minutes. It was extracted with ether and the combined organic extracts were dried over anhydrous sodium sulfate. The organic extracts were concentrated in vacuo. Purification by chromatography using 4:1 hexane:ethyl acetate elutes the ligand first followed by 1:1 mixture to elute the  $\beta$ -hydroxy ketone adduct (0.014 g, 72% yield).  $^1\text{H}$  NMR ( $\text{CDCl}_3$ , 400 MHz): same as in the previous case. Enantiomeric excess was determined by esterification with (*R*)-*O*-acetyl mandelic acid by the same method as described above. The CH proton adjacent to the chiral hydroxyl group in  $\beta$ -hydroxy ketone-(*R*)-*O*-acetyl mandelic acid adduct integrates in  $^1\text{H}$  NMR ( $\text{CDCl}_3$ , 400 MHz) at 3.47 and 3.72 ppm as multiplet with an intensity ratio of 1.0 to 3.38 (ee 54 %).

#### ***Reaction between benzaldehyde and 2-methoxy propene by catalyst C-4***

To a solution of Schiff's base ligand **3** (0.015 g, 0.028 mmol) in toluene (3 mL) was added  $\text{Ti}(\text{O}^i\text{Pr})_4$  (4.5  $\mu\text{L}$ , 0.014 mmol). The orange solution was stirred for 1 hr at 23 °C. The solvent was removed in vacuo and the solid orange residue was taken up in 2-methoxy propene (2mL) at 0 °C. 2,6-di-*t*-butyl 4 methyl pyridine (0.013 g, 0.056 mmol) and benzaldehyde (16.0  $\mu\text{L}$ , 0.14 mmol) were added sequentially. After 16 hrs, the reaction was concentrated in vacuo and the resulting residue was treated with a biphasic mixture of ether and aqueous 2(N) HCl for 30 minutes. It was extracted with ether and the combined organic extracts were dried over anhydrous sodium sulfate. The organic extracts were concentrated in vacuo. Purification by chromatography using 4:1 hexane:ethyl acetate elutes the ligand first followed by 1:1 mixture to elute the  $\beta$ -hydroxy ketone adduct (0.012 g, 70% yield).  $^1\text{H}$  NMR ( $\text{CDCl}_3$ , 400 MHz):  $\delta$  1.27 (t,

3H); 2.71 (dd, 1H); 2.78 (dd, 1H); 3.32 (s, 1H); 4.16 (q, 2H); 5.14 (m, 1H); 7.28-7.40 (m, 5H).  $^{13}\text{C}$  NMR ( $\text{CDCl}_3$ , 400MHz):  $\delta$  30.7, 51.9, 69.7, 125.5, 127.5, 128.4, 142.7, 209.0. Enantiomeric excess was determined by forming an ester with (*R*)-*O*-acetyl mandelic acid.

**Procedure for formation of (*R*)-*O*-acetylmandelic acid ester:** To a solution of (*R*)-*O*-acetyl mandelic acid (0.018 g, 0.086 mmol), 0.012 g of aldol product (0.079 mmol) and DMAP (0.003 g, 0.017 mmol) in 1mL of  $\text{CH}_2\text{Cl}_2$  at 0 °C was added dropwise over 10 minutes with stirring under Ar, DCC (0.021 g, 0.095 mmol) in 2mL of  $\text{CH}_2\text{Cl}_2$ . A white precipitate should observe before the addition is complete. The reaction then allowed to proceed at 25 °C for an additional 22 hrs. The urea was removed by filtration and the resulting solution was washed successively with 5ml of 0.5 N HCl, 2N  $\text{Na}_2\text{CO}_3$  and brine. The organic layer was dried over  $\text{MgSO}_4$ , and concentrated. The crude product was purified by flash column chromatography with 6:1 hexane:ethyl acetate mixture. The methyl proton in  $\beta$ -hydroxy ketone-(*R*)-*O*-acetyl mandelic acid adduct integrates in  $^1\text{H}$  NMR ( $\text{CDCl}_3$ , 400 MHz) at 2.19 and 2.22 ppm as singlets with an intensity ratio of 0.40 to 1.0 (ee 43 %).

#### **Reaction between benzaldehyde and 2-methoxy propene by catalyst C-5**

To a solution of Schiff's base ligand **5** (0.016 g, 0.029 mmol) in toluene (3 mL) was added  $\text{Ti}(\text{O}^i\text{Pr})_4$  (4.21  $\mu\text{L}$ , 0.014 mmol). The orange solution was stirred for 1 hr at 23 °C. The solvent was removed in vacuo and the solid orange residue was taken up in 2-methoxy propene (2mL) at 0 °C. 2,6-di- $^t$ butyl 4 methyl pyridine (0.012 g, 0.058 mmol) and benzaldehyde (14.6  $\mu\text{L}$ , 0.14 mmol) were added sequentially. After 16 hrs, the reaction was concentrated in vacuo and the resulting residue was treated with a biphasic mixture of ether and aqueous 2(N) HCl for 30 minutes. It was extracted with ether and the combined organic extracts were dried over anhydrous sodium sulfate. The organic extracts were concentrated in vacuo. Purification by chromatography using 4:1 hexane:ethyl acetate elutes the ligand first followed by 1:1 mixture to elute the  $\beta$ -hydroxy ketone adduct (0.011 g, 68% yield).  $^1\text{H}$  NMR ( $\text{CDCl}_3$ , 400 MHz): same as in the previous case. Enantiomeric excess was determined by esterification with (*R*)-*O*-acetyl mandelic acid by the same method as described above. The methyl proton in  $\beta$ -hydroxy ketone-(*R*)-*O*-acetyl mandelic acid adduct integrates in  $^1\text{H}$  NMR ( $\text{CDCl}_3$ , 400 MHz) at 2.19 and 2.22 ppm as singlets with an intensity ratio of 0.38 to 1.0 (ee 45 %).

### ***Reaction between 3-methyl butyraldehyde and 2-methoxy propene by catalyst C-4***

To a solution of Schiff's base ligand **3** (0.015 g, 0.031 mmol) in toluene (3 mL) was added  $\text{Ti}(\text{O}^i\text{Pr})_4$  (4.5  $\mu\text{L}$ , 0.015 mmol). The orange solution was stirred for 1 hr at 23 °C. The solvent was removed in vacuo and the solid orange residue was taken up in 2-methoxy propene (2mL) at 0 °C. 2,6-di-<sup>t</sup>butyl 4 methyl pyridine (0.013 g, 0.061 mmol) and 3-methyl butyraldehyde (16.6  $\mu\text{L}$ , 0.153 mmol) were added sequentially. After 20 hrs, the reaction was concentrated in vacuo and the resulting residue was treated with a biphasic mixture of ether and aqueous 2(N) HCl for 30 minutes. It was extracted with ether and the combined organic extracts were dried over anhydrous sodium sulfate. The organic extracts were concentrated in vacuo. Purification by chromatography using 4:1 hexane:ethyl acetate elutes the ligand first followed by 1:1 mixture to elute the  $\beta$ -hydroxy ketone adduct (0.010 g, 67% yield). <sup>1</sup>H NMR ( $\text{CDCl}_3$ , 400 MHz):  $\delta$  0.97-0.99 (d, 6H); 1.14 (m, 1H); 1.28 (dd, 2H); 1.5 (m, 1H); 1.56 (m, 1H); 1.59 (s, 3H); 1.62 (m, 1H); 1.76 (m, 1H). Enantiomeric excess was determined by forming an ester with (*R*)-*O*-acetyl mandelic acid.

***Procedure for formation of (*R*)-*O*-acetylmandelic acid ester:*** To a solution of (*R*)-*O*-acetyl mandelic acid (0.02 g, 0.011 mmol), 0.015 g of aldol product (0.010 mmol) and DMAP (0.003 g, 0.021 mmol) in 1mL of  $\text{CH}_2\text{Cl}_2$  at 0 °C was added dropwise over 10 minutes with stirring under Ar, DCC (0.024 g, 0.016 mmol) in 2mL of  $\text{CH}_2\text{Cl}_2$ . A white precipitate should observe before the addition is complete. The reaction then allowed to proceed at 25 °C for an additional 22 hrs. The urea was removed by filtration and the resulting solution was washed successively with 5ml of 0.5 N HCl, 2N  $\text{Na}_2\text{CO}_3$  and brine. The organic layer was dried over  $\text{MgSO}_4$ , and concentrated. The crude product was purified by flash column chromatography with 6:1 hexane:ethyl acetate mixture. The CH proton adjacent to the chiral hydroxyl group in  $\beta$ -hydroxy ketone-(*R*)-*O*-acetyl mandelic acid adduct integrates in <sup>1</sup>H NMR ( $\text{CDCl}_3$ , 400 MHz) at 1.82 and 1.89 ppm as multiplet with an intensity ratio of 1.0 to 3.61 (ee 55 %).

### ***Reaction between 3-methyl butyraldehyde and 2-methoxy propene by catalyst C-5***

To a solution of Schiff's base ligand **5** (0.016 g, 0.029 mmol) in toluene (3 mL) was added  $\text{Ti}(\text{O}^i\text{Pr})_4$  (4.21  $\mu\text{L}$ , 0.014 mmol). The orange solution was stirred for 1 hr at 23 °C. The solvent was removed in vacuo and the solid orange residue was taken up in 2-methoxy propene (2mL) at 0 °C. 2,6-di-<sup>t</sup>butyl 4 methyl pyridine (0.012 g, 0.058 mmol) and 3-methyl

butyraldehyde (16.6  $\mu\text{L}$ , 0.14 mmol) were added sequentially. After 20 hrs, the reaction was concentrated in vacuo and the resulting residue was treated with a biphasic mixture of ether and aqueous 2(N) HCl for 30 minutes. It was extracted with ether and the combined organic extracts were dried over anhydrous sodium sulfate. The organic extracts were concentrated in vacuo. Purification by chromatography using 4:1 hexane:ethyl acetate elutes the ligand first followed by 1:1 mixture to elute the  $\beta$ -hydroxy ketone adduct (0.010 g, 64% yield).  $^1\text{H}$  NMR ( $\text{CDCl}_3$ , 400 MHz):  $\delta$  1.82 (m, 3H); 1.89 (m, 3H); 3.65 (m, 1H); 3.95 (dd, 1H); 4.14 (m, 1H); 4.31 (dd, 1H); 4.68 (m, 1H). Enantiomeric excess was determined by esterification with (*R*)-*O*-acetyl mandelic acid by the same method as described above. The CH proton adjacent to the chiral hydroxyl group in  $\beta$ -hydroxy ketone-(*R*)-*O*-acetyl mandelic acid adduct integrates in  $^1\text{H}$  NMR ( $\text{CDCl}_3$ , 400 MHz) at 1.82 and 1.89 ppm as multiplet with an intensity ratio of 1.0 to 3.65 (ee 56 %).

#### ***Reaction between crotonaldehyde and 2-methoxy propene by catalyst C-4***

To a solution of Schiff's base ligand **3** (0.015 g, 0.028 mmol) in toluene (3 mL) was added  $\text{Ti}(\text{O}^i\text{Pr})_4$  (4.5  $\mu\text{L}$ , 0.014 mmol). The orange solution was stirred for 1 hr at 23  $^\circ\text{C}$ . The solvent was removed in vacuo and the solid orange residue was taken up in 2-methoxy propene (2mL) at 0  $^\circ\text{C}$ . 2,6-di- $^t$ butyl 4 methyl pyridine (0.013 g, 0.056 mmol) and crotonaldehyde (10.0  $\mu\text{L}$ , 0.14 mmol) were added sequentially. After 20 hrs, the reaction was concentrated in vacuo and the resulting residue was treated with a biphasic mixture of ether and aqueous 2(N) HCl for 30 minutes. It was extracted with ether and the combined organic extracts were dried over anhydrous sodium sulfate. The organic extracts were concentrated in vacuo. Purification by chromatography using 4:1 hexane:ethyl acetate elutes the ligand first followed by 1:1 mixture to elute the  $\beta$ -hydroxy ketone adduct (0.007 g, 71% yield).  $^1\text{H}$  NMR ( $\text{CDCl}_3$ , 400 MHz):  $\delta$  1.95 (m, 3H); 2.21 (s, 3H); 3.62 (m, 1H); 3.95 (dd, 1H); 4.14 (m, 1H); 4.31 (dd, 1H); 4.68 (m, 1H). Enantiomeric excess was determined by forming an ester with (*R*)-*O*-acetyl mandelic acid.

***Procedure for formation of (R)-O-acetylmandelic acid ester:*** To a solution of (*R*)-*O*-acetyl mandelic acid (0.015 g, 0.010 mmol), 0.015 g of aldol product (0.010 mmol) and DMAP (0.003 g, 0.020 mmol) in 1mL of  $\text{CH}_2\text{Cl}_2$  at 0  $^\circ\text{C}$  was added dropwise over 10 minutes with stirring under Ar, DCC (0.024 g, 0.016 mmol) in 2mL of  $\text{CH}_2\text{Cl}_2$ . A white precipitate should observe before the addition is complete. The reaction then allowed to proceed at 25  $^\circ\text{C}$  for an additional 22 hrs. The urea was removed by filtration and the resulting solution was washed successively

with 5mL of 0.5 N HCl, 2N Na<sub>2</sub>CO<sub>3</sub> and brine. The organic layer was dried over MgSO<sub>4</sub>, and concentrated. The crude product was purified by flash column chromatography with 6:1 hexane: ethyl acetate mixture. The methyl group in the  $\beta$ -hydroxy ketone-(*R*)-*O*-acetyl mandelic acid adduct integrates in <sup>1</sup>H NMR (CDCl<sub>3</sub>, 400 MHz) at 2.19 and 2.22 ppm as singlet with an intensity ratio of 0.53 to 1.00 (ee 31 %).

### ***Reaction between crotonaldehyde and 2-methoxy propene by catalyst C-5***

To a solution of Schiff's base ligand **5** (0.016 g, 0.029 mmol) in toluene (3 mL) was added Ti(O<sup>*i*</sup>Pr)<sub>4</sub> (4.21  $\mu$ L, 0.014 mmol). The orange solution was stirred for 1 hr at 23 °C. The solvent was removed in vacuo and the solid orange residue was taken up in 2-methoxy propene (2mL) at 0 °C. 2,6-di-<sup>*t*</sup>butyl 4 methyl pyridine (0.013 g, 0.058 mmol) and crotonaldehyde (10.0  $\mu$ L, 0.14 mmol) were added sequentially. After 20 hrs, the reaction was concentrated in vacuo and the resulting residue was treated with a biphasic mixture of ether and aqueous 2(N) HCl for 30 minutes. It was extracted with ether and the combined organic extracts were dried over anhydrous sodium sulfate. The organic extracts were concentrated in vacuo. Purification by chromatography using 4:1 hexane : ethyl acetate elutes the ligand first followed by 1:1 mixture to elute the  $\beta$ -hydroxy ketone adduct (0.0067 g, 67% yield). <sup>1</sup>H NMR (CDCl<sub>3</sub>, 400 MHz):  $\delta$  same as in the previous case. Enantiomeric excess was determined by the formation of ester with (*R*)-*O*-acetyl mandelic acid. The methyl group in the  $\beta$ -hydroxy ketone-(*R*)-*O*-acetyl mandelic acid adduct integrates in <sup>1</sup>H NMR (CDCl<sub>3</sub>, 400 MHz) at 2.19 and 2.22 ppm as singlet with an intensity ratio of 0.52 to 1.00 (ee 32 %).

## **5.6 References**

1. "Highly region and enantioselective palladium catalyzed allylic amination with sodium diformylamide" Wang, Y.; Ding, K. *J. Org. Chem.* **2001**, *66*, 3238.
2. "Catalytic asymmetric ring opening metathesis/cross metathesis (AROM/CM) reactions, mechanism and application to enantioselective synthesis of functionalized cyclopentanes" La, D. S.; Stately, E. S.; Ford, J. G.; Schrock, R. R.; Hoveyda, A. H. *J. Am. Chem. Soc.* **2001**, *123*, 7767.

3. "Total synthesis of macrolactin A with versatile catalytic, enantioselective dienolate aldol addition reactions" Kim, Y.; Singer, R. A.; Carreira, E. M. *Angew. Chem. Int. Ed.* **1998**, *37*, 1261.
4. "To probe the origin of activation effect of carboxylic acid and (+) NLE in tridentate titanium catalyst systems" Ji, B.; Ding, K.; Meng, J. *Chinese. J. Chem.* **2003**, *21*, 727.
5. "Synthesis of novel N, P chiral ligands for palladium catalyzed asymmetric allylations: the effect of binaphthyl backbone on the enantioselectivity" Wang, Y.; Guo, H.; Ding, K. *Tetrahedron: Asymmetry* **2000**, *11*, 4153.
6. Wang, Y.; Li, X.; Ding, K. *Tetrahedron Lett* **2002**, *4*, 99.
7. "Optical properties of (S)-NOBIN" Studentsov, E. P.; Piskunova, O. V.; Skvortsov, A. N.; Skvortsov, N. K. *Russian J. Gen. Chem.* **2009**, *79*, 962-966.



## CHAPTER 6 - Overall Conclusions and Future Work

Different helical tetradentate salen ligands with cyclohexyl and binaphthyl backbones and phenanthryl and benz[a]anthryl side arms were synthesized and characterized. These ligands possess unique stepped helical conformations. Vanadium(IV) complexes of these ligands with cyclohexyl backbone adopt *M* helical conformations in the solution as observed from the CD spectra of these complexes. However, in the solid state these complexes form 1:1 mixtures of both *M* and *P* conformations. Asymmetric sulfoxidations by these complexes showed moderate ee. We concluded that chiral cyclohexyl diamine or binaphthyl diamine is a weak director of chirality and this hypothesis was given by Fox et al.<sup>1</sup>

Initially we thought that these tetradentate salen ligands are too sterically congested around the metal center for the sulfoxidation to occur with high ee. So, we synthesized the tridentate Schiff base ligands with (*S*)-NOBIN backbone. These ligands were subjected to the complexation with V(IV)O acetylacetonate and they were characterized. These complexes have the potential to adopt square pyramidal geometry with one tridentate ligand and two monodentate ligands. Asymmetric sulfoxidation results suggest that these complexes are too open to provide any directionality for the incoming nucleophile to attack the metal bound sulfide. Also more extended side arms with greater helical nature do not improve the ee to a large extent.

We synthesized the imine bond reduced version of the tetradentate salen ligands. These ligands are called salan ligands. Due to the flexible nature of these ligands, they can adopt  $\beta$ -cis geometry. Complexes in this geometry are chiral and they can impose high chiral inductions in the asymmetric reactions. Titanium and vanadium complexes of these salan ligands were synthesized and characterized. They showed slightly better enantioselectivity than their unreduced version salen ligands. However, due to the fluxional character of these titanium salan complexes, they are difficult to characterize. Also, aluminum and iron complexes of these N-methylated salan ligands showed moderate activity in asymmetric sulfoxidation reactions.

We also, wanted to investigate the chiral induction ability of mixed salen complexes with two different side arms in the same ligand. However, we are unable to synthesize pure mixed salen ligands. They always formed in a mixture by our applied method. The vanadium complexes of these mixed salen ligands showed comparable activities as their  $C_2$ -symmetric counterparts in asymmetric sulfoxidations.

Lastly, we have synthesized and characterized (*S*)-NOBIN backbone tridentate Schiff base ligands. The titanium complexes of these ligands form octahedral complexes. These octahedral complexes can catalyze asymmetric aldol addition between 2-methoxy propene and different aldehydes. These helical titanium complexes showed moderate enantioselectivity in the asymmetric aldol addition reactions.

As we observed, helicity itself does not play an important role in the sulfoxidation reactions or asymmetric aldol addition reactions. So, we need to modify the ligands in future to obtain better control over the reaction in terms of enantioselectivity. Molecular modeling will be a good tool to understand the preferred molecular structure of a catalyst for a particular reaction. Changing or incorporating new functional groups may also have great impact in the catalysts in terms of enantioselectivity in a particular reaction. As we now know that only chiral cyclohexyl diamine is a weak director of chirality, and recently, Fox. et al. have observed that the chirality of the overall complex is being determined by an additional chirality in the side arm, which overshadows the backbone chirality. Hence, incorporation of an additional chirality may help to produce better ee.

## Reference:

1. “Control of absolute helicity in single stranded abiotic metallofoldamers” Dong, Z.; Karpowicz, R. J. Jr.; Bai, S.; Yap, G. P. A.; Fox, J. M. *J. Am. Chem. Soc.* **2006**, *128*, 14242-14243.

Note: Definitions and full names of some terms used:

NMR: nuclear magnetic resonance

IR: infra-red

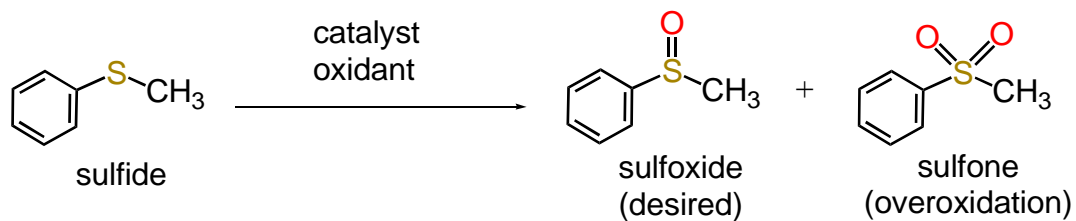
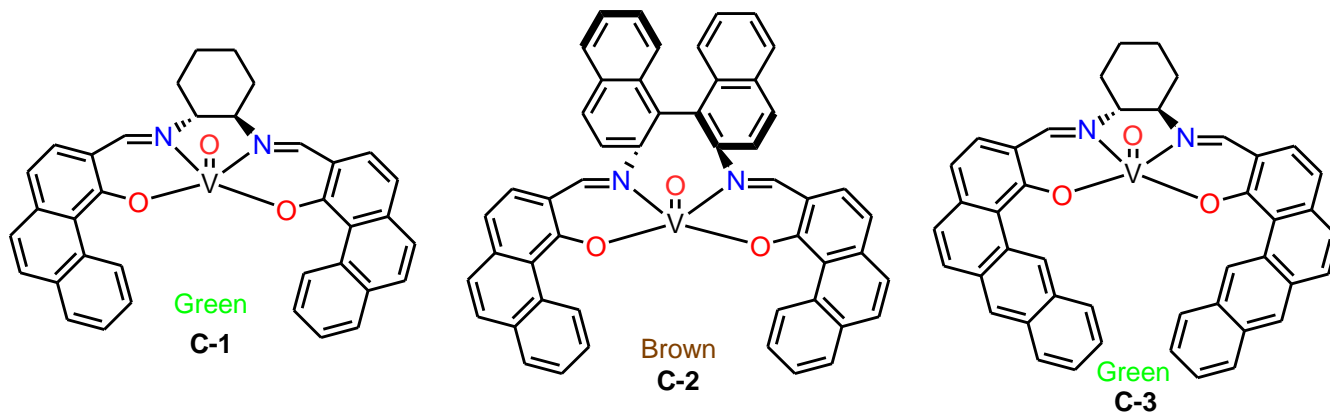
EPR: electron paramagnetic resonance

MALDI-TOF: matrix assisted laser desorption/ionization-time of flight

ee (enantiomeric excess): absolute difference between the mole fractions of each enantiomer.

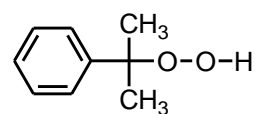
# Appendix A - Chapter 1

## Compounds and reactions

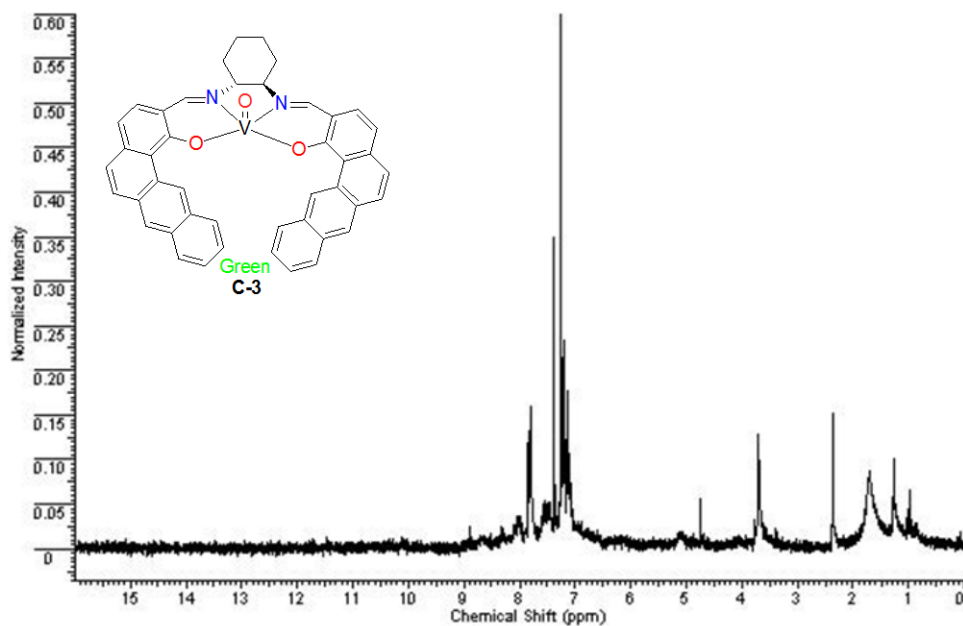


Oxidant:  $\text{H}_2\text{O}_2$

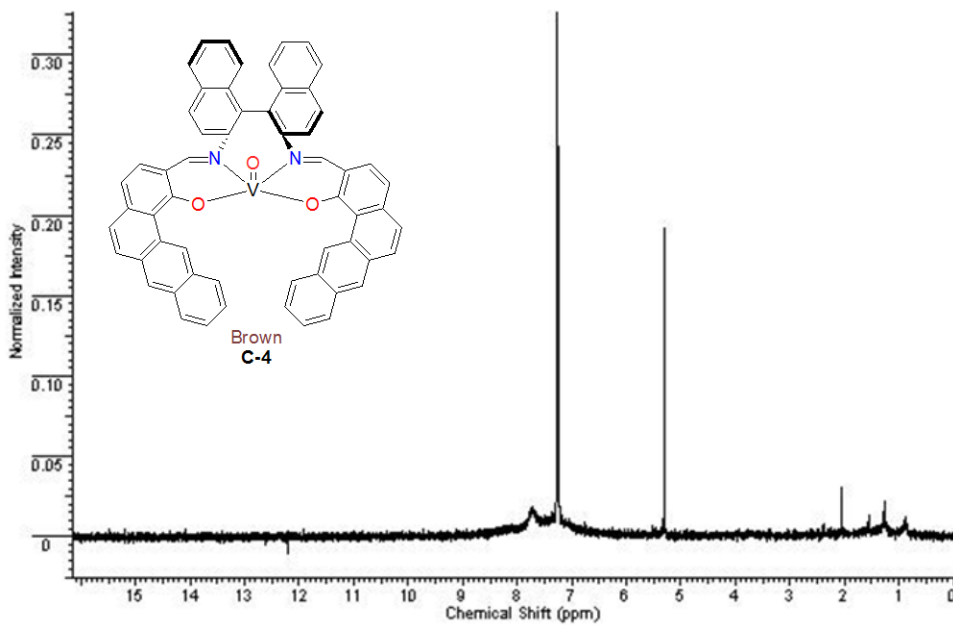
or



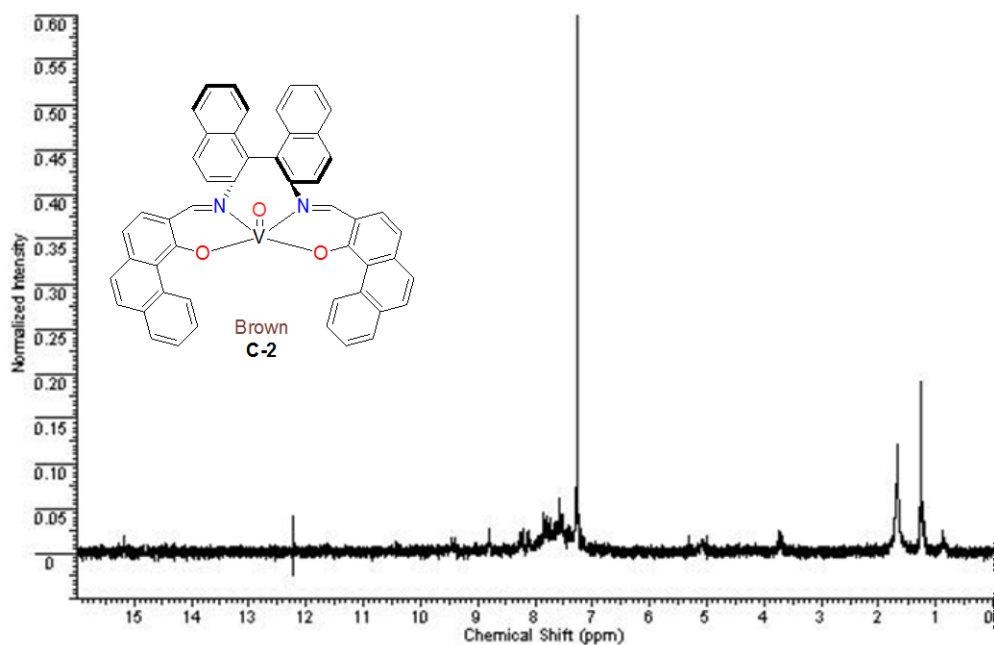
# $^1\text{H}$ NMR



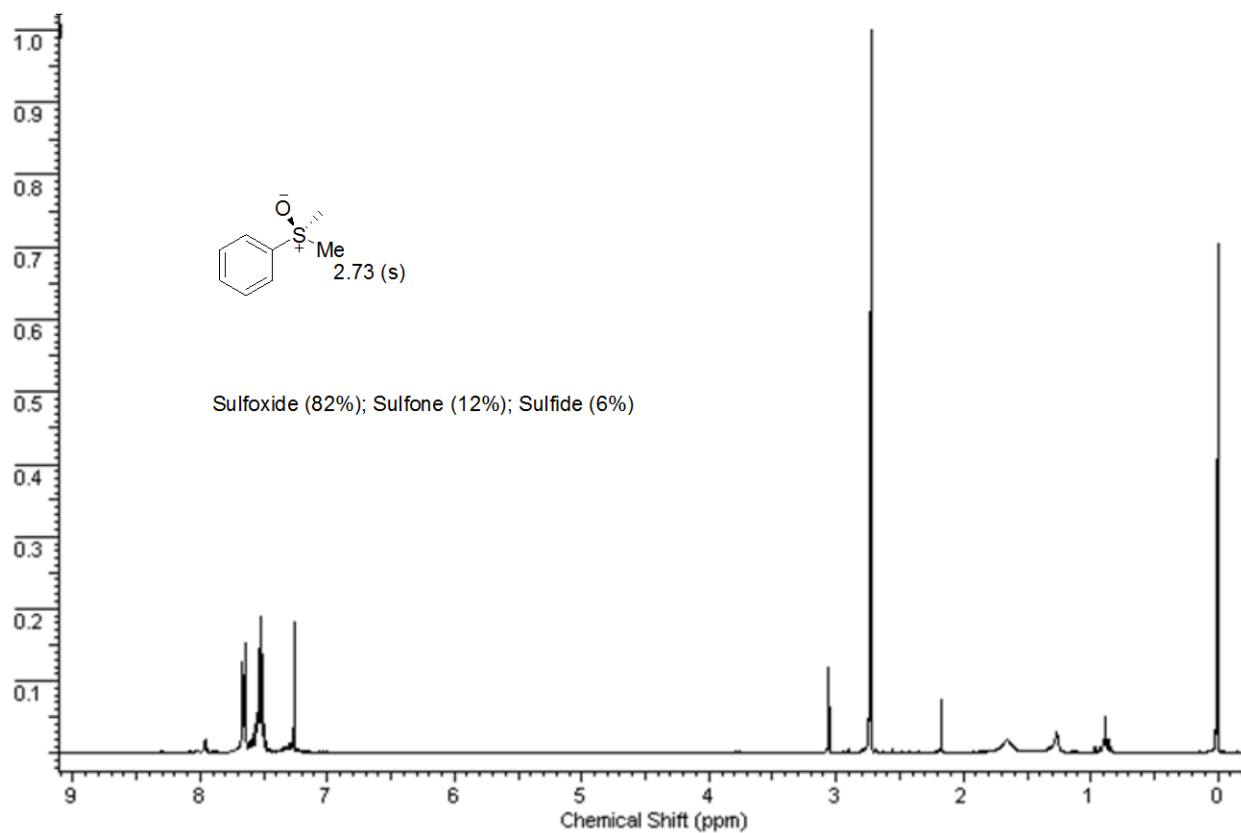
## $^1\text{H}$ NMR ( $\text{CDCl}_3$ , 400 MHz) of C-3



## $^1\text{H}$ NMR ( $\text{CDCl}_3$ , 400 MHz) of C-4

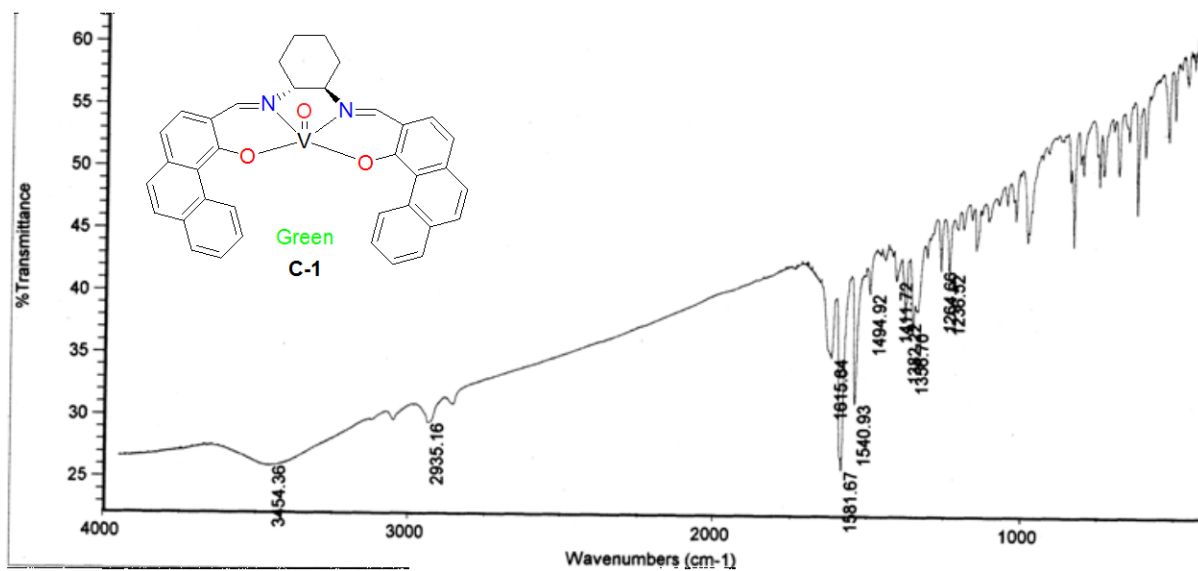


$^1\text{H}$  NMR ( $\text{CDCl}_3$ , 400 MHz) of C-2

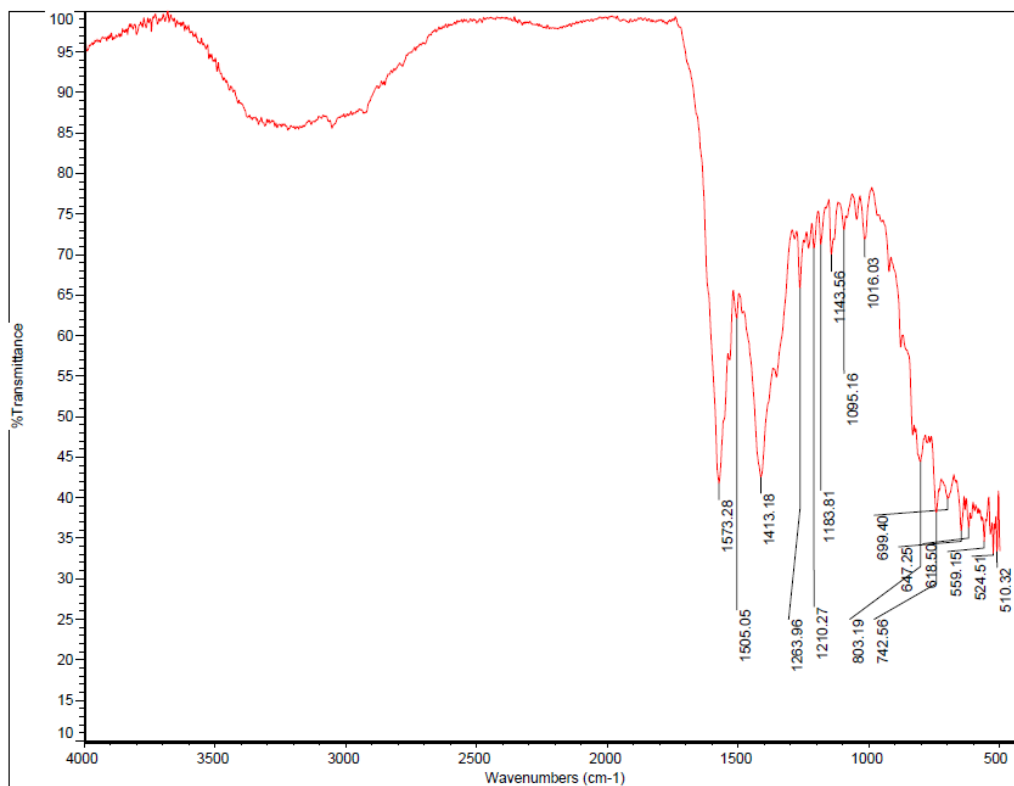


One example of  $^1\text{H}$  NMR ( $\text{CDCl}_3$ , 400 MHz) spectrum of the crude product mixture after sulfoxidation of thioanisole with  $\text{H}_2\text{O}_2$  in  $\text{CH}_2\text{Cl}_2$ .

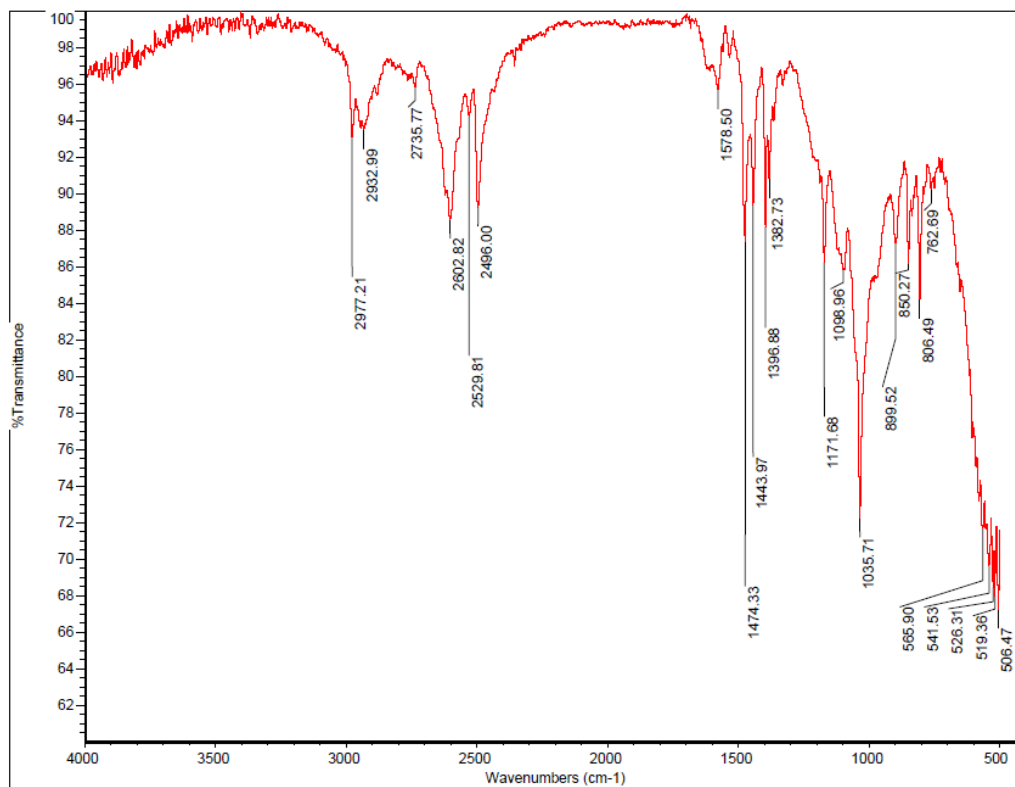
## IR of complexes



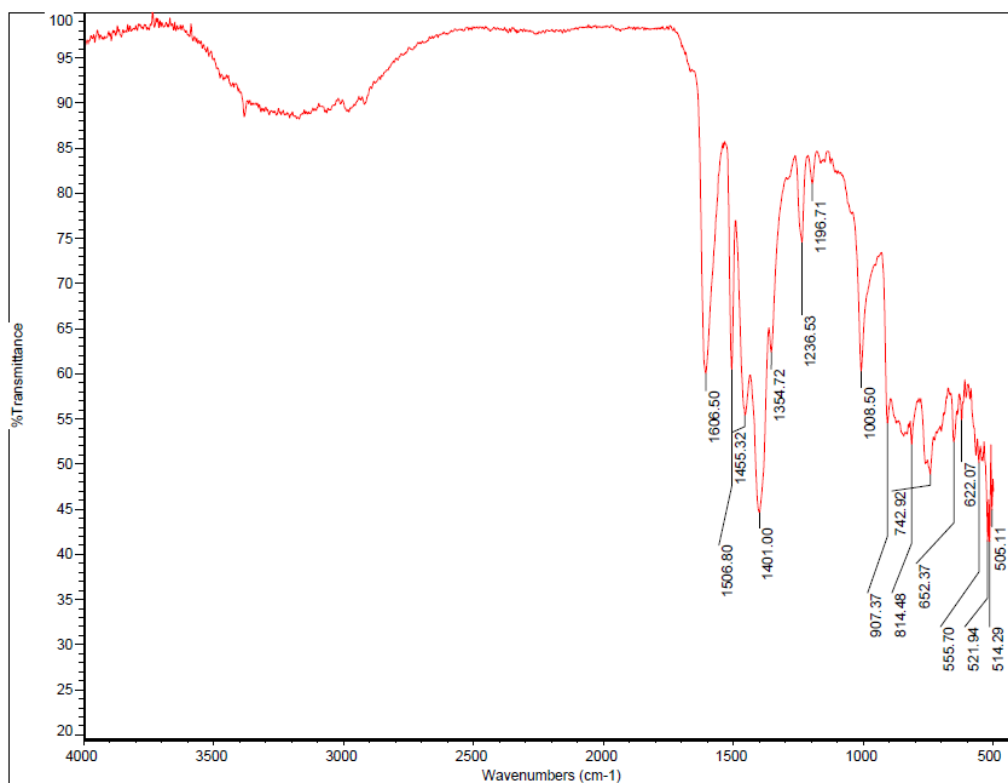
IR of C-1



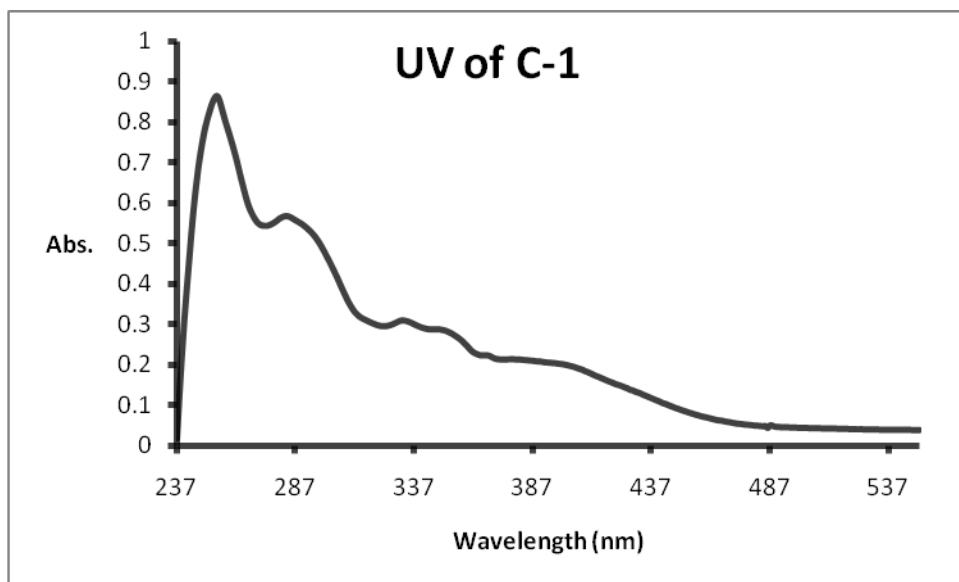
IR of C-2



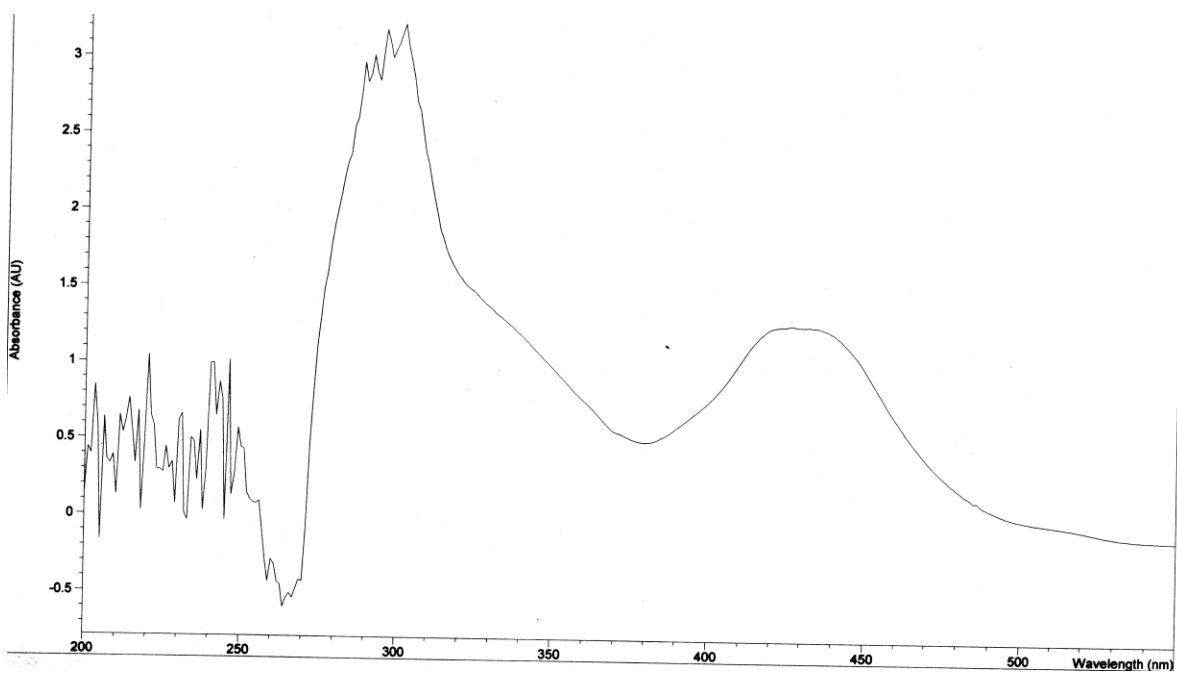
IR of C-3



IR of C-4

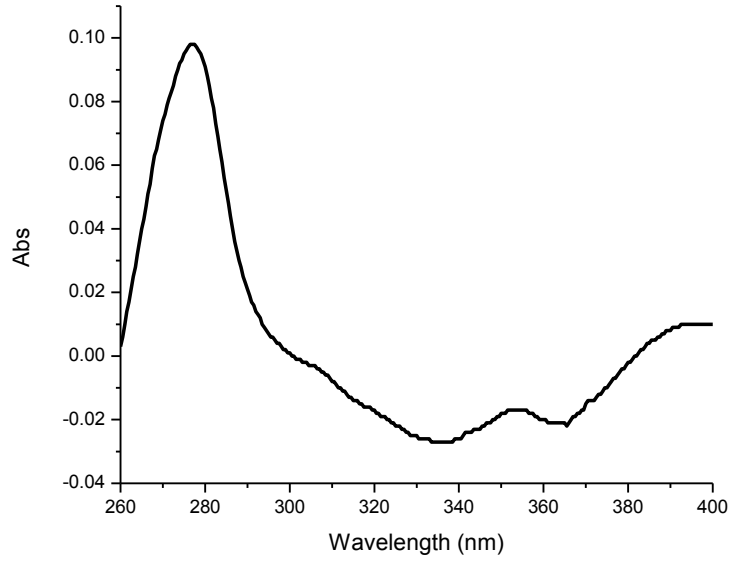


UV for C-1

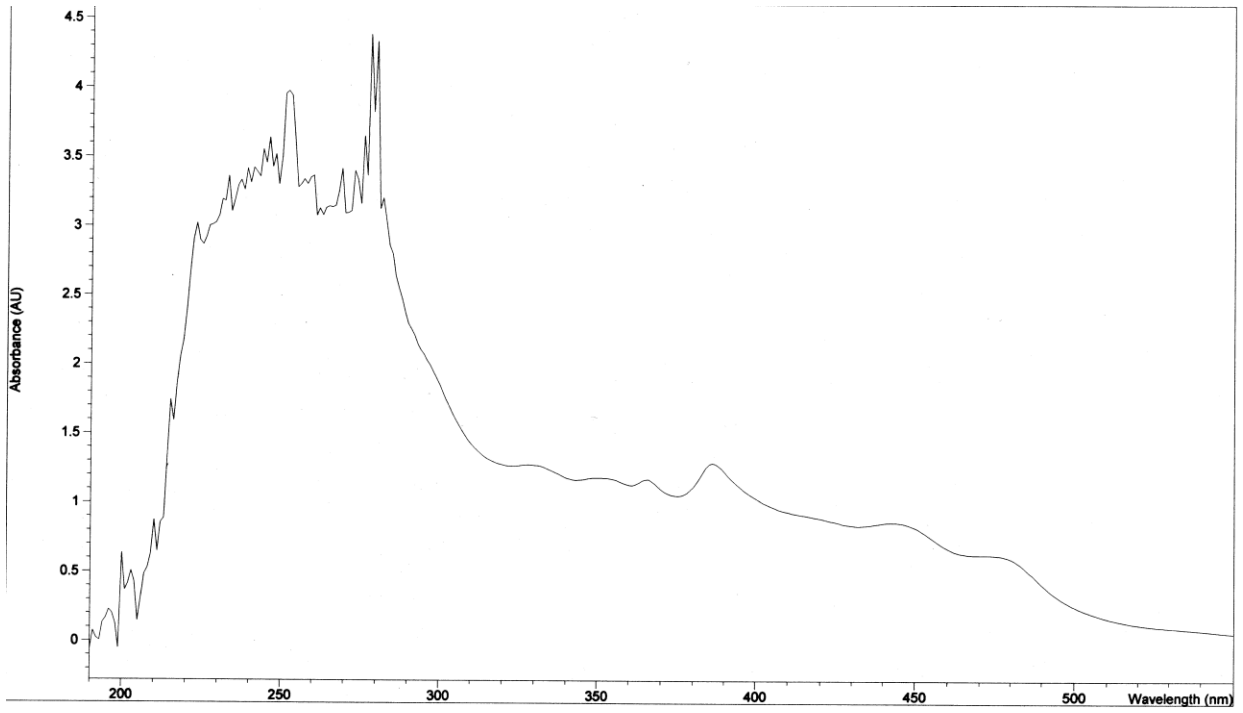


UV for C-2



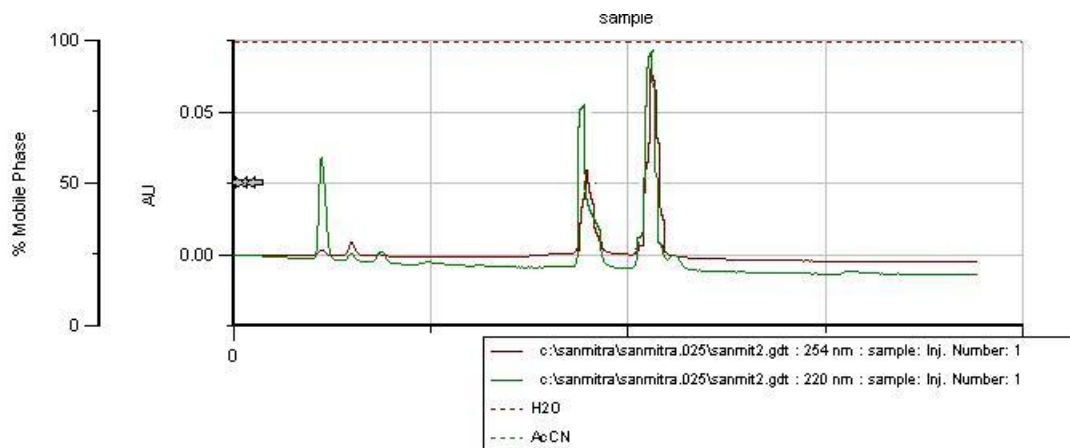
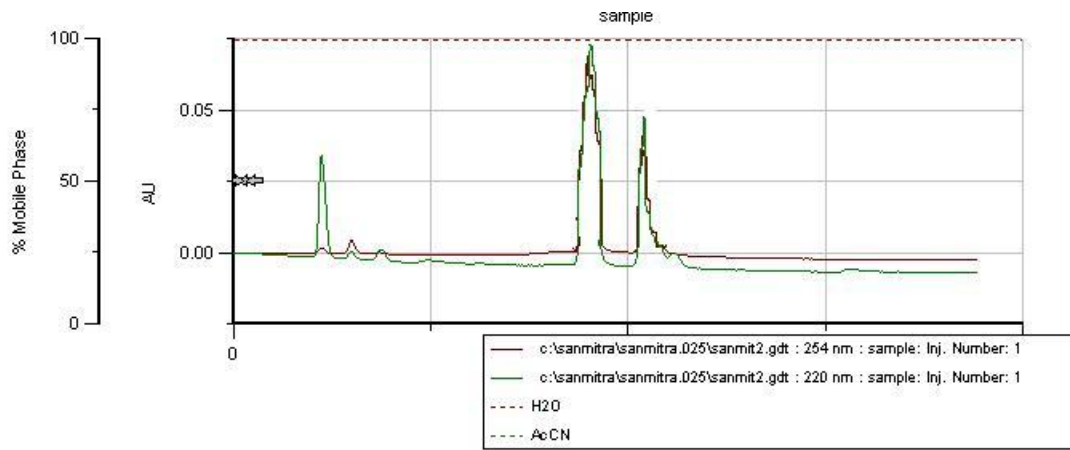
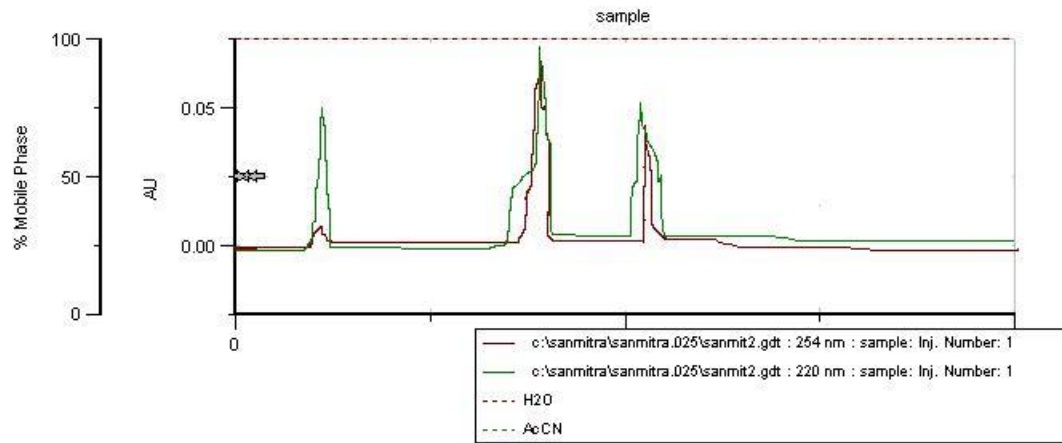


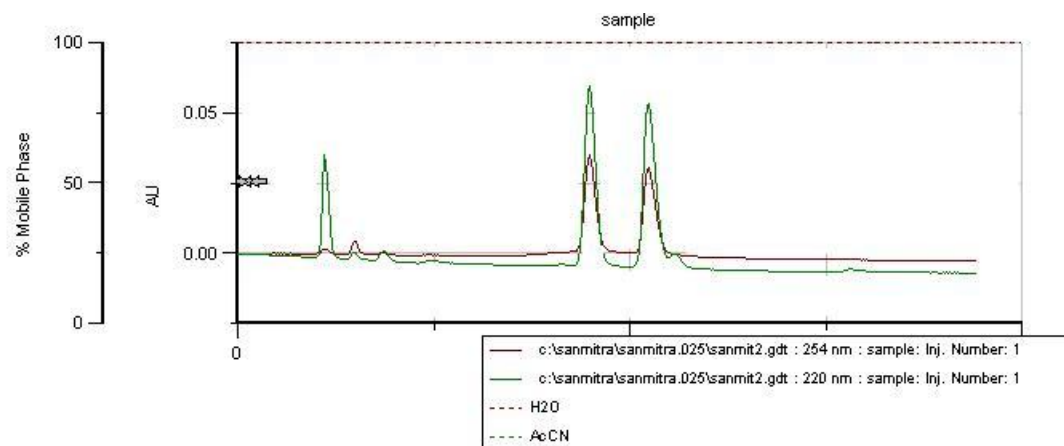
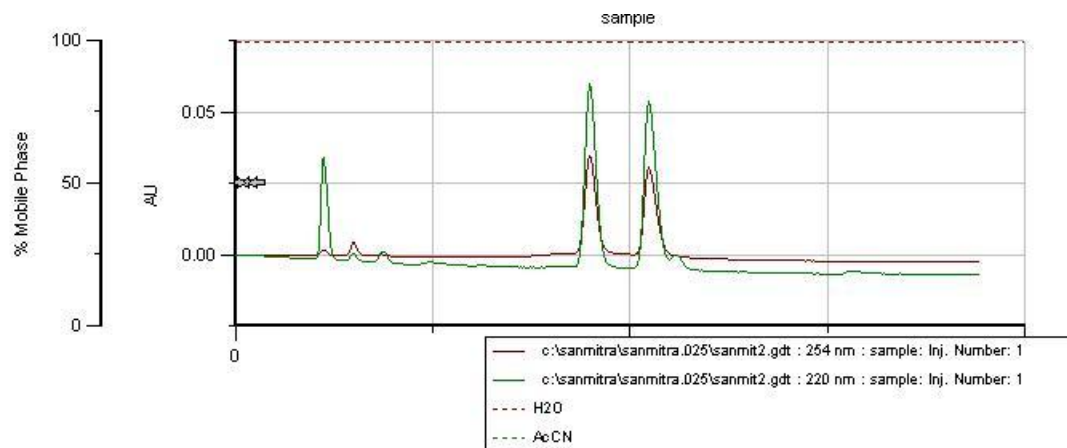
UV of C-3



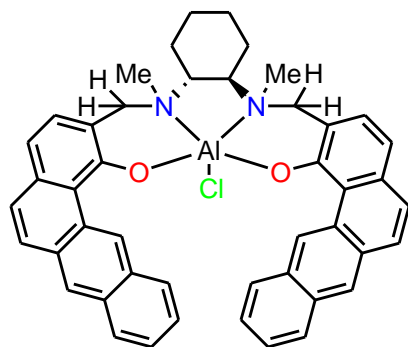
UV of C-4

# HPLC data showing the ratio between the two isomers



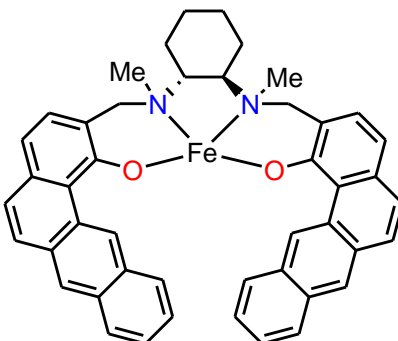


## Appendix B - Chapter 2

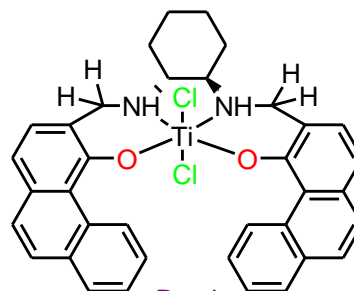


Off white

**C-3**

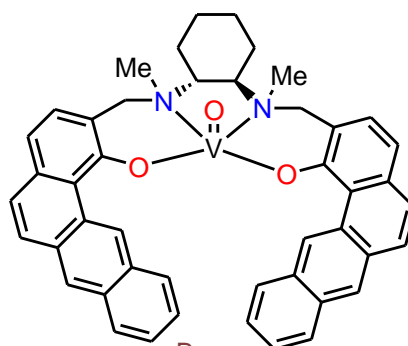


**C-1**



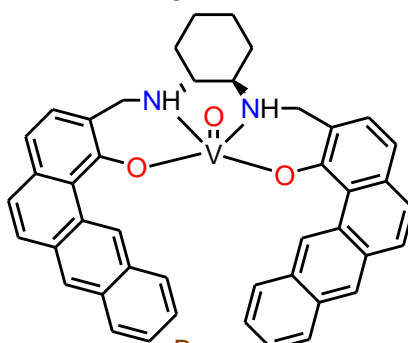
Purple

**C-6**



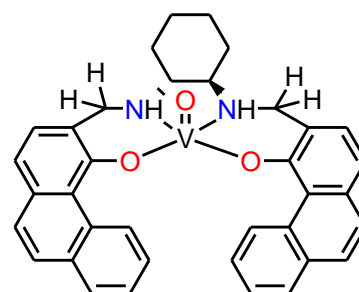
Brown

**C-2**



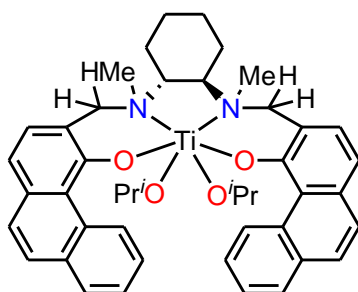
Brown

**C-4**



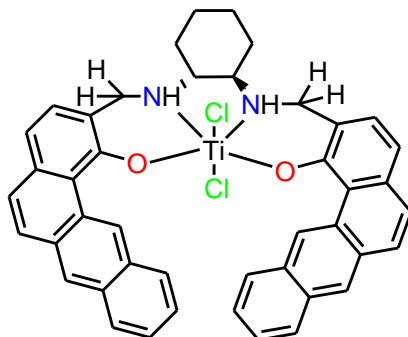
Brown

**C-5**



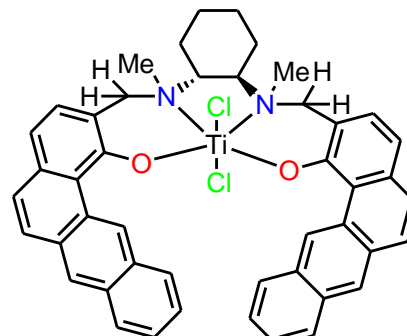
Yellowish brown

**C-7**



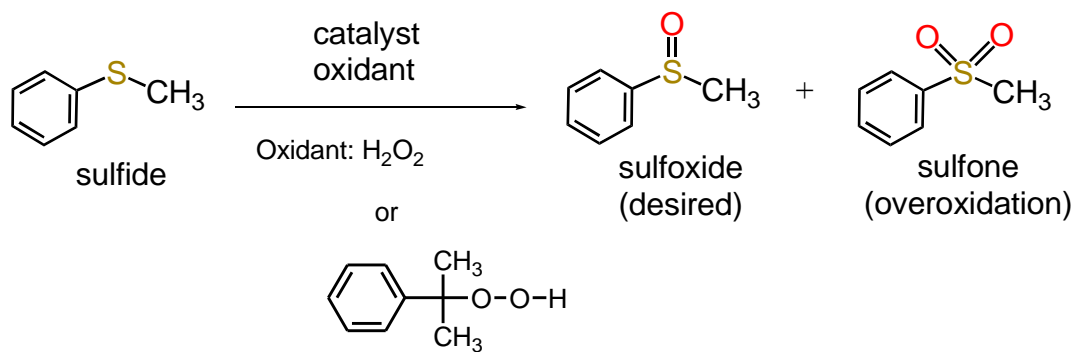
Dark purple

**C-8**

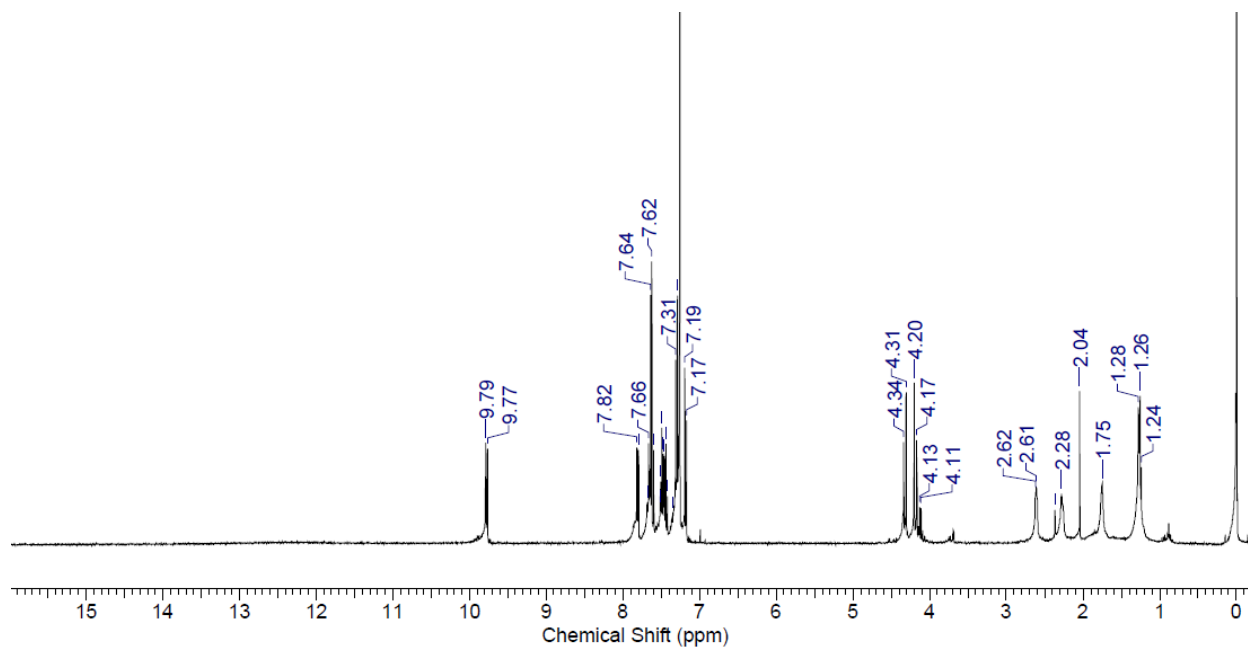


Dark purple

**C-9**

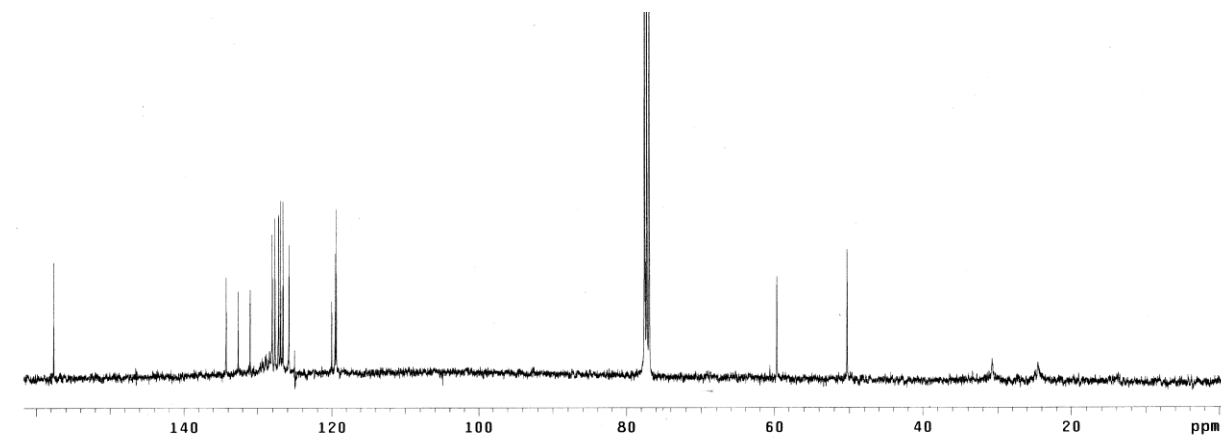


# $^1\text{H}$ NMR



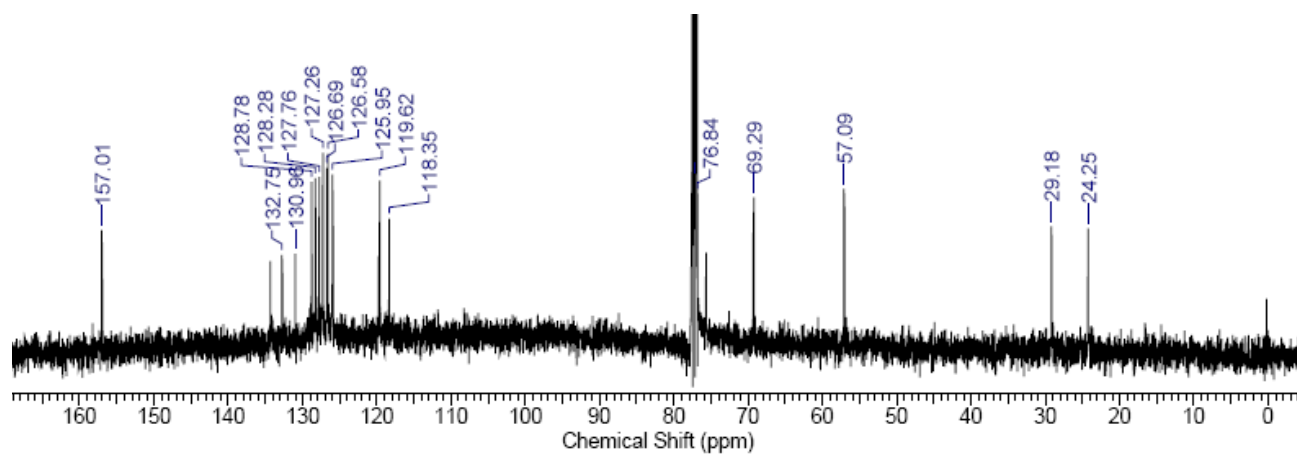
$^1\text{H}$  NMR ( $\text{CDCl}_3$ , 400 MHz) of ligand (*R,R*)-5

# $^{13}\text{C}$ NMR

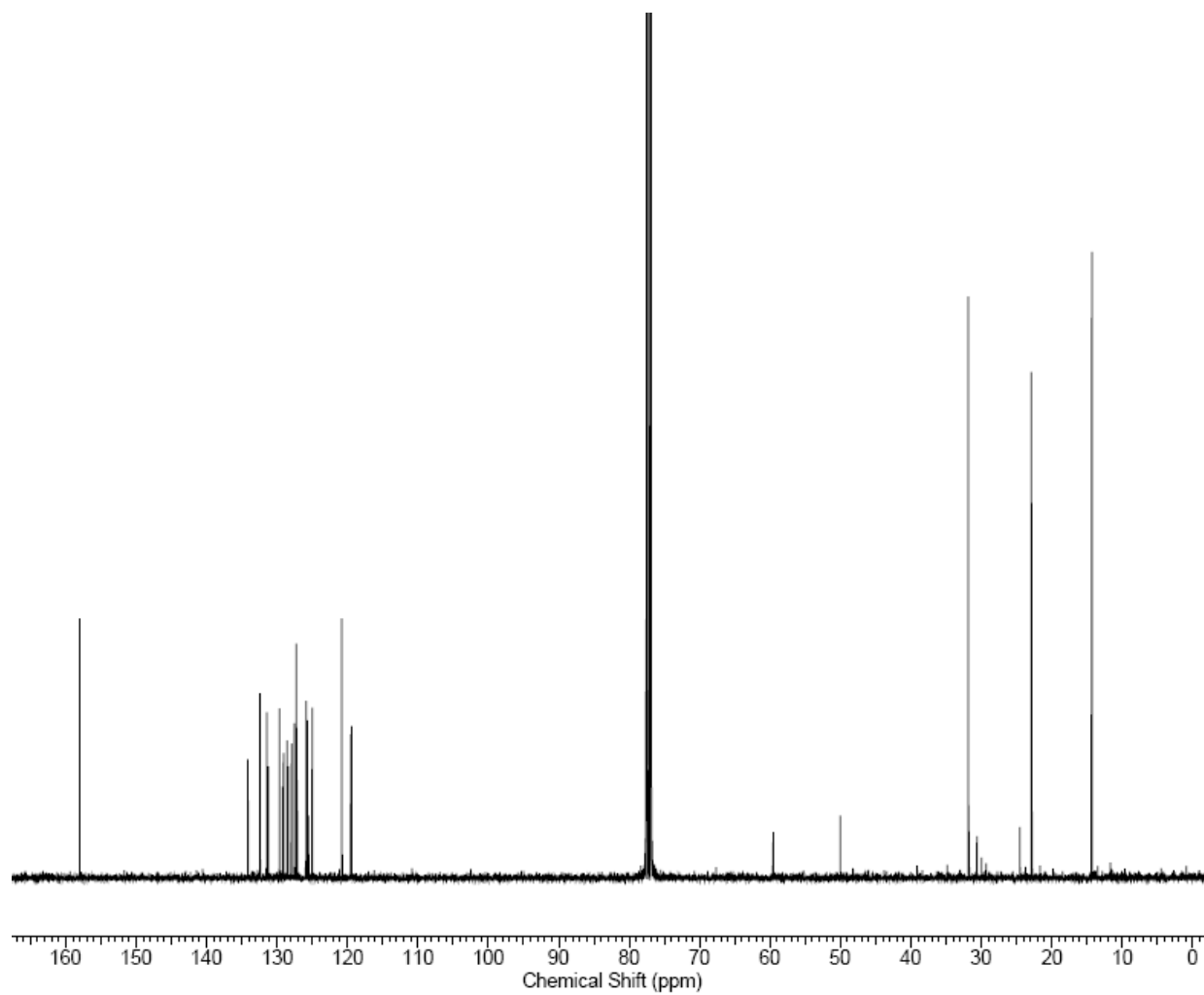


$^{13}\text{C}$  NMR ( $\text{CDCl}_3$ , 400 MHz) of ligand (*R,R*)-5

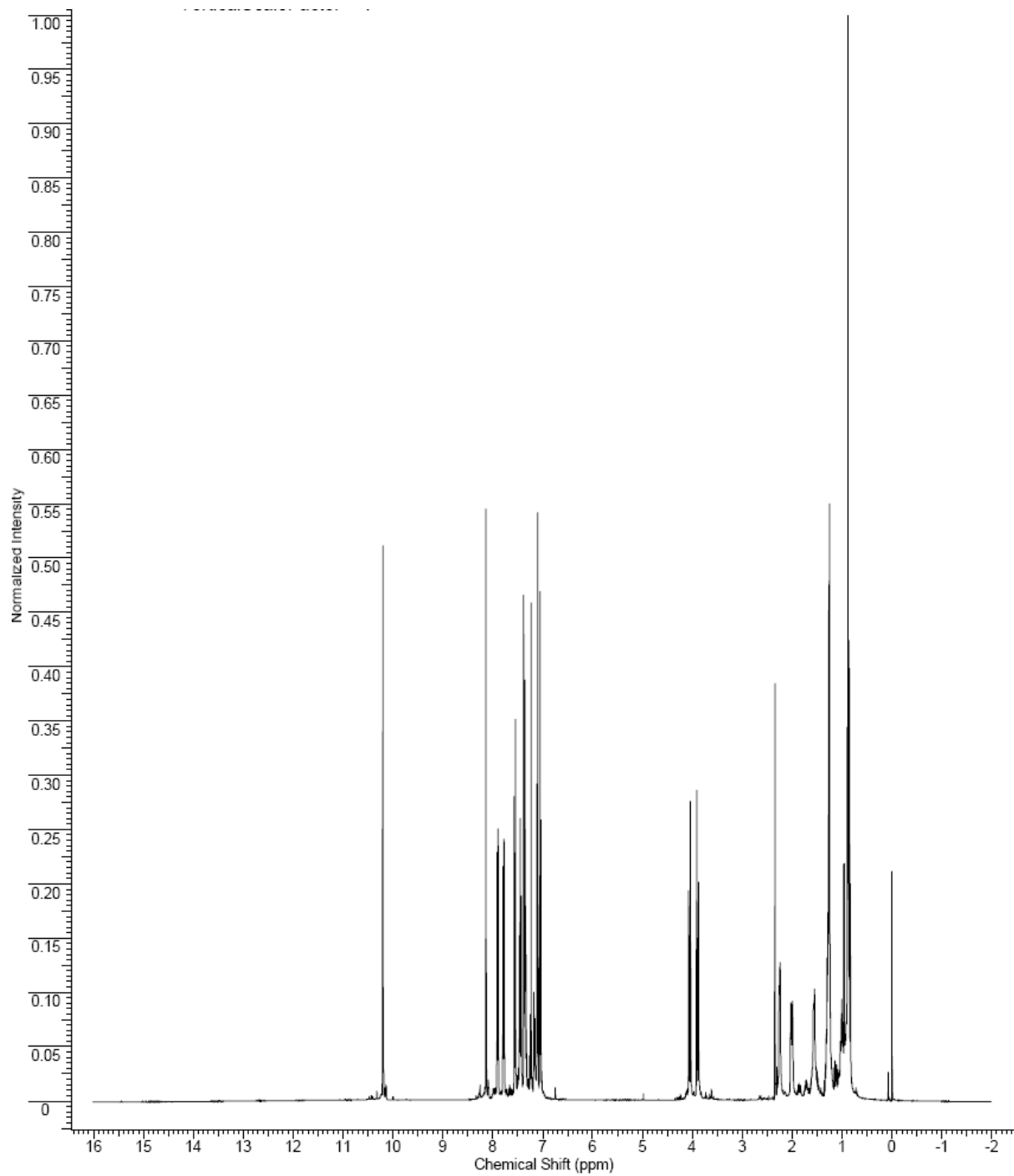
# $^{13}\text{C}$ NMR



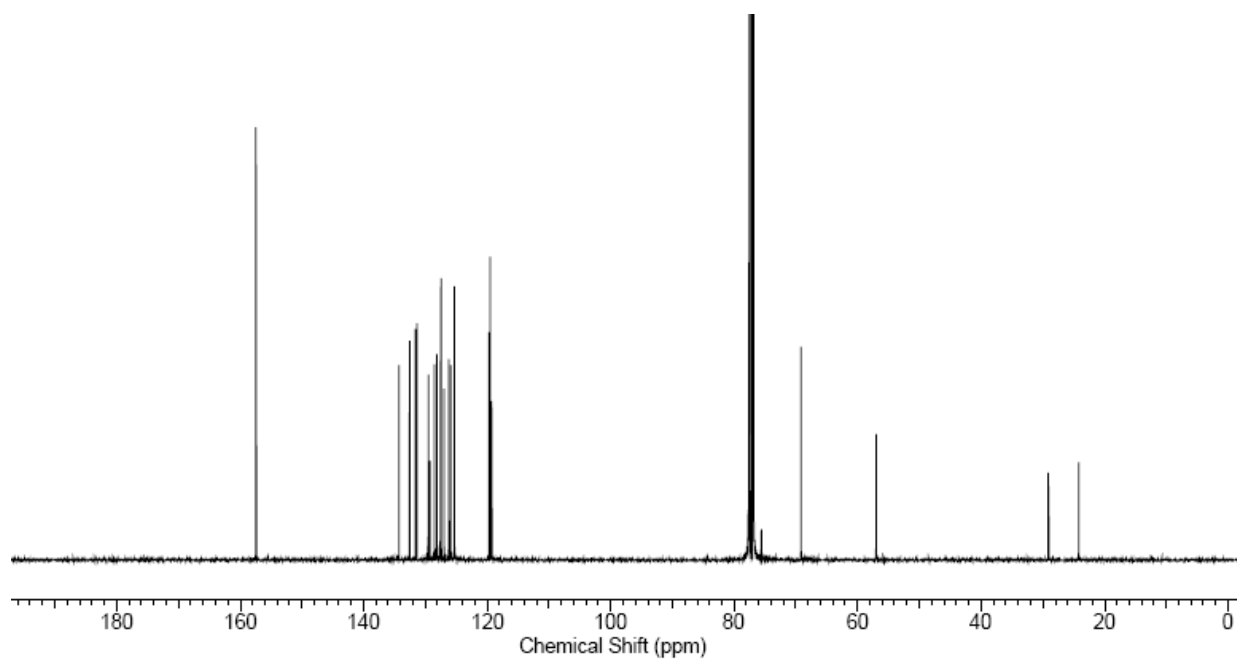
$^{13}\text{C}$  NMR ( $\text{CDCl}_3$ , 400 MHz) of  $(R,R)$ -6



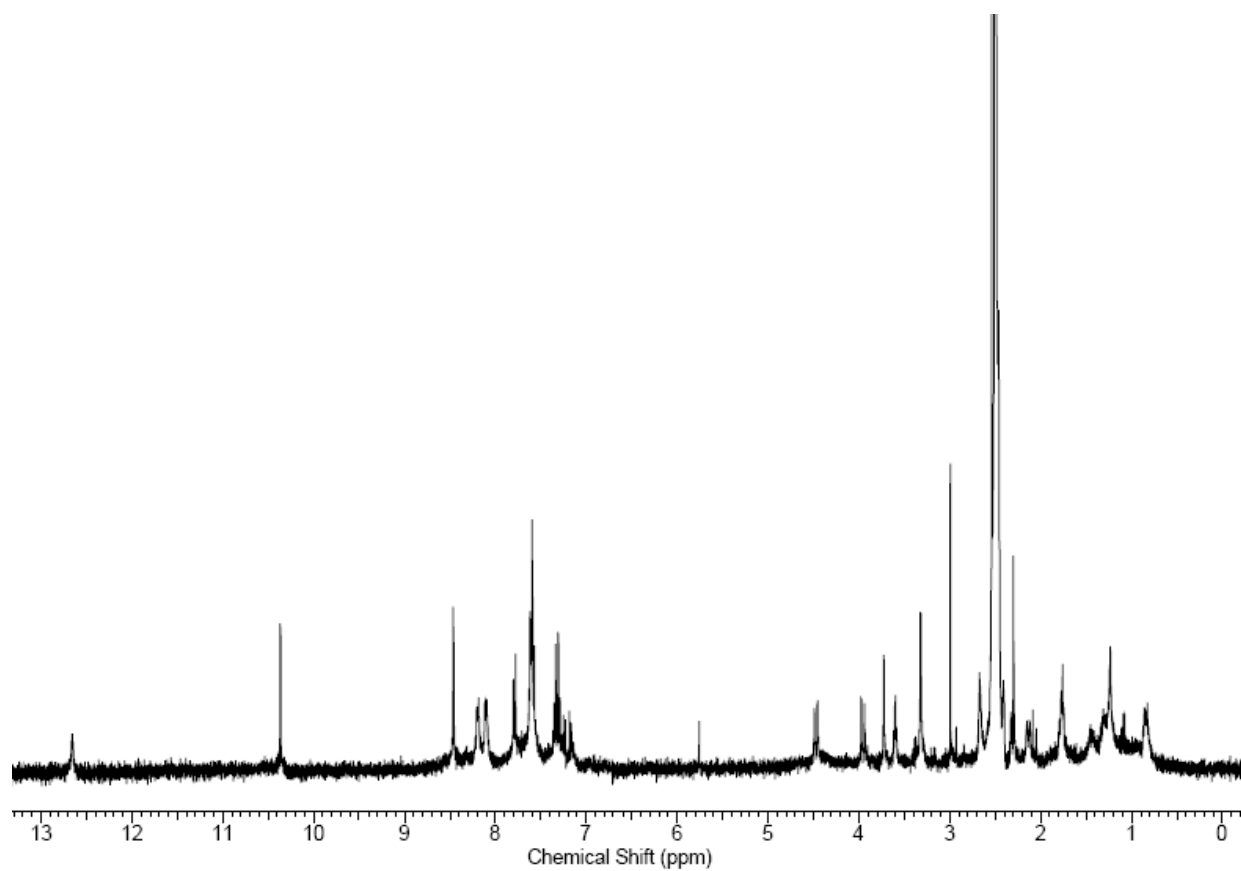
$^{13}\text{C}$  NMR ( $\text{CDCl}_3$ , 400MHz) of  $(R,R)$ -7



$^1\text{H}$  NMR ( $\text{CDCl}_3$ , 400 MHz) of ligand (*R,R*)-7

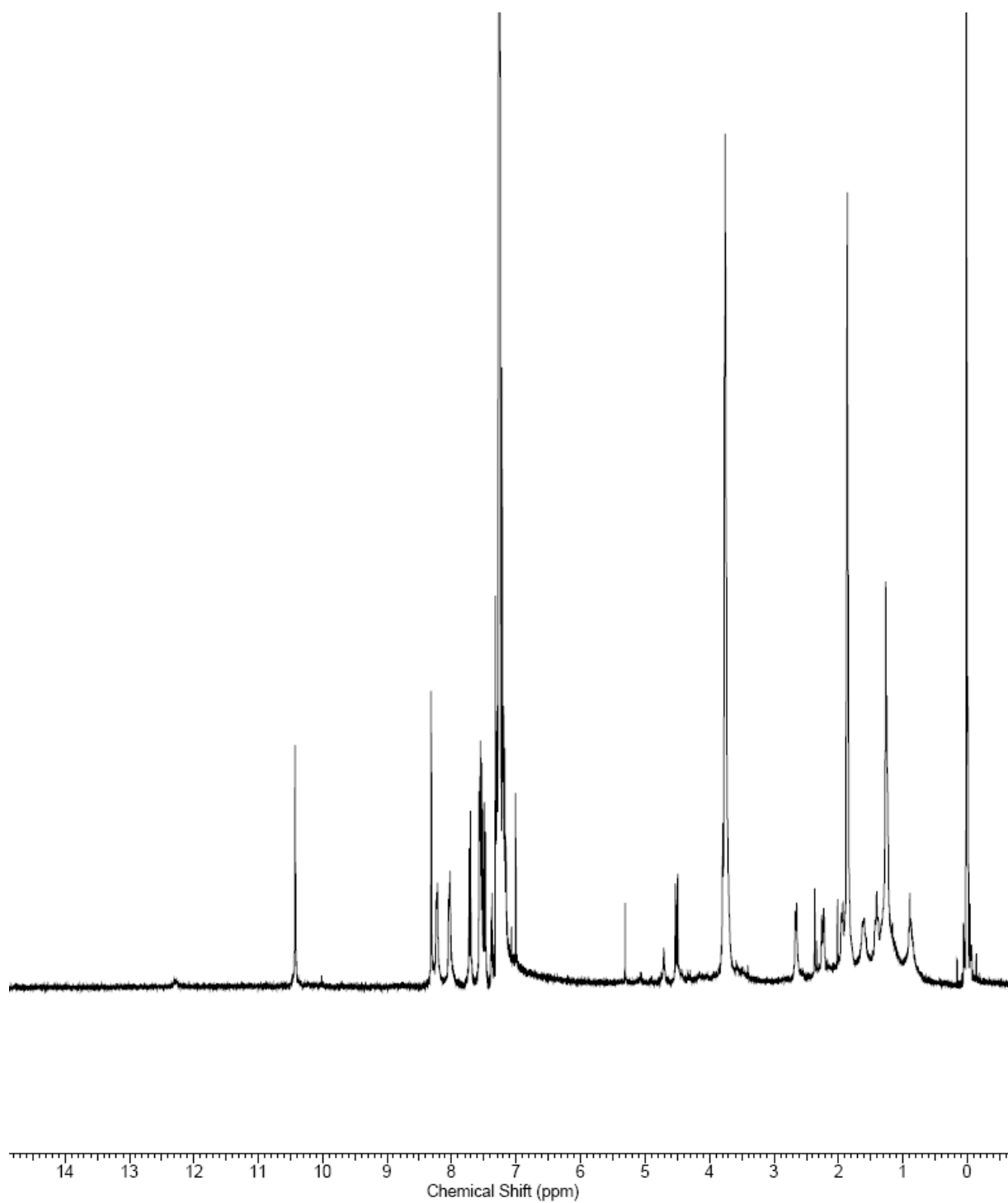


$^{13}\text{C}$  NMR ( $\text{CDCl}_3$ , 400 MHz) of **(*R,R*)-8**

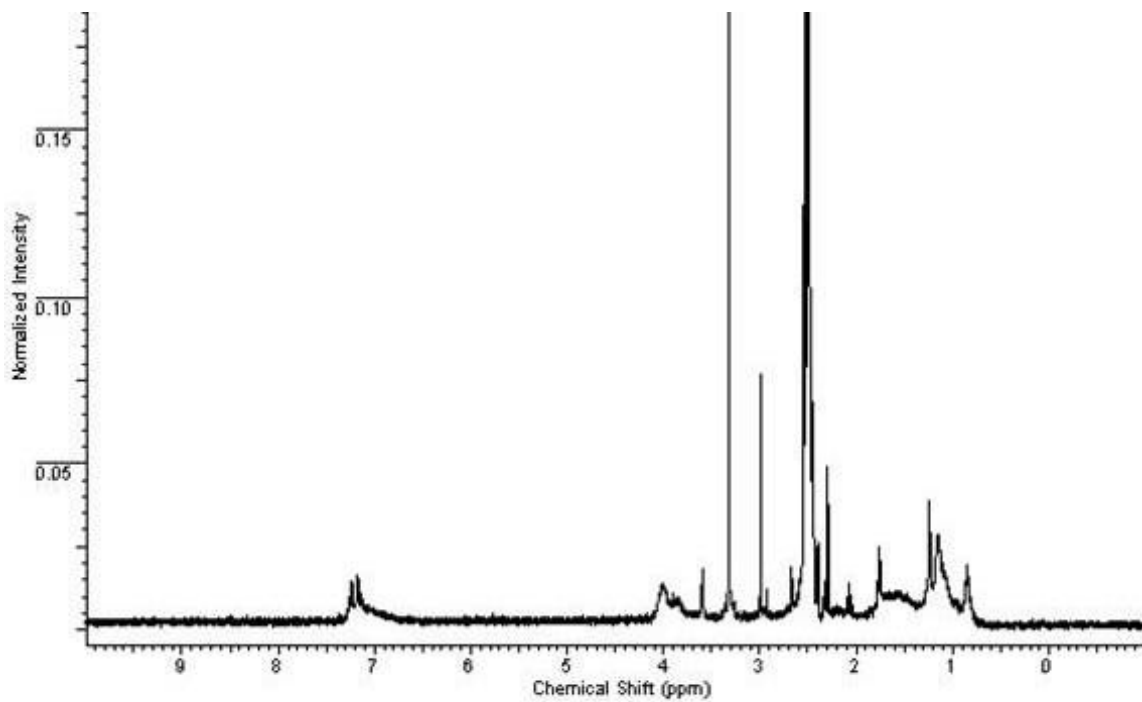


$^1\text{H}$  NMR ( $\text{CDCl}_3$ , 400 MHz) of complex **C-3**

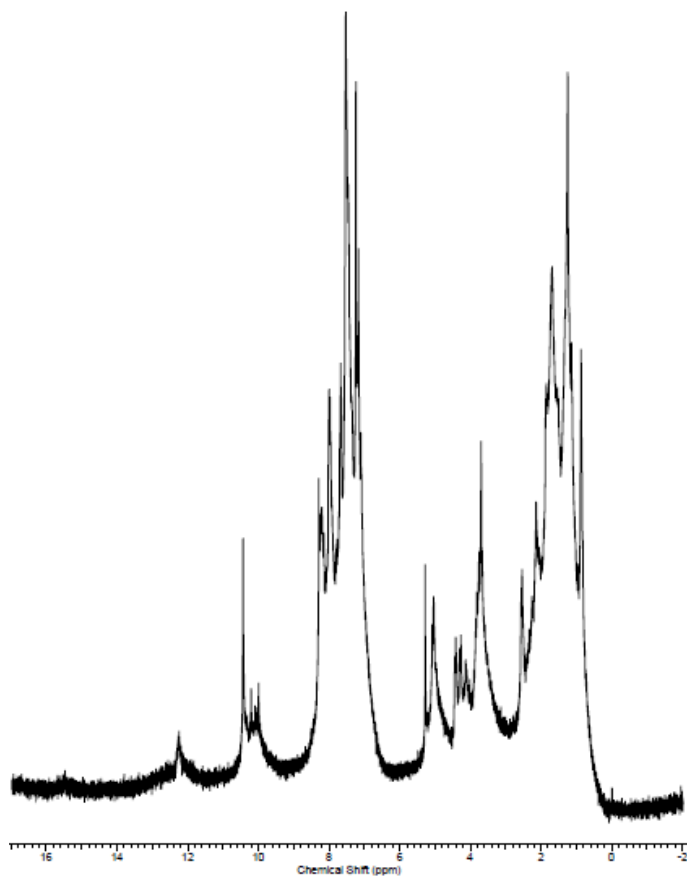




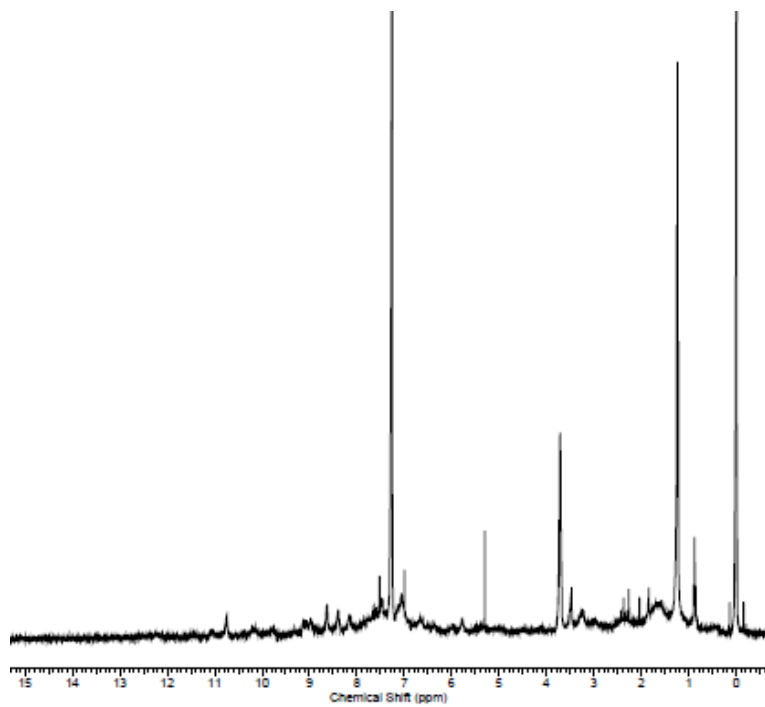
$^1\text{H}$  NMR ( $\text{CDCl}_3$ , 400 MHz) of complex C-1



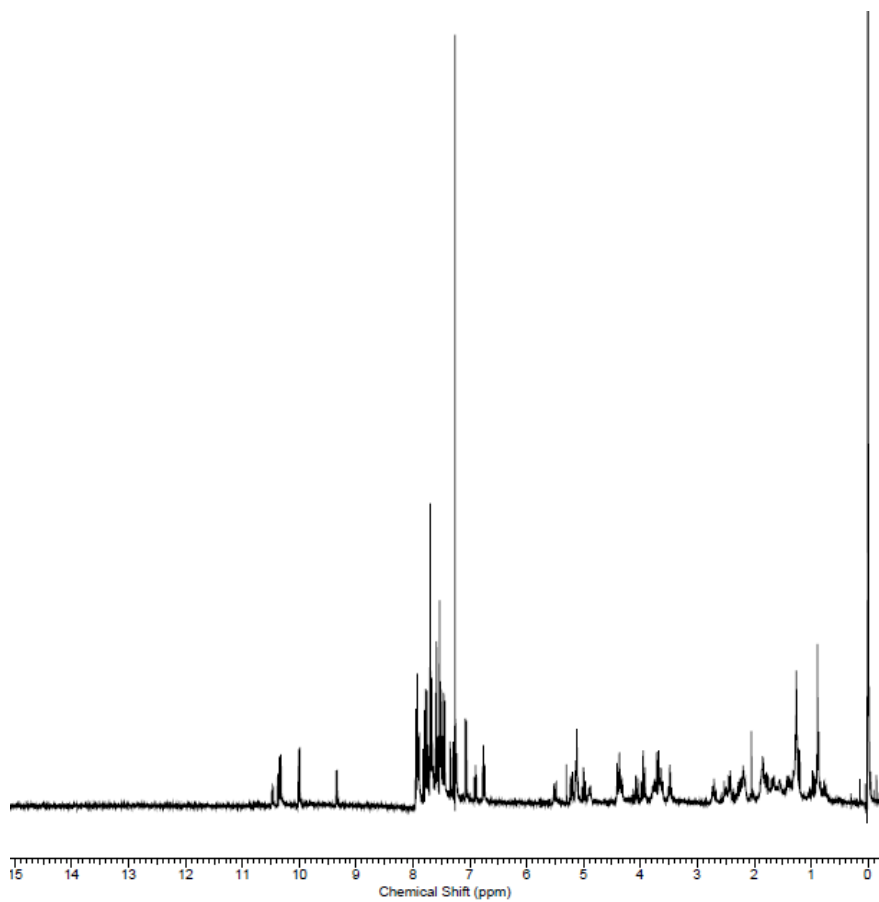
$^1\text{H}$  NMR ( $\text{CDCl}_3$ , 400 MHz) of complex C-2



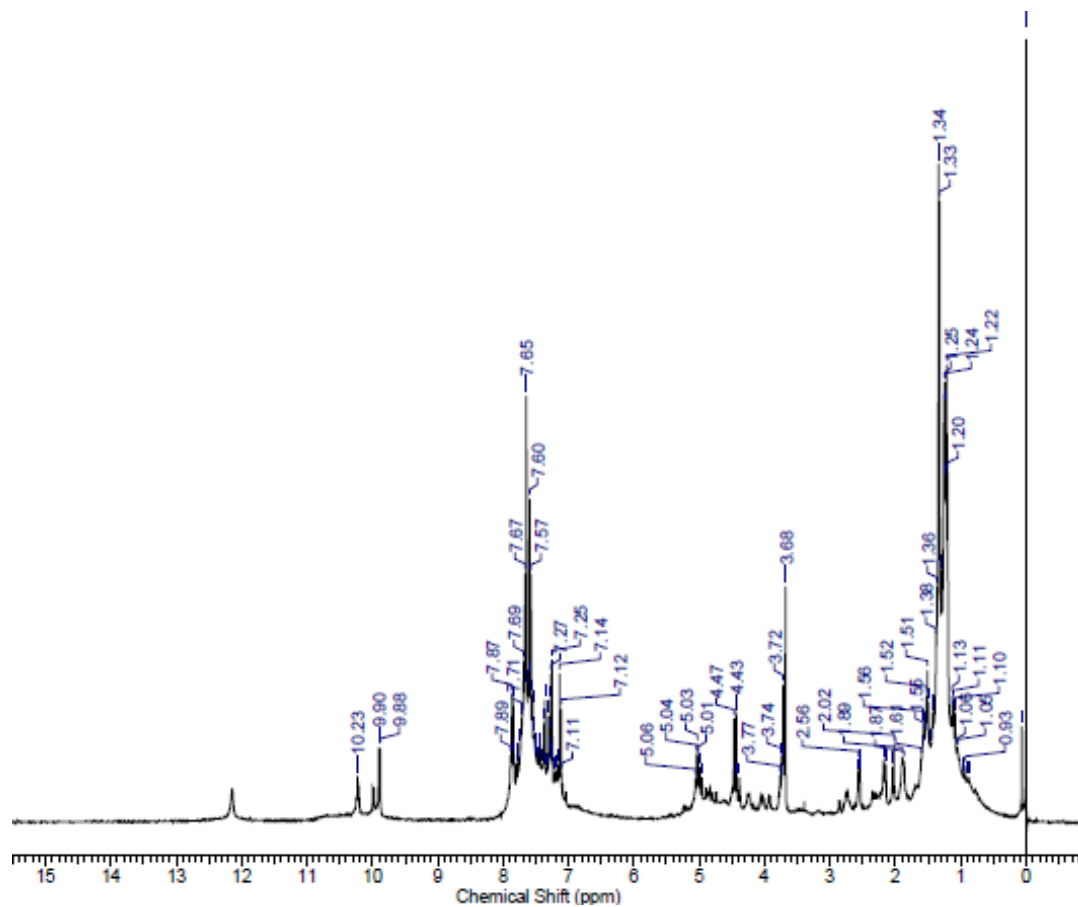
$^1\text{H}$  NMR ( $\text{CDCl}_3$ , 400 MHz) of complex C-4



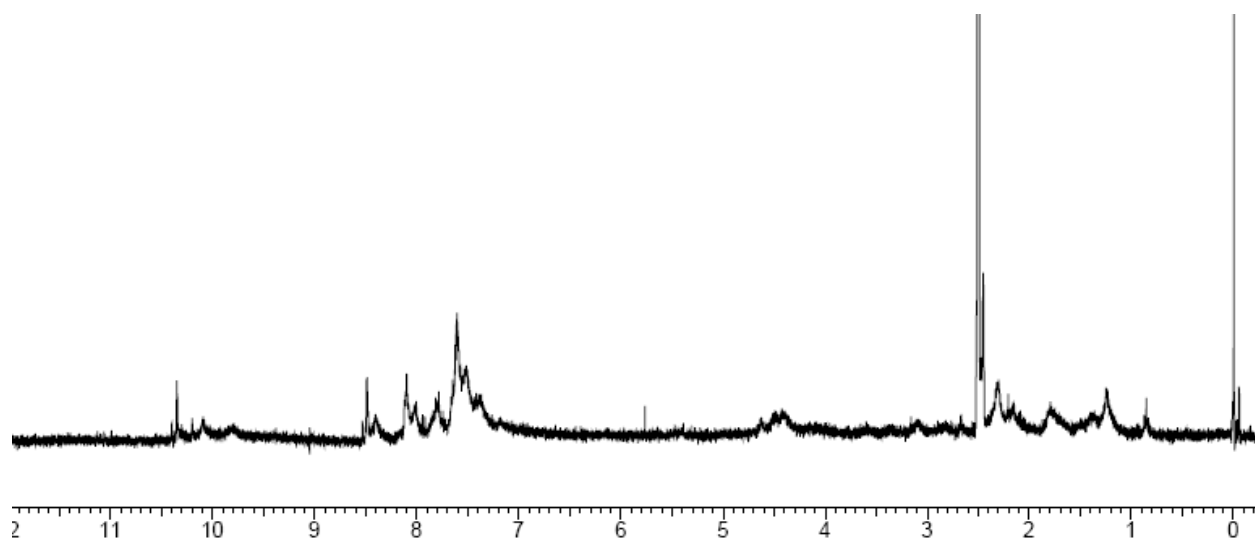
$^1\text{H}$  NMR ( $\text{CDCl}_3$ , 400 MHz) of complex **C-5**



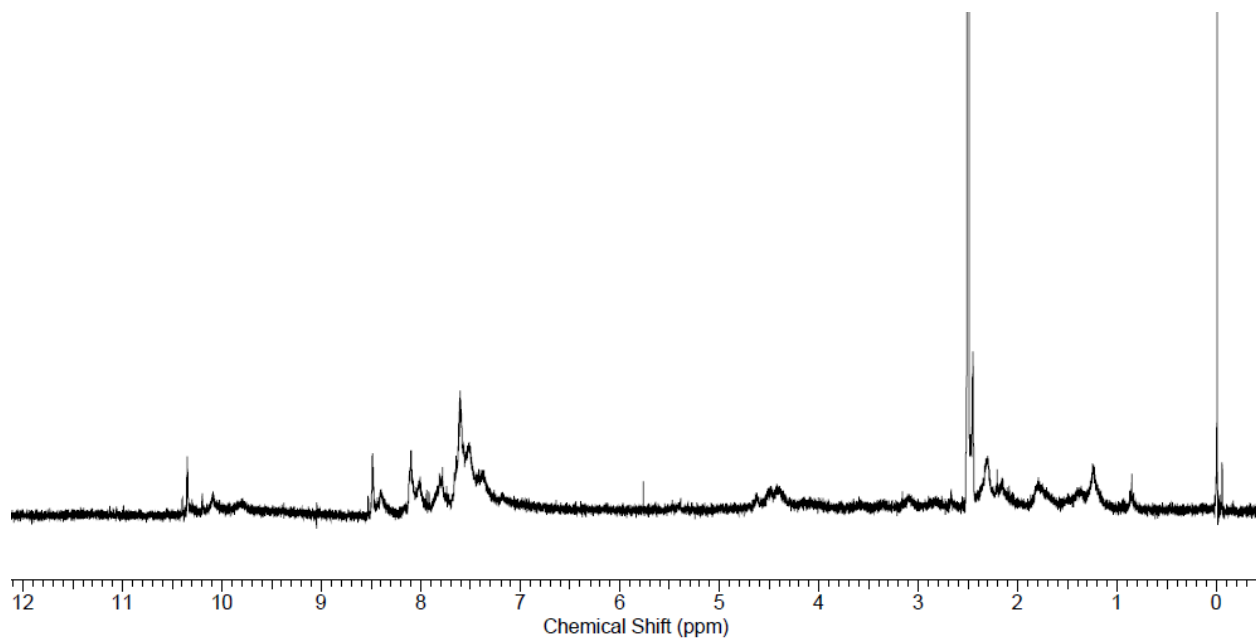
$^1\text{H}$  NMR ( $\text{CDCl}_3$ , 400 MHz) of complex **C-6**



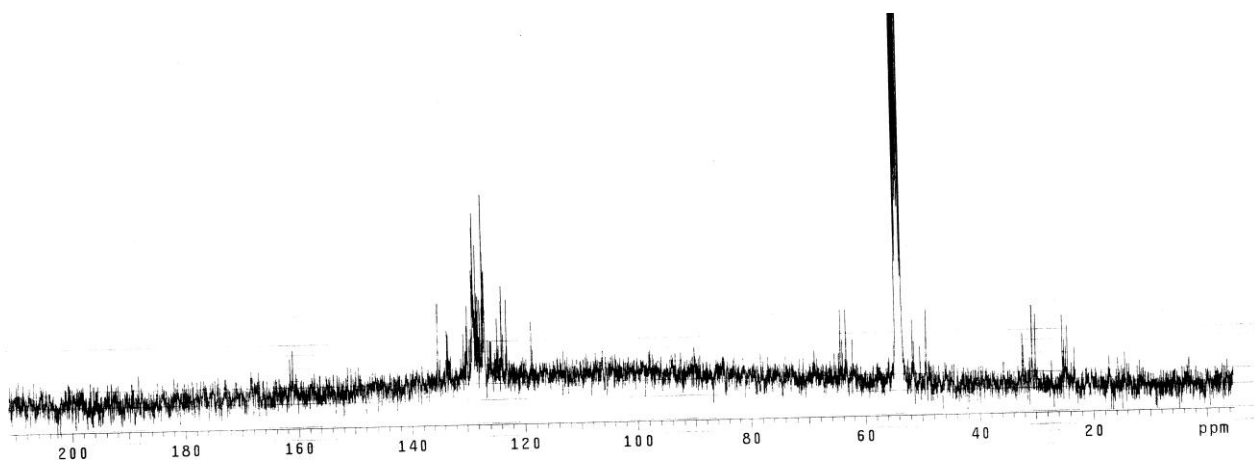
$^1\text{H}$  NMR ( $\text{CDCl}_3$ , 400 MHz) of complex C-7



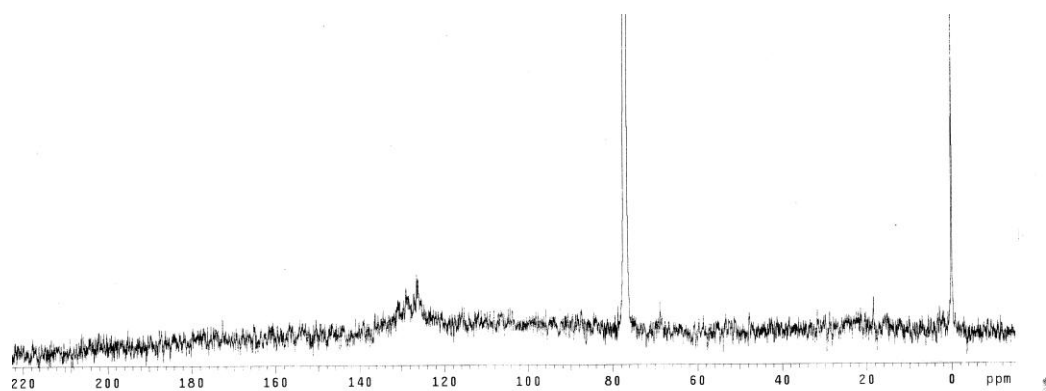
$^1\text{H}$  NMR ( $\text{DMSO}$ , 400 MHz) of complex C-8



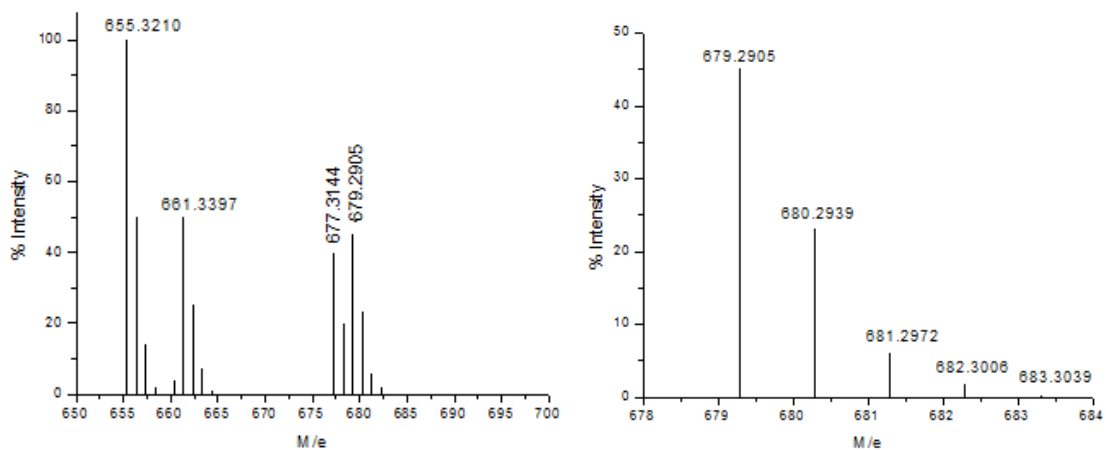
$^1\text{H}$  NMR (DMSO, 400 MHz) of complex **C-9**



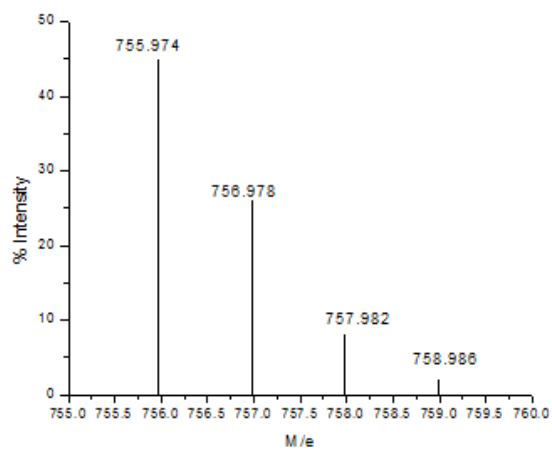
$^{13}\text{C}$  NMR ( $\text{CD}_2\text{Cl}_2$ , 400 MHz) of complex **C-6**



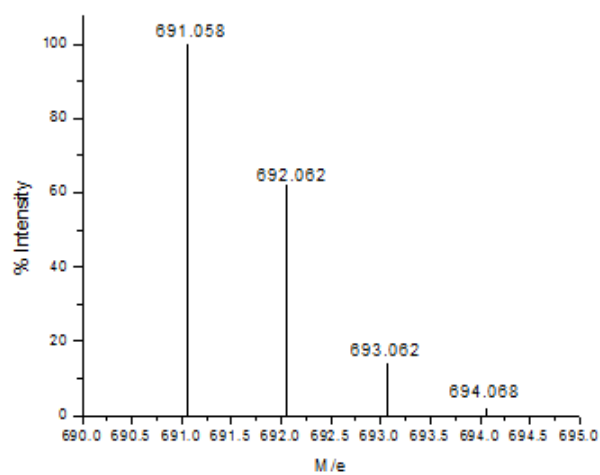
$^{13}\text{C}$  NMR ( $\text{CDCl}_3$ , 400 MHz) of complex **C-8**



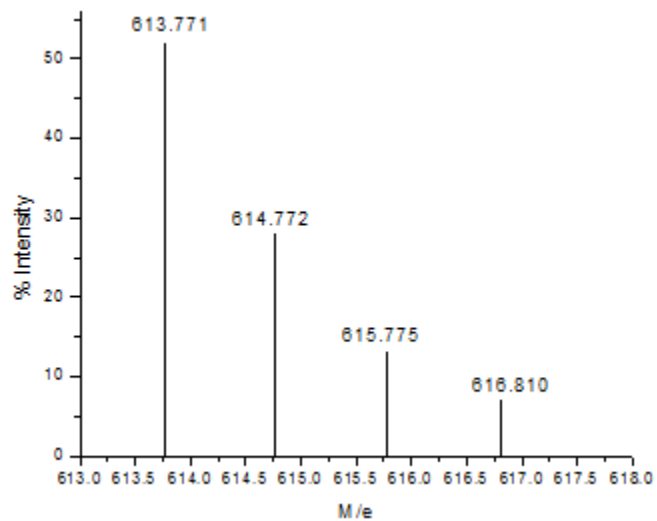
Entire mass spectrum (on left) and isotopic pattern of the molecular ion  $[M-Cl]^{+1}$  peak for complex **C-3** (on right)



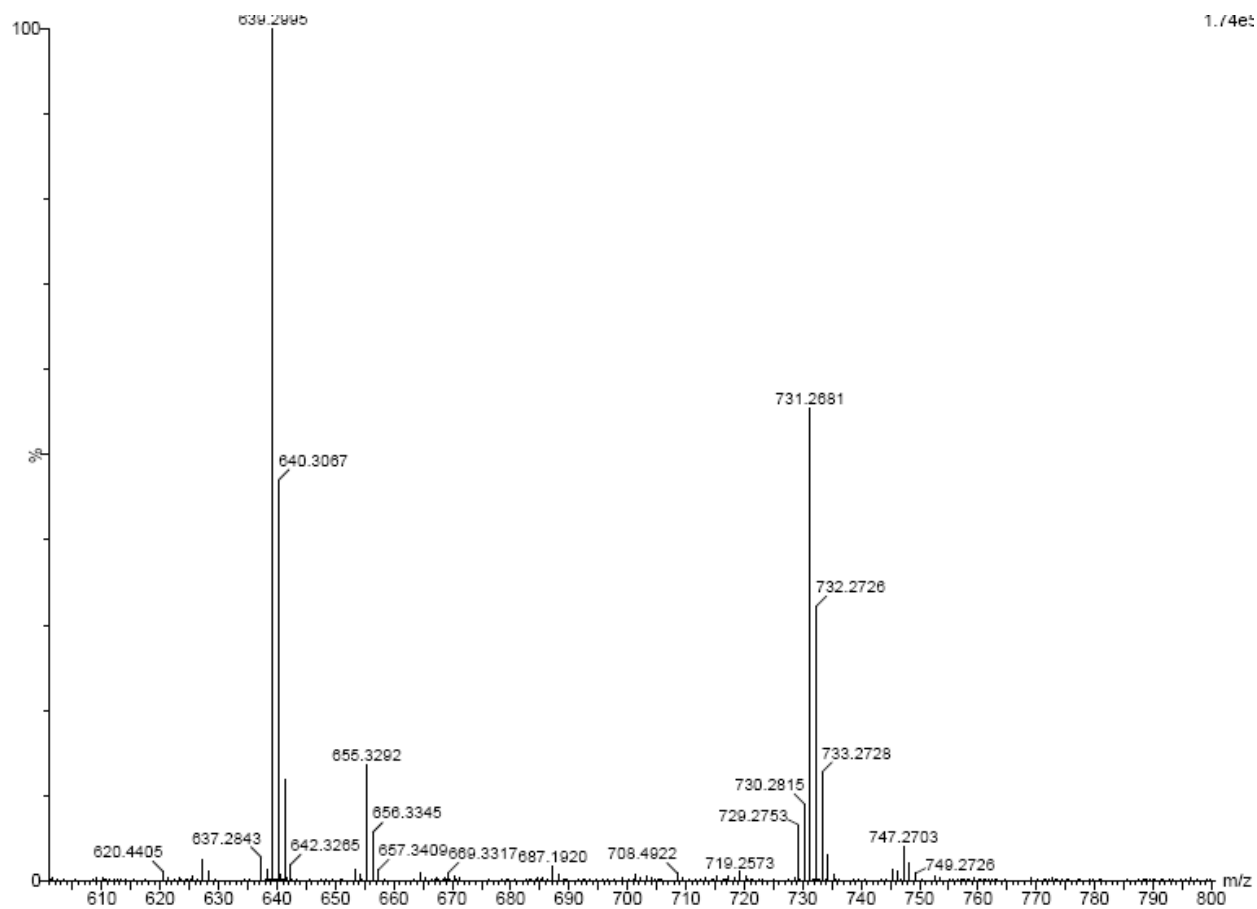
Isotopic pattern of the molecular ion peak for complex **C-2**  $[M+Cl]^{+1}$ .

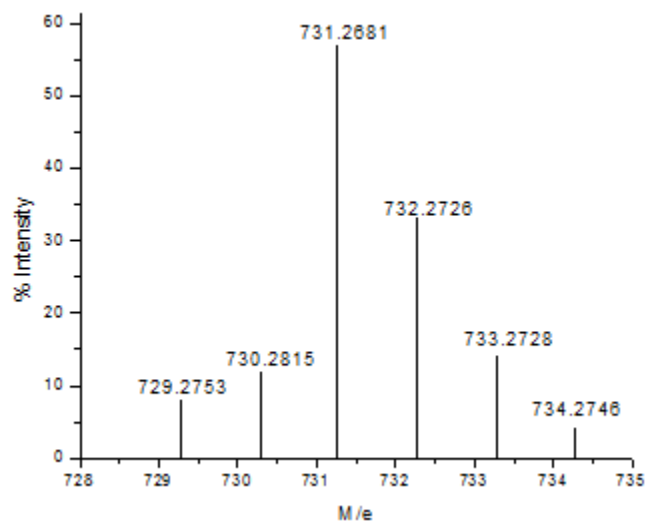


Isotopic pattern of the molecular ion peak for complex **C-4**  $[M]^{+1}$

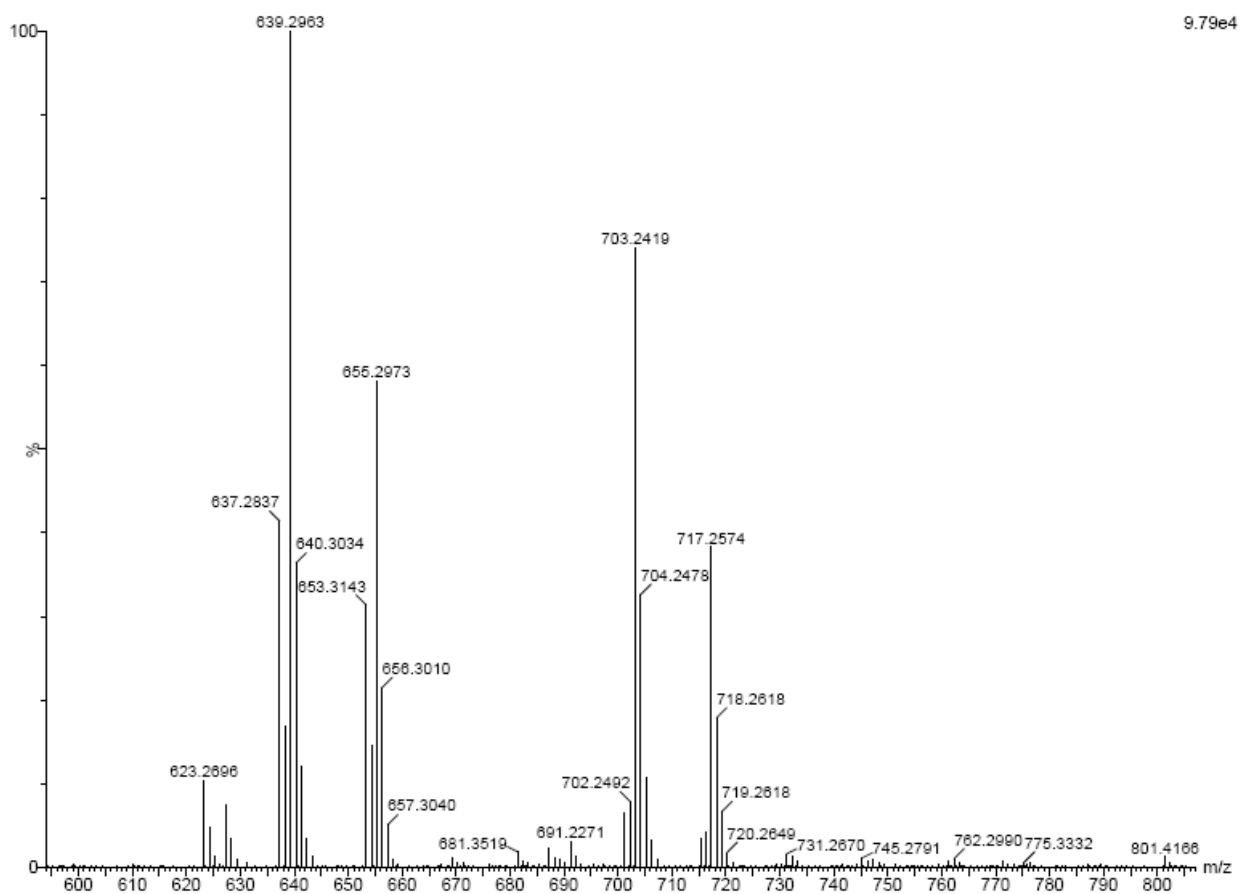


Isotopic pattern of the molecular ion peak for complex C-5 [M+Na]<sup>+1</sup>

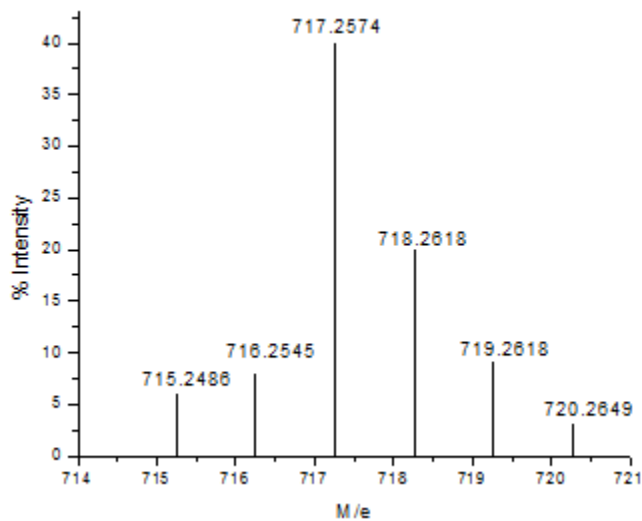




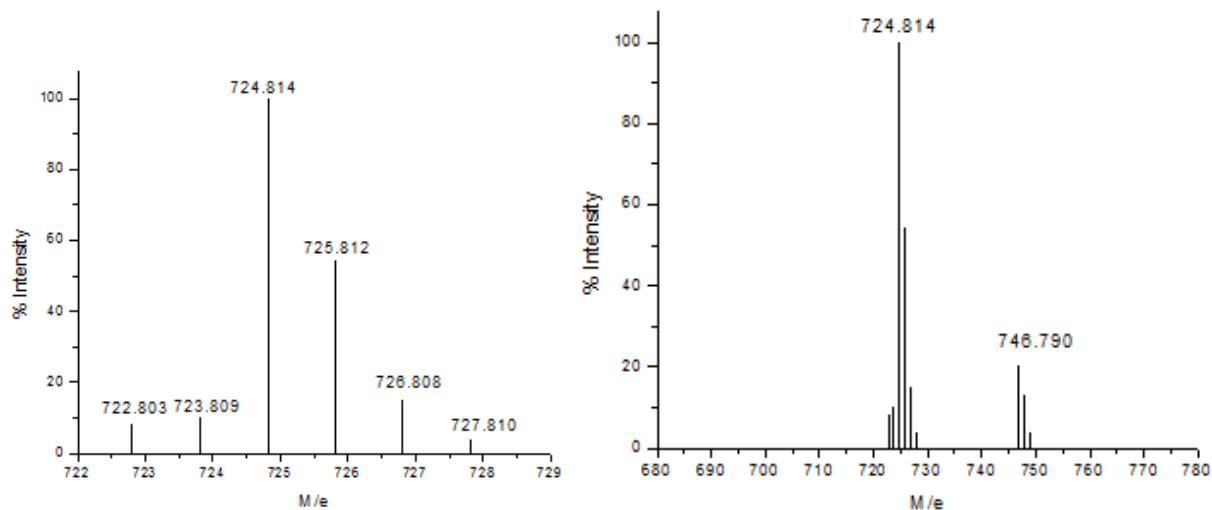
Entire mass spectrum of complex **C-9**  $[M-2Cl+OMe]^{+1}$  (on previous page), with isotopic pattern and molecular ion peak at 731.2691 (top).



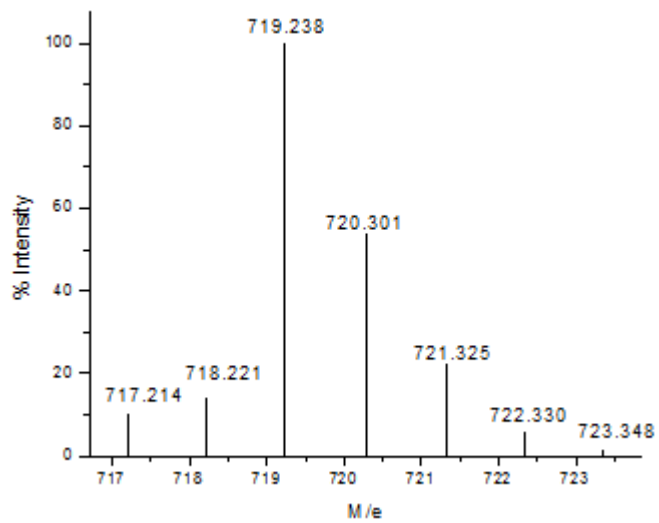




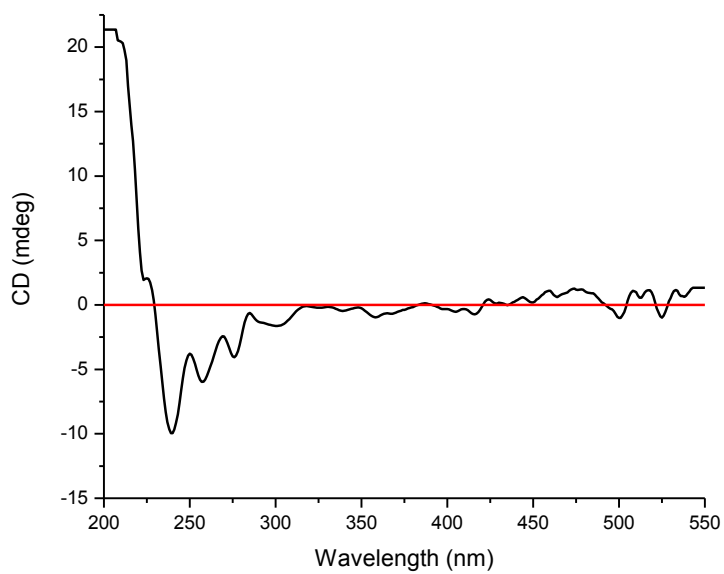
Entire mass spectrum of complex **C-8**  $[M-2Cl+OEt]^{+1}$  (on previous page), with isotopic pattern and molecular ion peak at 717.2574 (top).



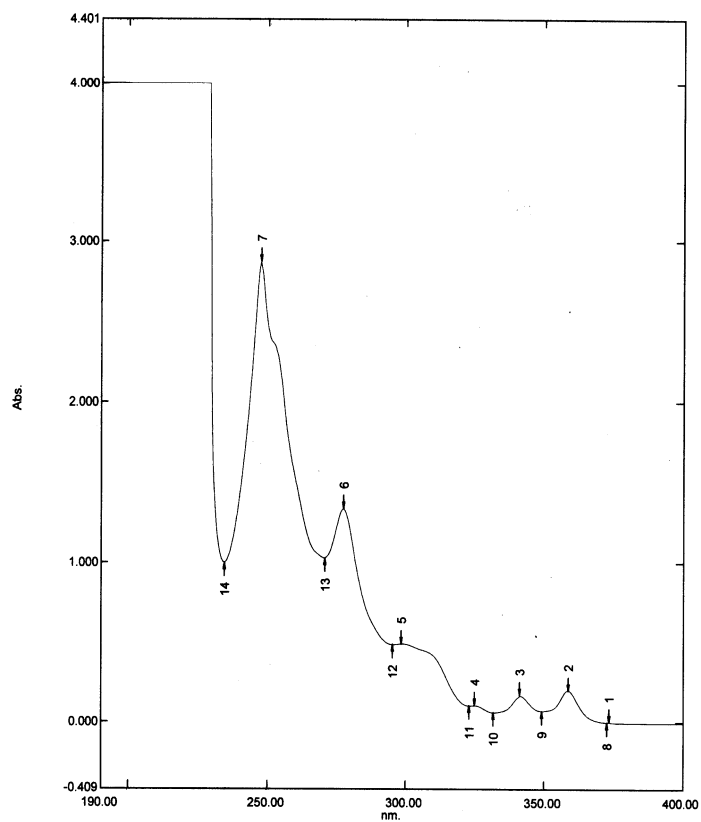
Entire mass spectrum (on the right) of complex **C-6**  $[M-2Cl+2\text{-hydroxy benzoic acid}]^{+1}$ , with isotopic pattern and molecular ion peak (on the left) centered at 724.814.



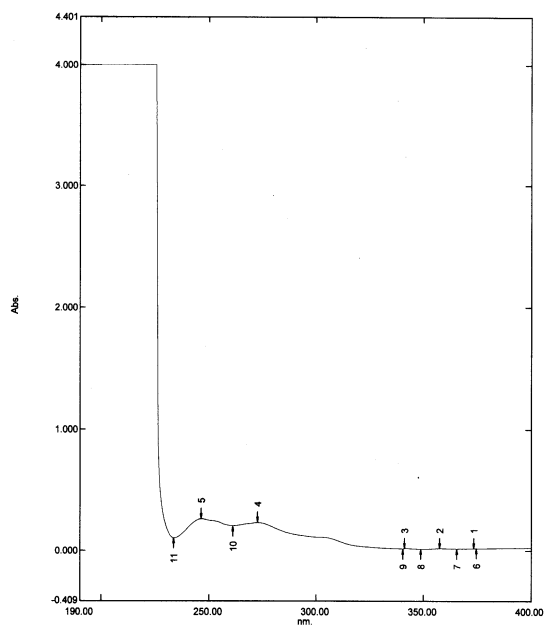
Isotopic pattern of the molecular ion peak of **C-7**  $[M+1]^{+1}$



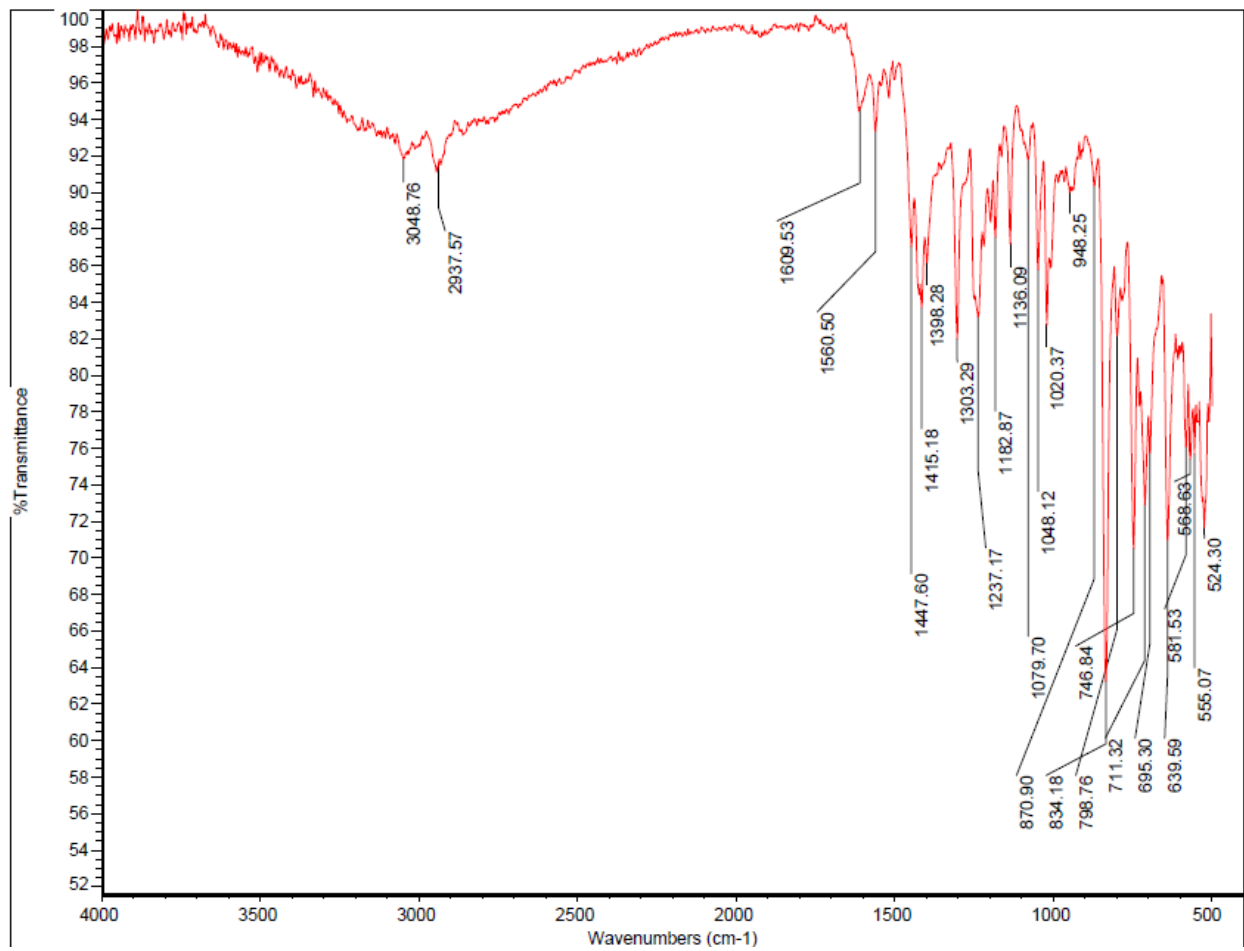
CD of (*R,R*)-**5** (THF,  $10^{-5}$  M)



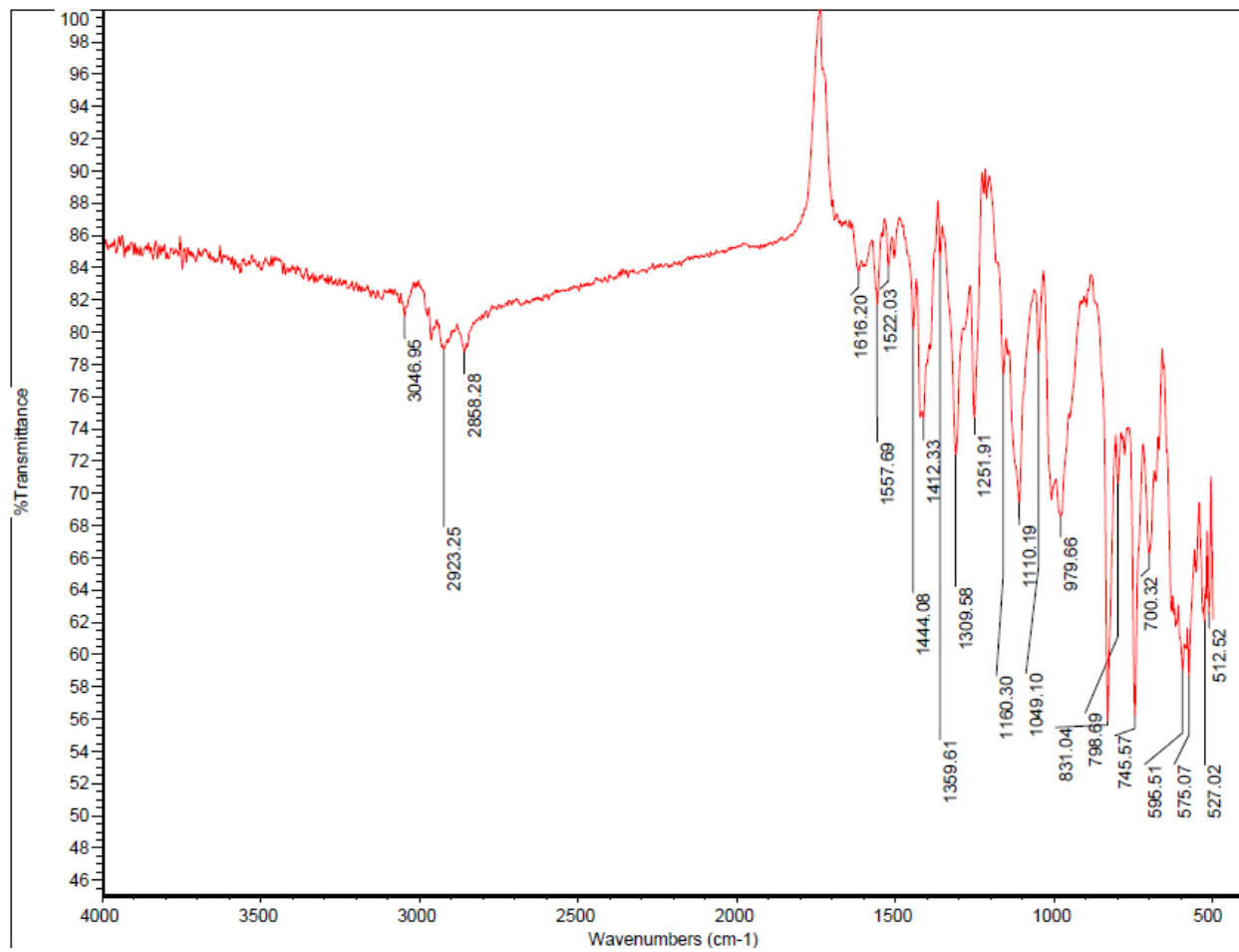
UV of **(*R,R*)-5** (THF,  $10^{-5}$  M)



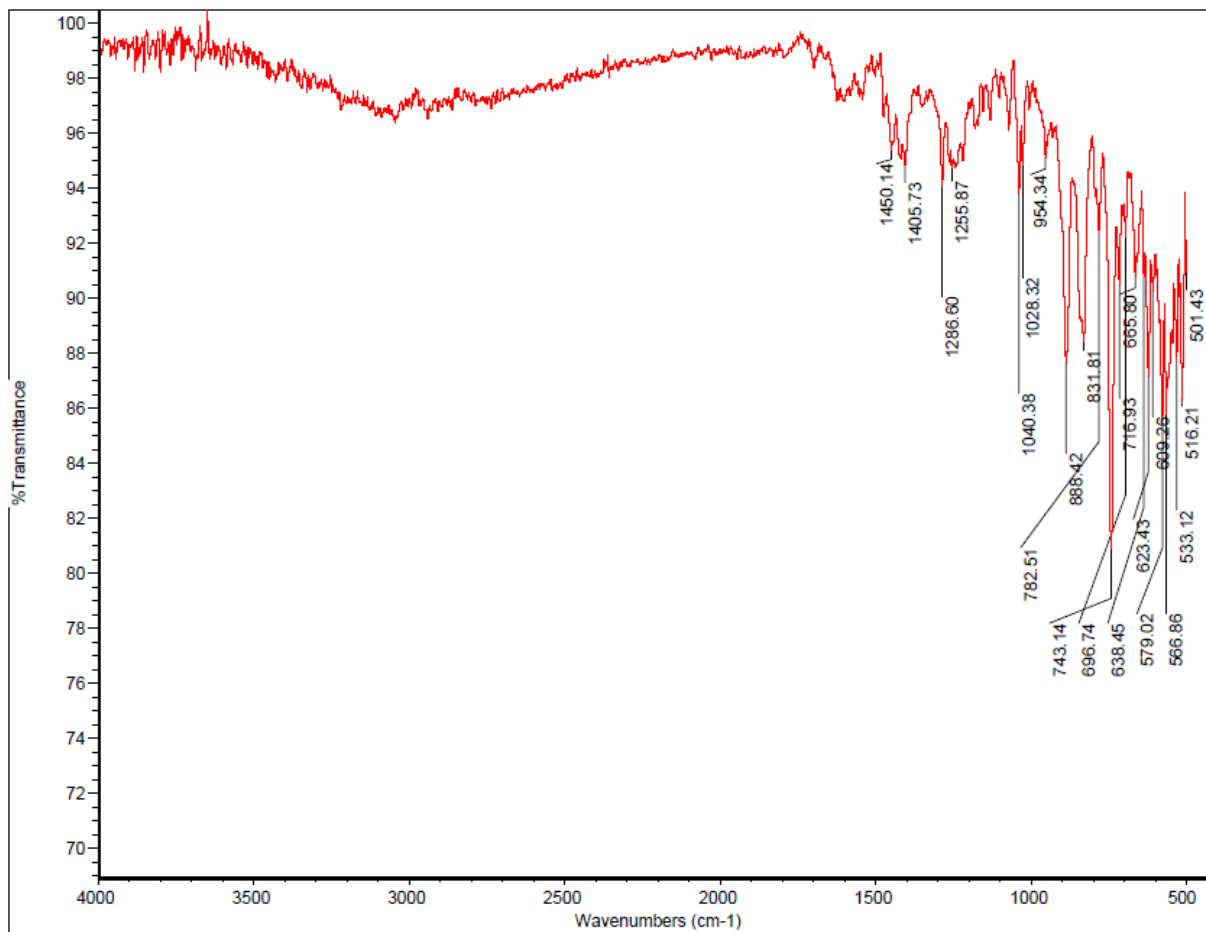
UV of **C-6** (THF,  $10^{-5}$  M)



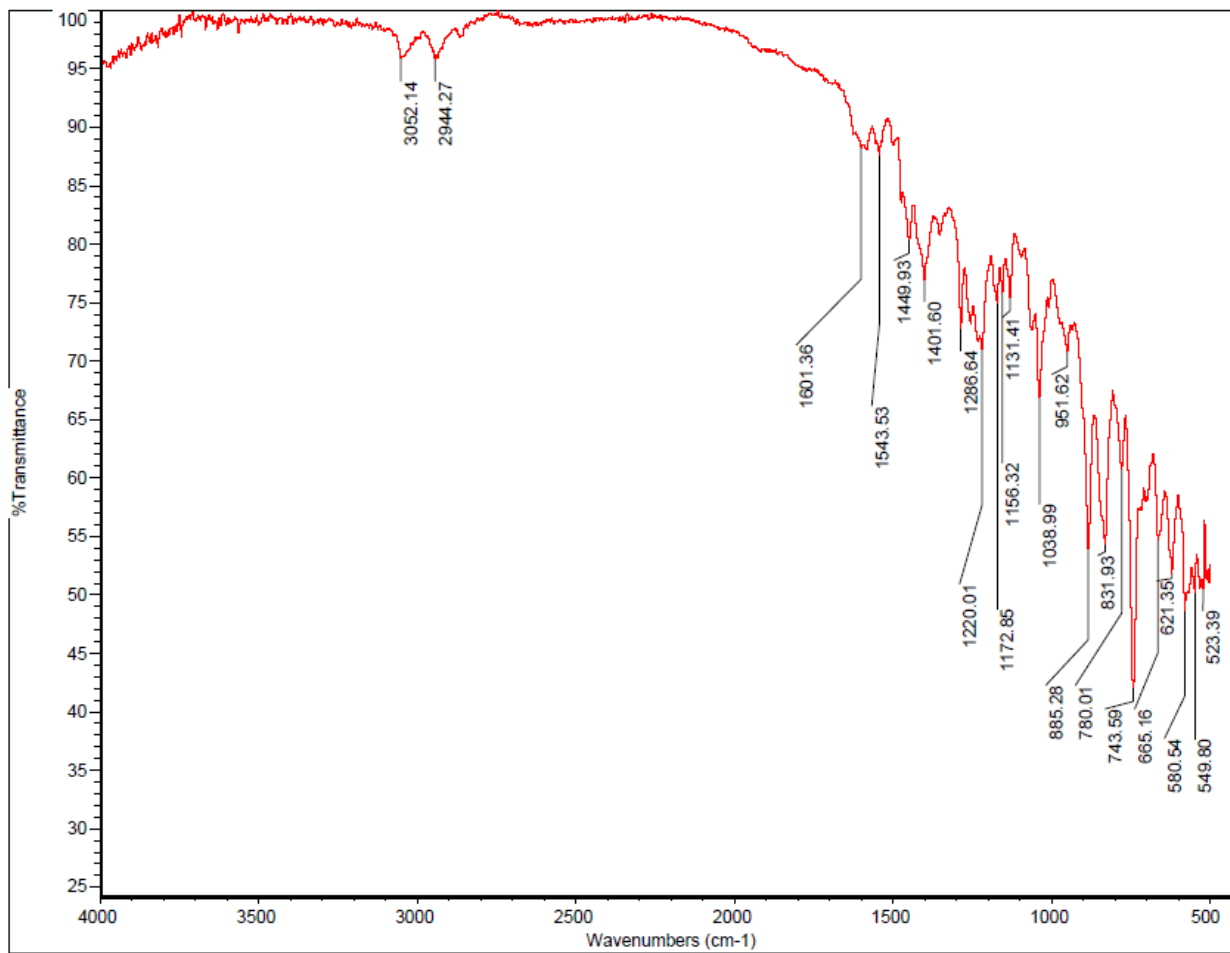
IR of C-6



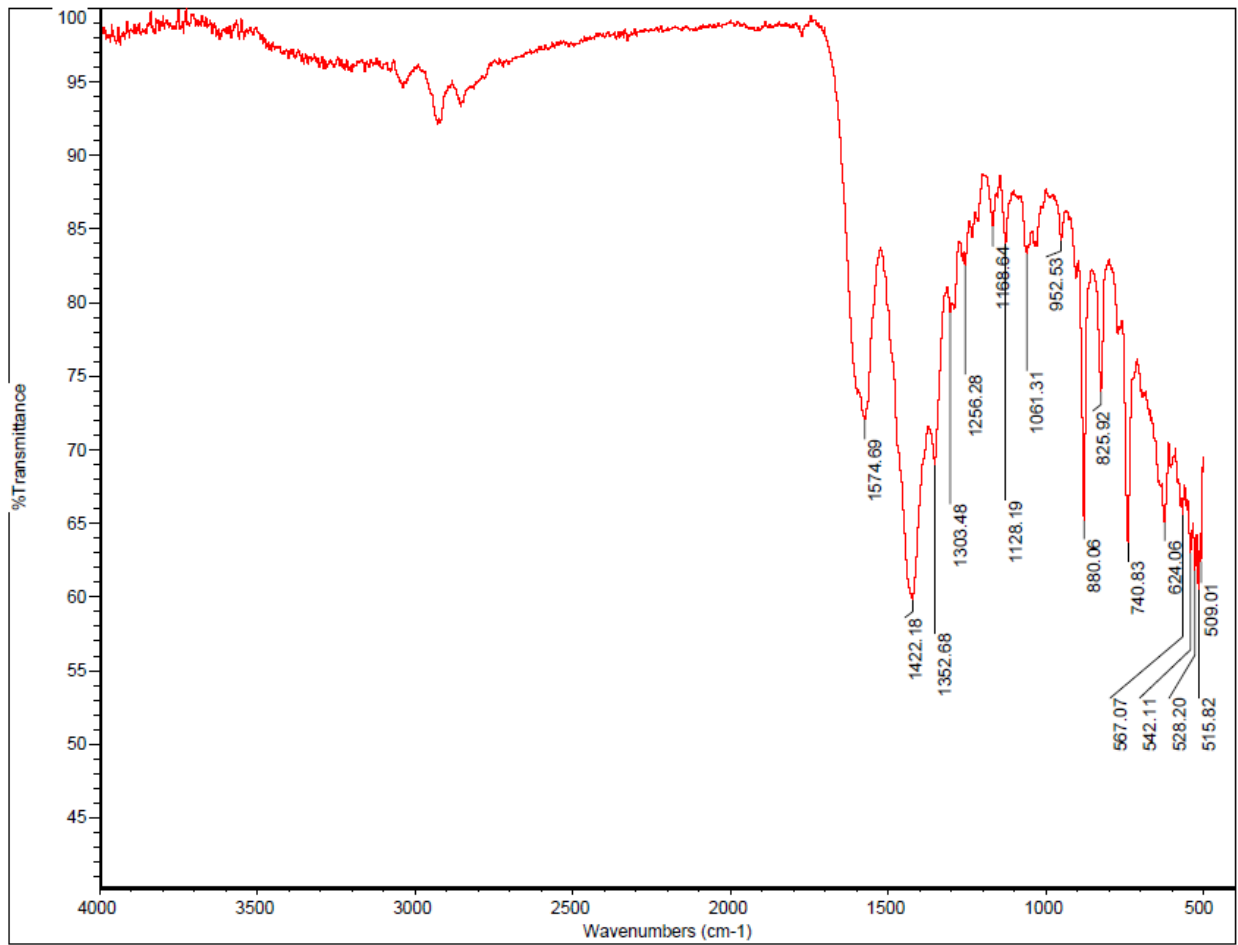
IR of C-7



IR of C-8

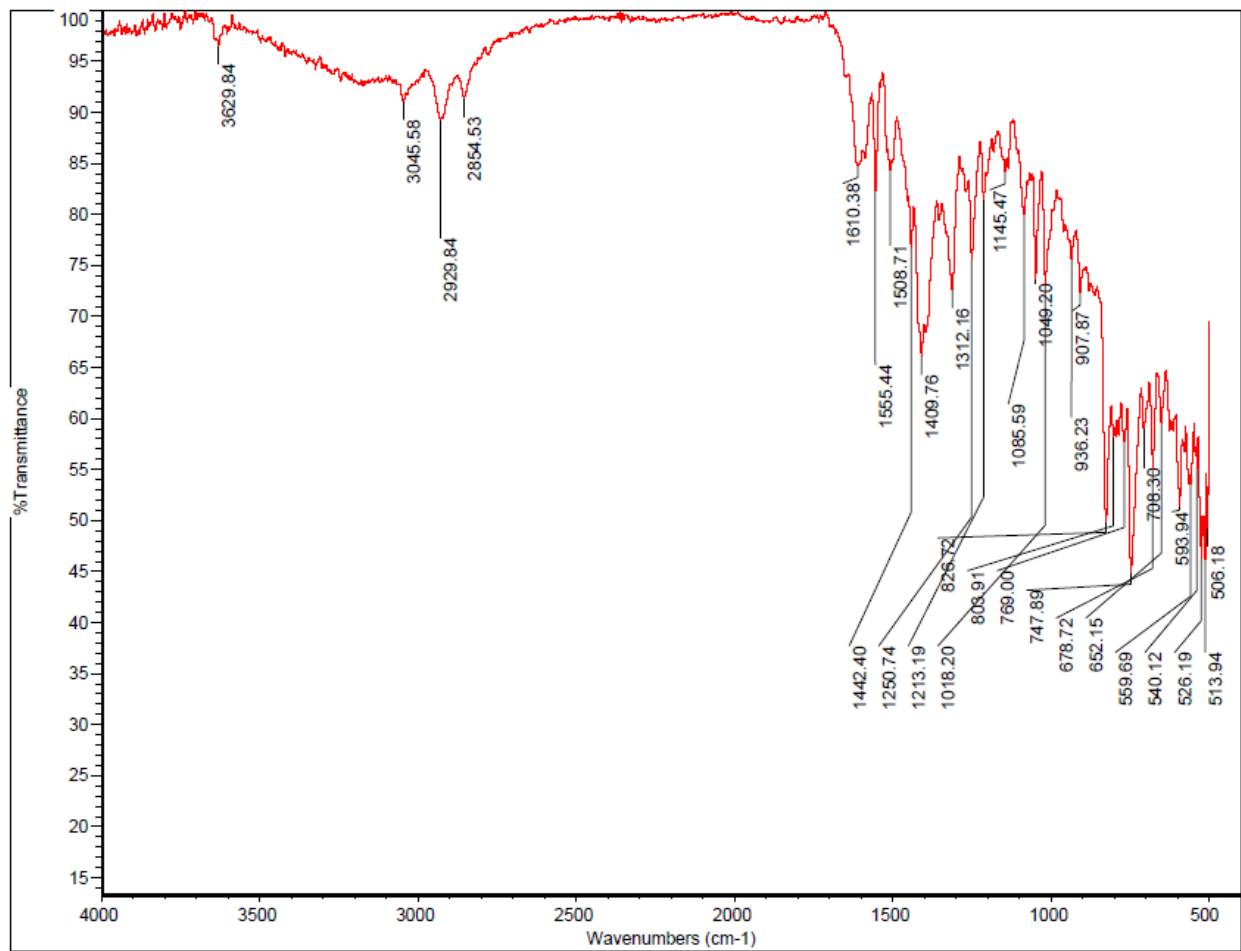


IR of C-9

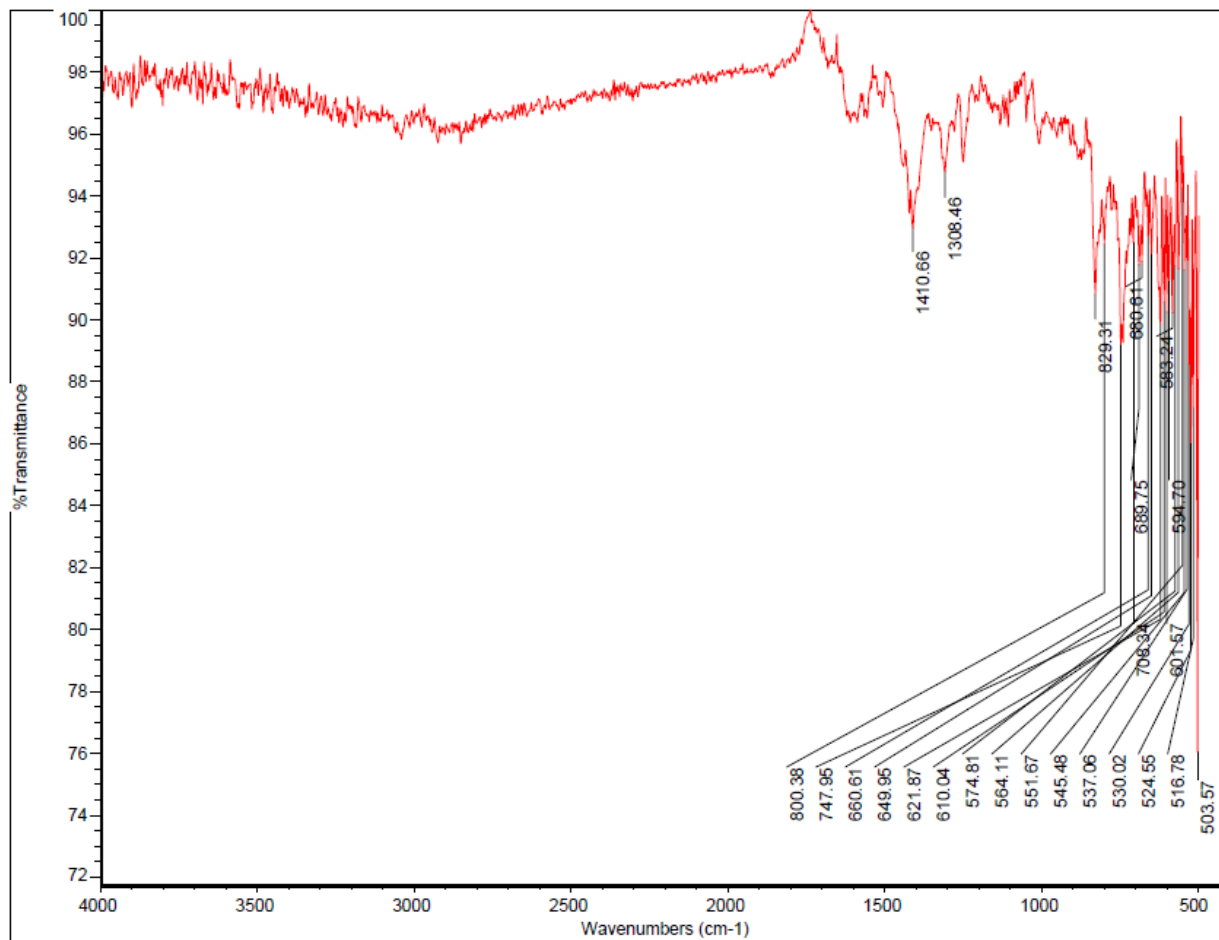


IR of C-1



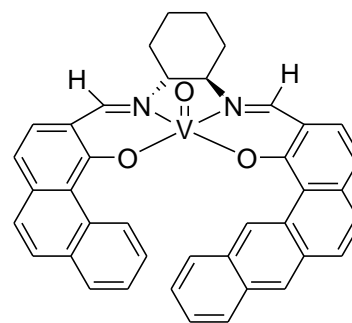
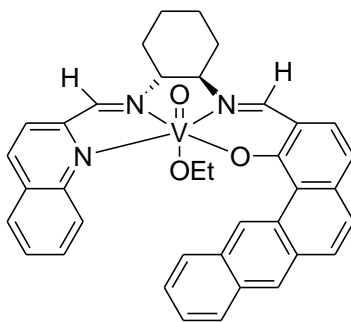
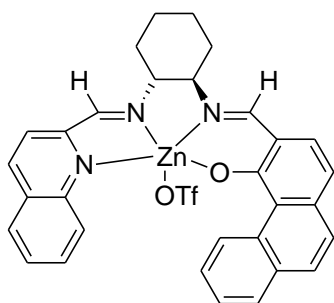
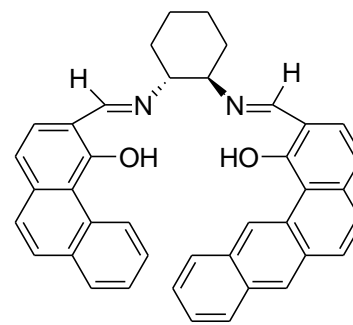
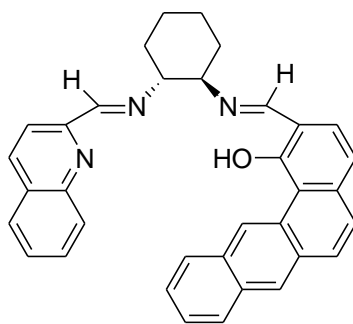
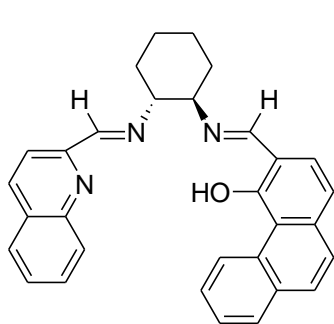


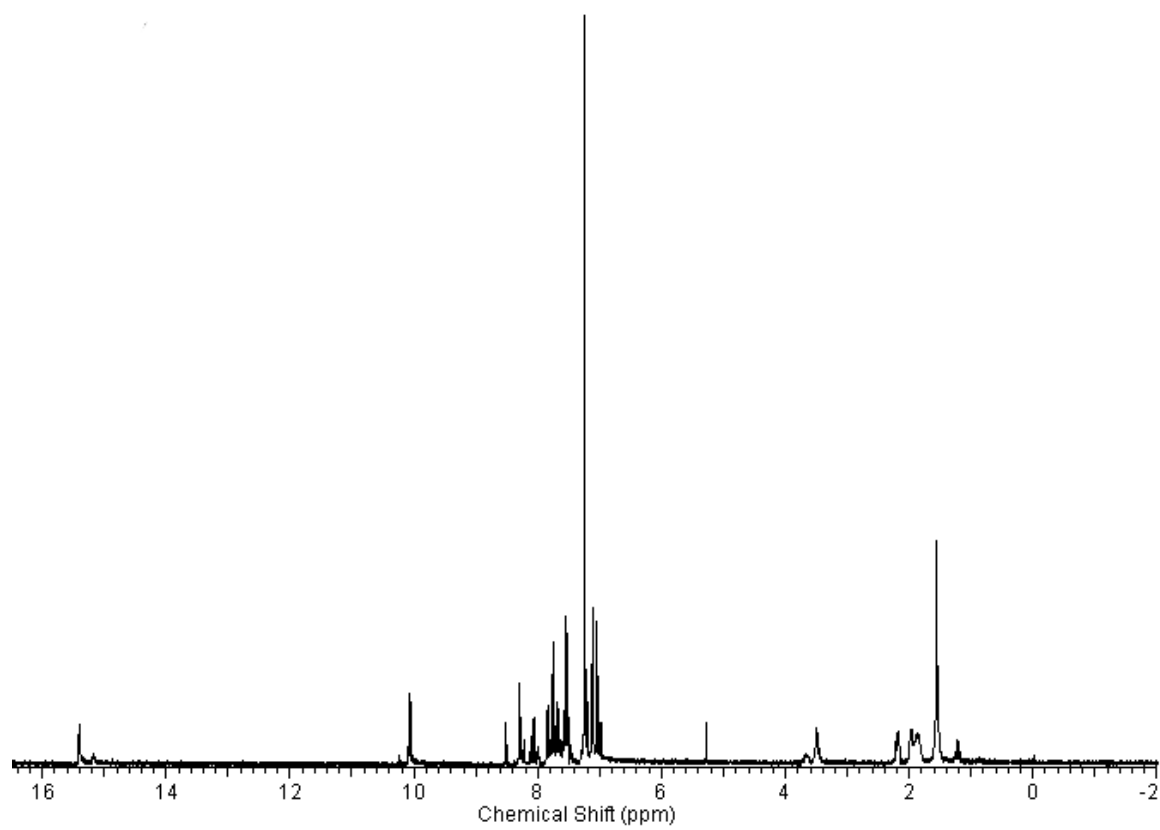
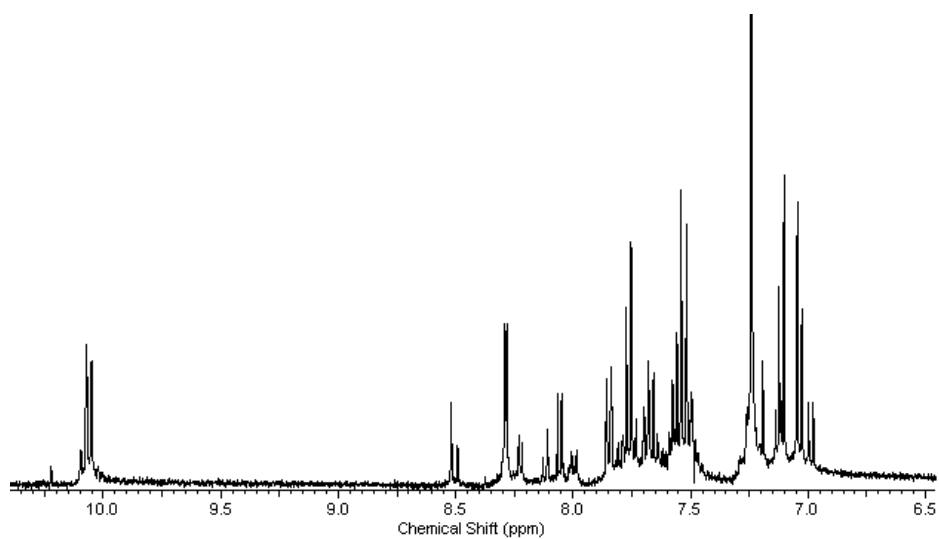
IR of C-5



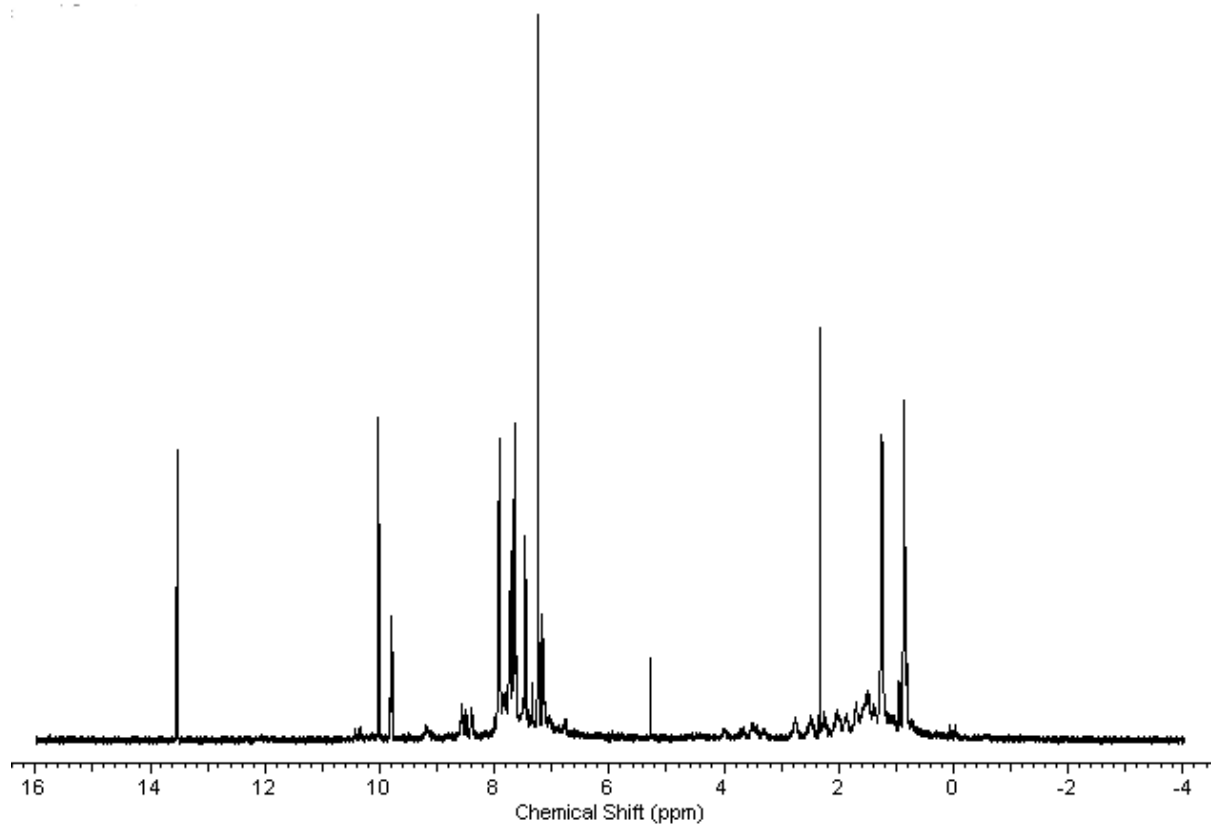
IR of C-4

## Appendix C - Chapter 3

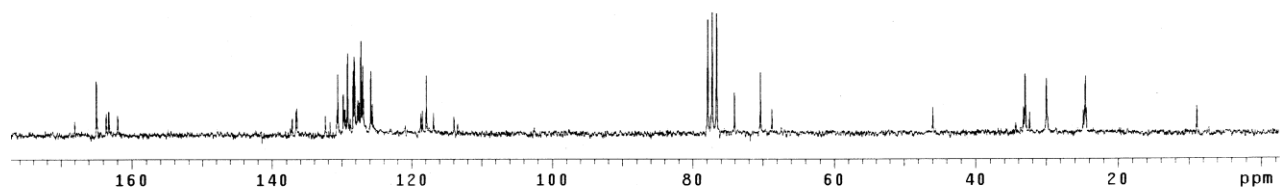




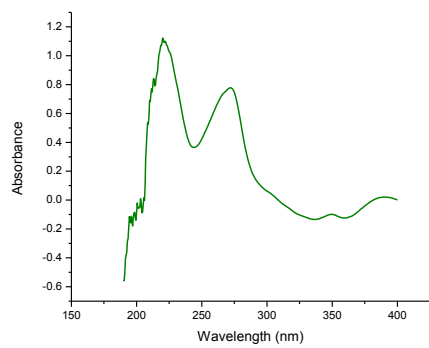
$^1\text{H}$  NMR ( $\text{CDCl}_3$ , 400 MHz) expanded (top) and full (bottom) of **(*R,R*)-2**



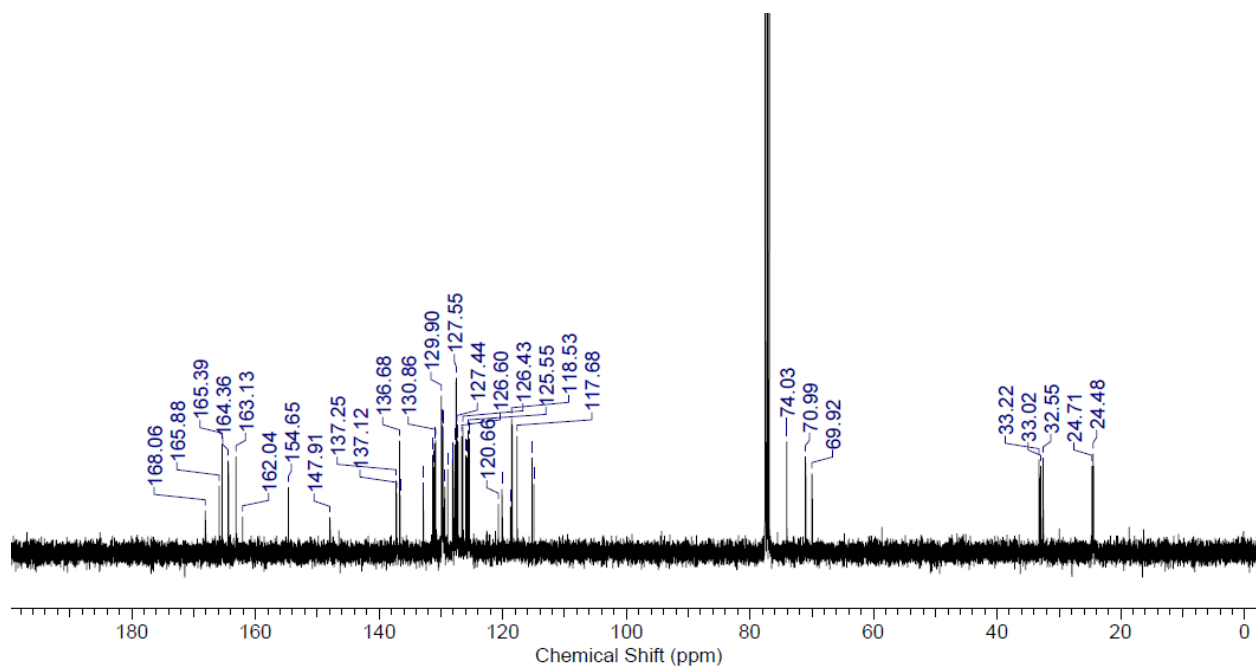
$^1\text{H}$  NMR ( $\text{CDCl}_3$ , 400 MHz) of **C-1**



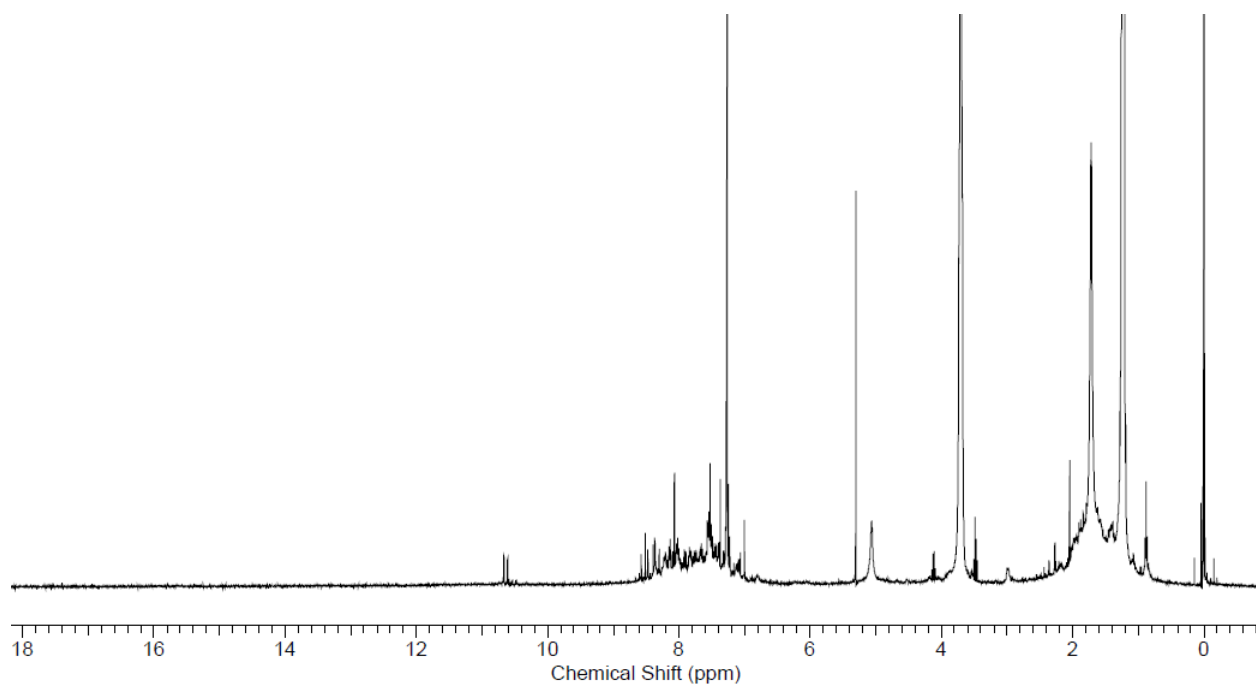
$^{13}\text{C}$  NMR ( $\text{CDCl}_3$ , 400 MHz) of **(R,R)-2**



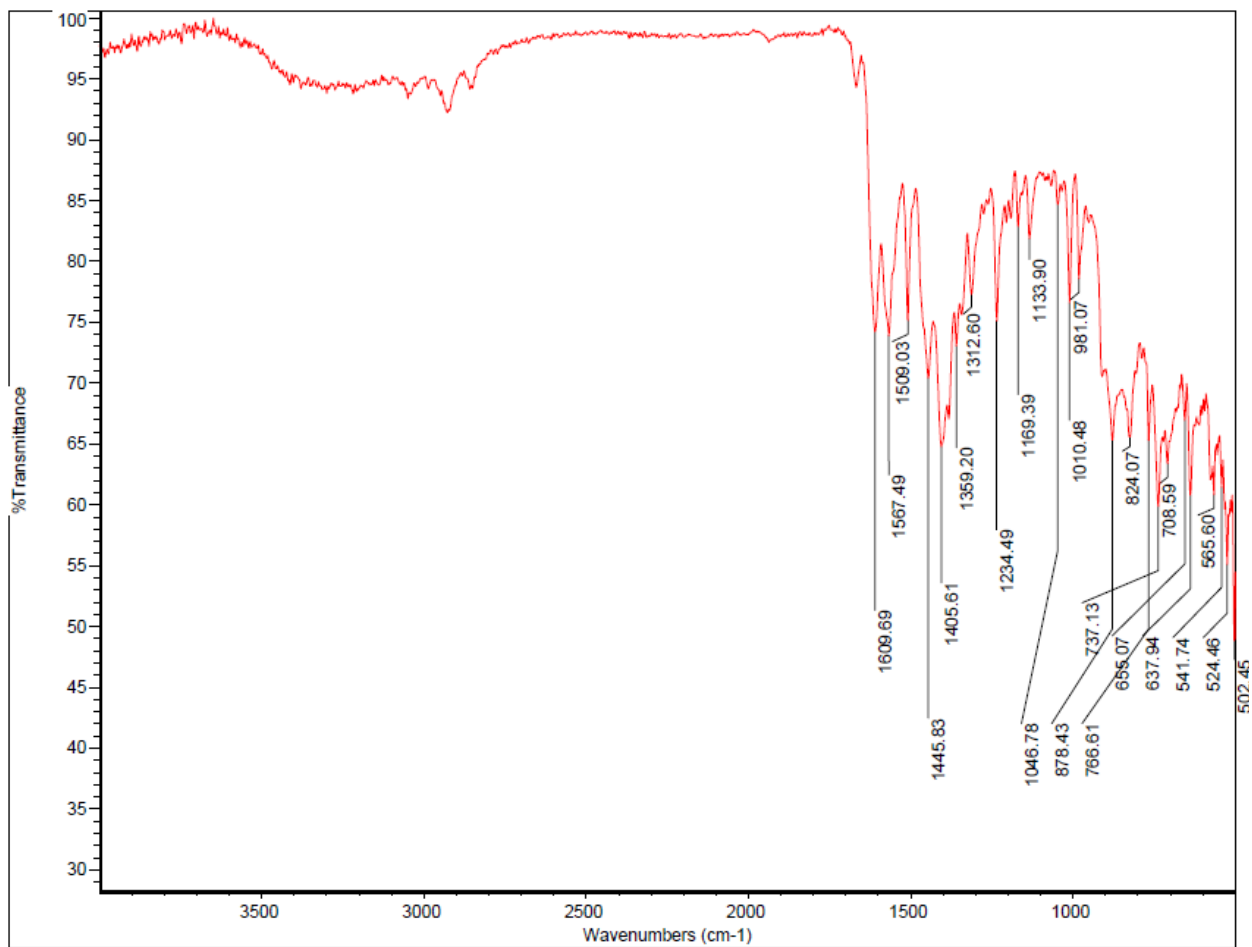
UV of **(R,R)-2**



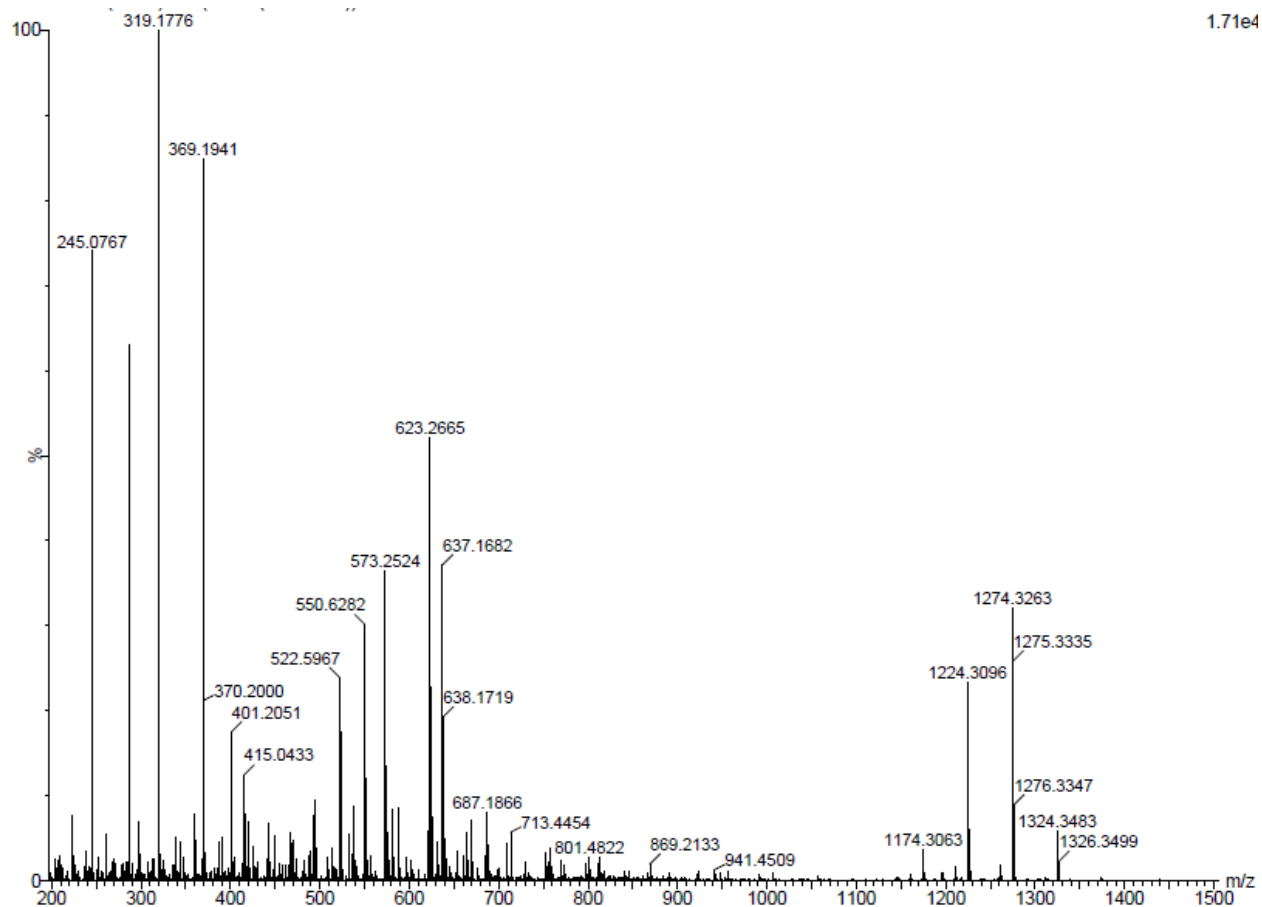
$^{13}\text{C}$  NMR (CDCl<sub>3</sub>, 400 MHz) of **(R,R)-3**



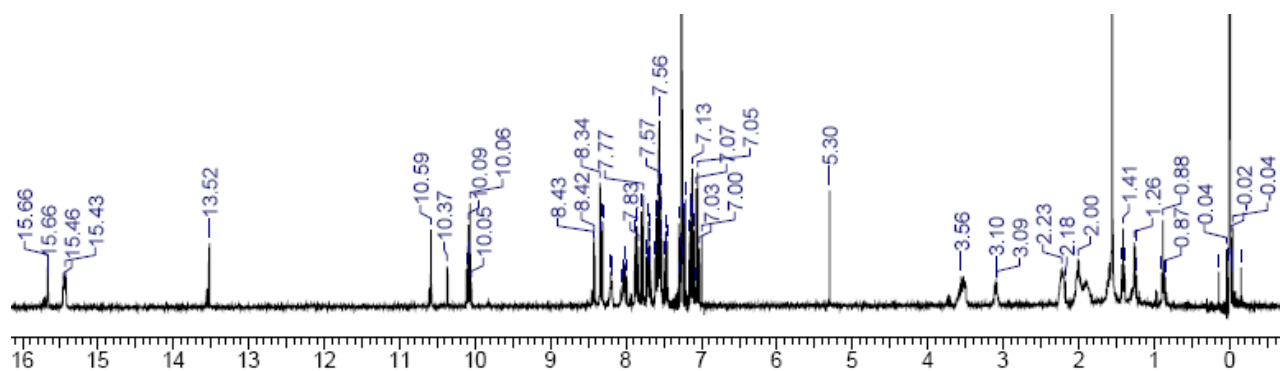
$^1\text{H}$  NMR (CDCl<sub>3</sub>, 400 MHz) of **C-2**



IR of C-2

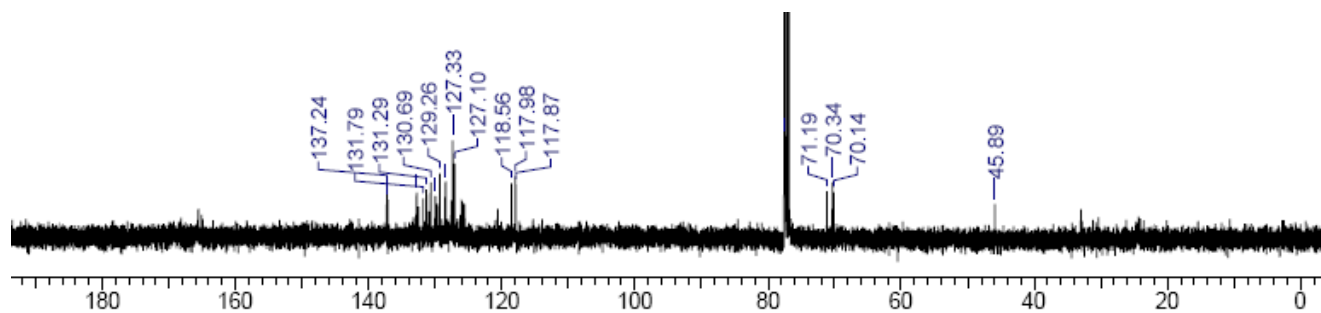


Entire mass spectrum of **C-2**

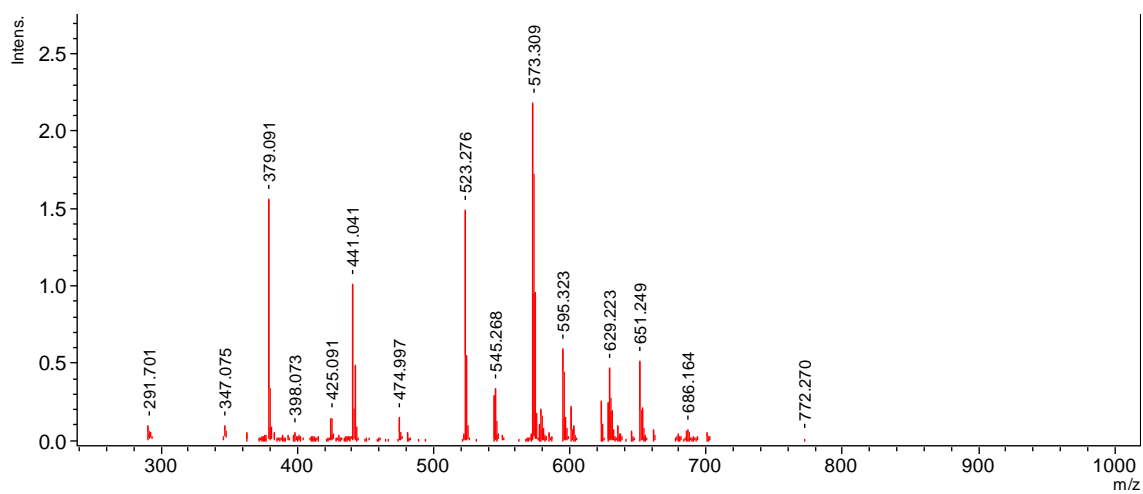


$^1\text{H}$  NMR (CDCl<sub>3</sub>, 400 MHz) of **(R,R)-4**

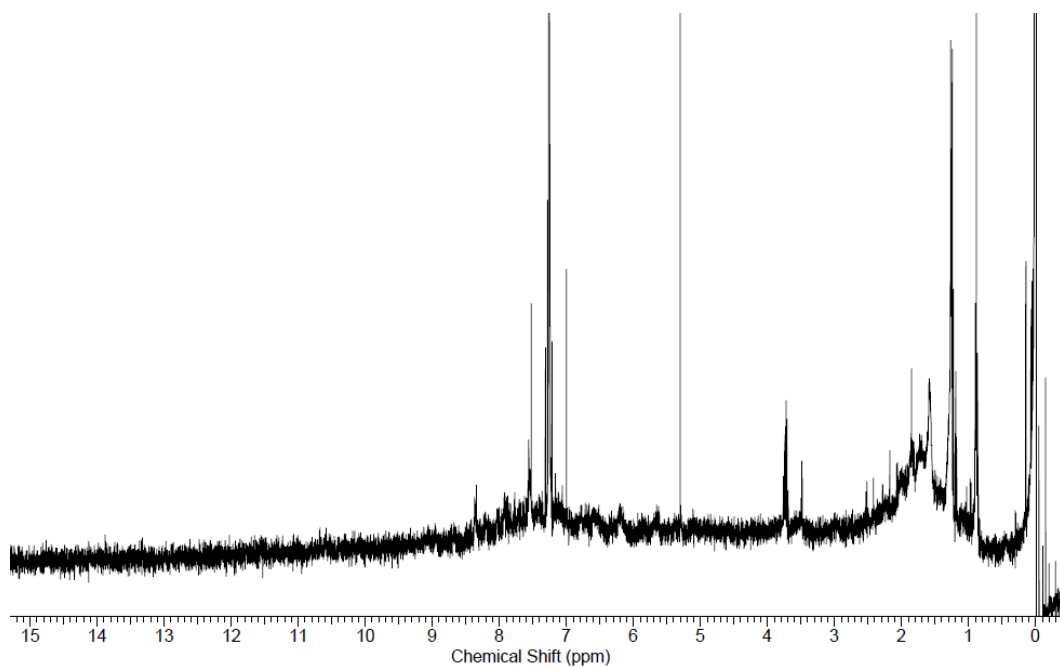




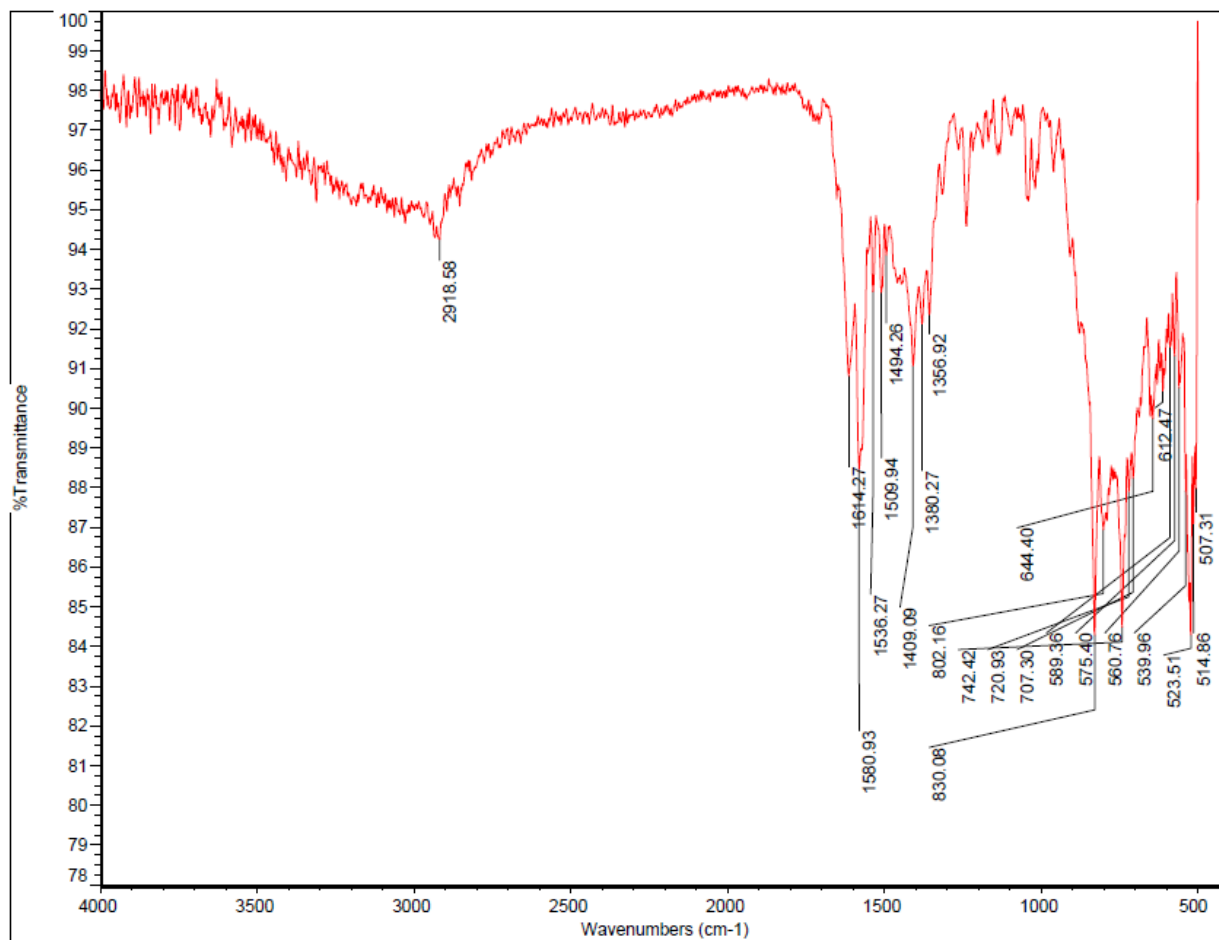
$^{13}\text{C}$  NMR ( $\text{CDCl}_3$ , 400 MHz) of  $(R,R)$ -4



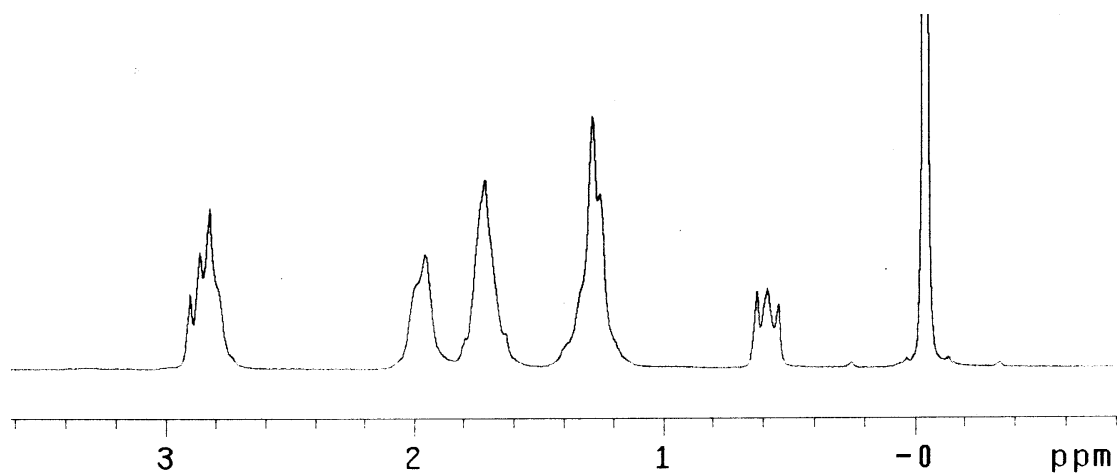
Entire mass spectrum of  $(R,R)$ -4



$^1\text{H}$  NMR ( $\text{CDCl}_3$ , 400 MHz) of  $\text{C-3}$

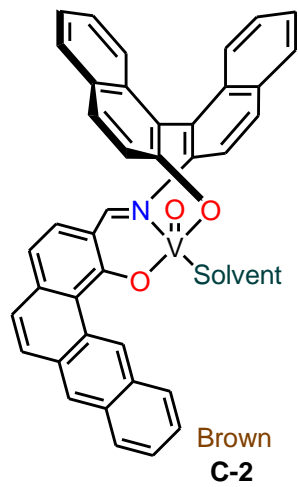
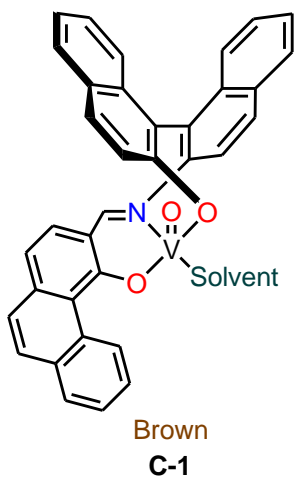
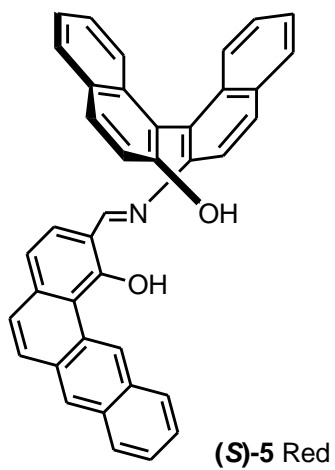
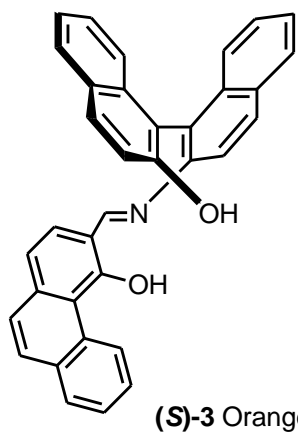


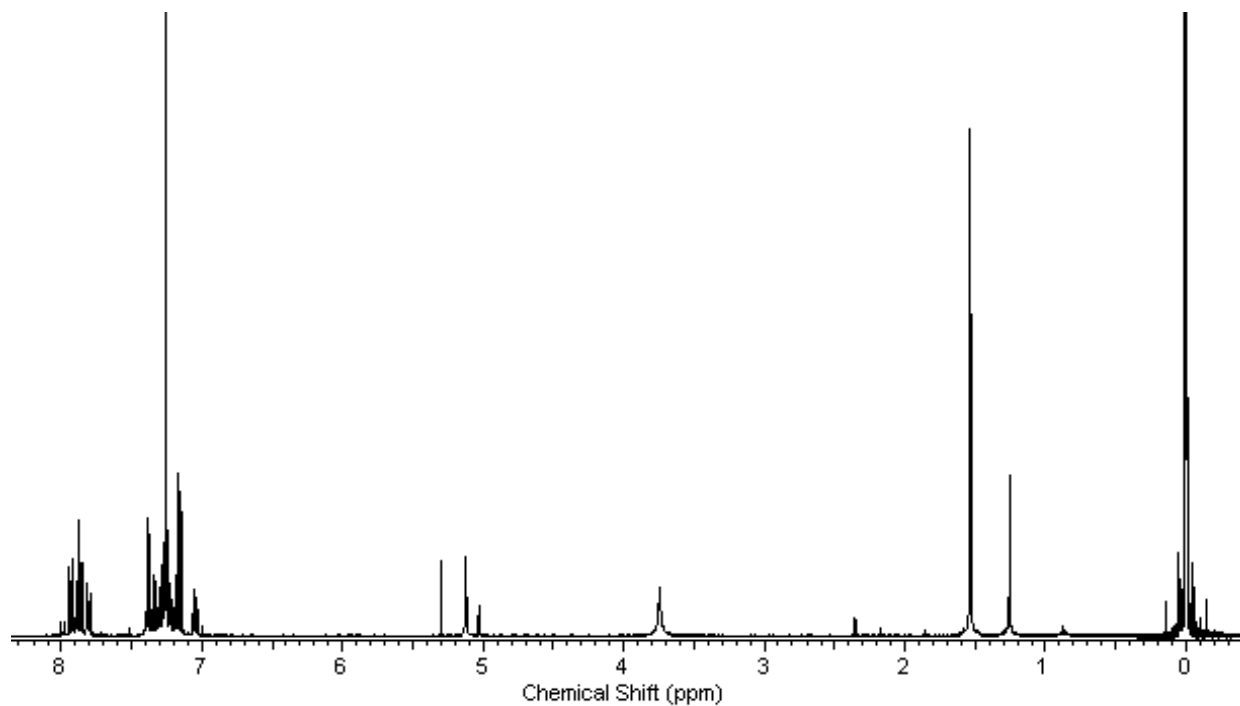
IR of C-3



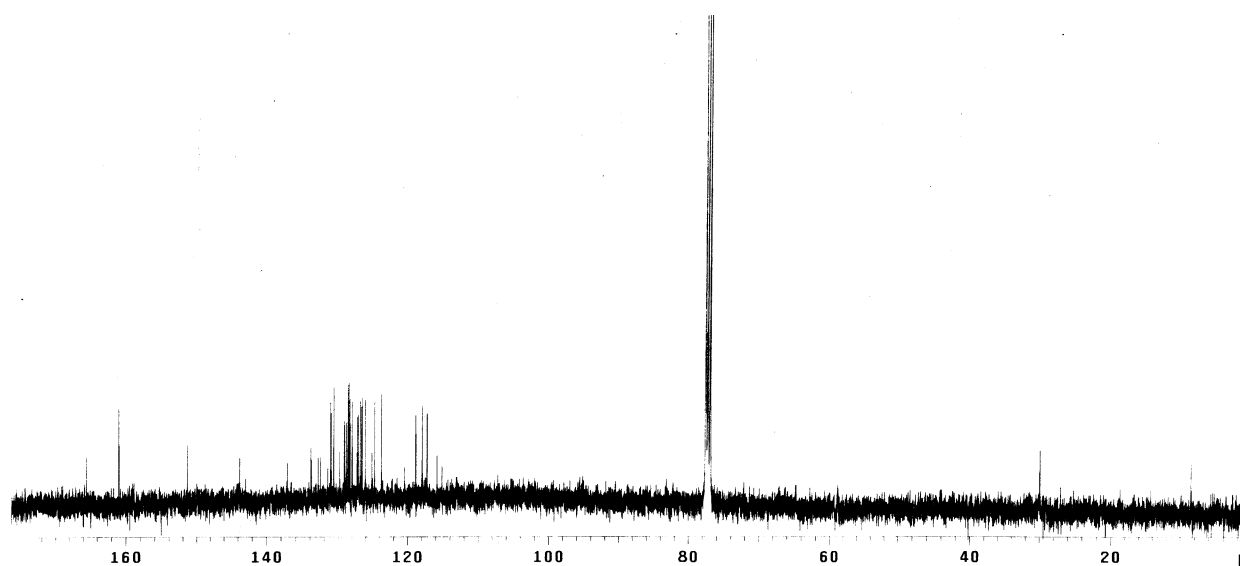
$^1\text{H}$  NMR ( $\text{CDCl}_3$ , 400 MHz) of monochloro-ammonium salt of chiral diamino-cyclohexane

## Appendix D - Chapter 4

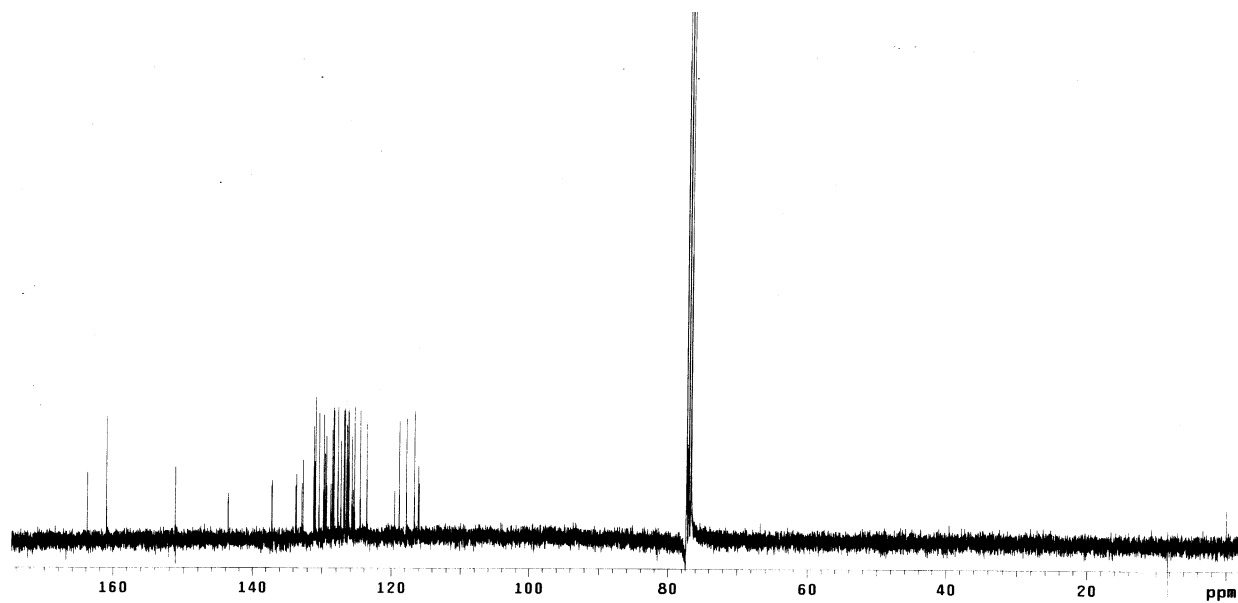




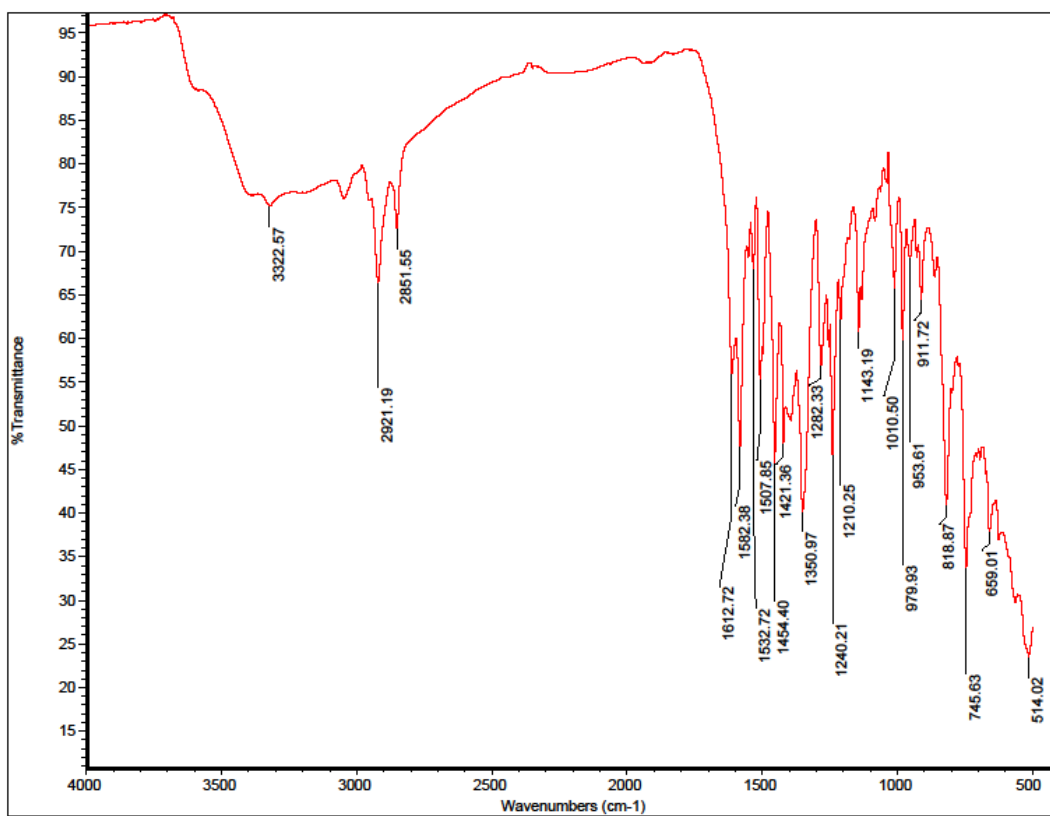
$^1\text{H}$  NMR ( $\text{CDCl}_3$ , 400 MHz) of (*S*)-NOBIN



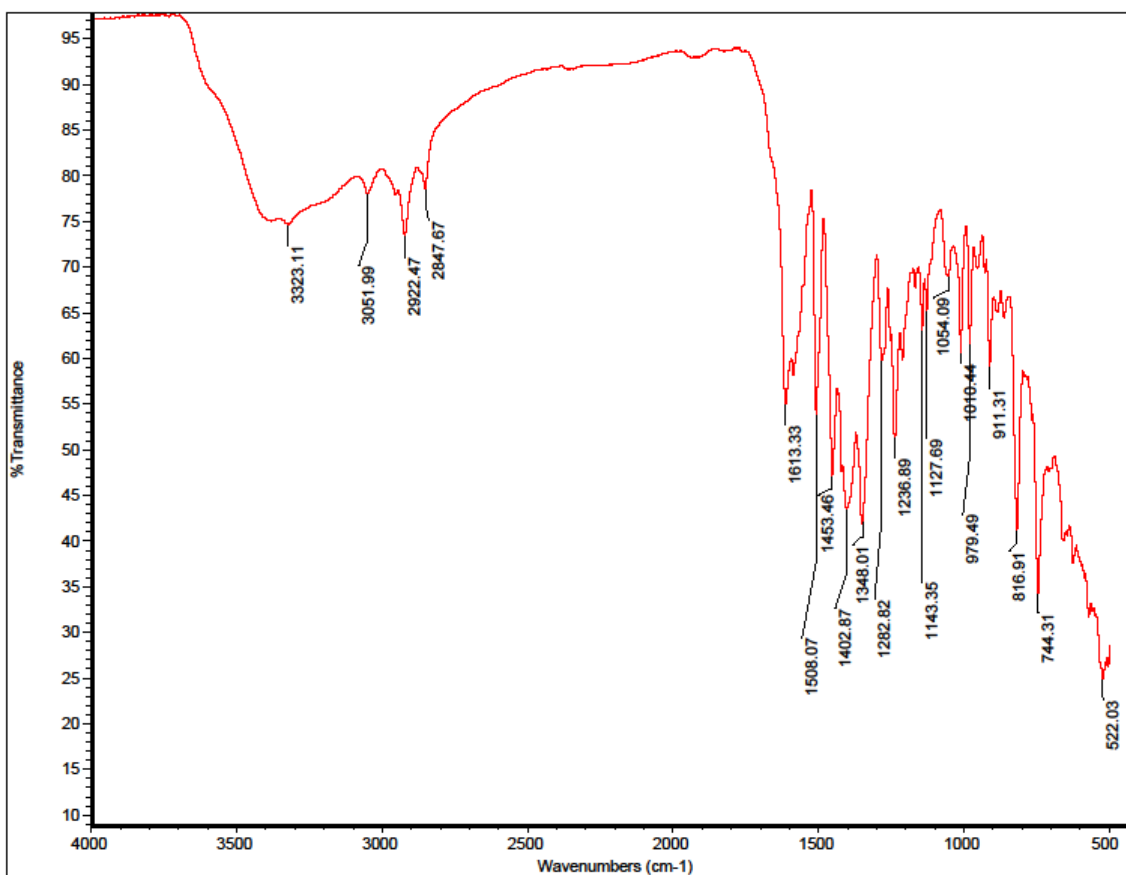
$^{13}\text{C}$  NMR ( $\text{CDCl}_3$ , 400 MHz) of (*S*)-3



$^{13}\text{C}$  NMR ( $\text{CDCl}_3$ , 400 MHz) of (S)-5

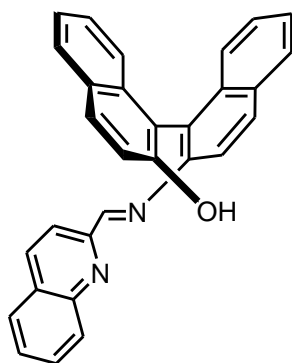


IR of C-1

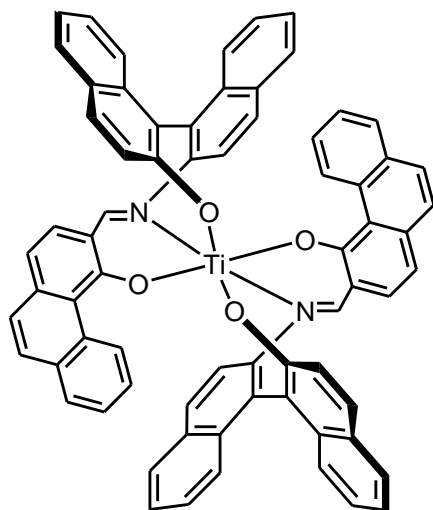


IR of C-2

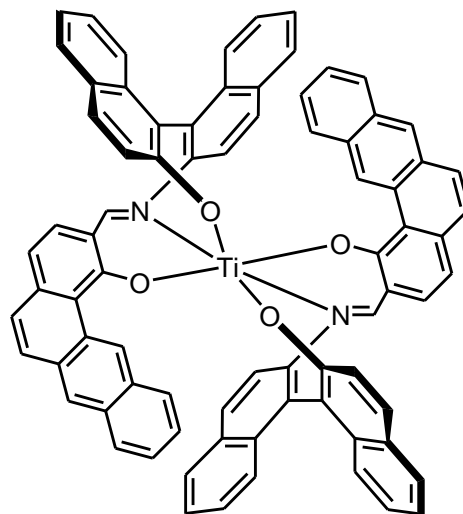
## Appendix E - Chapter 5



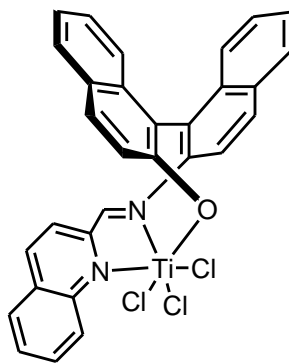
(S)-4



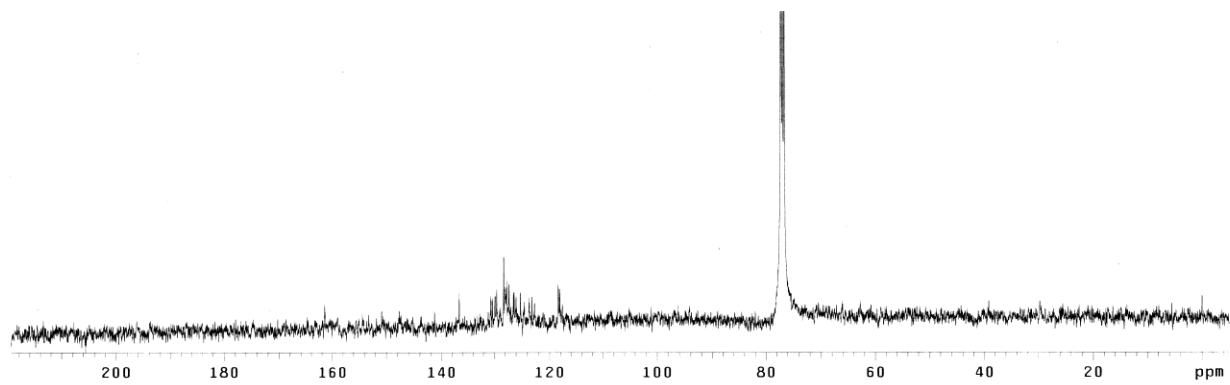
C-4



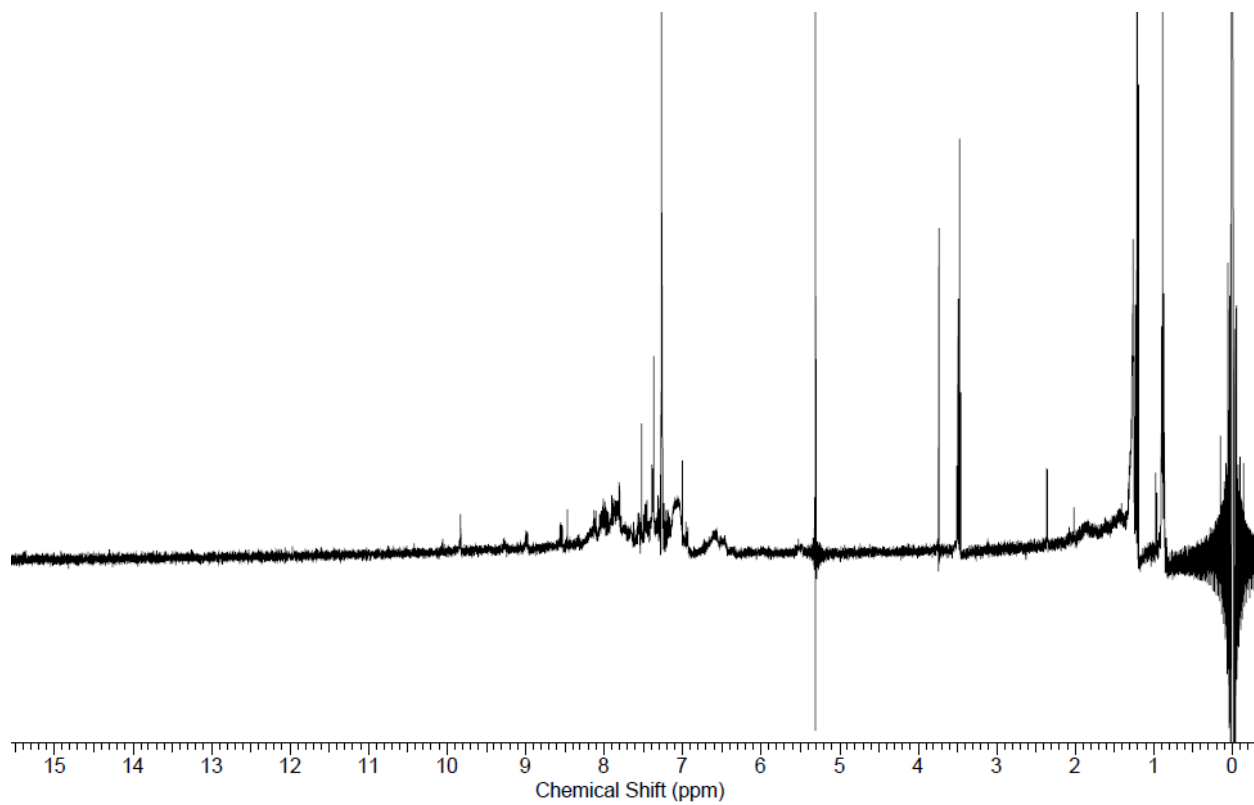
C-5



C-3

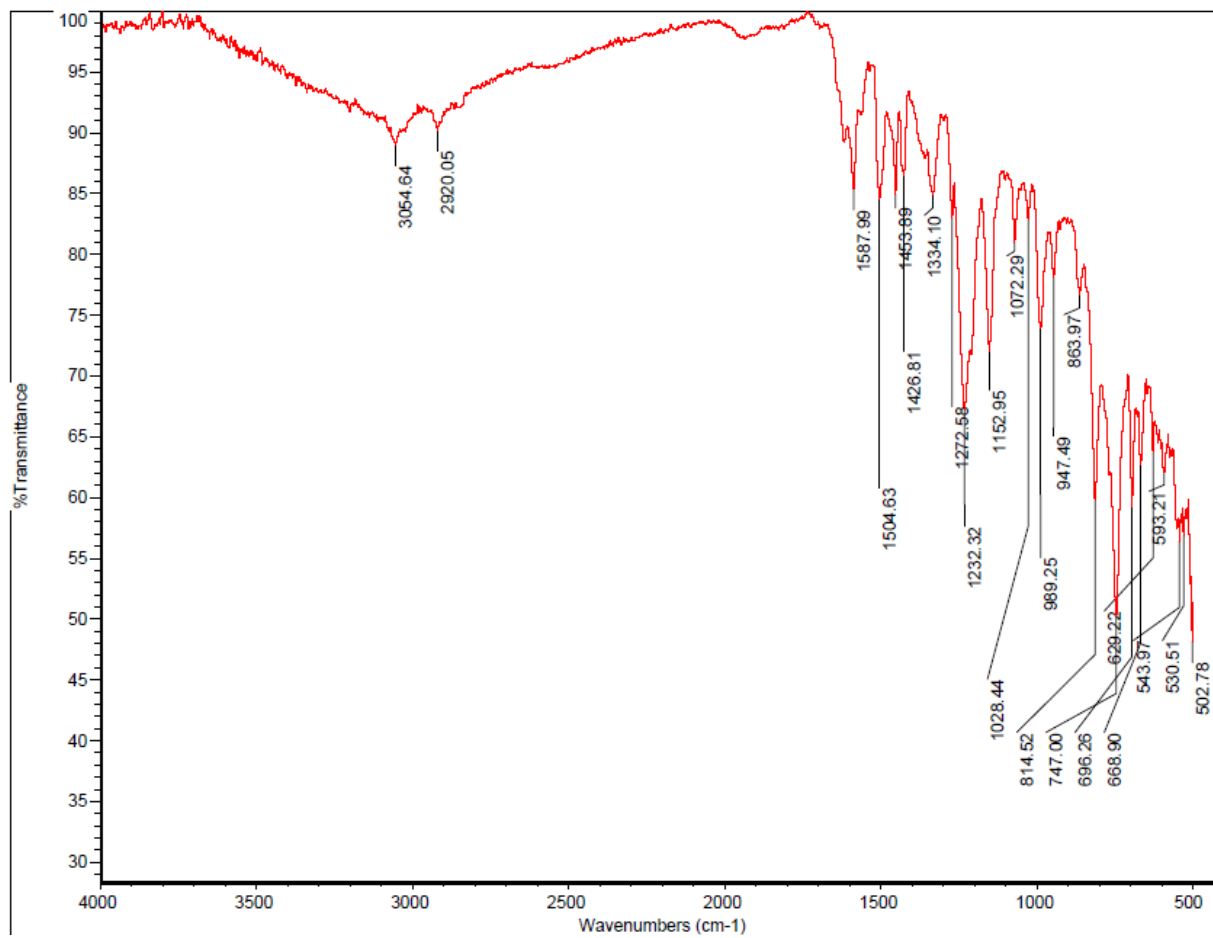


$^{13}\text{C}$  NMR ( $\text{CDCl}_3$ , 400 MHz) of (S)-4

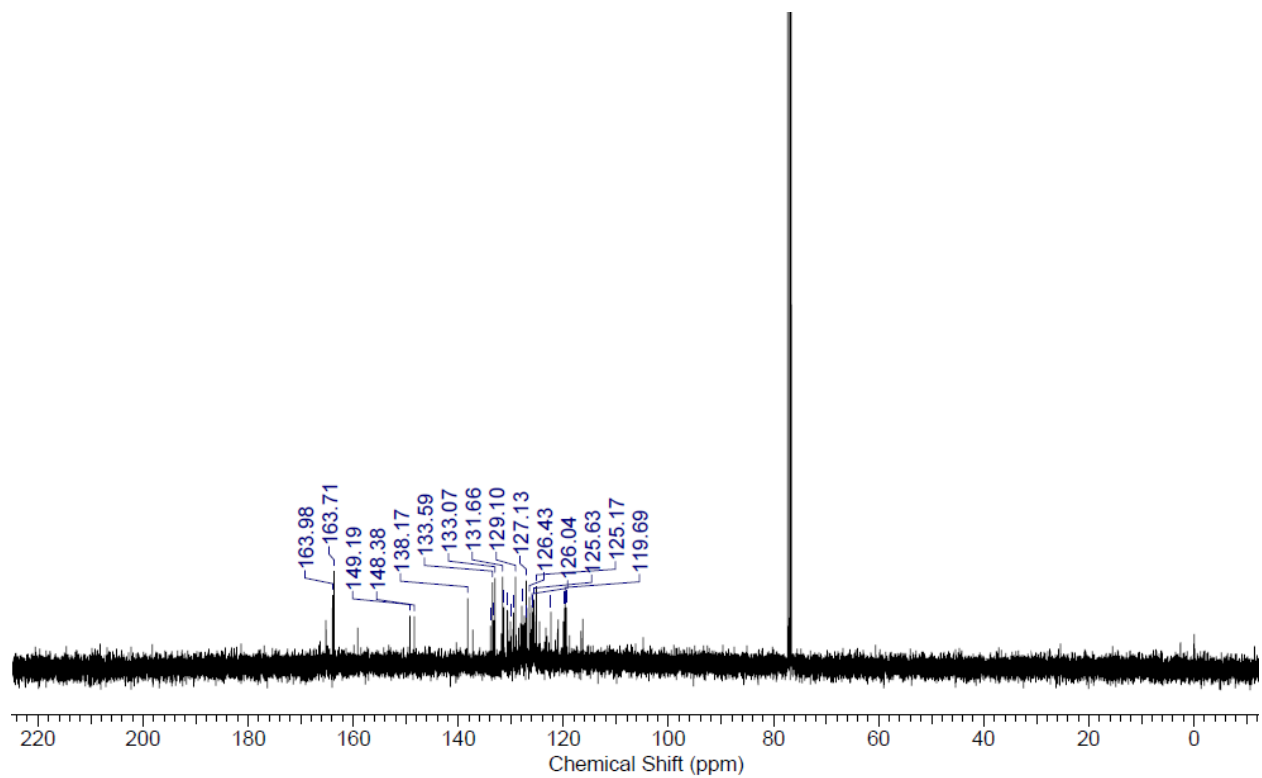


$^1\text{H}$  NMR ( $\text{CDCl}_3$ , 400 MHz) of C-3

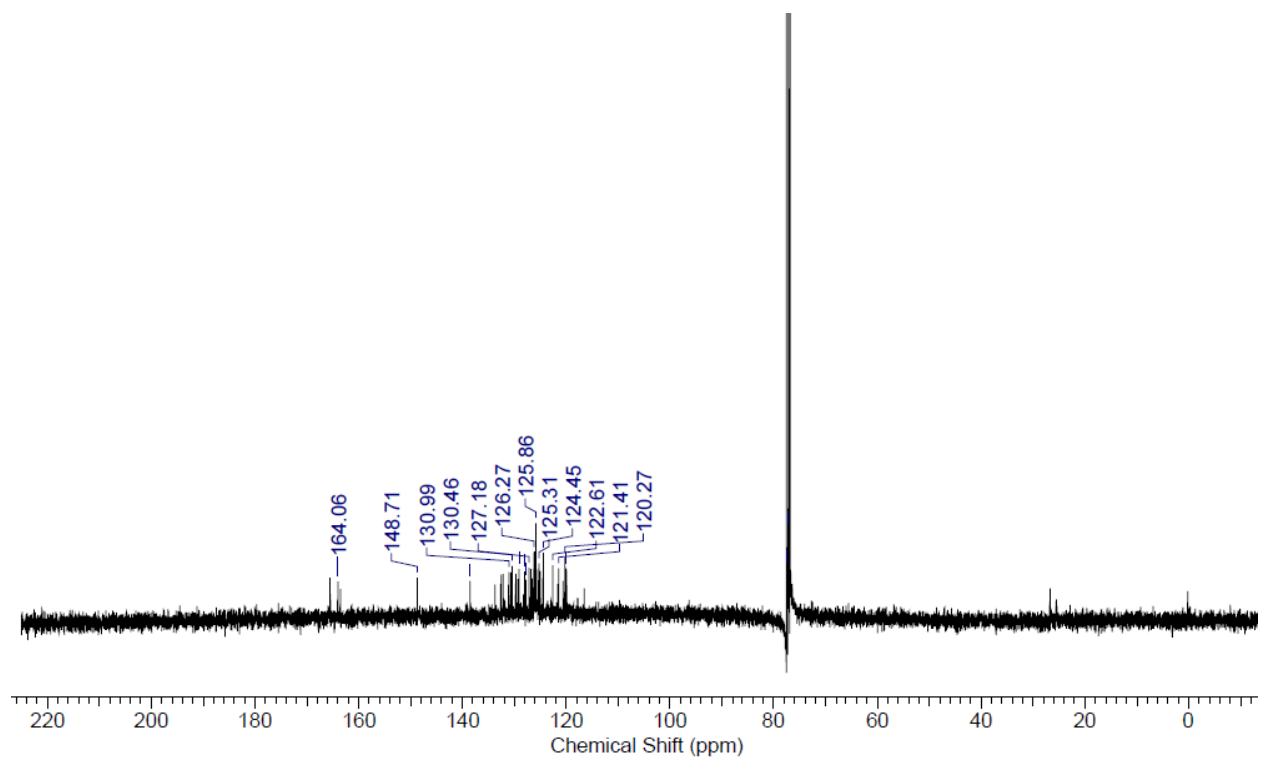




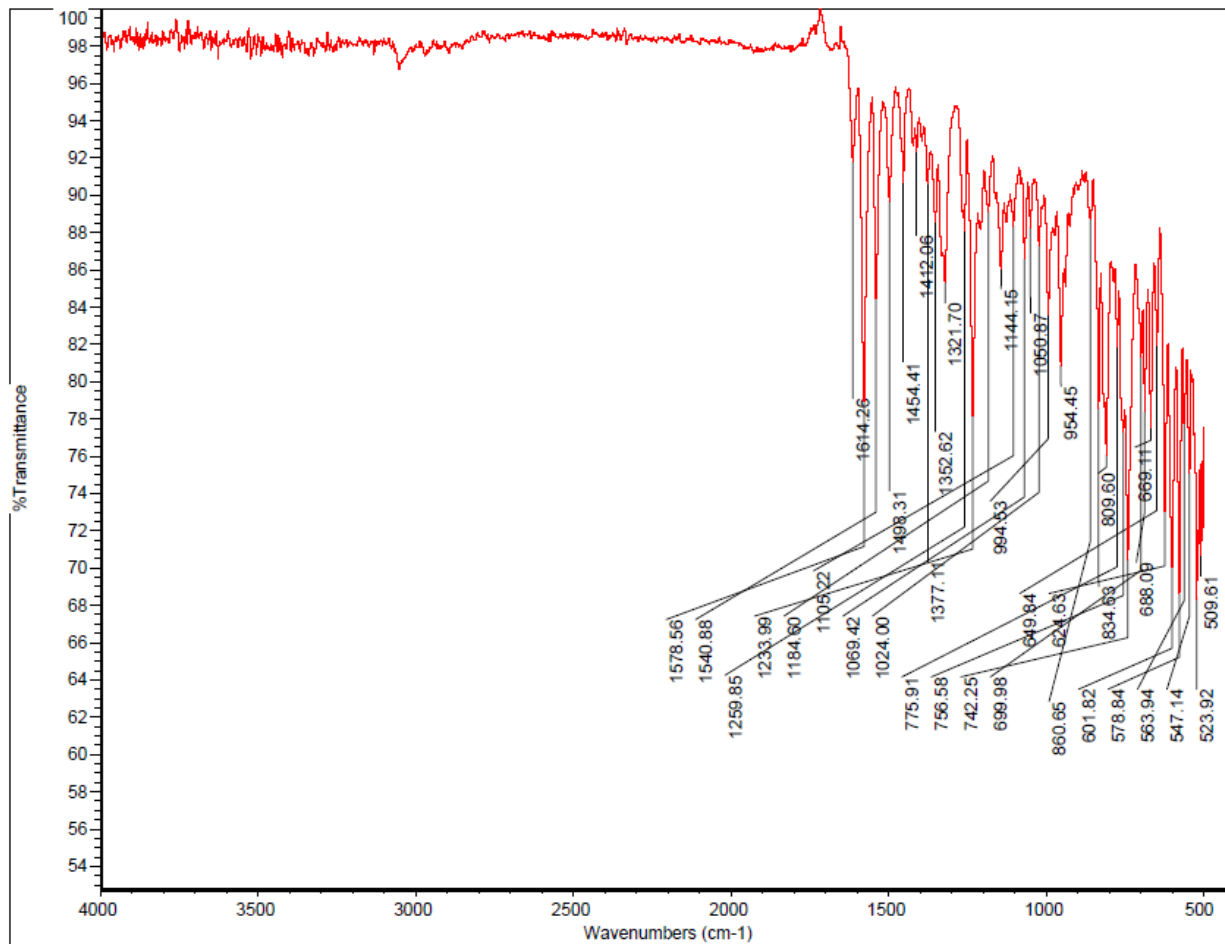
IR of C-3



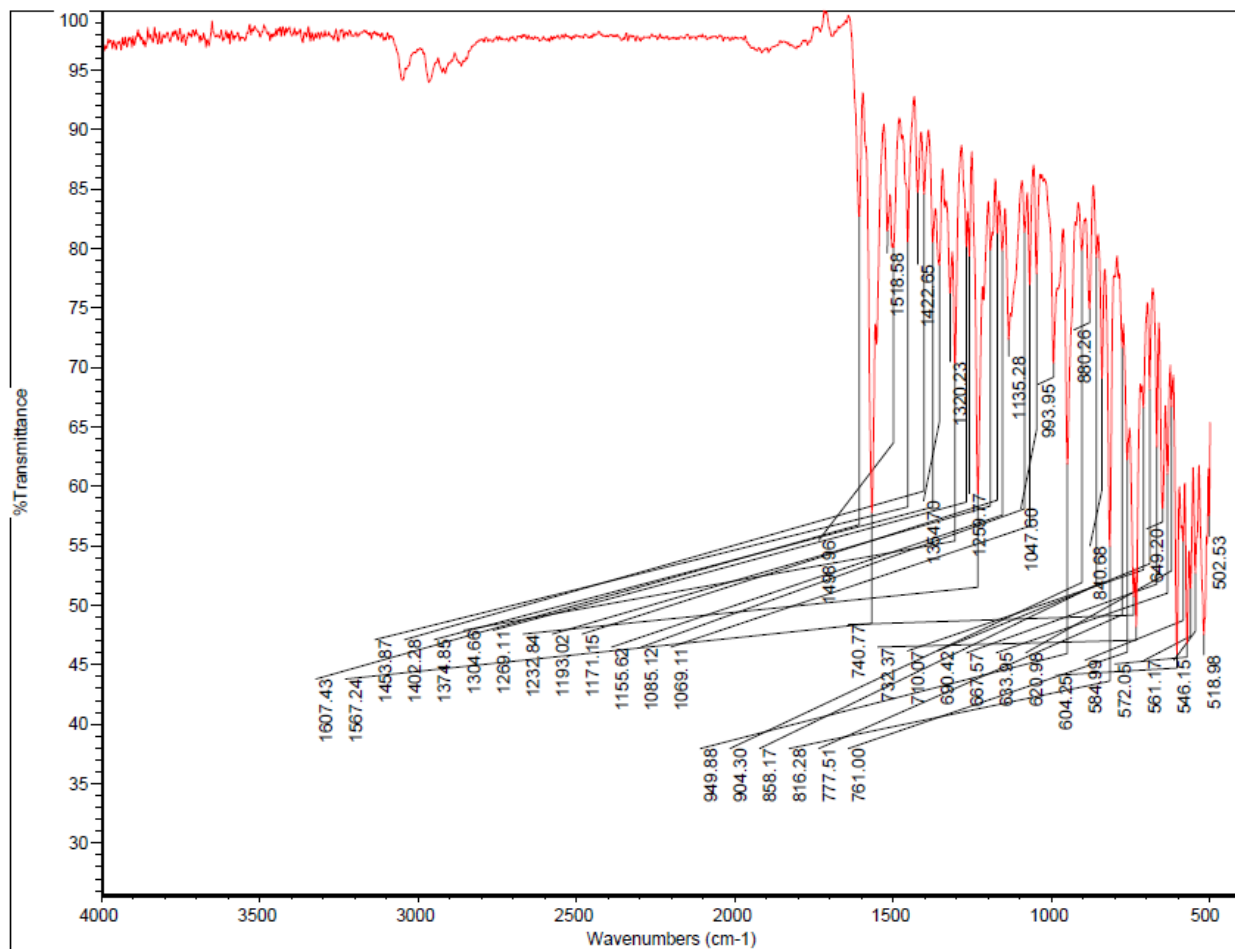
$^{13}\text{C}$  NMR ( $\text{CDCl}_3$ , 400 MHz) of **C-4**



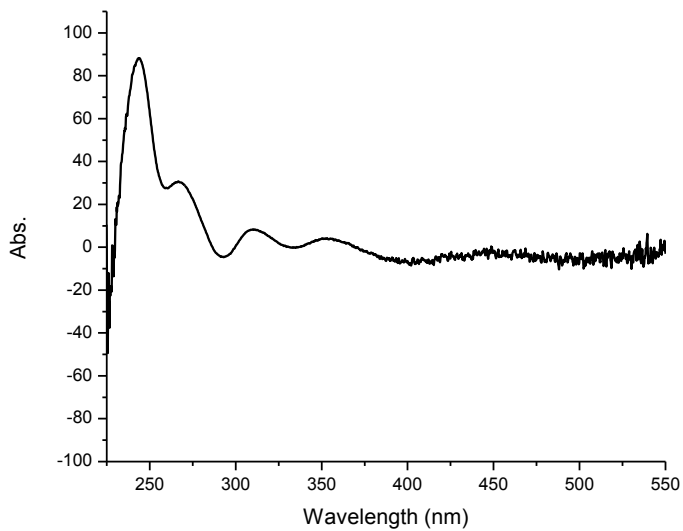
$^{13}\text{C}$  NMR ( $\text{CDCl}_3$ , 400 MHz) of **C-5**



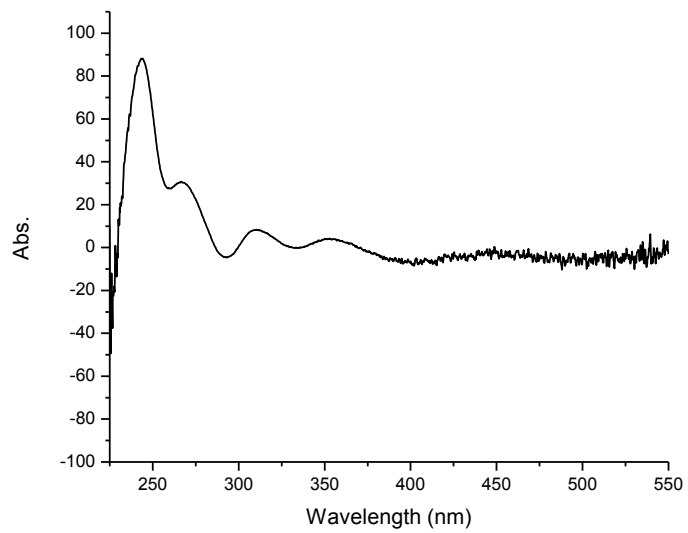
IR of C-4



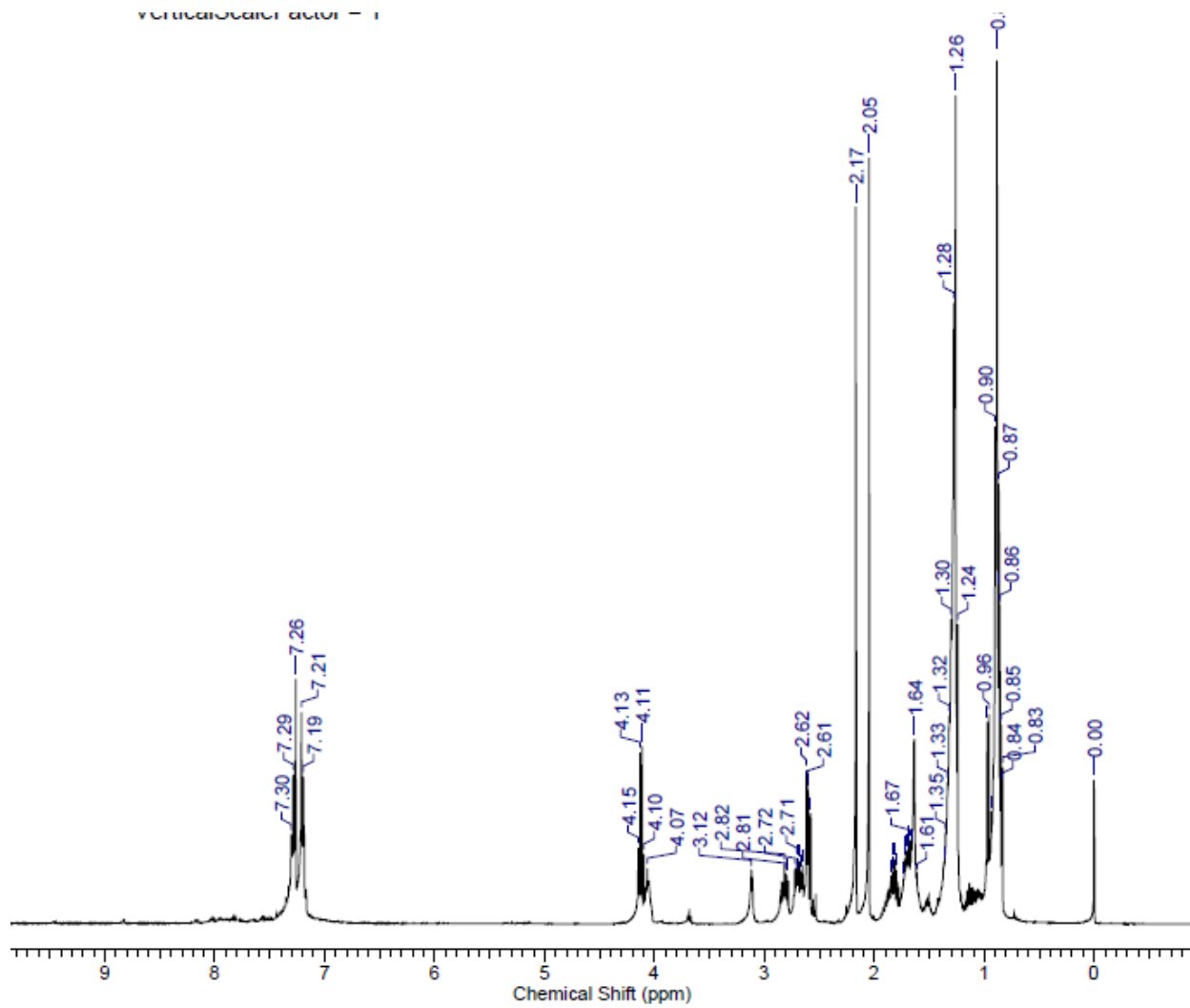
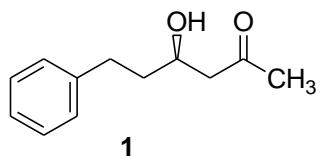
IR of C-5



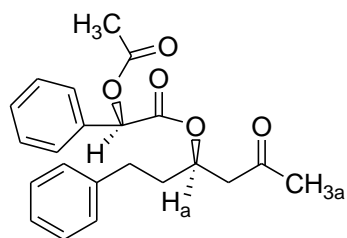
UV of C-4



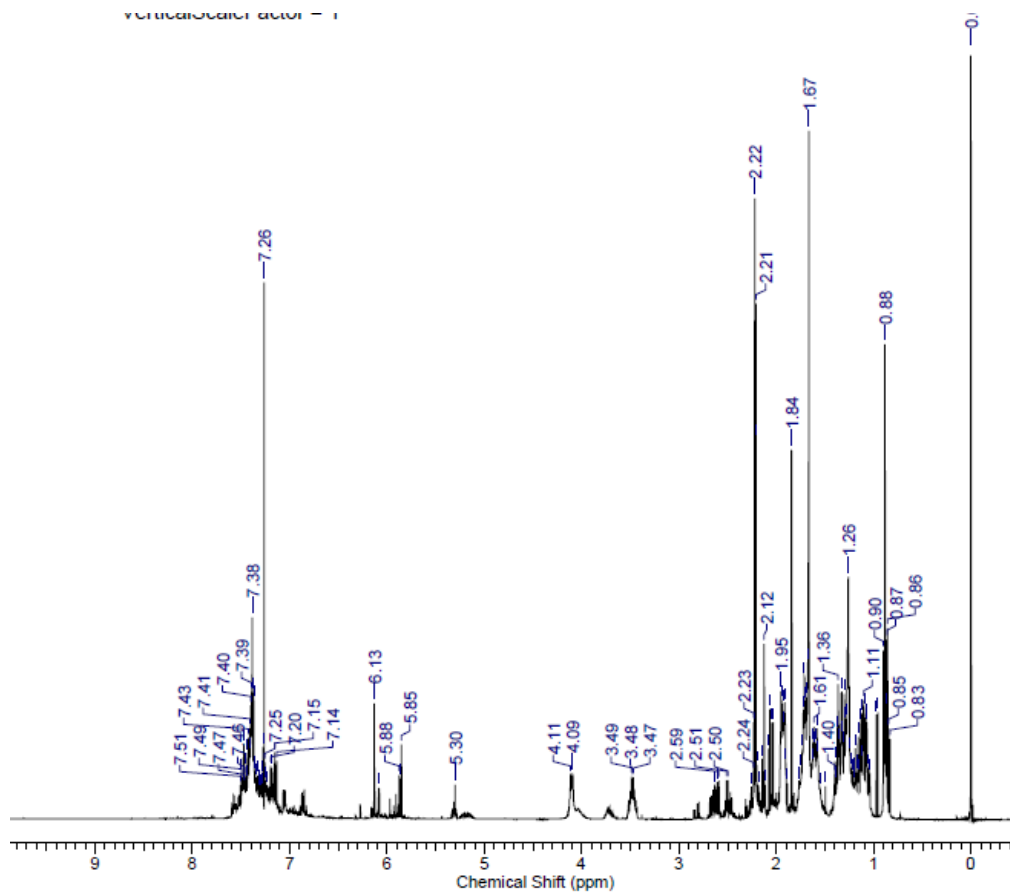
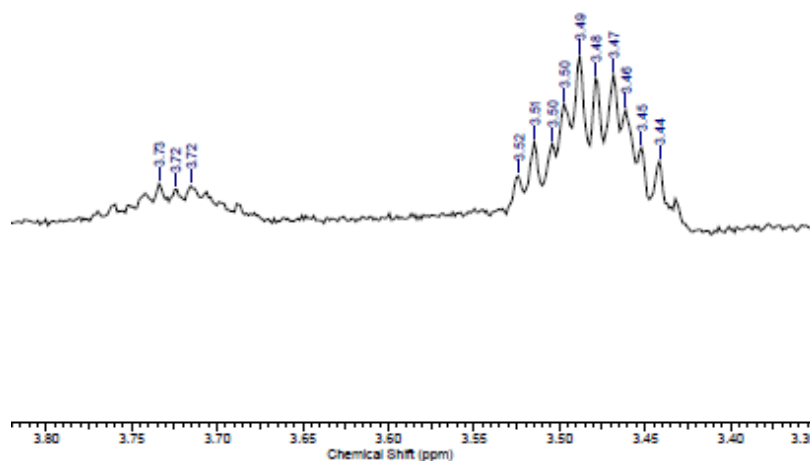
UV of C-5



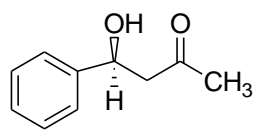
$^1\text{H}$  NMR ( $\text{CDCl}_3$ , 400 MHz) of **1**



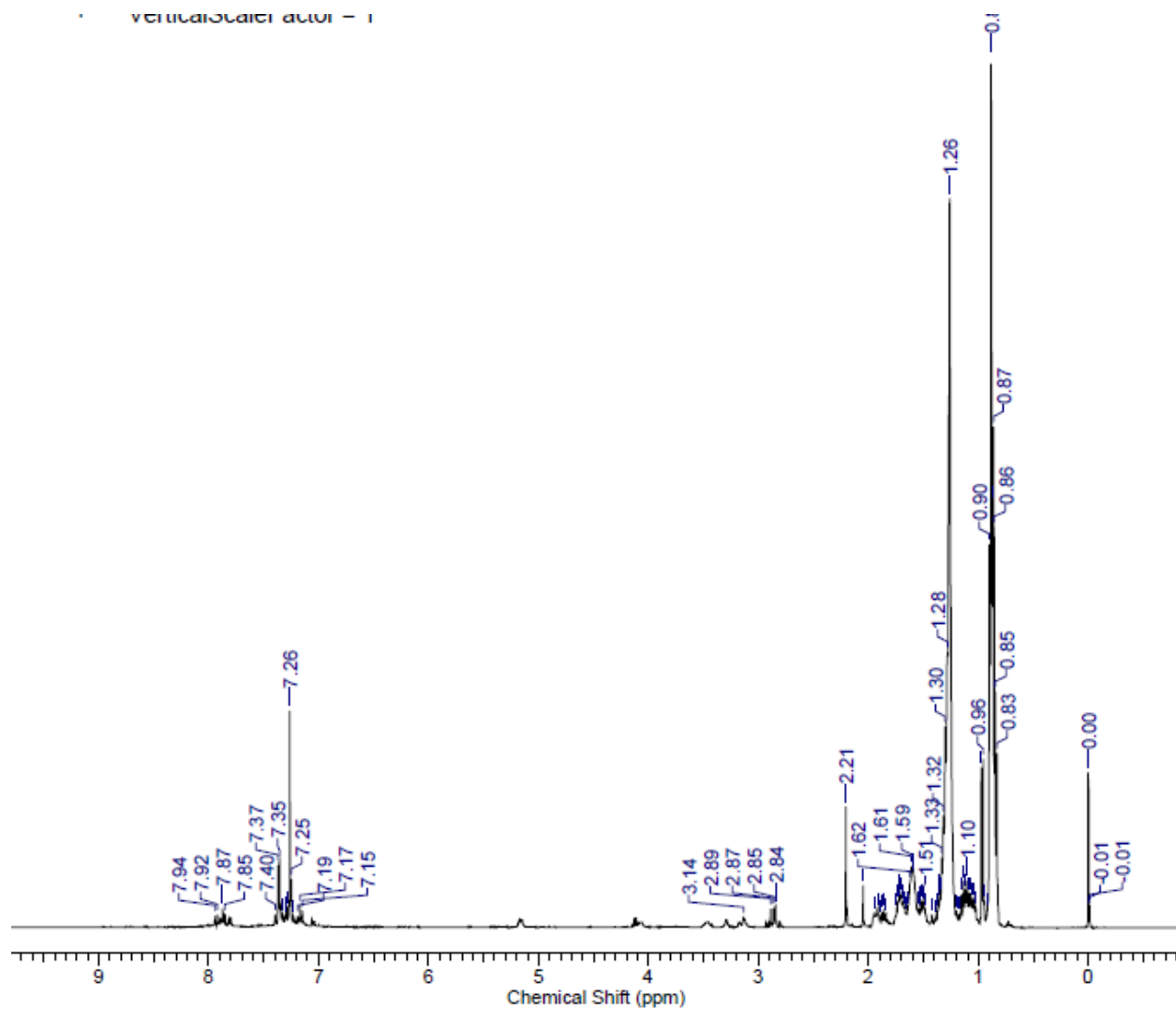
2



$^1\text{H}$  NMR ( $\text{CDCl}_3$ , 400 MHz) of 2

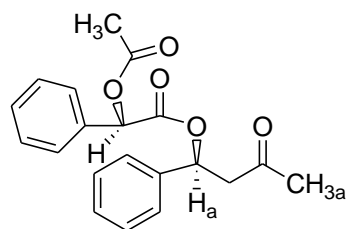


3

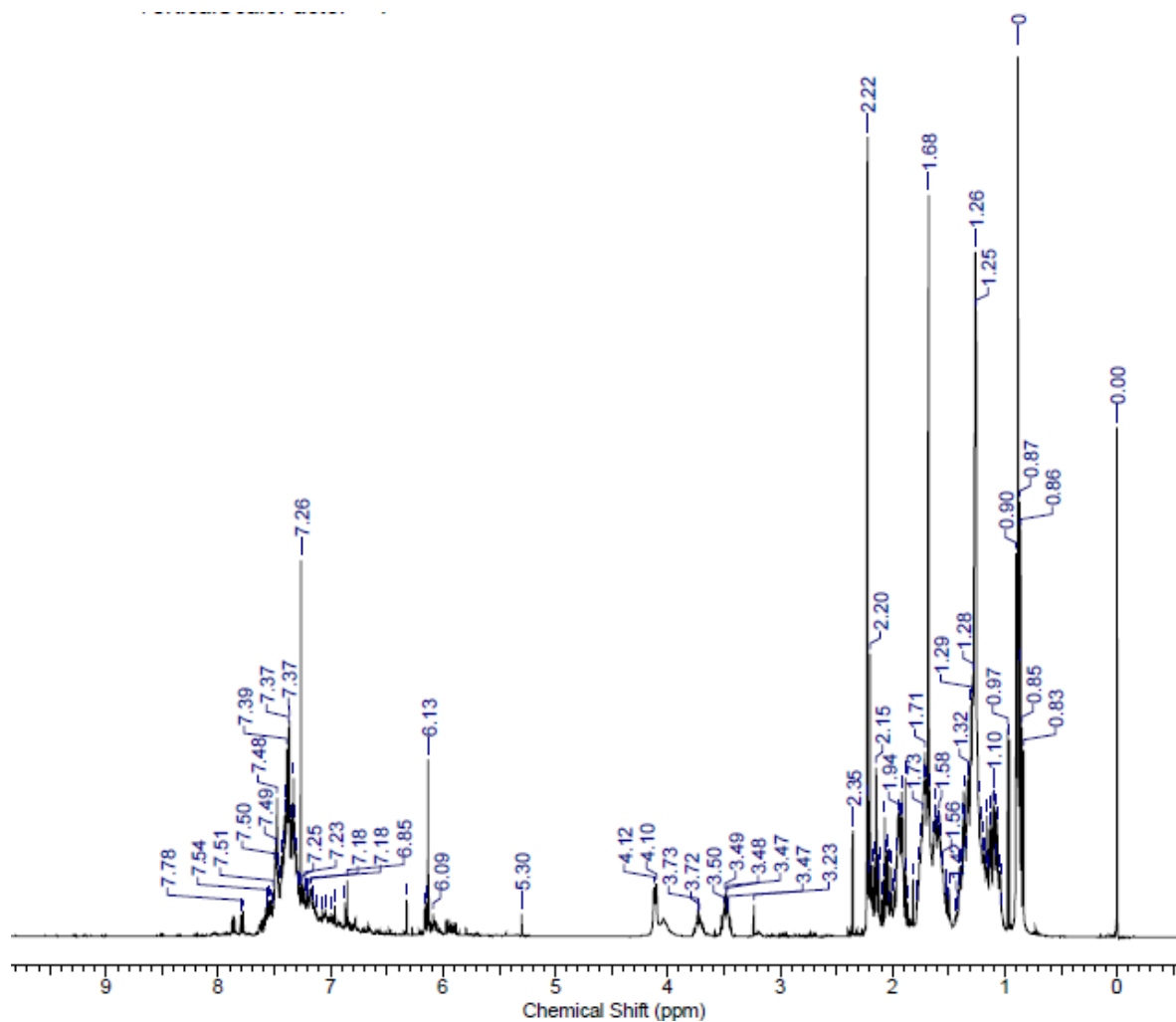
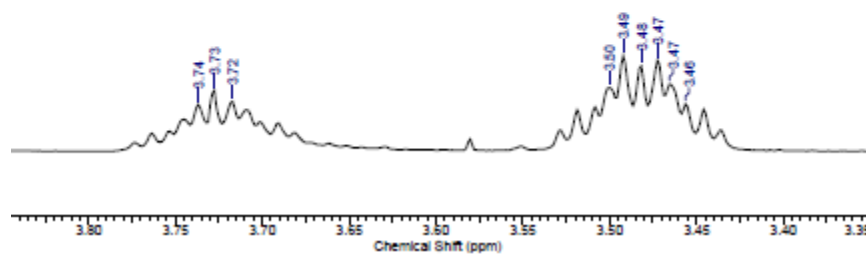


$^1\text{H}$  NMR ( $\text{CDCl}_3$ , 400 MHz) of **3**

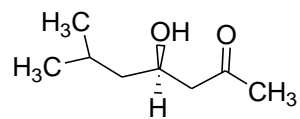




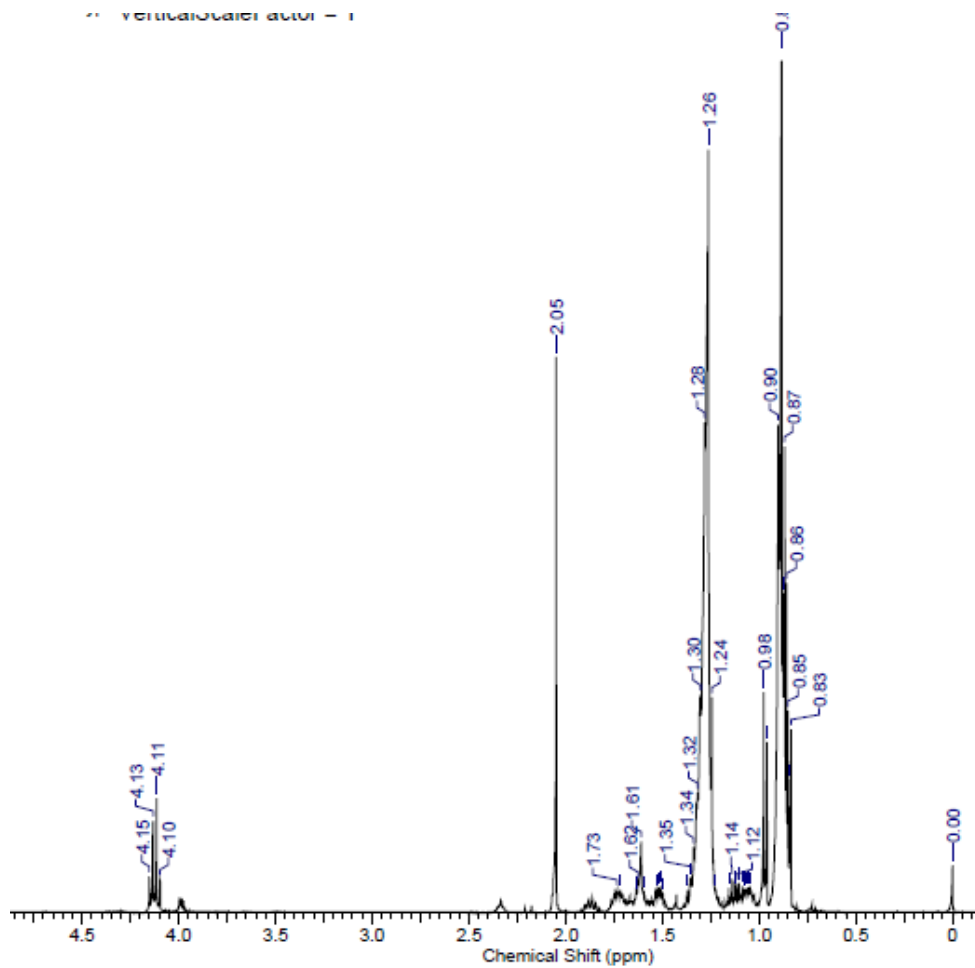
4



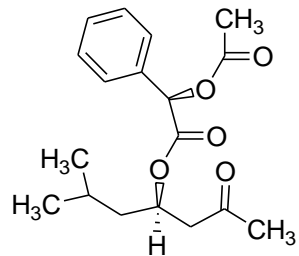
$^1\text{H}$  NMR ( $\text{CDCl}_3$ , 400 MHz) of **4**



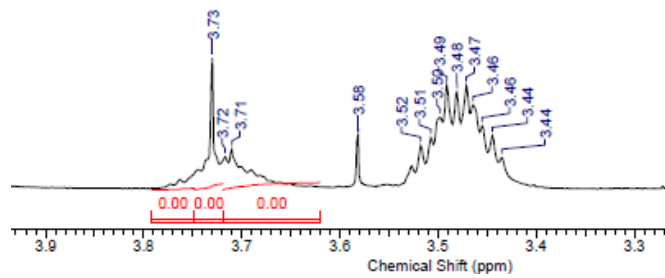
5



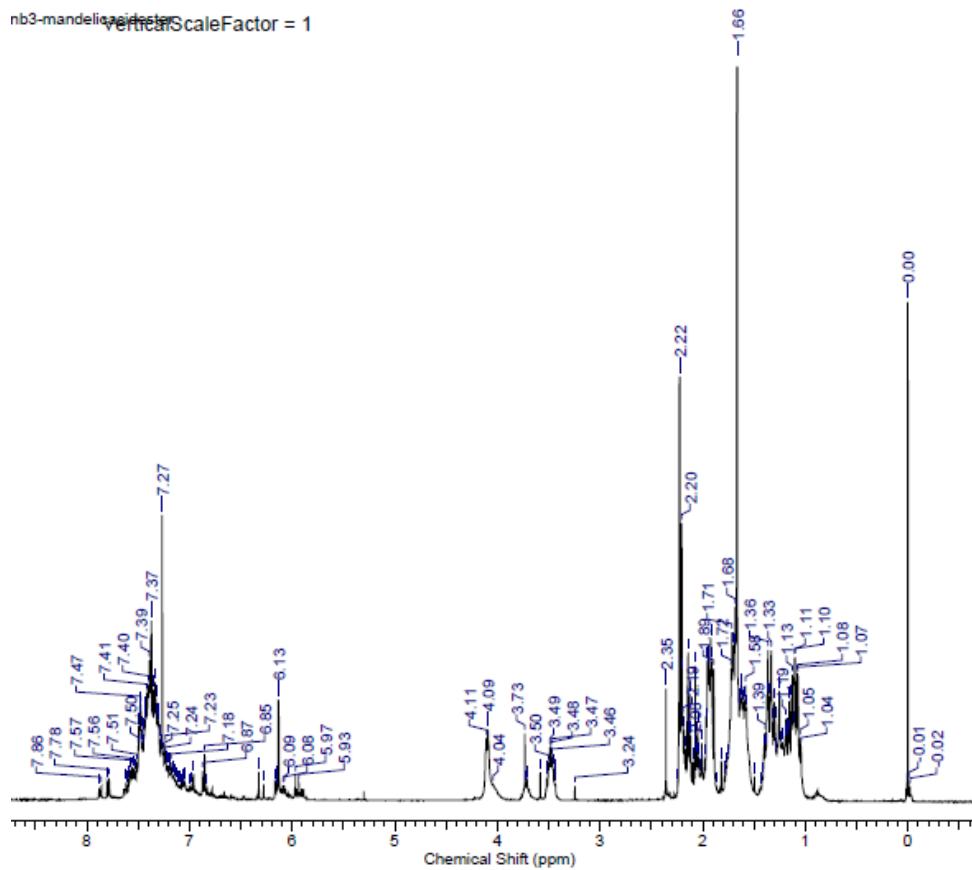
$^1\text{H}$  NMR ( $\text{CDCl}_3$ , 400 MHz) of 5



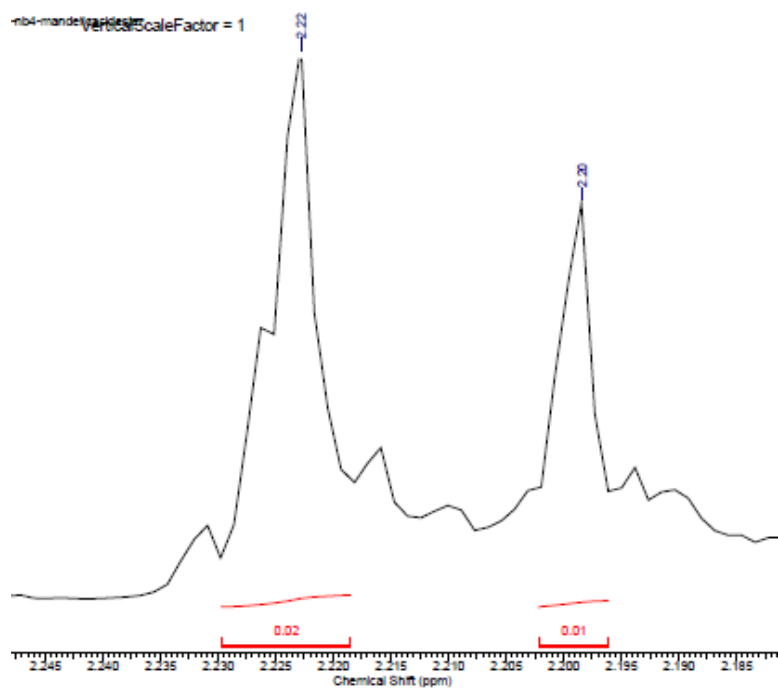
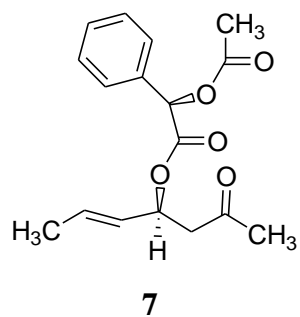
**6**



nb3-mandelic acid ester  
Vertical ScaleFactor = 1



$^1\text{H}$  NMR ( $\text{CDCl}_3$ , 400 MHz) of **6**



$^1\text{H}$  NMR ( $\text{CDCl}_3$ , 400 MHz) integration of **7**